# Cement chemistry

## 2nd edition

H.F.W. Taylor
Emeritus Professor of Inorganic Chemistry
University of Aberdeen

Thomas Telford

Published by Thomas Telford Publishing, Thomas Telford Services Ltd,
1 Heron Quay, London E14 4JD

First published 1990 by Academic Press
Thomas Telford edition published 1997

Distributors for Thomas Telford books are
*USA*: American Society of Civil Engineers, Publications Sales Department,
345 East 47th Street, New York, NY 10017-2398
*Japan*: Maruzen Co. Ltd, Book Department, 3Ã10 Nihonbashi 2-chome, Chuo-ku, Tokyo 103
*Australia*: DA Books and Journals, 648 Whitehorse Road, Mitcham 3132, Victoria

A catalogue record for this book is available from the British Library

ISBN: 0 7277 2592 0

# Preface

The previous edition of this book, published by Academic Press in 1990, is both out of print and out of date, and when Thomas Telford invited me to prepare a new edition I was delighted to comply. I am most grateful both to them and to Academic Press, whose release of the copyright made the present edition possible.

This book deals with the chemistry of the principal silicate and aluminate cements used in building and civil engineering. It is directed primarily to those whose background is in chemistry, materials science or related disciplines. Emphasis is placed throughout on the underlying science rather than on practical applications, which are well covered in other works. The cements considered fall into the category of hydraulic cements; they set and harden as a result of chemical reactions with water, and if mixed with water in appropriate proportions continue to harden even if subsequently placed in water. Much the most important is Portland cement. Chapters 1 to 4 deal mainly with the chemistry of Portland cement manufacture and the nature of the resulting product. Chapters 5 to 8 deal mainly with the processes that occur when this product is mixed with water and with the nature of the hardened material. Chapters 9 to 11 deal with the chemistry of other types of cement, of admixtures for concrete and of special uses for cements. Chapter 12 deals with chemical and microstructural aspects of concrete, including ones that affect its durability or limit its service life.

The literature of cement chemistry is voluminous; the abstracting journal, *Cements Research Progress*, has for some years listed around 1000 new contributions annually. The output of the seven years since the previous edition of this book appeared is reflected in the increased number of references to the literature, which is approximately 1500 compared with 1300 in that edition. Of necessity, coverage in the present book has been selective, but it is hoped that the most important contributions up to mid-1996 have been covered. The advances in some parts of the subject have been greater than in others, and this is reflected in the differences between this and the previous edition; some sections have been totally rewritten whereas others have changed relatively little.

As one who has seen the subject develop over a period of nearly 50 years, I am highly aware of the problems that those entering the subject

for the first time have in grappling with the previous literature. I have therefore tried not only to deal with recent research, but also to place the development of our knowledge in a historical perspective. I hope that the book will thereby serve both as an introduction that assumes no previous specialist knowledge of cements, and as a guide to further research.

**Acknowledgements**

I am most grateful to Sally Smith and her colleagues at Thomas Telford Publishing for their unfailing help and patience, and to my wife, Joan, for help in preparing the reference list and in other ways. I am also most grateful to former colleagues at the University of Aberdeen and friends elsewhere with whom I have had productive discussions over a period of many years. Professor F.P. Glasser was most helpful in suggesting that this edition be published. Others in Aberdeen to whom thanks are due include, notably, Dr J.A. Gard, Dr L.S. (Dent) Glasser and Dr E.E. Lachowski. Either indirectly through the previous edition, or directly in relation to the present one, many others have given invaluable assistance. Mr R.S. Gollop, Dr S. Kelham, Mr C.P. Kerton, Dr G.R. Long, Mr J.S. Lumley, Dr J.J. Kollek, Dr G.K. Moir and Mr M.S. Sumner, now or formerly of Blue Circle Industries plc, helped on many aspects of cement production, use and durability. My thoughts on the hydration chemistry of calcium silicates owe much to discussions with Drs P.W. Brown, G. Frohnsdorff and H.M. Jennings, then all at the National Bureau of Standards (now NIST), USA. Those on microstructural aspects of hydration similarly owe much to discussions with the late Professor P.L. Pratt and Dr K.L. Scrivener, then both at Imperial College, London. Dr L.J. Parrott (British Cement Association) helped greatly with a discussion on the pore structures of cement pastes. Drs A. Capmas, C.M. George, K.L. Scrivener, D. Sorrentino and F. Sorrentino (Lafarge Corporation) gave extensive and invaluable help in preparing the section on calcium aluminate cements. Professor J. Bensted, then at The British Petroleum Company plc, corrected some important errors on oil well cementing. Many of those mentioned above gave help that included comments on parts of the manuscript, but any errors are mine.

Many people, noted in the reference list, generously made results available in advance of publication. Dr D.C. Pomeroy, formerly at the British Cement Association, Drs K.L. Scrivener and M.C. Lewis (Imperial College) and Dr D. Sorrentino kindly provided some excellent light or electron micrographs. Mr C.P. Kerton freely gave extensive bibliographical assistance, and I thank Mr S. Black and Ms J. Kerr (University of Aberdeen) for photography of the line drawings.

I thank publishers (as copyright holders; italics) and authors for permission to reproduced the figures noted below. Authors and sources, including copyright years, are given in the captions and reference list and, where it was requested, the acknowledgment is expanded below. Reprinted by permission of the *American Ceramic Society*, Figs 5.5C and D (Ref. J11, Issue 10, Oct., on 'Morphological development of hydrating tricalcium silicate as examined by electron microscopy techniques'); Fig. 5.1 (Ref. M46, Issue 12, Dec., on 'Analytical electron

microscopy of cement pastes: IV, $\beta$-dicalcium silicate pastes'); Figs 5.7 and 5.9 (Ref. T21, Issue 6, June, on 'Proposed structure for calcium silicate hydrate gel'); Fig. 5.12 (Ref. J16, Issue 8, Aug., on 'Aqueous solubility relationships for two types of calcium silicate hydrate'); Fig. 9.3 (Ref. T39, Issue 12, Dec., on 'Analytical study of pure and extended Portland cement pastes: II, fly ash- and slag-cement pastes'). *American Concrete Institute*, Fig. 11.6. Reprinted by permission of *American Journal of Science*, Fig. 6.5. *British Cement Association*, Fig. 5.11. © *(British) Crown Copyright* 1970. Published by permission of the Controller of HMSO, and with thanks to the Institute of Materials, Fig. 2.9. *Cemento*, Fig. 11.4. *Chapman and Hall Ltd*, Figs 10.2 and 10.6. Reprinted from 'Cement and Concrete Research', with kind permission from *Elsevier Science Ltd*, The Boulevard, Langford Lane, Kidlington OX5 1GB, UK, Figs 1.2, 3.3, 5.4, 5.8, 5.14, 5.15, 8.9, 11.1, 11.5, 12.5 and 12.7. *International Cement Microscopy Association* from 'Proceedings of the 6th International Conference on Cement Microscopy, Albuquerque, NM, USA', Fig. 4.3. *8th International Congress on the Chemistry of Cement* (Vol. 3, Fig. 4, p. 231), Fig. 6.7. *Materials Research Society*, Figs 9.1, 9.2 and 12.1. *R. Oldenbourg Verlag*, Fig. 5.6. *Palladian Publications Ltd.*, Fig. 7.1. *RILEM Publications*, first published in 'The hydration of tricalcium silicate', RILEM committee 68-MMH, task group 3, 'Materials and Structures' **17**, (102) 458 (1984), Figs 5.10 and 5.13. *The Royal Society*, Fig. 7.7. *Editions Septima*, Fig. 10.7. *Society of Chemical Industry*, Fig. 5.2. *Stroyizdat*, Fig. 3.4. *Thomas Telford Publishing*, Figs 12.4 and 12.6. *Transportation Research Board, National Research Council, Washington, DC*, Fig. 4, p. 380 in Ref. L35, 'Changes in composition of the aqueous phase during hydration of cement pastes and suspensions', Fig. 7.8. Reprinted by permission of *John Wiley and Sons Ltd*, Fig. 8.4. I thank the National Bureau of Standards (now NIST) for the use of Figs 7.9 and 8.2. Figs 7.2, 8.8, 10.1, 11.3, 12.2, 12.3, 12.7, 12.8 and 12.9 did not appear in the previous edition of this book. The remaining figures were used in that edition, and I am most grateful to Academic Press for permission to reproduce them.

# Contents

# 1 Portland cement and its major constituent phases

## 1.1 Introduction

### *1.1.1 Portland cement: general*

Portland cement is made by heating a mixture of limestone and clay, or other materials of similar bulk composition and sufficient reactivity, ultimately to a temperature of about 1450°C. Partial fusion occurs, and nodules of clinker are produced. The clinker is mixed with a few per cent of calcium sulfate and finely ground, to make the cement. The calcium sulfate controls the rate of set and influences the rate of strength development. It is commonly described as gypsum, but this may be partly or wholly replaced by other forms of calcium sulfate. Some specifications allow the addition of other materials at the grinding stage. The clinker typically has a composition in the region of 67% CaO, 22% $SiO_2$, 5% $Al_2O_3$, 3% $Fe_2O_3$ and 3% other components, and normally contains four major phases, called alite, belite, aluminate and ferrite. Several other phases, such as alkali sulfates and calcium oxide, are normally present in minor amounts. Hardening results from reactions between the major phases and water.

Alite is the most important constituent of all normal Portland cement clinkers, of which it constitutes 50–70%. It is tricalcium silicate ($Ca_3SiO_5$) modified in composition and crystal structure by ionic substitutions. It reacts relatively quickly with water, and in normal Portland cements is the most important of the constituent phases for strength development; at ages up to 28 days, it is by far the most important.

Belite constitutes 15–30% of normal Portland cement clinkers. It is dicalcium silicate ($Ca_2SiO_4$) modified by ionic substitutions and normally present wholly or largely as the $\beta$ polymorph. It reacts slowly with water, thus contributing little to the strength during the first 28 days, but substantially to the further increase in strength that occurs at later ages. By one year, the strengths obtainable from pure alite and pure belite are about the same under comparable conditions.

Aluminate constitutes 5–10% of most normal Portland cement clinkers. It is tricalcium aluminate ($Ca_3Al_2O_6$), substantially modified in composition and sometimes also in structure by ionic substitutions.

It reacts rapidly with water, and can cause undesirably rapid setting unless a set-controlling agent, usually gypsum, is added.

Ferrite makes up 5–15% of normal Portland cement clinkers. It is tetracalcium aluminoferrite ($Ca_2AlFeO_5$), substantially modified in composition by variation in Al/Fe ratio and ionic substitutions. The rate at which it reacts with water appears to be somewhat variable, perhaps due to differences in composition or other characteristics, but in general is high initially and low or very low at later ages.

### *1.1.2 Types of Portland cement*

The great majority of Portland cements made throughout the world are designed for general constructional use. The standard specifications with which such cements must comply are similar, but not identical, in all countries and various names are used to define the material, such as Class 42.5 Portland cement in current European and British standards (42.5 is the minimum 28-day compressive strength in MPa), Types I and II Portland cement in the ASTM (American Society for Testing and Materials) specifications used in the USA, or Ordinary Portland Cement (OPC) in former British standards. Throughout this book, the term 'ordinary' Portland cements is used to distinguish such general-purpose cements from other types of Portland cement, which are made in smaller quantities for special purposes.

Standard specifications are, in general, based partly on chemical composition or physical properties such as specific surface area, and partly on performance tests, such as setting time or compressive strength developed under standard conditions. The content of MgO* is usually limited to 4–5%, because quantities of this component in excess of about 2% can occur as periclase (magnesium oxide), which through slow reaction with water can cause destructive expansion of hardened concrete. Free lime (calcium oxide) can behave similarly. Excessive contents of $SO_3$ can also cause expansion, and upper limits, typically 3·5% for ordinary Portland cements, are usually imposed. Alkalis ($K_2O$ and $Na_2O$) can undergo expansive reactions with certain aggregates, and some specifications limit the content, e.g. to 0·6% equivalent $Na_2O$ ($Na_2O + 0{\cdot}66\ K_2O$). Other upper limits of composition widely used in specifications relate to matter insoluble in dilute acid, and loss on ignition. Many other minor components are limited in content by their effects on the manufacturing process, or the properties, or both, and in some cases the limits are defined in specifications.

Rapid-hardening Portland cements have been produced in various ways, such as varying the composition to increase the alite content, finer grinding of the clinker, and improvements in the manufacturing process,

* Confusion can arise because the names or formulae of compounds can be used to denote either phases or components; this applies especially to CaO and MgO. Here and elsewhere, chemical or mineral names of oxides (e.g. calcium oxide, magnesium oxide, lime, periclase) will generally be used for phases, and formulae (e.g. CaO, MgO) for components. Mineral names or prefixed formulae (e.g. $\alpha$-$Al_2O_3$) are never used for components.

e.g. finer grinding or better mixing of the raw materials. The alite contents of Portland cements have increased steadily over the one and a half centuries during which the latter have been produced, and many cements that would be considered ordinary today would have been described as rapid hardening only a few decades ago. In the ASTM specifications, rapid-hardening Portland cements are called high early strength or Type III cements. For both ordinary and rapid-hardening cements, both lower and upper limits may be imposed on strengths at 28 days, upper limits being a safeguard against poor durability resulting from the use of inadequate cement contents in concrete.

Destructive expansion from reaction with sulfates can occur not only if the latter are present in excessive proportion in the cement, but also from attack on concrete by sulfate solutions. The reaction involves the $Al_2O_3$-containing phases in the hardened cement, and in sulfate-resisting Portland cements its effects are reduced by decreasing the proportion of the aluminate phase, sometimes to zero. This is achieved by decreasing the ratio of $Al_2O_3$ to $Fe_2O_3$ in the raw materials. In the USA, sulfate-resisting Portland cements are called Type V cements.

White Portland cements are made by increasing the ratio of $Al_2O_3$ to $Fe_2O_3$, and thus represent the opposite extreme in composition to sulfate-resisting Portland cements. The normal, dark colour of Portland cement is due to the ferrite, formation of which in a white cement must thus be avoided. It is impracticable to employ raw materials that are completely free from $Fe_2O_3$ and other components, such as $Mn_2O_3$, that contribute to the colour. The effects of these components are therefore usually minimized by producing the clinker under slightly reducing conditions and by rapid quenching. In addition to alite, belite and aluminate, some glass may be formed.

The reaction of Portland cement with water is exothermic, and while this can be an advantage under some conditions because it accelerates hardening, it is a disadvantage under others, such as in the construction of large dams or in the lining of oil wells, when a cement slurry has to be pumped over a large distance under pressure and sometimes at a high temperature. Slower heat evolution can be achieved by coarser grinding, and decreased total heat evolution by lowering the contents of alite and aluminate. The ASTM specifications include definitions of a Type II or 'moderate heat of hardening' cement, and a more extreme Type IV or 'low heat' cement. The Type II cement is also suitable for conditions exposed to moderate sulfate attack, and is widely used in general construction work. Heat evolution can also be decreased by partially replacing the cement by flyash (pulverized fuel ash; pfa) or other materials (Chapter 9), and this is today a widely used solution. The specialized requirements of oil well cements are discussed in Section 11.8.

### *1.1.3 Cement chemical nomenclature and other abbreviations*

Chemical formulae in cement chemistry are often expressed as sums of oxides; thus tricalcium silicate, $Ca_3SiO_5$, can be written as $3CaO \cdot SiO_2$. This does not imply that the constituent oxides have any separate

existence within the structure. It is usual to abbreviate the formulae of the commoner oxides to single letters, such as C for CaO or S for $SiO_2$, $Ca_3SiO_5$ thus becoming $C_3S$. This system is often combined with orthodox chemical notation within a chemical equation, e.g.

$$3CaO + SiO_2 \rightarrow C_3S \tag{1.1}$$

or even within a single formula, as in $C_{11}A_7 \cdot CaF_2$ for $Ca_{12}Al_{14}O_{32}F_2$. The abbreviations most widely used are as follows.

| | | | |
|---|---|---|---|
| $C = CaO$ | $S = SiO_2$ | $A = Al_2O_3$ | $F = Fe_2O_3$ |
| $M = MgO$ | $K = K_2O$ | $\bar{S} = SO_3$ | $N = Na_2O$ |
| $T = TiO_2$ | $P = P_2O_5$ | $H = H_2O$ | $\bar{C} = CO_2$ |

The formulae of the simple oxide phases (e.g. CaO) are usually written in full. Other abbreviations and units used in this book are as follows.

#### 1.1.3.1 Techniques

BEI = backscattered electron imaging. BSE = backscattered electron. DTA = differential thermal analysis. EPMA = electron probe microanalysis. ESCA = electron spectroscopy for chemical analysis (X-ray photoelectron spectroscopy). GLC = gas–liquid chromatography. GPC = gel permeation chromatography. IR = infrared. MIP = mercury intrusion porosimetry. NMR = nuclear magnetic resonance. QXDA = quantitative X-ray diffraction analysis. SEM = scanning electron microscop(e,y). STEM = scanning transmission electron microscop(e,y). TEM = transmission electron microscop(e,y). TG = thermogravimetry. TMS = trimethylsilyl(ation). XRD = X-ray diffraction. XRF = X-ray fluorescence.

#### 1.1.3.2 Materials

C–S–H = poorly crystalline or amorphous calcium silicate hydrate of unspecified composition. Ggbs = ground granulated blastfurnace slag. Hcp = hardened cement paste. Pfa = pulverized fuel ash (flyash).

#### 1.1.3.3 Properties or reactions

AR = alumina ratio (alumina modulus). ASR = alkali silica reaction. DEF = delayed ettringite formation. LSF = lime saturation factor. SR = silica ratio (silica modulus). $C_x$ = analytical (total) concentration of $x$, irrespective of species. $[x]$ = concentration of species $x$. $\{x\}$ = activity of species $x$. RH = relative humidity. $Na_2O_e$ = equivalent $Na_2O$ (mass % $Na_2O + 0{\cdot}66\ K_2O$). $(+)2V$, $(-)2V$, optic sign and optic axial angle.

#### 1.1.3.4 Pressure units

$1\,MPa = 1\,N\,mm^{-2} = 10\,bar = 9.87\,atm = 7500\,torr = 145{\cdot}0\,lb\,in^{-2} = 10{\cdot}198\,kg\,cm^{-2}$.

## 1.2 Alite

### 1.2.1 Polymorphism and crystal structure

On being heated, pure $C_3S$ undergoes a series of reversible phase transitions, which have been detected by a combination of DTA,

high-temperature XRD and high-temperature light microscopy (B1,G1, M1–M5,R1,R2,Y1):

$$T_1 \overset{620^\circ C}{\rightleftarrows} T_2 \overset{920^\circ C}{\rightleftarrows} T_3 \overset{980^\circ C}{\rightleftarrows} M_1 \overset{990^\circ C}{\rightleftarrows} M_2 \overset{1060^\circ C}{\rightleftarrows} M_3 \overset{1070^\circ C}{\rightleftarrows} R$$

(T = triclinic, M = monoclinic, R = rhombohedral)

The pure compound, when cooled to room temperature, is thus $T_1$. In production clinkers, due to the incorporation of substituent ions, the form present at room temperature normally approximates to $M_1$ or $M_3$ or a mixture of these; rarely, $T_2$ is found (M1–M5,T1). There has been some uncertainty as to the number and nomenclature of these polymorphs; reported $M_{1b}$ and $M_{2b}$ forms appear to be identical with $M_3$, leaving reported $M_{1a}$ and $M_{2a}$ forms to be called simply $M_1$ and $M_2$ respectively (M4,M5).

Jeffery (J1) made the first determination of the crystal structure. He showed that the forms now known as R, $T_1$ and $M_3$ had closely similar structures, and determined the approximate or pseudostructure common to all three; it was built from $Ca^{2+}$, $SiO_4^{4-}$ and $O^{2-}$ ions, the last being bonded only to six $Ca^{2+}$ ions, as in CaO. Later, more exact determinations were reported for $T_1$ (G2), $M_3$ stabilized by $Mg^{2+}$ (N1), $M_3$ with increased disorder isolated from a works clinker (M6), R at 1200°C (N2) and R stabilized with $Sr^{2+}$ (I1). Figure 1.1 shows the structure of the R form. The known structures are all closely similar as regards the positions of the $Ca^{2+}$ and $O^{2-}$ ions and of the Si atoms, but differ markedly in the orientations of the $SiO_4^{4-}$ tetrahedra, which show varying degrees of disorder.

The structural differences between the polymorphs affect the coordination of the $Ca^{2+}$ ions and the O atoms of the $SiO_4^{4-}$ tetrahedra. For each polymorph, there are several crystallographically distinct Ca sites, having different coordination, and for a given site, the coordination sometimes varies between individual atoms due to orientational disorder in the surrounding $SiO_4$ tetrahedra. Definitions of the Ca coordination numbers are somewhat arbitrary due to variations in the lengths of the bonds; e.g. in the R form at 1200°C, the Ca atoms in one of the sites could be regarded as 7 coordinated if bonds as long as 0·296 nm are counted, and 5 coordinated if they are not (N2). If such abnormally long bonds are excluded, the mean coordination number of the Ca is 5·66 in the R polymorph, 6·15 in $M_3$ and 6·21 in $T_1$ (M5). In relation to reactivity towards water, the coordination of the oxygen atoms is possibly more important than that of Ca. This has not been discussed in detail in the literature, but mean oxygen coordination numbers may be expected to increase with those of calcium.

Table 1.1 gives the crystal data for the $C_3S$ polymorphs that have been obtained using single-crystal methods. The literature contains additional unit-cell data, based only on powder diffraction evidence. Some of these may be equivalent to ones in Table 1.1, since the unit cell of a monoclinic or triclinic crystal can be defined in different ways, but some are certainly incorrect. Because only the stronger reflections are recorded, and for

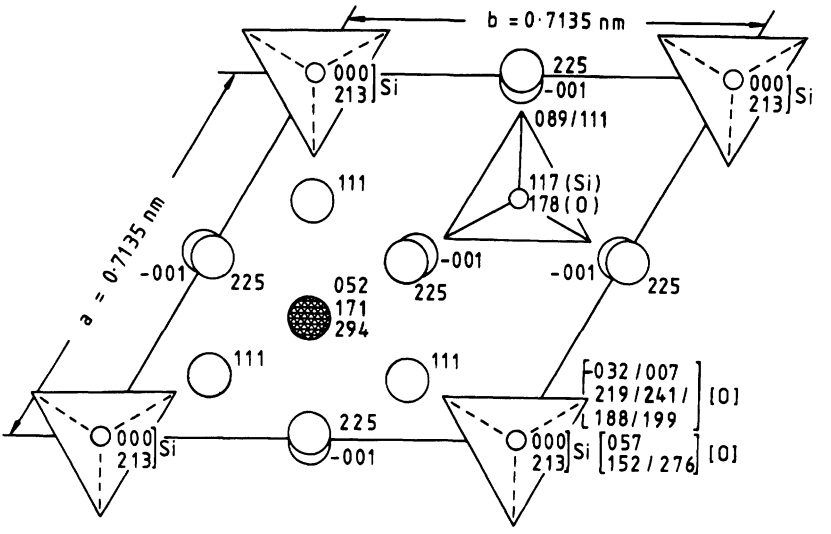


**Fig. 1.1** *Crystal structure of the R-modification of $C_3S$, based on the results of Nishi and Takéuchi (N2) and showing Ca atoms (large open circles), Si atoms (small open circles), oxide ions (large hatched circle) and oxygen tetrahedra (triangles). Heights of atoms are in thousandths of the cell height (c = 2·5586 nm), slashes denoting statistical alternatives. Oxygen tetrahedra are shown in averaged orientations; in reality, each is tilted around its enclosed Si atom statistically in any one of three directions so as to preserve the threefold symmetry. All tetrahedra point upwards excepting those surrounding the Si atoms at height 213, of which 70% point downwards and 30% upwards. Only the bottom third of the cell is shown, the middle and top thirds being derivable from it by translations of 1/3, 2/3, 1/3 and 2/3, 1/3, 2/3 parallel to the a, b and c axes respectively.*

**Table 1.1** *Crystal data for the $C_3S$ polymorphs*

| Polymorph | Space group | Cell parameters (*a*, *b*, *c* in nm) | | | | | | *Z* | Ref. |
|---|---|---|---|---|---|---|---|---|---|
| | | *a* | *b* | *c* | $\alpha$ | $\beta$ | $\gamma$ | | |
| Pseudostructure | R3m | 0·70 | | 2·50 | | | 120° | 9 | J1 |
| R (at 1200°C) | R3m | 0·7135 | | 2·5586 | | | 120° | 9 | N2 |
| R (stabilized with Sr) | R3m | 0·70567 | | 2·4974 | | | 120° | 9 | I1 |
| $M_3$ (stabilized with Mg) | Cm | 3·3083 | 0·7027 | 1·8499 | | 94·12° | | 36 | N1 |
| $M_3$ (ex clinker; less ordered) | Cm | 1·2235 | 0·7073 | 0·9298 | | 116·31° | | 6 | M6 |
| $T_1$ | $P\bar{1}$ | 1·167 | 1·424 | 1·372 | 105·5° | 94·3° | 90·0° | 18 | G2 |

other reasons, it is doubtful whether the unit cells of these complex structures can be reliably determined by powder methods. The unit cells of the $T_1$, $M_3$ and R forms are superficially somewhat different, but all are geometrically related; transformation matrices have been given (I2,H1).

### *1.2.2 Tricalcium silicate solid solutions*

Hahn *et al.* (H2) reported a detailed study of the limits of substitution in $C_3S$ of MgO, $Al_2O_3$ and $Fe_2O_3$, alone and in combination. They concluded that $Ca^{2+}$ could be partly replaced by $Mg^{2+}$ and that both $Ca^{2+}$ and $Si^{4+}$ could be partly replaced by $Al^{3+}$ or $Fe^{3+}$. They found the maximum content of MgO to be 2·0% at 1550°C, falling to 1·5% at 1420°C. The limits for $Al_2O_3$ and $Fe_2O_3$ were 1.0% and 1·1% respectively, but $Al^{3+}$ and $Fe^{3+}$ competed for sites, and the limit for each was lowered if the other was present. A subsequent study using $^{27}Al$ NMR indicated that the Al was present almost entirely in tetrahedral sites, thus excluding substitution of $Al^{3+}$ for $Ca^{2+}$ (S1). Woermann *et al.* (W1) found a limit of 1·4% for either $Na_2O$ or $K_2O$ at 1500°C.

Hahn *et al.* (H2) found that incorporation of $Mg^{2+}$, $Al^{3+}$ or $Fe^{3+}$ in sufficient quantity caused the higher temperature polymorphs to persist on cooling to room temperature. For each combination of substituents studied, increase in the total proportion of substituents led to the persistence of successively higher temperature polymorphs in the sequence $T_1 \rightarrow T_2 \rightarrow M_1$. In the system $CaO–MgO–Al_2O_3–SiO_2$, total contents of substituent oxides of about 1% caused $T_1$ to be replaced by $T_2$, and ones of about 2% caused $T_2$ to be replaced by $M_1$. Slightly higher total substituent contents were needed to effect each of these changes if $Fe_2O_3$ was present.

### *1.2.3 Compositions of alites in clinkers*

Pure $C_3S$ contains 73.7% of CaO and 26.3% of $SiO_2$. Alites in clinkers typically contain 3–4% of substituent oxides. Boikova (B2) found a positive correlation between the total percentage of substituent oxides in the alite ($I_a$) and the percentage of MgO in the clinker ($M_c$). Her results are approximately fitted by the equation $I_a = 0{\cdot}7M_c + 2{\cdot}1$.

Many workers have analysed alites from ordinary production clinkers by X-ray microanalysis (B3,B4,G3,G4,H3–H5,K1,M6,M7,S2,T2,T3,U1) or chemical analysis of separated material (U2,Y1). Alites in white (B4) and iron-rich (G5,H6) clinkers have been analysed. The most important substituents are $Mg^{2+}$, $Al^{3+}$ and $Fe^{3+}$, and there is wide agreement that the contents of MgO and probably also of $Fe_2O_3$ in the alite increase with those in the clinker. Since MgO replaces CaO, the content of CaO decreases with that of MgO in the clinker. Taking these relationships into account, as well as some less important variations with clinker composition and the errors inherent in either experimental method, the agreement between the various sets of data is generally good.

In the following discussion, symbols of the type $O_a$ and $O_c$ are used to denote the contents of oxide component $O$ in the alite and in the clinker,

**Table 1.2** *Typical compositions of phases in Portland cement clinkers (mass per cent)*

| | $Na_2O$ | MgO | $Al_2O_3$ | $SiO_2$ | $P_2O_5$ | $SO_3$ | $K_2O$ | CaO | $TiO_2$ | $Mn_2O_3$ | $Fe_2O_3$ |
|---|---|---|---|---|---|---|---|---|---|---|---|
| Alite* | 0·1 | 1·1 | 1·0 | 25·2 | 0·1 | 0·1 | 0·1 | 71·6 | 0·0 | 0·0 | 0·7 |
| Belite* | 0·1 | 0·5 | 2·1 | 31·5 | 0·1 | 0·2 | 0·9 | 63·5 | 0·2 | 0·0 | 0·9 |
| Aluminate (cubic)* | 1·0 | 1·4 | 31·3 | 3·7 | 0·0 | 0·0 | 0·7 | 56·6 | 0·2 | 0·0 | 5·1 |
| Ferrite* | 0·1 | 3·0 | 21·9 | 3·6 | 0·0 | 0·0 | 0·2 | 47·5 | 1·6 | 0·7 | 21·4 |
| Aluminate (orthorhombic)† | 0·6 | 1·2 | 28·9 | 4·3 | 0·0 | 0·0 | 4·0 | 53·9 | 0·5 | 0·0 | 6·6 |
| Aluminate (low Fe)‡ | 0·4 | 1·0 | 33·8 | 4·6 | 0·0 | 0·0 | 0·5 | 58·1 | 0·6 | 0·0 | 1·0 |
| Ferrite (low Al)§ | 0·4 | 3·7 | 16·2 | 5·0 | 0·0 | 0·3 | 0·2 | 47·8 | 0·6 | 1·0 | 25·4 |

* Typical values for an ordinary Portland cement clinker with 1·65% MgO, 3·1% $Fe_2O_3$ and molar $SO_3/(K_2O + Na_2O) < 1·0$. For clinkers not approximating to these conditions, the compositions of the phases may differ significantly from those given in the table, as explained in the text.

† Orthorhombic or pseudotetragonal forms, present in some clinkers high in alkalis. Na/K ratio varies with that of the clinker.

‡ Tentative composition for aluminate phase in white cement clinkers.

§ Values for the ferrite phase in a typical sulfate-resisting clinker (MgO, 2·1%; $Al_2O_3$, 3·8%; $Fe_2O_3$, 4·7%)(G5)· Compositions of other such clinkers may vary considerably (see text).

respectively. For MgO, Kristmann's (K1) data indicate the approximate relations $M_a = 0{\cdot}67 \times M_c$ for $M_c \leq 3{\cdot}0$ and $M_a \approx 2{\cdot}0$ for $M_c > 3{\cdot}0$. Yamaguchi and Takagi (Y1), Terrier (T2) and Maki *et al.* (M7) found similar correlations, but with slopes of 0·74, 0·45 and 0·58 respectively. For a series of clinkers of low Al/Fe ratio, Hall and Scrivener (H6) found $M_a = 0{\cdot}64 \times M_c - 0{\cdot}23$. For $Fe_2O_3$, Kristmann's data (K1) indicate the approximate relation $F_a = 0{\cdot}33 \times F_c$ for $F_c < 4\%$. There does not appear to be a significant correlation between $A_a$ and $A_c$. Boikova (B2) reported ratios of 0·34–0·82 for $M_a/M_c$, 0·09–0·23 for $A_a/A_c$ and 0·17–0·36 for $F_a/F_c$. The $SO_3$ contents of clinker alites are often very low, but values up to 0.9% have been reported for clinkers low in MgO and alkalis (G6) or high in $SO_3$ (M8).

Taken as a whole, the evidence indicates that the significant substitutions in clinker alites are of $Na^+$, $K^+$, $Mg^{2+}$ and $Fe^{3+}$ for $Ca^{2+}$ and of $Al^{3+}$, $P^{5+}$ and $S^{6+}$ for $Si^{4+}$. Observed contents of $K_2O$ and $Na_2O$ are much below the limits found by Woermann *et al.* (W1). Table 1.2 includes a typical composition for a clinker with 1·65% MgO and 3·1% $Fe_2O_3$, and Table 1.3 includes atomic ratios calculated from it.

### *1.2.4 Polymorphic modifications of the alites in clinkers*

Maki and co-workers (M2–M5,M9) studied the crystallization of alite by high-temperature light microscopy of thin sections together with thermal and X-ray methods. It crystallizes from the clinker liquid at about 1450°C as the R polymorph, which inverts to lower temperature forms on cooling. Due to the lowering of symmetry, each crystal usually contains several optically distinct domains, recognizable in thin section using polarized light. At the higher temperatures of formation or recrystallization within the normal range, small crystals, relatively high in substituent ions, are formed, which on cooling invert to $M_3$. Crystals formed at lower temperatures are larger and poorer in substituent ions, and may undergo further transition, partial or complete, to $M_1$ or, rarely, to $T_2$.

The MgO and $SO_3$ contents of the clinker are especially important in determining whether the transformation into $M_1$ occurs (Fig. 1.2; M7, M9–M11). High ratios of MgO to $SO_3$ promote nucleation rather than growth, resulting in formation of small, euhedral crystals of $M_3$. In contrast, low ratios favour rapid, unstable growth, giving rise to large, irregularly shaped crystals, often of $M_1$. These can be skeletal or dendritic, with relatively high contents of substituents and inclusions both of clinker liquid and of minute crystals of belite and free lime. High ratios of alkalis to $SO_3$ lessen the tendency to form $M_1$, as the $SO_3$ is then largely combined as alkali sulfates. Crystals containing both $M_3$ and $M_1$ can occur, and are often zoned, with cores of $M_1$ and peripheral regions of $M_3$. This is because the clinker liquid becomes richer in MgO as crystallization proceeds, causing the material deposited later to persist as $M_3$. The $M_3$ to $M_1$ transformation is also affected by the cooling rate, slow cooling favouring the transformation to $M_1$. In certain slowly cooled clinkers, further transformation may occur, giving $T_2$. This is likely to occur only if the alite is particularly low in substituents.

**Table 1.3** *Atomic ratios for phases in Portland cement clinkers, calculated from the typical compositions in Table 1.2 (see footnotes to Table 1.2)*

| | K | Na | Ca | Mg | Mn | Ti | Fe | Al | Si | P | S | O |
|---|---|---|---|---|---|---|---|---|---|---|---|---|
| Alite | <1 | 1 | 291 | 6 | | | 2 | 4 | 96 | <1 | <1 | 500 |
| | | | | | 300 | | | 100 | | | | |
| Belite | 3 | 1 | 194 | 2 | | | 2 | 7 | 90 | | 1 | 393 |
| | | | 200 | | | | | 100 | | | | |
| Aluminate (cubic) | 4 | 9 | 273 | 9 | | 1 | 17 | 166 | 17 | | | 600 |
| | | | 296 | | | | | 200 | | | | |
| Ferrite | 1 | 1 | 198 | 17 | 2 | 5 | 62 | 100 | 14 | | | 500 |
| | | | 200 | | | | 200 | | | | | |
| Aluminate (orthorhombic) | 23 | 5 | 265 | 8 | | 2 | 23 | 157 | 20 | | | 600 |
| | | | 303 | | | | | 200 | | | | |
| Aluminate (low Fe) | 3 | 3 | 276 | 7 | | 2 | 3 | 176 | 20 | | | 600 |
| | | | 291 | | | | | ~200 | | | | |
| Ferrite (low Al) | 1 | 3 | 197 | 22 | 3 | 2 | 75 | 75 | 20 | | | 500 |
| | | | ~200 | | | | | ~200 | | | | |

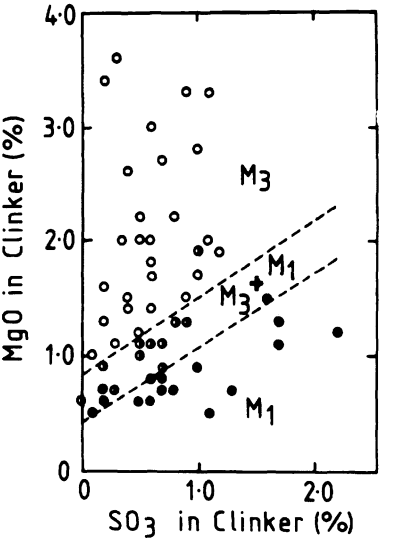


**Fig. 1.2** *Dependence of the polymorphic modification of alite in production clinkers on the MgO and $SO_3$ contents of the clinker (M9).*

On prolonged heating at high temperatures, the larger alite crystals grow at the expense of smaller ones, and in this process the content of substituent ions decreases, favouring inversion of $M_3$ to $M_1$ or $T_2$. Production clinkers are usually sufficiently high in MgO to prevent this inversion from taking place, even though considerable recrystallization may occur (M9). Recrystallization can thus markedly affect the relation between temperature of formation and crystal size.

Guinier and Regourd (G1) concluded from XRD evidence that the R polymorph occurred in certain clinkers. This view has been accepted by many other workers, but Maki and Kato (M4) concluded from thermal and other evidence that the supposed R form was really $M_1$, which had been misidentified because of the similarity of its XRD powder pattern to that of the R form. They gave two strong reasons in support of this view. Firstly, the clinkers contained less MgO than $M_3$ alites; for R to persist at room temperature it would have to contain more MgO than $M_3$, because it is a higher temperature form. Secondly, phase transitions were detected on heating; R, again because it is the high-temperature form, would not undergo these. Sinclair and Groves (S3) also described a case of the misidentification of an alite as rhombohedral; using single crystal electron diffraction, they found that some laboratory-prepared alites that had been regarded as rhombohedral were really either monoclinic or triclinic.

On present evidence, it is thus probable that the only alite polymorphs found in normal production clinkers approximate to $M_3$, $M_1$ or, occasionally, $T_2$, and that those that have been described as R are really $M_1$. However, both XRD and thermal evidence show that some alites formed

in the presence of fluoride are rhombohedral (M12). XRD and optical evidence indicates that the commonest polymorph in production clinkers is almost certainly $M_3$ or a less ordered form of it. The presence of $M_3$ in a works clinker has also been demonstrated using single crystal electron diffraction (H1).

### 1.2.5 *X-ray powder patterns and densities of tricalcium silicate and alites*

A number of experimentally determined XRD powder patterns have been reported for $C_3S$ and alite polymorphs (P1), but because of uncertainties in the indexing and sometimes in identification of the polymorph, these are usefully supplemented by patterns calculated from the crystal structures (Appendix; M6). The patterns of the polymorphs are closely alike, and interpretation is complicated in clinkers by the fact that many peaks overlap ones of other phases. The pattern depends not only on the polymorph or mixture of polymorphs present, but also on the nature and amounts of the substituent ions present in each. It is therefore not always

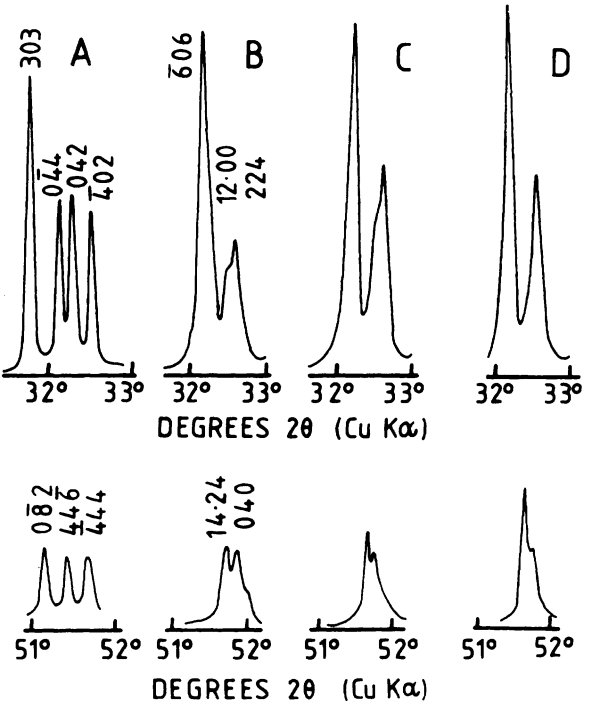


**Fig. 1.3** *Portions of XRD powder patterns of (A) the $T_1$ modification of $C_3S$ at 605°C (after R2); (B), (C) and (D) clinkers containing, respectively, $M_3$, ($M_3 + M_1$) and $M_1$ alites (after M4). Indexing of $T_1$ and $M_3$ patterns is based on the axes in Table 1.1 and calculated intensities.*

easy or even practicable to identify the polymorph or polymorphs in a clinker by the XRD powder pattern alone. The patterns differ principally in the fine structures of certain peaks (B2,G1,J1,M4,M5,R1). Figure 1.3 shows characteristic portions of the patterns of $T_1$ $C_3S$ and of some clinkers. $M_1$ alite, as present in clinkers, probably always has the maximum MgO content possible for this polymorph, and as such has a unit cell or pseudocell that is geometrically almost hexagonal. This causes the peak at about 51·7° $2\theta$ (Cu K$\alpha$ radiation) to be almost a singlet; the corresponding peak of the $M_3$ alite is a well-defined doublet, and those of $T_1$ $C_3S$ and $T_2$ alite are triplets. There are also differences in the peaks at 32–33° $2\theta$, but these are less useful because of overlaps with other phases. Because of their high relative intensities, care is needed with these latter peaks to avoid intensity errors from extinction.

The X-ray density of $T_1$ $C_3S$ is 3120 kg m$^{-3}$ (G2); that of $M_3$ alite, calculated assuming the atomic parameters of Nishi *et al.* (N1) and the composition $(Ca_{0\cdot98}Mg_{0\cdot01}Al_{0\cdot0067}Fe_{0\cdot0033})_3(Si_{0\cdot97}Al_{0\cdot03})O_5$, is 3150 kg m$^{-3}$.

### *1.2.6 Optical, thermal and other data*

$T_1$ $C_3S$ is biaxial with $(-)2V = 20–60°$, and $\alpha \wedge c_{hex} = 0–15°$ (O1); the refractive indices are $\alpha = 1\cdot7139$, $\gamma = 1\cdot7172$ for pure $C_3S$ and $\alpha = 1\cdot7158–1\cdot7197$, $\gamma = 1\cdot7220–1\cdot7238$ for typical clinker alites, all determined using sodium light (B5). In thin sections in polarized light, $M_1$ and $M_3$ are most readily distinguished by the maximum birefringence, which is 0·005 to 0·006 for $M_3$ and 0·003 for $M_1$ (M2–M5). Other differences in optical properties include the optic orientation referred to the hexagonal axes of the R form, whose shape persists through the transitions that occur on cooling, and the optic axial angle; Maki and Kato (M4) give details.

It is doubtful whether the polymorphs can be reliably distinguished by DTA, since both the $M_1$ and the $M_3$ forms are metastable at low temperatures and transform to $T_2$ at about 700°C (M4,M5). This effect is normally swamped by the endothermic $\beta$ to $\alpha'_L$ transition of the belite. Due to the effect of substituents, neither $T_3$ nor $M_2$ appears to form on heating. With alites relatively low in substituents, endotherms occur at 790–850°C, giving $M_1$ and at 950°C, giving $M_3$. Clinkers high in MgO, in which the alite is present entirely as $M_3$, normally show no thermal effects attributable to the alite until more than 1000°C, when transition to R occurs.

A substituted $C_3S$ has been found in nature and given the mineral name 'hatrurite' (G7). The rock containing it is interesting because it contains other phases present in clinker and appears to have been formed under conditions somewhat similar to those existing in a cement kiln.

## 1.3 Belite

### *1.3.1 Polymorphism and crystal structure*

Thermal and X-ray evidence (B6,N3,R1) shows that five polymorphs of $C_2S$ exist at ordinary pressures, viz.

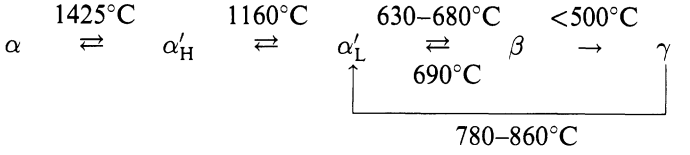


(H = high; L = low). The structures of all are built from $Ca^{2+}$ and $SiO_4^{4-}$ ions. The arrangements of these ions are closely similar in the $\alpha$, $\alpha'_H$, $\alpha'_L$ and $\beta$ polymorphs, but that in $\gamma$-$C_2S$ is somewhat different. As with $C_3S$, the higher temperature polymorphs cannot normally be preserved on cooling to room temperature unless stabilized by substituent ions. $\gamma$-$C_2S$ is much less dense than the other polymorphs, and this causes crystals or sintered masses of $\beta$-$C_2S$ to crack and fall to a more voluminous powder on cooling, a phenomenon known as dusting. If the crystallites of $\beta$-$C_2S$ are sufficiently small, the transformation does not occur, even if no stabilizer is present (Y2). In all normal Portland cement clinkers, the belite contains enough stabilizing ions to prevent the transformation to $\gamma$-$C_2S$ from taking place.

Many of the earlier crystal data reported for the $C_2S$ polymorphs were based on powder XRD patterns obtained either at high temperatures or from stabilized preparations at room temperature. As with the $C_3S$ polymorphs, such data are not always reliable. Table 1.4 gives data derived from single-crystal evidence, which do not suffer from this limitation.

The structures of the $\alpha$, $\alpha'_H$, $\alpha'_L$ and $\beta$ polymorphs (Figs 1.4A–C) all belong to a large family typified by that of glaserite, $K_3Na(SO_4)_2$ (M14).

**Table 1.4** *Crystal data for the dicalcium silicate polymorphs*

| Polymorph | Cell parameters (lengths in nm) | | | | Space group | Axial relation‖ | *Z* | Ref. |
|---|---|---|---|---|---|---|---|---|
| | *a* | *b* | *c* | Angle¶ | | | | |
| $\alpha$* | 0·5579 | | 0·7150 | $\gamma = 120°$ | $P6_3/mmc$(?) | $-ac$ | 2 | U3 |
| $\alpha'_H$† | 0·949 ($\sqrt{3} \times 0{\cdot}548$) | 0·559 | 0·685 | | Pcmn | *abc* | 4 | S4 |
| $\alpha'_L$‡ | 2·0871 ($3 \times 0{\cdot}6957$) | 0·9496 | 0·5600 | | $Pna2_1$ | *bca* | 12 | I2,I3 |
| $\beta$§ | 0·5502 | 0·6745 | 0·9297 | $\beta = 94{\cdot}59°$ | $P2_1/n$ | *cab* | 4 | J2 |
| $\gamma$ | 0·5081 | 1·1224 | 0·6778 | | Pbnm | *bac* | 4 | U4 |

* Stabilized with Ba. Other space groups ($P\bar{3}m1$, $P6_3mc$) have been proposed (M13). The space group $P6_3/mmc$ arises either from a domain structure (U5,U6) or from disorder in the orientations of the $SiO_4$ tetrahedra (M13).

† Stabilized with $P_2O_5$ and examined at 1200°C.

‡ Stabilized with Sr. A different superstucture can also form (K2,R3), in which the *a*, *b* and *c* axes of the $\alpha'_H$ form are respectively doubled, doubled and unchanged.

§ Crystal prepared from a $CaCl_2$ melt without additional stabilizer. Crystals showing a superstructure have been observed (K2).

¶ Where not 90°.

‖ Sequence of axes respectively equivalent to *a*, *b* and *c* of the $\alpha'_H$ polymorph.

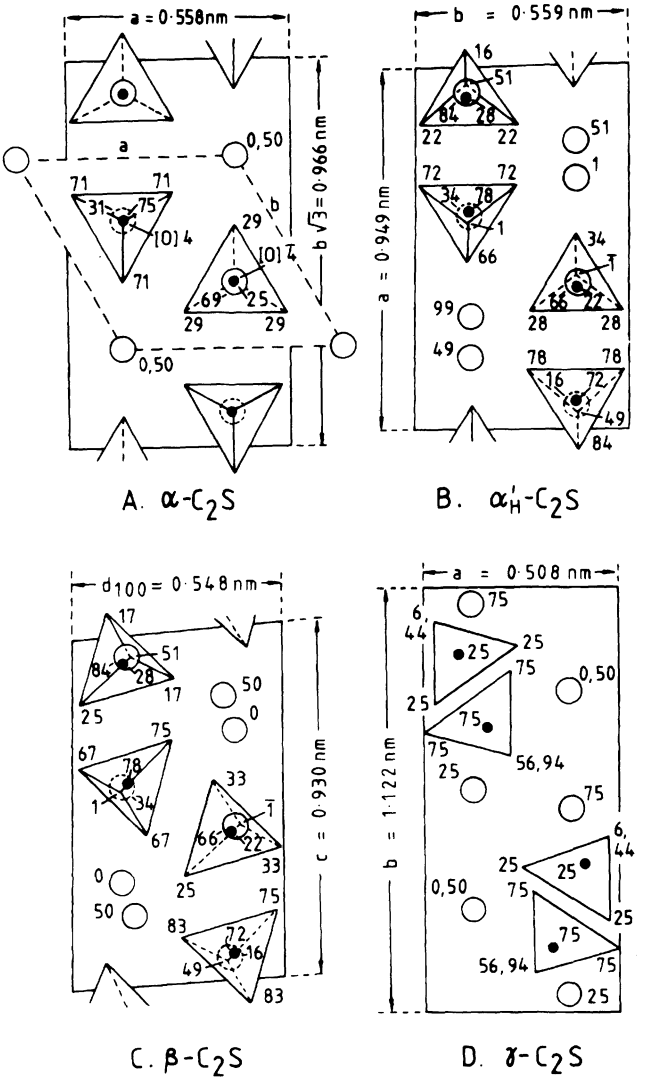


**Fig. 1.4** *Crystal structures of $C_2S$ polymorphs (after U7,U8). Large, open circles represent calcium atoms, small closed circles silicon atoms, and triangles tetrahedra of oxygen atoms. Heights of atoms are given as hundredths of the cell height (0·68–0·71 nm). For $\alpha$-$C_2S$, the structure shown is that of an individual domain of space group $P\bar{3}1c$. The structures are shown in the relative orientations found when they are interconverted, an unconventional choice of origin being adopted for $\gamma$-$C_2S$ to clarify the relation to the other polymorphs.*

As is apparent from the data in Table 1.4, the unit cells of all four are closely related. Structure determinations have been reported for the $\alpha$ (M13,U5,U7), $\alpha'_H$ (M13), $\alpha'_L$ (I2,I3,U9) and $\beta$ (D1,J2,M13,M15) polymorphs. The space group of the $\alpha$ form may vary according to the temperature and the nature of the stabiliser, if any (K2). $\alpha'_L$ is in practice a generic term for complex variants of $\alpha'_H$, as two different superlattices have been found to occur (K2,R3).

The structures of the $\alpha'_H$, $\alpha'_L$ and $\beta$ polymorphs are derived from that of $\alpha$-$C_2S$ by progressive decreases in symmetry, which arise from changes in the orientations of the $SiO_4^{4-}$ tetrahedra and small movements of $Ca^{2+}$ ions. The quantities of substituent ions needed to stabilize the higher temperature polymorphs at room temperature decrease along the sequence from $\alpha$- to $\beta$-$C_2S$. The situation parallels that existing with the $C_3S$ polymorphs, described in Section 1.2.2. Also as in the latter case, and for the same reason, these $C_2S$ polymorphs differ in calcium ion coordination. In $\beta$-$C_2S$, some of the $Ca^{2+}$ ions have 7, and others 8 oxygen atoms within 0·288 nm (J2). A modulated structure, i.e. one in which compositional or structural variations occur with a statistical periodicity that is not a rational multiple of that of the basic structure, has been observed in a polymorph of $C_2S$ (F1).

The crystal structure of $\gamma$-$C_2S$ is similar to that of olivine, $(Mg,Fe)_2SiO_4$ (Fig. 1.4D; M13,U4). The calcium is octahedrally coordinated. The unit cell and the arrangement of $Ca^{2+}$ and $SiO_4^{4-}$ ions show some similarities to those of the other polymorphs, but also important differences. It has often been supposed that transformations involving this form entail total reorganization of the structure, but single crystal high-temperature XRD evidence indicates that this is not correct; the products are formed topotactically (i.e. in a definite crystallographic orientation relative to the starting material; Fig. 1.4), but fragment because of the large volume change (B7,G8,K2,U8). $\gamma$-$C_2S$ scarcely reacts with water at ordinary temperatures.

### *1.3.2 Polymorphic forms and textures in clinker belites*

XRD powder evidence shows that in the majority of clinkers the belite is predominantly or entirely of $\beta$-$C_2S$ structure (G1,Y1), though some peaks are broadened (G1) and the presence also of both $\alpha$ and $\alpha'$ (presumably $\alpha'_L$) forms has been reported (G1,O1,R1,Y1). Characterization of the polymorphic form is rendered difficult by the similarities between their powder patterns (Fig. 1.5) and by overlaps between the peaks and ones of other phases, especially alite, but has been aided by examination of fractions in which the belite has been concentrated by chemical (R1) or heavy liquid (Y1) separation.

The belite grains in Portland cement clinkers frequently show complex, striated structures. These have been studied over a long period by workers using light microscopy; Yamaguchi and Takagi (Y1) and Ono *et al.* (O1), who also used XRD and other methods, gave the first substantially complete interpretations. Groves (G9) and Fukuda and Maki (F2,F3)

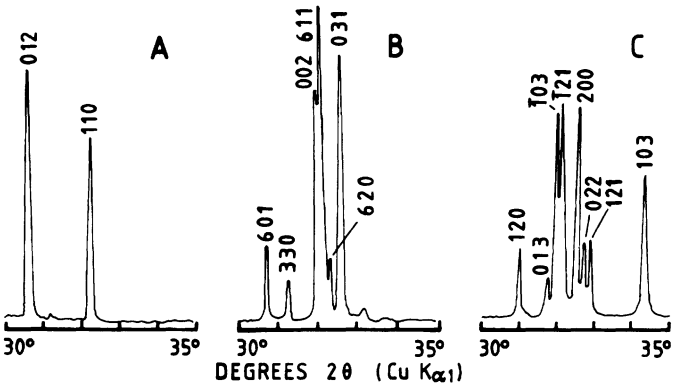


**Fig. 1.5** *Portions of XRD powder patterns (microdensitometer traces of Guinier photographs) of (A) α-$C_2S$ at 1500°C, (B) $\alpha'_L$-$C_2S$ at 1000°C and (C) β-$C_2S$. Indices are based on axes used in Table 1.4 (after R1).*

extended these results, using single-crystal electron diffraction and other methods. Kim *et al.* (K2) have discussed transformation mechanisms.

A very common type of belite grain in production clinkers, called Type I belite, is rounded, typically 20 to 40 $\mu$m in mean dimension, and shows several sets of parallel striations. Such crystals have formed as the $\alpha$ polymorph and the striations arise from the lowering of symmetry inherent in the $\alpha$ to $\alpha'_H$ and $\alpha'_L$ to $\beta$ transformations that occur on cooling. Type I belite crystals consist largely or wholly of the $\beta$ polymorph, though some $\alpha$ may remain. Other phases tend to be exsolved between the lamellae, since the lower-temperature polymorphs are less able to accommodate substituent ions.

Type II belite grains are typically irregular in shape and show only one set of striations. They are rare in modern clinkers. The striations arise from the $\alpha'_L$ to $\beta$ transformation. The restricted number of orientations can arise either because the crystals had formed below the $\alpha$ to $\alpha'_H$ transition temperature or because one of the twin components of the $\alpha'$ modification grew at the expense of the others (O1). Belite can form in clinkers by additional mechanisms, sometimes at lower temperatures than those discussed above, and may not then show any striations.

Chan *et al.* (C1) showed that material exsolved between lamellae or at grain boundaries in synthetic belites was often compositionally far removed from $C_2S$, and structurally either amorphous or composed of crystalline phases of entirely different structure, such as $C_2AS$, $C_3A$ or $C_3S_2$. They concluded that the possibilities of compositional variation in $\beta$-$C_2S$ were considerably narrower than had often been supposed, the grosser deviations from ideal composition being attributable to such effects. Evidence from $^{27}Al$ NMR is consistent with these results (S1). Chan *et al.* also concluded that, contrary to some earlier views, $\beta$-$C_2S$ cannot be stabilized by excess CaO alone, and that the role of ionic substitution in stabilizing forms other than $\gamma$ to room temperature

needed to be reassessed, mechanical constraints associated with exsolution providing a possible alternative explanation.

### 1.3.3 Compositions of belites in clinkers

Table 1.2 includes an average composition for belites in ordinary production clinkers, based on the results of many studies by X-ray microanalysis (B3,G3,G4,H3,H4,K1,S2,T2) or chemical analysis of separated material (D1,Y1). As with alite (Section 1.2.3), most of the results from different laboratories are in relatively close agreement. Belites in white (B4) and iron-rich (G5,H6) clinkers have also been analysed. Pure $C_2S$, for comparison, contains 34·9% of $SiO_2$ and 65·1% of CaO.

Clinker belites typically contain 4–6% of substituent oxides, of which the chief are usually $Al_2O_3$ and $Fe_2O_3$. The $Al^{3+}$ is in tetrahedral sites (S1). With clinkers high in $SO_3$, the belite tends to be high in that component; coupled substitution of $2Al^{3+} + S^{6+}$ for $3Si^{4+}$ probably occurs (B8). The $SO_3$ content of the belite ($\bar{S}_b$) is reported to be related to that of the clinker ($\bar{S}_c$) by the relation $\bar{S}_b = 1.23\bar{S}_c + 0{\cdot}24$, or, alternatively, $\bar{S}_b = 3.36\bar{S}_{c'} + 0{\cdot}55$, where $\bar{S}_{c'}$ excludes $SO_3$ present in soluble sulfate phases (H6). Correlations have been reported to exist between the MgO contents of the belite and the clinker (K1), and the $Al_2O_3/Fe_2O_3$ ratios of the belite and the clinker (F4,H6), but there is disagreement in the case of $Fe_2O_3$ (H6,K1). Early reports mention a compound $KC_{23}S_{12}$, but the $K_2O$ content of 3·5% corresponding to this formula is well above those found in clinker belites, and recent electron optical work indicates that the limit of $K_2O$ substitution is about 1·2% (C1).

Any interpretation of belite analyses is at present tentative because of the uncertainties arising from exsolution effects. From the practical standpoint, it may be necessary to regard the exsolved material as forming part of the belite. Clinker belite compositions seem often to indicate ratios of other atoms to oxygen above the theoretical value of 0·75. As Regourd *et al.* (R3) noted, the $C_2S$ structures are too densely packed for the presence of interstitial ions to appear likely, and it is possible that vacancies occur in the oxygen sites. Table 1.3 includes atomic ratios, with a possible allocation of atoms to sites, corresponding to the composition given in Table 1.2.

### 1.3.4 Cell parameters, X-ray powder patterns and other data

Regourd *et al.* (R3) synthesized several belites of $\beta$-$C_2S$ type with compositions similar to those found in clinkers and determined their cell parameters. With increased substitution the crystallinity tended to decrease, causing broadening of XRD powder peaks. Table 1.5 gives two of their results and one for a belite extracted from a Portland cement clinker. The Appendix includes a calculated pattern for a typical clinker belite. Assuming $a = 0{\cdot}550$ nm, $b = 0{\cdot}675$ nm, $c = 0{\cdot}933$ nm, $\beta = 94{\cdot}4°$, with the atomic parameters of Jost *et al.* (J2) and the site occupancies

$$(K_{0{\cdot}01}Na_{0{\cdot}005}Ca_{0{\cdot}975}Mg_{0{\cdot}01})_2(Fe_{0{\cdot}02}Al_{0{\cdot}06}Si_{0{\cdot}90}P_{0{\cdot}01}S_{0{\cdot}01})O_{3{\cdot}96}$$

**Table 1.5** *Cell parameters of belites*

| Composition | $a$ (nm) | $b$ (nm) | $c$ (nm) | $\beta$ |
|---|---|---|---|---|
| $Ca_2Fe_{0.035}Al_{0.035}Si_{0.93}O_{3.965}$* | 0·5502 | 0·6750 | 0·9316 | 94·45° |
| $Ca_2Fe_{0.050}Al_{0.050}Si_{0.90}O_{3.950}$* | 0·5502 | 0·6753 | 0·9344 | 94·19° |
| $Ca_2Mg_{0.044}K_{0.020}Fe_{0.032}Al_{0.043}Si_{0.933}O_4$† | 0·5504 | 0·6762 | 0·9328 | 94·17° |

* Laboratory preparation (R3).
† Isolated from a clinker; also, Na, Ti, Mn, P, each ≤ 0·01 (D1).

the X-ray density is 3300 kg m$^{-3}$. That for pure $\beta$-$C_2S$, based on Jost *et al.*'s data, is 3326 kg m$^{-3}$, and that for pure $\gamma$-$C_2S$, based on data of Udagawa *et al.* (U4), is 2960 kg m$^{-3}$.

Synthetic $\beta$-$C_2S$ is biaxial positive with high $2V$ and $\alpha = 1{\cdot}717$, $\gamma = 1{\cdot}735$; $\gamma$-$C_2S$ is biaxial negative with $2V = 60°$, $\alpha = 1{\cdot}642$, $\beta = 1{\cdot}645$, $\gamma = 1{\cdot}654$ (R4). In the Type I belites of clinkers, lamellae of $\beta$ structure have mean refractive index 1·720 and birefringence 0·015–0·018, while for the intervening material the corresponding values are 1·700–1·710 and 0·000–0·003 (O1). Ono *et al.* (O1) and Yamaguchi and Takagi (Y1) give further data on the optical properties of clinker belites.

Guinier and Regourd (G1) summarized the thermal behaviour of $C_2S$ polymorphs. On heating, $\beta$-$C_2S$ shows endotherms beginning at 693°C and 1450°C, due respectively to the $\beta \rightarrow \alpha'_L$ and $\alpha'_H \rightarrow \alpha$ transitions; with $\gamma$-$C_2S$, the 693°C endotherm is replaced by a broad one beginning at about 748°C due to the transition to $\alpha'_L$. The curve obtained on cooling $\alpha$-$C_2S$ from 1500°C shows exotherms beginning at about 1456°C, 682°C and 530°C, due respectively to the $\alpha \rightarrow \alpha'_H$, $\alpha'_L \rightarrow \beta$ and $\beta \rightarrow \gamma$ transitions. The $\alpha'_H \rightarrow \alpha'_L$ transition gives only a very weak effect at 1160°C.

$\beta$-$C_2S$, modified by solid solution, occurs in nature as larnite. Early identifications of $\alpha'$-$C_2S$ with bredigite were incorrect (B9,M16). $\alpha$-$C_2S$ has been assumed to resemble nagelschmidtite ($Ca_7Si_2P_2O_{16}$), but the unit cell of the latter seems to be more complex (G1).

## 1.4 Aluminate

### *1.4.1 Crystal structure: cubic, orthorhombic and monoclinic modifications*

Pure $C_3A$ does not exhibit polymorphism. It is cubic, with $a = 1{\cdot}5263$ nm, space group Pa3 and $Z = 24$; the structure is built from $Ca^{2+}$ ions and rings of six $AlO_4$ tetrahedra, of formula $Al_6O_{18}^{18-}$ (M17). These rings are highly puckered, such that the Al atoms lie near to six of the corners of a cube (Fig. 1.6). The unit cell is composed of 64 ($4_i^3$) subcells, of edge length 0·3816 nm. Of these subcells, 8 are occupied by $Al_6O_{18}$ rings; the $Ca^{2+}$ ions occur at the body centres of some of the remaining subcells and near the corners of others. The coordination of those near the corners is octahedral, while that of those at the body centres is irregular, with either 5 or 6 oxygen atoms within 0·28 nm.

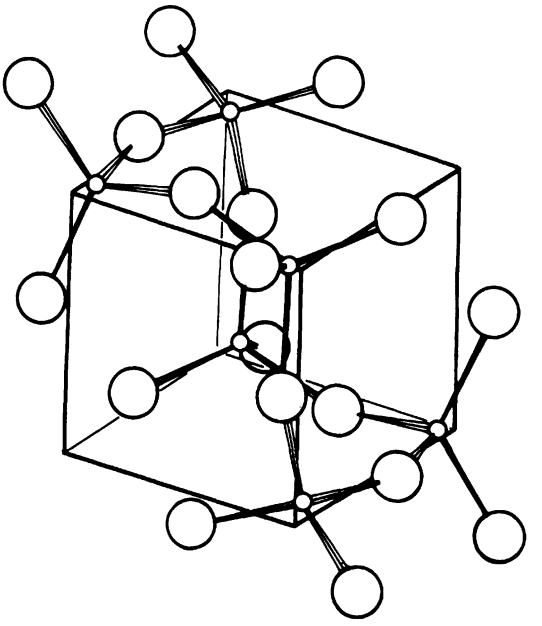

**Fig. 1.6** *$Al_6O_{18}$ ring in the structure of $C_3A$, showing the situations of the aluminium atoms near to the corners of a cube; based on the results of Mondal and Jeffery (M17).*

$C_3A$ can incorporate $Na^+$ by substitution of $Ca^{2+}$ with inclusion of a second $Na^+$ ion in an otherwise vacant site, thus giving solid solutions of general formula $Na_{2x}Ca_{3-x}Al_2O_6$ (F5,R1,R5,T4). The substitution occurs without change in structure up to a limit of about 1% $Na_2O$ ($x \approx 0{\cdot}04$). Higher degrees of substitution lead to a series of variants of the structure (Table 1.6). In the absence of other substituents, the upper limit of $Na_2O$ substitution is 5.7%.

The $C_I$ structure (Table 1.6) is the $C_3A$ structure, with up to about 1% of $Na_2O$ present as described above. The $C_{II}$ structure is a minor variant of it, of lower symmetry (T4); comparison of calculated XRD patterns

**Table 1.6** *Modifications of the $C_3A$ structure, of general formula $Na_{2x}Ca_{3-x}Al_2O_6$ (T4)*

| Approximate $Na_2O$ (%) | Compositional range ($x$) | Designation | Crystal system | Space group |
|---|---|---|---|---|
| 0–1·0 | 0–0·04 | $C_I$ | Cubic | Pa3 |
| 1·0–2·4 | 0·04–0·10 | $C_{II}$ | Cubic | $P2_13$ |
| 2·4–3·7 | 0·10–0·16 | $C_{II}+O$ | – | – |
| 3·7–4·6 | 0·16–0·20 | O | Orthorhombic | Pbca |
| 4·6–5·7 | 0·20–0·25 | M | Monoclinic | $P2_1/a$ |

(T5) shows that there is little possibility of distinguishing the two by powder XRD, unless by very precise determinations of the cell parameter, $C_{II}$ with 2·4% $Na_2O$ having $a = 1{\cdot}5248$ nm (T4). In $C_{II}$, and by analogy also in $C_I$, the additional $Na^+$ ions are located at the centres of the $Al_6O_{18}$ rings. The O structure (originally called $O_I$) resembles $C_I$ and $C_{II}$ in having a unit cell that is composed of pseudocubic subcells with edge lengths of approximately 0·38 nm, which contain $Ca^{2+}$ ions and $Al_6O_{18}$ rings, but the arrangement of the rings within the true unit cell is entirely different (N4,T4). A preparation of composition $Na_{0{\cdot}875}Ca_{8{\cdot}375}Al_{5{\cdot}175}Fe_{0{\cdot}450}Si_{0{\cdot}375}O_{18}$ (3·3% $Na_2O$) had $a = 1{\cdot}0879$ nm, $b = 1{\cdot}0845$ nm, $c = 1{\cdot}5106$ nm, $Z = 4$ (T4). The M structure, which was originally considered to be orthorhombic and called $O_{II}$ (R5), is a slightly distorted variant of the O structure; a preparation of composition $Na_{1{\cdot}50}Ca_{8{\cdot}25}Al_6O_{18}$ (5·7% $Na_2O$) had $a = 1{\cdot}0877$ nm, $b = 1{\cdot}0854$ nm, $c = 1{\cdot}5135$ nm, $\beta = 90{\cdot}1°$, $Z = 4$ (T4).

Substantial proportions of the Al in these structures can be replaced by other ions, of which $Fe^{3+}$ and $Si^{4+}$ are the most important. Lee *et al.* (L1) found the limits of substitution under equilibrium conditions to be around 2% for $SiO_2$ and 3–4% for $Fe_2O_3$, but higher degrees of substitution were obtainable under non-equilibrium conditions, such as crystallization from undercooled melts. If $Si^{4+}$ is present, fewer large cations are needed to maintain charge balance; this extends the solid solution range of the O structure to lower $Na_2O$ contents and that of the M structure to higher ones (T4). The literature contains many references to an supposed compound $NC_8A_3$. This formula corresponds to an $Na_2O$ content of 7·6%, which cannot be attained in $C_3A$ substituted only with $Na^+$, and it is reasonably certain that this compound does not exist (F5,M18,R5,T4); however, if Si is also present, the upper limit of Na substitution is near to this value (M18,T4).

Pollitt and Brown (P2) were unable to prepare an analogue of the orthorhombic phase with $K^+$ as the sole substituent, but obtained evidence that $K^+$ could stabilize it in clinker, probably because other substituents were also present. Maki (M18) also failed to prepare K forms of the orthorhombic or monoclinic phases under equilibrium conditions, but by moderately rapid cooling of melts he obtained orthorhombic crystals having cell parameters close to those of the corresponding sodium-containing phase. He considered that the presence of Si in the clinker liquid would favour supercooling and thereby also non-equilibrium formation of the orthorhombic or monoclinic phase.

### *1.4.2 Other modifications*

Two further modifications of the $C_3A$ structure have been described. One was obtained as a high-temperature polymorph of the O and M forms and was considered on the basis of powder XRD evidence to be tetragonal (R1,R5). It appeared to be metastable at room temperature but could be preserved by quenching. Later studies, using thermal analysis, high-temperature light microscopy and high-temperature single crystal XRD (M19,M20,T4) showed, however, that the O modification

was structurally unchanged up to its decomposition temperature and that the M modification was reversibly transformed on heating into the O form. A study of quenched material using powder XRD and single crystal electron diffraction (L2) confirmed that the supposed tetragonal form was really orthorhombic, though with $a$ equal to $b$ and thus geometrically tetragonal. The space group was considered to be probably Pcaa, which differs from that (Pbca) of the normal O form; however, three of the indices assigned to the XRD powder peaks (023, 045 and 047) are incompatible with this space group, though not with Pbca. The high-temperature material may thus have the normal O structure and a composition such that the $a$ and $b$ axial lengths are equal to within experimental error. Its persistence to room temperature appears to be favoured by relatively high contents of $Na_2O$ and $Fe_2O_3$ (L1).

The other $C_3A$ modification is a disordered, poorly crystalline form, called 'proto-$C_3A$', which was obtained metastably from simulated clinker liquids, either by rapid cooling or by static crystallization at low temperatures (B10). It gave an XRD powder pattern with broadened peaks, corresponding to the systematically strong reflections of cubic $C_3A$ indexable on the subcell with $a \approx 0{\cdot}39$ nm. Analytical electron microscopy of individual crystals showed it to be very high in substituents, one preparation, for example, having an Fe/Al ratio of 0·54 (H7).

### *1.4.3 Structural modifications of clinker aluminates*

Production clinkers have been found to contain cubic or orthorhombic forms of aluminate, alone or in combination. The monoclinic modification has not been observed. The orthorhombic modification is also known as the prismatic, dark interstitial material, and is sometimes pseudotetragonal. It can arise only if sufficient alkali is available, but its formation appears to be favoured also by rapid cooling and by bulk compositions potentially able to yield a relatively high proportion of aluminate (M18).

Cubic aluminate in clinker is often finely grained and closely admixed with dendritic crystals of ferrite; when it forms larger crystals, these tend to be equidimensional. The XRD powder pattern is characterized by strong, singlet peaks at approximately 33·3°, 47·7° and 59·4° $2\theta$ (CuK$\alpha$ radiation; Fig. 1.7A), whose indices are, respectively, 044, 008 and 448. Patterns obtained either from clinker or from material in which the aluminate and ferrite phases have been concentrated by chemical extraction of the silicates give $a = 1{\cdot}5223$–$1{\cdot}5255$ nm (R1). The slight decrease relative to the value of 1·5263 nm for pure $C_3A$ agrees with results for synthetic sodium-substituted preparations (R1,T4). These data are probably equally compatible with the presence of proto-$C_3A$, but the contents of substituents (Section 1.4.4) are considerably lower than those found in the latter material. There is probably not enough evidence to show whether the modification is $C_I$ (Pa3) or $C_{II}$ ($P2_13$).

The orthorhombic phase is recognizable in the light microscope or SEM by its occurrence as characteristic, lath-shaped crystals, which are often twinned (M18). An XRD powder pattern of material from which

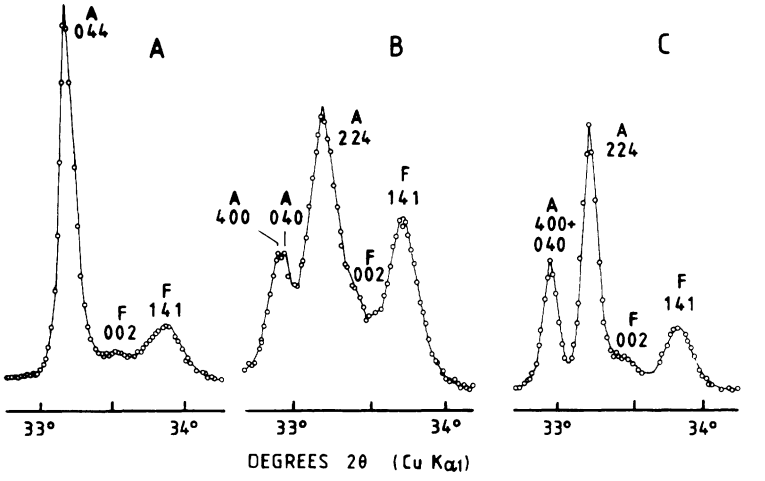


**Fig. 1.7** *Portions of XRD powder patterns of clinkers containing (A) cubic, (B) orthorhombic and (C) pseudotetragonal modifications of the aluminate phase. Peaks marked A and F are due to aluminate and ferrite phases respectively, and are reindexed, where necessary, to correspond to axes used in text and Table 1.7, and to calculated intensities (after R1).*

the silicate phases had been removed showed a splitting of the strong peak at 33·3° $2\theta$ into a strong singlet at approximately 33.2° and a weaker, close doublet at 32·9–33·0° (Fig. 1.7B). The unit cell parameters were $a = 1{\cdot}0874$ nm, $b = 1{\cdot}0860$ nm, $c = 1{\cdot}5120$ nm (R1). Another clinker, in which the aluminate was pseudotetragonal, gave a strong singlet peak at 33·2° and a weaker singlet at 33·0° (Fig. 1.7C), and the cell parameters were $a = b = 1{\cdot}0867$ nm, $c = 1{\cdot}5123$ nm.

### *1.4.4 Compositions of clinker aluminates*

Because of the close admixture with other phases, which is often on a scale of 10 $\mu$m or less, X-ray microanalysis of the aluminate in clinkers is frequently difficult or unreliable. Data have been reported for cubic, orthorhombic, pseudotetragonal or unspecified forms of the aluminate in ordinary clinkers (B3,H3,K1,R1), for aluminate in high-iron clinkers (H6) and for aluminate (B4,G3,G4,S2) and glass (B4) in white cement clinkers. A study of laboratory clinkers indicated that slow cooling decreased $Mg^{2+}$ substitution (I4). Tables 1.2 and 1.3 include, respectively, average compositions based on these somewhat scanty data, and suggested site occupancies based on them. The values in both tables take into account both the experimental data and the requirement of reasonable site occupancies.

Pure $C_3A$ contains 62·3% CaO and 37·7% $Al_2O_3$. Substantial proportions of both Ca and Al are thus replaced, the total content of substituent oxides being typically around 13% for the cubic and up to about 20% for the orthorhombic modification. The content of equivalent $Na_2O$

($Na_2O + 0{\cdot}66\ K_2O$) appears to be around 1% for the cubic form and 2–4% for the orthorhombic form. None of the analyses indicates alkali contents as high as that required by the formula $NC_8A_3$, even though considerable amounts of Si are present.

### 1.4.5 *X-ray powder data, densities and optical properties*

The Appendix includes calculated XRD powder patterns for cubic and orthorhombic clinker aluminates. The X-ray density of the cubic modification is 3064 kg m$^{-3}$, assuming $a = 1{\cdot}5240$ nm and composition $(K_{0{\cdot}03}Na_{0{\cdot}06}Ca_{2{\cdot}76}Mg_{0{\cdot}08}Ti_{0{\cdot}01})(Fe_{0{\cdot}22}Al_{1{\cdot}60}Si_{0{\cdot}18})O_6$. That of the orthorhombic modification is 3052 kg m$^{-3}$, assuming $a = 1{\cdot}0879$ nm, $b = 1{\cdot}0845$ nm, $c = 1{\cdot}5106$ nm and composition $(Na_{0{\cdot}292}Ca_{2{\cdot}792})\ (Fe_{0{\cdot}150}Al_{1{\cdot}725}Si_{0{\cdot}125})O_6$. For pure $C_3A$ with $a = 1{\cdot}5263$ nm, the value is 3029 kg m$^{-3}$. Pure $C_3A$ is optically isotropic, with refractive index 1·710 (R4); iron substitution can raise this value to 1·735 (H8). Maki (M19,M21) described the morphology and optical properties of the orthorhombic modification, including variations with composition.

## 1.5 Ferrite

### 1.5.1 *Crystal structure and composition in the $Ca_2(Al_xFe_{1-x})_2O_5$ series*

At ordinary pressures in the absence of oxide components other than CaO, $Al_2O_3$ and $Fe_2O_3$, the ferrite phase can be prepared with any composition in the solid solution series $Ca_2(Al_xFe_{1-x})_2O_5$, where $0 < x < 0{\cdot}7$. The composition $C_4AF$ is only a point in this series, with $x = 0{\cdot}5$. The end member, $C_2A$, with $x = 1$, has been prepared, but only at a pressure of 2500 MPa (A1). The series with $x < 0{\cdot}7$ is not quite isostructural, as the space group changes near $x = 0{\cdot}33$ (S5). Table 1.7 gives crystal data for various compositions. Care is needed in referring to the unit cell and space group, as some workers reverse the choice of $a$ and $c$ axes used here, with appropriate changes in space group symbol. There has also been uncertainty in the past as to the space group for the compositions with $x > 0{\cdot}33$.

**Table 1.7** *Crystal data for ferrites in the series $Ca_2(Al_xFe_{1-x})_2O_5$*

| $x$ | Unit cell parameters (nm)* | | | Space group | X-ray density (kg m$^{-3}$) | Ref. |
|---|---|---|---|---|---|---|
| | $a$ | $b$ | $c$ | | | |
| 0 | 0·55980 | 1·47687 | 0·54253 | Pcmn | 4026 | B13 |
| 0·285 | 0·5588 | 1·461 | 0·5380 | Ibm2 | 3862 | C2 |
| 0·36 | 0·5583 | 1·458 | 0·5374 | Ibm2 | 3812 | C2 |
| 0·50 | 0·55672 | 1·4521 | 0·5349 | Ibm2 | 3732 | C3,M22 |
| 1 | 0·541 | 1·445 | 0·523 | Ibm2(?) | 3480 | A1 |

* The unit cell is orthorhombic, with $Z = 4$.

Plots of unit cell parameters or XRD powder spacings against $x$ for the pure $Ca_2(Al,Fe)_2O_5$ series (S5) tend to show a change in slope near $x = 0{\cdot}3$, attributable to the structural change. Such plots may be used to determine composition only if oxide components other than CaO, $Al_2O_3$ and $Fe_2O_3$ are absent. They have often been applied to ferrites in clinkers, but this gives seriously inaccurate results because of the effects of other substituents (Sections 1.5.2 and 1.5.3).

Büssem (B11) determined the approximate crystal structure of $C_4AF$. Subsequent determinations or refinements were reported for preparations with $x = 0$ ($C_2F$) (B12,B13,C4), $x = 0{\cdot}285$ and $0{\cdot}36$ (C2) and $x = 0{\cdot}5$ (C3). Figure 1.8 shows the structure for the compositional range with $0{\cdot}33 < x < 0{\cdot}7$. It is derived from that of perovskite ($CaTiO_3$) by the substitution of Al and Fe for Ti, together with ordered omission of oxygen atoms, which causes one-half of the sheets of octahedra in perovskite to be replaced by chains of tetrahedra. The empirical composition may thus be written $Ca_2M_2T_2O_5$, where M and T represent octahedral and tetrahedral cations, respectively. The structure for compositions with $x < 0{\cdot}33$ differs from that shown in Fig. 1.8 in that one-half of the chains of tetrahedra have the opposite polarity.

Each $Ca^{2+}$ ion in $C_4AF$ has 7 oxygen neighbours at 0·23 to 0·26 nm (C3). The aluminium and iron atoms are both distributed between

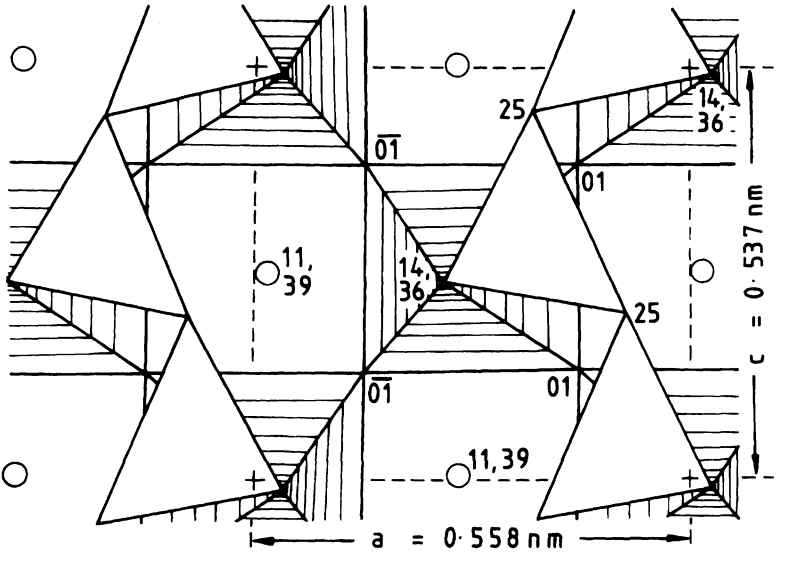


**Fig. 1.8** *Crystal structure of $C_4AF$, based on the results of Colville and Geller (C3) and showing calcium atoms (open circles), $(Al,Fe)O_4$ tetrahedra (triangles) and $(Fe,Al)O_6$ octahedra (hatched squares). Heights of atoms are given as hundredths of the cell height ($b = 1{\cdot}452$ nm). Atoms at heights outside the range of $-1$ to $+39$ are not shown, their positions being derivable from those shown by translations of 1/2 parallel to each of the axes.*

octahedral and tetrahedral sites, the fraction of the aluminium entering tetrahedral sites under equilibrium conditions decreasing with temperature. For the three preparations with $x = 0{\cdot}285$, $0{\cdot}36$ and $0{\cdot}5$ on which X-ray structure determinations were made, 75–76% of the total content of aluminium was found to be in tetrahedral sites. These preparations were shown to have been in equilibrium at about 750°C (C3); for a $C_4AF$ preparation quenched from 1290°C, the Mössbauer spectrum indicated that only 68% of the aluminium was in tetrahedral sites (G10). It was suggested that $x$ does not exceed the observed limit of about $0{\cdot}7$ because at this composition the tetrahedral sites are all occupied by aluminium (C2). There is evidence of clustering of aluminium and iron atoms to an extent depending on composition and conditions of formation (Z1).

### 1.5.2 Compositions of clinker ferrites

In many clinkers, the ferrite is closely mixed with aluminate; due to a similarity in cell parameters, oriented intergrowth can occur (M21). The close admixture often renders X-ray microanalysis difficult or unreliable. For ordinary Portland cement clinkers, the compositions found in different laboratories are nevertheless remarkably consistent. They show that there is little or no substitution for $Ca^{2+}$, the substituent ions being contained essentially in the octahedral and tetrahedral sites. Table 1.2 includes an average value based on the results of investigations using X-ray microanalysis (B2,B3,H3,H9,K1,S6,U2) or chemical analysis of separated material (Y1). Table 1.3 includes suggested site occupancies corresponding to these data. Data on the distribution of substituents between octahedral and tetrahedral sites (Z2) are insufficient to justify a distinction between them, as the preferences of some of the cations, especially $Mg^{2+}$, in this structure are unknown, as is the temperature at which equilibrium is attained. This temperature probably varies between clinkers, and may be expected to affect the distribution.

The typical composition differs markedly from that of $C_4AF$ (46·1% CaO, 21·0% $Al_2O_3$, 32·9% $Fe_2O_3$). It contains about 10% of substituent oxides and is much lower in $Fe_2O_3$. It approximates to $Ca_2AlFe_{0{\cdot}6}Mg_{0{\cdot}2}Si_{0{\cdot}15}Ti_{0{\cdot}05}O_5$, which is derived from that of $C_4AF$ by replacing some of the $Fe^{3+}$ by $Mg^{2+}$ and an equal amount by $Si^{4+}$ and $Ti^{4+}$. A conclusion (N5) based on Rietveld analysis of the XRD powder pattern that $Si^{4+}$ is not present in solid solution but in closely admixed belite appears incompatible with the observation that incorporation of $Si^{4+}$ markedly affects the colour and electrical conductivity (I5). A Mössbauer study also provided indirect evidence for silicon substitution (Z2).

Sulfate-resisting Portland cement clinkers, including those made for use in oil well cements, have relatively high ratios of Fe to Al, and if it is assumed that most of the iron is in the ferrite, the latter cannot have the composition given above. X-ray microanalyses (B14,G3–G5,H6,R6) indicate that, in contrast to the situation in normal Portland cement clinkers, there is substantial replacement of $Al^{3+}$ as well as, or even

instead of, $Fe^{3+}$ in the $C_4AF$ composition. Microanalyses show that there is much variation in composition, both between clinkers and within clinkers, especially at the micrometre level that can be studied using TEM (R6). The mean contents of MgO and $Fe_2O_3$ are related to those of the clinker, and the $SiO_2$ content tends to increase with that of MgO; $SO_3$ contents of up to 0·9% have been reported (B14, H6). The $Al_2O_3/Fe_2O_3$ ratio is probably also related to that in the clinker. Tables 1.2 and 1.3 include what is possibly a typical mean composition and atomic ratios calculated from it.

### *1.5.3 Crystal data and X-ray powder patterns for ferrites containing substituent ions*

$Mn^{3+}$ can replace all the $Fe^{3+}$ or up to 60% of the $Al^{3+}$ in $C_4AF$ (K3). Yamaguchi and Takagi (Y1) summarized data showing that incorporation of $Mg^{2+}$ or $Si^{4+}$ or both causes increases in cell parameters. Boikova (B2) determined the cell parameters of four preparations with compositions similar to those of typical clinker ferrites; the ranges were $a = 0{\cdot}5535$–$0{\cdot}5554$ nm, $b = 1{\cdot}4492$–$1{\cdot}4642$ nm, $c = 0{\cdot}5288$–$0{\cdot}5333$ nm. Marinho and Glasser (M23) found that $Ti^{4+}$ substitution caused stacking changes in $C_2F$ or $C_4AF$. It had negligible effect on the cell parameters and the charge was balanced by incorporation of additional oxygen atoms. This last conclusion may be irrelevant to clinker ferrites, since $Ti^{4+}$ is a relatively minor substituent and the charge can be balanced in other ways.

Regourd and Guinier (R1) reported unit cell parameters for the ferrite in five clinkers. The ranges observed were $a = 0{\cdot}5517$–$0{\cdot}5555$ nm, $b = 1{\cdot}455$–$1{\cdot}462$ nm, $c = 0{\cdot}5335$–$0{\cdot}5350$ nm. Boikova (B2) reported XRD powder spacings for clinker ferrites which indicate similar values. The similarity of these cell parameters to those of the laboratory preparations (B2) mentioned in the previous paragraph supports the results of X-ray microanalyses of clinker ferrites described in Section 1.5.2. Compared with pure $C_4AF$, typical clinker ferrites have smaller values of $a$ and $c$, but larger values of $b$.

The XRD powder patterns of clinker ferrites are affected by the cooling rate (I4,M24,O2). The effect is associated with differing uptake of MgO and $SiO_2$. Extreme values of the cell parameters were $a = 0{\cdot}557$ nm, $b = 1{\cdot}462$ nm, $c = 0{\cdot}532$ nm for a quenched sample, and $a = 0{\cdot}543$ nm, $b = 1{\cdot}465$ nm, $c = 0{\cdot}533$ nm for one that was slowly cooled (O2). The ferrite in the quenched samples was poorly crystalline, many peaks other than the three most intense (200, 141 and 202) disappearing (O2). Broadening of peaks of clinker ferrites (B2,M24,R1) might be caused not only by poor crystallinity, but also by zoning. The cell parameters observed by Regourd and Guinier (R1) and Boikova (B2) are near to those of the quenched sample.

The Appendix includes a calculated powder pattern for a ferrite having cell parameters and composition similar to those for the material in typical clinkers The X-ray density, assuming $a = 0{\cdot}5535$ nm, $b = 1{\cdot}4642$ nm, $c = 0{\cdot}5328$ nm and composition $Ca_2AlFe_{0{\cdot}6}Si_{0{\cdot}15}Ti_{0{\cdot}05}O_5$, is 3570 kg m$^{-3}$.

### 1.5.4 Optical, magnetic and other data

Ferrite of or near $C_4AF$ composition and free from substituent ions is yellowish brown in transmitted light. The optical properties of $C_4AF$ are as follows: biaxial, negative, with moderate $2V$; $\alpha$ 1·96, $\beta$ 2·01, $\gamma$ 2·04 in lithium light; pleochroic, with $\gamma$ brown, $\alpha$ yellowish brown; the refractive indices increase with Fe/Al ratio (H8). The optic orientation is $X=b$, $Y=c$, $Z=a$ (M25). The pleochroism of ferrite solid solutions has been studied (M25).

If clinker ferrites are cooled in air, they are commonly almost black. The dark colour is associated with markedly higher electrical conductivity (I5,M24). In the absence of other substituents, it arises if the ferrite contains an excess of small dipositive ions ($Mg^{2+}$ or $Zn^{2+}$) over tetrapositive ions ($Si^{4+}$ or $Ti^{4+}$) and is cooled in air (I5). If the substituted ferrite is cooled in $N_2$ or quenched in water, the dark colour disappears (M24). Its disappearance seems to be due to the absence of $Fe^{4+}$ rather than the presence of $Fe^{2+}$ (M25,S7). An excess of dipositive over tetrapositive substituents when all the iron is present as $Fe^{3+}$ implies the presence of oxygen vacancies; these can be filled during cooling, with concomitant oxidation of a little of the iron to $Fe^{4+}$. Clinker ferrites can apparently be dark even if there is not an excess of dipositive over tetrapositive substituents. This has yet to be explained.

The ferrite is ferromagnetic, and the more iron-rich members of the $Ca_2(Al_xFe_{1-x})_2O_5$ series have been studied for their magnetic properties, especially in regard to the coordinations of the Fe atoms (C4,G11). Ferrite with a composition near $C_4AF$ has been found in nature. The name brownmillerite, already in use in cement chemistry, was adopted as the mineral name (G7).

# 2 High-temperature chemistry

## 2.1 Introduction

A knowledge of the relevant high-temperature phase equilibria is necessary for understanding the factors that govern acceptable bulk compositions for Portland cement clinker, the conditions under which the latter can be manufactured, and the phase composition and microstructure of the resulting material. This chapter deals with these equilibria and with the phases to which they relate, with the exception of the major clinker phases, which were described in Chapter 1. Some anhydrous phases primarily of interest in relation to other types of cements are also considered here. Principles underlying the preparation of anhydrous silicate, aluminate and other high-temperature phases are outlined.

## 2.2 Systems containing CaO with $SiO_2$ or $Al_2O_3$ or both

### *2.2.1 The CaO–$SiO_2$ system*

Figure 2.1 shows the phase diagram. For clarity, the polymorphism of $C_3S$ and the distinction between $\alpha'_H$- and $\alpha'_L$-$C_2S$ are omitted. Calcium oxide (CaO) has the sodium chloride structure, in which all ions are octahedrally coordinated; the unit cell is cubic, with $a = 0{\cdot}48105$ nm, space group Fm3m, $Z = 4$, $D_x = 3345\,\text{kg m}^{-3}$ (S8). The refractive index is 1·837 (W3).

On equilibrium cooling below 1250°C, $C_3S$ decomposes to give CaO and $\alpha'_H$-$C_2S$; this process, which is always slow and below 700°C imperceptible, is considered in Section 3.5.5. $\beta$-CS, $\alpha$-CS and $C_3S_2$ are commonly known by their mineral names of wollastonite, pseudowollastonite and rankinite, respectively; none reacts significantly with water at ordinary temperatures. The crystal structures of $\beta$-CS (O4) and $\alpha$-CS (Y3) differ markedly from each other and the two polymorphs are easily distinguishable by powder XRD. Both exhibit polytypism ($\beta$-CS (H10,H11); $\alpha$-CS (Y3)); the polytypes of a given polymorph are barely distinguishable by this method. The name 'parawollastonite' has been used for the 2M polytype of $\beta$-CS. The $\beta$–$\alpha$ transition is reversible but slow in the $\alpha$ to $\beta$ direction, rendering $\alpha$-CS easily preservable by quenching. The structure of rankinite is known (S9); a polymorph, kilchoanite, is known only as a natural mineral and as a product of hydrothermal reactions.

The polymorphs of silica relevant to cement chemistry are briefly considered in Section 3.3.2.

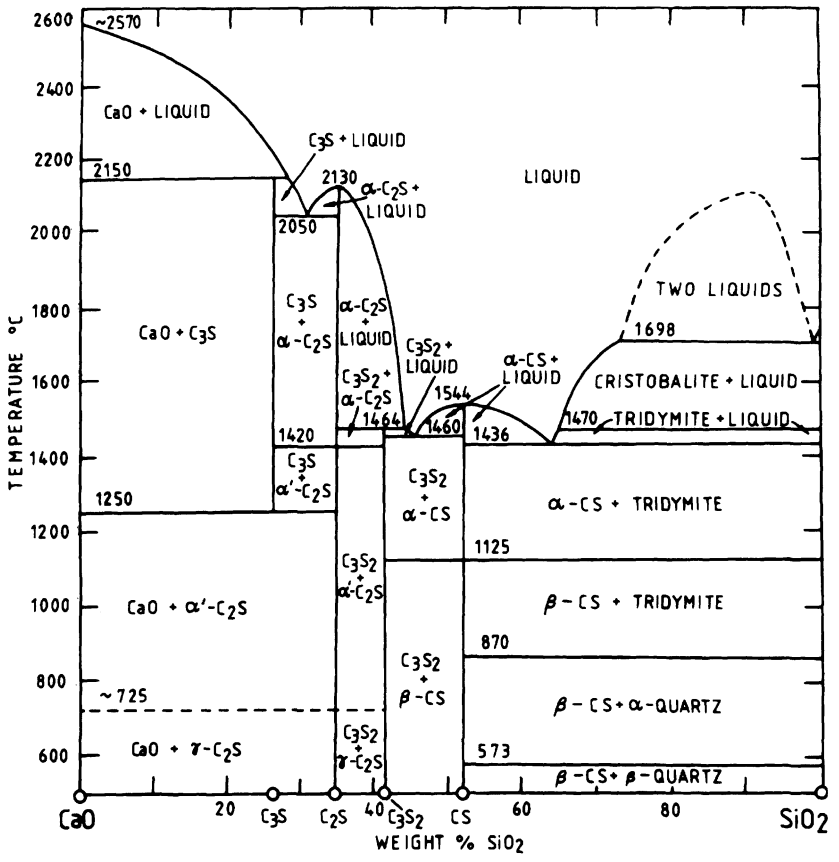


**Fig. 2.1** *The system CaO–$SiO_2$. After D2, with later modifications (G12,O3, R4,W2).*

### 2.2.2 *The CaO–$Al_2O_3$ system*

There have been many phase equilibrium studies on this system, and differences of opinion probably still exist on several points. In part, these differences arise because variations in the humidity and oxygen content of the furnace atmosphere markedly affect the phase relations for compositions in the region of $C_{12}A_7$. The phase diagram in Fig. 2.2 appears to provide the best description of the system modified by the presence of small amounts of water and oxygen, and thus represents the behaviour in air of ordinary humidity. With both CA and $CA_2$, opinions have differed as to whether melting is congruent or incongruent; Nurse *et al.* (N7), who found it to be incongruent in both cases, discussed earlier work. Of the five calcium aluminate phases appearing in Fig. 2.2, one, tricalcium aluminate ($C_3A$), is described in Section 1.4.

Monocalcium aluminate (CA), which is the main constituent of calcium aluminate cements (Section 10.1), reacts rapidly with water. It is

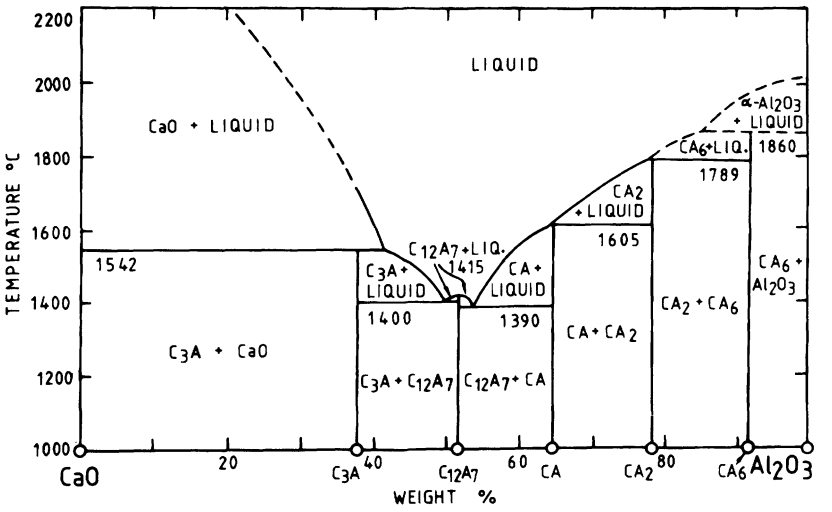


**Fig. 2.2** *The system $CaO–Al_2O_3$ modified by the presence of small amounts of $H_2O$ and $O_2$, and thus representing the behaviour in air of ordinary humidity. After R4, with later modifications (C5,N6,N7).*

monoclinic and pseudohexagonal, with $a = 0{\cdot}8700$ nm, $b = 0{\cdot}8092$ nm, $c = 1{\cdot}5191$ nm, $\beta = 90{\cdot}3°$, space group $P2_1/n$, $Z = 12$, $D_x = 2945\,kg\,m^{-3}$, and has a stuffed tridymite structure, composed of $Ca^{2+}$ ions and an infinite, three-dimensional framework of $AlO_4$ tetrahedra sharing corners (H12). It crystallizes as irregular grains, sometimes prismatic and often twinned, with $\alpha = 1{\cdot}643$, $\beta = 1{\cdot}655$, $\gamma = 1{\cdot}663$, $(-)2V = 36°$ (R4). Formation from $CaCO_3$ and $Al(NO_3)_3$ in the presence of organic reducing agents is reported to proceed through an amorphous material at 500°C and an orthorhombic polymorph at 850°C (B15).

Calcium dialuminate ($CA_2$) occurs in some calcium aluminate cements. It reacts only slowly with water. The formula was at one time wrongly considered to be $C_3A_5$. $CA_2$ is monoclinic, with $a = 1{\cdot}28398$ nm, $b = 0{\cdot}88624$ nm, $c = 0{\cdot}54311$ nm, $\beta = 106{\cdot}8°$, space group C2/c, $Z = 4$, $D_x = 2920\,kg\,m^{-3}$, and has a structure based on a framework of $AlO_4$ tetrahedra, in which some oxygen atoms are shared between two, and others between three tetrahedra (B16,G13). It crystallizes as laths or rounded grains, with $\alpha = 1{\cdot}6178$, $\beta = 1{\cdot}6184$, $\gamma = 1{\cdot}6516$, $(+)2V = 12°$ (B16). $CA_2$ has been found as a natural mineral (G7).

Calcium hexaluminate ($CA_6$) melts incongruently and does not react with water at ordinary temperatures. Its crystal structure is closely related to those of corundum and $\beta$-$Al_2O_3$.

### 2.2.3 $C_{12}A_7$ and derived structures

In air of ordinary humidities, a phase of approximate composition $C_{12}A_7$ is readily formed. It reacts rapidly with water and occurs in some calcium

aluminate cements. A related phase, $C_{11}A_7 \cdot CaF_2$, is similarly reactive and occurs in certain special cements. In early work, $C_{12}A_7$ was wrongly assigned the formula $C_5A_3$ and called 'stable $C_5A_3$' to distinguish it from another phase of that composition, described below, which was called 'unstable $C_5A_3$'. $C_{12}A_7$ is cubic, with $a = 1{\cdot}1983$ nm (J3), space group $I\bar{4}3d$ and $Z = 2$ (B11). Studies on $C_{12}A_7$ or closely related phases (B17,B18,F6,W4,W5) show the crystal structure to be built from $Ca^{2+}$ ions, an incomplete framework of corner-sharing $AlO_4$ tetrahedra and empirical composition $Al_7O_{16}^{11-}$, and one $O^{2-}$ ion per formula unit distributed statistically between 12 sites.

At temperatures above about 930°C, a reversible equilibrium exists between $C_{12}A_7$ and water vapour in the furnace atmosphere (J3,N6, N8,R7). Material prepared in ordinary air and quenched from 1360–1390°C is almost anhydrous; on being gradually reheated, it takes up water until at 950°C a maximum content of about 1·3% is attained, corresponding to the formula $C_{12}A_7H$. On further increase in temperature, the water is lost again, until by the melting point in the region of 1400°C the material is almost anhydrous. The sorbed water affects the cell parameter and refractive index. There was early disagreement as to the direction of the variations, but it appears established that $C_{12}A_7H$ has the smaller cell parameter and higher refractive index, Jeevaratnam *et al.* (J3) finding $a = 1{\cdot}1983$ nm, $n = 1{\cdot}611$ and $D_x = 2680\,kg\,m^{-3}$ for $C_{12}A_7$ and $a = 1{\cdot}1977$, $n = 1{\cdot}620$ and $D_x = 2716\,kg\,m^{-3}$ for $C_{12}A_7H$.

Jeevaratnam *et al.* (J3) suggested that $C_{12}A_7$ can take up water because the 12 sites per formula unit that are occupied statistically by one $O^{2-}$ ion can alternatively be occupied by two $OH^-$ ions, $C_{12}A_7H$ thus having the constitution $Ca_6Al_7O_{16}(OH)$. In support of this conclusion, they prepared the halide analogues $C_{11}A_7 \cdot CaF_2$ and $C_{11}A_7 \cdot CaCl_2$ of the latter compound. $C_{11}A_7 \cdot CaF_2$ was found to have a cell parameter of 1·1964 nm, giving $D_x = 2732\,kg\,m^{-3}$. It forms a continuous range of solid solutions with $C_{12}A_7$ (S10). Bromide, iodide, and sulfide analogues (T1,Z3) and a chloride analogue with partial replacement of Al by Si, balanced by additional occupancy by Cl of the statistically available sites (F6), have also been described.

Imlach *et al.* (I6) found that they could prepare $C_{12}A_7$ reproducibly by slowly cooling melts in dry oxygen and that samples obtained in this way, or by cooling melts in moist air, contained excess oxygen, which could be detected chemically and was possibly present as peroxide ion. If similar melts were cooled in very dry nitrogen, mixtures consisting of CA, $C_3A$ and, sometimes, $C_5A_3$ were obtained, with only poor yields of $C_{12}A_7$. These observations have since been confirmed and extended (B19,B20,Z3,Z4).

Zhmoidin and Chatterjee (Z3,Z4) concluded from density, viscosity and mass spectrometric evidence that melts of $C_{12}A_7$ composition contained regions of two kinds, differing in structure and density. The proportion of the less dense regions increased if the melt took up $H_2O$, $O_2$, CO, $CO_2$ or $SO_3$, or if $CaF_2$, $CaCl_2$, CaS, $CaSO_4$, or $CaCO_3$ was added; if this proportion was sufficiently high, $C_{12}A_7$ or a derivative was formed on freezing. The proportion of the denser regions in the

melt was increased by maintaining a dry and slightly reducing atmosphere and by increase in temperature; if the less dense regions were thus eliminated, the melt yielded a homogeneous glass on quenching, or $C_5A_3$ on slow cooling. The molecules that stabilized the less dense regions acted by surrounding themselves with a particular type of open structure, from which $C_{12}A_7$ readily nucleated; analogies were noted with the roles of hydrated alkali cations in the formation of zeolites and of water or organic molecules in that of compounds of the noble gases. With the exception of water, the molecules thus occluded in crystalline $C_{12}A_7$ could not be removed without destroying the structure. $C_{12}A_7$ melts are considerably denser (2870–2910 kg m$^{-3}$) than solid $C_{12}A_7$, especially if they have been kept in reducing atmospheres.

The derivatives of $C_{12}A_7$ melt in normal ways, $C_{11}A_7 \cdot CaF_2$ congruently at 1577°C and $C_{11}A_7 \cdot CaS$ incongruently to give CaS and liquid at 1482°C (Z3). In contrast, $C_{12}A_7$ stabilized only by water shows anomalous behaviour, one study (N8) showing a sharp melting point of 1392°C over a range of compositions, and another (S10,Z3) melting over a range from 1380 to 1415°C with evolution of gas and incipient formation of CA, $C_3A$ and $C_5A_3$. Figure 2.2 is thus approximate in this region. For practical purposes, the situation in air of ordinary humidities is more important than that in very dry and oxygen-free atmospheres, and the primary phase field of $C_{12}A_7$ will be included in the relevant ternary and quaternary phase diagrams presented below.

$C_{12}A_7$ or $C_{12}A_7H$ has been found as a natural mineral and named mayenite (G7,H13).

### 2.2.4 $C_5A_3$, $C_2A$ and $C_4A_3$

The conditions of formation of $C_5A_3$ are discussed in the preceding section; it is probably an equilibrium phase in the strictly binary system $CaO–Al_2O_3$ but does not form in atmospheres of normal humidity and oxygen content. $C_5A_3$ is orthorhombic, with $a = 1{\cdot}1253$ nm, $b = 1{\cdot}0966$ nm, $c = 1{\cdot}0290$ nm, space group $Cmc2_1$, $Z = 4$, $D_x = 3067$ kg m$^{-3}$, and a structure related to that of gehlenite (V1). The density is considerably higher than that of $C_{12}A_7$ and accords with the formation of the compound from the denser regions present in the melt. $C_5A_3$ reacts rapidly with water (B21).

Two other anhydrous calcium aluminates are known. $C_2A$, a high-pressure phase, is described in Section 1.5.1. $C_4A_3$ is formed as the dehydration product of a hydrothermally produced phase, $C_4A_3H_3$. Its structure is similar to that of sodalite ($Na_4(Al_3Si_3O_{12})Cl$); the constitutional formula is $Ca_4(Al_6O_{12})O$ (P3).

### 2.2.5 The $CaO–Al_2O_3–SiO_2$ system

The phase diagram was originally determined by Rankin and Wright (R4). Figure 2.3 is based on that of Muan and Osborn (M26), with further amendments mainly following from studies on the bounding $CaO–SiO_2$ and $CaO–Al_2O_3$ systems discussed in the preceding sections. It relates to atmospheric pressure in an atmosphere of normal humidity, the primary phase field of $C_{12}A_7$ thus being shown. Some phases probably

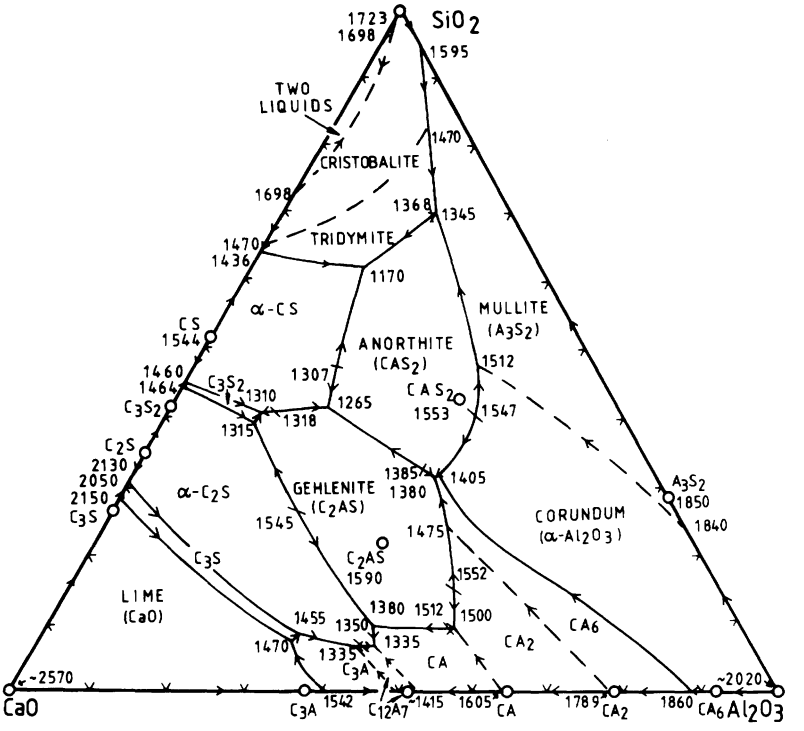


**Fig. 2.3** *The system $CaO–Al_2O_3–SiO_2$. After M26, with later modifications.*

form solid solutions within the system, $C_3S$, for example, being able to accommodate some $Al_2O_3$; this is not shown.

Two ternary compounds exist stably in the system under these conditions. Gehlenite ($C_2AS$; $Ca_2Al_2SiO_7$) belongs to the melilite family. In its structure, layers of 8 coordinated $Ca^{2+}$ ions alternate with ones of composition $Al_2SiO_7^{4-}$, in which both aluminium and silicon are tetrahedrally coordinated (L3). Gehlenite forms extensive solid solutions, e.g. with åkermanite ($C_2MS_2$; $Ca_2MgSi_2O_7$). In a modified form, it occurs in some calcium aluminate cement clinkers (Section 10.1.2). It is tetragonal, with $a = 0{\cdot}7716$ nm, $c = 0{\cdot}5089$ nm, space group $P\bar{4}2_1m$, $Z = 2$, $D_x = 3006\,kg\,m^{3-}$ (L3) and refractive indices $\omega = 1{\cdot}669$, $\varepsilon = 1{\cdot}658$ (W3). The unsubstituted compound does not appear to react with water at ordinary temperatures, but the Al-rich variety present in calcium aluminate cements shows some reactivity at 40°C (S11). Anorthite (a polymorph of $CAS_2$; $CaAl_2Si_2O_8$), which is less relevant to cement chemistry, is a triclinic felspar.

Several other anhydrous calcium aluminosilicates are known, including grossular or garnet ($C_3AS_3$), which is a high-pressure phase, various dehydration products of zeolites, and various products formed metastably by crystallization from melts or glasses. Most are too acid in composition

to be of clear relevance to cement chemistry, but some of the devitrification products, especially those with compositions near CA and structures similar to those of nepheline ($Na_3KAl_4Si_4O_{16}$) or kalsilite ($KAlSiO_4$) (Y4) are of possible interest in relation to the formation of calcium aluminate cements.

### 2.2.6 *Clinker formation in the $CaO–Al_2O_3–SiO_2$ system*

The $CaO–Al_2O_3–SiO_2$ diagram provides a basis for a preliminary understanding of the chemistry underlying the formation of Portland cement clinker, in which all but the three most important oxide components are ignored. The approximations are least for white cements. In a cement kiln, the maximum temperature reached by the mix, called the clinkering temperature, is commonly 1400–1450°C; at this temperature, the mix is partly molten. For a mix in the pure $CaO–Al_2O_3–SiO_2$ system, a somewhat higher temperature is required to give a comparable situation. In this discussion, it is assumed that equilibrium is attained at a clinkering temperature of 1500°C and the $CaO–Al_2O_3–SiO_2$ diagram is used to predict which solid phases will be present for various bulk chemical compositions. The processes by which this equilibrium is approached in cement making, and those taking place during the subsequent cooling, are discussed in Chapter 3.

The compositions in the pure $CaO–Al_2O_3–SiO_2$ system that correspond most nearly to those of typical Portland cement clinkers lie within the ringed area surrounding point P in Fig. 2.4. This point lies within the triangle whose apices are the compositions of $C_3S$, $C_2S$, and point X, which lies at the intersection of the boundary of the $C_3S$ and $C_2S$ primary phase fields with the 1500°C isotherm. For any bulk composition in this

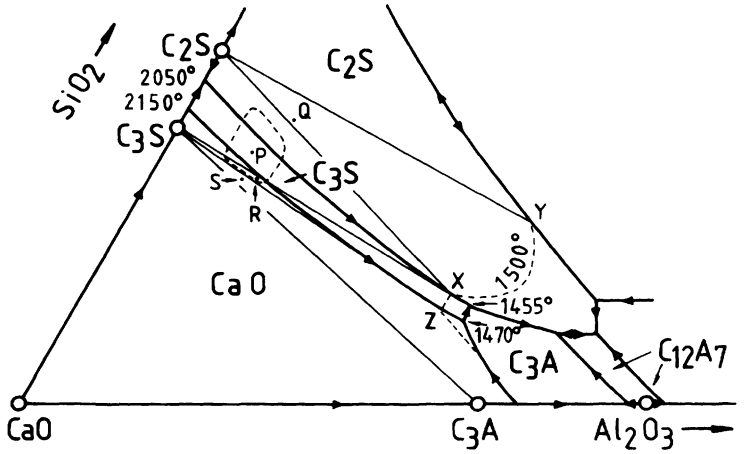


**Fig. 2.4** *Part of the system $CaO–Al_2O_3–SiO_2$, illustrating the formation of Portland cement clinker; for significance of lettered points and of thin full or broken lines, see text.*

triangle, the equilibrium phases at 1500°C will be $C_3S$, $C_2S$ and liquid of composition X. This may be understood by considering what happens if a melt of composition P is cooled. $C_3S$ first crystallizes, the liquid composition thus moving away from that of $C_3S$ until the boundary between the primary phase fields of $C_3S$ and $C_2S$ is reached. $C_3S$ and $C_2S$ then both crystallize, and the liquid composition moves along this boundary until the 1500°C isotherm is reached. For the conditions that exist in cement making, the entire mix is never molten, so that the path to equilibrium differs, but the resulting phase assemblage must be the same. The crystals of $C_3S$ and $C_2S$, being in contact with the melt, can grow to relatively large dimensions, which are typically around 30 $\mu$m. During the subsequent cooling the liquid solidifies, producing the more finely grained interstitial material.

Some other bulk compositions may be considered in the same way. A composition such as Q, lying within the triangle $C_2S$–X–Y, will at equilibrium at 1500°C give $C_2S$ and a liquid having a composition on the curve XY. One such as R, in the triangle $C_3S$–X–Z, will give $C_3S$ and a liquid having a composition on XZ. Any composition lying below the line $C_3S$–Z, such as S, will give an assemblage that includes calcium oxide as a solid phase.

In making Portland cement clinker, it is essential to avoid the presence of more than minimal amounts of free calcium oxide in the final product, and normally desirable to maximize that of $C_3S$. If equilibrium were continuously maintained during cooling, apart from decomposition of $C_3S$ into $C_2S$ and calcium oxide at sub-solidus temperatures, any bulk composition lying within the triangle $C_3S$–$C_2S$–$C_3A$ would yield a final product consisting of these three phases. For bulk compositions below the line $C_3S$–Z, this would require that the crystals of calcium oxide present at the clinkering temperature be redissolved. This process is slow, and one cannot assume that it will be substantially completed in the conditions existing in the kiln. The line $C_3S$–Z therefore sets a practical limit to the CaO content of the mix. For the temperature range in which clinkering is practicable, it virtually coincides with a line joining the $C_3S$ composition to the invariant point at 1470°C involving calcium oxide, $C_3S$, $C_3A$ and liquid, and that line may therefore be used to define the upper limit of acceptable CaO contents. This approach, modified as discussed in Section 2.3.3 to allow for the presence of $Fe_2O_3$, leads to the definition of a quantity called the lime saturation factor, which can be used in practice as an important parameter of the bulk chemical composition.

## 2.3 Systems containing $Fe_2O_3$

### *2.3.1 The $CaO$–$Al_2O_3$–$Fe_2O_3$ system*

This system includes the $Ca_2(Al_xFe_{1-x})_2O_5$ series of ferrite compositions. The bounding, binary system CaO–$Fe_2O_3$ includes three compounds, viz. $C_2F$, CF and $CF_2$. $C_2F$, as an end member of the above series, is discussed in Section 1.5. The other two compounds are of lesser importance to cement chemistry. Phillips and Muan (P4), in a study of the

binary system, found that CF melted incongruently at 1216°C to give $C_2F$ and liquid, and that $CF_2$ decomposed at 1155°C to give CF and hematite ($\alpha$-$Fe_2O_3$). In this and other systems containing $Fe_2O_3$, iron-rich mixes tend to lose oxygen when heated in air above 1200–1300°C, with consequent replacement of hematite by magnetite ($Fe_3O_4$). At lower partial pressures of oxygen, such as occur in a cement kiln, oxygen loss is significant even with compositions relatively low in iron.

Figure 2.5 shows part of the ternary system, $CaO–Al_2O_3–Fe_2O_3$. $C_3A$, $C_{12}A_7$ and CA can all accommodate some $Fe^{3+}$; for $C_3A$ under equilibrium conditions at 1325°C, the limit is about 4.5%, expressed as $Fe_2O_3$ (M27). The ferrite phase in equilibrium with Fe-substituted $C_3A$ can have compositions with $x$ between 0·48 and 0·7 in the formula $Ca_2(Al_xFe_{1-x})_2O_5$; if CaO is also present, $x$ is fixed at 0·48, i.e. the composition is close to $C_4AF$. Some reduction of $Fe^{3+}$ to $Fe^{2+}$ occurs when the ferrite phase is prepared from mixes with compositions in the $Ca_2(Al_xFe_{1-x})_2O_5$ series in air; it leads to the formation of minor amounts of other phases, which are not observed when similar experiments are carried out in oxygen (M27).

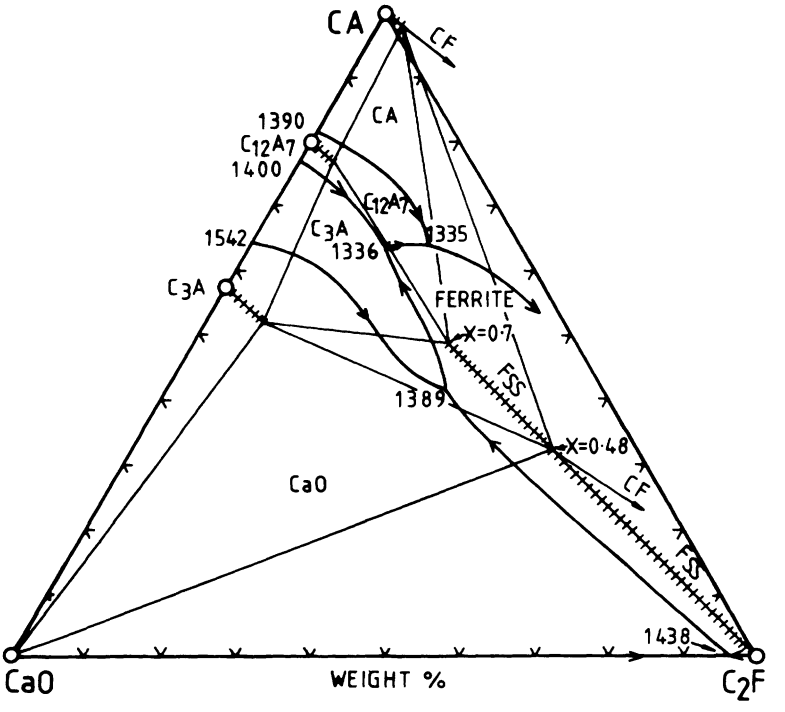


**Fig. 2.5** *Part of the system $CaO–Al_2O_3–Fe_2O_3$. Hatched lines indicate solid solutions. Ferrite phase compositions are indicated by the quantity $x$, which relates to the formula $Ca_2(Al_xFe_{1-x})_2O_5$. After N9 and M27.*

Swayze (S12) noted that equilibrium was often difficult to achieve in this system. One effect was the tendency for crystals of the ferrite phase to be zoned. For bulk compositions in the $Ca_2(Al_xFe_{1-x})_2O_5$ series, the liquid is of higher Al/Fe ratio than the ferrite phase with which it is in equilibrium; the crystals that are initially deposited on cooling such a liquid therefore have a lower Al/Fe ratio than the bulk composition of the mix. On further cooling, the Al/Fe ratio of the material deposited progressively increases. Equilibrium within the ferrite crystals is difficult to attain, causing them to remain zoned, with cores richer in $Fe^{3+}$ and outer regions richer in $Al^{3+}$ than the mean composition.

A second effect was the tendency for protected phases to be formed. If a liquid having a composition somewhat on the CaO-rich side of the boundary between the CaO and $C_3A$ primary phase fields (Fig. 2.5) is cooled, calcium oxide is initially deposited and the liquid composition moves away from CaO and towards that boundary. When the latter is reached, and assuming that equilibrium were to be maintained, calcium oxide would redissolve, $C_3A$ would be deposited, and the liquid composition would move along the boundary. In reality, the $C_3A$ quickly surrounds the particles of calcium oxide, which thus becomes a protected phase, effectively removed from the system. This can markedly affect the composition of the ferrite phase which is subsequently formed on further cooling.

### 2.3.2 *The $CaO–Al_2O_3–Fe_2O_3–SiO_2$ system*

This system comprises the four major oxide components of Portland cement. Lea and Parker (L4,L5) made a classic study of the subsystem $CaO–C_2S–C_{12}A_7–C_4AF$, which is the part directly relevant to cement production. Following Lea (L6), the formula $C_{12}A_7$ is substituted in the present description of this and related investigations for $C_5A_3$, which was used by the original authors in accordance with contemporary opinion on the composition of the phase now regarded as $C_{12}A_7$. Any errors arising from this compositional difference will be small. Lea and Parker assumed the ferrite phase to have the fixed composition $C_4AF$.

Lea and Parker began by studying the bounding ternary subsystems $CaO–C_2S–C_4AF$ and $C_{12}A_7–C_2S–C_4AF$. The first of these, which is the more important, is shown in Fig. 2.6, modified in accordance with later work on the $CaO–SiO_2$ system. In general form, it resembles the lime-rich corner of the $CaO–Al_2O_3–SiO_2$ system (Fig. 2.4), with $C_4AF$ in place of $C_3A$, the primary phase field of $C_3S$ thus being an elongated area extending away from the $CaO–C_2S$ edge of the diagram.

The quaternary system may be represented on a tetrahedral model, each face of which represents one of the bounding, ternary systems. Within the tetrahedron, primary phase fields and sub-solidus compatibility assemblages are represented by volumes, corresponding to the respective areas on the triangular diagram of a ternary system; correspondingly, isotherms are represented by surfaces. Figure 2.7 shows some important features of the $CaO–C_2S–C_{12}A_7–C_4AF$ subsystem, as found by Lea and Parker and modified to take account of later work (G12,M27,N9,S12,S13,W2).

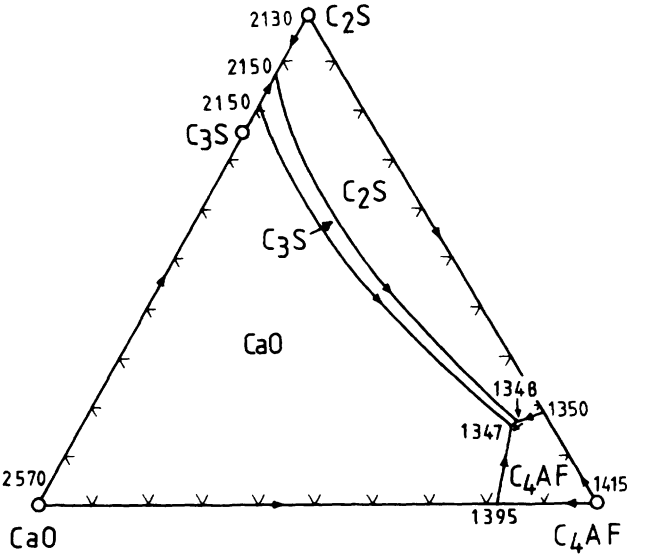


**Fig. 2.6** *The system $CaO–C_2S–C_4AF$. After L4, with later modifications.*

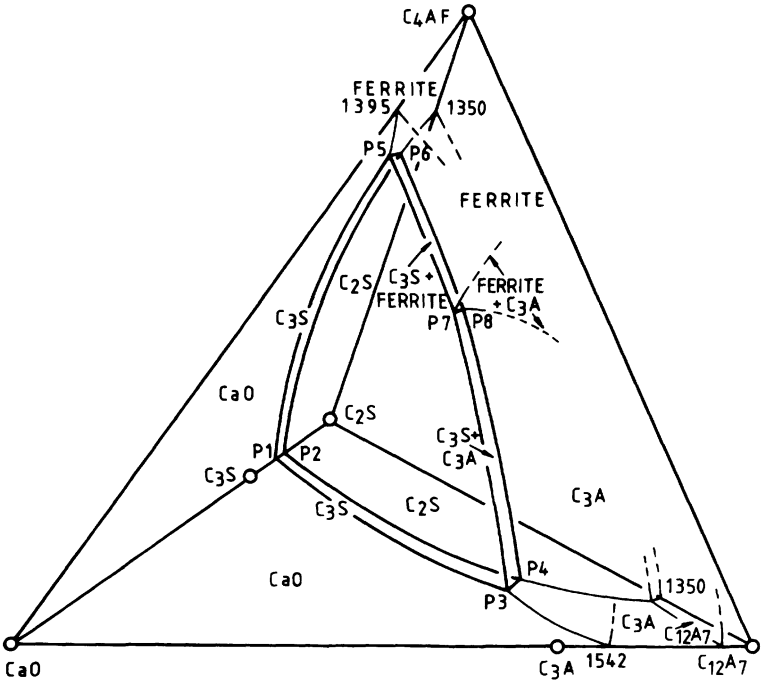


**Fig. 2.7** *The pseudosystem $CaO–C_2S–C_{12}A_7–C_4AF$, showing the primary phase volume of $C_3S$. For details of invariant points P1–P8, see Table 2.1. After L4, with later modifications.*

No quaternary compounds exist in this subsystem. The tetrahedron can therefore be divided into three smaller ones representing sub-solidus compatibility assemblages for $CaO–C_3S–C_3A–C_4AF$, $C_3S–C_3A–C_2S–C_4AF$ and $C_{12}A_7–C_3A–C_2S–C_4AF$. For clarity, these are not shown on Fig. 2.7. The most important feature of the subsystem is the primary phase volume of $C_3S$, which is a thin sliver, roughly parallel to the $C_2S–C_{12}A_7–C_4AF$ face of the tetrahedron and sandwiched between the larger phase volumes of CaO and $C_2S$. In accordance with the bounding subsystems (Figs 2.4 and 2.6), two of its edges lie on the $CaO–C_2S–C_4AF$ and $CaO–C_2S–C_{12}A_7$ faces of the tetrahedron, but it cannot extend to the $CaO–C_4AF–C_{12}A_7$ face. Table 2.1 gives details of the eight invariant points involving $C_3S$ in this subsystem.

Subsequent studies on the $CaO–Al_2O_3–Fe_2O_3$ (M27,N9) and $CaO–Al_2O_3–Fe_2O_3–SiO_2$ (S12,S13) systems have extended knowledge of the latter to a wider range of compositions, but have only slightly affected conclusions regarding the phase volume of $C_3S$. All indicate that the phase volume of $C_3A$ is larger, and that of the ferrite phase smaller than was shown in Lea and Parker's diagrams, which in this region partly rested on early results for the $CaO–C_{12}A_7–C_4AF$ system. To simplify the diagram, the volumes of phases other than $C_3S$ are indicated only in general terms on Fig. 2.7.

### 2.3.3 *Clinker formation in the $CaO–Al_2O_3–Fe_2O_3–SiO_2$ system*

Lea and Parker (L5) derived a formula giving the maximum acceptable content of CaO in a Portland cement clinker composition. If equilibrium was maintained during cooling, apart from decomposition of $C_3S$ into $C_2S$ and CaO at sub-solidus temperatures, any bulk composition within the tetrahedron $C_3S–C_2S–C_3A–C_4AF$ would yield a clinker consisting of those four phases. However, as in the $CaO–Al_2O_3–SiO_2$ system, it cannot be assumed that any calcium oxide present at equilibrium at the clinkering temperature will subsequently be reabsorbed. Following reasoning similar to that in Section 2.2.6, calcium oxide will not be present at equilibrium at the clinkering temperature of approximately 1450°C if the bulk composition lies on the lime-poor side of a plane defined by the compositions of $C_3S$, $C_4AF$ and the invariant point $P_3$ (Fig. 2.7 and Table 2.1). The oxide ratios by mass for these three compositions are given in Table 2.2. One may then set up three simultaneous equations of the type

$$(SiO_2/CaO)x + (Al_2O_3/CaO)y + (Fe_2O_3/CaO)z = 1{\cdot}0 \qquad (2.1)$$

where chemical formulae represent mass percentages of oxides in the clinker, and solve them to obtain an expression for the content of CaO at any point in the plane, viz.

$$CaO = xSiO_2 + yAl_2O_3 + zFe_2O_3 \qquad (2.2)$$

This gives $x = 2{\cdot}80$, $y = 1{\cdot}18$, $z = 0{\cdot}65$.

The ratio $[CaO/(2{\cdot}80SiO_2 + 1{\cdot}18Al_2O_3 + 0{\cdot}65Fe_2O_3)]$ is called the lime saturation factor (LSF). A mix having an LSF greater than unity will

**Table 2.1** *Invariant points involving $C_3S$ in the $CaO–Al_2O_3–Fe_2O_3–SiO_2$ system and in the same modified by 5% MgO*

| Point | Solid phases in addition to $C_3S$ | Liquid composition (mass per cent) | | | | | $x$ in ferrite phase* | Type of point† | Temp· (°C) | Ref. |
|---|---|---|---|---|---|---|---|---|---|---|
| | | CaO | $Al_2O_3$ | $Fe_2O_3$ | $SiO_2$ | MgO | | | | |
| P1 | CaO | 71·5 | – | – | 28·5 | – | – | P | 2150 | G12 |
| P2 | $C_2S$ | 69·5 | – | – | 30·5 | – | – | E | 2050 | G12 |
| P3 | $CaO + C_3A$ | 59·7 | 32·8 | – | 7·5 | – | – | P | 1470 | R4 |
| P4 | $C_2S + C_3A$ | 58·5 | 32·9 | – | 8·6 | – | – | P | 1455 | R4 |
| P5 | CaO + ferrite | 52·8 | 16·2 | 25·4 | 5·6 | – | 0·50 | E | 1347 | L4 |
| P6 | $C_2S$ + ferrite | 52·4 | 16·3 | 25·5 | 5·8 | – | 0·50 | P | 1348 | L4 |
| P7 | $CaO + C_3A$ + ferrite | 55·0 | 22·7 | 16·5 | 5·8 | – | 0·50 | P | 1341 | L4 |
| P7 | $CaO + C_3A$ + ferrite | 53·9 | 21·2 | 19·1 | 5·8 | – | 0·44 | P | 1342 | S12 |
| P7 | $CaO + C_3A$ + ferrite + MgO | 50·9 | 22·7 | 15·8 | 5·6 | < 5·0 | 0·47 | P | 1305 | S14 |
| P8 | $C_2S + C_3A$ + ferrite | 54·8 | 22·7 | 16·5 | 6·0 | – | 0·50 | ? | 1338 | L4 |
| P8 | $C_2S + C_3A$ + ferrite | 53·5 | 22·3 | 18·2 | 6·0 | – | 0·57 | P | 1338 | S12 |
| P8 | $C_2S + C_3A$ + ferrite + MgO | 50·5 | 23·9 | 14·7 | 5·9 | < 5·0 | 0·67 | P | 1301 | S14 |

* $x$ in formula $Ca_2(Al_xFe_{1-x})_2O_5$.
† E = eutectic; P = peritectic.

**Table 2.2** *Oxide ratios by mass for points on the surface bounding the region in which calcium oxide is an equilibrium phase at 1450°C*

| Point on surface | $SiO_2/CaO$ | $Al_2O_3/CaO$ | $Fe_2O_3/CaO$ |
|---|---|---|---|
| $C_3S$ | 0·357 | 0 | 0 |
| $C_4AF$ | 0 | 0·456 | 0·714 |
| $P_3$ | 0·126 | 0·549 | 0 |

yield free calcium oxide at the clinkering temperature, and this phase is liable to persist in the final product, irrespective of the degree of mixing of the raw materials and the time during which the clinkering temperature is maintained. The calculation is approximate, because of the neglect of minor oxide components and of ionic substitutions in the solid phases and for other reasons. For values below unity, the LSF provides a measure of the extent to which the maximum attainable content of $C_3S$ is approached. Values of 0·92–0·98 are typical of modern clinkers.

Lea and Parker considered that their calculations were valid only for $Al_2O_3/Fe_2O_3$ mass ratios in the clinker above that in $C_4AF$ (0·64), but this does not appear to be correct (W6). The plane within the $CaO–C_2S–C_{12}A_7–C_4AF$ tetrahedron defined by the compositions of $C_3S$, $C_4AF$ and the point $P_3$ passes close to the composition of $C_2A$, and therefore also to all other compositions in the $Ca_2(Al_xFe_{1-x})_2O_5$ series. Swayze's (S12) results, discussed in Section 2.4.2, show that the extension of the $CaO–C_3S$ boundary surface to more iron-rich compositions remains close to this plane, which therefore serves also for $Al_2O_3/Fe_2O_3$ ratios below that in $C_4AF$.

## 2.4 Systems containing MgO or FeO

### *2.4.1 General*

Portland cement raw materials contain small proportions of MgO; as noted in Section 1.1.2, they must be limited to avoid formation of more than a minor amount of periclase. The iron in Portland cement clinkers is normally present almost entirely as $Fe^{3+}$, but calcium aluminate cements may contain both $Fe^{3+}$ and $Fe^{2+}$.

Table 2.3 lists some phases containing MgO that are in varying degrees relevant to cement chemistry. It is not a complete list of phases with essential MgO in the $CaO–MgO–Al_2O_3–SiO_2$ system. As seen in Chapter 1, some MgO is also taken up by all four of the major clinker phases. Magnesium oxide (periclase), like calcium oxide, has the sodium chloride structure; it is cubic, with $a = 0{\cdot}4213$ nm, space group Fm3m, $Z = 4$, $D_x = 3581\ kg\ m^{3-}$ (S8) and refractive index 1·7366 (W3). FeO (wüstite) has the same structure, but always contains some $Fe^{3+}$, balanced by vacancies. It forms extensive solid solutions with MgO and can also accommodate some CaO.

Early studies of such systems as $MgO–C_2S–C_{12}A_7$ (H14), $CaO–MgO–C_2S–C_{12}A_7$ (M29) and $MgO–C_4AF$ (I7) indicated that periclase is the

**Table 2.3** *Some phases containing Mg relevant to cement chemistry*

| Name | Formula | Structure type |
|---|---|---|
| Periclase | MgO | Sodium chloride |
| Forsterite | $M_2S$ | Olivine |
| Monticellite | CMS | |
| Merwinite | $C_3MS_2$ | Related to alkali sulfate structures* |
| Bredigite | $C_7MS_4$ | |
| Åkermanite | $C_2MS_2$ | Melilite ($C_2AS$ etc.) |
| Enstatite | MS | Pyroxene† |
| Diopside | $CMS_2$ | |
| Spinel | MA | Spinel |
| – | $C_3A_2M$ | Related to $C_2AS$ and $C_5A_3$‡ |
| – | $C_7A_5M$ (?) | |
| 'Phase Q' | $C_{20}A_{13}M_3S_3$ | |

* 'Phase T', of approximate composition $C_{1.7}M_{0.3}S$ (G14,S15–S17), is identical with bredigite (B9,M28).
† Also, the MS polymorphs clinoenstatite and protoenstatite, which, too, are of pyroxene type.
‡ For references and descriptions, see Section 2.4.3. Phase Q is of variable composition; the formula given is a median.

only phase with essential MgO liable to be formed in Portland cement clinkers. A later study on the CaO–MgO–$Al_2O_3$–$SiO_2$ system suggested that bredigite and 'phase Q' could possibly occur in rapidly cooled clinkers (B9), but there is no convincing evidence that either of these phases is present in production clinkers.

Allen and Snow (A2) studied equilibria in the low-$SiO_2$ part of the CaO–'FeO'–$SiO_2$ system in the presence of metallic iron. The results are relevant to the formation of Portland cement clinkers under reducing conditions.

### 2.4.2 *Effect of MgO on equilibria in the CaO–$Al_2O_3$–$Fe_2O_3$–$SiO_2$ system*

Swayze (S12,S14) extended the work of Lea and Parker (L4,L5) by considering the effects of variable ferrite composition and of the presence of MgO as an oxide component. In the work with MgO, a constant 5% of the latter was present in all the compositions examined. This was considered sufficient to saturate the liquid, as small amounts of periclase were detected in nearly all the products. Figure 2.8 shows the results for the system in the presence of MgO, modified to take account of later work on the subsystems. The primary phase is always periclase, and the system is represented by using a tetrahedron whose edges correspond to a total mass percentage of 95%. Volumes within this tetrahedron relate to the second phase to crystallize.

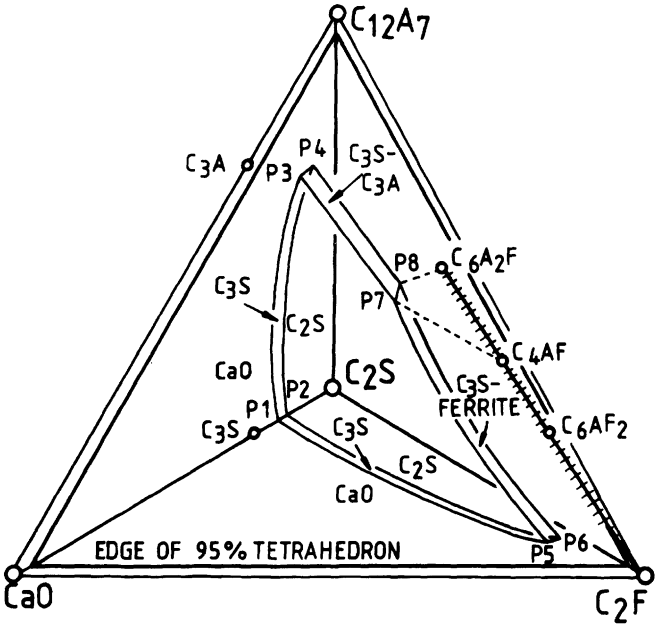


**Fig. 2.8** *The pseudosystem $CaO–C_2S–C_{12}A_7–C_2F$ modified by the presence of 5% of MgO, showing the phase volume of $C_3S$ and tie lines for the ferrite, the compositional range of which is represented by the hatched line. For details of invariant points P1–P8, see Table 2.1. After S14, with later modifications.*

The most important effects, whether of taking into account variable ferrite composition or the presence of MgO, concern the invariant points for $C_3S$, $C_3A$, ferrite phase, liquid and either CaO or $C_2S$, data for which are given in Table 2.1, where they may be compared with those of Lea and Parker. In the absence of MgO, the temperatures of the corresponding points agree well between the two studies, but the liquid compositions are slightly different. In the presence of MgO, the temperatures are each lowered by 37 K and the liquid compositions substantially affected, the $Al_2O_3$ concentrations being increased and those of CaO and $Fe_2O_3$ decreased. Swayze found the ferrite phase in equilibrium with $C_3A$, $C_3S$, $C_2S$ and liquid to have a composition slightly more iron-rich than $C_4AF$ if MgO was absent, and one close to $C_6A_2F$ if MgO was present.

Swayze pointed out that these results had important consequences for the composition of the ferrite phase in Portland cement clinkers, whose compositions normally include significant amounts of MgO. He concluded that, for $Al_2O_3/Fe_2O_3$ ratios above 1·6, the ferrite phase composition would be $C_6A_2F$. Most ordinary Portland cement clinkers have $Al_2O_3/Fe_2O_3$ ratios in this range. For ratios below 0·84, assuming no free calcium oxide to be present, no $C_3A$ would be formed, and the $Al_2O_3/Fe_2O_3$ ratio in the ferrite phase would be that of the bulk composition. For intermediate values, lack of information about the tie lines for the ferrite phase made it

impossible to predict the composition of the ferrite phase. Analyses of the ferrite phase in typical clinkers (Section 1.5.2) show that these conclusions are essentially correct, though the situation is complicated by the fact that the ferrite phase contains significant proportions of substituent oxide components, especially MgO, $SiO_2$ and $TiO_2$.

Swayze assumed that, for the bulk compositions that he studied, all the MgO was in the liquid phase at equilibrium, apart from the small proportions present as periclase. As noted in the preceding section, all four of the major clinker phases take up significant proportions of MgO. The contents of the latter component in the liquid phase were therefore probably substantially lower than 5%.

### 2.4.3 *Phases structurally related to gehlenite*

The phases $C_3A_2M$, $C_7A_5M$ and 'Q' are structurally related to each other and to $C_5A_3$ and gehlenite ($C_2AS$); this is shown by unit cell determinations (M30) and, for phase Q, by a structure determination (H15), which also yielded a probable structure for $C_3A_2M$. In all the known structures mentioned above, aluminium, magnesium, and, where present, silicon are tetrahedrally coordinated. Phase Q was originally assigned the formula $C_6A_4MS$ (P5), and it has also been suggested that two distinct quaternary phases exist, with compositions $C_{21}A_{14}M_7S$ and $C_{22}A_{13}M_3S_4$ (G15). The structure determination (H15) and an associated phase study (K4) indicated that there is only one such phase, and that its composition is $Ca_{20}Al_{32-2n}Mg_nSi_nO_{68}$ with $n$ variable between 2·5 and 3·5, a median formula thus being $C_{20}A_{13}M_3S_3$. The unit cell, for $n = 3{\cdot}0$, was found to be orthorhombic with $a = 2{\cdot}7638$ nm, $b = 1{\cdot}0799$ nm, $c = 0{\cdot}5123$ nm, space group Pmmn, $Z = 1$ and $D_x = 2985\,\mathrm{kg\,m^{-3}}$.

A phase known as pleochroite, of fibrous or acicular morphology, occurs in some calcium aluminate cements and is Phase Q modified by replacement of $Mg^{2+}$ by $Fe^{2+}$ and of $Al^{3+}$ by $Fe^{3+}$ (G15,P5). X-ray microanalyses by Conjeaud (C6) appear compatible with the approximate composition $Ca_{20}Al_{22{\cdot}6}Fe^{3+}_{2{\cdot}4}Mg_{3{\cdot}2}Fe^{2+}_{0{\cdot}3}Si_{3{\cdot}5}O_{68}$. Sourie *et al.* (S18) reported further analyses, most of which are compatible with phase Q, in which the $Al^{3+}$ is partly replaced by $Fe^{3+}$ and the $Mg^{2+}$ is completely replaced by $Fe^{2+}$, but with values of $n$ ranging from below 1 to more than 4. There were strong compositional variations both between and within samples. Electron diffraction showed no major abnormalities in the crystals low in silicon, but those high in silicon were ordered intergrowths at a unit-cell level of that phase with a melilite approximating to gehlenite. The results of another EPMA determination (M31) are of uncertain significance because they show improbably large deviations from charge balance.

Several phase equilibrium studies have been made on this part of the $CaO–MgO–Al_2O_3–SiO_2$ system (B9,G15,K4,P5). Phase Q has a primary phase volume in the system, but there are some uncertainties regarding the stable solid-phase assemblages that include it. $C_3A_2M$ has a primary phase field in the $CaO–MgO–Al_2O_3$ and $CaO–MgO–Al_2O_3–SiO_2$ systems (B9,H16,W7). $C_7A_5M$ is a metastable phase, and the formula given may be only approximate.

## 2.5 Systems containing alkalis or $SO_3$ or both

### *2.5.1 Phases*

Portland cement clinkers contain small amounts of alkalis and sulfates derived from the raw materials and fuel. Both alkalis and $SO_3$ can be present in the major clinker phases, but tend to combine preferentially with each other to form alkali or potassium calcium sulfates, and it is necessary to consider these components together. In addition, silicate and aluminate phases containing sulfate can form either as intermediates or in undesirable deposits in cement making, and a calcium aluminate sulfate is a major constituent of some expansive and other special cements.

The only phase containing essential alkali but not essential $SO_3$ known to occur in Portland cement clinkers in more than trace amounts is the orthorhombic aluminate phase described in Section 1.4. Trace amounts of alkali carbonates (P2) or potassium aluminate (F7) have been reported to occur in some clinkers, and some other alkali phases are formed as intermediates or deposits.

Tables 2.4 and 2.5 list the sulfate phases and give crystal data and optical properties, respectively. Arcanite is the polymorph ($\beta$) of potassium sulfate stable at room temperature; it transforms reversibly to $\alpha$-$K\bar{S}$ at 583°C and melts at 1069°C (R8). Thenardite is the polymorph (V) of sodium sulfate stable in presence of moisture at room temperature; on heating, it passes through a complex sequence of phase transitions and melts at 883°C (E1). Other polymorphs can persist to room temperature. Anhydrite is the polymorph ($\beta$) of calcium sulfate stable at room temperature, formed on heating the hydrates or the metastable $\gamma$-$C\bar{S}$ ('soluble anhydrite'). A thermal effect at 1195°C, generally attributed to polymorphic change to an $\alpha$-$C\bar{S}$, may be associated with onset of ionic rotation (F8). On heating in air, decomposition is detectable below 1000°C (K6), but slow below 1200°C; in a closed container, anhydrite melts at 1462°C (R8). Calcium langbeinite undergoes phase transitions at 200°C and 940°C and melts incongruently to give calcium sulfate and liquid at 1011°C (A3,R8). Aphthitalite is essentially a solid solution phase of general composition $(K,Na)_2SO_4$. When it is formed stably at room temperature, the composition does not vary much from $K_3N\bar{S}_4$, but at higher temperatures compositions much higher in sodium are possible, up to a limit near $KN_3\bar{S}_4$, and the resulting solid solutions can be quenched to room temperature. Glaserite is a varietal name for aphthitalite of or near $K_3N\bar{S}_4$ composition.

$C_4A_3\bar{S}$ $[Ca_4(Al_6O_{12})(SO_4)]$ is readily formed on heating mixtures of appropriate composition in air at 1350°C (H17,H18,R9). The crystal structure is a slightly distorted variant on that of sodalite $[Na_4(Al_3Si_3O_{12})Cl]$; it is composed of a three-dimensional framework of $AlO_4$ tetrahedra sharing corners, with $Ca^{2+}$ and $SO_4^{2-}$ ions in the cavities (H17). The distortion causes a change in symmetry and various larger, geometrically-related unit cells have been proposed (F9,H18,I8,Z5); two polymorphs, of closely similar structure, have been described (A4). $C_4A_3\bar{S}$ reacts readily with water, and melts at about 1600°C (H17).

**Table 2.4** *Crystal data for sulfate phases*

| Formula | Name | Crystal system* | Unit cell parameters (nm) | | | Space group | $Z$ | $D_x$ (kg m$^{-3}$) | Ref. |
|---|---|---|---|---|---|---|---|---|---|
| | | | $a$ | $b$ | $c$ | | | | |
| $K_2SO_4$ | Arcanite | Or | 0·7476 | 1·0071 | 0·5763 | Pnam | 4 | 2668 | M32 |
| $KC_2\bar{S}_3$ | Ca langbeinite | Or | 1·0334 | 1·0501 | 1·0186 | $P2_12_12_1$(?) | 4 | 2683 | S19 |
| $K_3N\bar{S}_4$ | Aphthitalite† | Tr | 0·5680 | – | 0·7309 | $P\bar{3}m1$ | $\frac{1}{2}$ | 2703 | O5 |
| $Na_2SO_4$ | Thenardite | Or | 0·5861 | 0·9815 | 1·2307 | Fddd | 8 | 2665 | M33 |
| $CaSO_4$ | Anhydrite | Or | 0·7006 | 0·6998 | 0·6245 | Amma | 4 | 2952 | K5 |
| $C_4A_3\bar{S}$ | 'Aluminosulfate' | Cu | 1·839 | – | – | $I4_132$‡ | 16 | 2607 | H17 |
| $C_5S_2\bar{S}$ | 'Silicosulfate' | Or | 1·0182 | 1·5398 | 0·6850 | Pcmn | 4 | 2973 | B22 |

* Or = orthorhombic, Tr = trigonal ($\gamma = 120°$), Cu = cubic.
† Data are for composition given; cell parameters decrease with increasing Na/K ratio (P2).
‡ The space group I23 has also been proposed (I8).

**Table 2.5** *Optical properties of sulfate phases*

| Formula | Name | Refractive indices | | | Character | $2V$ | Ref. |
|---|---|---|---|---|---|---|---|
| | | $\alpha$ | $\beta$ | $\gamma$ | | | |
| $K_2SO_4$ | Arcanite | 1·4935 | 1·4947 | 1·4973 | Biaxial + | 67° | W3 |
| $KC_2\bar{S}_3$ | Ca langbeinite | 1·522 | 1·526 | 1·527 | Biaxial − | Low | S19 |
| $K_3N\bar{S}_4$ | Aphthitalite* | 1·493 | – | 1·498 | Uniaxial + | – | W3 |
| $Na_2SO_4$ | Thenardite | 1·471 | 1·477 | 1·484 | Biaxial + | 84° | W3 |
| $C\bar{S}$ | Anhydrite | 1·5698 | 1·5754 | 1·6136 | Biaxial + | 43° | W3 |
| $C_4A_3\bar{S}$ | 'Aluminosulfate' | – | 1·569 | – | Isotropic | – | H17 |
| $C_5S_2\bar{S}$ | 'Silicosulfate' | 1·632 | 1·638 | 1·640 | Biaxial − | 60° | P6 |

* Data are for composition given; refractive indices decrease with increasing Na/K ratio (W3).

$C_5S_2\bar{S}$ [$Ca_5(SiO_4)_2(SO_4)$] has sometimes been called sulfospurrite. The name is misleading, because the structure is unrelated to that of spurrite [$Ca_5(SiO_4)_2(CO_3)$] and elemental prefixes conventionally denote similarity not only in formula type, but also in structure. $C_5S_2\bar{S}$ is isostructural with silicocarnotite, $Ca_5(PO_4)_2(SiO_4)$ (B22). It is obtained on heating mixtures of appropriate composition in air of ordinary humidity (G16,P7), and in this environment is stable up to 1298°C (P8). Pliego-Cuervo and Glasser (P7) were unable to prepare it in the absence of water vapour and obtained evidence that it contained a small amount of essential hydroxyl ion. They considered that the atmosphere in a cement kiln was sufficiently moist to stabilize it in the appropriate temperature range, but that this might not hold true for the centres of clinker lumps.

### 2.5.2 *Equilibria*

Considering first systems of sulfates alone, phase equilibria have been reported for $K\bar{S}$–$N\bar{S}$ (E1), $K\bar{S}$–$C\bar{S}$ (A3,P9,R8) and $K\bar{S}$–$N\bar{S}$–$C\bar{S}$ (B23). Melting of $K\bar{S}$–$N\bar{S}$–$C\bar{S}$ mixes begins below 800°C (R10). At high temperatures, $K\bar{S}$ is completely miscible with $N\bar{S}$ (E1) and accommodates up to 20 mole % of $C\bar{S}$ (A3) in solid solutions having the $\alpha$-$K\bar{S}$ structure. It can also dissolve some $CaCO_3$ (A3). With increase in temperature above ambient, the compositional range of aphthitalite solid solution rapidly broadens, extending much further in the direction of $N\bar{S}$ and contracting slightly in that of $K\bar{S}$; the maximum Na/K ratio of about 3 : 1 is attainable at 195°C (E1). At room temperature, all the phases other than metastable aphthitalites have essentially the fixed compositions shown in Tables 2.4 and 2.5.

A study of the CaO–$K\bar{S}$–$C\bar{S}$ system showed that the sulfate melts dissolved only a little CaO (P9). Alkali sulfate melts also show only limited mutual miscibility with oxide melts similar in composition to the main clinker liquid (P7,P10,T1,T6). For contents of alkali sulfates of 2–3% in the clinker liquid as a whole, the sulfate liquid is dispersed in the oxide liquid as microregions about 100 nm in diameter (T1), but with higher contents of alkali sulfates, the two liquids separate on a macroscopic scale (G17,T1). The partitioning of the components between sulfate melts and simulated clinker liquids at 1350°C has been studied (G17). $SO_3$ is virtually insoluble in the oxide liquid, and $SiO_2$, $Al_2O_3$ and $Fe_2O_3$ dissolve only to very minor extents in the sulfate liquid, but CaO, $Na_2O$ and $K_2O$ are appreciably soluble in both. For five mixes studied, the ratio of $K_2O$ to $Na_2O$ was between 1·9 and 4·6 times higher in the sulfate than in the oxide liquid.

Several early phase equilibrium studies on systems of calcium silicates or aluminates with alkalis were reported (N10), but their significance needs to be reassessed because they postulated the existence of the compounds $NC_8A_3$ or $KC_{23}S_{12}$, which in neither case is supported by more recent work.

Gutt and Smith (G18) reviewed earlier work on the effects of $SO_3$ on the formation of Portland cement clinker, and to augment the available

information studied part of the $CaO–Al_2O_3–Fe_2O_3–SiO_2–CaSO_4$ system at 1400°C. They concluded that, if $Al_2O_3$ was present and MgO absent, even small proportions of $SO_3$ could restrict or prevent formation of $C_3S$. The effect was lessened, but not eliminated, if MgO was present, and it was noted that other minor components, especially alkalis, might further modify the situation.

Pliego-Cuervo and Glasser (P8) determined sub-solidus phase assemblages in the CaO-rich part of the $CaO–Al_2O_3–SiO_2–SO_3$ system at 950–1150°C. Four-phase and three-phase assemblages defining the equilibria between CaO, $C_2S$, $C_3A$, $C_{12}A_7$, CA, $C_5S_2\bar{S}$ and $C_4A_3\bar{S}$ were established. This work was extended (P10) to cover parts of the $CaO–Al_2O_3–SiO_2–K\bar{S}$, $CaO–Al_2O_3–K\bar{S}–C\bar{S}$, $CaO–Al_2O_3–SiO_2–K\bar{S}–C\bar{S}$ and $CaO–Al_2O_3–Fe_2O_3–K\bar{S}–C\bar{S}$ systems, and the role of sulfur-containing species in the solid, liquid and vapour states in the formation of Portland cement clinker was discussed. Neither $C_5S_2\bar{S}$ nor $C_4A_3\bar{S}$ could occur in the final product, but both could play important parts in the kiln reactions.

Kaprálik *et al.* (K6,K7) studied equilibria in part of the $CaO–Al_2O_3–SiO_2–Fe_2O_3–MgO–C\bar{S}–K\bar{S}$ system at temperatures up to 1300°C with reference to the formation of clinkers designed to contain $C_4A_3\bar{S}$. Compatible phase assemblages were established. The authors noted that the subsystem $C_2S–C_4A_3\bar{S}–C\bar{S}$ included all the main compounds having hydraulic properties that were formed in clinkers of this type.

## 2.6 Systems with other components

### *2.6.1 Fluorides and fluorosilicates*

Small amounts of $F^-$ may occur in Portland cement clinkers, arising from raw materials or deliberate additions to lower the clinkering temperature. Two ternary phases are known to exist in the $CaO–C_2S–CaF_2$ system (B24). One, now known to be of formula $2C_2S \cdot CaF_2$ or $Ca_5(SiO_4)_2F_2$, has a structure analogous to that of chondrodite $[Mg_5(SiO_4)_2(OH,F)_2]$, with layers of $\gamma$-$C_2S$ structure alternating with ones containing $Ca^{2+}$ and $F^-$ (G19).

The second ternary phase has been described as $3C_3S \cdot CaF_2$ (G20), $C_{11}S_4 \cdot CaF_2$ (T7) and $C_{19}S_7 \cdot 2CaF_2$ (G21), but its probable formula is $Ca_{6-x/2}Si_2O_{10-x}F_x$ ($x \approx 1$), and the structure is related to that of $C_3S$ with partial replacement of $O^{2-}$ by $F^-$ balanced by omission of $Ca^{2+}$ (P11,P12). The arrangement of $Ca^{2+}$, $SiO_4^{4-}$ and $O^{2-}$ or $F^-$ ions differs from that in the $C_3S$ polymorphs, and is the simplest possible in the broader family of structures to which the latter belong (P11). There is a strongly marked pseudocell, which (for $x = 1{\cdot}0$) is hexagonal with $a = 0{\cdot}7099$ nm, $c = 0{\cdot}5687$ nm, space group $P6_3/mmc$ and atomic contents $\frac{1}{2}[C_{10}S_4 \cdot CaF_2]$, but the true cell is triclinic, with $a = 2{\cdot}3839$ nm, $b = 0{\cdot}7105$ nm, $c = 1{\cdot}6755$ nm, $\alpha = 90{\cdot}0°$, $\beta = 117{\cdot}3°$, $\gamma = 98{\cdot}56°$ and atomic contents $5[C_{10}S_4 \cdot CaF_2]$ (P11,P12). The X-ray density, for $x = 1{\cdot}0$, is 2936 kg m$^{-3}$. For brevity, this phase will be called $C_{10}S_4 \cdot CaF_2$.

In the $C_2S–CaF_2$ system, the two end members form a eutectic at 1110°C. $2C_2S \cdot CaF_2$ can be obtained by solid-state reaction at 950°C and decomposes at 1040°C to give $C_2S$ and $CaF_2$ (G20). Two phase

equilibrium studies of the $CaO–C_2S–CaF_2$ system (G22,T7) (Fig. 2.9) are in good agreement. $C_{10}S_4 \cdot CaF_2$ melts incongruently at 1170°C to give $C_3S$ and liquid. In the presence of $CaF_2$, $C_3S$ can thus be obtained at this temperature through the successive formation and decomposition at lower temperatures of $2C_2S \cdot CaF_2$ and $C_{10}S_4 \cdot CaF_2$ (B24,G23,T7).

There has been some uncertainty as to the extent to which $F^-$ enters the $C_3S$ structure (as opposed to that of $C_{10}S_4 \cdot CaF_2$) and also about the effectiveness of $C_3S$ produced in presence of $CaF_2$ as a cement. Welch and Gutt (W8) found that addition of $CaF_2$ to the starting materials caused the polymorph to change from triclinic to monoclinic, and obtained results suggesting that 0·74% of $F^-$ entered the $C_3S$; $CaF_2$ accelerated the formation of $C_3S$ but the compressive strengths of mortars made with the latter were reduced. Tanaka *et al.* (T7) found that $C_3S$ formed from $C_{10}S_4 \cdot CaF_2$ was trigonal (presumably rhombohedral), though it tended to invert to monoclinic on quenching. They found that $C_{10}S_4 \cdot CaF_2$ gave poor strengths and suggested that the poor hydraulic activity of Welch and Gutt's preparations might have been due to presence of this phase, formed from the $C_3S$ during cooling. Maki *et al.* (M34) described an alite prepared from a melt containing $F^-$; it was monoclinic ($M_3$) and contained 0·9% F and 3·4% $Al_2O_3$.

In contrast to some of these results, Moir (M12) described a clinker containing 1·8% $Al_2O_3$, 2·3% $SO_3$ and 0·16% F, which gave high early strengths; the $C_3S$ it contained was rhombohedral. Shame and Glasser (S20) found that little $F^-$ could enter the $C_3S$ structure in the absence of $Al^{3+}$, which permitted coupled substitution to occur, giving material of general formula $Ca_3(Al_xSi_{1-x})(O_{5-x}F_x)$. The upper limit of $x$ was 0·15 (1·2% F). At $x = 0{\cdot}15$, the material was rhombohedral, even if cooled rapidly, and gave high 28-day strengths. In the presence of $Al^{3+}$ and $F^-$, $C_3S$ could be made by solid-state reaction at temperatures as low as 1025°C, though reaction was slow below 1050°C. At higher temperatures,

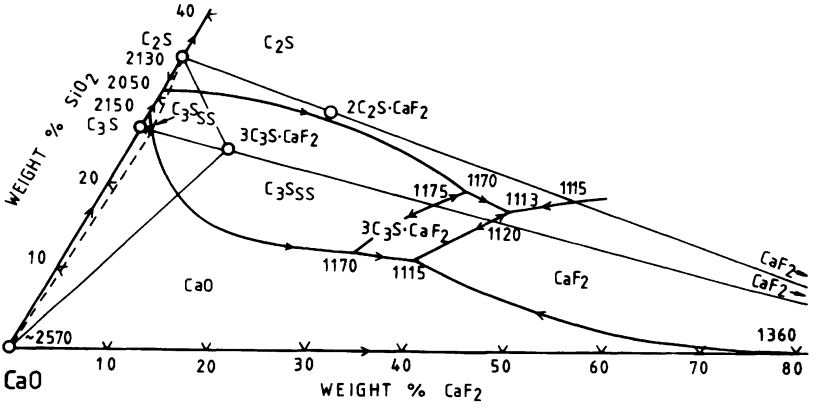


**Fig. 2.9** *The system $CaO–C_2S–CaF_2$. After G22.*

$F^-$ not lost by volatilization was mainly present in the melt, and thus acted as a flux rather than as a mineralizer.

Another calcium silicate fluoride, cuspidine [$Ca_4(Si_2O_7)F_2$] exists but is not formed under conditions relevant to clinker formation. Systems containing fluorosilicate ions [$SiF_6^{2-}$] and the possible use of calcium fluorosilicate as a flux have been investigated (S21).

In the $CaO–Al_2O_3–CaF_2$ system, the compound $C_{11}A_7 \cdot CaF_2$ is described in Section 2.2.3. One other ternary phase, $3CA \cdot CaF_2$, is known; it is hexagonal, with $a = 1{\cdot}729$ nm, $c = 0{\cdot}701$ nm, and refractive indices $\omega = 1{\cdot}628$, $\varepsilon = 1{\cdot}618$ (L7). Several studies on parts of the system have been reported (C5,C7,G24,Z6).

### 2.6.2 Carbonates

Spurrite [$Ca_5(SiO_4)_2(CO_3)$] is readily formed under suitably low partial pressures of $CO_2$; using oxalic acid as a source of $CO_2$, it has been obtained at 430°C (H19). At sufficiently low $CO_2$ pressures or sufficiently high temperatures, it decomposes to give $C_2S$ and CaO. Some other syntheses, and conditions under which it is formed or decomposed in the cement kiln, are mentioned in Sections 3.3.3 and 3.3.5. A pressure–temperature equilbrium curve for the reaction of wollastonite and calcite to give spurrite and $CO_2$ has been reported (H20). The crystal structure is known, and the unit cell is monoclinic, with $a = 1{\cdot}049$ nm, $b = 0{\cdot}6705$ nm, $c = 1{\cdot}416$ nm, $\beta = 101{\cdot}3°$; space group $P2_1/a$, $Z = 4$, $D_x = 3024\,kg\,m^{-3}$ (S22). The refractive indices are: $\alpha = 1{\cdot}638$, $\beta = 1{\cdot}671$, $\gamma = 1{\cdot}676$; $(-)2V = 40°$ (H20). Another calcium silicate carbonate, tilleyite [$Ca_5(Si_2O_7)(CO_3)_2$], occurs as a natural mineral and has been synthesized (H19), but is not known to form during the manufacture of clinker.

## 2.7 Laboratory preparation of high-temperature phases

In general, high-temperature phases are prepared in the laboratory by heating mixtures of appropriate composition at temperatures for which reference to the phase equilibria shows them to be stable. Platinum apparatus is normally required. Compounds having a lower temperature limit of stability (e.g. $C_3S$) may have to be cooled rapidly to a temperature at which they are kinetically stable. Some high-temperature polymorphs can be preserved by quenching, but with others it may be necessary to add a stabilizer. For $\beta$-$C_2S$, $B_2O_3$ (0·1–0·3%) has often been used, but it may be considered preferable to employ a composition closer to that of the material in clinker. As noted in Section 1.3.1, crystals of $\beta$-$C_2S$ below a certain size do not invert to $\gamma$-$C_2S$ on cooling. This makes it possible to prepare $\beta$-$C_2S$ without any stabilizer by first preparing $\gamma$-$C_2S$ and reheating at 1000°C (S23). For the same reason, $\beta$-$C_2S$ is the normal product when hydrated calcium silicates of appropriate composition, including the major hydration product of $C_3S$ or Portland cement, are decomposed at 800–1000°C.

As starting materials for high-temperature preparations, finely ground and well-mixed combinations of crystalline oxides (e.g. quartz) and carbonates (e.g. calcite) have been widely used. Mixtures containing

carbonates must initially be heated at a relatively low temperature (900–1000°C for calcite) to avoid violent decarbonation. Repeated heating and regrinding, followed each time by examination of the product by light microscopy, XRD or other methods, is often necessary to produce an acceptable product. Intermediate products are often formed; for example, in the $CaO–SiO_2$ system, $C_2S$ is formed initially, and reacts only slowly with any excess of calcium oxide or silica to give other phases. Some phases can be obtained by cooling of melts or devitrification of glasses. Particular care and choice of conditions may be needed if, as with the ferrite phase, protected phases or zoned crystals may be formed. More reactive starting materials can sometimes be used; for example, $C_3S$ of 99% purity has been obtained by a single heating of a mixture of freshly precipitated calcium oxalate and hydrous silica (O6). It may also be possible first to prepare a hydrated compound and then to heat it; for example, $C_3A$ can be obtained in this way via $C_3AH_6$.

If material can be lost by volatilization, as with phases containing alkalis, fluoride, or sulfate, it may be necessary to use a sealed platinum container and to test its effectiveness by chemically analysing the product. Control of the furnace atmosphere, e.g. by employing mixtures of CO and $CO_2$ to buffer the oxygen pressure, may be needed if variable oxidation states are possible, as with iron compounds. Special methods may be needed to make single crystals of sufficient size for X-ray structure determinations or other purposes. These are described in papers on X-ray structure determination. Single crystals of $C_3S$ can be obtained from $CaCl_2$ melts (N11).

# 3 The chemistry of Portland cement manufacture

## 3.1 General considerations

### *3.1.1 Summary of the reactions in clinker formation*

In the manufacture of Portland cement clinker, the raw materials, typically a limestone and a clay or shale, are intimately mixed and heated, ultimately to a temperature of about 1450°C. The principal reactions taking place are conveniently divided into three groups, as follows:

(1) Reactions below about 1300°C, of which the most important are (a) the decomposition of calcite (calcining), (*b*) the decomposition of clay minerals, and (*c*) reaction of calcite or lime formed from it with quartz and clay mineral decomposition products to give belite, aluminate and ferrite. Liquid is formed only to a minor extent at this stage, but may have an important effect in promoting the reactions. At the end of this stage, the major phases present are belite, lime, aluminate and ferrite. The last two may not be identical with the corresponding phases in the final product.

(2) Reactions at 1300–1450°C (clinkering). A melt is formed, mainly from the aluminate and ferrite, and by 1450°C some 20–30% of the mix is liquid. Much of the belite and nearly all the lime react in the presence of the melt to give alite. The material nodulizes, to form the clinker.

(3) Reactions during cooling. The liquid crystallizes, giving mainly aluminate and ferrite. Polymorphic transitions of the alite and belite occur.

Figure 3.1 shows these changes for a typical clinker. No attempt has been made to show a detailed sequence of phases below 1300°C, as sufficient data do not exist, and minor phases, including sulfates, are omitted. Quantitative phase compositions at various stages vary considerably with starting materials and other factors.

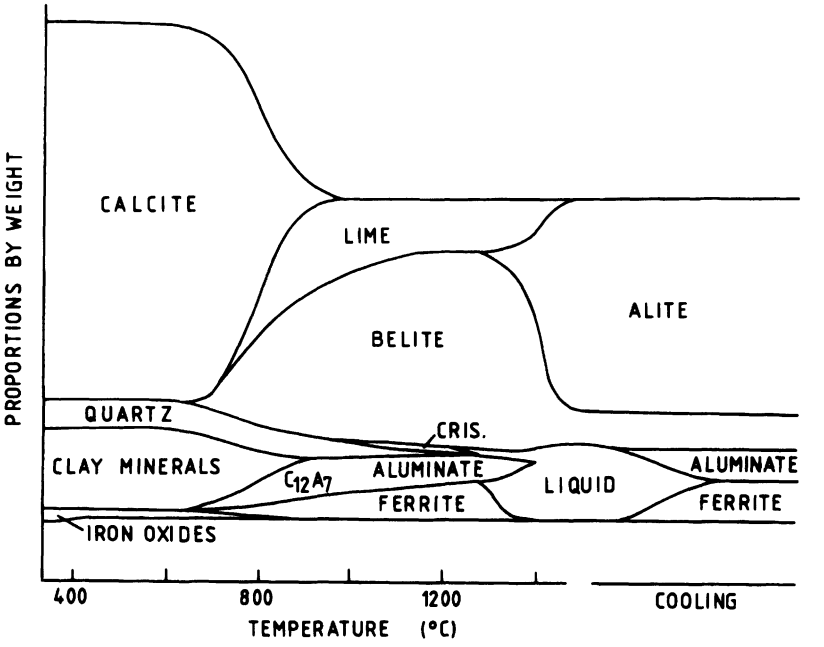


**Fig. 3.1** *Schematic diagram showing the variations in typical contents of phases during the formation of Portland cement clinker, loosely based on a figure by Wolter (W9).*

### *3.1.2 Lime saturation factor, silica ratio and alumina ratio*

Chemical analyses of cements, clinkers and individual phases are commonly expressed in terms of oxide components, but it is often useful to employ quantities derived from these. In the equations that follow, chemical formulae also denote mass percentages. The following parameters are widely used in the UK and elsewhere.

lime saturation factor (LSF)

$$= CaO/(2{\cdot}8SiO_2 + 1{\cdot}2Al_2O_3 + 0{\cdot}65Fe_2O_3) \quad (3.1)$$

$$\text{silica ratio (SR)} = SiO_2/(Al_2O_3 + Fe_2O_3) \quad (3.2)$$

$$\text{alumina ratio (AR)} = Al_2O_3/Fe_2O_3 \quad (3.3)$$

The definition of LSF is theoretically based (Section 2.3.3), and in the form given above applies to clinkers; if corrected by subtracting $0{\cdot}7SO_3$ from CaO, it may be applied to cements. It largely governs the ratio of alite to belite and also shows whether the clinker is likely to contain an unacceptable proportion of free lime, a value of 1·0 or above indicating that the latter will be present at equilibrium at the clinkering temperature and thus liable to persist in the product. In practice, values up to 1·02 may be acceptable; typical values for modern clinkers are 0·92–0·98.

Other parameters similar in function to LSF are used in some countries. A suggested modification to the LSF definition, intended to allow for Mg substitution in alite, replaces CaO by (CaO + 0·75MgO) for MgO ≤ 2%, or by (CaO + 1·5) for MgO > 2% (S24). In the German literature, Kalkstandard II corresponds approximately to LSF and Kalkstandard III to this modification of it.

The SR and AR, also respectively called silica modulus and alumina modulus, are empirically based. For normal types of Portland cement clinker, SR is usually 2·0–3·0, and AR 1·0–4.0, but these ranges do not apply to special types, such as sulfate-resisting or white cement clinkers. The SR governs the proportion of silicate phases in the clinker. Increase in SR lowers the proportion of liquid at any given temperature in the kiln, and thus makes the clinker more difficult to burn. The AR governs the ratio of aluminate to ferrite phases in the clinker, which has important effects on cement properties, and also determines the quantity of liquid formed at relatively low temperatures. At 1338°C, for a given total content of $Al_2O_3$ and $Fe_2O_3$, the quantity of liquid passes through a maximum at an AR of 1·38.

The proportions of raw materials are commonly calculated on the basis of the above parameters, most obviously by setting up and solving simultaneous equations; to fix $n$ parameters, $(n + 1)$ raw materials of appropriate composition are required. It is also necessary to consider the desired or allowable contents of minor components.

### *3.1.3 The Bogue calculation*

In another approach, the quantitative phase composition is estimated using a procedure due to Bogue (B25). The calculation, in the form commonly used in Europe, is as follows.

(1) Assume that the compositions of the four major phases are $C_3S$, $C_2S$, $C_3A$ and $C_4AF$.
(2) Assume that the $Fe_2O_3$ occurs as $C_4AF$
(3) Assume that the remaining $Al_2O_3$ occurs as $C_3A$.
(4) Deduct from the CaO content the amounts attributable to $C_4AF$, $C_3A$ and free lime, and solve two simultaneous equations to obtain the contents of $C_3S$ and $C_2S$.

This leads to the following equations, in which CaO is assumed to have been corrected for free lime:

$$C_3S = 4{\cdot}0710CaO - 7{\cdot}6024SiO_2 - 6{\cdot}7187Al_2O_3 - 1{\cdot}4297Fe_2O_3 \quad (3.4)$$

$$C_2S = -3{\cdot}0710CaO + 8{\cdot}6024SiO_2 + 5{\cdot}0683Al_2O_3 + 1{\cdot}0785Fe_2O_3$$
$$= 2{\cdot}8675SiO_2 - 0{\cdot}7544C_3S \quad (3.5)$$

$$C_3A = 2{\cdot}6504Al_2O_3 - 1{\cdot}6920Fe_2O_3 \quad (3.6)$$

$$C_4AF = 3{\cdot}0432Fe_2O_3 \quad (3.7)$$

As with LSF, the approach is applicable to cements if CaO is further corrected by deducting $0{\cdot}7SO_3$. Because minor oxide components are

ignored, the total for the four main phases plus free lime will not add up to 100%. It is implicit in the approach that all the MgO is assumed to occur as periclase. The phase composition calculated by Bogue's method is related to the LSF in that a ratio of $C_2S$ to $C_3A \leq 0{\cdot}546$, calculated without correcting the CaO content for free lime, corresponds to an LSF $\geq 1{\cdot}0$ (D3).

In a variant of the Bogue calculation used in US specifications (ASTM C-150), free lime is not deducted and $Al_2O_3$ is replaced by $Al_2O_3 + P_2O_5 + TiO_2$. This latter modification typically raises the calculated $C_3A$ content by some 1·1%.

The results of the Bogue calculation are often called potential phase compositions, because when the the procedure was devised, it was generally considered that the principal source of error was failure to reach equilibrium during cooling. The results do indeed differ, often markedly, from the true phase compositions, notably in underestimating alite and overestimating belite (Section 4.5.4), and it is unlikely that equilibrium is maintained during cooling, but the principal direct source of error is that the compositions of the clinker phases differ considerably from those of the pure compounds. In addition to their use in some specifications, Bogue compositions are used for proportioning by setting up and solving equations to calculate the relative amounts of raw materials needed to obtain given 'potential' contents of $C_3S$ or other phases. They have often been misused for other purposes on the assumption that they are close to the actual phase compositions. Spohn *et al.* (S24) have indicated the dangers of such uncritical use.

### *3.1.4 Enthalpy changes in clinker formation*

The enthalpy change on formation of Portland cement clinker cannot be calculated with high precision, mainly because of uncertainties associated with the clay minerals in the raw material. Table 3.1 gives data for the main thermochemical components of the reaction, almost all of which have been calculated from a self-consistent set of standard enthalpies of formation, and which are therefore likely to be more reliable than other values in the literature. The conversion of the clay minerals into oxides is an imaginary reaction, but valid as a component in a Hess's law calculation. Few reliable thermochemical data exist for clay minerals; those for pyrophyllite and kaolinite can probably be used with sufficient accuracy, on a mass basis, for other 2:1 and 1:1 clay minerals, respectively. The data for the pure compounds may similarly be used for the clinker phases. Table 3.2 illustrates the use of these data. The quantitative phase composition of the clinker was estimated from the bulk composition by the method described in Section 4.4. The overall enthalpy change is often calculated approximately from the bulk composition using a formula (Z7), and an experimental method for its determination has been described (C8).

The overall enthalpy change in forming clinker is dominated by the strongly endothermic decomposition of calcite. The component reactions

**Table 3.1** *Standard enthalpies of reaction*

| Reaction | ΔH (kJ) | For 1 kg of |
|---|---|---|
| $CaCO_3$ (calcite) → $CaO + CO_2$ (g) | +1782 | $CaCO_3$ |
| $AS_4H$ (pyrophyllite) → $\alpha$-$Al_2O_3 + 4SiO_2$ (quartz) + $H_2O$ (g) | +224 | $AS_4H$ |
| $AS_2H_2$ (kaolinite) → $\alpha$-$Al_2O_3 + 2SiO_2$ (quartz) + $2H_2O$ (g) | +538 | $AS_2H_2$ |
| $2FeO \cdot OH$ (goethite) → $\alpha$-$Fe_2O_3 + H_2O$ (g) | +254 | $FeO \cdot OH$ |
| $2CaO + SiO_2$ (quartz) → $\beta$-$C_2S$ | −734 | $C_2S$ |
| $3CaO + SiO_2$ (quartz) → $C_3S$ | −495 | $C_3S$ |
| $3CaO + \alpha$-$Al_2O_3 \rightarrow C_3A$ | −27 | $C_3A$ |
| $6CaO + 2\alpha$-$Al_2O_3 + \alpha$-$Fe_2O_3 \rightarrow C_6A_2F$ | −157 | $C_6A_2F$ |
| $4CaO + \alpha$-$Al_2O_3 + \alpha$-$Fe_2O_3 \rightarrow C_4AF$ | −105 | $C_4AF$ |

Values for starting materials and products at 25°C and 0·101 MPa, calculated from the data of Wagman *et al.* (W10), excepting those for the formation of $C_6A_2F$ (N12) and $C_4AF$ (T8). The value for $C_4AF$ is for 20°C.

for the replacement of clay minerals by oxides are endothermic, because the heat required for dehydroxylation exceeds that liberated on forming the products.

The formation of $\beta$-$C_2S$ from lime and quartz is moderately exothermic, but that of $C_3S$ from lime and $\beta$-$C_2S$ is endothermic, with $\Delta H = +59\,kJ\,kg^{-1}$. All these calculations refer to reactants and products at 25°C and 0·1 MPa. The enthalpy changes at the temperatures at which the reactions occur are somewhat different, because the specific heats of reactants and products are not the same. The reaction of lime with $C_2S$ giving $C_3S$ changes from endothermic to exothermic at 1430°C (J4). For the decomposition of calcite at 890°C, ΔH is $+1644\,kJ\,kg^{-1}$ (L6).

**Table 3.2** *Enthalpy of formation of 1 kg of a Portland cement clinker*

| Component of reaction | ΔH (kJ) |
|---|---|
| $CaCO_3 \rightarrow CaO + CO_2$ (g) | +2138 |
| $AS_4H$ (pyrophyllite) → $\alpha$-$Al_2O_3 + 4SiO_2$ (quartz) + $H_2O$ (g) | +34 |
| $AS_2H_2$ (kaolinite) → $\alpha$-$Al_2O_3 + 2SiO_2$ (quartz) + $2H_2O$ (g) | +21 |
| $2FeO \cdot OH$ (goethite) → $\alpha$-$Fe_2O_3 + H_2O$ (g) | +8 |
| $3CaO + SiO_2$ (quartz) → $C_3S$ | −333 |
| $2CaO + SiO_2$ (quartz) → $\beta$-$C_2S$ | −98 |
| $3CaO + \alpha$-$Al_2O_3 \rightarrow C_3A$ | −3 |
| $6CaO + 2\alpha$-$Al_2O_3 + \alpha$-$Fe_2O_3 \rightarrow C_6A_2F$ | −10 |
| *Total* | +1757 |

The contributions to ΔH are calculated assuming the starting materials to be: calcite, 1·20 kg; quartz, 0·10 kg; pyrophyllite, 0·15 kg; kaolinite, 0·04 kg; goethite, 0·03 kg. The products are assumed to be: $C_3S$, 0·673 kg; $\beta$-$C_2S$, 0·133 kg; $C_3A$, 0·118 kg; $C_6A_2F$, 0·064 kg; free CaO, 0·010 kg; total, 1·00 kg.

## 3.2 Raw materials and manufacturing processes

### *3.2.1 Raw materials and fuel*

These, and manufacturing processes, will be considered only to the extent needed for a basic understanding of their chemistry; fuller accounts are given elsewhere (D4,G25,K8,P13).

The raw mix for making Portland cement clinker is generally obtained by blending a calcareous material, typically limestone, with a smaller amount of an argillaceous one, typically clay or shale. It may be necessary to include minor proportions of one or more corrective constituents, such as iron ore, bauxite or sand, to correct the bulk composition. On the other hand, some argillaceous limestones and marls have compositions near to that required, making it possible to use a blend of closely similar strata from the same quarry.

Limestones vary in physical characteristics from compact rocks of low porosity to friable and highly porous ones, such as chalk, which may contain up to 25% of water. All consist essentially of calcium carbonate, normally in the polymorphic form of calcite. Other naturally occurring forms of $CaCO_3$, such as shell deposits, are sometimes used. Many limestones contain significant amounts of minor components, either as substituents in the calcite or in accessory phases, some of which are deleterious if present in amounts exceeding a few per cent (e.g. MgO, SrO), a few tenths of a per cent (e.g. $P_2O_5$, $CaF_2$, alkalis) or even less (some heavy metals).

Suitable shales and clays typically have bulk compositions in the region of 55–60% $SiO_2$, 15–25% $Al_2O_3$ and 5–10% $Fe_2O_3$, with smaller amounts of MgO, alkalis, $H_2O$ and other components. Mineralogically, their main constituents are clay minerals, finely divided quartz and, sometimes, iron oxides. The dominant clay minerals are usually of the illite and kaolinite families, but small amounts of smectites (montmorillonite-type minerals) may also be present. Kaolinite has a 1:1 layer silicate structure and ionic constitution $Al_2(Si_2O_5)(OH)_4$. Illites and smectites have 2:1 layer silicate structures, derived from those of pyrophyllite $[Al_2(Si_2O_5)_2(OH)_2]$ or talc $[Mg_3(Si_2O_5)_2(OH)_2]$ by various ionic substitutions and incorporation of interlayer cations and, in smectites, water molecules. In place of clays or shales, other types of siliceous rocks, such as schists or volcanic rocks of suitable compositions, are sometimes used.

Pulverized coal, oil, natural gas and lignite have all been widely used as fuels, but due to pressing environmental and economic requirements are increasingly being supplemented by waste materials. In 1995, Bannon (B26) reported that fuel usage in Europe was coal, 38%; petroleum coke, 36%; lignite, 8%; fuel-oil, 7%; natural gas, 2%; and various alternative fuels, 9%. Worn-out or reject tyres and many kinds of industrial and municipal wastes are often used. In addition to conserving non-renewable fossil fuels and in some cases lowering $CO_2$ emissions, the use of waste materials as fuels can provide a means of safe and environmentally acceptable disposal. Some waste materials can be used in the raw feed; energy can be saved and $CO_2$ emission decreased if even a part of the CaO can be provided by a material, such as blastfurnace slag, that does

not require decarbonation. Some materials, such as flyash (pulverized fuel ash, pfa) can serve as raw materials that also possess some fuel content. The contribution of the fuel to the clinker composition must be taken into account, especially with coal or lignite, which produce significant quantities of ash broadly similar in composition to the argillaceous component. Some fuels also contribute sulfur.

### 3.2.2 Dry and wet processes; energy requirements

Comminution and mixing of the raw materials may be carried out either dry or wet. The theoretical amount of heat needed to produce 1 kg of clinker from typical raw materials is about 1750 kJ (Section 3.1.4). Additional heat is required because heat is retained in the clinker, kiln dust and exit gases after they leave the system, lost from the plant by radiation or convection, and, in the wet process, used to evaporate water. Table 3.3 compares the heat requirements of the wet process and a modern version of the dry process, in each case assuming typical raw materials and proper plant design and operating conditions. The greater thermal efficiency of the dry process occurs largely because there is no added water to be evaporated. The total energy requirement of a cement works includes also electrical energy used in operating the plant, to which grinding of raw material and of clinker make important contributions. This is higher for the dry process than for the wet process, typical values being 120 kWh and 77 kWh per tonne of cement (432 kJ $kg^{-1}$ and 277 kJ $kg^{-1}$ respectively), including that used for grinding the clinker in each case (D5), but the difference is small compared with that in the amounts of fuel required.

The wet process has certain advantages if the raw materials are already soft and moist, but its low fuel efficiency has rendered it obsolescent, and the following description is of a modern version of the dry process.

### 3.2.3 The dry process; suspension preheaters and precalciners

The raw materials first pass through a series of crushing, stockpiling, milling and blending stages, which yield an intimately mixed and dry raw meal, of which typically 85% passes through a 90 $\mu$m sieve. With automated,

**Table 3.3** *Heat requirement in dry and wet process kilns (kJ/kg of clinker)*

| | Dry | Wet |
|---|---|---|
| Theoretical heat requirement for chemical reactions | 1807 | 1741 |
| Evaporation of water | 13 | 2364 |
| Heat lost in exit gases and dust | 623 | 753 |
| Heat lost in clinker | 88 | 59 |
| Heat lost in air from cooler | 427 | 100 |
| Heat lost by radiation and convection | 348 | 682 |
| *Total* | 3306 | 5699 |

Dry kiln with suspension preheater. Data adapted from Ziegler (Z8).

computer-controlled procedures, the LSF, SR and AR can be maintained constant to standard deviations of 1%, 0·1 and 0·1, respectively.

The raw meal passes through a preheater and frequently also a precalciner before entering a rotary kiln. A preheater is a heat exchanger, usually of a type called a suspension preheater in which the moving powder is dispersed in a stream of hot gas coming from the kiln. Figure 3.2 shows a common arrangement, which employs a series of cyclones. Heat transfer takes place mainly in co-current; the raw material passes through the preheater in less than a minute, and leaves it at a temperature of about 800°C. These conditions are such that about 40% of the calcite is

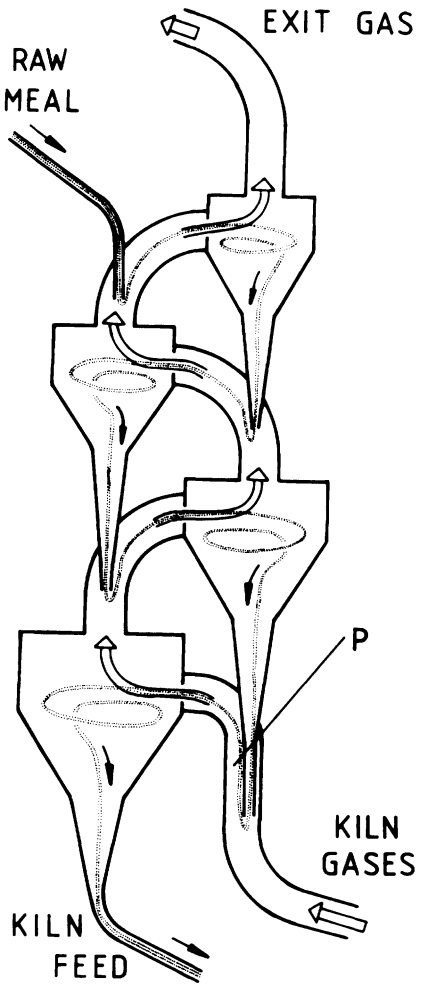


**Fig. 3.2** *Schematic diagram of a four-stage cyclone-type suspension preheater. P indicates the position at which a precalciner burner may be incorporated.*

decarbonated. It is possible to introduce a proportion of the fuel into a preheater, with a corresponding reduction in the quantity fed to the kiln; a precalciner is a furnace chamber introduced into the preheater into which 50–65% of the total amount of fuel is introduced, often with hot air ducted from the cooler. The fuel in a precalciner is burned at a relatively low temperature; heat transfer to the raw meal, which is almost entirely convective, is very efficient. The material has a residence time in the hottest zone of a few seconds and its exit temperature is about 900°C; 90–95% of the calcite is decomposed. Ash from the fuel burned in the precalciner is effectively incorporated into the mix.

Because less heat is supplied to the kiln, precalcination allows the rate at which material can be passed through a kiln of given size to be greatly increased, thus saving on capital cost. Alternatively, the rate of providing heat can be reduced, which lengthens the life of the refractory lining. Less $NO_x$ is formed, since much of the fuel is burnt at a low temperature, and with some designs $NO_x$ formed in the kiln may be reduced to nitrogen. Low-grade fuels can often be used in the precalciner. Precalcination may also make it economically feasible to deal with the problem, discussed in Section 3.2.5, of formation of deposits in the duct carrying the hot gases from the kiln to the preheater.

### 3.2.4 The rotary kiln

The rotary kiln is a tube, sloping at 3–4% from the horizontal and rotating at 1–4 rev/min, into which the material enters at the upper end and then slides, rolls or flows counter to the hot gases produced by a flame at the lower or 'front' end. In a system employing a precalciner, the kiln is typically 50–100 m long and its ratio of length to diameter is 10–15. The maximum material temperature, of about 1450°C, is reached near the front end of the kiln in the 'burning zone', also called the clinkering or sintering zone, in which the material spends 10–15 minutes. The kiln is lined with refractory bricks, of types that vary along its length in accordance with the varying gas and material temperatures. The bricks become coated with a layer of clinker, which plays an essential part in the insulation and in extending their life.

Nodules of clinker, typically 3–20 mm in diameter, are formed in a semi-solid state in the burning zone, and solidify completely on cooling, which begins in a short cooling zone within the kiln, and continues in a cooler. In modern plants, when the nodules leave the kiln, their internal temperatures are around 1350°C, but their surface temperatures are considerably lower.

Liquid or pulverized solid fuels are blown into the kiln through a nozzle with 'primary' air. Additional, 'secondary' air is drawn into the kiln through the clinker cooler. The flame in the rotary kiln must meet several requirements. The clinker must be correctly burned, so as to minimize its content of free lime, with the least expenditure of fuel. The ash from a solid fuel must be uniformly absorbed by the clinker. For normal Portland cements, the conditions must be sufficiently oxidizing that the iron is present in the cooled clinker almost entirely as $Fe^{3+}$;

however, for white cements, mildly reducing conditions may be preferable. Proper flame control also extends the life of the refractory lining of the kiln. Computer-aided or fully automated control of kiln operating conditions is increasingly used.

### 3.2.5 Circulation of volatiles; dust; cooling of clinker

In the hotter parts of the kiln, the K, Na, S, Cl and some other elements provided by the raw material or fuel are partly or wholly volatilized. The fractions that are not pass into the clinker. The volatilized material is swept back with the hot gases to the cooler parts of the system, where, assuming that a suspension preheater or precalciner is used, it is largely reabsorbed, so that cycles are set up. Material that is not reabsorbed may leave the system through the preheater as gas or dust, but some can form solid or semi-solid deposits. Deposits formed in this and other ways can seriously restrict the movement of material and gases; in the kiln, they form rings. They can form in the duct carrying the hot gases from the kiln to the preheater. With some raw materials or fuels, it is necessary to divert part of the gas through a bypass and to filter out the dust that it carries, and to accept the consequent losses of heat and material, but changes in the raw materials or fuel may sometimes be a preferable solution (D6).

Dust from the kiln is largely captured in a suspension preheater; that which is not is removed by an electrostatic precipitator before the gas passes up the chimney. The flow of gas is aided by an exhaust fan. The dust is as far as possible returned to the system by mixing with the raw meal or with the fuel (insufflation), though the extent to which either is possible may be restricted by its content of alkali sulfates or chlorides, which if high could lead to an unduly high recirculating load, conducive to the formation of deposits or undesirably high concentrations in the clinker.

The clinker cooler is essentially a heat exchanger that extracts heat from the clinker for return to the system; also, a cooled clinker is more readily transported, ground or stored. Rapid cooling from the clinkering temperature down to 1100°C produces a better quality clinker (Section 3.5.5), and the clinker should be effectively air-quenched as soon as it leaves the burning zone. When the clinker enters the grinding mill, its temperature should preferably be below 1100°C. Current practice favours grate coolers, in which the clinker passes over moving grates through which air is blown. More air is needed for cooling than for combustion in the kiln, especially with a fuel-efficient process. Some of the excess ('tertiary air') may be ducted to a precalciner or used to dry the coal and raw materials, but a quantity normally remains for which it has proved difficult to find economically viable uses, and which is therefore cleaned and exhausted; steam raising for electicity generation has been suggested as a possible use.

### 3.2.6 Other processes for clinker production; clinker grinding

In the wet process, the raw material is fed as a slurry directly to a rotary kiln, which typically has a length to diameter ratio of about 30 and may

be up to some 200 m long. In surviving wet process kilns, the slurry typically has a water content of 30–35%. A system of chains near the back end assists heat transfer. Cycling of volatiles and of dust is much less pronounced than with preheater systems. In the semi-wet process, some improvement in fuel efficiency is obtained by pressing out part of the water to produce a cake containing somewhat below 20% of water, which can be fed to the kiln directly or through certain types of preheater. In the semi-dry or Lepol process, the raw materials are made into nodules with just over 10% water content, which are fed to a moving grate preheater. The fuel efficiency is lower than that obtainable with a suspension preheater. Combined processes have been brought into operation in various countries for making cement and other materials, such as aluminium, iron or sulfuric acid (G26). While there are problems associated with such processes, the latter may become increasingly important as classical raw materials become scarcer and environmentally acceptable ways of disposing of industrial wastes more difficult.

To produce Portland cement, the clinker is ground together with gypsum. Portland cement clinker has a long storage life, and while it may be ground immediately, there are often good reasons for grinding it intermittently, and not necessarily in the same plant. Compositional and other variations in the clinker can be much reduced by using storage systems in which blending occurs. Natural gypsum, which is generally used, commonly contains significant proportions of such impurities as anhydrite, quartz, calcite and clay minerals. In some countries, by-product gypsums from various industrial processes are used. A proportion of anhydrite may also be added. Some national specifications permit the addition of materials other than calcium sulfate. To make interground composite cements, widely varying proportions of granulated blastfurnace slag, flyash or other materials are added (Chapter 9). Grinding typically requires a power consumption of 35–50 kW h tonne$^{-1}$ (125–180 kJ kg$^{-1}$), almost all of which is converted into heat, and cooling is required.

## 3.3 Reactions below about 1300°C

### *3.3.1 Decomposition of carbonate minerals*

The dissociation pressure of calcite reaches 0·101 kPa (1 atm) at 894°C (S25) and the decarbonation reaction is highly endothermic (Section 3.1.4). The rate of decarbonation becomes significant at 500–600°C if a sufficiently low partial pressure of $CO_2$ is maintained or if the calcite is intimately mixed with materials, such as quartz or clay mineral decomposition products, that react with the calcium oxide. Even in a precalciner such mixing occurs, aided by agglomeration caused by the presence of low-temperature sulfate melts.

In the absence of other substances, dolomite [$CaMg(CO_3)_2$] begins to decompose rapidly in air at about 750°C, giving initially periclase and a carbonate of higher Ca/Mg ratio. The decomposition temperature is much affected by the presence of other substances.

The mechanism and kinetics of calcite decomposition have been much studied. The reaction proceeds by the movement inwards from the surface of an interface, behind which the material is converted into lime, thus producing a highly porous pseudomorph. The interface moves at a constant rate, implying that the rate at any instant is proportional to the area of the interface. In principle, the rate is controlled by the slowest of the following five steps:

(1) transfer of heat to the exterior surface
(2) transfer of heat from the exterior surface to the interface
(3) chemical reaction at the interface
(4) transfer of carbon dioxide to the exterior surface
(5) transfer of carbon dioxide away from the exterior surface.

Hills (H21) showed that, contrary to some earlier opinions, it was not possible to determine which is the rate-controlling step either from the observed relationship between the extent of reaction and the time or from the apparent energy of activation, obtained by applying the Arrhenius equation to the rate constant determined at different temperatures. For large particles and low $CO_2$ pressures, the temperature within the sphere could be as much as 45 K below that of the surrounding gas, indicating that heat transfer controlled the rate. For the conditions existing in a rotary kiln, in which decomposition occurs in a deep, moving mass of material, heat transfer again determines the rate (B27). A rotary kiln is well suited to the later stages of clinker production, but much less so for calcination, which if carried out in it requires some tens of minutes for completion.

Very different conditions exist in a precalciner, where the raw meal is dispersed in hot gas. The reaction still proceeds by the movement of an interface inwards, but the rate is controlled by the chemical reaction and the temperature within the particle is virtually that of the surrounding gas (B28,V2). The rate is much higher than in a rotary kiln, and, as seen in Section 3.2.3, decomposition is normally 90–95% complete within a few seconds.

### *3.3.2 Decomposition of clay minerals and formation of products*

Laboratory experiments in which single substances or mixtures are heated in stationary containers in air provide a starting point for understanding the reactions that occur in manufacturing clinker, though caution is needed in applying the results because of the important differences in conditions.

The behaviour of clay minerals on heating depends on their structure, composition, crystal size and degree of crystallinity. In general, any interlayer or adsorbed water is lost at 100–250°C; dehydroxylation begins at 300–400°C and is rapid by 500–600°C. Clay minerals in which $Al^{3+}$ is the predominant octahedral cation do not form phases of radically different structure as the immediate products of dehydroxylation, but undergo varying degrees of structural modification and disorganization due to the replacement of $2OH^-$ by $O^{2-}$. Kaolinite gives a poorly crystalline product, called metakaolin; with illites, the structural disorganization

is less marked, perhaps because less water has to be lost. Above about 900°C, all begin to give new, crystalline phases, which are typically Al–Si spinel, cristobalite and, above 1100°C, mullite.

Quartz undergoes a minor, rapid and reversible phase transition to $\alpha$-quartz at 573°C. It is unstable relative to tridymite at 867–1470°C, and to cristobalite above 1470°C. These changes are slow in the absence of other materials, but many admixed materials accelerate them, and lead to formation not of tridymite, but of cristobalite at temperatures over about 1000°C.

As noted in Section 3.3.1, the decarbonation of calcite is greatly favoured by intimate mixing with quartz or clay minerals. Under these conditions, much $CO_2$ is lost before any free lime can be detected. The formation of $C_2S$ as an early product is well established, but the situation with the calcium aluminate phases is more complex, no one phase being dominant as an initial product (W11). The aluminate or aluminosilicate phases most often reported as early or intermediate products in laboratory experiments with pure chemicals or raw meals have been CA, $C_{12}A_7$ and, less frequently, gehlenite (C9,C10,D7–D9,I9,L8,L9,R11,W12,W13). $C_3A$ can form by 850°C (C10,L9) but seems usually to be a later product. Ferrite phase forms readily, and is initially of low Al/Fe ratio (D8,R11).

The reactions are notably accelerated by water vapour (C10). In the cement kiln or precalciner agglomeration may influence their course. Glasser (G27,G28) reviewed kinetic studies. The complexity of the mechanisms has not always been recognized, and it is doubtful whether kinetic data suffice to determine them, but electron microscopy and X-ray microanalysis are beginning to provide reliable information (R12).

### *3.3.3 Sampling from cement kilns or preheater outlets*

Several investigators have examined samples from rotary kilns during normal operation. In one such study, Weber (W13) obtained samples, and measured temperatures, mainly using sampling ports in the kiln walls. In all cases, the raw materials were limestone and marl, and the fuel was pulverized coal. CA and $C_{12}A_7$, but not gehlenite, were found as early products. As in the laboratory studies, much calcite decomposed before any free lime was detected. The free lime content passed through a maximum value of up to 17%, referred to the mass of clinker, about 15 m from the front end of the kiln. At this point, the measured temperature was about 1000°C. Laboratory studies (I9) and analyses of kiln input meals from precalciners, described below, show that the maximum content of free lime reached varies greatly with the nature of the raw material.

One may also examine samples from kilns that have been shut down, though uncertainties inevitably exist due to possible phase changes and movement of material during cooling, which is carried out with the kiln still rotating. Moore (M35) reported an XRD study of charge and coating samples taken from numerous points along the lengths of several kilns. Sulfate phases were prominent in both types of sample taken from the cooler parts of the kiln, and comprised anhydrite, $C_4A_3\bar{S}$, $C_5S_2\bar{S}$, calcium langbeinite and hydroxyl-ellestadite ($C_{10}S_3\bar{S}_3H$). KCl was

sometimes found. Spurrite ($C_5S_2\bar{C}$), $\beta$-$C_2S$, $C_{12}A_7$ and ferrite were usually also found before all the calcite had decomposed. Gehlenite was usually found in coating samples at intermediate temperatures, but rarely in the charge; CA was never found. $C_3A$ was a late product. Rarely, ferrite was found as a late product, being replaced earlier by iron-containing spinel, presumably indicating the existence of reducing conditions at the cooler end of the kiln. Moore concluded that sulfates and chlorides were important mineralizers and that both spurrite and $C_4A_3\bar{S}$ played parts in the normal reaction sequence. Later results probably do not exclude this latter conclusion, but both phases can undoubtedly be undesirable artefacts.

Wolter (W14) determined the phase compositions of kiln inlet meals from about 20 plants using cyclone preheaters, usually with precalciners. XRD showed that the decomposition products of the clay minerals were especially reactive, though some reaction of quartz also occurred. Phases detected, and some notable absences, were as follows.

(1) Unreacted phases from the raw meal: calcite, quartz, minor mica and felspars, traces of clay minerals.
(2) Product phases: free lime, periclase, poorly crystalline belite ($\beta$-$C_2S$), ferrite, $C_{12}A_7$ assuming that enough $Al_2O_3$ was present, and often spurrite. Gehlenite was possibly present but, if so, was minor compared with belite. Less basic silicates and aluminates (e.g. CA, $CA_2$) were absent.
(3) Condensed volatiles: arcanite ($K_2SO_4$), sylvine (KCl), aphthitalite (rare), NaCl (exceptionally), anhydrite (for high $SO_3$/alkali ratios, and then less than expected). Absences included thenardite, calcium langbeinite, alkali carbonates, $C_4A_3\bar{S}$ and $C_5S_2\bar{S}$.
(4) Clinker dust and coal ash: alite, flyash (rare).
(5) Secondary products formed on storage or treatment: calcium hydroxide, hemihydrate.

The quantitative composition varied widely, depending on the degree of calcination, heterogeneity of the raw meal, and whether kiln dust or volatiles were recirculated. $C_{12}A_7$ and ferrite formed easily. At high degrees of calcination, virtually all the $Al_2O_3$ and $Fe_2O_3$ had reacted, 10–60% of the total $SiO_2$ content was present as belite or spurrite and the content of free lime was 5–40%. The proportion of the CaO released from the calcite that was combined in other phases was high at low degrees of calcination, and decreased as the latter proceeded; at 40–70% calcination, it was 30–75%, or in rare cases over 90%.

### 3.3.4 Reaction mechanisms

The mechanisms of the reactions in cement raw meals (C9,C11,I9) and lime-silica composites (W15) have been studied using light and electron microscopy, XRD, high-temperature XRD and high-temperature light microscopy, EPMA and thermal analysis, and free lime determinations. Below about 1200°C reactions occur largely in the solid state, the first

visible effect in cement raw meals being the appearance of reaction rims around the larger quartz grains, which later become replaced by clusters of belite crystals. Chromý (C9) found that the rims comprised zones of cristobalite, isotropic material of refractive index 1·515–1·525 and (furthest out) belite. By 1200°C, the belite layer was up to 2–3 $\mu$m thick, and the isotropic material, which formed a thicker layer, was tending to break through, to form necks linking adjacent quartz grains. The isotropic material contained Ca and Si, and had Ca/Si < 1·0; it gave a diffuse XRD peak at 0·37 nm and was probably a glass. XRD and optical evidence also showed the presence of wollastonite and a little tridymite; in samples cooled from 1280°C, both were detectable optically, as needles dispersed in the amorphous material and as crystals on the border of the latter with the quartz, respectively. The wollastonite had presumably formed from $\alpha$-CS on cooling.

At 1200–1300°C, high-temperature light microscopy showed movement of the silica cores and CS crystals; the amorphous material was softening. Where the belite shell had burst, clusters of belite crystals with a central pore usually replaced the original quartz grain, but where it had not, these clusters only formed at a higher temperature and were more compact, with very little interstitial material.

Maki *et al.* (M36) studied the formation of belite clusters at 1400°C. Layers of belite and liquid formed within the quartz grains and grew out from them, so that the products of neighbouring grains coalesced. Three kinds of belite crystal, differing in origin, texture and composition, were distinguished in the clusters.

Rapid increase in temperature is desirable at temperatures below those at which substantial liquid formation occurs (B29,C9,C11,G28,S26,W9). Most of the belite, and almost all of the other product phases, subsequently either melt or react in the presence of the melt, and there is no merit in promoting crystal growth or removal of imperfections, which would impede these processes. Slow heating may also allow the decomposition products of the clay minerals to transform into less reactive phases. It can also lead to the formation of microstructures unfavourable to the later reactions; Chromý (C9) found that it allowed the belite shells around the silica particles to thicken, producing composites slow to react with lime. In contrast, rapid heating increases movement of the liquid phase, when this forms, and thus improves the mixing of the calcareous and siliceous constituents (C11).

### *3.3.5 Condensation or reaction of volatiles*

Bucchi (B30) reviewed the cycling of volatiles in kilns and preheaters. Condensation or reaction of species from the gas stream takes place below about 1300°C. The sulfate and chloride phases produced were noted in Section 3.3.3. Some of the material thus deposited is liquid, even at quite low temperatures: melting in the $Na_2SO_4$–$K_2SO_4$–$CaSO_4$–KCl system begins below 700°C (R10). These low-temperature melts have both good and bad effects. Deposition on the feed can promote reactions, as noted earlier. Deposition in the preheater or kiln can cause serious

obstructions, and condensation of volatiles is responsible for the formation of kiln rings and deposits in preheaters at temperatures below 1300°C (A5,B30,C12,S27,S28). Dust particles become coated with films of liquid condensate which cause them to adhere to obstacles or cooler surfaces. The temperature within a coating or deposit gradually falls as more material is deposited; this allows the formation of compounds within the body of the coating that differ from those present on the hot face.

Spurrite, if formed, reinforces deposits by producing a mass of interlocking crystals; $C_4A_3\bar{S}$ and $C_5S_2\bar{S}$ behave similarly. The kiln atmosphere is high in $CO_2$, and spurrite is readily formed on heating either clinker (A5) or raw meal (S27) in $CO_2$ at 750–900°C. It decomposes by 950°C (A5). In $SO_2$, either raw meal or clinker gives anhydrite at 550–1150°C, and silicosulfate at 1050–1150°C; in mixed gases, the reactions with $SO_2$ are favoured over those with $CO_2$, and if $K_2O$ is present in the solid, calcium langbeinite is formed at 600–900°C (A5). Formation of spurrite appears to be favoured by presence of $K_2O$ or chlorides and inhibited by phosphates (S27), which are, however, undesirable constituents of clinker. Fluoride also appears to favour formation of spurrite and silicosulfate.

Fluorides and compounds of Zn, Cd, Tl and Pb also undergo cycling and can be deposited in preheaters (K9). Emission of the toxic heavy metals must be avoided. Fluoride phases that have been reported in deposits include $KCa_{12}(SO_4)_2(SiO_4)_4O_2F$ (F10) and an apatite phase of composition $K_3Ca_2(SO_4)_3F$ (T9,P14).

## 3.4 Reactions at 1300–1450°C

### *3.4.1 Quantity of liquid formed*

The processes described in this section occur in the presence of substantial proportions of liquid. They comprise:

(1) melting of the ferrite and aluminate phases, and some of the belite
(2) nodulization
(3) reaction of the free lime, unreacted silica and some of the belite, to give alite
(4) polymorphic change of belite to the $\alpha$ form
(5) recrystallization and crystal growth of alite and belite
(6) evaporation of volatiles.

At the clinkering temperature, the principal phases present at equilibrium are alite, belite and liquid. For the pure $CaO–C_2S–C_3A–C_4AF$ system, this phase assemblage will, except at high $Al_2O_3/Fe_2O_3$ ratios, be reached by 1400°C (Section 2.3.3). Following Lea and Parker (L5), the quantity of liquid formed in a mix of given composition at this temperature may be calculated as follows.

(1) All the $Fe_2O_3$ is present in the liquid; hence the percentage of liquid is $100 \times Fe_2O_3/(Fe_2O_3)_l$, where $Fe_2O_3$ and $(Fe_2O_3)_l$ are the percentages of that component in the mix and in the liquid, respectively.

(2) The composition of the liquid is governed only by the $Al_2O_3/Fe_2O_3$ ratio of the mix, being represented by the point on the $C_3S$–$C_2S$ surface where the 1400°C isotherm is intersected by a plane corresponding to the value of that ratio. The intersection of the 1400°C isotherm with the $C_3S$–$C_2S$ surface runs near and approximately parallel to the boundaries between that surface and the $C_3A$ and $C_4AF$ surfaces. Table 3.4 gives liquid compositions for four values of the $Al_2O_3/Fe_2O_3$ ratio.

(3) The $Al_2O_3/Fe_2O_3$ ratios and $Fe_2O_3$ contents in these compositions are related by the empirical equation

$$Al_2O_3/Fe_2O_3 = -0{\cdot}746 + 33{\cdot}9/(Fe_2O_3)_l \qquad (3.8)$$

which may be rearranged to give

$$Fe_2O_3/(Fe_2O_3)_l = (Al_2O_3 + 0{\cdot}746Fe_2O_3)/33{\cdot}9 \qquad (3.9)$$

whence the percentage of liquid in the mix is $2{\cdot}95Al_2O_3 + 2{\cdot}20Fe_2O_3$.

(4) Lea and Parker (L5) corrected for the contributions to the liquid of MgO and alkalis. Assuming that the solubility of MgO in the liquid is 5–6%, and that the percentage of liquid is about 30%, the contribution from MgO was assumed to be the MgO content of the mix or 2%, whichever was smaller. The liquid was assumed to contain all the $K_2O$ and $Na_2O$.

Similar calculations were made for other temperatures. At lower temperatures, the relationship differs according to whether the $Al_2O_3/Fe_2O_3$ ratio is above or below 1·38, the value for the $C_3S$–$C_2S$–$C_3A$–$C_4AF$ invariant point. Formulae for the percentage of liquid for various combinations of temperature and $Al_2O_3/Fe_2O_3$ ratio are:

1450°C $\quad 3{\cdot}00Al_2O_3 + 2{\cdot}25Fe_2O_3 + MgO^* + K_2O + Na_2O$

1400°C $\quad 2{\cdot}95Al_2O_3 + 2{\cdot}20Fe_2O_3 + MgO^* + K_2O + Na_2O$

1338°C ($Al_2O_3/Fe_2O_3 \geq 1{\cdot}38$) $\quad 6{\cdot}10Fe_2O_3 + MgO^* + K_2O + Na_2O$

1338°C ($Al_2O_3/Fe_2O_3 \leq 1{\cdot}38$) $\quad 8{\cdot}20Al_2O_3 - 5{\cdot}22Fe_2O_3 + MgO^* + K_2O + Na_2O$

**Table 3.4** *Compositions of liquids in equilibrium with $C_3S$ and $C_2S$ in the $CaO$–$Al_2O_3$–$Fe_2O_3$–$SiO_2$ system at 1400°C*

| Mass ratio $Al_2O_3/Fe_2O_3$ | Mass percentage | | | |
|---|---|---|---|---|
| | CaO | $Al_2O_3$ | $Fe_2O_3$ | $SiO_2$ |
| 6·06 | 56·6 | 30·3 | 5·0 | 8·0 |
| 2·62 | 56·4 | 26·2 | 10·0 | 7·4 |
| 0·94 | 55·1 | 18·8 | 20·0 | 6·1 |
| 0·64 | 53·9 | 15·3 | 24·0 | 6·8 |

From Lea and Parker (L5), with corrections supplied by F.M. Lea and noted by Bogue (B31).

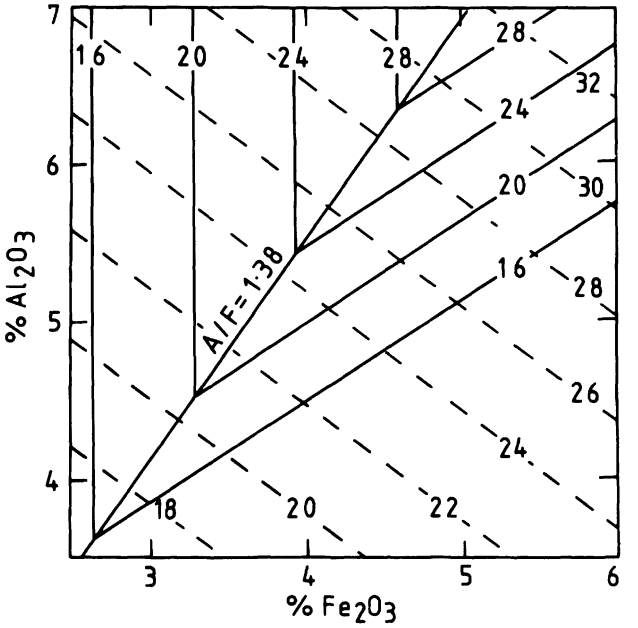


**Fig. 3.3** *Mass percentages of liquid at 1338°C (full lines) and 1400°C (broken lines) in the $CaO–Al_2O_3–Fe_2O_3–SiO_2$ system (B32).*

where MgO* denotes an upper limit of 2·0% to the term for MgO. Typical percentages of liquid (for a mix with 5·5% $Al_2O_3$, 3·5% $Fe_2O_3$, 1·5% MgO and 1·0% $K_2O$) are thus 24% at 1340°C, 26% at 1400°C and 27% at 1450°C.

Such results, omitting the contributions of MgO and alkalis, are conveniently represented as contours on plots of $Al_2O_3$ against $Fe_2O_3$ (Fig. 3.3). At 1400°C, the effects of the two oxides on the quantity of liquid are additive and fairly similar mass for mass. At 1338°C the effects are not additive, the maximum amount of liquid for a given total content of $Al_2O_3$ and $Fe_2O_3$ being obtained at an $Al_2O_3/Fe_2O_3$ ratio of 1·38.

The effects of the minor components on the quantity of liquid formed have not been thoroughly studied. Swayze's results (S14) indicate that the MgO depresses liquidus temperatures by about 50 K and increases the $Al_2O_3/Fe_2O_3$ ratio in the liquid at the $C_3S–C_2S–C_3A–C_4AF$ eutectic to 1·63. Alkalis and sulfate may depress the liquidus temperatures further, but the effects of liquid immiscibility must be taken into consideration.

### *3.4.2 Burnabilities of raw mixes*

The 'burnability' of a mix denotes the ease with which free lime can be reduced to an acceptable value in the kiln. For laboratory use, it has usually been defined either by the quantity of free lime present after a specified regime of heat treatment, or by the time of such treatment needed to reduce the free lime content to some specified value, though

some investigators have used dynamic heating or other regimes in attempts to simulate kiln conditions more closely. As Bucchi (B29) and Sprung (S26) have noted, none of the measures so far proposed has more than comparative significance, as they do not take into account such factors as the atmosphere, movement of material or rate of heat transfer in the kiln. The rate at which the free lime reacts depends not only on characteristics of the raw mix, but also on the effects on the latter of the heat treatment received before entering the clinkering zone and the conditions existing in that zone itself. The measures can strictly be justified only for a given kiln and set of operating conditions.

Many studies have shown that burnability decreases with increasing LSF or increasing SR. Increase in LSF implies more CaO that has to react, and increase in SR implies less liquid at a given temperature. These relationships have been discussed quantitatively (C13). The AR is relevant at low clinkering temperatures, because it then greatly affects the quantity of liquid (Section 3.4.1) and the temperature at which substantial formation of liquid begins, but at 1400°C and above its effect is smaller; however, in the extreme case of white cements, the AR is very high and burnability is low. The temperature at which melting begins is also affected by the contents of minor components, such as MgO, and by the addition of fluxes. Burnability is affected not only by the quantity of liquid, but also by its physical properties, some of which are considered in Section 3.6.

Burnability is affected by the particle size of the raw mix, and especially by the contents of coarse particles (C14,H22,L9). During calcination, large particles of calcite and of siliceous materials are converted into aggregates of lime crystals and clusters of belite crystals respectively. The size distributions of these large particles determine the time required during the last stages of clinkering, when the free lime content is falling to its final value. The fine end of any distribution likely to occur in practice is less important. For assessing burnability at 1400°C, the proportions of calcite particles larger than 125 $\mu$m, and of quartz particles larger than 44 $\mu$m, are particularly important (C14).

Burnability also depends on the nature, microstructures and intimacy of mixing of the raw materials and on the contents of minor components. Silica present as quartz is less reactive than that present in clay minerals, and a limestone high in silica or silicate minerals is likely to be more reactive than one that is nearly pure calcite. Inadequate mixing of the particles of the different constituent rocks present in the raw mix has effects broadly similar to those of too high a proportion of coarse particles. Petersen and Johansen (P15) discussed the mixing of particles from a statistical viewpoint.

Several workers have obtained expressions relating burnability to compositional and other parameters (C13–C15,F11,L9). Fundal (F11), defining burnability ($C_{1400}$) by the percentage of free lime remaining after 30 min at 1400°C, found that

$$C_{1400} = 0{\cdot}33(\mathrm{LSF} + 5{\cdot}1\mathrm{SR} - 107) + 0{\cdot}93S_{44} + 0{\cdot}56C_{125} + 0{\cdot}2A_q \quad (3.10)$$

where SR denotes silica ratio, $S_{44}$ and $C_{125}$ are the percentages of siliceous particles above 44 $\mu$m and of calcareous particles above 125 $\mu$m respectively, and $A_q$ is the percentage of acid-insoluble material, assumed to be quartz. This relation was considered to hold for LSF values of 88–100% and silica ratios of 2–6.

### 3.4.3 Nodulization

Nodule formation occurs through the sticking together of solid particles by liquid. Petersen (P16,P17) showed that the nodules grow partly by coalescence and partly by accretion, and developed a theory to predict the size distribution. Timashev (T1) regarded the process as one in which an initially relatively open assemblage of solid particles was compacted through the action of the liquid, initially by rearrangement of particles, and increasingly later by dissolution and crystallization processes. Nodulization requires an adequate proportion of liquid, and is favoured by low viscosity and high surface tension of the liquid and by small particle size of the solid (T1,P17). If there is not enough liquid, the outer parts of the nodules become enriched in silicates, some of which form dust (P15). Overburning can have a similar effect (L10). If the friable skin of large alite crystals remains on leaving the kiln, the clinker has a sparkling appearance. Much is abraded in the kiln, to form a dust that can cause rings or other deposits to form. It can also reaggregate to form porous, alite-rich lumps, which can incorporate small clinker nodules.

Nodulization, chemical reactions and evaporation of volatiles are interdependent. Alite formation and loss of volatiles affect nodulization, and the compaction that the latter entails must affect the kinetics of the former processes. Alite formation thus occurs in a changing environment. Initially, the clinker liquid is not a continuous and uniform medium enveloping the grains of lime, belite and other solid phases; rather, it fills separate pores and capillaries, forming thin films on the particles, and there are large local variations in composition (T1). As compaction proceeds, it becomes more continuous and more uniform.

### 3.4.4 Formation and recrystallization of alite

In the study described in Section 3.3.4, Chromý (C9) showed that a melt of low Ca/Si ratio began to form at 1200–1300°C around the original quartz grains, which were being converted into clusters of belite crystals. From 1300°C, a liquid also began to form around the grains of lime. It differed in reflectance from that surrounding the silica or belite crystals and was considered to be of higher Ca/Si ratio. Where it bordered on the belite clusters, alite was precipitated, initially as a compact layer. This later recrystallized, allowing the liquids to mix. Alite now formed more rapidly; the belite clusters contracted, and the crystals that remained recrystallized.

In further studies, Chromý and co-workers (C11,C15,C16) distinguished three stages in the reaction at clinkering temperatures. In the first, melt and belite are formed. In the second, belite continues to form; this stage yields a material consisting of isolated clusters of lime crystals

having thin layers of alite on their surfaces and dispersed in a matrix of belite crystals and liquid. In the third, the clusters of lime react with the surrounding belite to give alite, by a mechanism based on diffusion of CaO through the liquid. The temperature increases rapidly during the first stage, but the subsequent stages are isothermal.

Several workers have discussed the kinetics of the clinker-forming reactions (B33,C11,C15,C16,G28,J5,T1). Because the material is not uniform, different factors may dominate at different times and in different regions (T1) but the principal one appears to be diffusion of $Ca^{2+}$ through the liquid present between the alite crystals in the layers coating the lime clusters (C16).

From the standpoint of 28-day strength, the optimum size of the alite crystals appears to be about 15 $\mu$m, larger crystals containing fewer defects and thus being less reactive (L10). Ono (O7) considered that cannibalistic growth of alite crystals was unimportant, and that the size depended essentially on the rate of heating to the clinkering temperature; if this was low, the alite formed at relatively low temperatures as large crystals, and if it was high, it formed at higher temperatures as smaller crystals. This view has been only partially accepted by other workers, Hofmänner (H23), Long (L10) and Maki and co-workers (M5,M37,M38) all having found that alite crystals grow larger through recrystallization with increase in either time or temperature in the clinkering zone, and even (H23) during cooling. The rate of heating to the clinkering temperature is thus only one factor affecting alite size. In practice, few production clinkers contain alite with an average size as low as 15 $\mu$m.

Long (L10) noted that alite size is indirectly affected by both bulk composition and fineness of the raw feed. Increases in LSF, SR or AR all make a clinker harder to burn, which tends to increase the size, though with increased SR or AR the effect is counteracted by decreases in the quantity and mobility of the liquid, both of which tend to decrease the size. The presence of coarse particles, especially of silica, also demands harder burning and tends to increase the size. Coarse silica particles lead to increased alite size both for this reason and because they yield large, dense clusters of belite crystals, which on subsequent reaction with lime give large crystals of alite.

### 3.4.5 *Evaporation of volatiles; polymorphic transitions*

Miller (M39) summarized factors affecting the evaporation of volatile species in the burning zone. Much of the alkali and $SO_3$ is often present as sulfate melts. Alkali sulfates volatilize slowly because of their low vapour pressures, because diffusion within the clinker nodules is slow, and because the nodules do not spend all their time on the surface of the clinker bed. Evaporation is favoured by increased residence time or temperature, decreased size or increased porosity of the clinker nodules. Low partial oxygen pressure also favours evaporation through decomposition to give $SO_2$, $O_2$ and alkali oxides. Chloride favours it through formation of the much more volatile alkali halides. A high partial pressure of $H_2O$ favours it through formation and volatilization of alkali

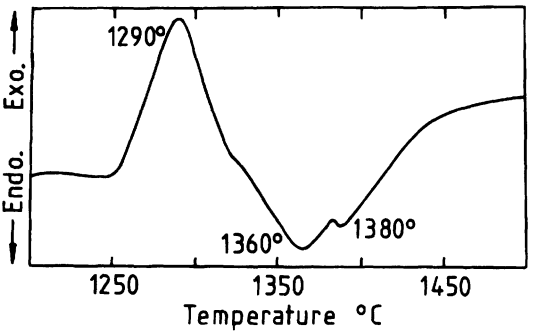


**Fig. 3.4** *DTA curve for a white cement clinker raw mix, obtained in air at 20 K min$^{-1}$. From C9.*

hydroxides. $SO_3$ present as anhydrite is more easily lost, because decomposition to $SO_2$ and $O_2$ occurs, and this is also true of sulfur present in the fuel as $FeS_2$ or organic compounds. Alkali present in the silicate or aluminate phases also appears to be more easily lost than that present as sulfates.

Alite may be expected to form in clinkers as the R polymorph, and belite as $\alpha'_L$, $\alpha'_H$ or $\alpha$, according to the temperature. Chromý (C9) and Hofmänner (H23) discussed DTA curves of raw meals (Fig. 3.4). The main exotherm is due to belite formation, and the main endotherm to melting. A small superimposed endotherm near 1380°C was attributed to the $\alpha'_H \rightarrow \alpha$ transition of the belite, at a temperature lowered by solid solution (C9). Curves for different raw meals show considerable variations.

### *3.4.6 Effects of reducing conditions; colour of clinker*

A cement kiln is normally operated with what is commonly described as an oxidizing atmosphere, but this term has purely relative significance and the equilibria in the burning zone are such that a significant fraction of the iron is present as $Fe^{2+}$. This is almost completely converted into $Fe^{3+}$ during cooling. Localized reducing conditions can, however, occur in the burning zone from such causes as deficiency of oxygen in the kiln gas, presence of reducing material in the raw feed, or entrapment of solid particles from the fuel. This can have major effects on the constitution of the clinker (C17,L11–L13,S7,S29,S30,W16). Decomposition of the alite is promoted, and more aluminate phase is formed at the expense of ferrite. Metallic iron, sulfides (CaS and $KFeS_2$) and wüstite can be produced. Some of the $Fe^{2+}$ that is formed replaces $Ca^{2+}$ in the solid phases; the Fe/Al ratio of the alite increases. For normal cements, the effects on properties are undesirable; strength development is impaired and setting time can be more difficult to control. For white cements, which contain very little Fe, reducing conditions may be preferred because they yield a whiter product. Locher (L12) concluded that the bad effects of reducing conditions were avoided so long as the clinker left the kiln at a temperature of at least 1250°C and thereafter cooled rapidly in air; however,

reoxidation of $Fe^{2+}$ in alite below 1300°C has been observed to cause the formation of exsolution lamellae consisting of $C_2F$ and belite (L11).

Portland cement clinker is normally almost black. The colour arises from the ferrite (Section 1.5.4). It has often been supposed that a brown or yellow colour is a sign of reducing conditions in the kiln, but this is not correct. The colour is determined by the extent of oxidation of the ferrite phase during cooling, and thus on the regime of time, temperature and oxygen supply at this stage (G29,J6,L12,L13,S6,S29). Especially in the centres of large nodules, it is possible to have a normal phase assemblage but a light colour. On the other hand, it is possible to have a highly reduced clinker in which oxidation of the ferrite during cooling has been sufficient to produce a dark colour (S7). Light colours can also arise from underburning.

## 3.5 Reactions during cooling, grinding or storage

### *3.5.1 Solidification of the clinker liquid: indications from pure systems*

In principle, the clinker liquid can behave in any of three ways during cooling, with intermediate possibilities. In the first, equilibrium between the liquid and the pre-existing solid phases (alite and belite) is continuously maintained. This implies the possibility of material transfer between these solids and the liquid in either direction for as long as any liquid remains. This situation will be called 'equilibrium crystallization'. In the second, the liquid does not crystallize but forms a glass. In the third, the liquid crystallizes independently, i.e. without interacting with the solid phases already present. Intermediate modes include, for example, equilibrium crystallization down to a certain temperature and independent crystallization below it.

Lea and Parker (L5) found that, in the pure $CaO–Al_2O_3–Fe_2O_3–SiO_2$ system, the compositions of the liquids in equilibrium with $C_3S$ and $C_2S$ at 1400°C lie within the $C_3S–C_2S–C_3A–C_4AF$ subsystem if the AR is between 0·7 and 1·7; for these compositions, equilibrium crystallization and independent crystallization lead to identical quantitative phase compositions. If the AR exceeds 1·7, the liquid composition is deficient in CaO relative to the above sub-system; this results in formation of a little $C_{12}A_7$ at the expense of $C_3A$ if crystallization is independent, and in reaction with some of the alite to form belite if it is not. Conversely, for an AR below 0·7, the liquid composition has a surplus of CaO relative to the $C_3S–C_2S–C_3A–C_4AF$ subsystem, resulting in formation of a little free lime if crystallization is independent and in reaction with some of the belite to form alite if it is not. Equations were derived for calculating the quantitative phase composition for various cooling conditions (B31,D3,L5).

### *3.5.2 Do Portland cement clinkers contain glass or $C_{12}A_7$?*

The applicability of these conclusions to production clinkers requires examination. The compositions of the aluminate and ferrite phases differ markedly from $C_3A$ and $C_4AF$ respectively (Chapter 1) and, because of

the presence of minor components, especially MgO, $TiO_2$ and alkalis, the compositions of the liquid phase differ from those in the pure system. We shall consider, in turn, first whether glass is formed, and if so, under what conditions; second, whether either $C_{12}A_7$ or free lime crystallizes from the liquid phase under appropriate conditions; and third, whether there is evidence of either equilibrium or independent cooling.

The early literature contains many references to the presence in production clinkers of glass, often in substantial proportions. This view was based partly on observations by light microscopy; however, this method cannot distinguish glass from crystalline solids of the cubic system unless crystals with distinct faces have been formed, nor from crystalline materials of any kind if the crystals are below a certain size. It was also found that if clinkers believed to contain glass were annealed, their heats of solution in an acid medium increased, and this method was used to obtain approximate estimates of the glass content (L14). This evidence, too, is inconclusive, because the same effect would arise from the presence of small or structurally imperfect crystals.

Quantitative XRD, SEM or X-ray microanalysis does not support the view that modern clinkers contain significant quantities of glass, except in rare cases. Regourd and Guinier (R1) found that a few clinkers gave a strong, diffuse XRD peak at 30–35° $2\theta$ (CuK$\alpha$), indicating the presence of glass or other amorphous material, but concluded that the amount of glassy or microcrystalline phase did not exceed a few per cent. An SEM and X-ray microanalytical study showed that white cement clinkers contained glass if quenched in water, but not if cooled in air (B4). A laboratory study on the cooling of simulated clinker liquids showed that glass, amorphous to X-rays, is formed on quenching small samples in water (B10). Somewhat slower cooling, from 1300 to 700°C in a few seconds, gave 'proto-$C_3A$', a poorly crystalline, iron-rich form of that phase; still slower cooling (1300–1100°C in 6 min) gave normally crystalline aluminate and ferrite phases. Material probably identical with proto-$C_3A$ was earlier obtained as a non-equilibrium quench growth (L14), and appears to form easily. The viscosity of the clinker liquid is near the lower limit for glass formation (B10). These observations suggest that glass may occur in clinkers that have been quenched in water, but is unlikely to be found with slower methods of cooling.

Neither XRD nor electron or light microscopy indicates that $C_{12}A_7$ is present in any modern clinkers, and when free lime is found, microscopic examination does not suggest that it has formed by precipitation from the liquid.

If clinkers of relatively high AR are cooled slowly, the effect of equilibrium cooling is detectable by light microscopy (L11). The alite crystals are eroded, and a layer of belite forms on their surfaces; 'pinhead' crystals of belite separate from the liquid. At AR values $> 2{\cdot}5$, slow cooling can cause a reduction of up to 10% in the concrete strength, attributable to the lowered content of alite. These effects are not observed at the moderately fast cooling rates more usual in practice. This evidence suggests that under normal conditions crystallization approximates to

independent, and that slower cooling is needed to achieve equilibrium crystallization. Production clinkers thus behave differently from mixes in the pure, quaternary system, which at AR > 1·7 give $C_{12}A_7$ on independent crystallization.

### 3.5.3 Evidence from X-ray microanalysis

X-ray microanalyses by many investigators (Chapter 1) also provide no indication that $C_{12}A_7$ occurs in normal clinkers. Ghose's (G4) results are of particular interest because he did not attempt to distinguish between the individual phases within the interstitial material, of which he thus obtained bulk analyses. Taken in conjunction with the results of other investigations in which individual phases were analysed, they are consistent with the hypothesis that for AR values between about 1 and 4 the interstitial material consists of aluminate and ferrite phases having the compositions given in Table 1.2, together with 4–10% of belite, the amount of which increases with AR. For lower AR values, the interstitial material consists essentially of ferrite of higher iron contents, and in white cements it consists of aluminate very low in iron, possibly together with glass. In each case, small amounts of silicate phases are probably also present.

The reason why mixes with AR > 1·7 do not yield any $C_{12}A_7$ on independent crystallization is that the solid phases are not pure $C_3A$, $C_4AF$ and $C_2S$. For AR = 2·71, the quaternary liquid in equilibrium with $C_3S$, $C_2S$ and $C_3A$ at 1400°C contains 55·7% CaO, 27·1% $Al_2O_3$, 10·0% $Fe_2O_3$ and 7.2% $SiO_2$ (S12). This composition can be closely matched by a mixture of aluminate (63%), ferrite (30%) and belite (7%), each having the compositions given in Table 1.2, the bulk composition of this mixture being 54·4% CaO, 26·4% $Al_2O_3$, 9·7% $Fe_2O_3$, 5·6% $SiO_2$ and 1·8% MgO, with <1% each of $TiO_2$, $Mn_2O_3$, $Na_2O$ and $K_2O$. Independent crystallization can thus yield a mixture of the three phases. The liquid composition cannot be matched by a mixture of pure $C_3A$, $C_4AF$ and $C_2S$, which is relatively too high in CaO, so that if no ionic substitutions occurred, some $C_{12}A_7$ would also be formed. A strict comparison would be with the actual composition of the clinker liquid, which is modified by minor components, but lack of adequate data precludes this.

### 3.5.4 Effects of cooling rate on the aluminate and ferrite phases

It follows from the above discussion that the compositions of the aluminate and ferrite phases in typical clinkers are controlled by the composition of the clinker liquid and the conditions under which the latter crystallizes. For clinkers with AR 1–4, their compositions are relatively constant because both phases are present, and because cooling rates are normally moderately fast. The compositions must nevertheless depend to some extent on the composition of the raw mix, especially in regard to minor components. The observation that resorption of alite occurs on slow cooling implies that their compositions, or their relative amounts, or both, depend on the cooling rate. They could also be affected by the clinkering temperature, and the time during which it is maintained. XRD

(B34,I4,O2) and microanalytical (I4) evidence shows that their compositions are affected by the cooling rate. IR evidence indicates the occurrence of structural and compositional variations in both phases dependent on cooling rate (V3).

The conditions of crystallization affect the ferrite and aluminate in ways other than in their mean compositions. Slow cooling produces relatively large crystals of each phase, while fast cooling produces close intergrowths; textures are discussed further in Section 4.2.1. Zoning occurs readily in the ferrite (Section 2.3.1), and may also occur in the aluminate. The distribution of atoms between octahedral and tetrahedral sites in the ferrite depends on the temperature at which internal equilibrium within the crystal has been achieved (Section 1.5.1). The degree of crystallinity of both phases appears to vary with cooling rate (V3). All these effects, and perhaps others, may affect the behaviour of the interstitial material on hydration.

### 3.5.5 *Other effects of cooling rate*

The behaviour of MgO in clinker formation depends markedly on the cooling rate (L11). If a clinker is burned at a high temperature (>1500°C), relatively high contents of MgO can enter the liquid, and on rapid cooling, much of it remains in the aluminate and ferrite phases and only a small quantity of periclase separates as small crystals. On slow cooling from high temperatures, only around 1·5% of MgO (referred to the clinker) is taken into solid solution, the excess forming large periclase crystals. At temperatures below 1450°C, the MgO is less readily taken into solution, and clusters of periclase crystals can remain; the crystals grow with time and even with temperature in this range.

The polymorphic transitions of the alite and belite that occur during cooling are discussed in Chapter 1. The belite of normal clinkers contains sufficient proportions of substituent ions to prevent dusting to give the $\gamma$ form; the mechanical constraint provided by the surrounding material may also contribute. The cooling rate affects the way in which the belite transitions occur, with effects recognisable microscopically (O2). Cooling rate is also reported to affect alite crystal size, rapid cooling giving smaller crystals, which are more easily ground (S31).

If a clinker is cooled too slowly in the region from 1250°C to about 1100°C, the alite begins to decompose. An intimate mixture of belite and lime forms as pseudomorphs after the alite, and the decomposition is especially likely to occur if the clinker has been fired under reducing conditions (L11). Mohan and Glasser (M40) reviewed and extended knowledge of the kinetics of this process. The kinetics follow a sigmoidal curve, in which an initial induction period merges into an acceleratory phase, followed by a deceleratory one as the process nears completion. These results can be explained by assuming that the rate is controlled by nucleation of the products on the surfaces of the $C_3S$ grains; in accordance with this, the reaction is accelerated, and the induction period largely eliminated, if the $C_3S$ is sufficiently intimately mixed with either $C_2S$ or CaO. Some substituent ions affect the rate: $Al^{3+}$ has little

effect, $Fe^{3+}$ markedly accelerates, $Na^{+}$ slightly retards, and $Mg^{2+}$ markedly retards decomposition. Where both $Mg^{2+}$ and $Fe^{3+}$ are present, the accelerating effect of the $Fe^{3+}$ is dominant. The decomposition is also accelerated by water vapour and, very strongly, by contact with sulfate melts; with a $CaSO_4$–$Na_2SO_4$ melt, decomposition was complete in 2 hours at 1025°C.

All the effects described above indicate that rapid cooling is desirable: the aluminate phase reacts more slowly with water when finely grained and intimately mixed with ferrite, making it easier to control the setting rate (S31), decrease in alite content either from reactions involving the interstitial material or from decomposition is avoided, a higher MgO content can be tolerated, and the clinker is easier to grind.

### 3.5.6 *Crystallization of the sulfate phases*

Much of the $SO_3$ is present at the clinkering temperature in a separate liquid phase, immiscible with the main clinker liquid (Section 2.5.2). The alkali cations are distributed between the two liquids and the alite and belite. During cooling, some redistribution of alkali cations and sulfate ions between the liquids may be expected to occur, the sulfate liquid finally solidifying below 900°C. The most usual sulfate phases to form are arcanite ($K_2SO_4$), which can accommodate some $Na_2SO_4$ or $CaSO_4$ or both in solid solution, and aphthitalite ($K_{4-x}N_x\bar{S}_4$, with $x$ probably usually near 1 but possibly sometimes up to 3). Clinkers relatively high in $K_2O$ and $SO_3$ may contain calcium langbeinite ($KC_2\bar{S}_3$), and those high in $SO_3$ (typically above about 2%) may contain anhydrite. Clinkers of unusually high Na/K ratio may contain thenardite (sodium sulfate). Because the sulfate phases are a late product, their crystals are in general to be found between those of the silicate phases, but, in clinkers of high $SO_3$ content, small amounts may also occur as inclusions in those phases.

### 3.5.7 *Quantitative estimation of the distributions of alkalis and $SO_3$ between phases*

Early work, reviewed by Newkirk (N10), indicated that the $SO_3$ combined as alkali sulfates, the excess of alkalis entering the silicate and aluminate phases, but subsequent work has shown that this is correct only for low ratios of $SO_3$ to alkalis. Pollitt and Brown (P2) made a systematic study of the distribution of alkalis and $SO_3$ in a number of works and laboratory-prepared clinkers. Figure 3.5 and the following discussion are based on their conclusions and the tabulated data in their paper. With reservations noted later, the sulfate and alkalis present in alkali sulfates or calcium langbeinite ($KC_2\bar{S}_3$) are rapidly extracted by water, and can thus be distinguished from those substituted in the silicate and aluminate phases or, for $SO_3$, in anhydrite.

The results of such extractions appear to depend significantly on the experimental procedure, and perhaps especially on the length of time during which the sample is in contact with the water. Gartner and Tang (G6) reported results broadly similar to those of Pollitt and Brown for the alkalis, but obtained generally lower results for the fractions of the $SO_3$

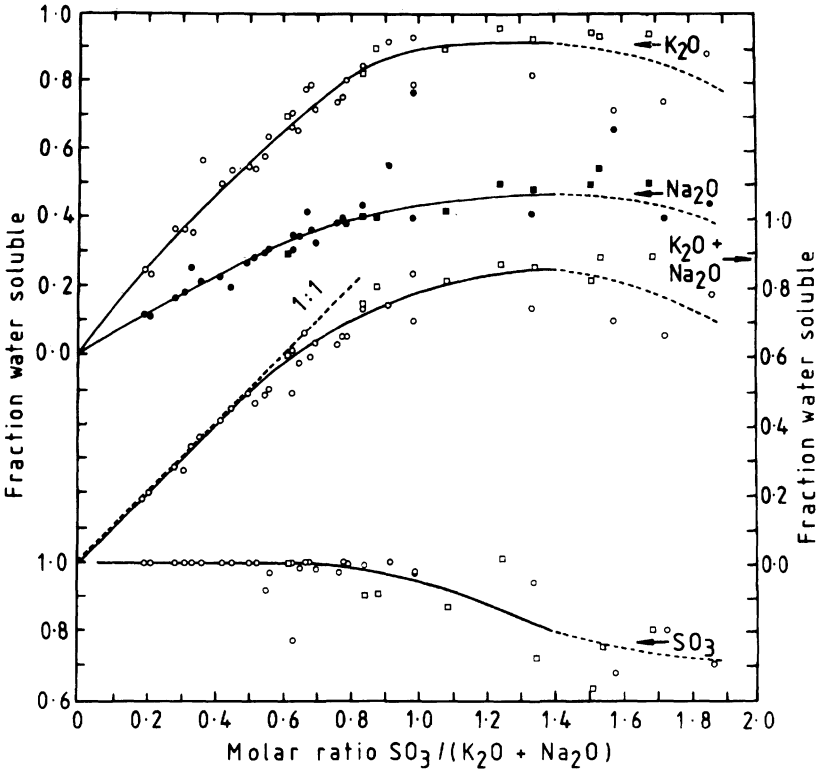


**Fig. 3.5** *Fractions of rapidly water-soluble $K_2O$, $Na_2O$, $K_2O + Na_2O$ (molar) and $SO_3$, plotted against the molar ratio of total $SO_3$ to (total $K_2O$ + total $Na_2O$) for production clinkers (circles) and laboratory clinkers (squares). Recalculated from the data of Pollitt and Brown (P2).*

that were rapidly soluble. This may have been because they used a 10 min treatment, whereas Pollitt and Brown used a method in which the water was drawn through the sample under suction on a filter in a period of 1.5–2.5 min (M41). A longer time may have allowed some sulfate to be precipitated in ettringite. Results of extraction tests do not necessarily have implications regarding the availability of the alkalis or $SO_3$ present in these latter phases during hydration, which occurs under different conditions.

Inspection of Fig. 3.5 indicates the following points.

(1) The fractions of the $SO_3$, $K_2O$ and $Na_2O$ that are rapidly water-soluble will be called $f(SO_3)$, $f(K_2O)$ and $f(Na_2O)$, respectively. They are largely determined by the molar ratio of $SO_3$ to $(K_2O + Na_2O)$ in the clinker, which will be called $R$. $f(K_2O)$ is always close to twice $f(Na_2O)$, showing that $Na^+$ tends more strongly than $K^+$ to enter the silicate or aluminate phases.

(2) For values of $R$ up to about 0·5, $f(K_2O)$ and $f(Na_2O)$ increase with $R$, and $f(SO_3) = 1{\cdot}0$. The rapidly soluble $SO_3$ is exactly balanced by rapidly soluble alkalis, showing that all the $SO_3$ is present as alkali sulfates.

(3) For values of $R$ between about 0·5 and 1·0, $f(SO_3)$ is still usually close to 1.0, but the contents of rapidly soluble alkalis tend to fall below that of the rapidly soluble $SO_3$. This can be attributed to formation of calcium langbeinite ($KC_2\bar{S}_3$). $f(K_2O)$ and $f(Na_2O)$ continue to increase with $R$, and reach limits of about 0·9 and 0·45 respectively at $R \approx 1{\cdot}0$.

(4) With increase in $R$ above about 1·0, $f(K_2O)$ and $f(Na_2O)$ tend to decrease. This might be explained by the presence of small proportions of the alkali sulfates as inclusions within the alite and belite. Alkali sulfates present as inclusions would be less accessible to water than crystals deposited between those of the silicate phases, which probably tend to become broken up and smeared over the surfaces of the cement grains during grinding.

(5) As $R$ increases above about 1·0, and sometimes at lower values, $f(SO_3)$ also shows an irregular decrease. This could be due to inclusion of alkali sulfate phases within the alite or belite, solid solution of sulfate in the major clinker phases, or formation of anhydrite.

Based on these considerations, the probable distribution of alkalis and $SO_3$ in a clinker can be estimated from the bulk analysis. The contents of rapidly soluble $K_2O$, $Na_2O$ and $SO_3$ are first estimated from the smoothed curves in Fig. 3.5. For the great majority of clinkers, they can be explained by assuming that any rapidly soluble $SO_3$ in excess of that equivalent to the rapidly-soluble alkalis is present in calcium langbeinite, the rest of the rapidly soluble $K_2O$ and all the rapidly soluble $Na_2O$ then being assigned to alkali sulfates. The relative amounts of rapidly soluble $K_2O$ and $Na_2O$ give an indication of the distribution within the alkali sulfates between arcanite, aphthitalite and, rarely, thenardite, but this can be of doubtful reliability because of uncertainties about the extents of solid solution in the first two of these phases. With a very few clinkers, there is not enough rapidly soluble $SO_3$ to balance the rapidly soluble alkalis. This has been attributed to the presence of traces of alkali carbonates (P2), or of potassium oxide and potassium aluminate (F7). The reverse situation, in which there is not enough $K_2O$ to allow the sulfate balance to be completed through formation of calcium langbeinite, can also occur. Pollitt and Brown's data show considerable scatter at high $SO_3$/alkali ratios, and the most likely explanation is perhaps that the smoothed curve in Fig. 3.5 does not correctly represent $f(SO_3)$ for the clinkers in question.

The less rapidly soluble alkalis could occur as substituents in the silicate or aluminate phases or in alkali sulfate inclusions in these phases. The less rapidly soluble $SO_3$ could occur in the same forms or as anhydrite. In neither case is it clearly possible to estimate the distributions

between these forms from the bulk analysis alone, though, as noted above, the decreases in $f(K_2O)$ and $f(Na_2O)$ at values of $R$ above about 1·5 suggest that alkali sulfate inclusions are a contributing effect. Tentative calculations based on the magnitudes of these decreases and on the $SO_3$ contents of the silicate phases suggest that, for clinkers relatively high in alkalis and of the commonly high $K_2O/Na_2O$ ratios, anhydrite is unlikely to be formed unless the $SO_3$ content of the clinker is greater than about 2·0%. Limited experimental data appear to be largely consistent with this conclusion (D10,G6,O8,P2).

### *3.5.8 Changes during grinding or storage*

Méric (M42) reviewed the grinding and storage of clinker. Factors influencing the ease with which a clinker can be ground include the size distribution of the nodules, the texture and phase composition, the cooling rate and the conditions under which it has been stored. Grindability increases with alite content and decreases with that of the interstitial phases. Hornain and Regourd (H24) defined a brittleness index, which they showed to have values of 4·7 for alite, 2·9 for aluminate, about 2 for ferrite and 1·8 for belite. They also found that microcracking produced by rapid cooling from 1250°C increased grindability. Some specifications allow the use of grinding aids (Section 11.3.2). The particle size distributions of cements are discussed in Section 4.1.

The heat produced on grinding can cause partial conversion of the gypsum into hemihydrate ($2CaSO_4 \cdot H_2O$) or $\gamma$-$CaSO_4$. The extent to which this occurs depends on the temperature reached and the relative humidity within the mill. The conversions affect the rate at which the calcium sulfate dissolves on hydration. Partial conversion to hemihydrate may be desirable, as the water present in gypsum can cause the particles of cement to adhere during storage, with formation of lumps (L12). To obtain an optimum rate of dissolution on hydration, part of the gypsum may be replaced by anhydrite. Lumpiness on storage can also result from the reaction of gypsum and potassium sulfate to form syngenite ($CK\bar{S}_2H$)(L11). Maultzsch *et al.* (M43) reported on the effects of prolonged storage; minor amounts of gypsum (from hemihydrate), syngenite, calcite and normal hydration products were present.

## 3.6 Effects of minor components

### *3.6.1 General*

Minor or trace components derived from raw materials, fuel, refractories or other plant materials, or added deliberately, can affect the reactions of clinker formation, or the properties of the product, or both. Their effects can be beneficial or harmful. Beneficial effects include acceleration of the clinkering reactions or lowering of the temperature at which they occur, or increase in the reactivity of the product leading to faster strength development. Harmful effects include decrease in alite content, volatilization in the kiln with consequent formation of kiln rings or other deposits, decrease in the durability of concrete made with the cement, or the introduction of poisonous elements. Some elements have beneficial effects

at low concentrations and harmful ones at higher concentrations. Bucchi (B30,B35) reviewed some of the effects on the manufacturing process.

The main clinker liquid can be affected through alteration in the temperature at which it begins to form or in its quantity or properties at a given temperature. A flux is an agent that promotes a reaction by increasing the quantity of liquid at a given temperature; $Al_2O_3$ and $Fe_2O_3$ are fluxes for the formation of alite. Butt, Timashev and co-workers studied the properties of clinker liquids (B33,T1). They found that the viscosity and surface tension of the liquid are markedly affected by relatively small additions of other ions. Species containing strongly electropositive elements increase the viscosity and ones containing strongly electronegative elements decrease it. This was attributed to changes in the distribution of $Al^{3+}$ and $Fe^{3+}$ between octahedral and tetrahedral coordination. The effects of adding more than one minor component are not additive, and can be complex, e.g. alkali sulfates decrease the viscosity, but even a small stoichiometric excess of alkali oxides over $SO_3$ increases it. Many species lower the surface tension, because ions that do not easily fit into the structure of the liquid tend to become concentrated near an interface, but the situation may be complicated by liquid immiscibility. Viscosity has a particularly important effect, a low value favouring alite formation by accelerating dissolution of lime and belite and diffusion through the liquid. Decrease in surface tension may be expected to favour wetting of the solids and penetration of the liquid into porous aggregates of lime crystals.

Effects of minor components on the solid phases are of various kinds. A mineralizer is an agent that promotes the formation of a particular solid phase by affecting the equilibria through incorporation in one or more of the solid phases. $CaF_2$ acts both as a mineralizer and as a flux in promoting the formation of alite. The mechanism of an observed effect is often not clear and, perhaps for this reason, the term 'mineralizer' is often used loosely. Other examples of action of minor components on solid phases include the stabilization of $M_3$ $C_3S$ and $\beta$-$C_2S$ at room temperature, the modification of the aluminate structure resulting from incorporation of alkali, and the non-formation of $C_{12}A_7$ in situations where it would be formed in the pure $CaO$–$Al_2O_3$–$Fe_2O_3$–$SiO_2$ system. Minor components can affect the properties of a clinker phase in other ways, such as by causing changes in crystal size, morphology or structural perfection, and can also modify the microstructure of the clinker as a whole.

The first 11 minor components of raw mixes, in sequence of decreasing median concentration, are MgO, $K_2O$, $SO_3$, $Na_2O$, $TiO_2$, $Mn_2O_3$, $P_2O_5$, SrO, fluorides, chlorides, and $Cr_2O_3$ (B29).

### 3.6.2 Effects of s-block elements

The effects of $K_2O$ and $Na_2O$ in producing low-temperature melts and volatile species have already been discussed. $K_2O$ and $Na_2O$ lower the temperature of formation of the melt but, in the absence of $SO_3$, increase its viscosity. If present in sufficient concentration, they lead to formation of orthorhombic or pseudotetragonal aluminate; this can have undesir-

able effects on the rheology of fresh concrete. High $K_2O$ contents can lead to syngenite formation and consequent lumpiness on storage. High contents of either $K_2O$ or $Na_2O$ can lead to destructive reactions with certain aggregates (Section 12.4). Alkalis increase early strength but often decrease late strength (Section 7.6.3).

MgO also lowers the temperature at which the main melt begins to form and increases the quantity of liquid; it slightly decreases the latter's viscosity (B33,T1). Its presence is probably the basic cause of the non-formation of $C_{12}A_7$ in normally cooled clinkers of high AR. It stabilizes $M_3$ alite (Section 1.2.4). It retards the decomposition of alite during cooling. These effects are beneficial, but the formation of periclase, discussed in Section 3.5.5, limits the permissible content, which most national specifications set at 4–5%.

Some limestones contain substantial proportions of SrO. Small contents favour alite formation, but phase equilibrium studies show that it increases the range of compositions at which free lime, with SrO in solid solution, is present at the clinkering temperature (B36,G30,G31). This limits the permissible content of SrO in mixes of normal LSFs to about 3%.

### 3.6.3 *Effects of p- and d-block elements*

The behaviour of $CaF_2$ as a flux and mineralizer is described in Section 2.6.1. In addition to promoting formation of alite at markedly lower temperatures, $CaF_2$ accelerates the decomposition of calcite. Volatilization does not cause serious problems in the kiln, and it has often been added to raw meals, typically in proportions below 0·5%. It retards setting, possibly through formation of $C_{10}S_4 \cdot CaF_2$ during cooling, and this limits its use. As with admixtures to the raw meal in general, it is also necessary to consider whether the resulting savings outweigh the extra costs. This is most likely to be the case with raw materials that would otherwise require a particularly high burning temperature.

Chloride contents must be kept low to avoid corrosion of steel in reinforced concrete (Section 12.3) and formation of kiln rings and preheater deposits. Contents below 0·02% are preferred, though higher ones can be acceptable if a sufficient proportion of the kiln gases is by-passed or in less energy-efficient (e.g. wet process) plants.

The effects of $SO_3$ include formation of alkali sulfates and other low melting phases and volatile species, discussed earlier in this chapter and in Section 2.5.2. Although much of the $SO_3$ is present in a separate liquid phase, the main melt begins to form at a lower temperature and its viscosity is reduced, rendering $CaSO_4$ an effective flux. Against this, it leads to the stabilization of belite and lime at clinkering temperatures, and consequent decrease in content or even disappearance of alite, though this effect is lessened if MgO is present (G18). Later work showed that high ratios of $SO_3$ to MgO promote the formation of large, irregularly shaped crystals of $M_1$ alite, which can engulf other phases (Section 1.2.4). Sulfate can be removed by increasing the burning temperature, but the inclusions of lime in alite that have formed at lower temperatures are not easily lost (L13).

Portland cement clinkers typically contain around 0·2% of $P_2O_5$; higher contents lead to decreased formation of alite, and if above about 2·5% to presence of free lime. An early conclusion that $\alpha$-$C_2S$ forms a continuous series of solid solutions with a ('super $\alpha$'-) $C_3P$ above 1450°C (N13) was modified by later work, which showed that a miscibility gap exists at 1500°C (G32). Solid solutions also exist between other combinations of $C_2S$ and $C_3P$ polymorphs, lowering the temperatures of the $C_2S$ transitions and, for some compositions, stabilizing $\alpha$ or $\alpha'$ forms at room temperature. In the $CaO–C_2S–C_3P$ system (G32), $C_3S$ has a primary phase field, but at a clinkering temperature of 1500°C, mixes with more than a few per cent of $P_2O_5$ do not yield $C_3S$. The tolerance for $P_2O_5$ is increased somewhat if $F^-$ is also present (G23).

The 3d elements from titanium to zinc all lower the viscosity of the clinker liquid in varying degrees, but their effects on clinker formation and properties present a confusing picture. It has been claimed that the content of alite in clinkers decreases with increase in that of $TiO_2$, but the effect is much less marked if the latter is regarded as replacing $SiO_2$ (B29). Chromium can enter the clinker from raw materials or refractories; cements high in it have been reported to give high early strengths, but toxicity renders their use impracticable. The enhanced early strength is possibly due to high defect concentrations in the alite (B29), in which the chromium occurs as $Cr^{4+}$ (J7). Both manganese and titanium occur in their highest concentrations in the ferrite phase, and probably for this reason yield darker coloured clinkers.

The cycling of zinc, cadmium, thallium, lead, sulfur, fluoride and chloride is noted in Sections 3.2.5, 3.3.5 and 3.4.5.

# 4 Properties of Portland clinker and cement

## 4.1 Macroscopic and surface properties

### *4.1.1 Unground clinker*

This chapter deals with chemical and physical properties other than ones for which the nature of the hydration products must be considered, which are treated in Chapters 5 to 8. In general, properties of the whole clinker or cement are alone considered, those of the constituent phases having been dealt with in Chapter 1, but factors affecting the reactivities of these phases are included as a link with the following chapters on hydration.

Portland cement clinker emerges from a dry process kiln as rounded pellets, or from a wet process kiln as irregularly shaped lumps, in either case typically of 3–20 mm dimensions. The colour, which is normally almost black, is discussed in Section 3.4.6. The bulk density, determined under standard conditions by rejecting material passing a 5 mm sieve, pouring the remainder into a conical container, and weighing, is called the litre weight. This quantity, which is typically 1·25–1·35 $kg\,l^{-1}$, gives some indication of the operating conditions. Its optimum value depends on the composition.

The measured true density of clinker is typically 3150–3200 $kg\,m^{-3}$; the value calculated from the X-ray densities and typical proportions of the individual phases is about 3200 $kg\,m^{-3}$. The difference is probably due mainly to the presence of pores inaccessible to the fluids used in the experimental determination. Using mercury intrusion porosimetry, Butt *et al.* (B37) determined pore size distributions and discussed their relations with burning and cooling conditions and grindability.

### *4.1.2 Particle size distribution of ground clinker or cement*

Allen (A6) discussed methods suitable for determining this important property. Sieving is suitable only for determining the proportions of particles in ranges above about 45 $\mu$m. In airjet sieving, jets speed the passage of material through the sieve and prevent the mesh from becoming blocked. For the entire range of size, the most widely used methods are ones based on either sedimentation in liquids or diffraction of light. In the X-ray sedigraph, the progress of sedimentation is

monitored by the absorption of an X-ray beam and the results calculated using Stokes's law. Because highly concentrated suspensions are used, there is some doubt as to whether this law is strictly applicable. An older method employs the Andreason pipette, by which samples are withdrawn from a suspension at a fixed depth after various times, so that their solid contents may be determined. In laser granulometry, light from a laser passes through a suspension and the particle size distribution (PSD) is calculated from the resulting diffraction pattern. Light microscopy can provide information on the distribution of both particle size and particle shape, and SEM with image analysis (Section 4.3.1) can provide additional information.

With all the methods, complications or uncertainties of interpretation arise due to effects associated with particle shape and with flocculation, so that the results given by different methods do not necessarily agree and usually have relative rather than absolute significance. Figure 4.1, curve R, shows the cumulative PSD, obtained using an X-ray sedigraph, for a typical Portland cement ground in an open-circuit mill (S32). In modern ordinary Portland cements, some 7–9% of the material is typically finer than 2 $\mu$m and 0–4% coarser than 90 $\mu$m.

Méric (M42) discussed analytical expressions used to represent the PSD of cements. Probably the most successful is the Rosin–Rammler function, which may be written in logarithmic form as

$$\ln \ln (100/R) = n(\ln x - \ln x_0) \tag{4.1}$$

where $R$ is the mass percentage of material of particle size greater than $x$. The constants $x_0$ and $n$ describe the distribution; $x_0$ is a measure of

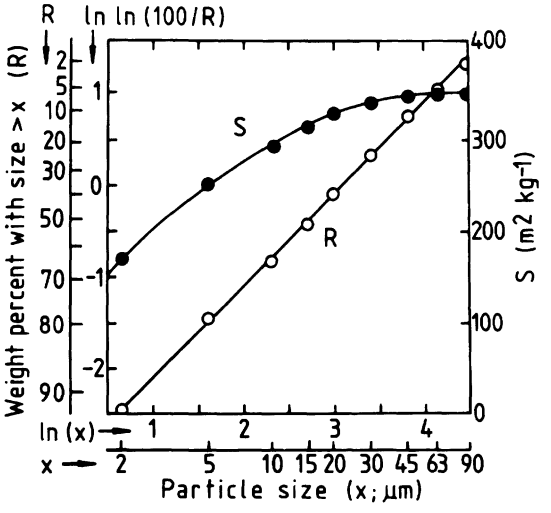


**Fig. 4.1** *Rosin–Rammler plot of the particle size distribution of a typical Portland cement. S = specific surface area attributable to particles of size smaller than x. Open circuit grinding; based on the data of S32.*

average size, 36·79% of the material being of size greater than $x_0$, and $n$ is a measure of breadth of distribution, increasing as the latter becomes narrower. For the example shown in Fig. 4.1, $x_0$ is 22 $\mu$m and n is 1·03. For open-circuit milling, the values of $n$ obtained using an X-ray sedigraph are 0·99–1·07; for closed-circuit milling, in which the fine material is separated and only the coarser material further ground, $n$ can be as high as 1·23–1·28 if the separation is efficient (S32). A narrow PSD can also be obtained using a vertical spindle mill. Laser granulometry typically gives values of $n$ lower by 0.15–0.20 (S32).

### *4.1.3 Specific surface area determination*

The specific surface area of cement is commonly determined directly by air permeability methods. In the Lea and Nurse method (L15), a bed of cement of porosity 0·475 is contained in a cell through which a stream of air is passed, and steady flow established. The specific surface area is calculated from the density of the cement, the porosity and dimensions of the bed of powder, the pressure difference across the bed, and the rate of flow and kinematic viscosity of the air. In the Blaine method (B38), a fixed volume of air passes through the bed at a steadily decreasing rate, which is controlled and measured by the movement of oil in a manometer, the time required being measured. The apparatus is calibrated empirically, most obviously using a cement that has also been examined by the Lea and Nurse method. The two methods gave closely similar results. The Blaine method, though not absolute, is simpler to operate and automated variants of it have been devised.

Other methods that have been used to determine specific surface areas of cements include the Wagner turbidimeter (W17) and BET (Brunauer–Emmett–Teller) gas adsorption. The former, as conventionally used, gives very low results because of a false assumption that the mean diameter of the particles smaller than 7.5 $\mu$m is 3.8 $\mu$m, which is much too high. The BET method gives results two to three times higher than the air permeability methods, because it includes internal surfaces present in microcracks or in pores open at only one end.

The specific surface area, like the PSD, is thus a quantity whose value depends on on how it is defined, and is liable to be affected by any pretreatment or conditions affecting the degree of flocculation. In practice, air permeability methods are widely used. Typical values are 300–350 $m^2\,kg^{-1}$ for modern ordinary Portland cements and 400–450 $m^2\,kg^{-1}$ for rapid-hardening Portland cements.

From a PSD curve, one may calculate the specific surface area, $S$:

$$S = 6 \times 10^6 \times F \times \Sigma f/(d \times \rho) \qquad (4.2)$$

where $f$ is the mass fraction of material consisting of grains assumed to have a diameter or edge length $d$ (in $\mu$m), $\rho$ is the density in $kg\,m^{-3}$, and the result is in $m^2\,kg^{-1}$. $F$ is an empirical constant which takes into account the differing assumptions regarding surface shape that are made implicitly or explicitly in the determination of PSD and the definition of specific surface area. This formula applies to both cubic and spherical

grains. For a calculation starting from a PSD obtained using an X-ray sedigraph to give a specific surface area comparable to that obtained by an air permeability method, $F$ is typically about 1·13. Figure 4.1, curve $S$, shows the contributions to the calculated specific surface area of particles of differing sizes, assuming that particles smaller than 2 $\mu$m have a mean size of 1 $\mu$m. About 40% of the total is provided by particles smaller than 2 $\mu$m.

In principle, the specific surface area may also be calculated from the PSD using analytical expressions derived from such functions as the Rosin–Rammler expression. In practice, this is not always satisfactory because the specific surface area is so highly dependent on the bottom end of the distribution.

### 4.1.4 *Particle size distribution, phase composition and cement properties*

Because the constituent phases of a cement are not equally easy to grind, different particle size fractions differ in composition. Gypsum, and its dehydration products, are concentrated in the finer fractions. Osbaeck and Jøns (O9) concluded that each 1% of gypsum contributed about 10 $m^2 kg^{-1}$ to the specific surface area; in a typical case, some 15% of the total specific surface area is thus due to gypsum. The content of alite decreases, and that of belite increases, with increasing particle size (G33,R13), the contents of aluminate and ferrite phases being little affected.

The depth of reaction of the cement grains after a given time has been determined by light microscopy; it may be expected to vary with the composition and microstructure of the clinker. Anderegg and Hubbell (A7,A8) found values of 0·43–0·47 $\mu$m at 1 day, 1·7–2·6 $\mu$m at 7 days, 3·5–5·4 $\mu$m at 28 days and 6·1–8·9 $\mu$m at 150 days. Zur Strassen (Z9) gave somewhat higher values (e.g. 6–7 $\mu$m at 28 days). From the depth of reaction and the PSD curve, and assuming the grains to be spherical, one may calculate the fraction $\alpha$ of cement that has reacted after a given time:

$$\alpha = \Sigma f \times [1 - (1 - 2h/d)^3] \qquad (4.3)$$

where $h$ is the depth of reaction in $\mu$m, $\Sigma$, $f$ and $d$ have the same meanings as in equation 4.2, and the quantity in square brackets cannot be less than zero. For the cement to which the data in Fig. 4.1 refer, and using the means of Anderegg and Hubbell's values, this gives 0·28 at 1 day, 0·63 at 7 days, 0·80 at 28 days and 0·90 at 150 days. These values are in reasonable agreement with those typically found using XRD (Section 7.3.1). Ritzmann (R13) determined the compressive strengths of pastes of a number of cements of known PSD, made by mixing separated fractions. For a given cement and water/cement (w/c) ratio, the strength was linearly related to the fraction of cement reacted, calculated in this way.

At 1 day, the reaction is primarily of the smaller particles, and the fine end of the PSD is therefore the important one for the strength. As the age increases, the coarser part of the distribution becomes progressivly more important; by 28 days the particles smaller than about 10 $\mu$m have

reacted completely, and the content of particles up to about 45 $\mu$m in size is of major importance. For a given specific surface area, narrowing the PSD increases the degree of reaction at 28 days, and thus also the strength (K10,L16,S32). The relation may be quantified using equation 4.3. Narrowing the PSD also saves energy in grinding (S32), but increases the amount of water needed to produce a mix of given workability (S32,S33); this latter effect can be compensated by adjusting the temperature during milling so as to increase the extent to which the gypsum is dehydrated to hemihydrate or $\gamma$-$CaSO_4$ ('soluble anhydrite') (S32).

### *4.1.5 Chemical analysis*

Ground clinker or cement may be analysed by standard methods, such as X-ray fluorescence (XRF). Determination of free lime is discussed in Section 4.3.3. With XRF or other methods in which no fraction of the material is excluded from the analysis, insoluble residue (determined separately) is included in the oxide components and therefore should be omitted from the total. Classical, wet analysis gives inaccurate results for $Al_2O_3$ unless the effects of $P_2O_5$ and $TiO_2$ are allowed for.

Chemical analysis, microscopy, XRD and other methods of examination should be carried out on the same, representative sample of material. A procedure for obtaining such a sample is described in the next section.

## 4.2 Light microscopy

### *4.2.1 General*

Light microscopy provides much information on clinker microstructure and thereby on the conditions existing at various stages of the manufacturing process. Much the most widely used technique has been the examination of polished and etched sections in reflected light, and the following sections refer to this unless otherwise stated, but additional information has been obtained from the examination of thin sections or powder mounts in transmitted light. Fuller accounts are given elsewhere (C18,G34,H23,L10).

It is vital to obtain a representative sample; the following procedure (L10) is typical. If a kiln is known to give a reasonably consistent product, samples taken at intervals over a suitable period are aggregated, but if not, they are examined separately. Each sample examined comprises at least 15 kg of clinker, and is first examined visually to distinguish kiln deposits or refractories. It is then crushed to below 6 mm and a representative sample obtained, e.g. by quartering. The 2–4 mm fraction of this sample is used. Ten to twelve samples of uncrushed nodules, covering the range of nodule sizes, are also examined, together with a sample of the material smaller than 2 mm, if much of this is present in the original clinker. The relative amounts of nodules of different sizes, and of the material below 2 mm, are noted.

For examination in reflected light, the sample is mounted in a plastic resin and is cut and polished using only non-aqueous lubricants. The most generally useful etchant is probably HF vapour, which has the merit of not removing alkali sulfates; the slide is inverted over a vessel

containing 40% aqueous HF for 10–20 s. Treatment with water followed by 0·25% $HNO_3$ in ethanol and finally ethanol is also widely used, and many other etchants have been employed for specific purposes. The etchants produce thin films of decomposition products, which yield interference colours when viewed in reflected light.

Figure 4.2 shows a polished and etched section of a production clinker. Crystals of alite and belite are embedded in a matrix of aluminate and ferrite phases. If HF vapour is properly used, the alite is yellowish brown, the belite is blue or red, and the aluminate is grey; the ferrite, which is unattacked, is brightly reflective. The alite crystals are angular, often pseudohexagonal; the belite crystals are rounded and normally striated, as described in Section 1.3.2. Ideally, the alite crystals are 15–20 $\mu$m in average size, though in practice they are usually much larger, and there should be no clustering of either alite or belite. The average size of the belite crystals is typically 25–40 $\mu$m.

A good clinker should have been rapidly cooled, and this will cause the ferrite and aluminate phases to be mixed on a scale of a few micrometres, the ferrite often forming dendrites or needles in a matrix of aluminate. In transmitted light, the ferrite is pleochroic. The normal, cubic aluminate tends to fill the spaces between the other phases and thus to exhibit

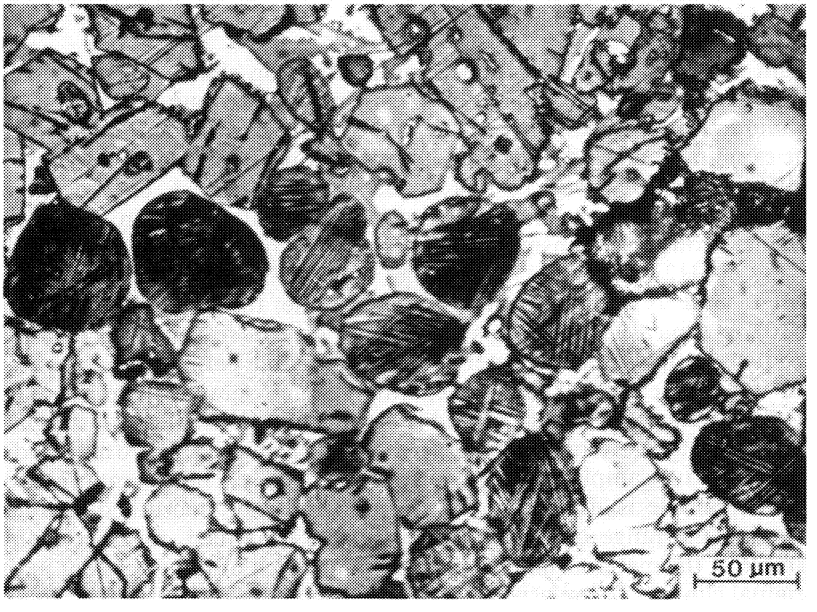


**Fig. 4.2** *Reflected light micrograph of a polished and etched section of a Portland cement clinker, showing crystals of alite (angular) and belite (rounded and striated) embedded in a matrix of interstitial material, itself composed mainly of ferrite (light) and aluminate (dark). Courtesy Materials Science Department, British Cement Association.*

no definite form; it is isotropic in transmitted light. In clinkers with an excess of alkali over $SO_3$, cubic aluminate may be partly or wholly replaced by the orthorhombic variety. This forms relatively large, prismatic crystals, which occur in a matrix of the other interstitial phases and are birefringent in transmitted light.

There should be little free lime. What there is should occur as rounded grains, typically 10–20 $\mu$m in size, and associated with alite and interstitial material. Lime appears cream in sections etched with HF vapour. Its presence may be confirmed by a microchemical test using White's reagent (5 g of phenol in 5 ml of nitrobenzene + 2 drops of water); long, birefringent needles of calcium phenate are formed. The test also responds to CH. Alkali sulfates occur in the clinker pore structure; they are etched black with HF vapour, and inhibit the etching of silicate phases with which they are in contact.

### *4.2.2 Effects of bulk composition, raw feed preparation and ash deposition*

The bulk composition affects the relative amounts of phases, the LSF, SR and AR affecting primarily the ratios of alite to belite, silicate phases to interstitial material and aluminate to ferrite phase, respectively. An LSF that is too high, either absolutely or in relation to the burning conditions, also gives rise to an excessive content of free lime. Belite may occur in such clinkers only as inclusions in alite.

Inadequate grinding of the raw meal is shown by the presence of large clusters of free lime or belite, up to several hundred micrometres in size and with defined outlines reflecting those of the original particles of calcareous or siliceous material respectively. Coarse fragments of dolomitic limestones similarly yield localized concentrations of periclase, usually intimately mixed with lime. Periclase crystals are characteristically angular, up to about 20 $\mu$m in size, and are unattacked by normal etchants. Due to their hardness, they stand out in high relief in unetched sections. Less sharply defined segregation indicates inadequate mixing, and is typically shown by the presence of regions rich in belite and in alite plus lime, in each case together with interstitial material. In extreme cases, entire nodules can depart seriously from the mean composition.

Incomplete assimilation of coal ash is shown by the existence of large regions high in belite, and containing also interstitial phases. The locations of these regions indicate the stage of the burning process during which the ash was deposited; if it was late, the belite-rich material forms coatings on clinker nodules, in which smaller nodules can be encapsulated, whereas if it is deposited earlier, it can form part of the kiln coating, which may later break away and form the centres of nodules. If the ash contains unburnt matter, localized reducing conditions can occur. Insufflation of materials into the kiln can produce similar effects (L10).

### *4.2.3 Effects of burning conditions and cooling rate*

Underburning is shown by the presence of abundant free lime and a low content of alite, the crystals of which are very small (<10 $\mu$m). The

average size and other characteristics of the alite and belite crystals provide much further information about the burning conditions; factors governing them are discussed in Chapters 1 and 3. Ono (O7) considered that alite size was an indication of the rate of heating to the clinkering temperature, which if high led to the formation of smaller crystals, but other studies indicate that many other factors are involved, and that overburning, in particular, can cause increase in size through recrystallization (Section 3.4.4). Another indication of excessively hard burning is the presence of material high in large alite crystals and low in interstitial material, formed by the withdrawal of the liquid into the centres of the clinker nodules (L10).

The effects of slow cooling (Section 3.5) are readily detectable by light microscopy. The most general are coarsening of the texture of the interstitial material and a change in the belite, when viewed in transmitted light, from colourless to yellow. The belite crystals may also develop ragged or serrated edges. Slow cooling can also cause resorption of alite, with deposition of small crystals of belite as fringes on the alite and in the body of the interstitial material, increase in alite crystal size and, if it occurs below 1200°C, decomposition of alite to an intimate mixture of lime and belite. The effects of reducing conditions (Section 3.4.6) are similarly detectable by light microscopy (L11,L13).

### *4.2.4 Applications of light microscopic investigations*

Light microscopy can be used to determine quantitative phase composition in clinkers, though it will often be impossible to determine aluminate and ferrite separately (Section 4.5.2). It has proved a highly effective means of finding the causes of unsatisfactory clinker quality or of determining what modifications in composition or plant operation are needed to change the clinker properties in a desired direction. It has also been used to predict strength development. Ono (O7) described results obtained from examinations of powder mounts. The values of four parameters, indicated in Table 4.1, were each estimated on a scale of 1–4 and the strength $R$, in MPa, of a mortar at 28 days then predicted using the regression equation:

$$R = 24{\cdot}8 + 0{\cdot}63\text{AS} + 2{\cdot}15\text{AB} + 0{\cdot}39\text{BS} + 2{\cdot}10\text{BC} \qquad (4.4)$$

The four parameters AS, AB, BS and BC were considered to be measures of heating rate, maximum temperature, time at that temperature and

**Table 4.1** *Parameters of Ono's method (O7) for predicting cement strength*

| | | | | |
|---|---|---|---|---|
| AS (alite size, $\mu$m) | 15–20 | 20–30 | 30–40 | 40–60 |
| AB (alite birefringence) | 0·008–0·010 | 0·006–0·007 | 0·005–0·006 | 0·002–0·005 |
| BS (belite size, $\mu$m) | 25–40 | 20–25 | 15–20 | 5–10 |
| BC (belite colour) | Clear | Faint yellow | Yellow | Amber |
| Hydraulic activity | Excellent | Good | Average | Poor |
| Value of parameter | 4 | 3 | 2 | 1 |

cooling rate, respectively. As noted in the preceding section, the first of these assignments is questionable, but this does not necessarily invalidate the results obtained by the method, which was tested by routine application in many plants of a major cement company over a long period. Some of the other workers using the method have, in contrast, had little success with it (e.g. S34), and the generality of the procedure, or of the coefficients, remains to be established. The constant term in the equation probably subsumes terms relating to composition and cement fineness, which would have to be taken into account if a wider range of samples was considered.

## 4.3 Scanning electron microscopy, X-ray diffraction and other techniques

### *4.3.1 Scanning electron microscopy*

Backscattered electron imaging of polished sections of clinkers in the scanning electron microscope (SEM) provides information essentially similar to that given by light microscopy, with two important additions (S35–S37). First, phases can be analysed chemically. Second, the image can be stored electronically and subsequently processed or analysed in various ways. The method can be used to study ground cements as well as clinkers by dispersing the cement in a resin, which is then allowed to harden. The residual, unhydrated cement grains in a hardened cement paste can also be examined.

In all cases, the polished section is coated with an electrically conducting layer, normally 30 nm of carbon, but not etched. A backscatter detector is used that maximizes contrast from compositional differences and minimizes that from topography. Provision for X-ray microanalysis is highly desirable and should include facilities both for obtaining X-ray images giving semi-quantitative information on the spacial distributions of individual elements ('dot maps'), and for obtaining complete and quantitative chemical analyses in regions of micrometre dimensions. Techniques are described in standard texts (e.g. G35), and the results of analyses of individual clinker phases are considered in Chapter 1.

Figure 4.3 shows backscattered electron images of a typical clinker and of a polymineralic cement grain present in a fresh paste. Cement grains larger than 2–3 $\mu$m are nearly always polymineralic (S37). Phases can, in general, be distinguished by their grey levels. The intensity of the electrons backscattered from a particular region of a specimen depends approximately on the mean atomic number of the material of which that region is composed; more precisely, it is represented by the backscattering coefficient $\eta$, which may be calculated from the formulae:

$$\eta = \Sigma C_i \eta_i \tag{4.5}$$

$$\eta_i = -0{\cdot}0254 + 0{\cdot}016 Z_i - 1{\cdot}86 \times 10^{-4} Z_i^2 + 8{\cdot}3 \times 10^{-7} Z_i^3 \tag{4.6}$$

where the summation is over elements and $C_i$ is the mass fraction of an element having atomic number $Z_i$ (G35). This equation assumes the accelerating voltage to be 20 kV. Assuming the typical compositions

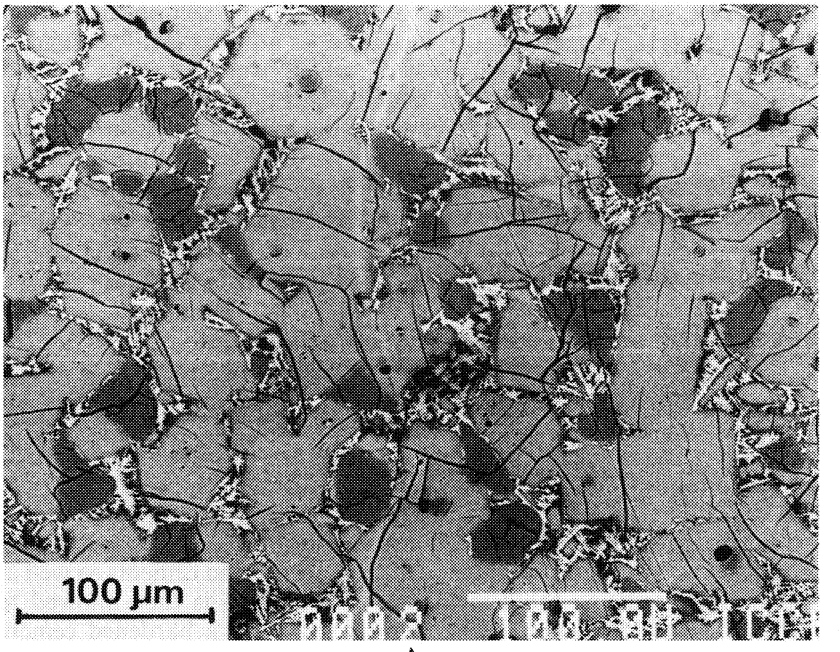


A

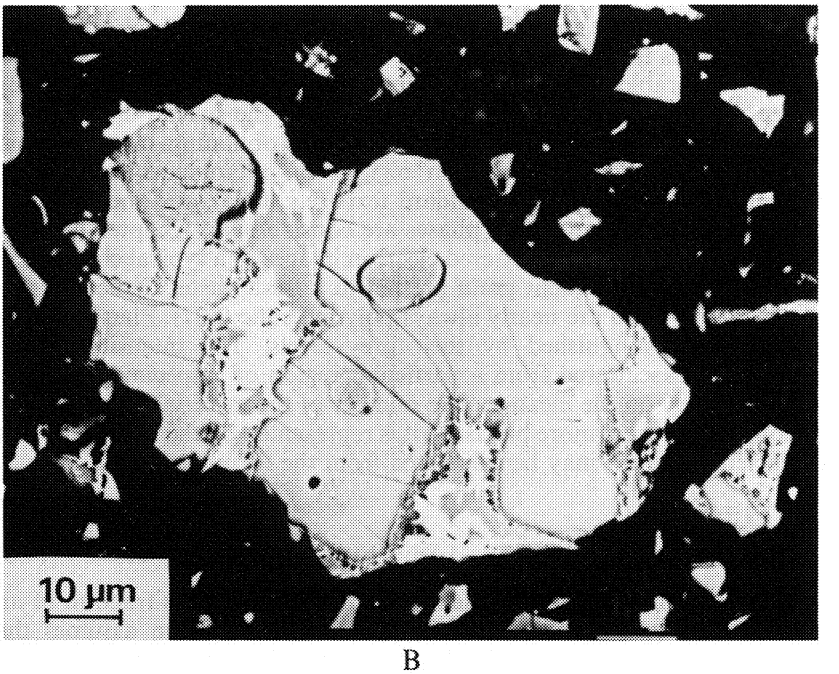


B

given in Table 1.2 for the individual phases, this gives values of 0·171 for alite, 0·167 for belite, 0·168 for cubic aluminate and 0·178 for ferrite. The differences between these values are such that the grey levels of the alite, belite and ferrite phases on micrographs are distinguishable to the eye, but those of belite and aluminate are not; however, the phase boundaries are normally visible, presumably due to slight topographical contrast or compositional irregularity. The resolution available is limited by the size of the region from which the backscattered electrons are produced, which is somewhat below 1 $\mu$m in each direction. Much higher resolution is obtainable using the secondary electron image, but this depends mainly on topographical contrast and thus gives, at best, poor definition of the phases. The resolution given by the X-ray image is poorer than that given by the backscattered electron image.

Image analysis makes it possible to quantify images produced by the SEM (D11,L17,S36–S39). It provides a means of quantitative phase determination and can also provide information on such matters as the distributions of shape, size and surroundings of particles and of phases and pores within them or the relative amounts of each of the phases exposed on the surfaces of polymineralic particles. It is, of course, essential to examine a sufficient number of samples and fields to ensure that the results are representative, but the labour and subjectivity associated with light microscopic studies of a comparable nature are largely eliminated.

Scrivener (S36) showed that it was possible to determine the total contents of silicate phases and interstitial material by image analysis of a combination of backscattered electron image and X-ray dot maps. She also showed that the proportions of interstitial phases exposed on the surfaces of the grains were significantly greater than those by volume in the bulk material. Overall, fracture during grinding appeared to be predominantly through alite, and to avoid phase boundaries. Subsequent developments in image-analysis systems have made it possible to determine the individual clinker phases quantitatively (D11,S38,S39).

### *4.3.2 X-ray diffraction*

The potential uses of XRD powder diffraction in the study of clinker or anhydrous cement include the qualitative and quantitative (QXDA) determination of phase composition, and the determination of polymorphic modification, state of crystallinity and other features of individual phases. In principle, information on compositions of phases is obtainable

**Fig. 4.3** *Backscattered electron images of polished sections of (A) a Portland cement clinker and (B) grains of a Portland cement in a fresh paste. In both sections, alite is the predominant clinker phase. In (A), the relatively large, darker areas are of belite and the interstitial material consists of dendritic ferrite (light) in a matrix of aluminate (dark); cracks and pores (black) are also visible. In (B), the belite forms well-defined regions, which are rounded, striated and darker than the alite; the interstitial material present, for example, in a vertical band left of centre within the large grain, consists mainly of ferrite (light) and aluminate (dark). From S35.*

**Table 4.2** *XRD powder pattern of a typical Portland cement (T5)*

| $2\theta°$ | $d$(nm) | $I_{pk}$ | Main phases | $2\theta°$ | $d$(nm) | $I_{pk}$ | Main phases |
|---|---|---|---|---|---|---|---|
| 11·7 | 0·756 | 5 | Gyp | 34·4 | 0·2607 | 83 | Ali, Bel |
| 12·1 | 0·731 | 6 | Fer | 36·7 | 0·2449 | 6 | Ali |
| 14·9 | 0·595 | 6 | Ali | 37·4 | 0·2404 | 2 | Bel |
| 20·7 | 0·429 | 7 | Gyp | 38·8 | 0·2321 | 12 | Ali |
| 21·9 | 0·406 | 2 | Alu | 39·5 | 0·2281 | 5 | Bel |
| 23·0 | 0·3867 | 7 | Ali | 41·3 | 0·2186 | 41 | Ali, Bel |
| 23·4 | 0·3802 | 3 | Bel | 41·6 | 0·2171 | 16 | Ali, Bel |
| 24·4 | 0·3648 | 3 | Fer | 44·1 | 0·2053 | 6 | Fer |
| 25·3 | 0·3520 | 4 | Ali | 44·5 | 0·2036 | 3(B) | Bel |
| 26·4 | 0·3376 | 2 | Bel | 44·7 | 0·2027 | 2 | Bel |
| 27·6 | 0·3232 | 2 | Bel, Ali | 45·8 | 0·1981 | 10 | Ali, Bel |
| 28·1 | 0·3175 | 4 | Ali, Bel | 47·0 | 0·1933 | 11 | Ali |
| 29·1 | 0·3069 | 5 | Gyp | 47·4 | 0·1918 | 8(B) | Fer |
| 29·4 | 0·3038 | 60 | Ali | 47·8 | 0·1903 | 7 | Alu |
| 30·1 | 0·2969 | 19 | Ali | 49·9 | 0·1828 | 5 | Ali, Fer |
| 31·1 | 0·2876 | 4 | Bel, Gyp | 51·7 | 0·1768 | 33 | Ali |
| 32·2 | 0·2780 | 100 | Ali, Bel, Fer | 51·8 | 0·1765 | 35 | Ali |
| 32·6 | 0·2747 | 85 | Ali, Bel | 56·0 | 0·1642 | 2 | Ali |
| 33·2 | 0·2698 | 40 | Alu, Ali | 56·6 | 0·1626 | 18 | Ali, Bel |
| 33·9 | 0·2644 | 23 | Fer | 58·7 | 0·1573 | 3 | Bel, Fer |
| | | | | 59·4 | 0·1555 | 3 | Alu |
| | | | | 59·9 | 0·1544 | 6 | Ali |

$CuK_\alpha$ radiation; $I_{pk}$ = relative peak height (B = broad); phases are given in decreasing order of their contributions to each peak, ones making only minor contributions being omitted. Ali = alite, Bel = belite, Alu = aluminate, Fer = ferrite, Gyp = gypsum.

through cell parameters, but due to the complexity of the problem and lack of adequate reference data, XRD is generally less satisfactory for the clinker phases than X-ray microanalysis. Table 4.2 gives the pattern of a typical Portland cement, with indications of the assignments of peaks to phases. Quantitative determination of phases is discussed in Section 4.5.3.

### *4.3.3 Chemical or physical methods for separation of phases*

Partial separations of the clinker phases can be effected by chemical extraction methods, which may be combined with XRD to identify and determine minor constituents. Of several reagents that have been used to dissolve the silicate phases, the most succesful has been a solution of salicylic acid in methanol (SAM), introduced by Takashima (T10). This reagent dissolves free lime, alite and belite, at rates decreasing in that order (H25). By adjusting its composition, it is possible either to remove much of the alite, so facilitating investigation of the belite, or all of the alite and belite, facilitating that of the remaining phases. The procedure is as follows (H25).

The clinker is ground in propan-2-ol to an average particle size of 5 $\mu$m. After evaporating off the propan-2-ol, the sample (5 g) is treated for 2 h at room temperature with the SAM reagent (300 ml), with constant stirring. The solution, which is now red, is filtered on a No. 4 sintered glass filter, and the residue washed with methanol and dried at 90°C. If the residue is to be examined by QXDA, the internal standard (e.g. rutile) may be mixed with the sample before the extraction. For removal of alite and belite, the salicylic acid content of the reagent is 20 g per 300 ml. For complete removal of the alite, leaving the maximum quantity of belite undissolved, it is 10–15 g, depending on the alite content; five times the mass of $C_3S$ in the sample, as given by the Bogue calculation, was found to be satisfactory.

A solution of maleic acid in methanol has also been used to dissolve the silicate phases (T11). This is quicker than the SAM method, but if the methanol contains water, ettringite may be formed and water-soluble phases, such as $K_2SO_4$, lost, while if it is anhydrous, gelling occurs; the SAM method is thus preferable (S40). Extraction of the silicate phases by the trimethylsilylation method of Tamás *et al.* (T12; Section 5.5.2) also leaves a residue containing the aluminate and ferrite phases.

Gutteridge (G36) found that a solution of sucrose in aqueous potassium hydroxide (KOSH reagent) dissolves the aluminate and ferrite, leaving the silicates and minor phases. The clinker or cement (10 g) is reduced to below 5 $\mu$m by grinding in cyclohexane (20 ml) for 40 min in an agate ball mill. After evaporating off the cyclohexane in a stream of $N_2$, the sample (9 g) is added to the KOSH solution (30 g of KOH and 30 g of sucrose in 300 ml of water) at 95°C and stirred for 1 min. The solution is then filtered and the residue washed in water (50 ml) followed by methanol (100 ml) and dried at 60°C. By using a combination of the SAM and KOSH procedures, it is possible to produce a residue consisting largely of belite.

Various solvents may be used to dissolve free lime, which can be determined by titrating the resulting solution with a suitable acid. In one procedure (J8), the clinker or cement (1·0 g), ground to about 300 $m^2\,kg^{-1}$ (Blaine), is treated with anhydrous ethylene glycol (50 ml) at 80–100°C for 5 min, using a magnetic stirrer. The solution is then filtered under suction and the residue washed at least twice with a further 10–15 ml of hot ethylene glycol. The filtrate and washings are diluted with 25 ml of water and titrated to phenolphthalein with 0·05M HCl. Other procedures employ mixtures of ethanol and glycerol (L18) or of acetoacetic ester and butan-2-ol (Franke solvent; F12). If properly used, all give similar results. They also dissolve CH, and have been used to determine this phase in hydrated cements, but their use for this purpose is questionable as they also appear to attack other hydration products.

Physical methods are of limited effectiveness for separating the phases in cement clinker because of the intimate scale on which the latter are mixed; however, Yamaguchi and Takagi (Y1) had some success with the use of dense liquids. Some concentration of the ferrite phase can be effected by magnetic separation (M44,Y1).

### 4.3.4 Other methods

Bensted (B39) described the use of TG in the study of clinkers or unhydrated cements. At 4 K $min^{-1}$ in $N_2$ with cements, losses normally occur at 100–200°C from gypsum or hemihydrate, 400–500°C from CH and 500–800°C from $CaCO_3$. If a normal, open sample cup is used, the losses from conversion of gypsum to hemihydrate and from dehydration of hemihydrate are poorly resolved, making interpretation difficult. Better separation can be achieved by using a sample cup with a top that is closed except for a narrow exit (S41).

Syngenite, if present, decomposes at 250–300°C. Small amounts of CH can occur due to hydration, and of $CaCO_3$ due to carbonation during milling or storage, impurity in the gypsum, or, where specification allows it, deliberate addition. The increasing tendency to allow additions of substances other than calcium sulfate may lead to the presence of other phases detectable by TG. A mass gain at 300–400°C in air that does not occur in $N_2$ normally indicates that the clinker was made under reducing conditions, but could also conceivably be due to the presence of an excessive quantity of metallic iron incorporated during milling. In this latter case it would, of course, not be shown by the clinker.

Applications of IR and Raman spectroscopy to the study of clinkers and unhydrated cements have been reviewed (B40,B41). The laser Raman microprobe, with which regions of micrometre dimensions on a polished surface may be examined, has been used to investigate structure and crystallinity, especially of the alite and belite (C19). Spectroscopic methods for studying the surface structures and compositions of cements are considered further in Section 5.8.2.

## 4.4 Calculation of quantitative phase composition from bulk chemical analysis

### 4.4.1 General

As seen in Section 4.5.4, there is wide agreement that the Bogue calculation gives seriously incorrect results, especially for alite. It has often been stated that the errors arise because equilibrium is not maintained during cooling, but this is only partly correct. Even if equilibrium was maintained, all the major phases would contain significant proportions of substituent ions. The calculation gives incorrect results mainly because the phases do not have the compositions assumed for them, and the absence of equilibrium conditions during cooling merely alters the errors that arise. In addition, the four major components are not completely contained in the four major phases, and errors arise because the bulk analysis is not fully corrected for this.

### 4.4.2 Modified Bogue calculation

The Bogue calculation is a solution of four linear simultaneous equations for four unknowns. Based on an approach due to Yamaguchi and Takagi (Y1), it may be modified (H3,T13) by using the best available estimates

of the compositions of the four phases instead of those of the pure compounds and by correcting the raw analysis more fully for the presence of major oxide components in phases other than the four major ones. For modern, rapidly cooled clinkers of ordinary Portland cements, the compositions of the phases do not seem to vary excessively, the most important variations in the present context being in the CaO and $Fe_2O_3$ contents of the alite (Chapter 1). By following these principles, one may expect to obtain results that are substantially more accurate than those given by the orthodox Bogue calculation.

Deductions from the bulk CaO content that may be needed comprise free lime and any CaO present in $CaCO_3$ (equivalent to the $CO_2$ content), clinker sulfates (calcium langbeinite or anhydrite or both) and, for a cement, added calcium sulfate ('gypsum'). Methods for estimating the amounts of CaO in clinker sulfates are suggested in Section 3.5.7. To obtain the content of CaO present in calcium sulfate added on grinding of a cement, it is necessary to know either the amount and composition of the added material or the $SO_3$ content of the clinker.

Assuming that a modern method of analysis (e.g. XRF) has been used, the $SiO_2$ and $Al_2O_3$ contents must be corrected for any material present in the insoluble residue. For a clinker, the latter usually consists largely of quartz ($SiO_2$), but for a cement it is likely to consist largely of impurities in the gypsum, and it is often reasonable to assume that the insoluble residue is two-thirds $SiO_2$ and one-third $Al_2O_3$. If classical, wet analysis was used, these deductions should not be made, but the apparent content of $Al_2O_3$ must be corrected for $TiO_2$ and $P_2O_5$.

Values are required for the contents of CaO, $SiO_2$, $Al_2O_3$ and $Fe_2O_3$ in each of the four major phases. For a modern, quickly-cooled ordinary Portland cement or clinker, the compositions given in Table 1.2 are probably often a sufficiently good approximation. It may be desirable to modify them in accordance with the bulk analysis, in ways suggested in Sections 1.2.3, 1.3.3, 1.4.4 and 1.5.2 for alite, belite, aluminate and ferrite respectively, those for the CaO and $Fe_2O_3$ in the alite being probably the most important. Alternatively, if they are available, compositions determined by X-ray microanalysis of the particular clinker or cement may be used. The situation with other types of Portland cements or clinkers is considered in Section 4.4.4.

It is then necessary to set up and solve four simultaneous equations, one for each of the four major oxide components. For each equation, there are four terms on the left-hand side, one for each of the four major phases. The coefficient in each term is the mass fraction of the oxide component in the phase, the unknown is the mass percentage of the phase in the clinker or cement, which has to be determined, and the right-hand side is the mass percentage of the oxide component in the material, corrected for any contributions from phases other than the four major ones. As an example, equation 4.7 might be that for CaO in a case for which the mass fractions of CaO in the alite, belite, aluminate and ferrite were respectively 0·710, 0·635, 0·566 and 0·475, the total mass percentage of CaO present in the four major phases was 64·7%, and $x_1$–$x_4$ are

respectively the mass percentages of alite, belite, aluminate and ferrite in the material.

$$0{\cdot}710x_1 + 0{\cdot}635x_2 + 0{\cdot}566x_3 + 0{\cdot}475x_4 = 64{\cdot}7 \qquad (4.7)$$

Similar equations are required for the other three major oxide components and the four equations are then solved to obtain values of $x_1$–$x_4$. Any standard method of matrix inversion, such as the Gauss–Jordan method (N14), may be used for this purpose.

### 4.4.3 *Mass balance calculations*

As a by-product of the modified Bogue calculation described in the preceding section, it is readily possible to calculate a mass-balance table showing how all the oxide components, both major and minor, are distributed among the major and minor phases. This requires values for the mass percentages of all the component oxides in each of the phases. Any MgO in excess of that assigned to the major phases is assumed to occur in periclase. Other constituent phases may include clinker sulfates, gypsum (for a cement), insoluble residue, $CaCO_3$ if present, and any part of the ignition loss not attributable to gypsum or $CaCO_3$. Table 4.3 is such a table for a typical clinker. The compositions assumed for the major phases were approximately those given in Table 1.2, and that of the sulfate was obtained as outlined in Section 3.5.7. The sulfate is probably largely $K_2SO_4$ with some $Na_2SO_4$ and $CaSO_4$ in solid solution, but could include some Ca langbeinite. The residual for each oxide component arises from incorrect assumptions regarding the compositions of phases together with contributions from any phases not included in the calculation.

### 4.4.4 *Limitations and modifications of the modified Bogue calculation*

The modified Bogue calculation described above appears to give satisfactory results for most modern Portland cement clinkers or cements having alumina ratios between about 1 and 4, but the following points should be noted.

(1) If the aluminate phase is orthorhombic, the appropriate composition (Table 1.2) should be used in the equations. If both cubic and orthorhombic forms are present, intermediate values could be used.

(2) For a sulfate-resisting Portland cement, an appropriate ferrite composition, such as that given in Table 1.2, should be used. If the result for aluminate is negative, this phase is absent and it may be useful to replace the coefficients for the aluminate composition by ones for a second ferrite composition. By bracketing the ferrite composition in this way, estimates of both the content and the composition of the ferrite can be obtained.

(3) The results will be less accurate for slowly cooled clinkers, as the compositions of the ferrite and possibly also the aluminate phases may differ significantly from those assumed here. At present, there are not enough data to deal with this problem. The

**Table 4.3** *Distribution of oxide components among phases in a typical Portland cement clinker, calculated from the bulk chemical analysis*

| | $Na_2O$ | MgO | $Al_2O_3$ | $SiO_2$ | $P_2O_5$ | $SO_3$ | $K_2O$ | CaO | $TiO_2$ | $Mn_2O_3$ | $Fe_2O_3$ | Total |
|---|---|---|---|---|---|---|---|---|---|---|---|---|
| Alite | 0·1 | 0·7 | 0·7 | 16·8 | 0·1 | 0·1 | 0·1 | 47·7 | 0·0 | 0·0 | 0·5 | 66·7 |
| Belite | 0·0 | 0·1 | 0·3 | 4·1 | 0·0 | 0·0 | 0·1 | 8·2 | 0·0 | 0·0 | 0·1 | 13·0 |
| Aluminate | 0·1 | 0·1 | 2·2 | 0·3 | 0·0 | 0·0 | 0·0 | 4·0 | 0·0 | 0·0 | 0·4 | 7·0 |
| Ferrite | 0·0 | 0·3 | 2·2 | 0·4 | 0·0 | 0·0 | 0·0 | 4·7 | 0·2 | 0·1 | 2·1 | 9·9 |
| Free lime | 0·0 | 0·0 | 0·0 | 0·0 | 0·0 | 0·0 | 0·0 | 0·9 | 0·0 | 0·0 | 0·0 | 0·9 |
| Periclase | 0·0 | 0·5 | 0·0 | 0·0 | 0·0 | 0·0 | 0·0 | 0·0 | 0·0 | 0·0 | 0·0 | 0·5 |
| Sulfates | 0·1 | 0·0 | 0·0 | 0·0 | 0·0 | 0·9 | 0·8 | 0·1 | 0·0 | 0·0 | 0·0 | 1·9 |
| Insol. res. | 0·0 | 0·0 | 0·0 | 0·1 | 0·0 | 0·0 | 0·0 | 0·0 | 0·0 | 0·0 | 0·0 | 0·1 |
| Residual | 0·0 | 0·0 | 0·0 | 0·0 | 0·0 | 0·0 | −0·1 | 0·0 | 0·0 | 0·0 | 0·0 | 0·1 |
| Total | 0·3 | 1·6 | 5·3 | 21·6 | 0·2 | 1·0 | 1·0 | 65·6 | 0·2 | 0·1 | 3·1 | 100·1 |

Results given as percentages on the ignited mass. Periclase calculated by difference. Discrepancies in totals arise from rounding.

method is not applicable without major modification to clinkers made under reducing conditions. It is doubtful whether the procedure is applicable to white cements, both for this reason and also because they may contain glass. In addition, the range of applicability of the composition given in Table 1.2 for the aluminate phase in such cements is uncertain.

## 4.5 Physical methods for determining quantitative phase composition

### *4.5.1 General*

The physical methods that have proved effective for quantitative determination of phases in clinkers are based on light microscopy (Section 4.2.1), scanning electron microscopy (Section 4.3.1) and X-ray diffraction (Section 4.3.2). The last of these, in common with calculation from the bulk chemical analysis (Section 4.4), is also applicable to cements. Other methods that have been investigated, such as IR spectroscopy, appear to have less potential.

### *4.5.2 Light microscopy*

The phases may be determined quantitatively by point counting (C20,H23). The areas of phases on a polished section of a cement clinker are proportional to the volumes in the material. Random and systematic errors arise from imperfect sampling, counting statistics, the presence of inclusions too small to be observed by this method and incorrect identifications of phases by the operator. Error from counting statistics depends on the number of points, the size of the grid and the grain sizes of the phases; 4000 points normally gives reasonable precision (H23). Systematic errors from incorrect identification of phases generally exceed errors from counting statistics, and give rise to differences in results between operators (C20). As an alternative to point counting, image analysis has been used (M45). With many clinkers, it is impracticable to determine the aluminate and ferrite phases separately by either method. For alite and belite, and for interstitial material as a whole, both are capable of giving highly reliable results, assuming in the case of the silicate phases that they do not contain inclusions of other phases too small to be observed.

### *4.5.3 Quantitative X-ray diffraction analysis (QXDA)*

The application of this method to clinkers or cements presents several problems. Alite is normally so much the predominant phase that its pattern tends to swamp those of the other phases. All the stronger peaks of belite are overlapped by ones of alite. Other difficulties in quantitative analysis are caused by variability of patterns of phases due to compositional or polymorphic variation, and, especially for the ferrite phase, peak broadening due to compositional zoning or imperfect crystallinity. Other problems in quantitative work are those of QXDA in general; e.g. the material must be ground sufficiently finely that primary extinction of the more intense peaks is minimized, and adequate mixing

with an internal standard is possible, if one is used, but not so strongly that crystallinity is reduced. Milling to below 5 $\mu$m in an agate ball mill with cyclohexane as grinding aid, followed by back loading into the sample holder of a diffractometer, has been found satisfactory for specimen preparation (G33).

Struble (S42) summarized early QXDA studies on clinkers and cements. Most investigators have used some form of the internal standard method (K11). Rutile ($TiO_2$) has been widely used as the internal standard, but other substances, such as Si, KBr, $CaF_2$ and corundum have also been employed; corundum has the advantage of giving no overlaps with important cement peaks up to 60° 2$\theta$. The method in its conventional form, in which only a single peak of the reference standard and of the phase to be determined is used, is moderately effective for alite, using the peak at approximately 51° 2$\theta$, assuming that a means of accommodating the splitting of this peak is found. It is less satisfactory for the aluminate and ferrite, and useless for belite, because of the weakness of their peaks and interference from those of alite.

Berger *et al.* (B42) pioneered a least-squares procedure in which the profile of a diffractometer trace was matched with a simulated trace summing the contributions from the component phases. In a development of this technique, Gutteridge (G33) collected data over the range of 24–39° 2$\theta$ by step counting at 0·05° intervals using Cu$K\alpha_1$ radiation. Data for the sample and pure phases, including known quantities of an internal standard, were stored in a computer and the least-squares calculation carried out. Auxiliary procedures were devised for dealing with background levels, adjusting the peak widths and, to some extent, peak positions in the reference patterns to match those in the clinker, and matching the observed and computed patterns. Minor phases, such as lime, periclase, calcium sulfate phases and mineral additions (Chapter 9) could be included in the analysis. Increased computing power has allowed later investigators to use wider ranges of 2$\theta$, with consequently improved precision and accuracy (S43,T14).

Instead of matching profiles, observed and calculated intensities integrated over selected ranges of 2$\theta$ can be matched by least-squares methods (K12,T15). In principle, this can avoid problems arising from variations in the patterns of the component phases, though at some loss of sensitivity.

With any form of QXDA, it is normally necessary to employ reference standards that are as near as possible to the phases in the material as regards composition, polymorphism and degree of crystallinity. This implies both knowledge of the characteristics of the particular clinker under examination and the ability to prepare the necessary specimens, or alternatively to isolate them physically from the clinker itself. One solution (G33) has been to prepare reference patterns for a wide range of specimens of each phase and to use those that appear to correspond most closely to those present in the clinker under examination. Clinkers for which results had been obtained by point counting have also been used

(K12). In another approach, a standard profile for alite was extracted mathematically from the observed patterns of several Portland cements (T14).

It is also possible to match the observed pattern against a simulated pattern obtained by summing patterns calculated from the known crystal structures. This procedure has been used (T15) to match intensities integrated over selected ranges of $2\theta$. For each calculated pattern, a 'reference intensity ratio' (H26) was calculated. This is the integrated intensity of the strongest individual reflection (which may be a component of an overlap) relative to that of the strongest peak of corundum in a 1:1 mixture by mass. The internal standard added to the clinker or cement need not be corundum, provided that its own reference intensity ratio is known.

If calculated patterns and reference intensity ratios are used, the relative proportions of the phases can be determined from the observed diffractometer trace for a clinker or cement to which no internal standard has been added. By normalizing the results to some assumed total (e.g. 98% for the four major phases in a clinker or 95% in a cement), it is thus possible to dispense both with reference standards and with an internal standard. The Appendix gives calculated patterns and reference intensity ratios for the four major phases.

### *4.5.4 Comparison of results of different methods*

From the results of a study in which six clinkers were examined in a number of different laboratories, Aldridge (A9) concluded that light microscopy gave accurate results for the quantitative determination of phases in clinkers, assuming an experienced operator and adequate sampling. Results obtained using QXDA varied widely between laboratories, and it was concluded that, as carried out in most of them, the method was of low accuracy. One laboratory, however, obtained results that agreed well with those given by microscopy, and which were considered to be accurate. In general, the contents of alite found by microscopy were higher than those given by the Bogue calculation.

The results of another cooperative study, in which microscopy and extraction methods were used, showed that the Bogue calculation always gives low results for alite and generally gives high ones for belite when compared with microscopy (C20). For the aluminate and ferrite phases, agreement was reasonably good. The total contents of silicates, determined by chemical extraction, agreed reasonably well with those found by microscopy.

Several early studies using QXDA gave results in fair agreement with those of the Bogue calculation, but in the light of the above and other recent evidence are of doubtful validity. Odler *et al.* (O10) found that alite contents found either by microscopy or by QXDA were always greater than those given by the Bogue calculation. Gutteridge (G33) reached the same conclusion for QXDA, and also noted that the total amounts of the crystalline phases did not vary significantly from 100%. Kristmann (K13) concluded from a study of 39 clinkers that alite and belite were determined more satisfactorily by microscopy than by QXDA, but that

aluminate and ferrite, due to their close admixture, were better determined by QXDA or by determining the total content of interstitial material by microscopy and the relative amounts of its constituent phases by QXDA of a residue from SAM extraction (Section 4.3.3). His results indicated that the values given by the Bogue calculation are low for alite and aluminate, high for belite, and reasonably satisfactory for ferrite. The mean discrepancy for alite was 8%.

The modified Bogue calculation described in Section 4.4.2 was tested using Kristmann's data (T13). Agreement was substantially better than with the Bogue calculation for alite, belite and aluminate, and about as good for ferrite. For alite and belite, there was no significant bias relative to Kristmann's results in either direction. For aluminate, there was a possible tendency to give high results; for ferrite, it was not possible to tell whether there was bias, due to inadequacies in the experimental data. Good agreement was also obtained in tests on a wide range of cements, using experimental data obtained by Gutteridge (G37) using QXDA.

Taken as a whole, the evidence indicates that all four major phases can be satisfactorily determined by QXDA if an adequate experimental procedure is employed (e.g. G33) or by calculation. Alite, belite and the total content of interstitial material can also be determined by microscopy. With any of these methods, assuming the best available procedures to be used, the absolute accuracy is probably not better than 2–5% for alite and belite, or 1–2% for aluminate and ferrite.

## 4.6 Reactivities of clinker phases

### *4.6.1 Effect of major compositional variation*

The ability of a substance to act as a hydraulic cement depends on two groups of factors. First, it must react with water to a sufficient extent and at a sufficient rate; $\gamma$-$C_2S$, which is virtually inert at ordinary temperatures, has no cementing ability. Second, assuming that an appropriate ratio of water to cement is used, the reaction must yield solid products of very low solubility and with a microstructure that gives rise to the requisite mechanical strength, volume stability, and other necessary properties. $C_3A$ reacts rapidly and completely with water, but the products that are formed when no other substances are present do not meet these criteria, and its ability to act as a hydraulic cement is very poor. $C_3S$, in contrast, satisfies both sets of conditions, and is a good hydraulic cement.

In this section, only the factors that control reactivity are considered. Any understanding of them must be based on a knowledge of the mechanisms of the reactions with water. It is highly probable that these are in all cases ones in which an essential step is transfer of protons to the solid from the water, which is thus acting as a Brønsted acid (B43,D12). As an initial approximation, one may consider the problem purely in terms of the idealized crystal structures. The reactivities of the oxygen atoms towards attack by protons depend on their basicities, i.e. the magnitudes of the negative charges localized on them. Any structural feature that draws electrons away from the O atoms renders them less reactive, the basicity thus depending on the electronegativities of the

atoms with which they are associated. In this respect, the nearest neighbours are the most important, but the effects of atoms further away are far from negligible. This hypothesis leads to the folowing predictions, all of which agree with the facts.

(1) O atoms attached only to atoms of a single element will be less reactive as the electronegativity of that element increases. Thus, $C_3S$ and lime both contain O atoms linked only to Ca, and are more reactive than $\beta$-$C_2S$, in which all the O atoms are also linked to Si, while $\alpha$-$Al_2O_3$, in which all are linked to Al, is inert. However, the reactivity of lime decreases if it is strongly burned; this is discussed below.

(2) O atoms forming parts of silicate, aluminate or other anionic groups will be less reactive as the degree of condensation with other such groups increases. $\beta$-$C_2S$, in which the tetrahedra do not share O atoms, is more reactive than any of the $C_3S_2$ or CS polymorphs, in which they do.

(3) O atoms forming parts of anionic groups similar as regards degree of condensation will be less reactive as the central atoms in the groups become more electronegative. In contrast to the $C_3S_2$ and CS polymorphs, CA, $C_{12}A_7$ and $C_3A$ are all highly reactive, even though the $AlO_4$ tetrahedra share corners in all cases.

Other hypotheses based on considerations of crystal structure have been proposed, and in varying degrees may account for second-order effects. Thus, Jeffery (J1) suggested that irregular coordination of Ca was responsible for the high reactivity of $C_3S$ as compared with $\gamma$-$C_2S$; however, lime reacts with water, but the coordination of its Ca atoms is highly symmetrical. Jost and Ziemer (J9), who noted the weaknesses in this and other earlier hypotheses, considered that high reactivity was associated with the presence of face-sharing polyhedra, but lime contains no such groupings, yet can be highly reactive.

*4.6.2 Effects of ionic substitutions, defects and variation in polymorph*

The considerations discussed in the preceding section suffice only to explain the effects on reactivity of major variations in composition. They do not, in general, explain the effects of variations in polymorph or introduction of substituent ions. These effects are often complex, and while in some cases the results appear clear-cut, there are many others in which they present a confusing and sometimes apparently contradictory picture. The probable reason is that many variables are involved, which are difficult or impossible to control independently. These include, besides chemical composition and polymorphic change, concentrations and types of defects; particle size distribution; textural features such as crystallite size and morphology, mechanical stress, presence of microcracks and the monocrystalline or polycrystalline nature of the grains; influences of reaction products, whether solid or in solution. In a cement as opposed to a pure phase, a foreign ion may not only substitute in a particular phase, but also influence the microstructure of the material in

ways unconnected with that substitution, *e.g.* by altering the physical properties of the high-temperature liquid present during its formation. For both microstructural and chemical reasons, the reactivity of a given phase in a cement may not be the same as that observed when it is alone.

Defects play a particularly important role. Sakurai *et al.* (S44) noted that $C_3S$, alite, $C_2F$ and $C_4AF$ could all take up $Cr_2O_3$ and that this greatly accelerated reaction at early ages. Electron microscopic studies showed that reaction began at grain boundaries and at points of emergence of screw dislocations, the concentration of which was greatly increased by $Cr_2O_3$ substitution. It was also shown that the substituted materials were semiconductors, and a mechanism of attack based on electron transfer processes was suggested. Fierens and co-workers (F13,F14) also found that the influence of substituent ions on the reactivity of $C_3S$ was due to the presence of defects, which could be studied using thermoluminescence, and which could also be introduced by suitable heat treatment.

The complex relations between content of substituent ions, polymorphism, defects and reactivity are well illustrated by the results of Boikova and co-workers (B2,B44) on ZnO-substituted $C_3S$. With increasing ZnO content, triclinic, monoclinic and rhombohedral polymorphs were successively stabilized. Curves in which the extent of reaction after a given time were plotted against ZnO content showed maxima corresponding approximately to the $T_2$–$M_1$ and $M_2$–R transitions, with intermediate minima. As in the work mentioned above, it was shown that these compositions were also ones in which the numbers of defects of a particular type were at a maximum. Reactivity thus depends not so much on the amount of substituent or nature of the polymorph as on the types and concentrations of defects.

Studies on the comparative reactivities of the $\beta$-, $\alpha'$- and $\alpha$-$C_2S$, reviewed by Skalny and Young (S45), have given contradictory results. As these authors conclude, reactivity probably depends on specimen specific factors other than the nature of the polymorph, and in the lower temperature polymorphs may be affected by the exsolution of impurities. This latter hypothesis receives strong support from subsequent observations that attack begins at exsolution lamellae and grain boundaries, and that these may contain phases, such as $C_3A$, that are much more reactive than the $C_2S$ (C1). Without these lamellae, $\beta$-$C_2S$ might be much less reactive than it is.

There is wide agreement that substitution of alkali metal ions retards the early reaction of the aluminate phase, which is thus less for the orthorhombic than for the cubic polymorphs (B45,R14,S46). The effect has been attributed to structural differences, but the early reaction of pure $C_3A$ is also retarded by adding NaOH to the solution, and the $OH^-$ ion concentration in the solution may be the determining factor (S46). The reaction of $C_3A$ is also retarded by iron substitution and by close admixture with ferrite; formation of a surface layer of reaction products may be a determining factor, at least in later stages of reaction, and the retarding effect of such a layer may be greater if it contains $Fe^{3+}$ (B46).

### 4.6.3 Ferrite reactivity; effect of complexing in solution

The reactivities of ferrite phases in the pure $Ca_2(Al_xFe_{1-x})_2O_5$ series have been widely found to increase with Al/Fe ratio, and material of composition similar to that in clinkers is more reactive than either $C_4AF$ or $C_6A_2F$ (e.g. B45,B46,D13). Anomalies in the relation between rate and Al/Fe ratio found by some workers can possibly be attributed to zoning or other variations in crystallinity. As with the aluminate phase, the decrease in reactivity with Fe content is possibly explainable by differences in the properties of a retarding layer of product. The relatively high reactivity of the clinker material may be related to its semiconducting properties (M24) and to disorder arising from the complex ionic substitutions (B46).

The rate of reaction of the ferrite phase is much increased by the presence of tri-isopropanolamine in the solution. This is not strongly adsorbed on the cement grains but complexes the iron in solution, thereby inhibiting the formation of a layer of reaction product and favouring the passage of iron into solution (G38). This illustrates the important fact that the rate of reaction is not solely controlled by properties of the solid phase but depends also on what is present in the solution.

# 5 Hydration of the calcium silicate phases

## 5.1 Introduction

### *5.1.1 Definitions and general points*

In cement chemistry, the term 'hydration' denotes the totality of the changes that occur when an anhydrous cement, or one of its constituent phases, is mixed with water. The chemical reactions taking place are generally more complex than simple conversions of anhydrous compounds into the corresponding hydrates. A mixture of cement and water in such proportions that setting and hardening occur is called a paste, the meaning of this term being extended to include the hardened material. The water/cement (w/c) or water/solid (w/s) ratio refers to proportions by mass; for a paste, it is typically 0·3–0·6. Setting is stiffening without significant development of compressive strength, and typically occurs within a few hours. Hardening is significant development of compressive strength, and is normally a slower process. Curing means storage under conditions such that hydration occurs; conditions commonly employed in laboratory studies include storage in moist air initially and in water after the first 24 h, storage in air of 100% relative humidity and, less favourable for reaction, storage in a sealed container.

Because Portland cement is a relatively complex mixture, many studies having the aim of elucidating its hydration chemistry have been made on its constituent phases. For a given particle size distribution and w/s ratio, tricalcium silicate or alite sets and hardens in a manner similar to that of a typical Portland cement. Using XRD or other methods, it may be shown that about 70% of the $C_3S$ typically reacts in 28 days and virtually all in 1 year, and that the products are calcium hydroxide (CH) and a nearly amorphous calcium silicate hydrate, called C–S–H, having the properties of a rigid gel. $\beta$-$C_2S$ behaves similarly, but much less CH is formed and reaction is slower, about 30% typically reacting in 28 days and 90% in 1 year. Figure 5.1 shows the XRD diffraction pattern of a 23-year old paste of $\beta$-$C_2S$. Patterns of fully reacted $C_3S$ pastes are similar, except that the CH peaks are much more intense. The only effects definitely attributable to the C–S–H are the diffuse peak at 0·27–0·31 nm and the somewhat sharper one at 0·182 nm.

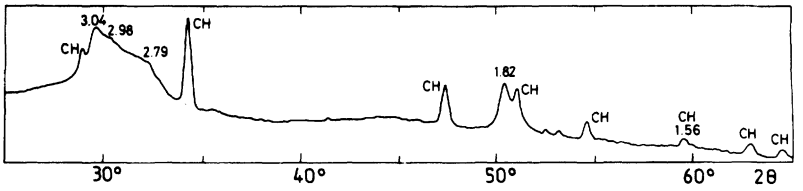


**Fig. 5.1** *XRD powder diffraction pattern (microdensitometer trace of Guinier film, $CuK_{\alpha 1}$ radiation, spacings in Å) of a fully reacted $\beta$-$C_2S$ paste. From M46.*

For both $C_3S$ and $\beta$-$C_2S$, reaction rates depend on particle size distribution and other factors. Development of compressive strength runs roughly parallel to the course of the chemical reactions, and the strengths at 1 year are comparable to those of Portland cements of the same w/s ratio and cured under the same conditions.

The calcium silicate hydrate formed on paste hydration of $C_3S$ or $\beta$-$C_2S$ is a particular variety of C–S–H, which is a generic name for any amorphous or poorly crystalline calcium silicate hydrate. The dashes indicate that no particular composition is implied, and are necessary because CSH in cement chemical nomenclature denotes material specifically of composition $CaO \cdot SiO_2 \cdot H_2O$. The term 'C–S–H gel' is sometimes used to distinguish the material formed in cement, $C_3S$ or $\beta$-$C_2S$ pastes from other varieties of C–S–H.

This chapter deals primarily with the reactions and products of hydration of $C_3S$ and $\beta$-$C_2S$ in pastes at ordinary temperatures. Some closely related studies on cement pastes are also considered. Most of the results for pastes of $C_3S$ or $\beta$-$C_2S$ are applicable also to the behaviour of those phases in cement pastes. Except where stated, a temperature of 15–25°C is assumed. Background information has been obtained from studies of $C_3S$ or $\beta$-$C_2S$ hydration at higher w/s ratios, i.e. in aqueous suspensions, or on C–S–H prepared in other ways, and the results of such studies are also considered.

### 5.1.2 Experimental considerations; carbonation

C–S–H reacts with $CO_2$ or $CO_3^{2-}$ ion with formation of $CaCO_3$. Initially, the Ca/Si ratio of the C–S–H decreases; further reaction destroys the C–S–H, with formation of hydrous silica. Contamination by atmospheric $CO_2$ ('carbonation') can probably be more serious in laboratory studies than in practical concrete mixes of lower surface to volume ratio. Many studies have been made under, as nearly as possible, $CO_2$-free conditions. This has the merit of simplifying interpretation, though the extent to which it corresponds to the situation in a real concrete mix is uncertain. To achieve a reasonable approximation to $CO_2$-free conditions, all operations, such as mixing, curing or drying of pastes, or preparation, filtration or drying of solid phases in suspensions, must be carried out in a $CO_2$-free atmosphere, either in a dry box or in apparatus otherwise designed to isolate the materials from the atmosphere. Wet or

moist materials are especially susceptible to attack, but dry ones are not immune. Water must be deionized and freshly boiled. Because of the alkaline nature of calcium silicate or cement mixes, prolonged contact with glass must also be avoided; wet curing may be carried out in the presence of a small excess of water in a sealed plastic container.

In any laboratory study, therefore, it is usually important to know how much $CO_2$ is present. This applies both to situations in which it is supposedly absent and to those in which an attempt has been made to include a controlled quantity. Jones's (J10) method, based on decomposition with dilute acid and absorption of the $CO_2$ in $Ba(OH)_2$ solution, which is then back-titrated with HCl, is simple and accurate. TG has often been used to determine $CO_2$, but is not satisfactory because the loss at 700–900°C is not wholly due to $CO_2$. Absence of calcite peaks from an XRD pattern is not a proof that $CO_2$ is absent, as $CO_2$ can occur in other forms, e.g. as vaterite ($\mu$-$CaCO_3$), in calcium aluminate hydrate phases and possibly within the C–S–H structure. Table 5.1 gives data for the three polymorphs of $CaCO_3$ that can form at ordinary pressures.

Especially with relatively young pastes, the problem often arises of removing excess water after a specified time of curing to stop the hydration reactions and to render the material less susceptible to carbonation. For this purpose, soaking or grinding in polar organic liquids, such as methanol, propan-2-ol or acetone has often been employed, but should

**Table 5.1** *Crystal and optical data for calcium carbonate polymorphs*

| | Calcite | Aragonite | Vaterite |
|---|---|---|---|
| *Crystal data* | | | |
| Crystal system | Trigonal (rhombohedral) | Orthorhombic | Hexagonal |
| Space group | $R\bar{3}c$ | Pmcn | $P6_3/mmc$ |
| $a$ (nm) | 0·4989 | 0·49623 | 0·71473* |
| $b$ (nm) | | 0·7968 | |
| $c$ (nm) | 1·7062 | 0·57439 | 1·6917* |
| Angles, where not 90° | 120° ($\gamma$) | | 120° ($\gamma$) |
| $Z$ | 6 | 4 | 12 |
| $D_x$ (kg m$^{-3}$) | 2711 | 2927 | 2664 |
| Reference | P1 (card 5-586) | P1 (card 41-475) | P1 (card 33-268) |
| *Optical properties* | | | |
| Refractive indices ($Na_D$) | $\omega$ 1·6584, $\varepsilon$ 1·4864 | $\alpha$ 1·5300, $\beta$ 1·681, $\gamma$ 1·6854 | $\omega$ 1·550, $\varepsilon$ 1·640–1·650 |
| Optic orientation | | $X=c$, $Y=a$, $Z=b$ | |
| Optic sign | Negative | Negative ($2V=18°$) | Positive |
| Morphology | Rhombs ($\alpha_R$ 101·9°) | Short columns, needles | Plates, radial aggregates |
| Reference | W3 | W3 | W3 |

* Other polytypes and disordered forms are known.

be used only in situations where it will not invalidate the results of subsequent tests. Organic substances can be completely removed from $C_3S$ or cement pastes only by drastic procedures that seriously alter the material. Their presence is especially undesirable if any form of thermal analysis (e.g. TG or DTA) is to be carried out, since on heating they react with C–S–H to give $CO_2$ (D14,T16). Acetone has especially complex effects, since in the alkaline medium it rapidly undergoes aldol condensations at room temperature, giving mesityl oxide, phorone and other relatively involatile products (T16). Some workers consider that primary aliphatic alcohols alter the pore structures of $C_3S$ or cement pastes or of synthetic C–S–H preparations (Section 8.4.1), and it has also been claimed that methanol reacts with CH at ordinary temperatures, giving calcium methoxide (B47).

In choosing a procedure to remove excess water, it is necessary to consider the likely effects on the tests subsequently to be performed. Retention of organic substances is not the only possible complication; unduly drastic drying procedures, e.g. heating at 105°C or equilibration to constant mass in atmospheres of low relative humidity, such as 'D-drying' (Section 5.2.2) partially dehydrate the C–S–H and, with cement pastes, also partially decompose the hydrated calcium aluminate or aluminate sulfate phases. For some procedures, such as XRD, the presence of organic material may not matter, but even here the possibility of decomposing or altering hydrated aluminate phases must be considered. For electron microscopy, including the preparation of polished sections for SEM, freeze-drying has been found satisfactory (J11). For many purposes, including thermal analysis above about 150°C, pumping with a rotary pump for 1 h is suitable. The drying of samples for studies on pore structure is considered in Section 8.4.1.

All analytical data on hydrated cements or cement constituents should normally be referred to the ignited mass. The original mass includes an arbitrary amount of water, and results referred to it, or to the mass after some arbitrarily chosen drying procedure (e.g. to constant mass at 105°C), are often impossible to interpret in detail.

### 5.1.3 Calcium hydroxide

CH has a layer structure (Fig. 5.2; B48,P18). The calcium atoms are octahedrally, and the oxygen atoms tetrahedrally, coordinated. The interlayer forces are weak, with negligible hydrogen bonding, thus giving good (0001) cleavage. The unit cell is hexagonal, with $a = 0{\cdot}3593$ nm, $c = 0{\cdot}4909$ nm, space group $P\bar{3}m1$, $Z = 1$, $D_x = 2242\,kg\,m^{-3}$ ; the optical properties are: uniaxial −, $\omega = 1{\cdot}573$, $\varepsilon = 1{\cdot}545$ (S8). Calcium hydroxide is often described by its mineral name, portlandite.

Under ideal conditions of crystallization, CH forms hexagonal plates. Admixtures greatly affect the morphology, and especially the $c:a$ aspect ratio (B49). Euhedral crystals are observed in young pastes and in pores of older pastes, but as hydration proceeds the main deposits of CH become massive and of indeterminate shape, though the good cleavage persists. There does not appear to be any convincing experimental

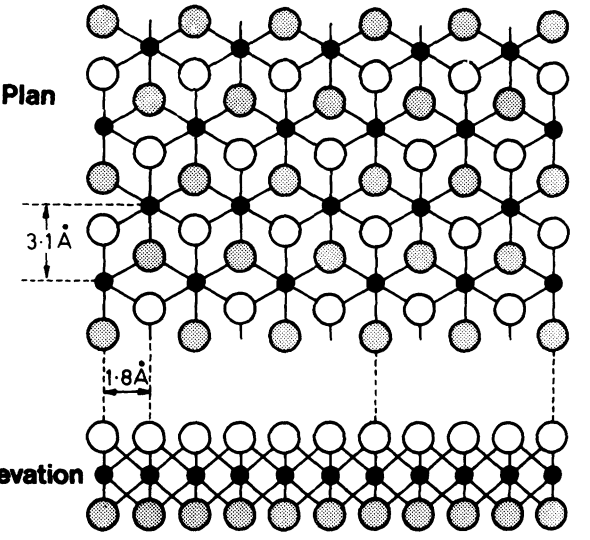


**Fig. 5.2** *Structure of a single layer of $Ca(OH)_2$. Small, solid circles represent calcium atoms, large open or shaded circles oxygen atoms; a hydrogen atom, not shown, completes the tetrahedral coordination of each oxygen atom. From T17.*

evidence for claims that some of the CH in calcium silicate pastes is amorphous. A TEM study of ion-thinned sections of a $C_3S$ paste of normal w/s ratio showed the CH to occur as large, imperfect crystals; no finely dispersed, microcrystalline materials were observed, though some crystals were only tens of nanometres thick (G39,G40). Cryptocrystalline CH has, however, been found in cement pastes and in pastes made from calcium oxide and silica of high w/s ratio and of blastfurnace slag activated by CH (Section 7.1.1).

Observations that the 0001 peak of CH in XRD powder patterns of calcium silicate or cement pastes is anomalously strong relative to the $10\bar{1}1$ peak (G41,Z10) have been attributed to overlap with a contribution from C–S–H, but probably arise from preferred orientation, which can be difficult to avoid. Stacking faults can also affect the CH pattern (S47).

The dissolution of CH in water is exothermic ($\Delta H = -13{\cdot}8\,kJ\,mol^{-1}$ at 25°C; G42), and the solubility therefore decreases with temperature (Table 5.2). The data given are for large crystals; higher apparent solubilities, up to at least 1·5 g CaO per l at 25°C, readily occur with finely crystalline material.

**Table 5.2** *Solubility of calcium hydroxide (S; g CaO $l^{-1}$; B50)*

| T(°C) | 0 | 5 | 10 | 15 | 20 | 25 | 30 | 40 | 50 | 60 | 80 | 99 |
|---|---|---|---|---|---|---|---|---|---|---|---|---|
| S | 1·30 | 1·28 | 1·25 | 1·21* | 1·17* | 1·13 | 1·09 | 1·00 | 0·92 | 0·83* | 0·66* | 0·52 |

* Interpolated values.

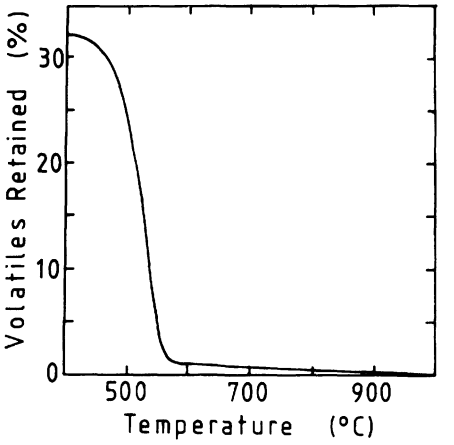


**Fig. 5.3** *Thermogravimetric curve of $Ca(OH)_2$ (0.2% $CO_2$); data are expressed as percentages on the ignited mass. 50 mg sample heated at 10 K min$^{-1}$ in dry, $CO_2$-free $N_2$ flowing at 15 ml min$^{-1}$. New data.*

Halstead and Moore (H27) reported thermal decomposition equilibria. The decomposition pressure reaches 101 kPa (1 atm) at 512°C and the mean enthalpy of decomposition at 300–510°C is 102·9 kJ mol$^{-1}$. When heated in a vacuum or in a stream of dry $N_2$, CH begins to decompose at an easily detectable rate at about 370°C. Under typical conditions for TG, decomposition is 98% complete at the end of the step at 580°C (Fig. 5.3). An earlier conclusion that only about 94% has decomposed at this point (T18) is incorrect. The finely divided CH available as a laboratory or analytical reagent normally contains several per cent of $CaCO_3$, and the curve in Fig. 5.3 is for coarsely crushed large crystals containing 0.2% $CO_2$.

## 5.2 Composition, density and other data for C–S–H gel

### *5.2.1 Calcium hydroxide content, thermal analysis and indirect determination of the Ca/Si ratio*

The Ca/Si ratio of the C–S–H in a fully reacted $C_3S$ or $\beta$-$C_2S$ paste may be calculated if the contents of CH and $CO_2$ are known, though an assumption must be made as to whether the $CO_2$ occurs in the C–S–H or as $CaCO_3$. If the content of unreacted $C_3S$ or $\beta$-$C_2S$ is also known, the method can be extended to incompletely reacted pastes, though small errors in the contents of CH or unreacted starting material greatly affect the result at low degrees of reaction. Quantitative XRD is probably the best method available at present for determining unreacted $C_3S$ or $\beta$-$C_2S$; the precision is probably not better than ±3% (O11). Methods used to determine CH have included TG, DTG, semi-isothermal DTG, thermal evolved gas analysis, DTA, differential scanning calorimetry (DSC), quantitative X-ray diffraction analysis (QXDA), IR spectroscopy, image

analysis of backscattered electron images and extraction methods using either aqueous media or organic solvents similar to those used to determine free lime in anhydrous cements.

Some workers studying pastes of $C_3S$ or cement have found significant differences between the results of thermal methods and QXDA, the latter usually giving lower results for the CH content (B51,D15,M47,O11,R15), but others have found no differences outside experimental error (L19,T19). There is broad agreement that extraction methods give higher results than either thermal methods or QXDA (B51,M47,O11,R15). It has been suggested that QXDA gives low results due to the presence of amorphous CH (R15). Thermal methods have also been considered to give low results for the same reason (O11), or because of CH adsorbed on the C–S–H (B51) or present as interlayer material (S48). Sources of error in CH determination by TG have been discussed (T18). As noted above, large errors can arise from use of thermal methods on material that has been in contact with organic liquids (T16). Preliminary results from image analysis did not correlate well with those from TG (S49).

The borderline between CH interlayered with C–S–H and that present as a separate phase is indistinct. The absence of evidence for amorphous or cryptocrystalline CH in $C_3S$ pastes is noted in Section 5.1.3. The higher results given by extraction methods are probably attributable to partial decomposition of the C–S–H. Of all the methods, TG or DTG is probably the least open to criticism, though, especially with cement pastes, precision and accuracy are limited by the difficulty of distinguishing sharply between the effects due to CH and to the other phases present. DTA is somewhat suspect, because the peak area for CH is reported to depend markedly on particle size (W18).

Figure 5.4 shows the TG and DTA curves of a fully reacted $C_3S$ paste, obtained under the same conditions as the TG curve of CH in Fig. 5.3. The paste had been prepared at w/s = 0·45 and stored wet, in a sealed container for 25 years at 25°C; it contained 0·8% of $CO_2$, referred to the ignited mass. The height of the CH step (mean from 7 determinations and estimated as shown in the inset) was 8·9%, referred to the ignited mass. Assuming that this step represents the decomposition of 98% of the CH and that the $CO_2$ occurs as $CaCO_3$, there is 1·15 mol CH and 0·04 mol $CaCO_3$ per mole of $C_3S$, and the Ca/Si ratio of the C–S–H is 1·81. Other recent investigations on $C_3S$ or $\beta$-$C_2S$ pastes have indicated Ca/Si ratios ranging from 1·6 to 2·0 (F15,K14,L19,O11,P19,S23). There is evidence of a lower Ca/Si ratio during the first few hours of reaction (O11), but with that reservation the more recent work (L19,O11,P19) does not support the conclusion of some earlier workers that the ratio changes markedly during the course of the reaction.

### *5.2.2 Water content*

Evidence considered in Sections 5.3 and 5.4 and Chapter 8 indicates that the C–S–H gel of calcium silicate or cement pastes has a layer structure, and that, together with a pore solution, it forms a rigid gel in which the pores range in size from macroscopic to enlarged interlayer spaces of

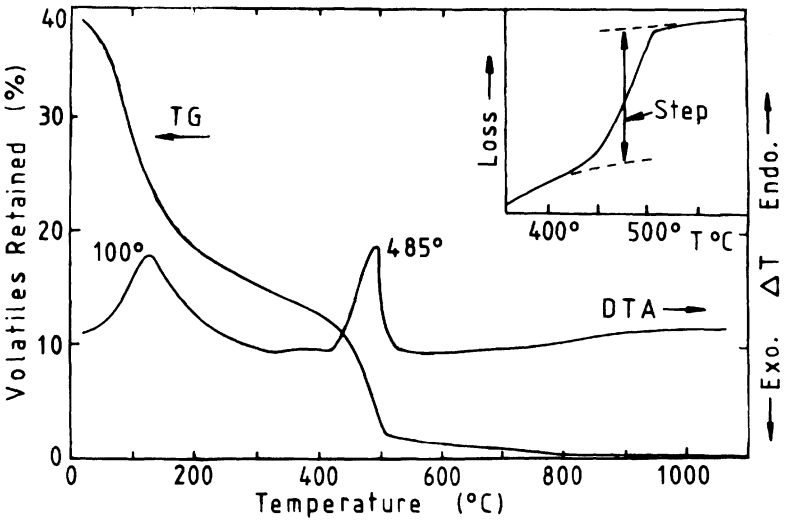


**Fig. 5.4** *Thermogravimetric and differential thermal analysis curves for a fully reacted $C_3S$ paste; experimental conditions as for Fig. 5.3. TG data are expressed as percentages on the ignited mass. After T16.*

nanometre dimensions. One can therefore define a water content only in relation to a specified drying condition. Three such conditions will be considered.

The most highly hydrated state is that existing in a saturated paste, i.e. one in which the pores are totally filled with water. According to the theory of Powers and Brownyard (P20; Section 8.2.1), the C–S–H in a cement paste can form only if sufficient space is available to permit it to be accompanied by a defined proportion of pore space. There is thus a certain w/c ratio below which complete hydration is impossible, and for which a mature paste consists entirely of hydration product, including this essential pore space. The total water content of such a paste in the saturated condition is typically 42–44%, referred to the ignited mass. For nearly saturated $C_3S$ pastes, Young and Hansen (Y5) concluded that the composition of the C–S–H was approximately $1{\cdot}7CaO \cdot SiO_2 \cdot 4H_2O$. Taking into account the water present in the CH, this corresponds to a w/c ratio of 0·42, which is similar to the values found for cement.

Chemically bound water is most reasonably defined as including that present in interlayer spaces, or more firmly bound, but not that present in pores larger than this. As will be seen in Chapter 8, the distinction between interlayer space and micropores is not sharp; water adsorbed on surfaces of pores further blurs the definition. From the experimental standpoint, the determination is complicated by the fact that the amount of water retained at a given RH depends on the previous drying history of the sample and on the rate at which water is removed. An approximate estimate is obtained by equilibrating a sample, not previously dried

below saturation, with an atmosphere of 11% RH (F16–F18). Saturated aqueous $LiCl \cdot H_2O$ gives the required RH (partial pressure of water vapour = 2·7 torr at 25°C). To achieve apparent equilibrium in a reasonable time (several days), the sample must be crushed and the system evacuated; the salt solution should be stirred, at least intermittently. Young and Hansen (Y5) found the composition of the C–S–H in $C_3S$ paste thus equilibrated to be $1{\cdot}7CaO \cdot SiO_2 \cdot 2{\cdot}1H_2O$.

As noted above, treatment of $C_3S$ pastes with methanol leaves some of the latter strongly sorbed. The methanol is removable only on heating at temperatures at which it reacts with the C–S–H, causing carbonation. However, the total mass of volatiles retained in a $C_3S$ paste that has been soaked in methanol and then pumped for about 1 h with a rotary pump is near that obtained on equilibration with saturated $LiCl \cdot H_2O$ (T16). Methanol treatment can thus be used as a rapid, though approximate method of determining chemically bound water. Other organic liquids could possibly be used in a similar way.

In a procedure known as 'D-drying', the sample is equilibrated with ice at −79°C by continuous evacuation with a rotary pump through a trap cooled in a mixture of solid $CO_2$ and ethanol (C21). The partial pressure of the water vapour is $5 \times 10^{-4}$ torr. Heating to constant mass at 105°C in an atmosphere of uncontrolled humidity, but free from $CO_2$, reduces the water content to approximately the same value, although it is not a strictly defined drying condition. The corresponding temperature on a TG curve obtained in dry and $CO_2$-free $N_2$ at 10 K $min^{-1}$ is about 145°C, but depends on the rate of gas flow and design of the apparatus. Water retained in pastes subjected to D-drying or equivalent procedures is known as 'non-evaporable' water. Contrary to some statements in the literature, it is not a measure of chemically bound water, as much water is lost from interlayer spaces under these conditions. It can nevertheless be used as an empirical measure of the degree of reaction. Typical values in the literature for the water contents of fully reacted $C_3S$ pastes dried by these procedures are 20·4–22·0% (O11), corresponding to C–S–H compositions of $1{\cdot}7CaO \cdot SiO_2 \cdot 1{\cdot}3–1{\cdot}5H_2O$.

Powers and Brownyard (P20) called the water lost from the C–S–H on passing from the saturated to the D-dry condition 'gel water'. It comprises part of the pore water plus an arbitrarily defined fraction of the interlayer water. Whatever procedure is used to dry or equilibrate a paste, $CO_2$-free conditions are essential, and the amount of water retained can be obtained accurately only if the ignition loss and $CO_2$ content are also determined. Calculations based on the initial w/s ratio are often unreliable due to changes in the water content during curing.

### *5.2.3 Density and infrared spectra*

The density of C–S–H gel depends on the water content. For strongly dried samples, it also depends on how the solid volume is defined, causing observed values to vary with the fluid used in their determination. Widely differing values can be equally meaningful, but for a given application the appropriate one must be used. Since the C–S–H of $C_3S$ or $\beta$-$C_2S$ pastes is

mixed with CH, it is necessary to correct for this phase ($D = 2242\,kg\,m^{-3}$) or to remove it. Ramachandran (R15) described a way of doing this.

At about 11% RH on first drying, the interlayer spaces are full of water and larger spaces are empty; $H_2O/SiO_2$ is approximately 2·0 (Section 5.2.2). Using helium pyknometry, Feldman (F19) obtained values of 2350–2360 $kg\,m^{-3}$ for fully reacted $C_3S$ pastes; correction for CH gave 2430–2450 $kg\,m^{-3}$ for the C–S–H. Determinations on C–S–H samples made by hydrating $C_3S$ in suspension showed that substitution of methanol or aqueous CH for helium as the fluid had no significant effect on the result. For a fully hydrated $C_3S$ paste with w/s = 0·4 from which the CH had been removed, Hansen (H28) found 2180 $kg\,m^{-3}$. For all these values, empty pores are excluded from the solid volume.

The C–S–H present in a saturated paste is assumed to include that part of the porosity, and its content of water, without which it cannot be formed. The $H_2O/SiO_2$ ratio is approximately 4·0. Assuming the water in excess of that present at 11% RH to have a density of 1000 $kg\,m^{-3}$, Hansen (H28) calculated the density of the C–S–H to be 1850–1900 $kg\,m^{-3}$. This value is near the values of 1900–2100 $kg\,m^{-3}$ for cement pastes under saturated conditions (P20), if allowance is made for the CH and other hydrated phases that they contain.

Helium pyknometry of D-dried samples has given values of 2320–2350 $kg\,m^{-3}$ for $C_3S$ pastes (F19) and of 2440 $kg\,m^{-3}$ for cement pastes (P20); correction for CH and other phases suggests values of 2400–2500 $kg\,m^{-3}$ for the C–S–H. For a $C_3S$ paste with w/s 0·4 from which the CH had been removed, Hansen (H28) found 2390 $kg\,m^{-3}$. With D-dried samples, methanol gives results similar to helium, but water or CH solution gives much higher values, Brunauer and Greenberg (B52) obtaining values around 2860 $kg\,m^{-3}$, after correction for CH, for the C–S–H of $C_3S$ or $\beta$-$C_2S$ pastes. Determinations using water on D-dried cement pastes, based on the difference between the masses of the D-dried and saturated materials, typically give values, uncorrected for CH and other phases, of 2500–2600 $kg\,m^{-3}$. Relis and Soroka (R16) found these to increase with the degree of hydration, an upper limit of 2700 $kg\,m^{-3}$ being found for a specific cement.

Feldman (F19) explained the difference between the values for D-dried samples obtained with aqueous and other fluids. When the material is dried, the layers partially collapse, and some empty spaces remain between them. Water penetrates into these spaces, and the density obtained, after correction for CH and any other phases present, is that of the layers themselves. Organic liquids do not penetrate, and helium penetrates only slowly. The empty interlayer space is counted as part of the solid volume, with a consequent decrease in the measured density.

The IR absorption spectra of pastes of $C_3S$, alite, or $\beta$-$C_2S$ (H29,L20,S50), are relatively diffuse, as would be expected from the poor crystallinity. Si–O stretching is represented by a single, broad band peaking at about 970 $cm^{-1}$; this is compatible with the existence of condensed silicate anions. Small amounts of carbonate are readily detectable by the absorption near 1400 $cm^{-1}$.

## 5.3 Microstructure, microanalysis and electron diffraction

### 5.3.1 Microstructure

The first effective studies of microstructural development in calcium silicate pastes were made using light microscopy of thin sections (B53). They showed that the CH grows from relatively few centres in the water-filled space, where it forms isolated masses typically some tens of micrometres in size. Much more CH is observed with $C_3S$ than with $\beta$-$C_2S$. At the same time, gel forms around the anhydrous grains and spreads into the remainder of the water-filled space. Early TEM examinations of ground and redispersed material showed the presence of acicular and rounded, platey particles, but could not show where these came from in the microstructure (C22,G43). SEM studies of fracture surfaces (C23,D16,G44,W19) confirmed these conclusions and showed also that the gel formed in situ from the larger anhydrous grains, called 'inner product', differed in texture from the 'outer product' formed in the water-filled space. It was massive and seemingly almost structureless, whereas the outer product appeared to form columns or fibres radiating from the anhydrous grains.

Diamond (D16) distinguished four morphological types of C–S–H gel visible by SEM on fracture surfaces of cement pastes; similar forms have been observed in calcium silicate pastes (Fig. 5.5). Type I, prominent at early ages, was the fibrous material, the fibres being up to about 2 $\mu$m long. Type II, described as forming honeycombs or reticular networks, was considered to be very rare in pure calcium silicate pastes, but later work showed that material resembling it is a normal early product. Type III, prominent in older pastes, was more massive and appeared to consist of tightly packed equant grains up to 300 nm across. Type IV, still more featureless and massive, was the inner product, and was also observed in older pastes.

SEM of fracture surfaces has provided valuable information, but its utility is lessened by the inherently unrepresentative nature of a fracture surface and by the effects of dehydration in the high vacuum of the instrument. Further information has come from the use of other techniques, especially high-voltage transmission electron microscopy (HVTEM) with environmental or 'wet' cells to reduce water loss (D17,G45,J12), examination of ion-thinned sections by TEM or scanning transmission electron microscopy (STEM) (D18,G39,R17,V4), and backscattered electron imaging (BEI) of polished sections with detectors that minimize contrast due to topography and maximize that due to compositional differences (S35,S37,S49). Scrivener and Pratt (S51) briefly described these techniques. Other methods have included X-ray imaging of polished surfaces (T20), SEM of polished surfaces impregnated and etched to reveal porosity (J13,J14) and use of a cryo stage in the SEM to avoid dehydration (B54). Each of these methods has its own limitations, but together they have yielded a reasonably clear picture.

### 5.3.2 Stages in microstructural development

Jennings *et al.* (J11) distinguished three principal stages of product formation in $C_3S$ pastes: an early product formed during the first 4 h, a

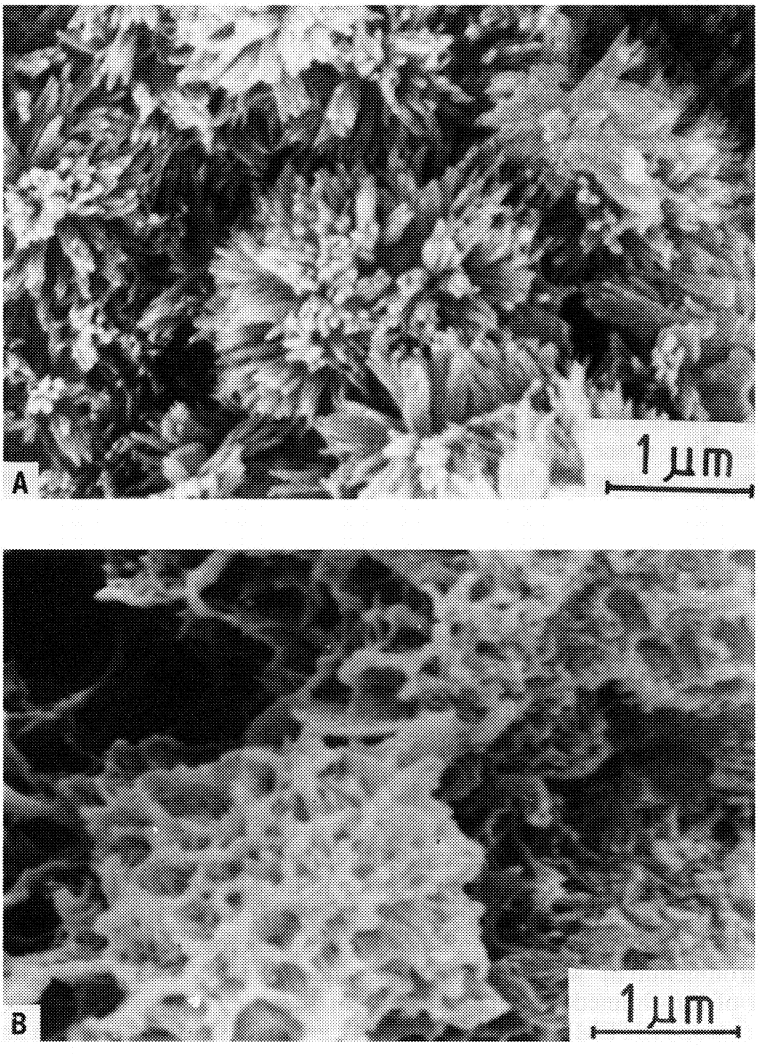


**Fig. 5.5** *(A,B) Types I and II C–S–H respectively (SEM of fracture surfaces, courtesy K.L. Scrivener). (C,D) SEM/STEM pair of ion-beam thinned section, showing Type III C–S–H (top, right) and Type IV C–S–H (top, left and bottom, right; J11). (A) is of an ordinary Portland cement paste, w/c = 0·5, aged 10 h. (B) is of a paste of an oil well cement, w/c = 0·44, with 2·4% of $CaCl_2$ on the mass of cement, aged 1 day. (C) and (D) are of a $C_3S$ paste, w/c = 0·47, aged 330 days.*

middle product formed at 4–24 h, and a late product formed subsequently. Several workers studying the hydration of $C_3S$ in pastes or compacted powders placed in water have described the early product as consisting of foils, flakes or honeycombs, which appear to exfoliate from the $C_3S$ surface,

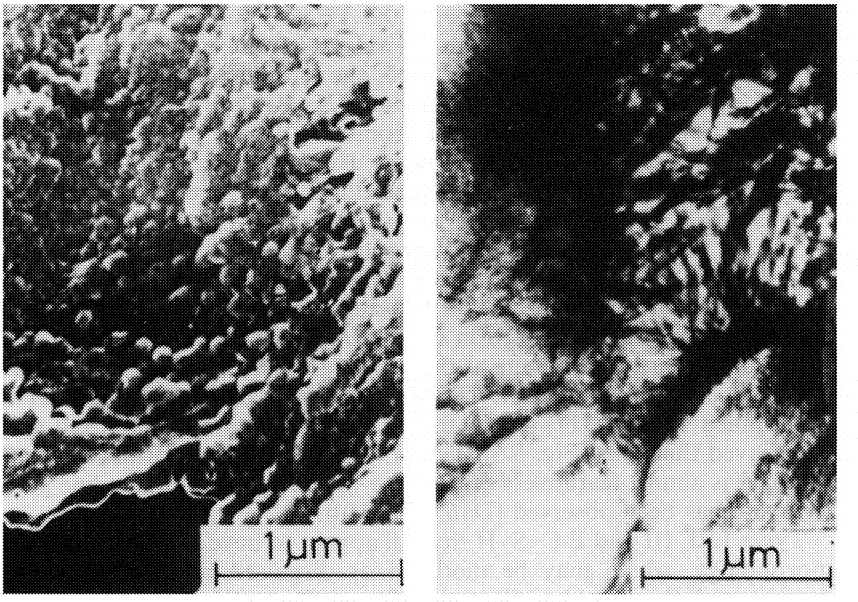


**Fig. 5.5** *(continued)*

probably together with some CH (F20,G40,H30,J11,M48,M49,S52). The honeycomb material is similar to 'Type II' C–S–H, and the foils have also been called 'Type E' C–S–H (J11). On drying, they collapse, crumple or roll up, forming fibres (J11). Broadly similar results have been obtained for $C_3S$ hydrated in CH solution (M49) or in the presence of gypsum (M50), sodium silicate or sodium aluminate (J15). The early hydration of $\beta$-$C_2S$ appears to follow a similar course to that of $C_3S$, but reaction is slower and begins preferentially at grain boundaries and exsolution lamellae (G45,M51).

The $C_3S$ surfaces are attacked unevenly (H30,M48,M49). Ménétrier *et al.* (M48,M49) reported that the first detectable product consisted of minute particles, some of which were probably CH. Continuous layers of product appear to be formed only at w/s ratios above those of normal pastes (G40,G46,L19). Ings *et al.* (I10) placed single crystals of $C_3S$ in an alite slurry with w/s = 2, and later removed them for SEM examination. A layer of apparently structureless material built up to a thickness of 5 $\mu$m in 30 min, together with cryptocrystalline CH; this later shrank, and acicular outgrowths were formed. The product layer contained aluminium, and had thus formed in part from the surrounding alite.

The middle stage of hydration is characterized by rapid formation of C–S–H and CH. In fracture surfaces of calcium silicate pastes, Type I C–S–H is prominent. Fibrillar material is also seen as the outer product

in ion-thinned sections examined in the TEM (G39). These fibrous or fibrillar materials may nevertheless be, at least in part, artefacts of drying. Unless a wet cell or cryo stage is used, the fine microstructure is much altered by dehydration in the instrument (J11,S53). HVTEM using wet cells (S37,S54) showed the undried product at 1 day to consist of foils, with no evidence of fibrillar outgrowths. However, localized drying may occur in any paste even before it is placed in a high vacuum, due to local exhaustion of water. The water is lost initially from the wider pores, which are probably represented disproportionately on fracture surfaces. The state of the cement paste in a practical concrete may thus vary on both a macro and a micro scale between dry and saturated. Fibrillar material is also reported to form during fracture (J11).

The characteristic products of the late stage of hydration are Types III and IV C–S–H and more CH. STEM examination of Type III material in ion-thinned section (J11) shows that it, too, consists of interlocked and interleaved thin foils (Fig. 5.5). Type IV material, which forms the inner product, is almost featureless even at the 100 nm level, though a fine pore structure has been observed (D16,G39,G40).

Types I, II, III and E C–S–H thus all appear to have an underlying foil morphology, which may be modified or disguised by compaction or drying, and this could well apply also to Type IV. The pastes may therefore contain only one type of C–S–H at the nanometre level. Against this, a less structured form of C–S–H has been observed as the very first product at high w/s ratios. A similar material, described as a viscous, gelatinous product and called 'Type 0' C–S–H', has also been reported to precede the formation of the other varieties in the middle stage of hydration (J11).

BEI of pastes of $C_3S$ mixed with $C_3A$ shows that no spaces develop between the hydrating $C_3S$ particles and the surrounding hydrate (S53). In this respect, $C_3S$ differs from Portland cement (Section 7.2.3).

### 5.3.3 *X-ray microanalysis*

Taylor and Newbury (T20) reviewed X-ray microanalysis (SEM or EPMA) studies of polished sections of mature $C_3S$ or $\beta$-$C_2S$ pastes and reported new results. The pastes show well-defined regions of C–S–H and CH. The Ca/Si ratios found for the C–S–H vary irregularly from point to point and increase with the voltage used to accelerate the electrons. As in all analyses of heterogeneous materials by this method, the choice of voltage rests on a compromise: it must be high enough to excite all the elements adequately, but low enough to produce an interaction volume sufficiently small that single phases can be analysed. The mean or median Ca/Si ratios reported for $C_3S$ pastes range from 1·4 at 6 kV to around 2·0 at 25 kV. It is questionable whether 6 kV is sufficient to ensure satisfactory analysis for Ca, and at 25 kV the volume analysed, taking into account the effect of porosity, is several micrometres in each direction, which may be too large to ensure absence of CH or unreacted $C_3S$. Working at 10 kV, Taylor and Newbury obtained mean values of 1·72 and 1·78 for mature pastes of $C_3S$ and $\beta$-$C_2S$, respectively. The range of values

was approximately 1·5–2·0 in both cases. The mean values are near to those obtained using the indirect methods described in Section 5.2.1.

The totals obtained in SEM or EPMA microanalyses of C–S–H in $C_3S$ or $\beta$-$C_2S$ pastes, after including oxygen equivalent to the calcium and silicon, should in theory fall below 100% by an amount equal to the water content under the conditions existing during the analysis, i.e. high vacuum and electron bombardment. The evidence from thermal dehydration and intensive drying at room temperatures (Section 5.2.2) indicates that this content is unlikely to exceed about 15% on the mass of material analysed, implying an analysis total of at least 85%. The totals are sometimes as high as this, but are more often 70–75%, and sometimes even lower (T20). A similar effect is observed with the C–S–H of cement pastes (Section 7.3.5), and appears to increase with the porosity of the region analysed. It has not been fully explained, and more than one cause may operate. Possibilities include retention of organic liquids used in preparing the polished section, carbonaceous residues formed under the action of the electron beam, superficial carbonation (R18) and loss of energy of the incident electrons through some ill-understood effect during passage through microporous material (H31).

### *5.3.4 Analytical electron microscopy*

X-ray microanalysis in transmission, also called analytical electron microscopy, allows regions in the order of tens of nanometres long in each direction to be analysed. Existing techniques give atom ratios but not absolute contents of individual elements. Early studies on ground and redispersed samples of $C_3S$ and $\beta$-$C_2S$ pastes (G47,M46) indicated variability of Ca/Si ratio on a micrometre scale, with ranges of 1·2–2·0 for $C_3S$ pastes and 1·1–1·6 for $\beta$-$C_2S$ pastes and means of 1·5 and 1·4 respectively. In a study using ion-thinned sections, Groves *et al.* (G39) found that a high-resolution probe caused the apparent Ca/Si ratio to decrease with time. The problem was avoided by scanning a 5 $\mu$m square raster, or by using a high voltage TEM, which gave a spot size of comparable dimensions. The mean values of Ca/Si thus obtained, for three groups of analyses, were 1·66–1·93, and the earlier values of 1·4–1·5 are probably incorrect. The marked local variability of Ca/Si ratio was confirmed. No significant compositional differences were observed between 'inner' and 'outer' products (Section 5.3.1). Crystals approximately 100 nm in size, identified by electron diffraction as calcite, were present.

A later study by Richardson and Groves (R17) on pastes of $C_3S$ and of cement showed that, at early ages, the range of Ca/Si ratios is typically 1·2–2·3 and that the distribution tends to be bimodal. As the pastes aged, the bimodal tendency disappeared and the spread of values slowly narrowed. With both $C_3S$ and cement, the mean Ca/Si ratio remained near 1·75 at all ages from 1 day onwards. Pastes aged up to 3·5 years for cement and 26 years for $C_3S$ were studied; in the 26-year-old $C_3S$ paste the range of Ca/Si ratios was approximately 1·60–1·85, with a modal value of 1·78. The C–S–H of the cement pastes contained small proportions of Al and other elements (Section 7.3.5).

Henderson and Bailey examined ground and redispersed $C_3S$ pastes (H30). They confirmed the wide local variability of Ca/Si ratio, and at 7 h obtained evidence of several distinct ranges between overall limits of 0·8–2·1. From 3 h onwards, there was evidence of structural variability, most of the material appearing amorphous but with regions of a more nearly crystalline appearance. Most of these were about 3 nm in longest dimension, but some were up to 5 nm × 15 nm, and were apparently composed of smaller segments of 3 nm dimensions. From a study of ion-thinned sections in the TEM, Viehland *et al.* (V4) also reported marked local variability both in the Ca/Si ratio and in the degree of crystallinity, with nanocrystalline regions some 5 nm across embedded in a matrix of seemingly amorphous material. Lattice imaging effects from the nanocrystalline regions were described. Most of Viehland *et al.*'s data were obtained from pastes cured at 80°C and subsequently stored at room temperature for approximately 5 years, but similar results were given by 8-month-old pastes cured at room temperature. The authors concluded that the strong local variations in composition and the slowness of long-range diffusion prevented the formation of nanocrystalline regions larger than about 5 nm.

### *5.3.5 Electron diffraction*

Attempts to obtain selected-area electron diffraction patterns from the C–S–H for calcium silicate or cement pastes have usually failed, but, occasionally, particles present in ground and redispersed material have yielded poorly defined patterns (C24,G43). These patterns are consistent with the XRD pattern (Fig. 5.1). Some have resembled patterns from tobermorite and others patterns from jennite (T21). These two crystalline calcium silicate hydrate phases are described in Section 5.4. A claim to have identified highly crystalline varieties of C–S–H in $C_3S$ pastes by electron diffraction (M52) was shown to be unsound (G48).

In the study mentioned in the previous section, Viehland *et al.* (V4) obtained both powder and preferred orientation electron diffraction patterns from the C–S–H of ion-thinned sections of cement pastes. The powder patterns were similar to those given by XRD and the preferred orientation patterns were broadly similar to those obtained by the previous workers (C24,G43). Inclusions of CH were identified by composition and diffraction pattern. Some of the nanocrystalline regions also yielded optical diffraction patterns, which were broadly similar to those obtained by electron diffraction.

## 5.4 More highly ordered phases related to C–S–H gel

### *5.4.1 General*

The XRD patterns given by the C–S–H gel of calcium silicate or cement pastes, of which that shown in Fig. 5.1 is typical, show that no long-range order exists in their structures. Such terms as 'crystal chemistry' or 'crystal structure' are therefore inapplicable to the material as a whole, and the term 'nanostructure' is more appropriate for describing the structure at this level. Because C–S–H gel is almost amorphous, currently

available techniques of X-ray diffraction have given only very general indications of its nanostructure. Slegers *et al.* (S50) described an early attempt to interpret the radial distribution function.

The first indications of the main features of the nanostructure of C–S–H gel (B55) were obtained from comparisons with crystalline calcium silicate hydrates, of which about 30 are known. It was considered that the local structures in C–S–H gel might resemble those in one or more of these crystalline compounds, the relationship thus being similar to that between vitreous silica and cristobalite.

The calcium silicate hydrate that appears to be thermodynamically stable in the presence of water and CH at ordinary temperature and pressure is afwillite ($C_3S_2H_3$) (L21). It has been prepared from $C_3S$ by ball-milling with water at ordinary temperature (K15) or by seeding (D19), but shows no similarities to C–S–H gel and nothing resembling it can be found in normal cement pastes. Two other crystalline phases that can be prepared in aqueous suspensions at temperatures somewhat below 100°C show much closer relationships. These are 1·4 nm tobermorite ($C_5S_6H_9$ approx.) and jennite ($C_9S_6H_{11}$). As will be shown below, the structures of both are based on layers derived from those in CH by substantial distortions of the Ca–O layer and replacement of some or all of the hydroxyl ions by silicate. The peaks in the XRD pattern of C–S–H gel in the region of 0·3 nm and near 0·18 nm correspond to important repeat distances in the Ca–O parts of these structures and also of CH (Fig. 5.2).

Reactions bringing together calcium and silicate ions in aqueous suspensions at ordinary temperature normally produce products which are intermediate in crystallinity and other respects between C–S–H gel and these crystalline phases. The most clearly defined of these semi-crystalline phases are C–S–H(I) and C–S–H(II), which are structurally imperfect foms of 1·4 nm tobermorite and jennite respectively. Contrary to some statements in the literature, these materials differ markedly in several respects from the C–S–H gel formed in cement or calcium silicate pastes, and should not be confused with it. From the compositional standpoint, jennite and C–S–H(II) are closer to C–S–H gel than are 1·4 nm tobermorite and C–S–H(I). On the other hand, 1·4 nm tobermorite and C–S–H(I) form more readily. A gelatinous calcium silicate hydrate, called plombierite, occurs in nature. It is of variable composition; some specimens resemble C–S–H(I) and others are probably closer to C–S–H gel (M53).

### *5.4.2 1·4 nm tobermorite*

1·4 nm tobermorite has a layer structure and the prefix refers to the layer thickness. On being heated at 55°C, it loses interlayer water and undergoes unidimensional lattice shrinkage, giving 1·1 nm tobermorite ($C_5S_6H_5$ approx.), often called, simply, tobermorite. 1·4 nm tobermorite occurs as a natural mineral (F21) and may be synthesized from CH and silicic acid in suspensions at 60°C (H32,K16). Table 5.3 gives crystal data. The crystal structure has not been determined, but may be inferred from that

**Table 5.3** *Crystal data for 1·4 nm tobermorite, jennite and related phases*

| Phase | 1·4 nm tobermorite | C–S–H(I) | Jennite | C–S–H(II) |
|---|---|---|---|---|
| *Molar ratios* | | | | |
| CaO | 5 | 5 | 9 | 9 |
| $SiO_2$ | 5·5 | 5 | 6 | 5 |
| $H_2O$ | 9 | 6 | 11 | 11 |
| *Pseudocell parameters* | | | | |
| $a$ (nm) | 0·5624 | 0·560 | 0·996 | 0·993 |
| $b$ (nm) | 0·3670 | 0·364 | 0·364 | 0·364 |
| $c$ (nm) | 2·797 | 2·5 | 2·136 | 2·036 |
| $\alpha$ | 90·0° | 90·0° | 91·8° | 90·0° |
| $\beta$ | 90·0° | 90·0° | 101·8° | 106·1° |
| $\gamma$ | 90·0° | 90·0° | 89·6° | 90·0° |
| Lattice type | I | I | A | A |
| $Z$ | 1 | 1 | 1 | 1 |
| $D_x$ (kg m$^{-3}$) | 2224 | 2250 | 2332 | 2350 |
| Reference | F21,T5 | T5,T22 | G49,T5 | G50,T5 |

All data are for the pseudocells and compositions stated· The true cells have doubled values of $b$ and can be in varying degrees disordered; $a$ and $c$ must often be differently defined· The structure of C–S–H(I) has little more than two-dimensional order, and that of C–S–H(II) has less than full three-dimensional order.

of 1·1 nm tobermorite (H33,M54), aided by evidence from dehydration and IR studies (F21), broad-line proton NMR and chemical determination of silicate anion type (W20) and $^{29}$Si NMR (C25,K17,W21). Each layer consists of a central part of empirical formula $CaO_2$, of which all the oxygen atoms are shared with Si–O chains, which form ribs covering each surface. Between these layers are water molecules and additional calcium atoms (Fig. 5.6). Some of the water molecules are also bonded to the calcium atoms in the central part of the layer. The idealized constitutional formula is possibly $Ca_5(Si_6O_{18}H_2)\cdot 8H_2O$, but the atomic contents of the unit cell in the natural mineral show that only 5·5 silicon atoms are present where 6 would be expected (M55), and synthetic studies also indicate that the Ca/Si ratio is higher than 0·83 (H32). Many silicate tetrahedra appear to be missing from the chains, and the actual formula may be nearer to $Ca_5Si_{5.5}O_{17}H_2\cdot 8H_2O$, corresponding to a mean chain length of 11 tetrahedra. A conclusion from $^{29}$Si NMR (K17) that little Si–OH is present is not supported by later work (C25).

The Ca–O parts of the layers have a pseudohexagonal, centred lattice with $a = 0{\cdot}56$ nm, $b = 0{\cdot}36$ nm, and may be regarded as layers of CH extremely distorted due to replacement of their OH groups by the silicate chains, the O–O distances of which have to be respected. CH, referred to orthogonal axes, has $a = 0{\cdot}62$ $(0{\cdot}36\sqrt{3})$ nm, $b = 0{\cdot}36$ nm. The Si–O chains are of a type called dreierketten, i.e. they are kinked so as to repeat at intervals of three tetrahedra. This conformation is imposed by the

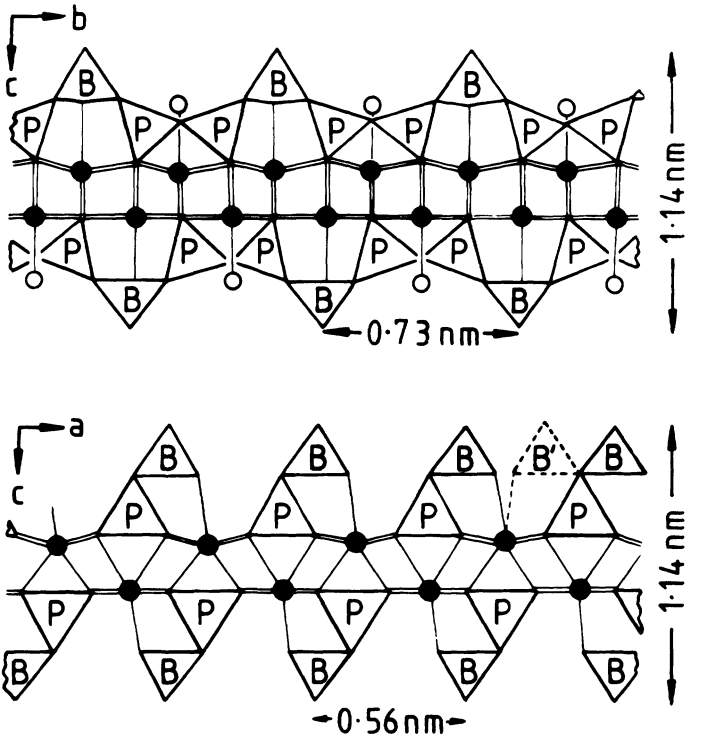


**Fig. 5.6** *Parts of the structure of a single layer of 1·4 nm tobermorite in bc- and ac-projections, based on the results of H33 for the 1·1 nm form. Solid circles represent calcium atoms, open circles $H_2O$ molecules, and P and B paired and bridging tetrahedra, respectively. In the bc-projection, only one-half of the cell in the direction of the a-axis is shown, and interlayer calcium atoms and $H_2O$ molecules other than those coordinated to the calcium atoms in the central part of the layer are omitted. In the ac-projection, the chains are seen end-on; B' represents a set of alternative positions for the bridging tetrahedra, made possible by disorder, and all $H_2O$ molecules and interlayer Ca atoms are omitted. From T23.*

coordination requirements of the calcium ions, and occurs in many crystalline calcium silicates. In 1·4 nm tobermorite, they are single, i.e. not condensed with other dreierketten to form double chains or more complex structures, and have the empirical formula $Si_3O_9H$. 1·1 nm tobermorite differs from 1·4 nm tobermorite in having lost some of its interlayer water molecules. Depending on how it is formed, it may or may not contain interlayer Si–O–Si linkages, which, if present, cause the single chains to be replaced by double chains (Section 11.7.4).

### 5.4.3 *Jennite*

Jennite ($C_9S_6H_{11}$) occurs as a natural mineral (C26,G49), and, like 1·4 nm tobermorite, may be synthesized from CH and hydrous silica in aqueous

suspensions below 100°C (C25,G51,H34,H35). In nature, it occurs in contact with 1·4 nm tobermorite (C26), with which it is probably in metastable equilibrium. Like 1·4 nm tobermorite, it has a layer structure, and at 70–90°C loses water with unidimensional lattice shrinkage, giving metajennite ($C_9S_6H_7$)(C26,H34). The layer thickness is 1·05 nm for jennite and 0·87 nm for metajennite (G49). Table 5.3 includes crystal data for jennite. The crystal structure has not been determined, but its major features may be inferred from the crystal data, dehydration behaviour, IR spectra and other evidence (C26,H34), which suggest that the constitutional formula is probably $Ca_9(Si_6O_{18}H_2)(OH)_8 \cdot 6H_2O$. Recent NMR evidence supports the conclusions that single dreierketten are present and that some silicon atoms carry OH groups (C25).

The structure almost certainly resembles that of 1·4 nm tobermorite, but with two important differences. One is that, for a given number of calcium atoms in the central part of the layer, there are only half as many silicate chains, the other half being replaced by hydroxyl ions. Possibly, silicate chains alternate with rows of hydroxyl ions on both sides of the layer. The other is that the central, Ca–O part of the layer is distorted from that in CH in a way that differs from that in 1·4 nm tobermorite. This follows from the different repeat distance in the direction perpendicular to the chains, which is 1·0 nm compared with 0·56 nm for 1·4 nm tobermorite. For the Ca–O part of the structure, this repeat distance is probably 0·50 nm in jennite, and thus shorter than that in 1·4 nm tobermorite, suggesting that the Ca–O part of the layer in jennite may be corrugated. The structure of metajennite is presumably derived from that of jennite by the omission of some of the interlayer water molecules.

### *5.4.4 C–S–H(I)*

Reaction between hydrous silica and CH in aqueous suspension at ordinary temperature gives a product called C–S–H(I), first adequately described by Zur Strassen and Strätling (Z11) and more fully by Taylor (T22). Similar but often less crystalline products are formed by mixing solutions of sodium silicate and calcium salts, or under certain conditions from $C_3S$ (B56,G52,J16,T22), and also as intermediate products of hydrothermal reactions at temperatures up to at least 180°C. C–S–H(I) is considerably more ordered than the C–S–H gel formed in calcium silicate or Portland cement pastes at ordinary temperature, but has been detected in pastes made from alkali-activated slag (Section 9.2.9). Pastes or suspensions made from Portland cement and reactive forms of silica, especially those cured at elevated temperatures, also give a product similar to C–S–H(I) under certain conditions (Section 11.7.2).

Table 5.4 gives the XRD powder pattern of a relatively highly ordered specimen of C–S–H(I). It consists largely of the hk0 reflections, or hk band heads, of 1·4 nm tobermorite, together with a broad, basal reflection. This last, which is absent in less ordered forms, corresponds to the mean layer thickness. C–S–H(I) may be prepared with Ca/Si ratios varying from 0·8 to about 1·5. Some recent studies have indicated minimum Ca/Si ratios of 0·6–0·7 (C27,G51). With increase in Ca/Si ratio,

**Table 5.4** *X-ray powder diffraction data for C–S–H(I)*

| $d$ (nm) | $I_{rel}$ | hkl | $d$ (nm) | $I_{rel}$ | hkl | $d$ (nm) | $I_{rel}$ | hkl | $d$ (nm) | $I_{rel}$ | hkl |
|---|---|---|---|---|---|---|---|---|---|---|---|
| 1·25 | vs | 002 | 0·24 | w,d | ? | 0·152 | vw | 22· | 0·111 | w | 42· |
| 0·53 | vvw | 10 1 | 0·21 | w,d | ? | 0·140 | w | 40· | 0·107 | vw | 51· |
| 0·304 | vs | 11· | 0·185 | s | 02· | 0·123 | vw | ? | | | |
| 0·280 | s | 20· | 0·167 | mw | 31· | 0·117 | vw | 13· | | | |

Pattern is for a relatively highly crystalline variety; all peaks are broad. s = strong, w = weak, m = moderately, v = very, d = diffuse. Indices relate to pseudocell in Table 5.3; hk· denotes a band head given by an essentially two-dimensional lattice (T24).

the degree of crystallinity tends to decrease, and the basal spacing, if present, also decreases, from about 1·3 nm at Ca/Si = 0·8 to about 1·1 nm at Ca/Si = 1·3 (T24). Later work showed also that, with increase in Ca/Si ratio, the repeat distance in the chain direction $b$ decreases while that in the plane of the layers and perpendicular to the chains $a$ increases (C27). The basal spacing also decreases on heating, values of 0·91–1·13 nm being obtained at 108°C (T25). TEM shows C–S–H(I) to consist of crumpled foils a few nanometres thick, with a tendency to elongation or fibrous character at the higher Ca/Si ratios (G43). These data show that C–S–H(I) is a structurally imperfect form of 1·4 nm tobermorite, with little or no more than two-dimensional order, i.e. each particle consists of a small number of layers that are relatively well-formed, and in approximately the same orientation in their own plane, but the distances between them are somewhat irregular. The cause of the high and variable Ca/Si ratio is described in Section 5.6.1.

DTA curves of C–S–H(I) preparations show endotherms at 100°–200°C and exotherms at 835°–900°C, the latter temperature increasing with Ca/Si ratio (K18). Curves have also been reported for apparently similar materials described as C–S–H(di,poly), formed at higher temperatures (S55). Solvents that dissolve lime, such as ethyl acetoacetate, have little action on preparations with Ca/Si ratios of 1·25–1·33, but remove CaO from ones of higher Ca/Si ratio until that composition is reached (K18,S55).

### 5.4.5 *Products formed in suspensions from $C_3S$ or $\beta$-$C_2S$; C–S–H(II)*

Many studies have been reported on the hydration of $C_3S$ or $\beta$-$C_2S$ in aqueous suspensions, often termed 'bottle hydration'. If the reaction is prolonged, so that no unreacted starting material remains, and the w/s ratio is sufficiently high that enough CaO is dissolved to lower the Ca/Si ratio of the product to below about 1·5, the product is C–S–H(I), essentially similar to that obtained by other methods (T22). At lower w/s ratios, such that the product contains CH, the C–S–H is usually similar in composition and crystallinity to that formed in pastes (F17). The products of bottle hydration for short times, such that unreacted starting material remains, are discussed in Sections 5.8.1 and 5.8.2.

**Table 5.5** *X-ray powder diffraction data for C–S–H(II)*

| $d$ (nm) | $I_{rel}$ | hkl | $d$ (nm) | $I_{rel}$ | hkl | $d$ (nm) | $I_{rel}$ | hkl |
|---|---|---|---|---|---|---|---|---|
| 0·96 | 85 | 002,100 | 0·312 | 100 | $\bar{1}13$ | 0·209 | 12 | 313(?) |
| 0·80 | 20 | $\bar{1}02$ | 0·307 | 95 | $\bar{3}04$ | 0·203 | 25 | $\bar{4}13,\bar{5}02,+$ |
| 0·48 | 12 | 004,200 | 0·294 | 90 | $\bar{2}11$ | 0·183 | 75 | $0\bar{2}0,\bar{4}17$ |
| 0·358 | 10 | 011 | 0·283 | 95 | $\bar{2}13$ | 0·1635 | 5 | $\bar{6}02$ |
| 0·340 | 12 | $\bar{1}11$ | 0·243 | 20 | $\bar{4}04,\bar{3}11,+$ | 0·1565 | 20 | $\bar{3}24,+$ |
| 0·335 | 25 | $\bar{3}02$(?) | 0·224 | 5 | $\bar{4}06$ | 0·1212 | 5 | 031 |
| 0·329 | 40 | 111,006 | 0·216 | 10 | 402(?) | 0·1174 | 5 | $231,\bar{8}15,+$ |

All peaks are broad; indexing, which relates to pseudocell in Table 5.3, is approximate as order is not fully three-dimensional. d = diffuse. Data are from P1, card 29–374, with peaks of $I_{rel} < 5$ omitted.

Under some conditions, prolonged reaction at room temperature gives a product differing from any of the above, which has been called C–S–H(II). This has been obtained from $C_3S$ by shaking with water and repeatedly replacing portions of the liquid with pure water until the bulk Ca/Si ratio has fallen to about 2·0 (T22) and by bottle-hydration of $\beta$-$C_2S$ (B52). C–S–H(II) has a Ca/Si ratio somewhat below 2·0, is seen in the TEM to consist of bundles of fibres (G43) and gives a characteristic XRD powder pattern (Table 5.5), which is different from that of C–S–H(I). The pattern shows similarities to that of jennite, and the unit-cell parameters, determined using electron diffraction, are also unlike those of 1·4 nm tobermorite or C–S–H(I) and near those of jennite (Table 5.3). C–S–H(II) appears to be a structurally imperfect form of jennite, related to it in the same way as C–S–H(I) is to 1·4 nm tobermorite, but somewhat better ordered (G50). Its Ca/Si ratio is higher than that of jennite; this resembles the situation for C–S–H(I) and 1·4 nm tobermorite, and is discussed in Section 5.5.4. Attempts to repeat these preparations of C–S–H(II) have failed, and the conditions under which the product is formed are obscure.

## 5.5 Silicate anion structure

### *5.5.1 Introduction*

It is noted in Section 5.4.2 that the Ca/Si ratios found for 1·4 nm tobermorite are higher than the idealized structure would suggest, apparently due to omission of $SiO_4$ tetrahedra from the structure. The Ca/Si ratios of most C–S–H(I) preparations and that of C–S–H(II) are higher than those of the crystalline phases (1·4 nm tobermorite and jennite respectively) of which they appear to be structurally imperfect forms, and that of C–S–H(I), at least, is variable over a considerable range. The Ca/Si ratio of the C–S–H gel of calcium silicate or cement pastes, which is approximately 1·75, is higher than that of jennite, and much higher than that of 1·4 nm tobermorite.

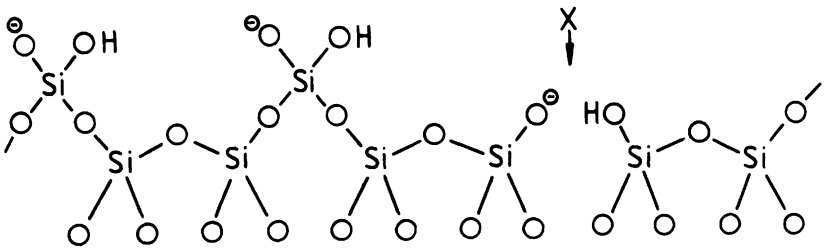


**Fig. 5.7** *Silicate chain of the type present in 1·4 nm tobermorite and jennite (dreierkette). In the tobermorite structure, and probably also in that of jennite, the oxygen atoms at the bottom of the figure are also part of a central $CaO_2$ layer. The tetrahedra in the lower row are described as paired and those in the upper row as bridging. A bridging tetrahedron is missing (at X). Suggested positions of hydrogen atoms and negative charges balanced by interlayer cations are included. From T21.*

An early study suggested that the increase in Ca/Si ratio in C–S–H(I) above that of tobermorite could arise from a combination of omission of tetrahedra from the chains and incorporation of additional calcium in the interlayer (T25). In a dreierkette (Fig. 5.7), the tetrahedra are of two types, which have been termed 'paired' and 'bridging'. In calcium silicate structures, the paired tetrahedra share oxygen atoms with columns of Ca–O polyhedra, which in 1·4 nm tobermorite, and by analogy also in jennite, are themselves condensed into Ca–O layers. If all the bridging tetrahedra are missing, a series of dimeric anions results. More generally, if some or all are missing, the theoretically infinite chain is split into fragments containing 2, 5, 8, ... $(3n - 1)$ tetrahedra (T21). This hypothesis was based on determinations of silicate anion structure, which are described in the sections that follow. It will be seen, however, that variations in the Ca/Si ratio of C–S–H, whether of pastes or more ordered varieties, cannot be wholly explained by omission of silicate tetrahedra.

### 5.5.2 *C–S–H gel of calcium silicate or cement pastes: chemical methods*

Chemical methods for determining the structures of the silicate ions have been based on either the kinetics of the reaction with molybdate (S56) or the preparation and characterization of trimethylsilyl (TMS) derivatives. In the TMS method, the sample is treated with a reagent that converts the silicate anions into the corresponding silicic acids, which then react further to replace Si–OH by $Si–OSi(CH_3)_3$. The resulting TMS derivatives can be identified and semi-quantitatively determined by various methods, of which the most widely used have been differential evaporation to isolate the higher molecular weight species, gas liquid chromatography (GLC) and gel permeation chromatography (GPC). It has to be assumed that conversion of the silicic acids into their TMS derivatives is sufficiently rapid to preclude side-reactions in which they are altered by hydrolysis or condensation. In practice, such side-reactions have never been totally eliminated, though the technique of Tamás *et al.* (T12) was

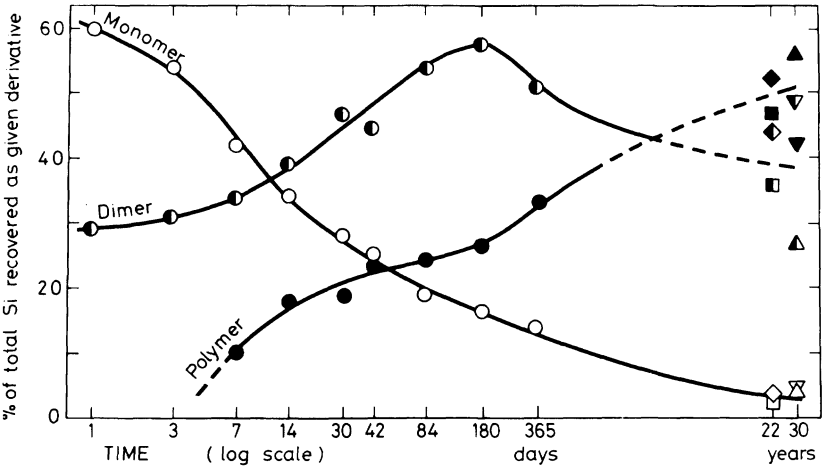


**Fig. 5.8** *Percentages of the total silicon in $C_3S$ or alite pastes recovered as monomer (open symbols), dimer (half-open symbols) and 'polymer' (closed symbols) by a trimethylsilylation method. Differently shaped symbols denote different $C_3S$ or alite specimens. From M56.*

a major advance on that originally used by Lentz (L22). Because of side-reactions, and because it is rarely possible to account for more than 80–90% of the total silicon, the absolute accuracy of percentages of individual anionic species is at best a few per cent.

In the remainder of this section, some of the results that are described relate to cement pastes, and are in general closely similar to those obtained for $C_3S$ pastes. Chemical formulae of silicate ions are written with negative charges and any attached hydrogen atoms omitted. Most of the chemical investigations on pastes hydrated for more than a few hours at 15–25°C have shown that any monomer ($SiO_4$) present is attributable within experimental error to unreacted $C_3S$, and that the products formed during the first few days contain dimer ($Si_2O_7$), which is first supplemented and later replaced by larger species, collectively called polymer (B57,D20,H36,L22,M56–M58,T12,W22). Subsequent NMR studies (Section 5.5.3) showed that a little monomer is also present in the hydration products at both early and late ages. Figure 5.8 gives typical results obtained by the TMS method. The percentage of the silicon present as dimer passes through a maximum at about 6 months, but even after 20–30 years it is still around 40%.

GLC, GPC, mass spectrometry and chemical analyses of TMS derivatives established the nature and size distribution of anion sizes within the polymer (D20,H36,M56,U10). From chemical analyses, one may calculate the mean connectivity of the $SiO_4$ tetrahedra, i.e. the number of other $SiO_4$ tetrahedra with which each one shares oxygen atoms; typical values are 1·6–2·0 (M56,M57). The anions are linear, with pentamer ($Si_5O_{16}$) the most important (after $Si_2O_7$) at all ages, the next most important being

linear octamer ($Si_8O_{25}$). As the paste ages, the mean size of the anions increases, this process continuing until long after all the $C_3S$ has reacted. At ages up to 6 months, the polymer fraction consists largely of pentamer and octamer, and even after 20–30 years these species account for a substantial fraction of the total silicon, though larger anions, containing some tens of tetrahedra, are also present (M56). These data are consistent with the $(3n - 1)$ sequence of chain lengths mentioned above.

Studies at 2–5°C have given divergent results. Two investigations suggested that the initial products contain substantial proportions of monomer (B57,S56), but later ones did not confirm this (H36,P21). With increase in temperature above ambient, condensation is increasingly rapid, and anions containing $\geq$100 tetrahedra are reportedly formed (B57,H36,S56). Early conclusions that admixtures such as $CaCl_2$ affect the degree of polymerization for a given degree of reaction of the $C_3S$ were not confirmed (H36). Early conclusions that the average size of the silicate anions in pastes increases on drying (B58,M59) were also not supported by later work (P21). The behaviour of $\beta$-$C_2S$ is similar to that of $C_3S$, apart from the rate of reaction (M57). A conclusion that three-dimensional cluster ions are formed (C28) is incompatible with observed connectivities and with the NMR evidence discussed below, and can probably be attributed to occurrence of side-reactions.

### 5.5.3 *C–S–H gel of calcium silicate or cement pastes: nuclear magnetic resonance*

$^{29}Si$ 'magic-angle spinning' (MAS) NMR complements the TMS method in several ways. It is a purely physical method, in which there is no possibility of altering the structure through side-reactions. Except with very young samples, no preliminary drying is needed. It gives different data, which relate directly not to the fractions of the silicon present in different anionic species, but to the local environments of individual silicon atoms. Quantitatively, it is more reliable than the TMS method. It has been applied mainly to pure calcium silicate pastes, because the substituent ions present in Portland cements cause the peaks in the spectra to be broadened.

The terms $Q^0 \ldots Q^4$ refer to the connectivities, $Q^0$ thus denoting isolated tetrahedra, $Q^1$ end-group tetrahedra (and thus including silicon present in $Si_2O_7$ groups), $Q^2$ middle groups, and so on. For $C_3S$ or $\beta$-$C_2S$ pastes, the content of $Q^0$ begins to decrease after a few hours, with formation of $Q^1$, later accompanied by $Q^2$; no $Q^3$ or $Q^4$ is detected (C29,C30,L23,R19–R21). This result is compatible with the formation of dimer, later accompanied by either single chains or rings, but not with that of double chains, clusters or more complex species. Clayden *et al.* (C29) found high correlations between the relative intensities of the $Q^0$ and $Q^1$ peaks in the NMR spectrum, the amount of CH indicated by TG and the cumulative heat evolution. After 23 years, a $C_3S$ paste had a $Q^1/Q^2$ ratio of 42/58, indicating a mean chain length of 4·8 tetrahedra (R20).

The TMS method is insufficiently precise to show whether the hydration products contain a small amount of monomer. Cross-polarization

magic-angle spinning (CPMAS) NMR can distinguish between silicon atoms that are near hydrogen atoms and ones that are not. This gives a strong, though not always unequivocal, indication as to whether silicon atoms in tetrahedra of a given connectivity carry OH groups. Monomer in a hydration product is almost certain to carry hydrogen, and can thus be distinguished from that in the anhydrous compounds. With one exception (Y6), the results have shown that the product formed in $C_3S$ pastes during the first few hours contains only monomeric ions, dimer beginning to form only later (B59,C30,R19,R21). The hydrated monomer accounts for some 2% of the total silicon at 24 h and remains detectable at 6 months (R19). Its formation agrees qualitatively with some of the results at low temperatures mentioned above (B57,S56). The hydrated monomer has been attributed to superficial hydration of the $C_3S$ (R21), or, alternatively, thought to occur either in a distinct phase or at defect sites in the C–S–H (B59).

Brough *et al.* (B59) described experiments which showed that rapid quenching of hydration with propan-2-ol followed by evacuation had no detectable effect on spectral line widths or chain lengths, and that the high stresses due to spinning had only minimal effect on the reaction. At 20°C, the mean chain length was approximately 2·4 at 50% hydration, 2·6 at 80% hydration and nearly 3·0 at 90% hydration; at 75°C, the corresponding values were approximately 2·6, 3·3 and 3·8. They also concluded from contents of $Q^1$ and $Q^2$ and maximum mean chain lengths that the polymerization of the silicate ions probably occurred through addition of monomer (i.e. separate tetrahedra) to form linkages between dimeric groups, which were thereby converted into pentamer, octamer and longer chains in the $(3n - 1)$ series.

Magic-angle spinning NMR has also been used to study the environments of hydrogen atoms (R21) and oxygen atoms (C30) in $C_3S$ or $\beta$-$C_2S$ pastes. The $^{17}O$ NMR showed the presence of OH groups attached to calcium and possibly also of OH groups attached to silicon.

### 5.5.4 C–S–H(I) and other products made in suspension

Stade and co-workers (S55,S57,S58) studied preparations of 'C–S–H (di,poly)', obtained in suspension at 80° or 150°C, and apparently similar to C–S–H(I). They used chemical methods and NMR. For Ca/Si ratios of 1·1–1·5, the anion-size distribution varied little with either Ca/Si ratio or temperature of preparation, 40–50% of the silicon being in dimeric and 50–60% in polymeric single-chain anions. Grutzeck *et al.* (G51), using NMR, obtained similar results for C–S–H(I) preparations having Ca/Si ratios of 1·1–1·3. At lower Ca/Si ratios, down to 0·71, they found the anions to be, essentially, long chains, as in 1·4 nm tobermorite; they concluded that a distinct phase change occurred at a ratio near 1·0. Damidot *et al.* (D21) studied products formed from $C_3S$ in very dilute suspensions. They obtained results similar to those of Grutzeck *et al.* (G51) and also concluded that a further phase change occurred at a Ca/Si ratio of 1·5. A preparation with an estimated Ca/Si ratio of 2·0 showed a $Q^1/Q^2$ ratio significantly higher than those with Ca/Si ratios of 1·0–1·5,

indicating a higher proportion of dimer. The formation of C–S–H with a Ca/Si ratio above 1·5 is explained by the use of $C_3S$ as the starting material. This material was possibly similar to the variety of C–S–H gel, containing mainly dimeric silicate ions, that is present in young pastes.

In contrast to these results, Cong and Kirkpatrick (C27) found only a continuous increase in $Q^1/Q^2$ ratio in C–S–H(I) preparations as the Ca/Si ratio increased over the range 0·8–1·5. Some preparations with Ca/Si ratios of 0·6–0·8 contained $Q^3$ in addition to the usual $Q^1$ and $Q^2$, which was believed to be present in the C–S–H and not in admixed hydrous silica.

Some other observations confirm the variability of C–S–H preparations of a given Ca/Si ratio. The silicate anion structures of C–S–H(I) preparations appear to be affected by how long the material remains in contact with its mother-liquor and by how strongly it is subsequently dried. Experiments using the molybdate method showed that the anions in precipitates obtained by mixing $CaCl_2$ and sodium silicate solutions at 0°C were mainly those present in the silicate solution, and were thus monomeric if the latter was sufficiently dilute (S57). By letting such products stand in contact with their mother-liquors at 0°C and drying at −10°C, preparations with Ca/Si ratios of 1·2–1·5 were obtained that contained only dimeric silicate anions. Another study, in which C–S–H preparations with Ca/Si ratios of 1·14–1·55 were obtained by mixing solutions high in $Ca^{2+}$ and in silicate, showed the anions to be almost entirely dimeric (M58).

Macphee *et al.* (M60) made an NMR study of C–S–H samples prepared in aqueous suspension. In preparations with Ca/Si = 1·8 that had been in contact with mother-liquor for 88 weeks the anions were almost wholly dimeric irrespective of drying condition between 10% and 50% RH, but in a preparation with Ca/Si = 1·1 that had been in contact with solution for only 4 weeks the ratio of $Q^2$ to $Q^1$ increased on drying. The C–S–H with Ca/Si = 1·8 thus differed in silicate anion structure from that of similar composition and age formed in $C_3S$ pastes. The authors suggested that, in freshly formed C–S–H, drying caused increased condensation. If the material was formed in suspension, the free supply of water ensured that little condensation beyond the stage of dimer occurred in the presence of mother liquor, and the aged material was less susceptible to the effect of drying. In a $C_3S$ or cement paste, the demand for water caused localized drying in the inner product, with consequent increase in condensation. The inner product could thus be less hydrated and more highly condensed than the outer product. In contrast to these results, Cong and Kirkpatrick (C31) concluded that reduction of the RH had little effect on the degree of condensation, though this was increased on heating at 110–200°C.

Gard and Taylor (G50) reported that studies of a C–S–H(II) preparation by the TMS and other chemical methods showed the silicate anions to be a mixture of $Si_2O_7$ groups and larger species, and concluded that this was compatible with the view that this material is derived from jennite by omission of silicate tetrahedra.

At Ca/Si ratios above about 1·5 it is impossible to obtain material giving the tobermorite-like XRD pattern of C–S–H(I). For such materials, there

are several possibilities. CH may be formed as a separate phase, as for example in the preparations studied by Cong and Kirkpatrick (C27). Less ordered material may be formed; this is the case in pastes of $C_3S$ or cement, or in the high Ca/Si preparations obtained in suspension such as those described by Damidot *et al.* (D21). Finally, conditions favouring the formation of an ordered structure can lead to the formation of C–S–H(II) or, at higher temperatures, jennite.

## 5.6 The nanostructures of C–S–H gel and related materials

### *5.6.1 Broad features and tobermorite-based models for C–S–H(I)*

In principle, increase in Ca/Si ratio above the theoretical value of 5 : 6 for 1·4 nm tobermorite could result from at least three types of modification to the structure, as follows.

(1) Omission of bridging tetrahedra, resulting in a decrease in chain length. As the evidence in the preceding sections shows, this plays a major role, both in the C–S–H gel of calcium silicate and cement pastes and in preparations obtained in suspensions, which are usually more highly ordered. This effect increases the Ca/Si ratio.

(2) Decreased content of Si–OH, balanced by increased content of interlayer calcium. For a tobermorite structure modified only by this effect, the limiting Ca/Si ratio would be 1·0, arising from the ionic constitution $[Ca_4(Si_6O_{18})]Ca_2 \cdot xH_2O$, where the material outside the square brackets is assumed to be in interlayer sites.

(3) Incorporation of additional $Ca^{2+}$ ions, balanced by $OH^-$. This is the effect responsible for the higher Ca/Si ratio of jennite as compared with that of 1·4 nm tobermorite. In both C–S–H(I) of the higher Ca/Si ratios and C–S–H gel formed in pastes, it is a major effect. Opinions differ as to whether it occurs through the incorporation of regions of jennite-type structure or by the substitution of silicate ions by hydroxyl in a less ordered fashion, within a structure essentially of tobermorite type.

Decrease in Ca/Si ratio below the theoretical value for 1·4 nm tobermorite might occur by increased content of Si–OH. This is the reverse of the effect descibed under (2) above, and the limiting Ca/Si ratio would be 0·67, arising from the constitution $[Ca_4(Si_6O_{18}H_4)] \cdot xH_2O$. A decrease to the same value could also occur through the presence of interlayer Si–O–Si linkages, which decrease the negative charge that has to be balanced by interlayer calcium. This effect is known to occur in one form of 1·1 nm tobermorite (Section 11.7.4). Cong and Kirkpatrick (C27) concluded that preparations with Ca/Si ratios below 0·8 contained $Q^3$ silicate tetrahedra, indicating the presence of interlayer linkages, and the spectrum of a preparation with Ca/Si 0·71 reported by Grutzeck *et al.* (G51) suggests the same conclusion.

Cong and Kirkpatrick (C27) concluded that, in their C–S–H(I) preparations, omission of bridging tetrahedra, variability in Si–OH content and the presence of OH groups attached to calcium all contributed to the

variation in Ca/Si ratio. Charge-balance calculations based on Ca/Si and $Q^1/Q^2$ ratios showed that the preparations with Ca/Si > 1·2 must contain Ca–OH and that those with Ca/Si < 1·2 must contain Si–OH. They indicated a minimum molar ratio of Si–OH to total Si of 0·43 at Ca/Si 0·88, decreasing to 0·13 at Ca/Si 1·56, and a molar ratio of Ca–OH to total Ca that was very low at Ca/Si ratios under 1·2, increasing to about 0·64 at Ca/Si 1·56. The Si–OH/Si ratio at Ca/Si 0·88 is distinctly higher than the theoretical value of 0·33 for 1·4 nm tobermorite. Such calculations can show only the minimum contents of Si–OH or Ca–OH, because additional protons attached to Si–O can be balanced by additional OH groups attached to $Ca^{2+}$.

The evidence from cross-polarization $^{29}Si$ NMR was compatible with the presence of Si–OH, but is not unequivocal because it shows only that the protons are near the Si, and not necessarily that they are bonded to it through oxygen atoms. Interpretation is further complicated by the fact that the protons are in rapid motion (C32). More definite information was obtained from $^{17}O$ NMR, which showed that both Si–OH and Ca–OH were present at all the Ca/Si ratios examined (0·7–1·5, ignoring CaO or $SiO_2$ present in admixed phases). The contents of both were higher than the minimum values calculated from the Ca/Si ratios and $^{29}Si$ NMR data (C33).

The existence of three different ways by which a given Ca/Si ratio higher than that of 1·4 nm tobermorite can be achieved may account for the differences between the results of different investigators. Very possibly, a given Ca/Si ratio is compatible with differing distributions of silicate anion size, and this distribution could depend on the conditions under which the material was formed.

### 5.6.2 *Tobermorite-based models for the C–S–H of calcium silicate and cement pastes*

Several models based on the tobermorite structure have been suggested for the structure of the C–S–H of calcium silicate and cement pastes or related materials. Kantro *et al.* (K19) proposed that tobermorite-type layers were interstratified with CH layers, while Stade and Wieker (S57) concluded that both $Ca^{2+}$ and $OH^-$ could be present in the interlayer region of a tobermorite-type structure. Stade (S55) suggested that, in 'C–S–H(di,poly)' one surface of a tobermorite-type layer was composed of dimeric and the other surface of polymeric ions, thus accounting for the near constancy of dimer/polymer ratio. Fujii and Kondo (F22) regarded C–S–H gel as a solid solution of 1·4 nm tobermorite and CH. Cong and Kirkpatrick (C27) considered that the C–S–H gel formed in calcium silicate or cement pastes was essentially similar C–S–H(I).

Richardson and Groves (R22) proposed a generalized model for the C–S–H gel formed in $C_3S$ or $\beta$-$C_2S$ pastes. They expressed the general formula as

$$Ca_XH_{(6n-2X)}Si_{(3n-1)}O_{(9n-2)} \cdot zCa(OH)_2 \cdot mH_2O$$

In this formula, the $Si_{(3n-1)})O_{(9n-2)}$ represents the average silicate anion, and the $H_{(6n-2X)}$ hydrogen atoms that are directly attached to them. $Ca^{2+}$ ions in the central part of a layer are not distinguished from those in an interlayer. With that reservation, this model is implicitly based on the three ways of altering the structure and composition of 1·4 nm tobermorite described in the previous section. The model was extended to cement pastes, by allowing the possibility of various ionic substitutions, of which the most important were of $Si^{4+}$ by $Al^{3+}$ or $Fe^{3+}$ and of interlayer $Ca^{2+}$ by $Na^{+}$ or $K^{+}$ (R23).

In some cement-based materials, the principal hydration products are forms of C–S–H closely similar to the C–S–H(I) formed in aqueous suspensions, and having Ca/Si ratios ranging from 0·9 to about 1·3. The materials giving such products include alkali-activated slags (Section 9.2.9) and autoclaved materials made using cement and siliceous additions (Section 11.7.2). Models based purely on a tobermorite-type structure appear to be appropriate in these cases. It is questionable whether they are appropriate to the C–S–H gel formed in normal pastes of calcium silicates or cement.

### 5.6.3 *A mixed tobermorite–jennite model for for the C–S–H of calcium silicate and cement pastes*

In models that are based strictly on a tobermorite-type structure, it is implicitly assumed that any Ca–OH that is present substitutes for silicate ions in a random manner. This is reasonable if the content of Ca–OH is relatively small, but scarcely so in materials, or individual regions of them, in which the content of Ca–OH is substantial. The conformation of the Ca–O cores of the layers that occurs in tobermorite results from the fact that all the O atoms are shared with silicate chains. If only one-half of them are thus shared, the conformation changes to that in jennite. It therefore seems more likely that, if the content of Ca–OH is substantial, a jennite-type conformation and not a tobermorite-type conformation will occur. One might also expect a tendency for the silicate ions and $OH^{-}$ groups to be arranged in whatever ordered way occurs in jennite.

Taylor (T21) suggested that C–S–H gel, assumed to have been equilibrated at 11% RH, contained elements of both 1·4 nm tobermorite and jennite structure. These were originally considered to form separate layers, but it was later suggested (T26) that the regions could be poorly defined, perhaps merging into each other within individual layers. The material was seen as being highly disordered, and small amounts of monomeric silicate ions could be present.

In Fig. 5.9, the Ca/Si ratio is plotted against the mean chain length for each type of structure. It is assumed that each bridging tetrahedron carries one H atom and one of the two end-group tetrahedra of each anion also carries an H atom. The observed Ca/Si ratio of about 1·8 can arise in two extreme ways, with intermediate possibilities. One is a mixture of tobermorite-type and jennite-type structures, both with dimeric anions; the other is a purely jennite-type structure, with a mean chain length of 5 tetrahedra. Initial formation of the first, followed by gradual

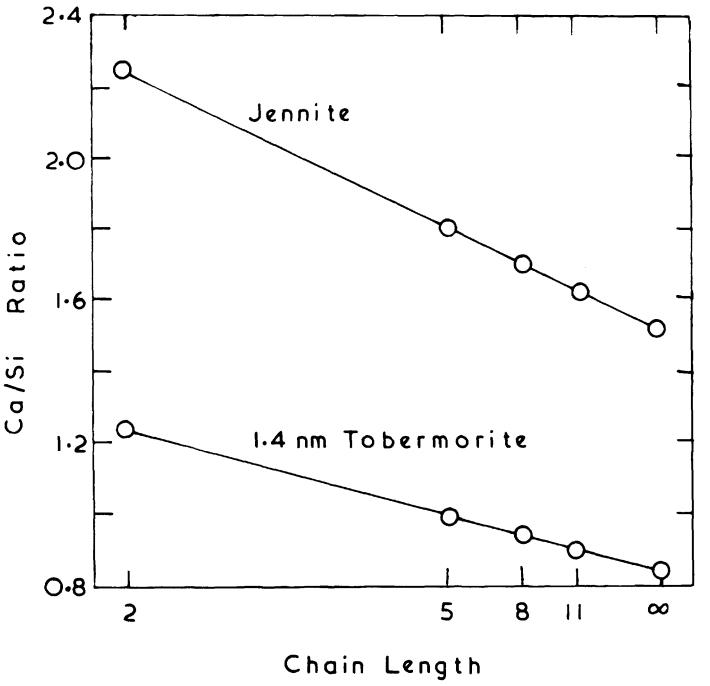


**Fig. 5.9** *Calculated Ca/Si ratio plotted against a function of chain length for jennite and 1·4 nm tobermorite modified by omission of bridging tetrahedra. From T21.*

transition to the second, would explain the observed changes in anion-size distribution with time. Since it would be a change towards a more highly ordered structure, it might also explain the direction taken by the process. Several other lines of evidence were cited in support of the hypothesis, based on data from TG, densities and water contents under various drying conditions, electron-diffraction patterns and the local variation in composition observed in electron-optical analyses.

The model would account for the changes in distribution of local Ca/Si ratio observed by Richardson and Groves (R17). The bimodal distributions observed at early ages had ranges typically around 1·2–2·3; the lower value is close to that calculated for a tobermorite-type structure with dimeric ions, and the higher one is close to the value of 2·25 calculated for a jennite-type structure with dimeric ions. The observed narrowing of the distribution and change towards unimodal character with a modal value near 1·75 is what would be expected for a change towards a structure purely of jennite type.

The model differs from those assuming a structure based purely on the tobermorite structure in that, in regions having a Ca/Si ratio above 1·5, the conformation of the Ca–O cores of the layers is assumed to be of the jennite and not the tobermorite type. It is also assumed that, in these regions, the silicate ions and $OH^-$ groups are arranged in an ordered

way, as in jennite. A particular assumption was made concerning the content of Si–OH; this appears to give the best agreement with the data, but is not an essential feature of the model.

### 5.6.4 *Other models for the C–S–H of calcium silicate and cement pastes*

The mixed tobermorite–jennite model described above takes account of local variability in composition and structure. The results of Henderson and Bailey (H30) and of Viehland *et al.* (V4) suggest that it may also be necessary to take into account local variability in crystallinity. The possibility of transitional structures intermediate between those of the calcium silicate hydrate and calcium hydroxide may also need to be considered.

Some other models for the structure of C–S–H gel that have been proposed appear incompatible with the evidence. They include an identification with natural tobermorite, based on IR and extraction results (S48), one assuming a close relation to the CH structure, with incorporation of monomeric silicate ions (G41), and, as noted in Section 5.5.2, one assuming three-dimensional anionic clusters (C28).

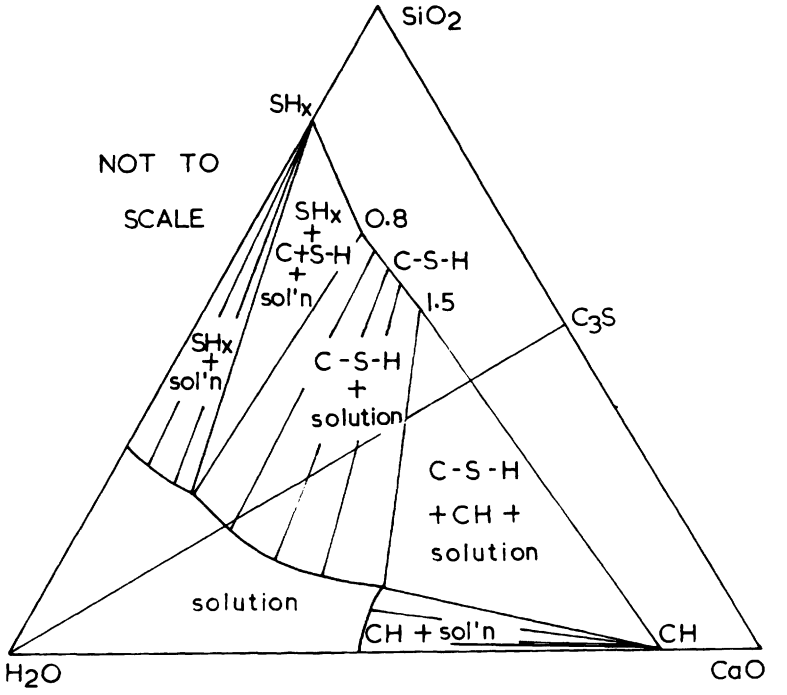


**Fig. 5.10** *The system $CaO–SiO_2–H_2O$ at ordinary temperatures (schematic). From T27.*

## 5.7 Equilibria

### 5.7.1 Solubility relations

Equilibria in the $CaO–SiO_2–H_2O$ system at ordinary temperatures have been widely studied for the light they may cast on cement hydration and on leaching of concrete by ground waters. Steinour (S59,S60) reviewed early work and Jennings (J16) discussed later studies. If C–S–H(I) is placed in water or CH solutions, its Ca/Si ratio changes until equilibrium is reached. Except at low CaO concentrations, the $SiO_2$ concentrations in solution are very low, so that transfer between solid and solution is almost entirely of CaO. The data may be plotted schematically on a triangular diagram (Fig. 5.10), but because of the low concentrations it is more useful to employ separate plots of the Ca/Si ratio of the solid or $C_{SiO_2}$ against $C_{CaO}$ (Figs 5.11 and 5.12).

In most of the investigations, the solid starting materials were either CH and hydrous silica, or C–S–H prepared either from those materials or by mixing solutions of sodium silicate and a soluble calcium salt, followed by washing to remove the soluble product. In some, anhydrous calcium silicates were used. The various sets of data represented by Figs 5.11 and 5.12 show considerable divergencies; a few studies suggested the existence of a step in the curve of Fig. 5.11 at Ca/Si $\approx$ 1·1 (S59). With the important exceptions of some of the data obtained using $C_3S$ or $C_2S$, none of these differences is clearly related to ones in starting material. They may be associated with differences in structure; Grutzeck *et al.* (G51) found a similar step in the related curve of Ca/Si ratio against pH, and concluded that it represented the change from a tobermorite-type structure with long chains to a jennite-type structure containing shorter chains and dimeric silicate groups (Section 5.5). XRD powder evidence shows that the central part of the curve in Fig. 5.11 ($C_{CaO} \approx 2$ to 22 mol $l^{-1}$) and curve A of

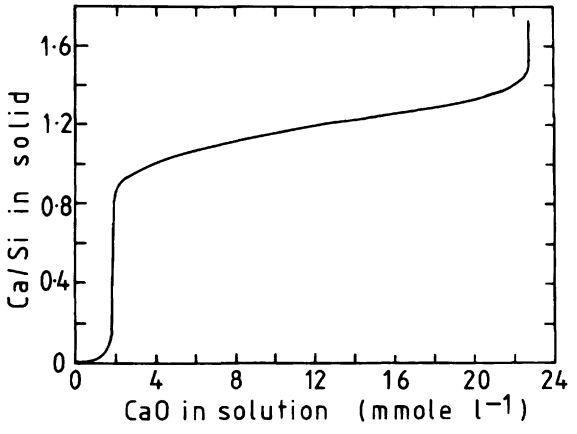


**Fig. 5.11** *Metastable equilibrium curve relating the Ca/Si ratios of C–S–H preparations to the analytical concentration of CaO in the solution, selected as typical from the results of many investigations. After S60.*

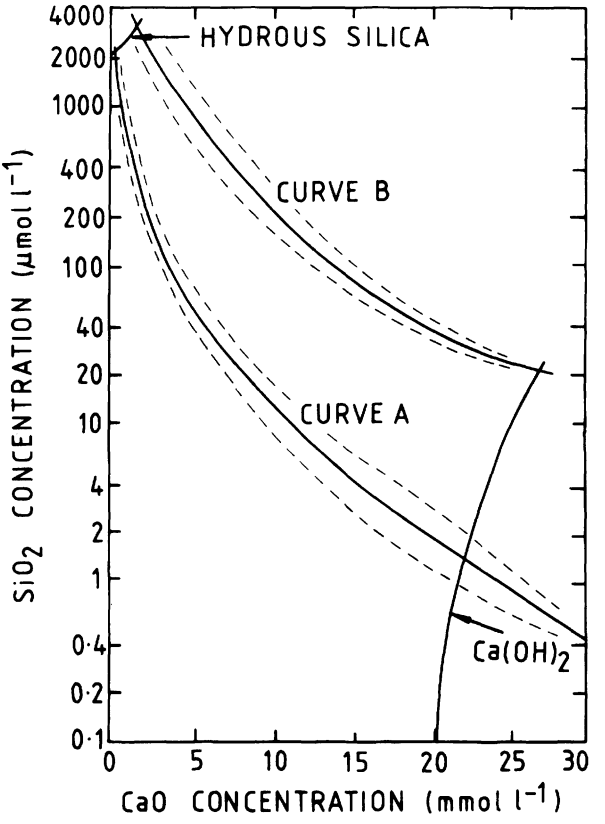


**Fig. 5.12** *Concentration data for C–S–H based on the results of many investigations; for explanation of curves, see text. Broken lines give an indication of the scatter of the data. After J16.*

Fig. 5.12 represent the solubilities of C–S–H(I) preparations and that there are invariant points for hydrous silica, C–S–H(I) with Ca/Si $\approx 0{\cdot}8$ and solution with $C_{CaO} \approx 1\,\text{mmol}\,l^{-1}$ and $C_{SiO_2} \approx 2\,\text{mmol}\,l^{-1}$, and for CH, C–S–H(I) with Ca/Si $\approx 1{\cdot}4$ and solution with $C_{CaO} \approx 22\,\text{mmol}\,l^{-1}$ and $C_{SiO_2} \approx 1\,\mu\text{mol}\,l^{-1}$ (J16,S60,T22). Figure 5.12 includes metastable solubility curves for hydrous silica and CH.

Jennings (J16) noted that observed points on plots of $C_{SiO_2}$ vs. $C_{CaO}$ tended to fall on one or other of two curves, with relatively few in between (Fig. 5.12). Of those that fell between, some were obtained using $\beta$-$C_2S$ and others were suspect from carbonation or for other reasons. Those falling on the upper curve, B, had all been obtained by reaction of $C_3S$ with water for periods not exceeding a few days; probably in all cases, unreacted $C_3S$ was present. Some of the experiments using $C_3S$, and all of those using other starting materials other than $\beta$-$C_2S$, gave points lying on

the lower curve, A. Of the experiments using $C_3S$ that gave points on curve A, some were of durations of 4 h or less (B56), but most appear to have been of long duration, and in at least one case, points lying on curve A were obtained only if no unreacted $C_3S$ remained (T22).

Curve A is clearly the solubility curve of C–S–H(I); scatter at the CaO-rich end may arise because a given Ca/Si ratio can be associated with more than one structural arrangement. However, any form of C–S–H that is structurally derived from 1·4 nm tobermorite or jennite or, perhaps more widely, that is based on Ca–O sheets, probably has a solubility lying on or close to this curve. There are no solubility data for C–S–H(II), 1·4 nm tobermorite or jennite, but one might expect the curves for the crystalline phases to lie below the relevant parts of curve A, and that of C–S–H(II) to lie near or slightly below the high CaO portion of that same curve.

Curve B is most unlikely to represent the metastable solubility of anhydrous $C_3S$; thermodynamic calculations (S61) indicate that such a curve would be very much higher, as would be expected from the high reactivity. Jennings (J16,J17) and Gartner and Jennings (G52) considered it to be the metastable solubility curve of a product formed as a layer on the $C_3S$ surface. Thermodynamic calculations based on this assumption indicated Ca/Si ratios of 1·1 at low and 1·65 at high CaO concentrations; these values are broadly compatible with ESCA evidence (Section 5.8.2). Barret and Bertrandie (B60,B61) considered that curve B was not a solubility curve, but represented a quasisteady state in which the concentrations were such as to equalize the rate of dissolution of a hydroxylated surface layer on the $C_3S$ and the rate of precipitation of C–S–H. Both views associate the curve, though in different ways, with the presence of an altered surface layer on the $C_3S$ that is metastable relative to the C–S–H whose solubility is represented by curve A. Experiments using $\beta$-$C_2S$ give compositions lying on a curve between curves A and B (B60,G53) and which may similarly be associated with an altered surface layer on the $\beta$-$C_2S$.

There are few data on the concentrations of CaO and $SiO_2$ in the pore solutions of $C_3S$ pastes (w/s < 1·0), as opposed to suspensions, and those that exist are conflicting as regards $C_{SiO_2}$ (B56,O12). The values of $C_{CaO}$ after long times (e.g. 27 mmol $l^{-1}$; O12) appear to be significantly above the solubility of CH; this has been attributed to incorporation of $SiO_2$ in the CH (W23), but might also be due to the small crystal size of some of this phase.

### 5.7.2 *Species in solution*

Barby *et al.* (B62) summarized data for silicate species in alkali silicate solutions. Monosilicic acid, $H_4SiO_4$, has $pK_{a1} = 9{\cdot}46$, $pK_{a2} = 12{\cdot}56$, and $pK_{a3}$ probably about 15. Monomeric species are overwhelmingly predominant at $C_{SiO_2}$ below about 2 mmol $l^{-1}$ at pH values up to 9, and up to higher concentrations at higher pH. The solubility product of CH, in terms of activities, is $9{\cdot}1 \times 10^{-6}$ $mol^3$ $l^{-3}$ at 25°C (G42), and the stability constant of the complex $CaOH^+$ is 20 mol $l^{-1}$ (S62). Undissociated CH is

not a significant species in saturated CH solution (G52). In saturated CH at 25°C, the activities of $Ca^{2+}$ and $CaOH^+$ are roughly equal, and the pH is 12·45. The stability constants of $CaH_2SiO_4^0$ and $CaH_3SiO_4^+$ are reported to be 1240 mol $l^{-1}$ and 2.5 mol $l^{-1}$ respectively (S62), but some doubt has been cast on these values by the results of thermodynamic calculations using them (G52).

Using the equilibrium constants given above, together with standard expressions to calculate ionic strength and activity coefficients, one may calculate the species concentrations and species activities in a system of given bulk composition. For $C_{CaO} = 28{\cdot}0$ mmol $l^{-1}$, $C_{SiO_2} = 20{\cdot}0$ $\mu$m $l^{-1}$, and assuming that calcium silicate complexes are not present, the species concentrations (in mol $l^{-1}$) are $Ca^{2+}$, $1{\cdot}90 \times 10^{-2}$; $CaOH^+$, $8{\cdot}98 \times 10^{-3}$; $OH^-$, $4{\cdot}70 \times 10^{-2}$; $H_4SiO_4$, $4{\cdot}19 \times 10^{-9}$; $H_3SiO_4^-$, $6{\cdot}82 \times 10^{-6}$; $H_2SiO_4^{2-}$, $1{\cdot}30 \times 10^{-5}$; $HSiO_4^{3-}$, $1{\cdot}46 \times 10^{-7}$ (G52). The activity of $OH^-$ is $3{\cdot}78 \times 10^{-2}$ mol $l^{-1}$; this corresponds to a pH of 12·58. If the complexes $CaH_2SiO_4^0$ and $CaH_3SiO_4^+$ are assumed to occur, with stability constants of 2000 and 20 mol $l^{-1}$, respectively, the concentrations of the $SiO_2$-containing species become (mol $l^{-1}$): $CaH_3SiO_4^+$, $2{\cdot}01 \times 10^{-7}$; $CaH_2SiO_4^0$, $1{\cdot}61 \times 10^{-5}$; $H_4SiO_4$, $7{\cdot}75 \times 10^{-10}$; $H_3SiO_4^-$, $1{\cdot}26 \times 10^{-6}$; $H_2SiO_4^{2-}$, $2{\cdot}41 \times 10^{-6}$; $HSiO_4^{3-}$, $2{\cdot}70 \times 10^{-8}$, the neutral complex $CaH_2SiO_4^0$ thus being the principal $SiO_2$-containing species. The concentrations of $Ca^{2+}$, $CaOH^+$ and $OH^-$ are not significantly affected.

### 5.7.3 *Thermochemistry and thermodynamics*

Using a heat of solution method, Lerch and Bogue (L24) found the enthalpies of hydration of $C_3S$ and $\beta$-$C_2S$ in pastes to be $-115$ kJ $mol^{-1}$ and $-45$ kJ $mol^{-1}$ respectively. Similar values have been reported by other investigators, e.g. $-118$ kJ $mol^{-1}$ and $-45$ kJ $mol^{-1}$ by Brisi (B63) and $-121$ kJ $mol^{-1}$ and $-46$ kJ $mol^{-1}$ by Fujii and Kondo (F22), who recalculated data obtained by Brunauer *et al.* (B64) for dried products. Brunauer *et al.* noted that, if the hydration products of $C_3S$ and $\beta$-$C_2S$ were identical apart from the quantities of CH formed, the enthalpy of hydration of $C_3S$ should equal the sum of the enthalpies of hydration of $\beta$-$C_2S$, hydration of CaO ($\Delta H_{298} = -65{\cdot}2$ kJ $mol^{-1}$; W10), and reaction of $\beta$-$C_2S$ and CaO to give $C_3S$ ($\Delta H_{298} = -13{\cdot}4$ kJ $mol^{-1}$; W10). For the moist material, this sum is $-124$ kJ $mol^{-1}$, which is near the observed value.

Fujii and Kondo (F22) calculated the thermodynamic properties of C–S–H, using solubility data and properties of 1·4 nm tobermorite and CH given by Babushkin *et al.* (B65). The C–S–H was treated as equivalent to a solid solution of these two compounds. For the composition $1{\cdot}7CaO \cdot SiO_2 \cdot 2{\cdot}617H_2O$, they found $\Delta H_f^0 = 2890$ kJ $mol^{-1}$, $\Delta G_f^0 = -2630$ kJ $mol^{-1}$ and $S^0 = 200$ J $mol^{-1}$ $K^{-1}$. They showed that these values were consistent with data for the enthalpies of hydration of $C_3S$ and $\beta$-$C_2S$. The free energy of formation of C–S–H from 1·4 nm tobermorite and CH was shown to become increasingly negative with increasing Ca/Si ratio, but to tend towards a limit at ratios approaching 2·0; this is consistent with the observed upper value of this quantity.

Glasser *et al.* (G54) calculated the activities of the principal ionic species in solutions in equilibrium with C–S–H of various Ca/Si ratios, and solubility products defined in terms of those species. Using values of $\Delta G_f^0$ for the ionic species (B65), values of $\Delta G_f^0$ for the solids were then calculated. The results depended somewhat on the set of solubility data used, but were broadly similar to those obtained by Fujii and Kondo (F22). Using one set of data, values ranged from $-1720\,\text{kJ mol}^{-1}$ at Ca/Si = 0·93 to $-2350\,\text{kJ mol}^{-1}$ at Ca/Si = 1·63, referred to formulae containing one silicon atom in each case.

The Gibbs–Duhem equation has been used to calculate Ca/Si ratios of solids from the CaO and $SiO_2$ concentrations in solutions with which those solids are in equilibrium (F23,G52). Gartner and Jennings (G52) showed that, at the low concentrations involved, this equation reduces to the approximate form $(Ca/Si)_{solid} = -d\mu_s/d\mu_c$, where $\mu_s$ and $\mu_c$ are the chemical potentials of $SiO_2$ and CaO respectively. The calculations were carried out for curve B and three variants of curve A on Fig. 5.12. For points along each curve, activities of the ionic species in solution were calculated, and from these, values of $\mu_s$ and $\mu_c$; these were plotted against each other to give curves on a chemical potential phase diagram. From the slopes at points along these curves, the Ca/Si ratios of the solids were obtained. For one variant of curve A, the calculated Ca/Si ratios at $C_{CaO} = 3\,\text{mmol l}^{-1}$ and $14{\cdot}4\,\text{mmol l}^{-1}$ were 1·0 and 1·45 respectively. These values agree well with typical experimental results shown on Fig. 5.11. For curve B, the calculated Ca/Si ratios were 1·1 at $5\,\text{mmol l}^{-1}$, 1·65 at $13\,\text{mmol l}^{-1}$ and 1·65 at $22\,\text{mmol l}^{-1}$.

### 5.7.4 *Effects of alkalis and of gypsum*

Brown (B66) reviewed studies on the $Na_2O$–CaO–$SiO_2$–$H_2O$ system at 25°C, based largely on the results of Kalousek (K20) and Macphee *et al.* (M61). The crystallization surfaces of the solid phases on the quaternary diagram were partially or completely defined. The quaternary solid phases comprised a sodium-substituted form of C–S–H, which was termed C–'N'–S–H, a calcium-substituted sodium silicate hydrate and a compound of composition $0{\cdot}25Na_2O \cdot CaO \cdot SiO_2 \cdot 3H_2O$. Brown noted that the concentrations in the pore solutions of cement pastes tended to fall along the curve bounding the surfaces for CH and C–'N'–S–H, but that there was a problem in reconciling the alkali content of the C–S–H with Kalousek's equilibrium data. In further work, Brown (B67) modelled the changes in solution composition during $C_3S$ hydration. A small content of $Na_2O$ in the $C_3S$ greatly increased the concentrations of $OH^-$ and decreased those of $Ca^{2+}$. In the presence of a limited amount of gypsum, the concentrations of $Ca^{2+}$ and $SO_4^{2-}$ were significant so long as any gypsum remained but decreased due to uptake of $SO_4^{2-}$ by the C–S–H, leaving a solution that was essentially one of NaOH. This behaviour resembles that found with cement pastes (Section 7.5.1). Other studies bearing on equilibria in the CaO–$SiO_2$–$H_2O$ system in the presence of alkalis have been reported (B68,S63).

## 5.8 Kinetics and mechanisms

### *5.8.1 $C_3S$: experimental data*

Figure 5.13 shows the general form of the curve relating the fraction of $C_3S$ consumed ($\alpha$) to time in a paste of w/s $\approx$ 0·5 at about 25°C and with moist curing. Such curves have been determined using QXDA for unreacted $C_3S$ (e.g. K21,O11), though the precision is low for values of $\alpha$ below about 0·1. At low values of $\alpha$, other methods are available, such as conduction calorimetry (e.g. P22), aqueous phase analyses (e.g. B69) or determinations of CH content or of non-evaporable water. At very early ages, it may be necessary to allow for the fact that the property determined depends on the nature of the hydration products, e.g. precipitation of C–S–H begins before that of CH.

The rate, as followed from that of heat evolution (Fig. 5.14), passes through an initial maximum, decreases to a minimum during a so-called induction period, passes through a second maximum and then gradually declines. Kondo and Ueda (K21) described five periods of reaction, viz.: (1) the initial reaction, (2) the induction period, (3) the acceleratory period, in which the main reaction first begins to occur rapidly, (4) the deceleratory period and (5) a period of slow, continued reaction. Periods 1 and 2 correspond to the early stage of reaction as defined from microstructural studies (Section 5.3.2), periods 3 and 4 to the

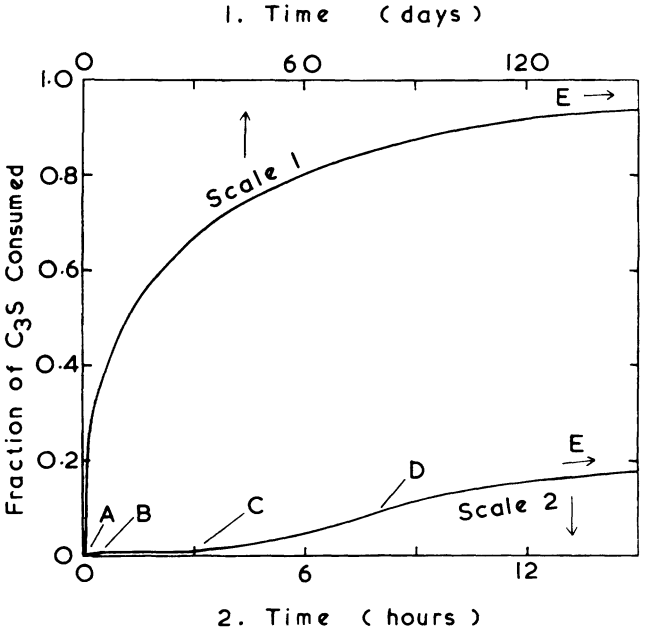


**Fig. 5.13** *General form of curves relating the fraction of $C_3S$ consumed to time in a paste. AB: initial reaction. BC: induction period. CD: acceleratory period. DE: deceleratory period and continuing slow reaction. From T27.*

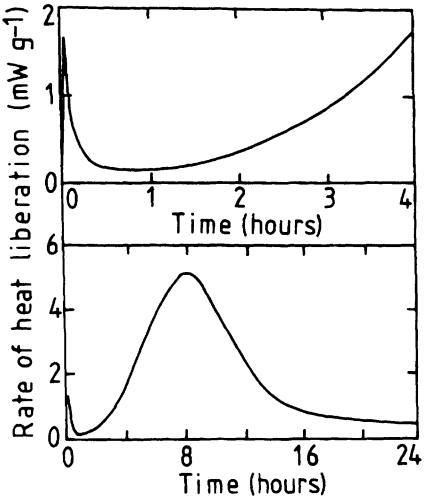


**Fig. 5.14** *Typical calorimetric curve relating the rate of heat liberation to time for a $C_3S$ paste. After B70.*

middle stage, and period 5 to the late stage. Setting takes place during the acceleratory period.

Many investigators have followed the changes in $C_{CaO}$ and $C_{SiO_2}$ or $[OH^-]$ with time in the course of the reaction of water with $C_3S$ or $\beta$-$C_2S$ in suspensions (e.g. B56,B69,G55; Fig. 5.15). The curves for $C_{CaO}$ or $[OH^-]$ typically show a steep rise during the initial reaction and a more gradual one of uniform slope during the induction period. Significant

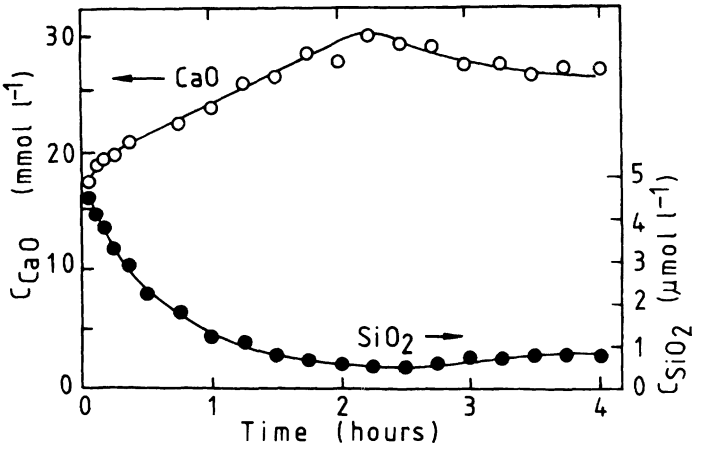


**Fig. 5.15** *Plots of the analytical concentrations of CaO and $SiO_2$ against time for a $C_3S$ paste ($C_3S$ 352·5 $m^2 kg^{-1}$, w/s 0·7, 24°C). After B56.*

precipitation of CH begins just before the maximum concentrations are reached, and is rapid when they decrease, during the acceleratory period (W23). Some of the curves reported in the literature show a plateau in the early part of the induction period, followed by a rise (e.g. B60). In the most marked cases of this behaviour, the maximum is unusually high ($\sim$40 mmol $l^{-1}$) and unusually delayed (24–36 h; e.g. F24). As noted in Section 5.7.1, the final values reported for pastes tend to be well above the solubility of CH. The $SiO_2$ concentration passes through a maximum in the order of 1 mmol $l^{-1}$ during the initial reaction. Brown *et al.* (B56) found the solution compositions to lie exclusively on curve A of Fig. 5.12, but other workers have found the paths followed by the concentrations to cross curve A, passing through maxima near (G55) or beyond (B60,B61) curve B and then falling back to curve A.

At early ages, $d\alpha/dt$ increases markedly with w/s ratio above 0·7 (B56). Moderate variations in specific surface area have little effect on the length of the induction period, but with finer grinding, $d\alpha/dt$ during the acceleratory period increases (B56,K21,O13). The rate of reaction increases with temperature up to the end of the the acceleratory period, but is much less affected thereafter (K19), suggesting a change from chemical to diffusion control. Introduction of defects into the $C_3S$ shortens the induction period (F24,M62,O13).

The results of experiments at high w/s ratios have been interpreted assuming superficial hydroxylation of the $C_3S$ followed by congruent dissolution and subsequent precipitation (B60,B69). Damidot and co-workers (D22–D24) followed the hydration of $C_3S$ using a technique that allowed simultaneous monitoring of the heat flow and electrical conductivity. The use of high w/s ratios also greatly facilitated the study of the earlier stages of the reaction, and made it possible to distinguish endothermic blips on the generally exothermic calorimetric curve, attributable to the onset of precipitation first of C–S–H and later of CH. From their results, the authors concluded that the initial process was one of congruent dissolution of $C_3S$. When the limiting supersaturation of C–S–H had been reached, this phase began to precipitate, initially by homogeneous nucleation and later by heterogeneous nucleation and growth on a hydroxylated $C_3S$ surface. During this stage, $C_{CaO}$ and the Ca/Si ratio of the C–S–H increased; when the limiting supersaturation of CH had been reached, that phase also precipitated. Three distinct forms of C–S–H were considered to form over different ranges of $C_{CaO}$ (Section 5.5.4).

Reaction in pastes must also occur at least partly by dissolution and precipitation, since much of the product is deposited at a distance from the starting material, and because both $C_{CaO}$ and $C_{SiO_2}$ pass through maxima. Topochemical mechanisms, defined as ones in which the material does not pass through a true solution phase, may also occur, especially in the late stage of reaction (T28).

The kinetics up to the middle of the acceleratory period are discussed in the following sections. Those of the later stages have been more thoroughly studied with cement (Section 7.7) and only some aspects are considered here.

### 5.8.2 $C_3S$: the initial reaction

Two ESCA studies of the hydration of $C_3S$ pastes or compacts showed an initial surface Ca/Si ratio of 3·0, which within the first minute fell sharply and then increased again; it then fell more slowly, reaching a value of 1·5–2·0 in 15–30 min (M48,R24,T29). Allowing for the fact that the region analysed will include unreacted $C_3S$ until the layer of hydration product is sufficiently thick and continuous, these results may be interpreted in terms of the formation of an initial hydrate of low Ca/Si ratio, which rapidly increases (R24). Another study (B71), in contrast, showed an unreacted $C_3S$ sample to have a low surface Ca/Si ratio. ESCA results also indicate a change in the environment of the silicon atoms at the end of the induction period, possibly associated with the formation of dimeric silicate ions (R24). Secondary-ion mass spectrometry (SIMS) is a possible alternative method for studying surface compositions, but has not yet given information on that of the hydrated material (G56). Electron diffraction shows that an amorphous surface layer can be produced by grinding (K21,U11); this may explain some of the reported differences in behaviour between apparently similar specimens.

Calculations of $\alpha$ from concentrations in the bulk solution indicate values of around 0·3% at the start of the induction period (B56,B69). These are likely to be minimum estimates, because they assume that no CH is formed; in reality, small amounts may be, on account of concentration gradients, which will themselves introduce an error in the same direction. Reported values of $\alpha$, summarized by Odler and Dörr (O11), range from 0·1% to an improbable 8%. Their own estimate of 1–2% is supported by subsequent evidence from cross-polarization $^{29}Si$ NMR (R19). Assuming a specific surface area of $300\,m^2\,kg^{-1}$, a value of 1% corresponds to a mean depth of attack of about 10 nm.

### 5.8.3 $C_3S$: the induction period

The causes of the induction period and of its termination have been the subject of much debate. Hypotheses have been reviewed in a collaborative paper (T27). The main ones are as follows.

(1) The product of the initial reaction forms a protective layer on the $C_3S$ particles; the induction period ends when this is destroyed or rendered more permeable by ageing or phase transformation (B72,J16,S64).

(2) The product of the initial reaction forms a semipermeable membrane which encloses an inner solution and is destroyed by osmotic bursting (D25).

(3) The rate of reaction in the induction and acceleratory periods is controlled by nucleation and growth of the C–S–H formed in the main reaction, the induction period ending when growth begins (B69,F24,O14,S65).

(4) The induction period occurs because the CH nuclei are poisoned by $SiO_2$ and cannot grow, and ends when the level of supersaturation is sufficient to overcome this effect (G57,T30,W23).

The induction period is shortened by adding prehydrated $C_3S$ (O14), but additions of lime or CH, including that formed from $C_3S$, are variously reported to be ineffective (B73,O14) or to lengthen it, though shortening it with cement (U12). In cement mixes, additions of flyash or some other finely divided materials accelerate hydration after the first day, apparently by acting as nucleation sites for C–S–H (Section 9.3.3). Additions of reactive silica markedly accelerate hydration (S64). Most of this evidence supports hypothesis 3 and tells against hypothesis 4. Hypothesis 3 does not exclude hypothesis 1, as the breakdown of a protective layer could be associated with formation of a new product.

The recent microstructural evidence (Section 5.3.2) gives no indication that a membrane or other product distinct from that formed later is formed during the initial reaction in $C_3S$ pastes, though a gelatinous coating is formed in cement pastes, which show an induction period similar to that observed with $C_3S$ (Section 7.5.1). For $C_3S$ pastes, this evidence excludes hypothesis 2, and gives no positive support to hypothesis 1. It does not exclude the formation of an altered layer on the $C_3S$ surface, no more than a few nanometres thick. Tadros *et al.* (T30) postulated the formation of an $SiO_2$-rich layer with chemisorbed $Ca^{2+}$, and Barret *et al.* (B69) that of a superficially hydroxylated $C_3S$, formed by protonation of the $O^{2-}$ and $SiO_4^{4-}$ ions, balanced by loss of $Ca^{2+}$.

The calculated solubility of $C_3S$ is about 1 molal (S61). In the absence of an altered or protective layer, the observed low rate of reaction during the induction period could be explained only if the concentrations close to the $C_3S$ surface were of this order of magnitude. It is doubtful whether the very high concentration gradients that this implies could exist (G53,J16).

The balance of the evidence favours a combination of hypotheses 1 and 3. The following model is essentially that of Gartner and Gaidis (G53), but has features in common with those of Barret and Bertrandie (B60) and of Grutzeck and Ramachandran (G55).

(1) In the initial reaction, $C_3S$ dissolves and a material is deposited, which will be termed Product B. The dissolving $C_3S$ probably has a hydroxylated surface, as proposed by Barret *et al.* (B69). Under typical paste conditions, Product B forms an overlying surface layer about 1 nm in average thickness, though it is likely to be non-uniform and thicker around active sites. It may be capable of existence only on a $C_3S$ surface and similar to a passive layer on a metal. Within 30 s the $C_3S$ is almost isolated from the solution, and an unstable equilibrium, represented by curve B of Fig. 5.12, is established between the solution and Product B.

(2) Product B is unstable with respect to the material represented by curve A of Fig. 5.12, for which we shall reserve the term C–S–H. During the early part of the induction period, C–S–H nucleates and begins to grow. This implies dissolution of Product B, and increased access of solution to the $C_3S$, which thus dissolves more rapidly. The rate of reaction in this stage is controlled

by the growth of C–S–H, the rate of which increases with the amount already formed.

The amount of Product B at any given stage in the reaction must depend on the relative rates of its formation and dissolution. It may or may not disappear completely when the latter is sufficiently high. The NMR evidence (Section 5.5.3) indicates that the hydrated material formed up to the end of the induction period contains only monomeric silicate ions and that the latter persist alongside larger ions when the latter are formed. This suggests that the silicate ions are monomeric both in Product B and in C–S–H in the early stages of formation of the latter product. The Ca/Si ratio of Product B is possibly about 1 initially, increasing to about 1·7 as equilibrium with CH is approached.

### *5.8.4 The main reaction ($C_3S$ and $\beta$-$C_2S$)*

From the kinetic standpoint, there is probably no distinction between the induction period and the early part of the acceleratory period; indeed, as Gartner and Gaidis (G53) noted, there is strictly no induction period in the absence of retarding admixtures. Throughout both stages, growth of C–S–H proceeds at an increasing rate, which is reflected in increasingly rapid dissolution of the $C_3S$. The $Ca^{2+}$ and $OH^-$ concentrations in the bulk solution increase steadily, and when a sufficient degree of supersaturation has been reached, CH begins to precipitate in quantity, causing these concentrations to fall. Its formation is not normally rate-determining, but could become so in the presence of admixtures that retard its growth. The kinetic data for this stage can be fitted by Avrami-type equations, but the assumptions underlying the latter (formation of a product within an initially homogeneous material) do not correspond to the situation existing in the hydration of $C_3S$ or cement.

The smaller grains of $C_3S$ probably react completely, by dissolution and precipitation, during the acceleratory period. In the final, slow periods of hydration, the remaining grains of $C_3S$, which are relatively large, are gradually replaced by C–S–H through the inward movement of an interface. It is difficult to believe that such a process occurs by dissolution into a true liquid phase, followed by precipitation. Following earlier studies (F25,K21,K22,M53), Taylor (T28) suggested that a topochemical reaction may occur with both $C_3S$ and $\beta$-$C_2S$. Comparison of the numbers of atoms of each element in the initial and product phases shows that to convert either $C_3S$ or $\beta$-$C_2S$ into C–S–H, relatively little $O^{2-}$ must be gained or lost; much of the $Ca^{2+}$ and smaller proportions of the $Si^{4+}$ must be lost, and equivalent amounts of $H^+$ gained (Table 5.6). At the interface, a narrow zone could exist, in which the necessary atomic rearrangements take place. It is not necessary to postulate any migration of water molecules through the inner product; instead, $Ca^{2+}$ and $Si^{4+}$ move outwards, and $H^+$ inwards. At the surface, the $Ca^{2+}$ and $Si^{4+}$ enter the solution, and ultimately precipitate, along with the $OH^-$ ions released from the $H_2O$ molecules, as CH and outer product C–S–H. Migration of silicon was suggested as the probable rate-determining step; however, at

**Table 5.6** *Numbers of atoms in $1000/N_0$ ml*

| Phase | Density (kg $m^{-3}$) | Ca | Si | H | O |
|---|---|---|---|---|---|
| $C_3S$ | 3120 | 41·0 | 13·7 | | 68·3 |
| $\beta$-$C_2S$ | 3326 | 38·6 | 19·3 | | 77·2 |
| C–S–H (90% RH) | 1900 | 14·4 | 8·2 | 66·0 | 63·9 |

Slightly modified from T28; C–S–H composition assumed $C_{1.75}SH_{4.0}$.

low w/s ratios, reaction stops because there is no more space in which the outer product can be formed, and in this case, control presumably shifts to some process related to deposition of outer product. Barret (B74) discussed topochemical mechanisms and their relation to dissolution–precipitation processes.

### 5.8.5 *Early hydration of $\beta$-$C_2S$*

The kinetics and mechanism of $\beta$-$C_2S$ hydration are similar to those for $C_3S$, apart from the much lower rate of reaction (F15,F26,M62,O15,T31), and as noted earlier, the products are similar apart from the much smaller content of CH. Preparations appear to be more variable in reactivity than those of $C_3S$; this is partly attributable to differing stabilizers (F27), but could also be due to differing amounts or natures of phases in intergranular spaces or exsolution lamellae. Preparations made at low temperatures are especially reactive (F26). Because of the low rate of heat evolution, conduction calorimetry is difficult, but shows the existence of an induction period similar to that found with $C_3S$ (M62), which is also indicated by QXDA (O15). ESCA, SEM and solution studies show that behaviour during the early period is similar in principle to that of $C_3S$ (M63). The ESCA data show that the connectivity of the silicate tetrahedra increases within 24 h at 50°C; this behaviour resembles that of $C_3S$ at the end of the induction period. They show the approximate depth of the hydrated layer to be 5 nm after 15 s, and 15 nm after 6 h at 25°C. The rate of reaction is increased in presence of $C_3S$ (O15,T31).

# 6 Hydrated aluminate, ferrite and sulfate phases

## 6.1 AFm phases

### *6.1.1 Compositional and structural principles*

AFm ($Al_2O_3$–$Fe_2O_3$–mono) phases are formed when the ions they contain are brought together in appropriate concentrations in aqueous systems at room temperature. Some can also be formed hydrothermally, i.e. in the presence of water under pressure above 100°C. They are among the hydration products of Portland cements. Under favourable conditions, they form platey, hexagonal crystals with excellent (0001) cleavage. Some of the AFm phase formed in Portland cement pastes is of this type, but much is poorly crystalline and intimately mixed with C–S–H. AFm phases have the general formula $[Ca_2(Al,Fe)(OH)_6]\cdot X\cdot xH_2O$, where X denotes one formula unit of a singly charged anion, or half a formula unit of a doubly charged anion. The term 'mono' relates to the single formula unit of $CaX_2$ in another way of writing the formula, viz. $C_3(A,F)\cdot CaX_2\cdot yH_2O$ [or $C_4(A,F)X_2\cdot yH_2O$], where $y = 2(x + 3)$. Many different anions can serve as X, of which the most important for Portland cement hydration are $OH^-$, $SO_4^{2-}$ and $CO_3^{2-}$. A crystal may contain more than one species of X anion. AFm-type phases can also be prepared in which other tripositive cations, such as $Cr^{3+}$, replace the $Al^{3+}$ or $Fe^{3+}$.

AFm phases have layer structures derived from that of CH by the ordered replacement of one $Ca^{2+}$ ion in three by $Al^{3+}$ or $Fe^{3+}$ (Fig. 6.1; A10–A12). The principal layers thus defined alternate with interlayers containing the X anions, which balance the charge, and $H_2O$ molecules. The replacement of $Ca^{2+}$ by the smaller $Al^{3+}$ or $Fe^{3+}$ ions distorts the structure of the principal layer, alternate $Ca^{2+}$ ions moving in opposite directions from its central plane. This allows each to coordinate the oxygen atom of an interlayer $H_2O$ molecule in addition to its six $OH^-$ ions. The principal layer, together with the $H_2O$ molecules thus bonded to the $Ca^{2+}$ ions, has the composition $[Ca_2(Al,Fe)(OH)_6\cdot 2H_2O]^+$. In the simpler AFm structures, these units are stacked in such a way as to produce octahedral cavities surrounded by three $H_2O$ molecules from

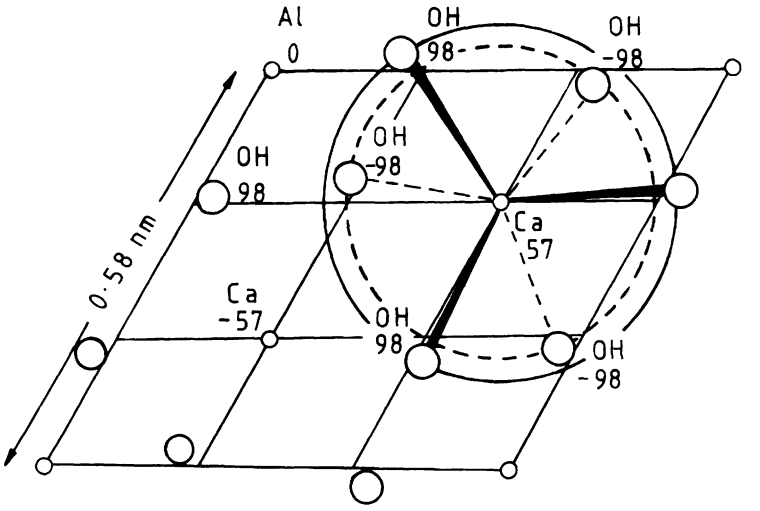


**Fig. 6.1** *Structure of a single principal layer of composition* $[Ca_2Al(OH)_6]^+$ *in an AFm phase, in ab-projection. Distances of calcium, aluminium and oxygen atoms above or below the central plane of the layer are in pm. Hydrogen atoms are not shown. Large circles illustrate the distortion of the* $CaO_6$ *octahedra, which allows the coordination of each calcium atom to rise to 7 through the addition of a water molecule (not shown) directly above or below it in this projection.*

each of the adjacent layers. These cavities may contain X anions, $H_2O$ molecules, or both. In $C_3A \cdot CaCl_2 \cdot 10H_2O$ (or $[Ca_2Al(OH)_6 \cdot 2H_2O]Cl$), each cavity contains a $Cl^-$ ion. In $C_3A \cdot CaSO_4 \cdot 12H_2O$, one half contain $SO_4^{2-}$ anions and the remainder contain two $H_2O$ molecules. In $C_4AH_{13}$, all contain one $OH^-$ anion and one $H_2O$ molecule.

The unit cells of all AFm phases are based on hexagonal structural elements with $a = 0{\cdot}57$–$0{\cdot}59$ nm. These values are somewhat less than $\sqrt{3}$ times that of CH. The layer thickness $c'$ depends on the nature of the X anion and the amount of interlayer water, which can be varied by stepwise dehydration from the highest hydration state. AFm phases exist in which a complete, additional layer of $H_2O$ molecules is present between the principal layers. There is no restriction on the separation between adjacent layers; this allows large anions, and also intercalated neutral molecules (D26,D27), to be present in interlayer sites. Many AFm phases readily undergo changes in water content and anion exchange (D27,F28), the latter including that of $CO_3^{2-}$ for $OH^-$. Due care must therefore often be taken to exclude $CO_2$, and where necessary also to control the humidity.

Complex sequences of stacking the layers, or ordered patterns of filling of the cavities where their contents are not all the same, lead to unit cells that are larger or of lower symmetry than the structural element. Some AFm phases show polytypism, arising from differences in layer stacking.

### 6.1.2 The $C_4AH_x$, $C_4A\bar{C}_{0.5}H_x$ and $C_4A\bar{C}H_x$ phases

Fischer and Kuzel (F29) summarized and extended earlier work on these groups of AFm phases, which are listed in Table 6.1. In the pure $CaO$–$Al_2O_3$–$H_2O$ system, the phase in metastable equilibrium with solutions of appropriate composition at temperatures up to at least 50°C is $C_4AH_{19}$, of which two polytypes ($\alpha_1$ and $\alpha_2$) are known. On decreasing the RH or increasing the temperature, lower hydrates are reversibly formed, with decrease in layer thickness; a decrease in RH to 81% is sufficient to produce $C_4AH_{13}$ (R25). $C_4AH_{19}$ is structurally derived from $C_4AH_{13}$ by the addition of an extra layer of $H_2O$ molecules. A high degree of crystallinity is needed to allow this extra layer to form (D28), and it is doubtful whether it could occur in the material in a cement paste. In $C_4AH_{11}$, the contents of the octahedral cavities in the interlayers are reduced from $(OH^- + H_2O)$ to $OH^-$, and in $C_4AH_7$, which is a poorly crystalline material, the $H_2O$ molecules attached to the $Ca^{2+}$ ions have also been lost.

The layer thicknesses indicate that the $CO_3^{2-}$ ions are oriented parallel to the layers in $C_4A\bar{C}H_{11}$, and perpendicular to them in $C_4A\bar{C}_{0.5}H_{12}$. In all these $CO_3^{2-}$-containing phases, some octahedral cavities contain a $CO_3^{2-}$ ion, and others varying combinations of $H_2O$ molecules and $OH^-$ ions. In the early literature, $C_4A\bar{C}H_{11}$ (or $C_3A \cdot C\bar{C} \cdot H_{11}$) was incorrectly identified as a $C_3A$ hydrate, and $C_4A\bar{C}_{0.5}H_{12}$ as a polymorph of $C_4AH_{13}$. Both phases readily form on carbonation of the $C_4A$ hydrates.

**Table 6.1** *AFm phases of the $C_4AH_x$, $C_4A\bar{C}_{0.5}H_x$ and $C_4A\bar{C}H_x$ groups*

| Composition (F29) | Drying conditions | Ref. | Layer thickness (nm) (F29) | Interlayer contents* | | |
|---|---|---|---|---|---|---|
| | | | | $OH^-$ | $CO_3^{2-}$ | $H_2O$ |
| $C_4AH_{19}$ | 25°C, >88% RH | R25 | 1·068 | 1 | 0 | 6 |
| $C_4AH_{13}$ | 25°C, 11–81% RH<br>40°C, 25% RH | R25<br>R25 | 0·794 | 1 | 0 | 3 |
| $C_4AH_{11}$ | 25°C, anhydrous $CaCl_2$<br>50–90°C | R25<br>B75 | 0·735 | 1 | 0 | 2 |
| $C_4AH_7$ | 25°C, $P_2O_5$<br>110–120°C | R25<br>B75 | 0·56 | 1 | 0 | 0 |
| $C_4A\bar{C}_{0.5}H_{12}$ | 22°C, ≥36% RH<br>40°C, 25% RH | F29<br>R25 | 0·8193 | 1/2 | 1/4 | 11/4 |
| $C_4A\bar{C}_{0.5}H_{11.25}$ | 35°C | F29 | 0·763 | 1/2 | 1/4 | 19/8 |
| $C_4A\bar{C}_{0.5}H_{10.5}$ | 25°C, anhydrous $CaCl_2$<br>80°C | R25<br>F29 | 0·726 | 1/2 | 1/4 | 2 |
| $C_4A\bar{C}_{0.5}H_{6.5}$ | 25°C, $P_2O_5$<br>105°C | R25<br>F29 | 0·66 | 1/2 | 1/4 | 0 |
| $C_4A\bar{C}H_{11}$ | 25°C, saturated $CaCl_2$ | F29 | 0·756 | 0 | 1/2 | 5/2 |
| $C_4A\bar{C}H_8$ | 95°C | F29 | 0·72 | 0 | 1/2 | 1 |
| $C_4A\bar{C}H_6$ | 130°C | F29 | 0·66 | 0 | 1/2 | 0 |

* Per formula unit of $Ca_2Al(OH)_6^+$.

**Table 6.2** *Crystal data for AFm phases*

| Phase | Crystal system† | Space group | Unit cell parameters | | | | $Z$ (kg m$^{-3}$) | $D_x$ | Ref. |
|---|---|---|---|---|---|---|---|---|---|
| | | | $a$ (nm) | $b$ (nm) | $c$ (nm) | Angle | | | |
| $\alpha_1$-$C_4AH_{19}$ | H | R$\bar{3}$c or R3c(?) | 0·577 | – | 6·408 | $\gamma = 120°$ | 3 | 1803 | A13 |
| $\alpha_2$-$C_4AH_{19}$ | H | $P6_3/m$ or $P6_322$ | 0·577 | – | 2·137 | $\gamma = 120°$ | 1 | 1802 | A13 |
| $C_4AH_{13}$ | H | R– – | 0·5752 | – | 9·527 | $\gamma = 120°$ | 6 | 2046 | F29 |
| $C_4A\bar{C}_{0.5}H_{12}$ | H | R$\bar{3}$ c or R3c | 0·5770 | – | 4·9159 | $\gamma = 120°$ | 3 | 1984 | F29 |
| $C_4A\bar{C}H_{11}$ | T | P$\bar{1}$ or P1 | 0·5781 | 0·5744 | 0·7855 | ‡ | 1/2 | 2170 | F29 |
| $C_4A\bar{S}H_{12}$ | H | R$\bar{3}$ | 0·576 | – | 2·679 | $\gamma = 120°$ | 3/2 | 2014 | A14 |
| $\alpha$-$C_3A \cdot CaCl_2 \cdot H_{10}$ | M | C2/c or Cc | 0·998 | 0·574 | 1·679 | $\beta = 110{\cdot}2°$ | 2 | 2065 | K23 |
| $\beta$-$C_3A \cdot CaCl_2 \cdot H_{10}$ | H | R$\bar{3}$c or R3c | 0·574 | – | 4·688 | $\gamma = 120°$ | 3 | 2090 | K23 |
| $C_3A \cdot CaCl_2 \cdot H_6$ | H | R$\bar{3}$c or R3c | 0·5729 | – | 4·1233 | $\gamma = 120°$ | 3 | 2080 | K24 |
| $C_2AH_{7.5}$* | M | C2/c or Cc | 0·993 | 0·574 | 4·22 | $\beta = 97.0°$ | 8 | 1943 | S66 |
| $C_2AH_5$ | H | R$\bar{3}$c | 0·573 | – | 5·22 | $\gamma = 120°$ | 6 | 2042 | S66 |
| $C_2ASH_8$ | H | R$\bar{3}$ or R3 | 0·5747 | – | 3·764 | $\gamma = 120°$ | 3 | 1936 | K25 |

* For $C_2AH_8$, only the structural element ($a = 0{\cdot}574$ nm, $c = 1{\cdot}07$ nm, $Z = 1$) and X-ray density (1950 kg m$^{-3}$) are known (S66).
† H = hexagonal or trigonal; M = monoclinic; T = triclinic.
‡ $\alpha = 92{\cdot}61°$, $\beta = 101{\cdot}96°$, $\gamma = 120{\cdot}09°$.

Table 6.2 includes crystal data for $C_4AH_x$, $C_4A\bar{C}_{0.5}H_x$ and $C_4A\bar{C}H_x$ groups. Only data based on single-crystal studies are included. Solid solutions in these groups of phases appear to be very limited, only $C_4A\bar{C}_{0.5}H_{12}$ showing some variation in layer thickness up to a maximum of about 0·825 nm associated with partial replacement of $CO_3^{2-}$ by $2OH^-$ together with variations in $H_2O$ content (D28,F29). The limiting composition is $C_4A\bar{C}_{0.25}H_x$. More extensive solid solution may occur in the poorly crystalline material formed in cement pastes.

### 6.1.3 *The $C_4A\bar{S}H_x$ phases*

Tables 6.2 and 6.3 give data for these phases. $C_4A\bar{S}H_{12}$ (or $C_3A \cdot C\bar{S} \cdot H_{12}$) is variously known as monosulfate, monosulfoaluminate, or, in the early literature, low-sulfate calcium sulfoaluminate. The water contents of the two highest hydrates are uncertain, values of 16 for the 0·95 nm hydrate (T32) and of 15 for the 1·03 nm hydrate (R25) having also been reported. An alternative formula with $18H_2O$ (M64) for the 0·95 nm hydrate implies an impossibly high density for the additional water.

$C_4A\bar{S}H_{12}$ forms solid solutions in which the $SO_4^{2-}$ is partly replaced by $OH^-$. The maximum replacement is 50% at 25°C, 33% at 45°C, 17% at 60°C and nil at 80°C. The layer thickness $c'$ decreases with increasing $OH^-$ content, to a value of 0·879 nm at 50% replacement (P23). Early reports that a continuous solid solution series exists with $C_4AH_x$ are incorrect. They were based on observations by light microscopy, which with layer structures of this type cannot distinguish between a true solid solution, in which the components are mixed at or below a nanometre level within each layer, an oriented intergrowth consisting of blocks each containing many layers of one or other component, or intermediate possibilities, such as random interstratification of layers of different types. Distinction can be made by XRD. $C_4A\bar{S}H_{12}$ and $C_4A\bar{C}H_{11}$ appear to be immiscible, but $C_4A\bar{C}_{0.5}H_{12}$ can accommodate a limited amount of sulfate (K26).

A compound of approximate composition $C_4A_{0.9}N_{0.5}\bar{S}_{1.1}H_{16}$, known as U-phase, was reported to form at high concentrations of $Na_2O$, $Al_2O_3$ and $SO_3$ (D29). Three hydration states, with $c' = 1{\cdot}00$, 0·93, and 0·81 nm, and 16, 12 and 8 moles of $H_2O$, respectively, were described, and it was suggested that the structure was derived from that of $C_4A\bar{S}H_x$ by the omission of some of the $Al^{3+}$ ions, balanced by the inclusion of $Na^+$, in addition to anions, in the interlayer. Several other investigations have confirmed the existence of this phase (B76,L25,S67,W24). Supporting evidence that AFm phases can accommodate cations as well as anions in the interlayer is provided by the existence of a compound $[Ca_2Al(OH)_6]K \cdot (ClO_4)_2 \cdot xH_2O$ (D27).

### 6.1.4 *Other AFm phases containing aluminium*

The range of anions that can occupy the X positions is very wide (A14,D27); even anions that form Ca salts of very low solubility, such as $F^-$, can be introduced using special techniques. We shall consider only those most relevant to cement chemistry. Tables 6.2 and 6.3 include data.

**Table 6.3** *AFm phases with $[Ca_2Al(OH)_6]^+$ principal layers and interlayer sulfate, chloride, aluminate or aluminosilicate anions*

| Composition | Drying conditions | Layer thickness (nm) | Interlayer contents† | | Ref. |
|---|---|---|---|---|---|
| $C_4A\bar{S}H_{16}$* | <10°C at 100% RH | 1·03 | $1/2SO_4^{2-}$ | $5H_2O$ | D28 |
| $C_4A\bar{S}H_{14}$* | >10°C at 100% RH | 0·95 | $1/2SO_4^{2-}$ | 4H2O | D28 |
| $C_4A\bar{S}H_{12}$ | >10°C at 20–95% RH | 0·893 | $1/2SO_4^{2-}$ | $3H_2O$ | D28 |
| $C_4A\bar{S}H_{10}$ | >10°C at <20% RH | 0·815 | $1/2SO_4^{2-}$ | $2H_2O$ | D28 |
| $C_4A\bar{S}H_8$ | 30°–50°C over $P_2O_5$ | 0·795 | $1/2SO_4^{2-}$ | $1H_2O$ | D28 |
| $C_3A \cdot CaCl_2 \cdot H_{10}$ ($\alpha$) | <28°C at 35% RH | 0·788 | $1Cl^-$ | $2H_2O$ | K23 |
| $C_3A \cdot CaCl_2 \cdot H_{10}$ ($\beta$) | >28°C at 35% RH | 0·781 | $1Cl^-$ | $2H_2O$ | K23 |
| $C_3A \cdot CaCl_2 \cdot H_6$ | 120–200°C | 0·687 | $1Cl^-$ | | K24 |
| $C_2AH_8$ | <26°C at 45% RH | 1·07 | $1Al(OH)_4^-$‡ | $3H_2O$ | S66 |
| $C_2AH_{7.5}$ | >26°C at 45% RH | 1·04 | $1Al(OH)_4^-$ | $5/2H_2O$ | S66 |
| $C_2AH_5$ | Room temp. over $P_2O_5$ | 0·87 | $1Al(OH)_4^-$ | | S66 |
| $C_2ASH_8$ | Room temp. at 37% RH | 1·255 | $1AlSiO_8H_8^-$ | $1H_2O$ | K25 |
| $C_2ASH_4$ | >135°C | 1·12 | $1AlSiO_5H_2^-$ | | K25 |

* Water contents uncertain; see text.
† Per formula unit of $Ca[Al(OH)_6]^+$.
‡ Al is 4 coordinated in $C_2AH_{7.5}$ (R26,S66) and possibly 6-coordinated in $C_2AH_8$ (G58).

$C_3A \cdot CaCl_2 \cdot 10H_2O$ or $[Ca_2Al(OH)_6]Cl \cdot 2H_2O$ (Friedel's salt) can be formed in concrete exposed to chloride solutions. Two polytypes are known; $\beta$ is the higher temperature form, produced reversibly from $\alpha$ at 28°C. $C_3A \cdot CaCl_2 \cdot 10H_2O$ does not form solid solutions with the sulfate AFm phases, but an ordered compound $C_6A_2 \cdot C\bar{S} \cdot CaCl_2 \cdot 24H_2O$ exists, in which interlayers containing $Cl^-$ probably alternate with ones containing $SO_4^{2-}$ (K23).

The $C_2A$ hydrates are AFm phases with aluminium-containing species in the interlayer. The hydrate formed in metastable equilibrium with aqueous solution at 18°C is $C_2AH_8$. Scheller and Kuzel (S66) found that, contrary to some earlier opinions, $C_2AH_8$ shows neither polymorphism nor polytypism, but that below 45% RH at 26°C it is converted into $C_2AH_{7.5}$. The transition temperature depends on the RH. An X-ray structure determination on the lower hydrate, $C_2AH_5$, showed that this had the constitution $[Ca_2Al(OH)_6][Al(OH)_4]$, the interlayer Al and some of the interlayer OH groups being statistically distributed. Because of poor crystallinity, it was not possible to obtain such detailed information about the higher hydrates, but some evidence was obtained for a similar constitution, with $H_2O$ molecules added, in $C_2AH_{7.5}$. A study using $^{27}Al$ NMR and EXAFS (extended X-ray absorption fine structure spectroscopy) confirmed this conclusion (R26). In contrast, an earlier study of $C_2AH_8$ (or $C_2AH_{7.5}$?) using $^{27}Al$ NMR showed that all the Al was octahedrally coordinated (G58), and the constitution $[Ca_2Al(OH)_6][Al(OH)_3(H_2O)_3]OH$ was proposed. The Al coordination might differ in the two hydrates, but further work on the 8-hydrate is needed. $C_2AH_8$ is reported to form solid solutions with $C_4AH_{19}$, but there is disagreement as to the end of the series at which these occur (D27,J18).

An early report of the formation of $C_4ASH_x$ was not supported by later work (C34), but three subsequent investigations have shown that such a phase can be prepared, though it is unstable at ordinary temperatures, and possibly so even in contact with its mother-liquor at 5°C. The anion is probably $H_2SiO_4^{2-}$, and hydration states with $c' \approx 1{\cdot}01$ nm and 0·89 nm, presumably analogous to those of $C_4A\bar{S}H_x$, have been observed. It was obtained by anion exchange (D27), in reaction rims around $C_3A$ grains in pastes made from $C_3A$, $C_3S$ and gypsum (R27) and by reaction between $C_4AH_{19}$ and amorphous silica in presence of water at 5°C (V5). Because of its instability, it is unlikely to be more than a transient hydration product of cement, at least at ordinary temperatures, but the possibility of partial replacement of $SO_4^{2-}$ by $H_2SiO_4^{2-}$ in an AFm phase cannot be excluded.

$C_2ASH_8$, known by its mineral name of strätlingite and also as 'gehlenite hydrate', is well established as a natural mineral, hydration product of certain types of composite cements and laboratory product. Its crystal data (Table 6.2) show it to be an AFm phase having an aluminosilicate anion as interlayer. The interlayer Al is tetrahedrally coordinated (G59,K25,K27,R28). Rinaldi *et al.* (R28) showed that, both in strätlingite and in a polytype, vertumnite, the interlayer is a double tetrahedral sheet of composition $[(T,\square)_4(OH,O)_8]^-$, where $\square$ represents

a vacant tetrahedral site and T can be Si or Al, with embedded water molecules. Compared with vertumnite, strätlingite tends to have a higher proportion of vacant tetrahedral sites and a higher degree of hydration; for $C_2ASH_8$, of every four tetrahedral sites, one would be occupied by aluminium, one by silicon and two would be vacant. The result appears to imply the possibility of variable Al/Si ratio. Kwan *et al.* (K27) studied the distribution of interlayer silicon and aluminium by NMR.

Naturally occurring AFm phases, called hydrocalumite, appear to vary in composition. The original specimen was reported to have a composition near $C_4AH_{12}$ with some $CO_3^{2-}$ and a monoclinic unit cell similar to that of $\alpha$-$C_3A \cdot CaCl_2 \cdot 10H_2O$ (T33), but others have proved to be either the $\alpha$- or the $\beta$-polymorph of that compound or members of a $C_3A \cdot CaCl_2 \cdot 10H_2O$–$C_4AH_{13}$ solid solution series (F30).

### 6.1.5 *AFm phases containing iron*

Iron(III) analogues of many of the phases described above have been obtained. Unless the anion imparts colour, AFm phases containing $Fe^{3+}$ are colourless, brown colours being due to iron(III) oxide or hydroxide impurity. They have *a*-axial lengths of approximately 0·589 nm (K28,S68).

$C_4FH_{13}$ has been obtained by many investigators (e.g. R29,S68). It has $c' = 0{\cdot}7902$ nm and forms a continuous series of solid solutions with $C_4AH_{13}$ (S68). As in the corresponding system with $Al_2O_3$, the phase existing in contact with solution is the 19-hydrate (R29). $C_4F\bar{S}H_x$ phases are also well established (M65). Kuzel (K28) found that $C_4F\bar{S}H_{12}$ is isostructural with its $Al^{3+}$ analogue, and has $c' = 0{\cdot}8875$ nm; a higher hydrate with $c' = 1{\cdot}021$ nm and probably containing $14H_2O$ exists above 90% RH. $C_4F\bar{S}H_{12}$ and $C_4A\bar{S}H_{12}$ form a continuous solid solution series at 100°C, but at 25°C or 50°C, miscibility is incomplete. At 25°C, $C_4F\bar{S}H_{12}$ accommodates up to about 50 mole % $C_4A\bar{S}H_{12}$, and the latter up to about 10 mole % $C_4F\bar{S}H_{12}$, and an intermediate phase with $Fe/Al \approx 0{\cdot}33$ exists (K28). $C_3F \cdot CaCl_2 \cdot 10H_2O$ similarly shows only limited miscibility with $C_3A \cdot CaCl_2 \cdot 10H_2O$ (K28).

Schwiete *et al.* (S69) found no solid solution between $C_4FH_{13}$ and $C_4F\bar{S}H_{12}$, but in preparations made from $C_4AF$ or $C_6A_2F$ limited miscibility occurred at the sulfate-rich end of the series as with $C_4AH_{13}$ and $C_4A\bar{S}H_{12}$. $Fe^{3+}$ analogues of the $Al^{3+}$ phases containing $CO_3^{2-}$ appear to exist (R30,S67).

### 6.1.6 *XRD patterns, thermal behaviour, optical properties and IR spectra*

Strong peaks in the XRD powder patterns of AFm phases normally include the first and second orders of the layer thickness, and the $11\bar{2}0$ and $30\bar{3}0$ reflections, which for the $Al^{3+}$ compounds have d-spacings at or near 0·2885 nm and 0·1666 nm, respectively. In mixtures, it is sometimes difficult to distinguish between AFm phases of similar layer thickness, and in such cases, examination of the patterns of heated samples is often useful.

Weight loss curves under either static or dynamic (TG) conditions or both have been reported for $C_4AH_{13}$ (B75,L6), $C_4A\bar{C}H_{11}$ (F29,T34), $C_4A\bar{C}_{0.5}H_{12}$ (F29), $C_4A\bar{S}H_{12}$ (T18), $C_3A \cdot CaCl_2 \cdot 10H_2O$ and other phases (A12,K24), $C_2AH_8$ (L6) and $C_2ASH_8$ (K25). The curves for $C_4AH_{13}$ and $C_4A\bar{S}H_{12}$ (Fig. 6.2) and of $C_2AH_8$ are all fairly similar if the quantity plotted against temperature is moles of $H_2O$ retained per mole of CaO, and allowance is made for the effect of differing heating rates. With the carbonate, nitrate and bromide, and on static heating also with the chloride, volatiles in addition to $H_2O$ are lost. All the curves show steps in varying degrees. Those at the lower temperatures are associated with the changes in hydration state of the AFm phase; loss of molecular water is complete by about 150°C on static, or 250°C on dynamic heating. XRD evidence showed that, for $C_4AH_{13}$, the plateau at about 350°C corresponds to formation of a poorly crystalline mixture of CH and $C_4A_3H_3$, and the steps at about 410°C and 630°C to decomposition of these phases to CaO and $C_{12}A_7H$ plus CaO, respectively (B75). The curve for $C_4A\bar{S}H_{12}$ shows similar features, but their significance has not been determined.

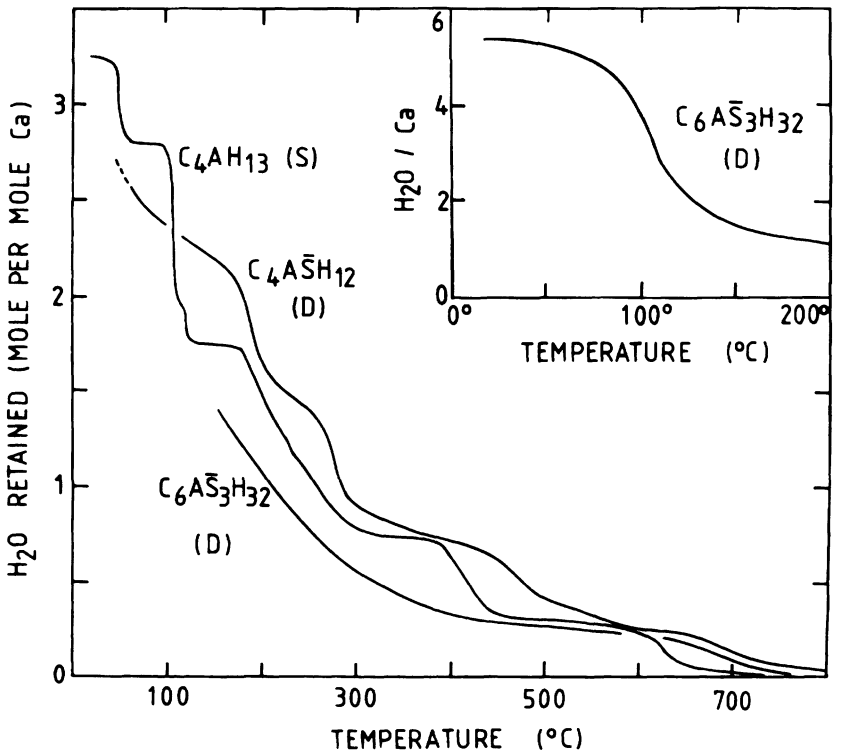


**Fig. 6.2** *Weight loss curves for $C_4AH_{13}$ (static; B75) and monosulfate and ettringite (TG; 10 K min$^{-1}$; T18).*

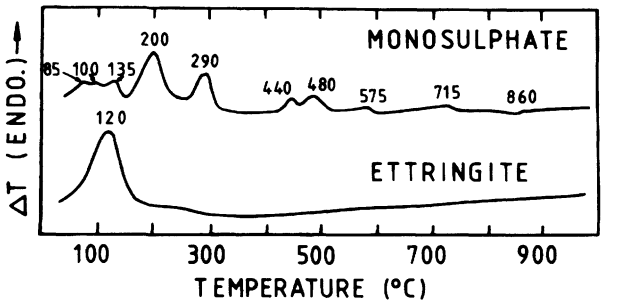


**Fig. 6.3** *DTA curves for monosulfate and ettringite (10 K min$^{-1}$) (New data).*

The DTA curves of $C_4AH_{13}$ and $C_4A\bar{S}H_{12}$ are characterized by a series of endotherms below 300°C, which correspond to the steps in the TG curve (K29,M66). Figure 6.3 includes a typical curve for $C_4A\bar{S}H_{12}$; that of $C_4AH_{13}$ is similar, but with peak temperatures some 10 K lower. The peak temperatures depend on the technique and amount present, and probably on the degree of crystallinity, the 200°C peak being typically shifted to 180–190°C for the material present in cement pastes (B77). DTA curves have been reported for other AFm phases, including $C_4A\bar{C}H_{11}$ (T34), $C_3A \cdot CaCl_2 \cdot 10H_2O$ (A12,K24) and $C_2ASH_8$ (K25).

As would be expected from their layer structures, AFm phases are optically negative. The $Al^{3+}$ phases typically have $\omega = 1{\cdot}50$–$1{\cdot}56$, $\varepsilon$ 1·49–1·54; for the $Fe^{3+}$ phases, $\omega$ is typically 1.56–1.61 and $\varepsilon$ is typically 1·54–1·60.

Henning (H37) reviewed IR spectra of hydrated calcium silicates and aluminates; data for $C_4AH_x$ and $C_2AH_x$ phases, $C_4A\bar{S}H_{12}$, $C_4A\bar{C}H_{11}$ and $C_4F\bar{S}H_{12}$ were included. Other data for phases in the $CaO$–$Al_2O_3$–$H_2O$ system (B78) and for $C_4A\bar{S}H_{12}$ (B79) have been reported.

## 6.2 AFt phases

### *6.2.1 Compositions and crystal structures*

AFt ($Al_2O_3$–$Fe_2O_3$–tri) phases have the general constitutional formula $[Ca_3(Al,Fe)(OH)_6 \cdot 12H_2O]_2 \cdot X_3 \cdot xH_2O$, where $x$ is, normally at least, $\leq 2$ and X represents one formula unit of a doubly charged, or, with reservations, two formula units of a singly charged anion. The term AFt refers to the three units of CX in an alternative way of writing the formula, $C_3(A,F) \cdot 3CX \cdot yH_2O$ [or $C_6(A,F)X_3 \cdot yH_2O$], where $y = x + 30$. AFt phases are formed under broadly similar conditions to AFm phases, but at higher ratios of CaX to $C_3(A,F)$ and rarely above about 90°C. The range of anions that can occupy the X sites is smaller, and singly charged anions can possibly only be accommodated to a limited extent. The most important AFt phase is ettringite, $[Ca_3Al(OH)_6.12H_2O]_2 \cdot (SO_4)_3 \cdot 2H_2O$ or $C_3A \cdot 3CaSO_4 \cdot 32H_2O$; a phase of or near this composition is formed during the early hydration of most Portland cements. In the early literature, it was often called high-sulfate calcium sulfoaluminate.

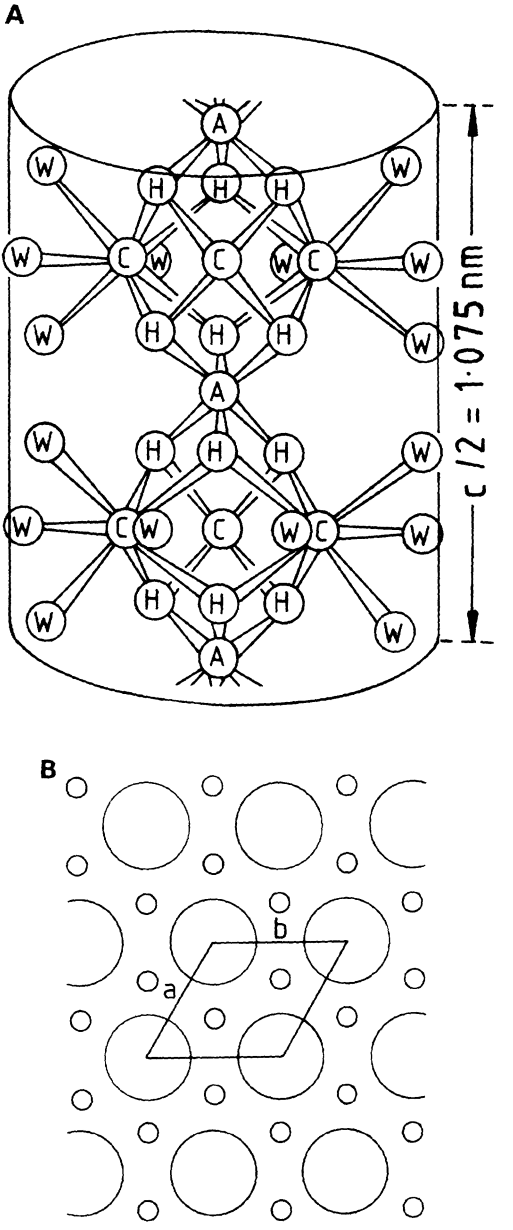


**Fig. 6.4** *Crystal structure of ettringite. (A) Part of a single column in (11$\bar{2}$0) projection; A = Al, C = Ca, H = O of an OH group, W = O of an $H_2O$ molecule. Hydrogen atoms are omitted, as are the $H_2O$ molecules attached to those calcium atoms lying in the central vertical line of the figure. (B) Projection on the ab-plane, showing columns (large circles) and channels (small circles); the unit cell, with a = 1·123 nm, is outlined. Modified from S70.*

Ettringite also occurs as a natural mineral. Phases of AFt type also exist in which other cations replace the $Ca^{2+}$ or $Al^{3+}$ or both; an important example is thaumasite, $Ca_3[Si(OH)_6 \cdot 12H_2O](CO_3)(SO_4)$.

AFt phases form hexagonal prismatic or acicular crystals. Their structures (C35,M67,M68) are based on columns in hexagonal array, running parallel to the prism ($c$) axis, with the X anions and, usually, $H_2O$ molecules in the intervening channels (Fig. 6.4B). The columns, which are of empirical formula $[Ca_3(Al,Fe)(OH)_6 \cdot 12H_2O]^{3+}$, are composed of $(Al,Fe)(OH)_6$ octahedra alternating with triangular groups of edge-sharing $CaO_8$ polyhedra, with which they share $OH^-$ ions (Fig. 6.4A). Each calcium atom is also coordinated by four $H_2O$ molecules, the hydrogen atoms of which form the nearly cylindrical surface of the column. Per formula unit with six calcium atoms, the channels contain four sites, of which, in ettringite, three are occupied by sulfate and one by two water molecules. The repeat distance along the column is approximately 1·07 nm.

Ettringite is trigonal, with $a = 1{\cdot}123$ nm, $c = 2{\cdot}150$ nm, $Z = 2$, $D_x = 1775\,\mathrm{kg\,m^{-3}}$ (S70); the space group is P31c, apparent higher symmetry being due to twinning or disorder (M68). It is optically negative, with $\omega = 1{\cdot}463$, $\varepsilon = 1{\cdot}459$ (M69). The doubling of $c$ is due to ordering of the $SO_4^{2-}$ ions and $H_2O$ molecules in the channels. A higher hydrate, $C_6A\bar{S}_3H_{36}$, is reported to exist at high relative humidities (P24).

### 6.2.2 *Ettringite analogues and solid solutions*

A carbonate analogue, $C_6A\bar{C}_3H_{32}$, is well established (C34). Its unit cell ($a = 1{\cdot}0834$ nm, $c = 2{\cdot}1250$ nm; S70) and refractive indices ($\omega = 1{\cdot}480$, $\varepsilon = 1{\cdot}456$) are near those of ettringite, but the cell parameters differ sufficiently to permit distinction by XRD. Hollow, tubular crystals have been observed (C34).

Pöllmann *et al.* (P24) showed that the fully $OH^-$-substituted phase, $C_6AH_{36}$, exists but is easily carbonated. Midgley and Rosaman (M66) concluded from DTA evidence that $SO_4^{2-}$ can be partly replaced by $OH^-$ in the AFt phase of cement pastes. An XRD study (P25) confirmed that up to approximately one-half of the $SO_4^{2-}$ in ettringite can be replaced by $2OH^-$, and showed that up to two-thirds of the $SO_4^{2-}$ can be replaced by $CO_3^{2-}$, but neither $C_6A\bar{C}_3H_{32}$ nor $C_6AH_{36}$ can accommodate any $SO_4^{2-}$. $C_6A\bar{C}_3H_{32}$ and $C_6AH_{36}$ are completely miscible.

Material described as a silicate analogue was later shown to have also contained $CO_3^{2-}$ (C34) but a product identified by X-ray microanalysis as $C_6AS_3H_{31}$ has since been found in reaction rims around $C_3A$ particles in pastes of that compound with $C_3S$ and gypsum (R27). The compound $C_3A \cdot 3CaCl_2 \cdot 30H_2O$ has been reported to form at temperatures below 0°C, but to be unstable at 20°C (S71,S72). A later attempt to prepare it failed (P24). Analogues of ettringite with $Fe^{3+}$, $Mn^{3+}$, $Cr^{3+}$ or $Ti^{3+}$ in place of $Al^{3+}$ exist (B80,B81,S70); solid solution in the $Fe^{3+}$–$Al^{3+}$ series is almost continuous, but there is probably a small gap at 70–80 mole % $Fe^{3+}$ (B80). The $Fe^{3+}$ phase has $a = 1{\cdot}1182$ nm, $c = 2{\cdot}2008$ nm (S70). Analogues also exist with $CrO_4^{2-}$ replacing $SO_4^{2-}$ (B80,B82) and with $Sr^{2+}$

replacing $Ca^{2+}$ (B83). Several other AFt phases have been described (J19,P24). Solid solutions occur between ettringite and its chromate and borate analogues, as well as ternary solid solutions including $OH^-$ (P26).

Thaumasite, $[Ca_3Si(OH)_6 \cdot 12H_2O](SO_4)(CO_3)$ or $C_3S\bar{S}\bar{C}H_{15}$, has a structure similar to that of ettringite, with $Si^{4+}$ replacing $Al^{3+}$ and $SO_4^{2-}$ and $CO_3^{2-}$ groups in the channel sites (E2,E3). The octahedral coordination of the Si was first established from IR evidence (M70). Thaumasite is hexagonal, with space group $P6_3$, $a = 1{\cdot}104$ nm, $c = 1{\cdot}039$ nm, $Z = 2$, $D_x = 1886\,kg\,m^{-3}$ (E2); the refractive indices are $\omega = 1{\cdot}470$, $\varepsilon = 1{\cdot}504$. An $Mn^{4+}$ analogue, jouravskite, exists (G60). Thaumasite and ettringite are not completely miscible, but limited solid solutions probably occur (E2).

### *6.2.3 Properties*

If crystals of natural ettringite are dehydrated, lattice shrinkage occurs, mainly in the *ab* plane, giving a product with $a \approx 0{\cdot}84$ nm, $c \approx 1{\cdot}02$ nm and probable constitution $[Ca_3Al(OH)_6 \cdot 3H_2O]_2(SO_4)_3$; this has been observed using crystals of the natural mineral heated at 110°C and subsequently examined by XRD (B84), or examined by electron diffraction, dehydration then occurring in the high vacuum (G61). Most of the molecular water has been lost, and the columns have fused together. Several phases of similar structure, such as despujolsite, $[Ca_3Mn(OH)_6 \cdot 3H_2O](SO_4)_2$ (G62), occur as natural minerals. Synthetic ettringite becomes almost amorphous when heated or subjected to a high vacuum, and gross morphological changes are easily effected in the electron microscope. The differing behaviour may be related to defect concentrations.

At ordinary humidities, ettringite begins to lose water rapidly at about 50°C. Figure 6.2 includes a TG curve, determined at $10\,K\,min^{-1}$. Curves obtained at lower heating rates for ettringite and its $Fe^{3+}$ and $Cr^{3+}$ analogues have been reported (B80). Thaumasite is thermally more stable, rapid weight loss beginning only at 110°C (B85). DTA curves have been reported for ettringite (B80,M66), its $Fe^{3+}$ (B80,M66) and $CO_3^{2-}$ (C34) analogues and thaumasite (B85). Figure 6.3 includes a curve for ettringite. All show strong endotherms at 110–150°C, the temperature varying somewhat with the composition, technique and amount present. When present in cement pastes, ettringite typically gives a peak at 125–130°C (B77).

In XRD powder patterns, ettringite is readily recognized by its strong, low-angle peaks at 0·973 nm ($10\bar{1}0$) and 0·561 nm ($11\bar{2}0$), which disappear on heating or intensive drying at room temperature. The corresponding peaks of thaumasite have spacings of 0·956 nm and 0·552 nm. The quantitative determination of ettringite is, at best, difficult because of the ease with which water is lost and crystallinity decreased during isolation or grinding, and opinions have differed as to whether it can be satisfactorily determined in hardened cement pastes by QXDA (C36,L26,M71,O16). Ettringite has also been determined by DTA or DSC (O16). IR spectra of ettringite, thaumasite and related phases have been reported (B77,B80–B82,B85,M70,S70).

## 6.3 Other hydrated phases

### 6.3.1 Hydrogarnet phases

These phases have structures related to that of grossular or garnet ($Ca_3Al_2Si_3O_{12}$). The latter has a cubic structure, in which the silicon, aluminium and calcium are in tetrahedral, octahedral and distorted cubic coordination, respectively; each oxygen is bonded to one silicon, one aluminium and two calcium atoms. In the hydrogarnets, this structure is modified by omission of some or all of the silicon, the charge being balanced by replacing each of the oxygen atoms to which it was attached by hydroxyl. The $Al^{3+}$ may be partly or wholly replaced by $Fe^{3+}$. Complete replacement of $Si^{4+}$ by $4H^+$ in grossular thus gives $Ca_3[Al(OH)_6]_2$ or $C_3AH_6$, and solid solutions exist within a compositional region bounded by $C_3AH_6$, $C_3FH_6$, $C_3AS_3$ and $C_3FS_3$. In recent mineralogical nomenclature, phases in the $C_3AH_6$–$C_3AS_3$ series are collectively called hydrogrossular, and the names katoite and hibschite are used more specifically to denote those with $SiO_2/Al_2O_3$ molar ratios below and above 1·5, respectively (P27).

$C_3AH_6$ is the only stable ternary phase in the $CaO$–$Al_2O_3$–$H_2O$ system at ordinary temperatures, but neither it nor any other hydrogarnet phase is formed as a major hydration product of typical, modern Portland cements under those conditions. Minor quantities of hydrogarnets are formed from some composite cements and, in a poorly crystalline state, from Portland cements. Larger quantities were given by some older Portland cements, and are also among the normal hydration products of autoclaved cement-based materials. $C_3AH_6$ is formed in the 'conversion' reaction of hydrated calcium aluminate cements (Section 10.1.4).

Hydrogarnet phases crystallize in various cubic forms, of which at ordinary temperatures icositetrahedra are probably the most usual. The space group is Ia3d, with $Z = 8$; $C_3AH_6$ has $a = 1{\cdot}25755$ nm, $D_x = 2527\ kg\ m^{-3}$ (K30). Detailed structural studies have been reported on $C_3AH_6$ or $C_3AD_6$ (B86,F31,K31,L27) and on phases in the $C_3AH_6$–$C_3AS_3$ (B87,S73) and $C_3FH_6$–$C_3FS_3$ (C37) series. The hydrogen atoms lie outside the tetrahedra of oxygen atoms to which they are attached, and which surround the empty silicon sites. They form neither hydrogen bonds nor, contrary to some early views, $H_4$ clusters.

The compositions of naturally occurring specimens indicate that the $C_3AH_6$–$C_3AS_3$ solid solution series is continuous (P27), but synthetic studies show that it is unlikely that all compositions in this series can be obtained at any one temperature and pressure (R7). At 95°C and 1 bar, solid solutions can be prepared with $SiO_2/Al_2O_3$ ratios of 0·00–0·42 and 0·76–0·99; there is a miscibility gap at ratios of 0·42–0·76 (J20). Contrary to many earlier opinions, $C_3FH_6$ can be prepared in the absence of $SiO_2$, though it is metastable and easily decomposed at ordinary temperatures (R29).

Equations relating the cell parameter and coordinates of the oxygen atoms in hydrogarnets to composition have been proposed (B87,B88), but give mediocre agreement with the observed cell parameter for $C_3AH_6$. The equations implicitly assume that Végard's law is obeyed over

the entire $C_3AH_6$–$C_3AS_3$ series, but the existence of miscibility gaps indicates that this may not be the case. An empirical equation giving better agreement over the more highly hydrated compositions relevant to cement chemistry is

$$a = 1{\cdot}171 + 0{\cdot}016Fe_2O_3 + 0{\cdot}0144H_2O \qquad (6.1)$$

where $a$ is the cell parameter in nm and $Fe_2O_3$ and $H_2O$ are the values of $x$ and $y$, respectively, in the formula $C_3A_{1-x}F_xS_{3-y/2}H_y$. In order to determine the composition of a phase of this general composition from the XRD powder pattern, a second quantity must be used. Zur Strassen (Z12) showed that the intensity ratio of the 022 peak to the 116 peak ($d = 0{\cdot}4445$ nm and $0{\cdot}2040$ nm, respectively, for $C_3AH_6$) was suitable. Table 6.4 gives some values of $a$ and of this ratio, calculated from equation 6.1 and from the crystal structure respectively (T5).

Studies by weight loss, XRD and IR spectroscopy show that, on static heating, $C_3AH_6$ decomposes at 200–250°C to a mixture of $C_{12}A_7H$ and CH, of bulk composition $C_3AH_{1.43}$ (B86,B89). At 500–550°C, the CH decomposes to CaO and on prolonged heating at 810°C, $C_3A$ is formed (K30). The $C_{12}A_7$ and $C_3AH_6$ structures are closely related (B11) and the $C_{12}A_7H$ forms topotactically, with all three axes parallel to those of the $C_3AH_6$ (B86). The $a$-axis of $C_{12}A_7H$ (1·198 nm) is only slightly shorter than that of $C_3AH_6$ (1·258 nm), and the lattice shrinkage at 200–250°C is gradual.

Passaglia and Rinaldi (P27) discussed IR spectra and TG curves for $C_3AH_6$ and other hydrogarnet phases. The TG curve of $C_3AH_6$ shows major loss at 250–310°C and further loss at 450–550°C, but in that of a katoite specimen the two steps were barely distinguishable. There is disagreement as to whether the temperature of the principal step varies systematically with $SiO_2/Al_2O_3$ ratio (L27,P27). Majumdar and Roy (M72) reported DTA and IR data for $C_3AH_6$. The refractive indices of $C_3AS_3$ and $C_3AH_6$ are 1·734 and 1·604 respectively; those of the solid solutions are linearly related to the composition (P27).

### 6.3.2 $CAH_{10}$

This phase is formed as a hydration product of calcium aluminate cements (Section 10.1.4). The crystals are hexagonal prisms, but none

**Table 6.4** *Calculated values of the cell parameter a and ratio of intensities of the 022 to the 116 XRD powder reflections for some hydrogarnet phases (T5)*

| $x$ (moles $Fe_2O_3$ in formula) | $C_3A_{1-x}F_xH_6$ | | $C_3A_{1-x}F_xSH_4$ | | $C_3A_{1-x}F_xS_2H_2$ | |
|---|---|---|---|---|---|---|
| | $a$ (nm) | $I_{022}/I_{116}$ | $a$ (nm) | $I_{022}/I_{116}$ | $a$ (nm) | $I_{022}/I_{116}$ |
| 1·0 | 1·273 | 2·22 | 1·245 | 1·77 | 1·216 | 1·36 |
| 0·5 | 1·265 | 1·15 | 1·237 | 0·78 | 1·208 | 0·43 |
| 0·0 | 1·257 | 0·41 | 1·229 | 0·17 | 1·200 | 0·03 |

large enough for single-crystal X-ray structure determination have been obtained. Evidence from XRD powder diffraction and thermal dehydration behaviour suggested a tentative unit cell and ionic constitution $Ca_3[Al_6(OH)_{24}] \cdot 18H_2O$, in which the anions are rings of six edge-sharing octahedra (B90). A $^{27}Al$ NMR study confirmed that the Al is octahedrally coordinated (G58). Richard *et al.* (R26) determined the principal features of the crystal structure, which confirmed and extended these results. In addition to powder XRD and $^{27}Al$ NMR, they used XANES (X-ray absorption near edge spectroscopy) to obtain information on the environments of the calcium and aluminium atoms. There was some uncertainty regarding the positions of the water molecules, but comparisons of observed and calculated XRD powder intensities confirmed the essential correctness of the proposed structure. The hexagonal unit cell has $a = 1{\cdot}6381$ nm, $c = 0{\cdot}8317$ nm, $Z = 6[CAH_{10}]$, $D_x = 1743\,kg\,m^{-3}$, prism axis $c$, and the pattern of linked $Al(OH)_6$ octahedra is related to that of the infinite sheets of such octahedra in gibbsite.

Much of the water in $CAH_{10}$ is very loosely bound; water loss begins on drying at 80% RH, and the H/A ratio is about 7 at 45% RH or 5·5 on drying over $P_2O_5$. TG curves at 0·5 or $5\,K\,min^{-1}$ (L28) show no definite steps; at 110°C, H/A is about 4 for the lower or 6 for the higher heating rate. On static heating at $p(H_2O) = 6$ torr, H/A is about 6 at 50°C, 3 at 110°C and 1 at 200°C.

The products of thermal decomposition depend on how easily the water can escape (B90). If escape is easy, a nearly amorphous product retaining some of the structural features of $CAH_{10}$ is formed, but if it is not, $C_3AH_6$ and gibbsite ($AH_3$) are formed. The latter situation can occur if a hardened paste of a calcium aluminate cement containing $CAH_{10}$ is heated. Under conditions not giving $C_3AH_6$, the XRD pattern varies continuously with temperature; the crystallinity deteriorates, the cell parameters decrease slightly and relative intensities change markedly. Little change occurs up to about 70°C, but by 120°C (H/A ≈ 2·5), only the 1·4 nm peak and a close doublet near 0·7 nm remain, and the relative intensity of the 1·4 nm peak is much reduced. By 200–350°C, the material is amorphous; by 1000°C, CA is formed. The marked loss in crystallinity that occurs when H/A falls below 4 can be attributed to the fact that further loss entails dehydroxylation. With some preparations small amounts of $C_2AH_8$ and $AH_3$ are also formed. The rehydration behaviour has been studied (B91).

DTA curves at $10\,K\,min^{-1}$ show a large endotherm at 130–150°C and a smaller one at about 290°C. Since the first of these is due to loss of molecular water, its height is affected by any preliminary drying that the specimen may have undergone. DTA has been used to determine the relative amounts of $CAH_{10}$ and $AH_3$, and thus indirectly also of $C_3AH_6$, in calcium aluminate cement concretes, but caution is needed because the $CAH_{10}$ may have undergone partial dehydration and also because its thermal decomposition can itself yield $AH_3$. To some extent, this caution also applies to the determination of $CAH_{10}$ by QXDA.

Henning (H37) reported IR spectra for $CAH_{10}$, $CAH_7$ and $CAH_4$.

### 6.3.3 Brucite, hydrotalcite and related phases

Brucite (magnesium hydroxide; $Mg(OH)_2$) is isostructural with CH. It is formed in Portland cement concrete that has been attacked by Mg salts, and on hydration of Portland cements high in MgO and possibly of Portland cements in general. It has $a = 0{\cdot}3147$ nm, $c = 0{\cdot}4769$ nm, $Z = 1$, $D_x = 2368\,kg\,m^{-3}$, $\omega = 1{\cdot}561$, $\varepsilon = 1{\cdot}581$ (S74). The three polytypes of aluminium hydroxide [$Al(OH)_3$], known as gibbsite, bayerite and nordstrandite, contain layers essentially similar to those in brucite, but with an ordered pattern of cation vacancies and a different relationship between adjacent layers, resulting from hydrogen bonding.

Hydrotalcite-type phases are structurally related to brucite as the AFm phases are to CH; that is, some of the $Mg^{2+}$ ions are replaced by tripositive ions, typically $Al^{3+}$ or $Fe^{3+}$, and the charge is balanced by anions which, together with $H_2O$ molecules, occupy interlayer sites. Hydrotalcite itself occurs as a natural mineral of composition $[Mg_{0{\cdot}75}Al_{0{\cdot}25}(OH)_2](CO_3)_{0{\cdot}125}(H_2O)_{0{\cdot}5}$. Many other phases of this type are known, as other cations of similar size can replace the $Mg^{2+}$ or $Al^{3+}$ or both, and other anions can replace the $CO_3^{2-}$. Allmann (A14) reviewed them. Hydroxyl ions can replace the $CO_3^{2-}$ in hydrotalcite, giving a phase called meixnerite, but this is very easily carbonated (K32). The basic features of the crystal structure common to the group as a whole were originally determined from studies on sjögrenite, which is a polytype of the $Fe^{3+}$ analogue of hydrotalcite (A15,I11). Phases approximating to hydrotalcite are formed on hydration of slag cements, and as minor products in the hydration of Portland cements.

Because the dipositive and tripositive cations in these phases are similar in size, their relative numbers are not fixed, as in AFm phases. Brindley and Kikkawa (B92) discussed the factors limiting the $M^{2+}/(M^{2+} + M^{3+})$ ratio. The minimum value is 2/3, and could be set by a requirement to avoid the occurrence of $M^{3+}$ ions in adjacent sites; in phases of this ratio, the cations are ordered (H38), giving unit cells with $a$ approximately $\sqrt{3}$ times that of brucite. At higher ratios, the cations are disordered, though ordered regions may occur locally, and the upper limit of the ratio may be set by nucleation of pure brucite layers if the proportion of tripositive ions falls below a certain value. In a study of synthetic meixnerites, pure phases were obtained only at Mg/(Mg + Al) ratios between 0·67 and 0·76, suggesting an upper limit close to 0·75 (M73), and it may be significant that this ratio is much the most usual in the natural minerals.

As with the AFm phases, anion exchange reactions occur (H38). Among the natural minerals of the group, ones with interlayer $CO_3^{2-}$ are relatively common, and ones with interlayer $OH^-$ very rare. This may be a further indication that replacement of $OH^-$ by $CO_3^{2-}$ occurs easily. Differing schemes for the packing of $H_2O$ molecules and $CO_3^{2-}$ ions in the interlayer have been proposed (A15,I11).

Layer thicknesses are similar to those of the AFm phases, and it would be difficult to distinguish the two groups of phases by XRD if only the basal reflections could be observed. Polytypism is common; e.g. sjögrenite, with a two-layer structure, has a three-layer polytype, called pyroaurite.

Three-layer structures are the ones normally formed at room temperature. Meixnerite, which is a three-layer form, has $a = 0{\cdot}30463$ nm, $c = 2{\cdot}293$ $(3 \times 0{\cdot}764)$ nm, space group $R\bar{3}m$, $Z = 3$, $D_x = 1950\,kg\,m^{-3}$ (K32). IR spectroscopic studies on Mg–Al phases of this group have been reported (H38), and there is an extensive literature on synthesis and thermal behaviour, arising largely from various applied chemical applications (e.g. B93,M74,M75). DTA curves typically show endotherms at about 285°C and 440°C; samples relatively high in aluminium (e.g. with Mg/Al = 2·0) also show a smaller endotherm at about 390°C. The 285°C endotherm is due mainly to loss of molecular water, that at 390°C, when it occurs, mainly to loss of hydroxyl water associated with aluminium, and that at 440°C mainly to loss of hydroxyl water associated with magnesium and of $CO_2$.

### 6.3.4 Sulfate phases

Table 6.5 lists these phases and gives crystal and optical data. The gypsum used in cement manufacture is usually of natural origin, but by-product gypsums produced by the chemical industry have also been used. The most important is phosphogypsum, resulting from manufacture of phosphoric acid by the wet process. It contains impurities, especially phosphate and fluoride, that retard setting and which, if present in relatively high proportions, may have to be partially removed by appropriate pretreatments (M76). Another by-product gypsum, which may be produced in increasing quantity, is that resulting from flue-gas desulfurization.

Dehydration of gypsum in air at 70–200°C gives hemihydrate ($CaSO_4 \cdot \sim 0{\cdot}5H_2O$) or $\gamma$-$CaSO_4$ ('soluble anhydrite'), the extent of dehydration depending on the temperature and duration of heating and RH of the surrounding atmosphere. $\gamma$-$CaSO_4$ is probably never completely anhydrous (B95). These products have essentially identical crystal structures, which are hexagonal or pseudohexagonal, with the $H_2O$ molecules in channels parallel to the hexagonal $c$ axis. The channels can accommodate methanol (R31). Hemihydrate is known as a natural mineral, called bassanite. Above about 200°C, anhydrite (also called 'insoluble anhydrite'; Section 2.5.1) is formed.

Reported $\alpha$ and $\beta$ forms of hemihydrate appear to differ only in degree of crystallinity or crystal size, the more crystalline $\alpha$ form being obtained by dehydration of gypsum in presence of liquid water or aqueous solutions and the $\beta$ form by heating in air (B96). $\gamma$-$CaSO_4$ is readily rehydrated to hemihydrate. There has been uncertainty as to the maximum $H_2O$ content of these products and whether variation in this quantity is continuous. Kuzel (K33), studying highly crystalline preparations, found that variation was continuous from 0·53 to 0·62 $H_2O$, but that a miscibility gap existed at 0·03–0·53 $H_2O$; the space group was $P3_121$ for 0·62 $H_2O$ and I2 for 0·53 $H_2O$. Some studies indicate a maximum $H_2O$ content well above 0·5; thus Abriel (A16) reported a crystal structure refinement for a preparation with 0·8 $H_2O$, for which the space group was $P3_121$. The $H_2O$ molecules were found to be statistically

**Table 6.5** *Crystal and optical data for hydrated sulfate phases*

| | | Hemihydrate | | $\gamma$-$CaSO_4$ | Syngenite |
|---|---|---|---|---|---|
| | $CaSO_4 \cdot 2H_2O$ | $CaSO_4 \cdot 0{\cdot}8H_2O$ | $CaSO_4 \cdot 0{\cdot}5H_2O$ | $CaSO_4 \cdot <0{\cdot}05H_2O$ | $K_2Ca(SO_4)_2 \cdot H_2O$ |
| *Crystal data* | | | | | |
| Crystal system | Monoclinic | Trigonal | Monoclinic | Hexagonal | Monoclinic |
| Space group | I2/a | $P3_121$ | I2 | $P6_222$ | $P2_1/n$ |
| *a* (nm) | 0·5679 | 0·6968 | 0·6930 | 0·69695 | 0·6225 |
| *b* (nm) | 1·5202 | – | 1·2062 | – | 0·7127 |
| *c* (nm) | 0·6522 | 0·6410 | 1·2660 | 0·63033 | 0·9727 |
| Angles (°)* | $\beta = 118{\cdot}43°$ | $\gamma = 120°$ | $\alpha = 90°$ ‡ | $\gamma = 120°$ | $\beta = 104{\cdot}15°$ |
| *Z* | 4 | 3 | 12 | 3 | 2 |
| $D_x$ (kg m$^{-3}$) | 2310 | 2783 | 2733 | 2558 | 2607 |
| Reference† | P28 | A16 | L29 | L29 | B94 |
| *Optical data and morphology (W3)* | | | | | |
| $\alpha$ | 1·5205 | ~1·56 | 1·559 | 1·505 | 1·5010 |
| $\beta$ | 1·5226 | – | 1·5595 | – | 1·5166 |
| $\gamma$ | 1·5296 | ~1·59 | 1·5836 | 1·548 | 1·5176 |
| Optic sign and 2*V* | (+)58° | + | (+)14° | + | (−)28·3° |
| Morphology | Tablets, (010) cleavage | Hexagonal prisms (length *c*); rarely, hexagonal plates | | | Tablets or prisms |

* Where not 90°.

† Also to crystal structure refinements.

‡ Axes chosen to clarify relation to the trigonal and hexagonal modifications; $b = 0{\cdot}696\sqrt{3}$ nm, $c = 2 \times 0{\cdot}633$ nm.

distributed, with four molecules among five positions. Abriel concluded that larger unit cells arose through ordering of the $H_2O$ molecules, which was possible only at $H_2O$ contents of or below 0·5. This would account for the larger cell with space group I2 found at $H_2O$ contents around 0·5 and for the reversion to a smaller cell in $\gamma$-$CaSO_4$. The extent to which these structural distinctions are relevant to the less crystalline products obtained by heating gypsum in air is uncertain.

Reaction in presence of water between $K_2SO_4$ and $CaSO_4$ can produce syngenite, $KCS_2H$, data for which are included in Table 6.5.

## 6.4 Equilibria and preparative methods

### 6.4.1 *The $CaSO_4$–$H_2O$, $CaSO_4$–$Ca(OH)_2$–$H_2O$ and $CaSO_4$–$K_2SO_4$–$H_2O$ systems*

At ordinary temperatures, the metastable solubility of hemihydrate or $\gamma$-$CaSO_4$ is considerably higher than the solubility of gypsum, which is thus precipitated on mixing either of the former materials with water (Fig. 6.5); the setting of plaster is based on this reaction. Anhydrite displaces gypsum as the stable phase above 42°C, or at somewhat lower temperatures if other solutes are present, but is not readily precipitated, and gypsum can persist metastably up to at least 98°C, above which temperature hemihydrate is stable relative to gypsum.

The solubility of gypsum is only slightly decreased in presence of CH, and vice versa (Table 6.6). This effect can be explained by the strong association of $Ca^{2+}$ in the solution with both $OH^-$ and $SO_4^{2-}$, which can be described in terms of the formation of $CaOH^+$ (Section 5.7.2) and neutral $CaSO_4$ respectively. The formation constant of the latter species is 204 mol $l^{-1}$ (S62).

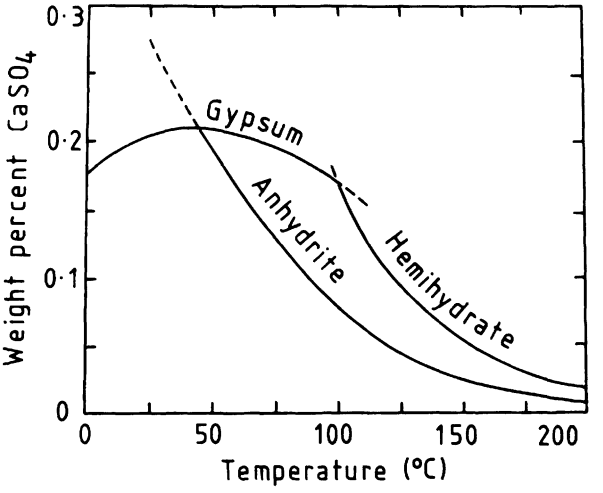


**Fig. 6.5** *The $CaSO_4$–$H_2O$ system. After P29.*

**Table 6.6** *Invariant points in the system $CaO–Al_2O_3–SO_3–H_2O$ at 20°C (B97,D30): Labelling of points as in Fig. 6.7*

| Point | Solid phases | Concentrations ($mmol\,l^{-1}$) | | |
|---|---|---|---|---|
| | | CaO | $Al_2O_3$ | $CaSO_4$ |
| w | $Ca(OH)_2$ | 20·7 | – | – |
| o | Hydrous alumina | – | ~0·01 | – |
| b | Gypsum | – | – | 15·2 |
| v | $Ca(OH)_2$, $C_4AH_{19}$ | 21·5 | 0·0329 | – |
| y | $C_4AH_{19}$, $C_2AH_8$ | 10·9 | 0·94 | – |
| p | $C_2AH_8$, hydrous alumina | 5·79 | 6·74 | – |
| c | CH, gypsum | 19·7 | – | 12·4 |
| j | Hydrous alumina, gypsum | – | ~0·01 | 15·2 |
| f | Ettringite, gypsum, $Ca(OH)_2$ | 20·6 | 0·0272 | 12·2 |
| e | Ettringite, gypsum, hydrous alumina | 0·151 | 0·103 | 15·1 |
| d | Ettringite, monosulfate, $Ca(OH)_2$ | 21·1 | 0·022 | 0·0294 |
| n | Ettringite, monosulfate, hydrous alumina | 5·98 | 1·55 | 5·88 |

Gartner *et al.* (G63) discussed equilibria governing precipitation of gypsum, calcium hydroxide and syngenite with reference to the early stage of cement hydration. They concluded that the equilibrium activity products at 25°C were $(2{\cdot}547 + 2{\cdot}258I) \times 10^{-5}\,mol^2\,l^{-2}$ for gypsum, $8{\cdot}25 \times 10^{-6}\,mol^3\,l^{-3}$ for calcium hydroxide and $(13{\cdot}9I - 0.3) \times 10^{-8}\,mol^5\,l^{-5}$ for syngenite, where $I$ is the ionic strength. Bailey and Hampson (B98) noted the need to take into account both complex formation and activity coefficients.

### 6.4.2 *The $CaO–Al_2O_3–H_2O$ and $CaO–Al_2O_3–SO_3–H_2O$ systems*

Aspects of equilibria in these systems that are mainly relevant to Portland cement hydration are considered in this section; those that are mainly relevant to calcium aluminate cements are discussed in Sections 10.1.4 and 10.1.5. Figure 6.6 shows equilibria in the $CaO–Al_2O_3–H_2O$ system mainly as found by Jones and Roberts (J18) at 25°C and reported by Jones (J21), who also reviewed earlier studies. Table 6.6 gives invariant concentrations at 20°C. The stable phases in contact with solution at 25°C are gibbsite ($AH_3$), $C_3AH_6$ and CH, but metastable solubility curves for AFm phases, $CAH_{10}$ and hydrous alumina can also be obtained.

The curve shown for AFm phases contains a discontinuity at Y. Jones and Roberts considered that the curve CY related to $C_4AH_{19}$, and the curve YT to a solid solution of $C_4AH_{19}$ with $C_2AH_8$ which had C/A = 2·0 at T and C/A = 2·4 at Y; the prolongation TT′ of this latter curve related to $C_2AH_8$. The results of Dosch and Keller (D27) do not support the conclusion that solid solutions with C/A ratios of 2·0–2·4 exist, but the data of Jones and Roberts could probably be equally well explained by the

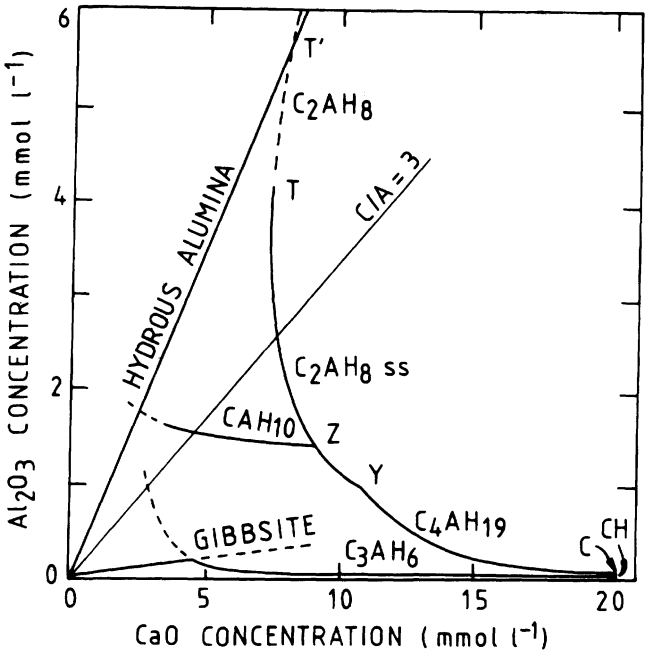


**Fig. 6.6** *The $CaO–Al_2O_3–H_2O$ system at 25°C, mainly after J18; $CAH_{10}$ solubility curve at 21°C, P30.*

formation of oriented intergrowths on a submicrometre scale. Not all workers have observed the discontinuity at Y. The curve for the AFm phases may be slightly variable, as small changes in conditions could determine whether separate crystals of $C_4AH_{19}$ and $C_2AH_8$, intergrowths or solid solutions are formed.

Data have also been obtained at other temperatures from 1°C to 50°C (J21); some are considered in Section 10.1.5. At 50°C or above, the other ternary phases are rapidly replaced by $C_3AH_6$.

Equilibria in the $CaO–Al_2O_3–SO_3–H_2O$ system were studied at 25°C by Jones (J22) and at 20°C by d'Ans and Eick (D30). Following Brown (B97), the latter's results are shown on a three-dimensional diagram in which the functions plotted are the tenth roots of the concentrations (Fig. 6.7). This figure represents the metastable equilibria involving AFm phases and hydrous alumina. The stable equilibria, which involve $C_3AH_6$ and crystalline $AH_3$, were also studied but are less relevant to cement hydration chemistry. Table 6.6 gives data for the invariant points.

The use of thermodynamic calculations to systematize and clarify equilibrium data in the $CaO–Al_2O_3–H_2O$ and related systems is outlined in Section 10.1.5. It was pioneered by Nikushchenko *et al.* (N15) and was later used by Dron (D31) and, notably, by Barret and co-workers (B99–B102) and by Glasser, Damidot and co-workers (A17,D32–D38).

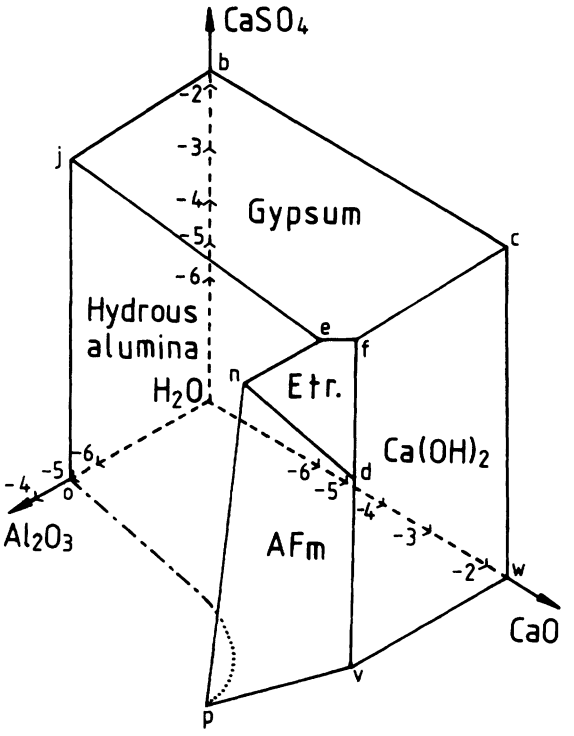


**Fig. 6.7** *Metastable equilibria in the $CaO–Al_2O_3–SO_3–H_2O$ system at 20°C, showing crystallization surfaces, based largely on the data of d'Ans and Eick (D30). Concentrations are expressed as logarithms to the base 10 of values in mol $l^{-1}$ and, following B97, are plotted on scales proportional to their tenth roots. Concentrations at the lettered invariant points are given in Table 6.6.*

Equilibrium solubility surfaces were thus calculated for the $CaO–Al_2O_3–SO_3–H_2O$ system at 25°C, 50°C and 85°C (A17,D32,D33). If allowance was made for the effects of different forms of $AH_3$, the results at 25°C agreed well with those found experimentally. Contrary to an earlier suggestion (S67), they showed that monosulfate was always metastable relative to $C_3AH_6$ and ettringite in the system at 25°C, but that at temperatures above 45°C monosulfate became stable at the expense of ettringite over an increasingly wide range of concentrations. Ogawa and Roy (O17) studied the stability of ettringite in the presence of water at higher temperatures and summarized earlier work. Ettringite appears to be stable in water up to at least 90°C at atmospheric pressures, 130°C at 6·7 MPa or 145°C at 27 MPa. The principal decomposition product is monosulfate. In cement pastes, it normally decomposes at about 70°C, because the C–S–H competes strongly for $SO_4^{2-}$ ions (B76), but if sufficient $SO_4^{2-}$ is present, it persists to higher temperatures (H39,K34).

### 6.4.3 Systems including $Na_2O$, $K_2O$, $SiO_2$, $CaCO_3$ or $CaCl_2$

The $CaO–Al_2O_3–SO_3–H_2O$ system modified by various additions of alkalis has been studied both experimentally (J23) and by thermodynamic calculation (D33,D34). In the main, the general form of the phase relations appears to be unchanged, but the invariant concentrations are considerably altered. In the presence of $K_2O$, syngenite and, at high $K_2O$ concentrations or high temperatures, $K_2SO_4$, KOH and 'pentasalt' ($C_5K\bar{S}_6$) may have to be considered (D34). Ettringite is stable over the pH range 10·43–12·52 at 25°C or 10·87–12·25 at 85°C. Monosulfate is stable at pH 11·80–12·25 at 85°C; an extrapolation suggests that it is likely to persist at 25°C only at or above pH 12 (D32). Experimental data are in reasonable agreement with these conclusions (G64).

Dron (D31) calculated the general form of the solubility surfaces in the $CaO–Al_2O_3–SiO_2–H_2O$ system at ordinary temperatures (Fig. 6.8). The phases considered were C–S–H, strätlingite, $C_4AH_x$, $C_2AH_8$, CH, hydrous silica and hydrous alumina. Damidot and Glasser (D35) made more detailed calculations, in which $C_3AH_6$ and hydrogarnet phases were introduced in place of $C_2AH_8$ and $C_4AH_{13}$. Both studies showed that strätlingite cannot coexist stably with CH, but a hydrogarnet phase can coexist with CH or with strätlingite. Neither study took into account the incorporation of sulfate or aluminate ions into the C–S–H; results described in Section 6.5.3 show that this can be of major importance in application of the $CaO–Al_2O_3–SiO_2–H_2O$ system to Portland cement hydration.

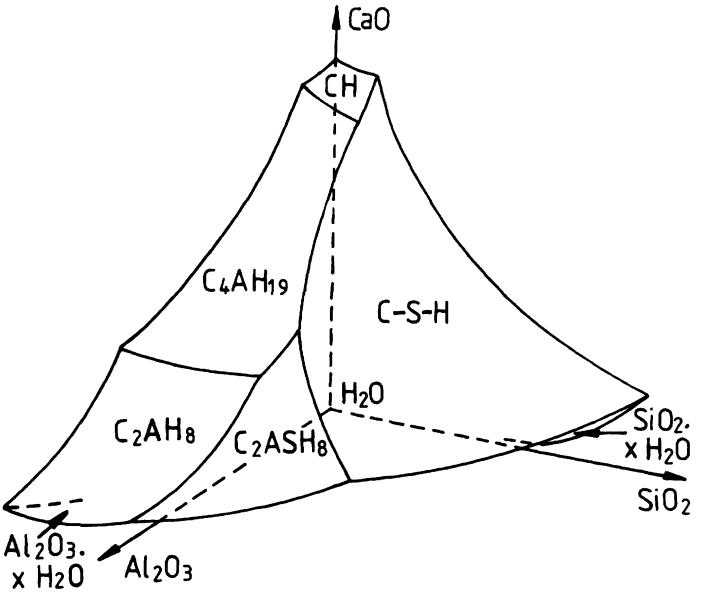


**Fig. 6.8** *General form of the metastable equilibria in the $CaO–Al_2O_3–SiO_2–H_2O$ system at ordinary temperature, showing solubility surfaces. Modified from D31.*

The $CaO–Al_2O_3–CaCO_3–H_2O$ system has been studied by thermodynamic calculation (B101,B102,D36,D37,S75), as has the $CaO–Al_2O_3–CaCl_2–H_2O$ system (D38). In the latter system at 25°C, $C_3A \cdot CaCl_2 \cdot 10H_2O$ has a stable phase field (A18,D38).

### *6.4.4 Preparative methods*

Mylius (M69) described the preparation of many calcium aluminate hydrates and related compounds. As with C–S–H, it is normally essential to exclude atmospheric $CO_2$ and to avoid prolonged contact with glass apparatus. Dosch and Keller (D27) described methods for obtaining many AFm phases by anion exchange or other special procedures.

The $C_4A$ and $C_2A$ hydrates are most conveniently prepared by adding calcium oxide or saturated CH solution to a supersaturated calcium aluminate solution obtained by shaking CA or white calcium aluminate cement (Section 10.1.1) with water. Such solutions typically contain up to about 1·2 g CaO $l^{-1}$ and 1·9 g $Al_2O_3$ $l^{-1}$, these concentrations depending on the shaking time, temperature, proportioning and particle size of the starting material. The amount of calcium oxide or CH solution added must be such as to produce the desired compound and a solution in metastable equilibrium with it, in accordance with the solubility relations (Fig. 6.6 and Table 6.6). $CAH_{10}$ may be prepared in this way at 5°C, no calcium oxide or CH being added to the supersaturated solution. $C_3AH_6$ may be prepared from metallic aluminium and CH solution at 50°C, or by hydrothermal treatment of $C_3A$ or a mixture of calcium oxide and $AH_3$ with water at 150°C.

Ettringite may be prepared by mixing solutions of CH, gypsum and $Al_2(SO_4)_3$. Mylius used 1000 ml of saturated CH (1·2 g CaO $l^{-1}$) diluted to 1200 ml (A), 530 ml of saturated gypsum (2·05 g $CaSO_4$ $l^{-1}$; B) and a solution of 1·78 g of $Al_2(SO_4)_3 \cdot 18H_2O$ in 770 ml of water (C). Solutions A and B were first mixed, and solution C then added, with shaking. The mixed solution was shaken at 18°C until an initially precipitated gel had been replaced by crystalline material. The molar proportions are $8CaO : 1Al_2(SO_4)_3 : 3CaSO_4$.

Monosulfate is troublesome to prepare. Mylius mixed 500 ml of a supersaturated calcium aluminate solution (649 mg CaO and 969 mg $Al_2O_3$ $l^{-1}$) at 18°C, with shaking, with 2924 ml of saturated CH (1·25 g CaO $l^{-1}$) and 334 ml of saturated gypsum (1·93 g $CaSO_4$ $l^{-1}$). After 30 min, crystallization was complete; the mixture was filtered, washed four times with a little water followed by 96% ethanol and ether, and dried over $CaCl_2$ and soda lime without evacuation. Monosulfate may also be prepared hydrothermally (A11).

Carlson and Berman (C34) described the preparation of $C_4A\bar{C}H_{11}$ and $C_6A\bar{C}_3H_{32}$. $C_4A\bar{C}H_{11}$ was obtained using a supersaturated calcium aluminate solution, saturated CH and $Na_2CO_3$. The most satisfactory method for preparing $C_6A\bar{C}_3H_{32}$ employed a supersaturated calcium aluminate solution, $NH_4HCO_3$ and a concentrated CH solution containing sucrose.

Crammond (C38) reviewed reports of the formation of thaumasite in the laboratory and in deteriorated building materials. It forms readily at 4°C from mixtures that contain the appropriate ions and also 0·4–1·0% of reactive alumina. It does not form at 25°C or above. A little $Al^{3+}$ may be essential, and reported failures to reproduce published syntheses may be due to the use of Al-free materials.

## 6.5 Hydration reactions of the aluminate and ferrite phases

### *6.5.1 Reaction of $C_3A$ with water or with water and calcium hydroxide*

The reactions of $C_3A$ and $C_4AF$ with water, alone or in the presence of calcium hydroxide or sulfate or both, have been widely studied for the light they may cast on the mechanism of Portland cement hydration, and especially on the action of gypsum in controlling setting. The results of such studies must be interpreted with caution. The aluminate and ferrite phases in Portland cement clinker differ greatly in composition from the pure compounds. In normal clinkers, they are intimately mixed with each other and react in an environment chemically and microstructurally influenced, and perhaps dominated, by the silicate phases, and which is further affected by the presence of alkalis. Small quantities of $CO_2$, which are likely to be present in real concretes, have important effects on the reactions.

Many studies have shown that the reaction of $C_3A$ with water in suspensions at ordinary temperatures gives $C_2AH_8$ and $C_4AH_{19}$, which are subsequently converted into $C_3AH_6$. At temperatures above about 30°C or in pastes, conversion is rapid and the AFm phases may not be observed; local temperature increase due to the strongly exothermic nature of the reaction probably has an important effect. Studies using SEM and XRD (B103) or HVTEM (S53) indicate that an amorphous gel is formed as a precursor to the crystalline phases; it appears to consist of thin foils growing on the $C_3A$ surface. Direct evidence on its composition, obtained using ESCA, is conflicting (B104,J24); indirect evidence from the $CaO/Al_2O_3$ ratio of the solution suggests that the initial ratio in the solid product is below 3·0 (B105,G65). In agreement with this conclusion, inspection of Fig. 6.6 indicates that the first product to form might be either $C_2AH_8$ or hydrous alumina, the latter tending to redissolve later.

In pastes, the hydration of $C_3A$, as followed calorimetrically, is slightly retarded if CH is present (C39). The products are essentially the same as those formed in the absence of CH, but the crystals of AFm phases are smaller (G66). In dilute suspensions, the first crystalline product to form is $C_4AH_{19}$; this causes the $CaO/Al_2O_3$ ratio in the solution to decrease (B105).

### *6.5.2 Reaction of $C_3A$ with water in the presence of calcium sulfate*

Studies using calorimetry, electron microscopy, XRD and DTG (C39,S76,S77) have shown that this reaction occurs in two stages, both of which are strongly exothermic. The first stage is characterized by a peak in the heat evolution curve during the first 30 min, and yields ettringite. In the second stage, which is characterized by a peak typically

occurring at 24–48 h, the ettringite reacts further and AFm phases are formed. The reactions may be represented by the following equations:

$$C_3A + 3C\bar{S}H_2 + 26H_2O \rightarrow C_6A\bar{S}_3H_{32} \quad (6.2)$$

$$2C_3A + C_6A\bar{S}_3H_{32} + 4H_2O \rightarrow 3C_4A\bar{S}H_{12} \quad (6.3)$$

$$C_3A + CH + 12H_2O \rightarrow C_4AH_{13} \quad (6.4)$$

where the $C_4AH_{13}$ forms a solid solution with monosulfate. Each of these reactions occurs to an extent that depends on the ratio of gypsum to $C_3A$. $C_4AH_{13}$ can form only if calcium hydroxide is also present.

Studies by TEM (B106) and HVTEM (S53) show that, as in the absence of gypsum, the formation of a distinctly crystalline reaction product is preceded by that of a layer of amorphous or poorly crystalline material having a foil or irregular, platey morphology on the surface of the grains. There is no direct evidence concerning the composition of this material, but Brown (B97) concluded from a consideration of the phase equilibria (Fig. 6.7) that, depending on the concentrations in the solution in contact with the $C_3A$ when the latter began to react, the first $Al_2O_3$-containing phase to form might be either $AH_3$ or ettringite. The morphology of the product does not support the view that it is ettringite, though it might be an amorphous material of similar composition. Formation of a crystalline precursor to the ettringite has also been reported (C40).

The ettringite produced in the first stage of reaction tends to form as stubby, prismatic crystals up to 1 $\mu$m long and close to the $C_3A$ surfaces, but it is also formed away from these surfaces, thus indicating a through-solution mechanism (M77,S53). Further evidence for the latter is provided by the observation that, in pastes of $C_3A$ and $C_3S$ with gypsum, some of the $C_3A$ grains form hollow shells only partly occupied by unreacted starting material or hydration products (S53). The ettringite crystals are readily damaged by the electron beam. Longer needles, of high aspect ratio, can also form. The amount of available space (M77), pH (B106) and sulfate ion concentration (S53) have been variously considered to control the morphology.

Addition of gypsum substantially retards reaction of the $C_3A$ in the pure system; CH increases the effect (C39). Gypsum also retards $C_3A$ hydration in cement pastes (T35; section 7.6.1). The effect of gypsum has been attributed to the protective action of a layer of ettringite (C39,S77), but it has been queried whether this layer is sufficiently impermeable to have such an effect (M77). Retardation has also been attributed to an underlying layer of hydrous alumina (C41) or AFm phase (G67,P31); this view is consistent with the electron microscopic evidence mentioned earlier. The retarding properties of such a layer might well depend on its composition, thus explaining the different rates of reaction observed in the absence of admixtures and with CH or gypsum or both. Retardation has also been attributed to the blocking of active sites on a modified $C_3A$ surface by adsorbed sulfate ions (F32,S78); however, $Na_2SO_4$ has no significant effect on the rate of reaction (C39).

### 6.5.3 Effects of temperature, alkali, tricalcium silicate and $CO_2$

Brown and Bothe (B76) studied the formation of ettringite from $C_3A$ and gypsum in systems including KOH or $C_3S$ or both at temperatures up to 80°C. Important results included the following.

(1) Elevated temperature in the range studied did not prevent ettringite formation.
(2) KOH retarded, but did not prevent, ettringite formation. At concentrations above 1 mol $l^{-1}$, syngenite was also formed. KOH accelerated the hydration of the $C_3S$.
(3) In the presence of $C_3S$, ettringite was formed at all temperatures provided that KOH was absent.
(4) At elevated temperatures in the presence of 0·5 mol $l^{-1}$ KOH and $C_3S$, little or no ettringite was formed.

The effect of alkali in depressing ettringite formation confirms an earlier observation by Ghorab and El Fetouh (G68). These observations show that, in any use of equilibria in the $CaO–Al_2O_3–SO_3–H_2O$ system in relation to Portland cement hydration at elevated temperatures, the effects of $K_2O$ and of the C–S–H cannot be ignored. Absence of ettringite or other hydrated aluminate or sulfoaluminate phases implies that the aluminate and sulfate ions have been incorporated into the C–S–H. Alkali favours this effect both by accelerating the formation of C–S–H and by retarding that of ettringite.

Monosulfate reacts with $CO_3^{2-}$ in the presence of CH to give ettringite and, initially, hemicarbonate (K35,S67,V6). Finely ground $CaCO_3$ is effective as a source of $CO_3^{2-}$. This reaction may play an important part in the hydration of $C_3A$ in practical concretes. It is discussed in Sections 7.1.2 and 9.6.3.

### 6.5.4 Reaction of the ferrite phase

Many investigations have shown that the hydration products of phases in the $C_2(A,F)$ series are essentially similar to those formed from $C_3A$ under comparable conditions (C42–C44,D13,S68). The experimental evidence includes XRD, DTA, DTG, TEM, SEM, IR and calorimetry. The first crystalline products to form in the absence and presence of $CaSO_4$ are AFm and AFt phases, respectively, the AFt phases being later replaced by AFm phases, as in the case of $C_3A$. Both types of product phase contain $Fe^{3+}$ as well as $Al^{3+}$, and tend to undergo further change to give hydrogarnet phases. ESCA evidence (B104) indicates that the surface of $C_4AF$ is hydroxylated and deficient in Ca and Fe before contact with liquid water. The deficiency in Fe possibly arises from zoning, considered in Section 2.3.1.

Different preparations of ferrite phase of a given composition and particle size distribution appear to vary greatly in reactivity (e.g. S53), perhaps because of zoning and differences in distribution of cations among tetrahedral and octahedral sites (Section 1.5.1). Some of the earlier studies indicated that reaction is accelerated in presence of CH, but later work showed that, as with $C_3A$, reaction is retarded by CH, more

strongly by gypsum and still more strongly by the two together. Under comparable conditions, $C_4AF$ appears normally to react more slowly than $C_3A$, though, initially at least, the reverse may sometimes be the case (S53). It appears generally agreed that the rate of reaction of the ferrite phase decreases with the Fe/Al ratio.

Several investigators have noted that the ratio of Al to Fe in the product phases tends to be higher than that of the starting material, and have concluded that an iron(III) oxide or hydroxide is also formed. Teoreanu *et al.* (T36), using Mössbauer spectroscopy and XRD, concluded that the hydration products formed from $C_2F$ or $C_4AF$ at ordinary temperatures included $FH_3$. With $C_2F$ above 75°C, this was replaced by hematite. Fukuhara *et al.* (F33) concluded from calorimetric evidence that the AFt phase formed from $C_4AF$ in pastes at 20°C had an Al/Fe ratio of about 3 and postulated that $FH_3$ was also formed. Rogers and Aldridge (R29) found that in $C_2(A,F)$ preparations hydrated at 4°C the only product detectable by XRD was $C_4(A,F)H_{19}$, but evidence from X-ray microanalysis showed that an amorphous iron oxide or hydroxide was also formed. In products formed at 80°C hematite was identified by XRD, microanalysis and Mössbauer spectroscopy. Hydrogarnet phases formed from $C_6A_2F$ or $C_4AF$ contained only small proportions of iron, as did that formed from $C_6AF_2$ at 150°C; those formed from $C_6AF_2$ at 21°C or 80°C had Fe/(Al + Fe) ratios of 0·30–0·35. Fortune and Coey (F34), using XRD and Mössbauer spectroscopy, similarly found that hydrous iron(III) hydroxide was present among the products of $C_4AF$ hydrated at 72°C. The hydrogarnet phase that was the main product had an Fe/(Al + Fe) ratio of 0·22. If CH was added, this ratio was increased to 0·32, but the hydrogarnet formed in presence of gypsum was almost free from $Fe^{3+}$.

Brown (B107) concluded that in $C_4AF$ hydration in presence of $CaSO_4$ the early product was $C_2AH_8$ or hydrous alumina, and that it was followed by formation of an AFt phase containing little or no $Fe^{3+}$; an

**Table 6.7** *Standard enthalpies of formation ($\Delta H_f^0$; kJ mol$^{-1}$) for some compounds relevant to hydration of the aluminate and ferrite phases (25°C except where otherwise stated)*

| Compound | $\Delta H_f^0$ | Ref. | Compound | $\Delta H_f^0$ | Ref. |
|---|---|---|---|---|---|
| $C_3A$ | −3587·8 | W10 | $C_6A\bar{S}_3H_{32}$ | −17 539 | W10 |
| | | | | −17 528 | S68 |
| $C_4AF$ (20°C) | −5090·3* | T8 | $C_4A\bar{S}H_{12}$ | −8778 | W10 |
| | | | | −8752 | S79 |
| $C_6A_2F$ | −8104·9 | N12 | $C_4AH_{13}$ | −8318 | H40 |
| $C\bar{S}H_2$ | −2022·6 | W10 | $C_4A\bar{C}H_{10·68}$ | −8176 | W10 |
| $C\bar{S}H_{0·5}$ ($\beta$) | −1514·65 | W10 | $C_3AH_6$ | −5548 | W10 |
| CH | −986·1 | W10 | $H_2O$ (liquid) | −285·83 | W10 |

* Using data for oxides, from W10.

**Table 6.8** *Enthalpy changes for some hydration reactions of $C_3A$, calculated from the data in Table 6.7*

| Reaction | $\Delta H$ (kJ per mole of $C_3A$) |
|---|---|
| $C_3A + 3C\bar{S}H_2 + 26H_2O \rightarrow C_6A\bar{S}_3H_{32}$ | −452 |
| $C_3A + C\bar{S}H_2 + 10H_2O \rightarrow C_4A\bar{S}H_{12}$ | −309 |
| $C_3A + CH + 12H_2O \rightarrow C_4AH_{13}$ | −314 |
| $C_3A + 6H_2O \rightarrow C_3AH_6$ | −245 |
| $2C_3A + C_6A\bar{S}_3H_{32} + 4H_2O \rightarrow 3C_4A\bar{S}H_{12}$ | −238 |

iron oxide gel containing some $Ca^{2+}$ was also formed. The conclusion regarding the later products agrees substantially with that of Fukuhara *et al.* (F33). The tendency to form iron oxide or hydroxide may be connected with the fact that species containing $Al^{3+}$ can migrate in pastes relatively easily, whereas those containing $Fe^{3+}$ cannot, and are thus largely confined to the space originally occupied by the anhydrous material from which they come (T37).

### 6.5.5 Enthalpy changes

Table 6.7 gives standard enthalpies of formation of some relevant compounds, and Table 6.8 gives enthalpy changes for hydration reactions of $C_3A$ calculated from them. The strongly exothermic nature of these reactions is apparent. Lack of data for the standard enthalpies of the hydration products containing iron precludes similar calculations for the ferrite phase. For the hydration of $C_3A$ to give $C_3AH_6$, Lerch and Bogue (L24) obtained an experimental value of $-234\,kJ\,mol^{-1}$; other workers have obtained similar results. Experimental determinations of the enthalpy of hydration of $C_4AF$ have given $-203\,kJ\,mol^{-1}$ (products not established; L24), and, in the presence of excess CH to give hydrogarnets, $-193\,kJ\,mol^{-1}$ for $C_4AF$ and $-208\,kJ\,mol^{-1}$ for $C_4A_{0.68}F_{0.32}$ (B63). For $C_4AF$ in the presence of gypsum to give ettringite and $FH_3$, a value of $-352\,kJ\,mol^{-1}$ has been reported (F33). Houtepen and Stein (H40) gave standard enthalpies of formation of some other AFm phases determined experimentally, and Babushkin *et al.* (B65) gave values for other compounds estimated on the basis of crystal chemistry.

# 7 Hydration of Portland cement

## 7.1 Evidence from X-ray diffraction, thermal analysis and infrared spectroscopy

### *7.1.1 Introduction; formation of calcium hydroxide and C–S–H*

Study of the hydration process and products in concretes, and even in mortars, is complicated by the presence of the aggregate. Some concentration of the paste can usually be effected by crushing, mild grinding and sieving, but with most experimental techniques, much more detailed information can be obtained from studies on pastes. Because of this, most investigations have related to pastes and, unless otherwise stated, this chapter relates to ordinary Portland cements hydrated in pastes at 15–25°C and w/c ratios of 0·45–0·65. However, data for pastes stored under constant external conditions may not be fully applicable to the paste fraction of concrete. Much of the paste in a normal concrete is close to aggregate surfaces and differs from bulk paste; in real concretes, temperature and other parameters inevitably vary both with age and with location within the material. Of the various experimental approaches, microstructural studies are probably the ones for which the presence of an aggregate interferes least with the quality of the data that can be obtained.

XRD powder studies on cement pastes have been reported by many investigators (e.g. C45,M78). Gypsum and other calcium sulfate phases are usually no longer detectable after, at most, 24 h, and the clinker phases are consumed at differing rates, alite and aluminate phase reacting more quickly than belite and ferrite. The ratio of belite to alite thus increases steadily, and after about 90 days at most, little or no alite or aluminate phase is normally detectable. The rates of disappearance of the phases present in the unreacted cement are considered more fully in Section 7.3.1. As with pure calcium silicate pastes, the principal products are C–S–H and CH.

TEM studies show that a small proportion of the CH in cement pastes is cryptocrystalline and intimately mixed with the C–S–H (G69,V4). This contrasts with the situation in pure $C_3S$ pastes (Section 5.1.3). Cryptocrystalline CH was also found in pastes made from calcium oxide and silica of high w/s ratio and of blastfurnace slag activated by CH (G70). These observations may explain ones, reviewed by Barker (B108), that

the CH in cement pastes appears to contain small amounts of $SiO_2$. A reported occurrence of amorphous CH in a Renaissance lime plaster (M79) was disproved (N16), but a natural occurrence of amorphous CH has been described (N17).

*7.1.2 Formation of hydrated aluminate or sulfoaluminate phases*

The phases of these types that are observed depend on the cement composition, the time and other conditions of hydration, the presence or otherwise of $CO_2$ and the drying conditions. With most ordinary Portland cements at ordinary temperatures, ettringite peaks are detectable in the XRD pattern within a few hours and increase in intensity to a maximum, often at about 1 day. The 0·973 and 0·561 nm peaks are especially prominent, but many other peaks can often be detected, indicating that at least some of the ettringite is highly crystalline. Subsequently, peaks of AFm phases usually appear and are somewhat variable. Where present, they normally comprise hk.0 peaks at about 0·288 nm (11·0) and 0·166 nm (30·0) and the first- and second-order basal reflections corresponding to one or more layer thicknesses. The AFm peaks tend to be broad and, taking into account also the amounts likely to be present, the XRD evidence suggests that much of the AFm material is poorly crystalline. The AFm peaks may be observed within 24 h, but are sometimes only observed after some days or even months.

In one type of behaviour, the ettringite peaks weaken after about 24 h and may ultimately disappear, while peaks of monosulfate ($c' = 0{\cdot}89$ nm) or a monosulfate solid solution appear and gradually become stronger. This behaviour is common in laboratory-prepared pastes from which $CO_2$ has as far as possible been excluded, and arises from the reactions represented by equations 6.2–6.4 (Section 6.5.2). Sulfate ion is released rapidly from the clinker sulfates and calcium sulfate, whereas $Al(OH)_4^-$ is released, mainly from the aluminate phase, more slowly, and the resulting high ratio of available $SO_4^{2-}$ to available $Al(OH)_4^-$ favours the formation of ettringite. By about 24 h, substantially all the $SO_4^{2-}$ has been released, and the continuing supply of $Al(OH)_4^-$ leads to the dissolution of ettringite and precipitation of monosulfate. The reactions are in reality more complex than the above. An amorphous gel is formed in addition to the ettringite; it seems to be high in $Al_2O_3$ and $SiO_2$, but also to contain significant proportions of $Ca^{2+}$ and $SO_4^{2-}$ (Section 7.2.2). In addition, the C–S–H takes up some of the $SO_4^{2-}$ ions. Not all of the sulfate released from the gypsum and clinker sulfates thus enters the ettringite directly. Because of the lower rate of release of the $Al(OH)_4^-$, sulfate may enter the amorphous gel and the C–S–H, from which it is partly or wholly transferred to ettringite as more $Al(OH)_4^-$ becomes available.

The AFm phase ultimately formed in these reactions will only have the monosulfate composition if the effective ratio of $SO_3$ to $Al_2O_3$ is 1·0. With cements of relatively high $SO_3/Al_2O_3$ ratio not all of the ettringite may disappear; conversely, with those in which this ratio is low, the monosulfate may undergo anion exchange, giving a solid solution in

which the $SO_4^{2-}$ is partly replaced by $OH^-$. With a sulfate-resisting Portland cement, ettringite has been reported to persist for periods of up to 1 year, but eventually to disappear, probably due to incorporation of $SO_4^{2-}$ and $Al(OH)_4^-$ in the C–S–H (G5). Monosulfate was not detected. In another study, substantial contents of ettringite were found at ages up to 60 days, together with poorly crystalline AFm phase (H41).

Petrographic studies on field concretes appear very commonly to show the presence of ettringite, but monosulfate has rarely been reported. Ettringite could persist, even with cements of low $SO_3/Al_2O_3$ ratio, because of a reaction with $CO_3^{2-}$, which reacts with monosulfate in the presence of $Ca(OH)_2$ to produce ettringite and hemicarbonate (S67,S80):

$$3C_4A\bar{S}H_{12} + 2Ca^{2+} + CO_3^{2-} + 2OH^- + 19H_2O \rightarrow C_6A\bar{S}_3H_{32} + 2C_4A\bar{C}_{0.5}H_{12} \qquad (7.1)$$

Of every three moles of $C_4A\bar{S}H_{12}$, one is decomposed, its content of $Al_2O_3$ going to form ettringite, and two undergo anion exchange, giving hemicarbonate. Further reaction with $CO_3^{2-}$ causes the hemicarbonate to be replaced by monocarbonate, and, ultimately, the AFm and AFt phases are destroyed. In a cement paste, ettringite and hemicarbonate may be formed directly. Kuzel and Meyer (K35) noted that a few tenths of a per cent of $CO_2$ (referred to the mass of cement) could suffice to prevent the formation of monosulfate in a typical cement paste, and concluded that, as a result, ettringite was likely to persist indefinitely. The extent to which this happens in field concretes is largely a matter for conjecture.

In those cement pastes in which monosulfate is formed, XRD usually shows this to be the 12-hydrate, with $c' \approx 0{\cdot}89$ nm. Intensive drying can cause dehydration to the 10-hydrate, with $c' \approx 0{\cdot}82$ nm, and can also cause the ettringite peaks to disappear (C45). On the other hand, it has been reported that the 14-hydrate is present in undried pastes (K35).

With the probable exception of sulfate-resisting types (G5), modern Portland cements do not yield amounts of hydrogarnet detectable by XRD on hydration at ordinary temperatures, though a poorly crystalline product probably approximating to a hydrogarnet has been found by TEM (Section 7.4.2). Luke and Glasser (L30) found a hydrotalcite-type phase by XRD in a residue from which the other phases had been removed by chemical extraction. Calcite, if present, is detectable by a sharp peak superimposed on the maximum in the C–S–H band at 0·3035 nm, and if in sufficient quantity by additional peaks.

### *7.1.3 Evidence from differential thermal analysis and infrared spectroscopy*

Bensted and Varma (B109) summarized the use of DTA and IR spectroscopy for the examination of cement pastes. Both are mainly useful for following the phase changes in relatively young pastes. Figure 7.1 shows DTA curves for pastes of a typical Portland cement at ages up to 7 days. The peaks at 145°C and 165°C given by the unhydrated cement are due to gypsum, and that at 485°C to a small amount of CH formed during

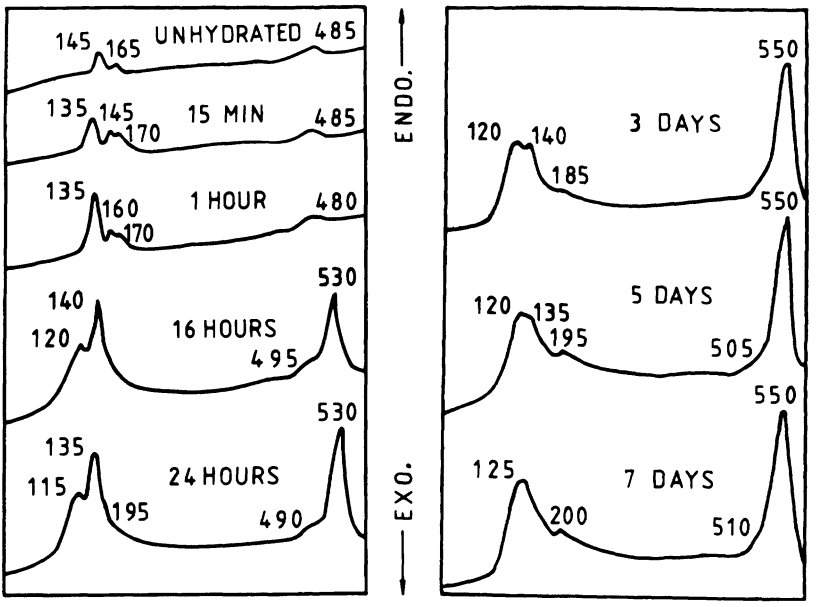


**Fig. 7.1** *DTA curves for pastes of a typical Portland cement. From B109.*

storage, probably by hydration of free lime. The peak at 135–140°C that appears within 15 min is due to ettringite; its intensity passed through a maximum at 16–24 h. The peak at 115–125°C is due to C–S–H or cement gel, and that at 530–550°C to CH. The relatively large crystals of this phase that are formed on hydration in the paste decompose at a higher temperature than the smaller ones formed on hydration during storage. The peak at 185–200°C is due to an AFm phase or phases. One would expect all these peak temperatures to vary with the technique used, but that their relative positions would be essentially unchanged.

In the first effective studies of hydrated cements by DTA, Kalousek and co-workers (K29,K34,K36) observed the early formation of ettringite and its subsequent replacement by monosulfate, or a monosulfate solid solution. This later disappeared, and the authors concluded that all the oxide components were ultimately taken up by a material which they termed 'Phase X'. Subsequent work indicates that this was essentially C–S–H. No $C_3AH_6$ or other hydrogarnet phases were detected. Quantitative or semi-quantitative determinations of gypsum and ettringite indicated that less than half the total $SO_3$ present could be accounted for by AFm and AFt phases. The successive formation of ettringite and AFm phase, and the disappearance of the latter, took place more rapidly as the temperature increased, and at 100°C the entire sequence appeared to be completed in 3–4 h.

Infrared absorption spectra (B109) of unhydrated cements typically show moderate to strong bands at 525 and 925 $cm^{-1}$ due to alite, and at

1120 and 1145 $cm^{-1}$ from S–O stretching vibrations, and weak bands in the 1650 and 3500 $cm^{-1}$ regions due to $H_2O$ molecules. The early formation of ettringite on hydration is shown by a change in the sulfate absorption to a singlet centred at 1120 $cm^{-1}$, and the subsequent replacement of ettringite by monosulfate by a further return to a doublet at 1100 and 1170 $cm^{-1}$. The hydration of the silicate phases causes a shift in the broad Si–O absorption band from 925 to 970 $cm^{-1}$. After several days, the silicate absorption tends to obscure that from sulfate. Changes also occur in the $H_2O$ bending band near 1650 $cm^{-1}$ and in the $H_2O$ or OH stretching bands at 3100–3700 $cm^{-1}$; in the latter region, CH gives a peak at 3640 $cm^{-1}$, ettringite one at 3420 $cm^{-1}$ and a weaker one at 3635 $cm^{-1}$ and monosulfate ones at 3100, 3500 (broad), 3540 and 3675 $cm^{-1}$. The complexity and partial overlapping of these absorptions lessens their utility. The IR spectra also indicate that both the ettringite and the AFm phases formed in cement pastes are less crystalline than the pure materials, and that the AFm phases become poorer in $SO_4^{2-}$ as hydration proceeds.

## 7.2 Microstructure

### *7.2.1 Evidence from light and electron microscopy*

Studies on the microstructures of cement pastes have given results broadly similar to those on calcium silicate pastes (Section 5.3.1), though with some important differences at early ages. As with calcium silicate pastes, the first effective studies were made using light microscopy of thin sections (B53), which were successively augmented by TEM of ground and redispersed material (C22,G42), SEM of fracture surfaces (C23,D16,W19), X-ray (T37,U13,U14) or backscattered electron imaging (D39,S35,S37,S51,S81) of polished sections, TEM examination of ion-thinned sections (R17,R32,V4) and other techniques.

The development of microstructure is considered in Sections 7.2.2–7.2.4. The broad microstructures of pastes more than about 28 days old, first described by Scrivener and Pratt (S35), are similar to those of $C_3S$ pastes. Figure 7.2 shows a typical backscattered electron image, obtained under conditions maximizing contrast from compositional differences. The following types of region are distinguishable by their differing grey levels.

(1) The brightest areas are of unreacted clinker phases. Individual cement grains are usually polymineralic and, as in a clinker (Section 4.3.1), the different phases within them can be distinguished by their differing grey levels or by X-ray microanalysis.

(2) To varying extents, the clinker phases are replaced by hydration products that have formed in situ, and which appear darker on the backscattered electron image. Most noticeably, the alite and belite are replaced by material approximating in composition to the C–S–H of calcium silicate pastes, but which tends to have a higher Ca/Si ratio and contains small amounts of other elements, especially Al, Fe and S. Initially, these hydration products are

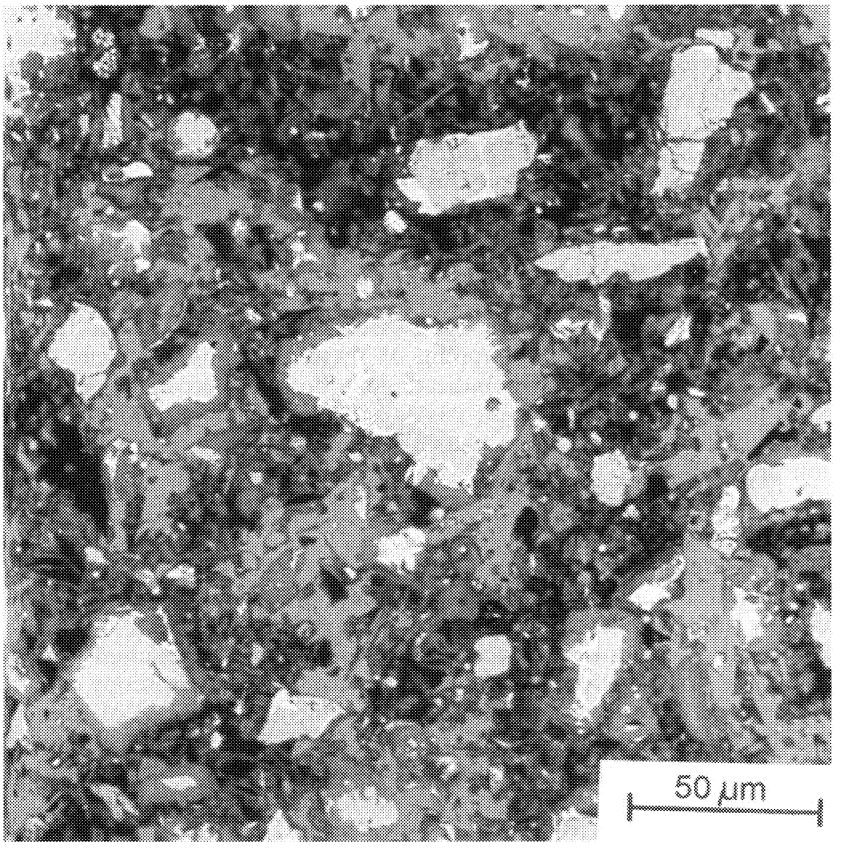


**Fig. 7.2** *Backscattered electron image of a Portland cement paste ($w/c = 0{\cdot}5$), aged 7 days. Successively darker areas are of unreacted cement grains (bright), calcium hydroxide, undesignated product and pores (black). Most of the larger cement grains are polymineralic, and many have rims of inner product. Courtesy M.C. Lewis and K.L. Scrivener, Imperial College, London.*

observed as rims on the unhydrated material. As the paste ages, the latter is progressively replaced, until ultimately no significant quantity may remain. As in the case of calcium silicate pastes (Section 5.3.1), the terms 'inner product' and 'outer product' are used to denote material formed in situ from the clinker grains and in the initially water-filled space, respectively. Only the larger cement grains, unreacted or otherwise, can be clearly distinguished on a backscattered electron image in this way.

(3) Calcium hydroxide can be observed as areas darker than the unreacted clinker phases but brighter than the other hydration products. As in calcium silicate pastes, these appear to have grown in regions initially occupied by water. Although the areas

appear discrete on two-dimensional sections, they are not necessarily so in the three-dimensional material. They can engulf small cement grains. The CH tends to be more finely dispersed in pastes of low w/c ratio.

(4) The remaining space, which forms the matrix in which the above regions appear to be embedded, consists of material varying in grey level from material similar to the in situ product to darker regions, representing pores. Like the CH, these appear discrete in two dimensions, but are not necessarily so in three. This material is often called 'outer product', but in reality includes not only products formed in what was originally water-filled space, but also that formed in space initially occupied by the interstitial material or by the smaller cement grains, the outlines of which can no longer be distinguished. Various other terms, such as 'undesignated product', matrix material' and 'groundmass' have been used. For laboratory-prepared pastes of most cements, the majority of individual microanalyses of the hydration product in these regions have shown compositions varying between those of C–S–H and either AFm phase or CH (H4). Regions large enough for accurate microanalysis on polished surfaces ($\sim 5\,\mu$m) are rarely of pure AFm phase.

### *7.2.2 The early period of hydration*

Many features of the development of microstructure in cement pastes are similar to those observed in $C_3S$ pastes (Section 5.3.1), but there are some important differences. As with $C_3S$ pastes, it is convenient to consider the process in terms of early, middle and late periods of hydration, with divisions at approximately 3 and 24 h after mixing. Figure 7.3 shows diagrammatically the sequence of changes undergone by a typical, polymineralic cement grain, as given by Scrivener, on whose conclusions (S37) the following is largely based.

Studies by HVTEM show that at high dilutions a gel layer or membrane forms over the surfaces of the grains soon after mixing (D17,G45). A product of similar appearance has been observed in pastes of $C_3A$ with gypsum (S53), and, less distinctly, in pastes of cement of normal w/c ratios (J25,S37). It is probably amorphous, colloidal and rich in alumina and silica, but also containing significant amounts of calcium and sulfate, the composition varying with that of the underlying surface. Within about 10 min, stubby rods of AFt phase are also seen (D40,D41). They are typically some 250 nm long and 100 nm thick. Studies using wet cells show them to occur both on the surfaces of the grains, and at some distance away (S37,S53; Fig. 7.3b). They are probably more abundant near the surfaces of the aluminate phase, and appear to nucleate in the solution and on the outer surface of a layer of gel. On drying, this layer shrinks, and the AFt crystals fall back onto the surfaces of the cement grains. The early products thus differ in morphology and composition from the exfoliating foils or honeycombs of C–S–H that have been observed in $C_3S$ pastes.

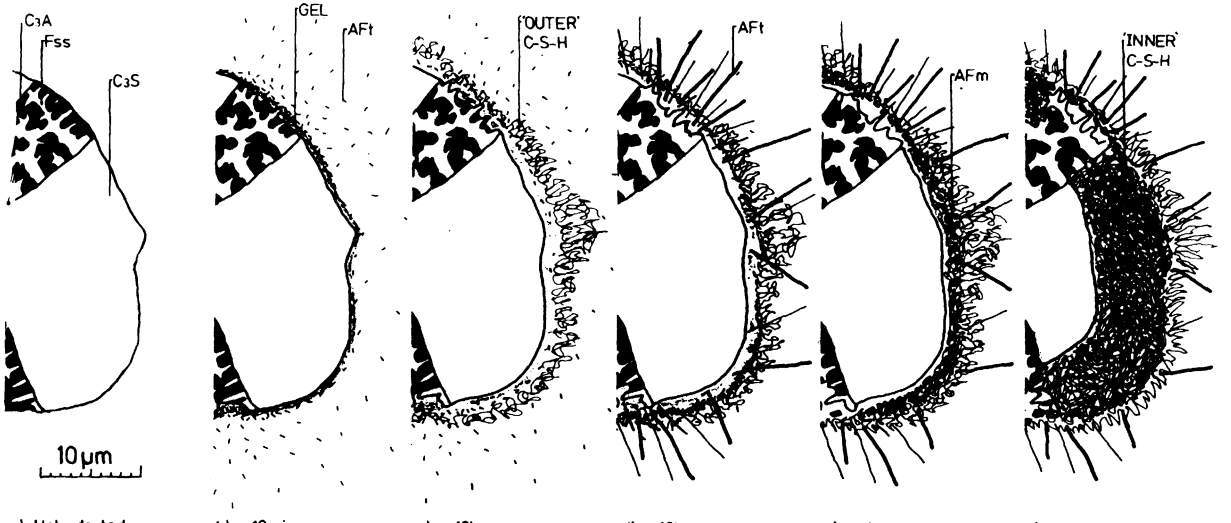


a) Unhydrated
Section of polymineralic grain (scale of interstitial phase is slightly exaggerated).

b) ~10min
Some $C_3A$ (&/or Fss) reacts with calcium sulphate in solution. Amorphous, aluminate-rich gel forms on the surface and short AFt rods nucleate at edge of gel and in solution.

c) ~10h
Reaction of $C_3S$ to produce 'outer' product C-S-H on AFt rod network leaving ~1μm between grain surface and hydrated shell.

d) ~18h
Secondary hydration of $C_3A$ (&/or Fss) producing long rods of AFt. C-S-H 'inner' product starts to form on inside of shell from continuing hydration of $C_3S$.

e) 1-3days
$C_3A$ reacts with any AFt inside shell forming hexagonal plates of AFm. Continuing formation of 'inner' product reduces separation of anhydrous grain and hydrated shell.

f) ~14days
Sufficient 'inner' C-S-H has formed to fill in the space between grain and shell. The 'outer' C-S-H has become more fibrous.

**Fig. 7.3** *Development of microstructure during the hydration of Portland cement. From S54.*

Early work using a wet cell, made at high w/c ratios, showed tubular growths radiating from the cement grains, which were considered to have formed by a 'silicate garden' mechanism (D17). Later work showed that they were rich in calcium, aluminium and sulfur, and that they did not form if $C_3S$ was substituted for cement (B110). They have not been observed in the more recent studies made at normal w/c ratios, and do not appear to be a significant feature of normal cement hydration.

### *7.2.3 The middle period of hydration*

During this period, which begins at about 3 h and ends at about 24 h, some 30% of the cement reacts. It coincides with the period of strong heat evolution and is characterized by the rapid formation of C–S–H and CH. Studies using wet cells show that the undried C–S–H has a filmy, foil-like morphology (P32,S51), which on drying changes to give fibres ('Type I C–S–H'), where space is freely available, or honeycombs or reticular networks ('Type II C–S–H'), where it is more restricted (Section 5.3.1). The morphology is also affected by the presence of foreign ions, such as $Cl^-$. Spherical aggregates of fibres some 2 $\mu$m in diameter, observed in dried material, probably result from the rapid reaction of small cement grains consisting only of alite (S37). The CH forms massive crystals in the originally water-filled space. Nucleation sites appear to be relatively few in number, and the growing crystals may engulf some of the smaller cement grains. All these features of the process are similar to those observed in $C_3S$ pastes.

The C–S–H forms a thickening layer around the cement grains (D40,P32), which engulfs and perhaps nucleates on the AFt rods (Fig. 7.3c). A significant amount has formed by 3 h, and the grains are completely covered by 4 h. The shells grow outwards; by about 12 h they are some 0·5–1·0 $\mu$m thick, and those surrounding adjacent grains are beginning to coalesce. At this stage, which was called the cohesion point, fracture through the shells begins to supplant fracture between them. It coincides with the maximum rate of heat evolution and corresponds approximately to the completion of setting. The structure of interconnected shells has been considered to play an important part in determining the mechanical and other properties, which thus depend on the particle size distribution of the cement (D40).

Studies using ion-thinned sections, wet cells and backscattered electron images of polished sections show that a space develops between the shell and the anhydrous material (K37,S37,S51,S53; Fig. 7.3c). In this respect, the hydration of cement differs from that of $C_3S$, in which the C–S–H grows directly over the $C_3S$ surfaces, without any detectable separation (S53). By 12 h, the spaces are up to 0·5 $\mu$m wide. They are likely to be filled with a highly concentrated or colloidal solution, and the shells are evidently sufficiently porous at this stage that ions can readily migrate through them (S37). The existence of spaces shows that reaction proceeds by dissolution and precipitation; further evidence for this is provided by the fact that the C–S–H also deposits on the surfaces of flyash particles, if

these are mixed with the cement (D42). Some other relatively unreactive or inert admixtures behave in the same way.

Towards the end of the middle period, a renewed growth of AFt crystals takes place (D41,P32,S53; Fig. 7.3d). They are markedly more acicular than those formed earlier; their lengths are typically 1–2 $\mu$m, but sometimes up to 10 $\mu$m. Their formation is associated with a shoulder on the heat evolution curve (Section 7.5.1). Their formation implies an increase in the rate of reaction of the aluminate, or less probably the ferrite phase, which is probably related to the reaction of the alite (S37).

### 7.2.4 *The late period of hydration*

With the decreasing permeability of the shells, C–S–H begins to deposit also on their insides, and its surface advances inwards more quickly than that of the alite retreats. Grains smaller than about 5 $\mu$m appear to react completely before the end of the middle period, and before much material has deposited inside the shells; many that originally contained aluminate phase are empty (S37). The outer product from such grains is often absorbed in the shells surrounding adjacent, larger grains. With larger grains, the spaces between shell and core fill up, and by about 7 days they have disappeared; at this stage, the shells are typically some 8 $\mu$m thick and consist mainly of material that has been deposited on their inner surfaces (Figs 7.3e and f; S37). The separations between shell and core seen on polished or ion-thinned sections rarely exceed about 1 $\mu$m.

Separated shells, up to at least 10 $\mu$m across and sometimes completely hollow, were originally observed on fracture surfaces (B111) and have been called 'Hadley grains'. These are not observed on ion-thinned sections, and possibly result from the core falling out during specimen preparation (S37). It would be difficult to reconcile any widespread occurrence of such cavities in a mature paste with the bulk density of the material (P32).

The concentration of $SO_4^{2-}$ must drop rapidly inside the shells as the aluminate phase reacts, and AFm phase often forms within the shells, any AFt phase formed there initially being replaced by AFm as a result of continued reaction of the aluminate phase (S37,S53). A single specimen may show AFm phase within the shells and AFt phase outside them. The XRD evidence (Section 7.1.2) shows that significant quantities of AFt phase may persist, apparently indefinitely; this is presumably material that has been precipitated outside the shells. If the $SO_4^{2-}$ concentration in the solution outside the shells drops before these have sufficiently isolated the anhydrous grains, relatively large ($\sim$10 $\mu$m) crystals of AFm phase can form throughout the paste (S37).

After the spaces between shells and cores have filled up, reaction is slow and, in contrast to that occurring earlier, appears to occur by a topochemical mechanism (Section 5.8.4). In old cement pastes, three regions of C–S–H can thus be distinguished in the relicts of the larger fully reacted grains (S81), viz. (*a*) an outer layer some 1 $\mu$m thick that has formed through solution in originally water filled space, (*b*) a middle layer some 8 $\mu$m thick that has been deposited, also through solution, on the inside of the shell and thus in space originally occupied by the cement

grain, and (*c*) a central core, that has formed topochemically. As with $C_3S$ pastes, all the C–S–H probably has a foil morphology, which is modified in varying ways by the effects of drying and in accordance with the amount of space available.

Except in pastes many years old, the hydration of belite has proved difficult to observe by electron microscopy (S37), although XRD evidence shows that considerable reaction has occurred within 14 days. In a 23-year-old paste studied by backscattered electron imaging, the belite grains had reacted completely, but the original lamellar structure remained, providing further evidence of a topochemical mechanism (S81). The belite appears to react preferentially along the exsolution lamellae. The reaction of the ferrite phase has similarly proved difficult to observe, though backscattered electron imaging showed the formation in the same sample of rims high in iron, and TEM examination has provided further data (Section 7.4.2).

## 7.3 Analytical data for cement pastes

### *7.3.1 Unreacted clinker phases*

The experimental considerations applying to calcium silicate pastes (Sections 5.1 and 5.2) are equally relevant to cement pastes. Of the methods so far used in attempts to determine the degrees of reaction of the individual clinker phases as a function of time, QXDA (C46,D15, P33,T35) has proved much the most satisfactory. Procedures are essentially as for the analysis of a clinker or unreacted cement (Section 4.5.3), but it is necessary to take account of overlaps with peaks from the hydration products, and especially with the C–S–H band at 0·27–0·31 nm. The water content of the sample must be known, so that the results can be referred to the mass of anhydrous material. If a sample of the unhydrated cement is available, and its quantitative phase composition has been determined, it may be used as the reference standard for the individual clinker phases in the paste.

The precision and accuracy of the technique are often overestimated. If a cement paste contains 50% of alite initially, an error of 3% in the determination of that phase leads to one of 6% in the percentage reaction; if it contains 5% of aluminate phase initially, an error of 1% leads to one of 20% in the percentage reaction. With existing techniques, errors much smaller than these are unlikely to be achieved for untreated pastes. The precision may be greatly increased for the aluminate and ferrite by first removing the silicates by chemical extraction methods (Section 4.3.3). Figure 7.4 shows some results from the literature. Asaga *et al.* (A19) reported broadly similar results. The considerable differences between the results of different investigations are no doubt partly due to the limitations of the technique, but also to differences between cements or curing conditions, which are discussed in Section 7.7.

### *7.3.2 Non-evaporable and bound water*

As with calcium silicate pastes, the gelatinous nature of the principal reaction product renders any definition of chemically bound water

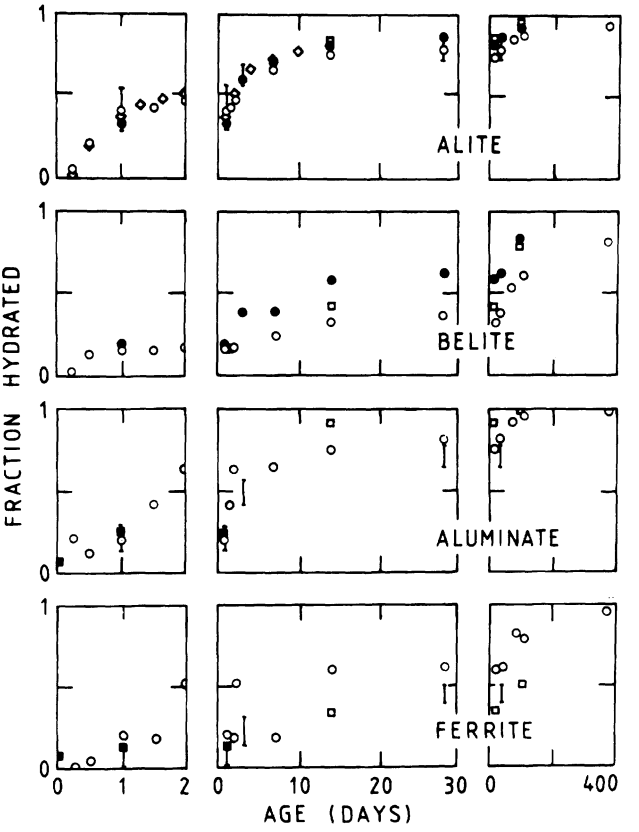


**Fig. 7.4** *QXDA results for the fractions of the clinker phases reacted in Portland cement pastes. Solid circles: C46, w/c = 0·65. Diamonds: B112, sample C2. Vertical lines: O9, range for 7 samples. Open circles: D15. Open squares: P33, samples cured at 100% RH. Solid squares: T35, clinker interground with gypsum.*

somewhat arbitrary. The three definitions of water content given in Section 5.2.2 for calcium silicate pastes are relevant to cement pastes, viz. non-evaporable water, chemically bound water and water seemingly essential to the formation of the hydration products in a saturated paste.

Water retained after D-drying, known as non-evaporable water, has often been wrongly identified with chemically bound water. It excludes much of the interlayer water in C–S–H, AFm and hydrotalcite-type phases and much of the water contained in the crystal structures of AFt phases. It is often used as a measure of the fraction of the cement that has reacted, but can only be approximate in this respect, because the clinker phases react at different rates and yield products containing different amounts of non-evaporable water. Fully hydrated cement pastes typically contain about 23% of non-evaporable water, referred to the ignited mass. Copeland *et al.* (C45) determined the non-evaporable water contents of a

series of mature cement pastes and carried out regression analyses on the cement composition. For pastes of w/c ratio 0·8 and aged 6·5 years, they obtained the approximate expression:

$$H_2O = CaO - 0{\cdot}5SiO_2 + 5Al_2O_3 - 5Fe_2O_3 - 2SO_3 \qquad (7.2)$$

where $H_2O$ represents the quantity of non-evaporable water and all quantities are in moles. The coefficient for $SO_3$ was of low reliability, and other sets of data given in the same paper suggest a value nearer to $-1$. For a typical cement composition (65% CaO, 21% $SiO_2$, 5·5% $Al_2O_3$, 3·0% $Fe_2O_3$, 2·3% $SO_3$), and using a coefficient of $-1$ for $SO_3$, this gives a non-evaporable water content of 20·4%.

The content of chemically bound water is approximately that retained on equilibration at 11% RH of a sample not previously dried below saturation. For fully hydrated pastes of typical cements, it is about 32%, referred to the ignited mass (F17,T38). There are no systematic data relating this quantity to cement composition. The total content of water essential for complete hydration in a saturated paste is defined as that present in such a paste having the minimum w/c ratio at which complete hydration is possible (Section 8.2.2). For typical Portland cements, it is 42–44% referred to the ignited mass.

### *7.3.3 Thermogravimetry and calcium hydroxide content*

The discussion of methods for determining CH in calcium silicate pastes (Section 5.2.1) applies also to cement pastes; TG and QXDA are probably the most satisfactory methods. Figure 7.5 shows a typical TG curve for a mature cement paste. The step at 425–550°C is due primarily to decomposition of CH, and its height, estimated as shown in Fig. 5.4, probably affords the best available method for determining this phase. It is nevertheless subject to several sources of error. TEM evidence indicates that cement pastes (unlike $C_3S$ pastes) may contain significant amounts of cryptocrystalline CH intimately mixed with the C–S–H (Section 7.1.1), and this may not be determined by thermal methods or QXDA. Curves for AFm phases show a step in the same range (Fig. 6.2) and the decomposition of CH is not quite complete within this range (Section 5.1.3). It is probably not practicable in the present state of knowledge to correct for these errors, and doubtful whether either TG or QXDA gives results with an accuracy better than $\pm 1\%$.

The loss above 550°C is due partly to $CO_2$ and partly to the final stages of dehydration of C–S–H and the hydrated aluminate phases. It is doubtful whether the contributions can be distinguished from TG evidence alone, and, unless evolved gas analysis is used, a separate determination of $CO_2$ is needed in order to interpret the data fully. As with calcium silicate pastes, errors arise if TG determinations are carried out on material that has been treated with an organic liquid, for example, to stop hydration. Losses above 550°C of more than about 3%, referred to the ignited mass, usually indicate serious carbonation from this or other causes.

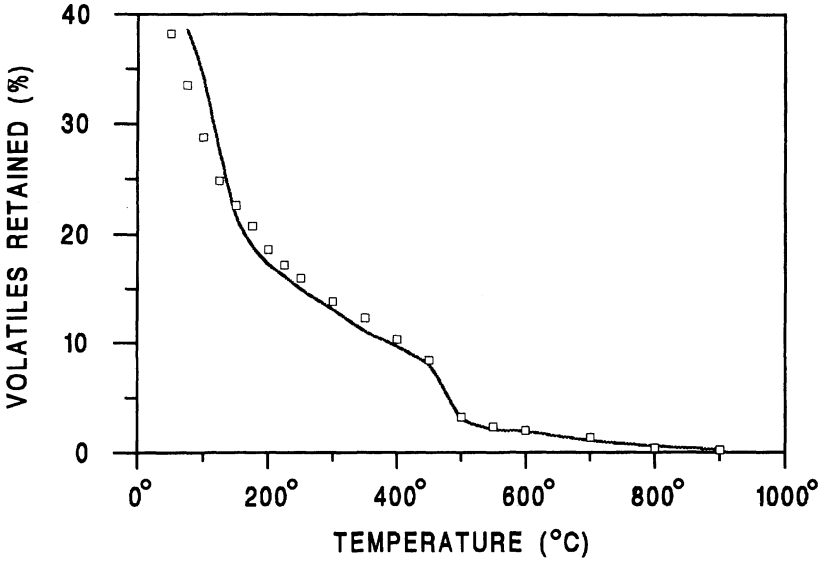


**Fig. 7.5** *TG curve for a Portland cement paste (w/c = 0·5), moist cured at 25°C for 14 months. Data are given as percentages on the ignited mass. Open squares represent points calculated as described in the text. Heating rate, 10 K min$^{-1}$; flow rate of dry, $CO_2$-free $N_2$, 15 ml min$^{-1}$; sample mass, 50 mg. New data.*

The loss below the CH step is due to decomposition of C–S–H and the hydrated aluminate phases. Although the TG curves of pure AFm phases are markedly stepped in this region (Fig. 6.2), those of cement pastes normally show only slight indications of steps. Weak peaks can, however, sometimes be seen on DTG curves. The absence of steps is probably due to a combination of low crystallinity, the presence of other phases and the presence of AFm phases of different compositions in mixture or solid solution or both. For typical experimental conditions with a 50 mg sample, heating rate of 10 K min$^{-1}$ and $N_2$ flow rate of 15 ml min$^{-1}$, the volatiles retained at about 150°C, after correction for $CO_2$, correspond approximately to the non-evaporable water, and those retained at about 90°C to the bound or 11% RH water, but both temperatures depend on experimental conditions (T5).

For pastes of typical ordinary Portland cements cured for 3–12 months, the CH content found by thermal methods or QXDA is typically 15–25%, referred to the ignited mass (D15,H42,M47,P34,R15,T19). Pressler *et al.* (P34) found that for pastes of various ages of ordinary (ASTM Type I) Portland cements, it was linearly related to the content of non-evaporable water, but that for cements high in belite (ASTM Type IV), it tended to a maximum while the latter continued to increase. This is readily explained, since belite yields only a little CH on hydration. The present author has noticed similar behaviour even with modern cements high in alite, and that the CH content can possibly even decrease slightly after 28–91 days (T5).

### 7.3.4 Hydrated aluminate and silicate phases

Opinions have differed as to the possibility of determining the hydrated aluminate phases by thermal or X-ray methods. The determination of ettringite is discussed in Section 6.2.3. A recent investigation (O18) showed good agreement between XRD and DTA results, with contents in pastes of four cements of widely differing composition cured at 20°C passing through maxima of 7–11% at 1–7 days, falling to 3–10% after 2 years. There are probably no effective direct methods at present for determining either C–S–H or AFm phases in cement pastes; in both cases, this is probably attributable to the low degree of crystallinity. Odler and Abdul-Maula (O16) found that determination of AFm phase by QXDA was only semi-quantitative.

### 7.3.5 Analyses of individual phases

The general considerations mentioned in Section 5.3.3 in relation to calcium silicate pastes apply equally to cement pastes. Figure 7.6 shows a plot of Al/Ca ratios against Si/Ca ratios for individual microanalyses from varying parts of the microstructures of typical Portland cement pastes (H4). Most of the analyses clustering near the lower right-hand corner are of the inner product from the larger alite or belite grains. The

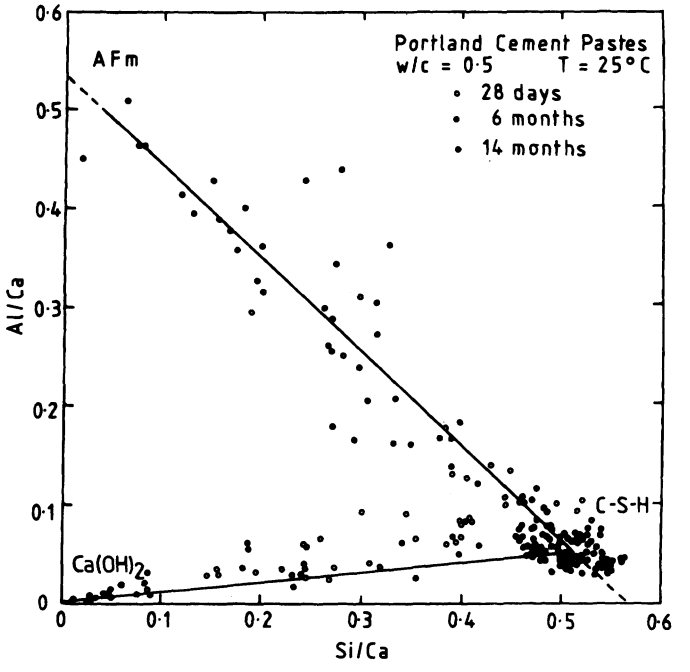


**Fig. 7.6** *Al/Ca ratios plotted against Si/Ca atom ratios for individual X-ray microanalyses of typical Portland cement pastes. Modified from H4.*

spots analysed were not chosen at random, and CH is much under-represented. The analyses intermediate between those of the inner product and either CH or AFm phase were, in general, obtained from the undesignated product, suggesting that the latter was largely a mixture on or below a micrometre scale of C–S–H with CH or AFm phase. Other workers have obtained broadly similar results, but have used different means to express them (B113,R17,R33,R34). Table 7.1 gives results of X-ray microanalyses of the inner product formed from the larger alite or belite grains, obtained by analysis of polished sections in the EPMA or SEM. The reported mean Si/Ca ratios are 0·48–0·61 (Ca/Si 1·6–2·1). Most of the investigators reported considerable scatter between the results of individual analyses. In one investigation (R34), bimodal distributions were reported. Results for a paste hydrated at 45°C (U13) do not differ significantly from those for ones hydrated at lower temperatures.

Several investigators have reported X-ray microanalyses of polished sections of the 'undesignated product' formed in space formerly occupied by water, interstitial material or small cement grains (B113,H4,R17,R33, R34,T37). From a study using both EPMA and TEM microanalyses, Richardson and Groves (R17) concluded that EPMA could yield analyses of C–S–H unmixed with other phases for inner but not outer product. Such analyses could be obtained by TEM for both inner and outer product C–S–H. Even for the inner product, TEM showed the presence of phases other than C–S–H. These included AFt, AFm, $Ca(OH)_2$ and phases high in magnesium (hydrotalcite-type?) or in iron. The analyses in Table 7.1 showing the higher contents of aluminium or other foreign ions probably do not represent C–S–H unmixed with other phases.

Early TEM analyses of ground and redispersed cement pastes (L31–L33,T19) showed wide variations between individual analyses, even within single particles of micrometre dimensions, but, as with parallel studies on C–S–H pastes, the mean Ca/Si ratios obtained were probably low (Section 5.3.4). These studies, and a later one on ion-thinned sections (R32), also showed that some particles contained small proportions of aluminium, sulfur and other elements but that others were essentially unsubstituted calcium silicate hydrate. A further study on ion-thinned sections (R17) confirmed this observation and also the wide distribution of Si/Ca ratios. As in the C–S–H of $C_3S$ pastes, the distribution of Si/Ca ratios tended to be bimodal at early ages and to become unimodal at later ages. For inner and outer product C–S–H alike, at all ages from 1 day to 3·5 years, the mean Ca/Si ratios were in the range 1·57–1·90, with no systematic variation with age. The mean Al/Ca ratio was 0·033 for the inner product and 0·052 for the outer product. These results, which were obtained for mature pastes, agreed well with those obtained in the same investigation by EPMA.

Regions of AFt phase of sufficient size for analysis on polished sections are rare in most cement pastes, and the most reliable results are probably those obtained using TEM. Richardson and Groves (R17) found that the (Al + Fe)/Ca and S/Ca ratios were close to the theoretical values of 0·33 and 0·5 respectively. Only about 30% of the analyses showed a detectable

**Table 7.1** *Results of X-ray microanalyses by EPMA or SEM of the C–S–H gel formed from alite or belite in Portland cement pastes**

| Na | Mg | Al | Si | S | K | Fe | w/c | Temp. (°C) | Age | Ref. |
|---|---|---|---|---|---|---|---|---|---|---|
| tr. | 0·05 | 0·07 | 0·59 | 0·01 | 0·02 | 0·01 | 0·5 | 20 | 8 days | R35 |
| n.d. | n.d. | n.d. | 0·59 | n.d | n.d | n.d. | 0·5 | 25 | 28 days | R36 |
| n.d. | 0·02 | 0·06 | 0·49 | 0·02 | n.d. | 0·03 | 0·3 | ? | 5 years | R37 |
| n.d. | n.d. | 0·06 | 0·60 | 0·02 | n.d. | 0·02 | 0·6 | ? | 5 years | R33 |
| n.d. | 0·03 | 0·08 | 0·60 | 0·03 | n.d. | 0·015 | 0·45 | 25 | 23 years | T37 |
| n.d. | 0·05 | 0·10 | 0·49 | 0·01 | n.d. | 0·05 | ? | ? | 136 years | R37 |
| 0·01 | 0·02–0·08 | 0·05–0·07 | 0·50–0·53 | 0·01–0·03 | 0·01–0·02 | 0·01–0·02 | ? | 20–25 | 3–180 days | H4¶ |
| n.d. | n.d. | 0·12(?) | 0·49 | n.d. | n.d. | n.d. | 0·40 | 25 | 4 years | U13 |
| n.d. | n.d. | 0·14(?) | 0·53 | n.d. | n.d. | n.d. | 0·40 | 45 | 60 days | U13 |
| 0·001 | 0·022 | 0·034 | 0·610 | 0·011 | 0·004 | 0·016 | 0·40 | 20 | 'mature'† | R17 |
| 0·002 | 0·000 | 0·051 | 0·564 | 0·032 | 0·009 | 0·015 | 0·40 | 20 | 'mature'‡ | R17 |
| n.d. | n.d. | 0·036 | 0·478 | 0·042 | n.d. | 0·017 | 0·40 | 23 | 3 days§ | B113 |

* Means or other measures of central tendency, expressed as atom ratios relative to Ca. n.d. = not determined or not reported; tr. = trace.
† Inner product; also, Ti/Ca, 0·000, Mn/Ca, 0·000.
‡ Outer product, defined as having Ca/Si < 2 and Mg/Ca = 0·0; also, Ti/Ca, 0·000, Mn/Ca, 0·000.
§ Inner product in fully reacted grains.
¶ Data for six pastes from three cements.

Fe content; for those that did, the mean Fe/(Al + Fe) ratio was approximately 0·25. Reports that the AFt phase in cement pastes often contains Si or that it has a S/Ca ratio below 0·5 (B113,L33,T39) can perhaps be attributed to admixture with C–S–H.

Particles of AFm phase large enough to be analysed free from other phases are also rare in most cement pastes. One investigation (G71) gave no indication of any deviation from unsubstituted monosulfate composition, but others have indicated lower mean S/Ca ratios (B113,H4). AFm phase closely mixed with C–S–H has been reported to have a higher S/Ca ratio than that present in larger regions (H4). For some ordinary Portland cements, at least, the mean Fe/Al ratios were less than 0·1 (B113,H4).

### 7.3.6 *Silicate anion structure*

Silicate anion structures in Portland cement pastes have been studied by the methods described in Section 5.5 for calcium silicate pastes. Trimethylsilylation (TMS) studies (L22,L34,M56,M57,S82,T12,T40) show that, as with $C_3S$, the proportion of the silicon present as monomer decreases with age and that the hydration products contain dimer, which is later accompanied and eventually partly replaced by polymer (≥5 Si). Two studies showed proportions of Si remaining as monomer in mature Portland cement pastes that were greater than those in mature $C_3S$ pastes (M57,S82). The differences are probably within the experimental error of the method. In addition, the cement pastes may have contained some unreacted belite.

A study (L34,M56) in which the TMS derivatives were examined by gel permeation chromatography and other methods gave the results shown in Table 7.2. There are no significant differences between the distributions

**Table 7.2** *Comparison of silicate anion structures in pastes of $C_3S$ and Portland cement (M56)*

| | Starting material | | |
|---|---|---|---|
| | $C_3S$ | Cement | Cement |
| Curing time (months) | 12·0 | 9·5 | 13·5 |
| % of total Si recovered as: | | | |
| monomer | 14 | 11 | 11 |
| dimer | 50 | 34 | 36 |
| polymer | 34 | 34 | 34 |
| Molecular weights of polymer TMS derivatives: | | | |
| mode | 1300 | 1300 | 1300 |
| number mean | 1700 | 1650 | 1700 |
| weight mean | 2900 | 2950 | 2700 |
| Mean connectivity of $SiO_4$ tetrahedra in polymer anions | 1·8 | 1·8 | 1·8 |

of anion size within the polymer fractions of the cement and $C_3S$ pastes, and, though the lower totals for the cement pastes impede comparison, probably none between the relative proportions of monomer, dimer and polymer that cannot be explained by kinetics, side-reactions or other experimental inaccuracies. In all cases, the data for the molecular weights of the polymer TMS derivatives, and the mean connectivities of the polymeric anions, are consistent with the hypothesis that the latter are linear, with pentamer as the major component and little of the material in chains containing more than 11 tetrahedra. A study in which the TMS derivatives were examined using high-pressure liquid chromatography and other methods confirmed that the principal species were dimer and linear pentamer (D20).

Due to ionic substitutions and other effects, $^{29}Si$ NMR spectra are less well resolved for cement pastes than for $C_3S$ pastes. A study (B114) nevertheless showed that, as for $C_3S$ pastes, the content of $Q^0$ silicate tetrahedra decreases with time and that those of $Q^1$ and later of $Q^2$ tetrahedra increase. After 180 days, the degree of hydration, estimated from the intensities of the NMR peaks, was approximately 90%. These results are consistent with those obtained by the TMS method, and suggest that the hydration products present after 180 days contain at most only a small proportion of monomer. As with $C_3S$ pastes (Sections 5.5.2 and 5.5.3), the rate of polymerization increases with temperature; after 31 days at 80°C, 42% of the silicon was in $Q^2$ tetrahedra, compared with 22% at 21°C (A20). The possible effects on the silicate anion structure of drying, whether during hydration as a result of localized water shortage or subsequently, were considered in Section 5.5.4.

## 7.4 Interpretation of analytical data

### *7.4.1 Substitution or admixed phases?*

As noted in Section 7.1.3, Kalousek and co-workers (K29,K34,K36) concluded from DTA observations that both AFm and AFt phases ultimately disappeared from cement pastes, their ions being apparently incorporated into what would now be called C–S–H gel. Copeland *et al.* (C24,C46) later treated $C_3S$ pastes, and C–S–H prepared in other ways, with various sources of $Al^{3+}$, $Fe^{3+}$ or $SO_4^{2-}$ ions, including $C_4AH_{13}$. The XRD peaks of the phases providing the ions disappeared, and changes occurred in the micromorphology of the gel, the non-evaporable water content and the fraction of the CaO extractable with an organic solvent. It was concluded that the ions were taken up by the C–S–H and that up to about one silicon atom in six could be replaced by aluminium, iron or sulfur, and that aluminium and iron could also replace calcium. These results suggested that the principal hydration product in Portland cement pastes was a substituted C–S–H, a conclusion that later appeared to be supported by the results of X-ray microanalyses. However, none of the evidence shows that the substitutions occur at the crystal-chemical level postulated by Copeland *et al.*, and there are indications that this is only partly the case.

Stade and Müller (S83) concluded from $^{27}Al$ NMR that the Al in pastes of alite or $C_3S$ plus a little $C_3A$ was largely in octahedral coordination, and a related study using electron-spin resonance and Mössbauer spectra showed that $Fe^{3+}$ in C–S–H preparations was entirely in octahedral coordination (S84). It is unlikely that sulfur would substitute for silicon in C–S–H, as S–O–Si bonds would probably be very easily hydrolysed. $CaSO_4$ taken up by C–S–H is, moreover, very easily removed, and this led Odler (O19) to suggest that the sulfate ion was adsorbed. These and other considerations led Taylor (T41) to suggest that the C–S–H was substantially unsubstituted, the foreign ions being contained in closely admixed AFm and other phases. It was also noted that TMS methods showed that the distribution of silicate anion size and mean connectivity in mature cement pastes were similar to those in mature $C_3S$ pastes. Since substituents for silicon are not part of the silicate anions from the standpoint of TMS methods, this would not be the case if there was any substantial degree of substitution, and the $(3n-1)$ sequence of chain lengths would not be maintained if substitution of the silicon atoms took place other than in the bridging tetrahedra.

Subsequent work indicates that substitution of silicon by aluminium does occur, and that it is confined to the bridging tetrahedra, but that it is less extensive in normal pastes of Portland cements than was suggested by Copeland *et al.* Richardson and Groves (R17) showed that in individual TEM microanalyses of single-phase C–S–H in mature cement pastes, the Al/Ca ratio increased linearly with the Si/Ca ratio. This also applied to the mean analyses of the C–S–H in a range of slag cement pastes, which had a wide range of Ca/Si ratios (R23,R38). The R/Ca ratio (where R was mainly Al but included a little Fe) was related to the Si/Ca ratio by the equation

$$\mathrm{Si/Ca} = 0{\cdot}444 + 2{\cdot}25\mathrm{R/Ca} \qquad (7.3)$$

The authors noted that an increase in Al/Ca with increasing Si/Ca was not consistent with the hypothesis that the aluminium was present in admixed AFm phase; it was consistent with a fixed Al/Si ratio in a series of C–S–H particles of varying Si/Ca ratio. Studies on the C–S–H formed in pastes of alkali-activated slags or synthetic glasses indicate that Al substitutes for Si in the bridging tetrahedra (Section 9.2.9). As substitution is confined to these sites, the Al/Ca ratios in young pastes may be lower than those found for mature pastes.

A number of problems remain. In particular, the results obtained by Kalousek and co-workers (K29,K34,K36) and by Copeland and co-workers (C24,C46) indicate that substantially more AFm phase can be apparently consumed by the C–S–H in a Portland cement paste than can be accounted for by substitution of the $Al^{3+}$ for $Si^{4+}$. This is true even for a mature paste in which the content of C–S–H has been maximized. C–S–H thus appears to have the ability to destroy AFm phases, or at least to lower their crystallinity so that they can no longer be detected by XRD or DTA. The same effect could account for the fact that, even when

they are detected by these methods, AFm phases in cement pastes seem always to be poorly crystalline. The explanation of the effect is not known. One possibility is based on the fact that the main layers in C–S–H and AFm phases are oppositely charged; this might produce strong mutual attraction, sufficient to destroy crystals of AFm phases and to disperse their constituent layers, or groups of layers, in the C–S–H gel (T42). AFm phases, crystalline or otherwise, are likely to occur predominantly in the outer product.

The general conclusion from the evidence at present available is that, in the hydration products of Portland cement pastes, $Al^{3+}$ can occur as a substituent in C–S–H, in AFm or AFt phases sufficiently crystalline to be detectable by XRD or thermal methods, and in AFm phases that are so poorly crystalline that they cannot be so detected. The crystallinity of the AFm phases decreases with age. A little $Al^{3+}$ is probably present in hydrotalcite-type phases and in a poorly crystalline hydrogarnet-like phase (Sections 7.4.2 and 7.4.3).

### *7.4.2 $Fe_2O_3$ in cement hydration products*

Most of the studies on the hydration of $C_4AF$ with or without gypsum (Section 6.5.4) have indicated that the hydration products are AFm, AFt or hydrogarnet phases of higher Al/Fe ratio, together with an iron(III) hydroxide gel. It has also been suggested that a calcium ferrite gel is formed (B107). There is, however, no experimental evidence that an iron hydroxide gel is formed in cement pastes, and Harchand *et al.* (H43) concluded from a Mössbauer study that it was absent and that the $Fe^{3+}$ entered the AFm phase. The ferrite phase in cement may well behave differently from pure $C_4AF$, because of the large difference in composition and the effects of other constituents.

Studies of polished sections by X-ray (T37) and backscattered electron (S37) imaging indicated that the $Fe^{3+}$ in Portland cement does not migrate through the pore solution on hydration, but remains in products formed in situ. In 1960, Copeland *et al.* (C45) observed that the XRD patterns of many pastes included many peaks of a hydrogarnet in addition to those of other hydrated aluminate phases, and obtained evidence that this had formed by hydration of the ferrite. The unit cell parameter was 1·24 nm. SEM microanalyses of one of these pastes confirmed that the principal hydrated aluminate phase was a hydrogarnet of approximate composition $Ca_3Al_{1.2}Fe_{0.8}SiO_{12}H_8$ (T37). The formation of hydrogarnet in these cements may have been due to the fact that they were manufactured many years ago and were much lower in $SO_3$ than modern cements (H44). With the probable exception of sulfate-resisting types (G5), the latter do not yield amounts of hydrogarnet detectable by XRD on hydration at ordinary temperatures. However, Rodger and Groves (R32) described regions which had probably formed in situ from the ferrite phase, and which consisted of C–S–H, a hydrotalcite-type phase and a poorly crystalline iron-containing phase that could have been the precursor of a hydrogarnet. The particles of this last constituent were almost spherical and some 200 nm in diameter.

In an ordinary Portland cement, only some two-thirds of the $Fe^{3+}$ occurs in the ferrite, the rest being contained largely in the alite and aluminate (Table 4.3). On hydration, the $Fe^{3+}$ in these other phases probably does not enter a hydrogarnet. If it enters the AFm phase or C–S–H, this would account for observations by analytical electron microscopy that small amounts of $Fe^{3+}$ are present in these phases.

### *7.4.3 MgO, $SO_3$ and alkalis in cement hydration products*

One would expect that any relatively large crystals of periclase in a clinker would hydrate to give brucite. However, in modern clinkers, much or all of the $Mg^{2+}$ is not present in this form, but in the major clinker phases, especially alite and ferrite, and, if the MgO content exceeds about 1·5%, in small crystals of periclase intimately mixed with aluminate and ferrite in the interstitial material. In all these cases, it is associated with comparable or larger amounts of $Al^{3+}$, and one would then expect that a hydrotalcite-type phase would be formed. XRD and TEM evidence (Sections 7.1.2 and 7.4.2) indicates that this is the case. $Mg^{2+}$, like $Fe^{3+}$, does not readily migrate through the pore solution, and the formation of a hydrotalcite-type phase in the inner product of the ferrite (Section 7.4.2) is readily explained by the substantial Mg content of that phase. Small amounts of a hydrotalcite-type phase have also been found embedded in inner-product C–S–H (R17).

Sulfate could be accommodated as interlayer anions present in AFm phases. C–S–H can, however, take up $CaSO_4$ in the absence of $Al^{3+}$ or $Fe^{3+}$, and thus of AFm layers (C24). Odler (O19) showed that $CaSO_4$ taken up by C–S–H was very readily removed, and his conclusion that the $Ca^{2+}$ and $SO_4^{2-}$ ions are sorbed seems very probable. The $K^+$ and $Na^+$ ions that are found in the cement gel by X-ray microanalysis result partly from evaporation of the pore solution during specimen preparation, but are partly contained in the C–S–H, where they probably occupy interlayer sites. After deducting the fractions deposited from the pore solution, the K/Ca and Na/Ca ratios in the gel are typically ~0·01 and <0·01 respectively (Section 7.5.2).

The considerations discussed in this and the preceding section suggest that the cement gel is a complex material, comprising several types of solid constituent together with the pore solution. While the foreign ions are partly present in the C–S–H, either as substituents at a crystal-chemical level or sorbed, some are present in other phases mixed with the C–S–H on scales probably varying from the nanometre to the micrometre level. In addition to AFm, AFt and hydrotalcite-type phases, these include cryptocrystalline $Ca(OH)_2$ (G69,V4) and poorly crystalline hydrogarnet formed from the ferrite. The scale of mixing is often sufficiently fine that SEM or EPMA microanalyses do not relate to single phases, especially in the undesignated product. This leads to some ambiguity in nomenclature; C–S–H or C–S–H gel is often used to describe the multi-phase material, but a case could be made for restricting these terms to the pure phase and using cement gel for the more complex material.

### 7.4.4 The stoichiometry of cement hydration

Many attempts have been made to formulate the stoichiometry of cement hydration (e.g. J26,P35,T19,T38). The following treatment incorporates features of those in the references mentioned. Because of uncertainties in the compositions of phases and differences between cements, many variants of the calculation are possible, and the example is intended to be illustrative rather than definitive.

The essential input data are (*a*) the bulk chemical composition of the cement, (*b*) the quantitative phase composition of the cement and the approximate chemical compositions of its individual phases, (*c*) the fraction of each phase that has reacted and (*d*) the composition of each hydrated phase for the specified drying condition. If (*b*) is unknown it may be estimated from a modified Bogue calculation as described in Section 4.4, and if (*c*) is unknown it may be estimated from the age as described by Parrott and Killoh (P35), or, more simply though less precisely, by using empirical equations (D15,T43). Steps (1)–(7) of the calculation, listed below, are best carried out on an ignited mass basis.

(1) Calculate the quantity of each component oxide that has been released into the hydration products. In each of the succeeding steps, the composition of the relevant hydration product must be assumed, and the contents of all the component oxides present in it calculated and deducted from the total amounts available.
(2) Assume that MgO in the products occurs as a hydrotalcite-type phase.
(3) Assume that the $Fe_2O_3$ from the ferrite phase occurs in a hydrogarnet-type phase.
(4) Assume that the remaining $SiO_2$ occurs in C–S–H.
(5) Assign the remaining $Al_2O_3$, $Fe_2O_3$ and $SO_3$ to AFm and AFt phases. No fixed rule can be given for doing this. Part or all of the $CO_2$ may be assigned to AFm phases.
(6) Assign any remaining $CO_2$ to $CaCO_3$.
(7) Assume that the remaining CaO is present as $Ca(OH)_2$.

A mass-balance table may now be completed, showing the assignments of each of the oxide components to phases. The water contents are inserted at this stage, assuming any desired drying conditions. Table 7.3 is such a table for a mature paste of an ordinary Portland cement. Such tables often show higher contents of $Ca(OH)_2$ than are found by XRD or thermal methods. This is the case whatever reasonable assumptions are made about the nature and compositions of the hydration products, and may be due to the presence of cryptocrystalline $Ca(OH)_2$ closely mixed with the C–S–H. If the w/c ratio and the densities of the phases are introduced, it is also possible to calculate volume percentages of phases and porosities (Section 8.3.2).

Table 7.4 contains reference data for volatiles retained by each of the hydration products at a series of temperatures under conditions typically used in thermogravimetric analysis. These data may be used in conjunction with a mass balance table of the type represented by Table 7.3.

**Table 7.3** *Calculated mass balance table for a 14-month-old Portland cement paste**

| | $Na_2O$ | MgO | $Al_2O_3$ | $SiO_2$ | $SO_3$ | $K_2O$ | CaO | $TiO_2$ | $Fe_2O_3$ | $H_2O$ | $CO_2$ | Total |
|---|---|---|---|---|---|---|---|---|---|---|---|---|
| Alite | | | | 0·7 | | | 1.9 | | | | | 2.6 |
| Belite | | | | 0·5 | | | 1.1 | | | | | 1.6 |
| Aluminate | | | | | | | 0·1 | | | | | 0·1 |
| Ferrite | | 0·1 | 0·7 | 0·1 | | | 1.4 | 0·1 | 0·6 | | | 3.0 |
| Insol. res. | | | 0·1 | 0·2 | | | | | | | | 0·3 |
| Hydrotalcite | | 1.1 | 0·6 | | | | | | | 1.2 | | 2.9 |
| Hydrogarnet | | | 0·3 | 0·3 | | | 2.1 | 0·1 | 1.5 | 1.2 | | 5.5 |
| C–S–H | 0·1 | | 1.1 | 19.2 | 0·5 | 0·2 | 31.4 | | | 12.1 | | 64.6 |
| $C_4(A,F)\bar{S}H_{12}$ | | | 1.1 | | 1.1 | | 3.1 | | 0·5 | 3.0 | | 8.8 |
| $C_4(A,F)\bar{C}H_{11}$ | | | 1.3 | | | | 3.6 | | 0·5 | 3.2 | 0·7 | 9.3 |
| $C_6A\bar{S}_3H_{32}$ | | | 0·4 | | 1.0 | | 1.4 | | | 2.4 | | 5.2 |
| $Ca(OH)_2$ | | | | | | | 19.2 | | | 6.2 | | 25.4 |
| Residual† | 0·1 | | | | | 0·2 | | 0·1 | | | | 0·7 |
| Total‡ | 0·2 | 1.2 | 5.6 | 21.0 | 2.6 | 0·4 | 65.3 | 0·3 | 3.1 | 29.3 | 0·7 | 130·0 |

* Data relate to paste equilibrated at 11% RH and are expressed as percentages on the ignited mass. Total (non-evaporable plus gel) water, 40·6%; chemically bound water, 29·3%; non-evaporable water, 21·7%.

† Pore solution and unassigned; total also includes $P_2O_5$ and $Mn_2O_3$.

‡ Also, $P_2O_5$, 0·2% and $Mn_2O_3$, 0·1%.

**Table 7·4** *TG data and water contents for phases in Portland cement pastes**

| | Phase and mass of water retained at given temperature¶ | | | | | | $CO_2$** |
|---|---|---|---|---|---|---|---|
| Temp. (°C) | C–S–H | CH | AFm | AFt | Hgt§ | Htc‖ | Any |
| 50 | (0·643) | 0·321 | 0·964 | 1·671 | 0·565 | 1·115 | 1·000 |
| 75 | (0·514) | 0·321 | 0·900 | 1·446 | 0·565 | 1·105 | 1·000 |
| 100 | (0·418) | 0·321 | 0·758 | 0·964 | 0·565 | 1·034 | 1·000 |
| 125 | 0·315 | 0·321 | 0·732 | 0·626 | 0·565 | 0·992 | 1·000 |
| 150 | 0·263 | 0·321 | 0·704 | 0·427 | 0·565 | 0·908 | 1·000 |
| 175 | 0·215 | 0·321 | 0·671 | 0·386 | 0·565 | 0·830 | 1·000 |
| 200 | 0·186 | 0·321 | 0·514 | 0·337 | 0·565 | 0·757 | 1·000 |
| 225 | 0·167 | 0·321 | 0·479 | 0·292 | 0·321 | 0·749 | 1·000 |
| 250 | 0·148 | 0·321 | 0·447 | 0·244 | 0·161 | 0·736 | 1·000 |
| 300 | 0·119 | 0·321 | 0·286 | 0·177 | 0·129 | 0·702 | 1·000 |
| 350 | 0·087 | 0·321 | 0·254 | 0·138 | 0·096 | 0·534 | 1·000 |
| 400 | 0·058 | 0·305 | 0·231 | 0·116 | 0·064 | 0·120 | 1·000 |
| 450 | 0·045 | 0·247 | 0·193 | 0·103 | 0·048 | 0·055 | 1·000 |
| 500 | 0·032 | 0·022 | 0·129 | 0·090 | 0·032 | 0·037 | 1·000 |
| 550 | 0·022 | 0·006 | 0·096 | 0·077 | 0·026 | 0·016 | 1·000 |
| 600 | 0·016 | 0·003 | 0·084 | 0·071 | 0·016 | 0·010 | 1·000 |
| 700 | 0·013 | 0·002 | 0·045 | 0·022 | 0·000 | 0·005 | 0·800 |
| 800 | 0·010 | 0·001 | 0·010 | 0·013 | 0·000 | 0·000 | 0·000 |
| 900 | 0·006 | 0·000 | 0·003 | 0·000 | 0·000 | 0·000 | 0·000 |
| *Data for standard drying conditions* | | | | | | | |
| Total† | 0·739‡ | 0·321 | 0·964 | 1·713 | 0·565 | 1·115 | 1·000 |
| 11% RH | 0·386 | 0·321 | 0·964 | 1·713 | 0·565 | 1·067 | 1·000 |
| D-dried | 0·273 | 0·321 | 0·643 | 0·386 | 0·565 | 0·830 | 1·000 |

* TG with heating rate 10 K $min^{-1}$, 50 mg specimen, flow rate of dry $N_2$, 15 ml $min^{-1}$.
† Non-evaporable and gel water.
‡ Of uncertain significance for w/c < 0·4.
§ Hydrogarnet-type product from ferrite phase.
¶ Grams retained per gram of CaO present in the given phase, except for the hydrotalcite-type phase, for which it is grams per gram of MgO present in that phase.
** Fraction of the $CO_2$ retained, irrespective of the phase in which it is present.
‖ Hydrotalcite-type phase.

In most cases, they are given as mass ratios of $H_2O$ to CaO, so that, in order to calculate the amount of $H_2O$ in a given phase at a particular temperature, it is necessary only to multiply the mass of CaO present in that phase by the relevant entry in the table. By summing the quantities of volatiles retained by each of the phases at each temperature, a simulated TG curve is obtained. The data points in Fig. 7.5 were calculated by this procedure using the data in Table 7.3, and the continuous curve was obtained experimentally for the paste to which those data relate. It is thus possible to account for the general form of the observed curve. The level of agreement between observed and calculated

curves is limited by several factors, including uncertainties and approximations in the reference data, the poor crystallinity of most of the hydrated phases and their intimate admixture with each other. Table 7.4 also contains data for the three definitions of the water content described in Section 5.2.2 and Table 7.3 includes the values obtained for the example given.

## 7.5 Calorimetry, pore solutions and energetics

### *7.5.1 The early and middle periods*

Figure 7.7 shows the heat evolution curve for a typical Portand cement paste, determined by conduction calorimetry. It broadly resembles those given by $C_3S$ (Fig. 5.14), and comparison with the microstructural evidence (Section 7.2) shows that it can largely be explained in a similar way. The initial peak (1) is attributable to a combination of exothermic wetting and the early-stage reactions, which with cement give a gelatinous coating and rods of AFt phase. Rehydration of hemihydrate to give gypsum may contribute. The main peak (2) corresponds to the middle-stage reaction, in which the main products, as with $C_3S$, are C–S–H and CH. The gradually decreasing rate of heat evolution after 24 h corresponds to the continuing slow reactions of the late stage, which again give mainly C–S–H and CH. As with $C_3S$, the process may be divided into the five stages of initial reaction, induction, acceleratory and decelerating periods, and the final period of slow reaction.

Many cements show a shoulder or more definite peak (3) at about 16 h. This has often been associated with the replacement of AFt by AFm phase, but comparison with the microstructural evidence shows that this is incorrect (P32); it is associated with renewed formation of ettringite. A further, less distinct shoulder (4) has been associated with hydration of the ferrite phase (P32) or conversion of AFt to AFm phase (S37). It may

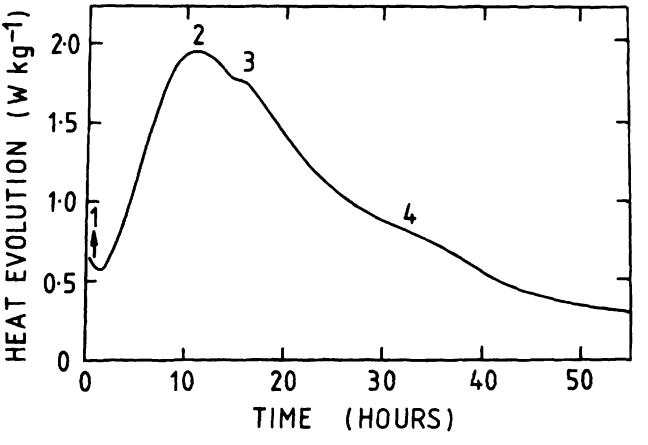


**Fig. 7.7** *Rate of heat evolution at 20°C for a typical Portland cement; for significance of numbered peaks, see text. After P32.*

correspond to a peak at about 50 h observed by Stein (S85). In all these reactions involving the aluminate or ferrite phases, the principal exothermic component is probably the reaction of the anhydrous compound with water and not the precipitation or subsequent reactions of hydrated compounds.

Many studies of concentrations in the pore solution during the early and middle periods have been reported (G63,L35,L36,T44,U13). Figure 7.8 shows typical results. Relatively high concentrations of $Ca^{2+}$, $K^+$, $Na^+$, $SO_4^{2-}$ and $OH^-$ are quickly reached. Between 2 and 12 h in the example given, the concentrations change relatively little, indicating an approximate balance between the continued dissolution of the cement phases and the precipitation of products. At 12–16 h, the concentrations of $Ca^{2+}$ and $SO_4^{2-}$ fall sharply, and the solution thereafter is essentially one of alkali hydroxides. The sharp fall at 12–16 h corresponds to the renewed growth of ettringite observed in the SEM and to shoulder (3) on the heat evolution curve. Concentrations of $SiO_2$ and $Al_2O_3$ are low throughout, values of 0·03–0·05 mmol $l^{-1}$ for Si and below 5 ppm for Al having been reported for times from 20 s to 45 min (T44).

Any more detailed interpretation demands that both activity coefficients and the existence of complex species be taken into account (B98,G63). Gartner *et al.* (G63) showed that, for most cements, the

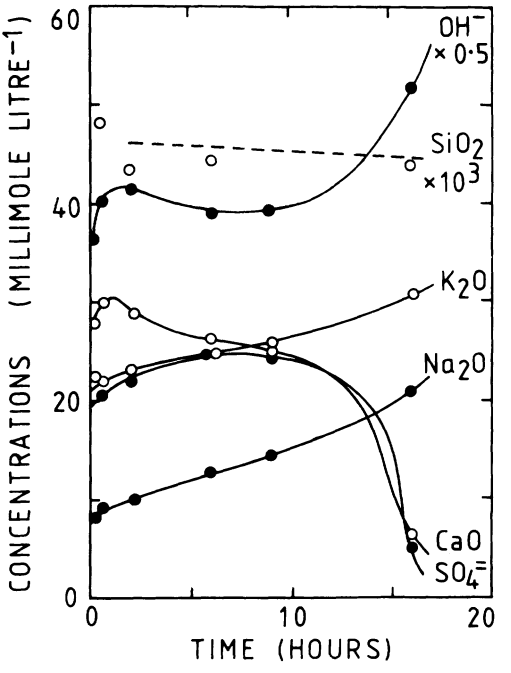


**Fig. 7.8** *Concentrations in the pore solution (scaled as indicated in the cases of $OH^-$ and $SiO_2$) of a Portland cement paste of w/c ratio 0·5. After L35.*

solution is saturated in CH within 12 min and that the saturation factor (defined as the activity product divided by its value at saturation) reaches a maximum of 2–3 within 2 h. For gypsum, saturation is reached within 6 min, but the saturation factor never exceeded 1·3 in the cases studied. With cements high in $K_2O$, the solution can become saturated in syngenite. Gartner *et al.* found that the $K^+$ and $Na^+$ concentrations increased rapidly during the first 12 min and only slowly, or not at all, during the subsequent period up to 3 h.

One may calculate a partial mass balance for the reaction at an age of 30 min. QXDA of a typical cement retarded with gypsum showed that, at this age, 11% of the aluminate and 8% of the ferrite phase had reacted (T35). Assuming from the bulk analysis that the cement contained 12% of aluminate and 7% of ferrite, and that these phases had the typical compositions given in Table 1.2, a total of 1·0 g of CaO and 0·5 g of $Al_2O_3$ are released from them per 100 g of cement. For broadly similar cements at the same age, ettringite contents of about 2% have been typically reported (B115,U14). These appear to be referred to masses of paste, and suggest values of about 3% referred to that of cement. This quantity of ettringite, ignoring any iron substitution, contains 0·8 g of CaO, 0·2 g of $Al_2O_3$ and 0·6 g of $SO_3$. It thus appears that, of the $Al_2O_3$ released, less than half enters the ettringite. Apart from small amounts in solution, the remainder and the CaO, $SiO_2$ and part of the $SO_3$ released from other phases presumably enter the amorphous gel that is also formed.

The evidence from microstructure, calorimetry and other sources suggests that the hydration processes of cement and $C_3S$ are essentially similar. There are important differences in the nature of the early product and in where the C–S–H formed in the middle stage of reaction begins to deposit, but in both cases it would appear that the early reaction slows down because of the deposition of a layer of product, which either isolates parts of the anhydrous surfaces from the main solution or allows the concentrations close to those surfaces to rise to values approaching the theoretical solubilities of the anhydrous compounds. In both cases, the initiation of the main reaction and the kinetics in its acceleratory phase appear to be controlled by the nucleation and growth of C–S–H.

### 7.5.2 *Pore solutions after the first day*

Apparatus for extracting pore solution from hardened cement pastes by applying pressures of some 375 MPa was first described by Longuet *et al.* (L37), and many other investigators have reported analyses of solutions thus obtained (e.g. D43,X1); for further references see T43). With pastes of normal Portland cements more than about 1 day old, the only ions present in concentrations above a few mmol $l^{-1}$ are $K^+$, $Na^+$ and $OH^-$. Most studies show the concentrations of these ions to rise with time, and to approach a limit after 28–90 days. Some show concentrations passing through maxima, with subsequent decreases that are usually slight. Typical concentrations after 180 days for pastes of w/c ratio 0·5 are 0·08 mol $l^{-1}$ for $Na^+$ and 0·24 mol $l^{-1}$ for $K^+$ for a low-alkali cement (X1)

and 0·16 mol $l^{-1}$ for $Na^+$ and 0·55 mol $l^{-1}$ for $K^+$ for a high-alkali cement (L37). The corresponding $OH^-$ concentrations are 0·32 mol $l^{-1}$ and 0·71 mol $l^{-1}$ respectively. Differing views have been expressed as to the validity of the method, mainly because of the possibility that high concentration gradients exist (e.g. D44, L38).

The $K^+$ and $Na^+$ are present in the cement partly as sulfates and partly in the major clinker phases (Section 3.5.7). When the phases containing them react, the accompanying anions enter products of low solubility and equivalent quantities of $OH^-$ are produced. The $K^+$, $Na^+$ and $OH^-$ ions are partitioned between the pore solution and the hydration products. Some estimates of the fractions remaining in solution have been too high because non-evaporable water was used as a measure of bound water and the quantity of pore solution thereby overestimated.

Taylor (T43) described a method for predicting the concentrations at any desired age after 1 day from the w/c ratio and the contents of total $Na_2O$, total $K_2O$, water-soluble $Na_2O$ and water-soluble $K_2O$ in the cement. It was assumed that the amount of each alkali cation taken up be the products is proportional to its concentration in the solution and to the quantity of products (C–S–H and AFm phase) taking it up. This led to the equation

$$c = m_r/[V + (b \times P)] \tag{7.4}$$

where $c$ is the concentration in mol $l^{-1}$, $m_r$ the quantity in millimoles of alkali cation released, $V$ the volume of pore solution in ml, $P$ the quantity of relevant products (C–S–H + AFm phase) relative to that formed on complete hydration, and $b$ an empirical constant, called the binding factor, equal to 20·0 ml for $K^+$ and to 31·0 ml for $Na^+$. $V$ was taken to be the total volume of water less the volume of bound water, i.e. that retained at 11% RH. The latter quantity, and $m_r$ and $P$, were estimated using empirical equations.

For a Portland cement with 0·2% total $Na_2O$ and 0·6% total $K_2O$, at w/c = 0·5 and an age of 1 year, calculation by the above method indicated that 59% of the $Na^+$ released and 48% of the $K^+$ released were taken up by the products. The ratios of alkali cations to $Ca^{2+}$ in the products are sufficiently low (typically <0·01 for $Na^+$ and ~0·01 for $K^+$) to suggest that the ions, with an equivalent quantity of $OH^-$, are adsorbed. As Glasser and Marr (G72) concluded earlier, $Na^+$ appears to be more strongly held than $K^+$. As noted in Section 7.4.3, the ratios of alkali cations to calcium found in the cement gel by X-ray microanalysis are higher than those in the solid products, because they include the materials dissolved in the pore solution, which are deposited when the latter evaporates.

### *7.5.3 Energetics of cement hydration*

Copeland *et al.* (C45) reviewed the energetics of cement hydration. After the first few days, the rate of heat liberation is too low for conduction calorimetry to be a practicable means of investigation, but the total amount of heat liberated after any desired time can be determined from

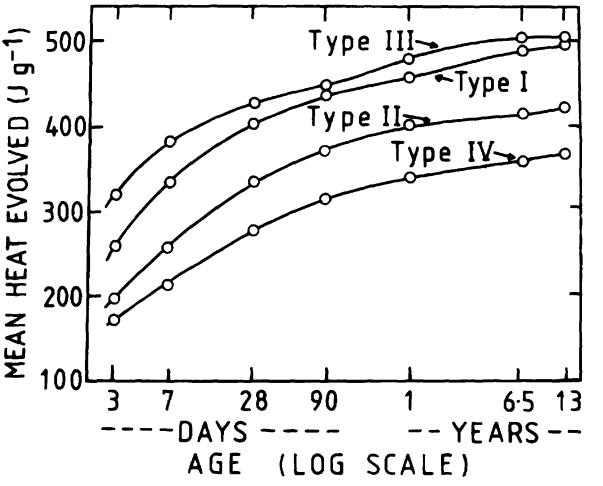


**Fig. 7.9** *Average cumulative heat evolution for a total of 20 Portland cements of ASTM Types I, II, III and IV, hydrated at w/c = 0·4 and 21°C. After C45.*

the heat of solution in acid, which is compared with that of the unhydrated cement. Figure 7.9 gives average results thus obtained for different ASTM types of Portland cements.

With any Portland cement, the amount of heat evolved by a given time is directly related to the amounts of the clinker phases that have reacted, and thus depends on such factors as the particle size distribution, w/c ratio and temperature and RH of curing. As the results in Fig. 7.9 show, it also depends on the cement composition. At all ages, the amount of heat liberated is greatest for the Type III (high early strength) cements and least for the Type IV (low heat) cements. The differences reflect the different average potential phase compositions, which show progressively lower contents of $C_3S$ and $C_3A$, and progressively higher ones of $C_2S$, along the sequence from Type III to Type IV.

Using least-squares regression analysis, the heat liberated at any given age was predicted from the potential phase composition by equations of the type

$$H_t = a(C_3S) + b(C_2S) + c(C_3A) + d(C_4AF) \qquad (7.5)$$

where $H_t$ is the amount of heat evolved in kJ kg$^{-1}$, the formulae denote the mass fractions of the phases calculated by the Bogue equations and the coefficients $a$, $b$, $c$ and $d$ have the values given in Table 7.5, which also includes values for the enthalpies of hydration of the pure clinker compounds, taken from the data in Sections 5.7.3 and 6.5.5. The agreement between the least-squares coefficients and the enthalpies of hydration is good for mature pastes, but there are some anomalies for younger pastes.

In principle, it should be possible to calculate the heat of hydration from the quantitative phase compositions of the unreacted mix and of the

**Table 7.5** *Coefficients in equation 7.5 for predicting the cumulative heat evolution in a cement paste of given age from the potential phase composition of the cement (for w/c = 0·4 and 21°C) (C45)*

| Compound | Coefficient | Value of the coefficient ($kJ\,kg^{-1}$) for age given below | | | | | | | Enthalpy of complete hydration* ($kJ\,kg^{-1}$) |
|---|---|---|---|---|---|---|---|---|---|
| | | 3 d | 7 d | 28 d | 90 d | 1 yr | 6·5 yr | 13 yr | |
| $C_3S$ | *a* | 243 | 222 | 126 | 435 | 490 | 490 | 510 | $-517 \pm 13$ |
| $\beta$-$C_2S$ | *b* | 50 | 42 | 105 | 176 | 226 | 222 | 247 | −262 |
| $C_3A$ | *c* | 887 | 1556 | 1377 | 1301 | 1167 | 1372 | 1356 | −1144†; −1672‡ |
| $C_4AF$ | *d* | 289 | 494 | 494 | 410 | 377 | 464 | 427 | −418§ |

* From data in Chapters 5 and 6.
† Reaction with gypsum to give $C_4A\bar{S}H_{12}$.
‡ Reaction with gypsum to give ettringite.
§ Reaction in presence of excess CH to give a hydrogarnet.

paste, using standard enthalpies of formation. The sensitivity of such calculations to small errors in the latter data probably renders this approach unsatisfactory with existing data.

## 7.6 Actions of calcium sulfate and of alkalis

### *7.6.1 Setting*

Setting times are commonly defined empirically, using a Vicat needle. In this device, weighted needles of standard design are allowed to sink into the paste, and initial and final set defined as the times when the degree of penetration falls below specified levels. In the British standard, which is typical, initial set must occur not earlier than 60 min (45 min for the highest strength classes).

In contrast to some earlier observations (L36,L39,O20), Tang and Gartner (T35) found that the amounts of both aluminate and ferrite phases reacting during the first 30 min were substantially decreased in presence of gypsum or other forms of calcium sulfate, and evidence from XRD, DTA, IR spectroscopy, conduction calorimetry and SEM shows that setting occurs during the acceleratory period and thus corresponds to a period of rapid formation of C–S–H and CH (B116). The microstructural evidence (Section 7.2.3) shows that little change occurs in the amount or morphology of the ettringite during this period, the secondary growth of ettringite occurring later. The concept of a cohesion point, at which the shells surrounding individual cement grains coalesce (D40), further indicates the importance of the relation between C–S–H formation and both setting and the initial stages of strength development. The close similarity in setting behaviour between pastes of cement and $C_3S$, and the relation between setting and microstructural development in $C_3S$ pastes, provide further evidence that normal setting depends primarily on the silicate reactions.

If too little gypsum is added, or none at all, many cements undergo what is termed 'flash' or 'quick' set. This is a rapid set, with much evolution of heat; plasticity is not regained on continued mixing, and the subsequent development of strength is poor. It is associated with increased early reaction of the aluminate and ferrite phases (T35), and with the formation of plates of AFm phase throughout the paste. These can be 5–10 $\mu$m in size (L39). The meshwork of plates, which may be contrasted with the much more compact coatings of gel and small rods of AFt phase formed in the presence of an adequate supply of gypsum, accounts for the rapid stiffening, but the reason for the subsequent poor strength development is less clear. Possible explanations include the formation during the initial reaction of strongly protective layers of product around the cement grains, and the existence of a microstructure weakened by the large plates of AFm phase. Some cements low in aluminate phase do not show flash set even if no gypsum is added.

Another undesirable condition is called 'false set'. This is also a rapid set, but there is no abnormally high evolution of heat, plasticity is regained on further mixing, and subsequent strength development is not markedly affected. The most usual cause of false set is the presence of too

much calcium sulfate in the form of hemihydrate, which is rehydrated to give gypsum (called 'secondary' gypsum). The setting is attributable to the interlocking of the gypsum crystals, which are tabular and can be 5–10 mm in longest dimension (L39). If the quantity of secondary gypsum is not too great, it redissolves on further mixing, and the reactions then follow their normal course. Dehydration of gypsum to hemihydrate can occur during milling; hemihydrate may also be added deliberately, if a more reactive form of calcium sulfate is required. With cements high in $K_2O$, syngenite can be precipitated; this also can cause false set, and, due to the removal of $CaSO_4$ from the system, even flash set (J27).

### 7.6.2 Optimum gypsum

The gypsum in cement affects not only the setting time, but also the strength development and the volume stability. Locher *et al.* (L36,L40), Kanare and Gartner (K38) and Tang and Gartner (T35) have discussed factors governing the optimum content and the effects of varying the source of the sulfate. The situation is complicated by the fact that, contrary to some early conclusions, the amounts needed to optimize different properties, such as strength at various ages and drying shrinkage, are not necessarily the same; also, the amount needed to optimize a given property in a concrete may not be the same as that required in a paste or mortar (K38).

During the early and middle periods of reaction in a cement paste, gypsum or other forms of calcium sulfate dissolve and react at or close to the surfaces of the clinker grains, or more specifically those of the aluminate and ferrite phases. The factor most directly influencing the course of the early reactions is not so much the relative amounts of calcium sulfate, aluminate and ferrite phases, as the rates at which the relevant ionic species are made available at the surfaces of the cement grains. The rates at which $Ca^{2+}$ and $SO_4^{2-}$ ions are supplied by the calcium sulfate thus depend both on the amount of the latter and on its physical and chemical nature. Hemihydrate or $\gamma$-$CaSO_4$ supply ions more quickly than does gypsum, which in turn supplies them more quickly than anhydrite. Other major factors affecting the supply of these ions are the particle size distribution of the calcium sulfate and the distribution in space of the particles; Tang and Gartner (T35) found that a given proportion of gypsum added by intergrinding was much more effective than the same proportion added by blending, all other conditions being as nearly as possible equal. Intergrinding presumably brings the gypsum particles into more intimate contact with those of the clinker. Increase in any of the factors rendering the $CaSO_4$ more readily available will tend to decrease the amount that is needed to produce a given effect in the early stage of reaction. Increase in temperature has a similar effect (C46).

Factors affecting the rate at which $Al_2O_3$ is supplied include its content in the clinker, its distribution among the clinker phases and especially the amount present in the aluminate phase, the specific surface area of the ground clinker, the reactivities of the aluminate and ferrite, and the

microstructure of the clinker particles, or, more specifically, the areas of surface composed of aluminate and ferrite phases and the manner in which these phases are intergrown with each other and with the silicate phases. Any factor increasing the availability of the $Al_2O_3$ will tend to increase the amount of gypsum that is required to produce a given effect in the early reactions.

Sulfate ion is also supplied by the clinker, especially as alkali sulfates or calcium langbeinite, and $Ca^{2+}$ ions are supplied by the clinker phases, including free lime. The alkali sulfates provide a highly available source of $SO_4^{2-}$, but the alkali cations, or more probably the $OH^-$ ions that they produce, have additional effects (Section 7.6.3).

The minimum content of $SO_3$ required to control setting is typically around 2%. Increase in $SO_3$ content beyond the minimum required has little effect on setting unless the proportion of hemihydrate or $\gamma$-$CaSO_4$ is so high as to cause false set. It causes a progressive decrease in the shrinkage that occurs in dry atmospheres (e.g. at 50% RH) and a progressive increase in the expansion that occurs in water. If expansion is excessive, the concrete disintegrates; this limits the permissible $SO_3$ content, which, in typical specifications, is set at 2·5–4·5%. The $SO_3$ content above which damaging expansion is liable to occur depends on cement composition and fineness, but seems rarely to be under 5–6% (H45,H46,L41,T45).

For any particular clinker and source of $SO_3$ there is an optimum content of $SO_3$ for strength at early ages. In a careful study, in which strengths were corrected empirically for the effects of differing particle size distributions and contents of entrapped air, Osbaeck and Jøns (O9) found maximum 1-day strengths at 3–5% $SO_3$ for a number of cements having different alkali contents and clinker $SO_3$/alkali ratios. At later ages, somewhat variable results have been reported; in general, the optimum seems to shift to higher values but to become less pronounced. The results of Osbaeck and Jøns, and of Jelenić *et al.* (J28), indicate that it is more definitely upwards if the alkali content is high. In evaluating the effect of gypsum content on strength or other properties, it is necessary to ensure that other relevant factors are as far as possible kept constant. Thus, if cements with the same clinker but different gypsum contents are ground to the same specific surface area, the clinker will be less finely ground the more gypsum is present, and this will tend to decrease the rate of strength development.

Calcium sulfate additions probably affect both the quantities of products that are formed, especially at early ages, and the microstructure at all ages. Addition of $CaSO_4$ is reported to increase the rate of hydration, both of pure $C_3S$ and of the alite in cement (B117,C46,J28,J29,L39). This could explain an increase in strength at early ages due to additions below the optimum, but not a decrease with larger amounts. The fact that calcium sulfate additions affect the drying shrinkage also suggests that the microstructure is modified. This could occur in various ways, e.g. by changes in the micromorphology of the C–S–H or by incipient precipitation of ettringite throughout the gel. The latter effect, if it happened at

an early age or to a limited extent, could augment strength through a decrease in porosity, but if it happened later or to too large an extent could decrease strength through localized expansions.

Attempts to formulate equations relating optimum gypsum content to composition and particle size distribution have proved of little practical value, and gypsum contents are normally decided on the basis of empirical strength tests. In practice, the molar ratios of total $SO_3$ to total $Al_2O_3$ in modern cements range from 0·5 to 0·9, with an average of about 0·6 (K38). In order to adjust the supply of $SO_4^{2-}$ to that required at different stages of the hydration process, it may be desirable to use mixtures of different forms of calcium sulfate; for example, with cements high in aluminate phase, a mixture of anhydrite and hemihydrate, the latter produced by dehydrating gypsum during milling, has been recommended (L39).

### 7.6.3 *Effects of alkalis*

Alkali cations normally occur in cements either as sulfates or in the major clinker phases. In either case, the balancing anion sooner or later enters a hydration product of low solubility, and an equivalent amount of $OH^-$ ion is released. Apart from syngenite precipitation, mentioned above, the effects of alkali cations on cement hydration are likely to be predominantly those of the $OH^-$ ion. Jawed and Skalny (J27) reviewed these effects, both on the hydration process and on the properties of the hardened product. In general, early strengths are increased and late strengths decreased. Some other properties, such as drying shrinkage, are affected, and the optimum gypsum content is increased. This last effect must be taken into account when effects on strength are considered. Lerch (L41) attributed it to accelerated early reaction of the clinker phases.

The results obtained by Osbaeck and Jøns (O9) in the study mentioned in the previous section are probably typical. They show the effects of alkali sulfates on early and late strengths and on optimum gypsum contents mentioned above. The effects on strength were diminished or absent at gypsum contents above the optimum. QXDA showed that the increased early strengths were associated with increased reaction of the alite, aluminate and ferrite phases. This effect was quite marked; for example, at 1 day, the reaction of the alite increased from 26% for a cement low in soluble alkalis to 56% for an otherwise similar cement high in them. There were less definite indications of an association between the decreased strength at 28 days and decreased consumption of the clinker phases, and the authors were uncertain whether the decrease in strength was due to this or to the formation of a less favourable microstructure.

Bezjak *et al.* (B112) similarly found that the fractions of alite reacting at early ages were substantially increased in the presence of alkali sulfate, both in Portland cement and in mixtures of alite with $C_3A$. After 10 days, which was the longest time studied, the fraction reacting was still enhanced in presence of alkali sulfate in the case of a cement low in aluminate phase, but was slightly lowered in that of a cement higher in aluminate. Applying a theory of the kinetics of hydration described in Section 7.7.2, they attributed the acceleration at early ages primarily to

an increase in the permeability of the layer of hydration products surrounding the alite at a stage soon after the rate of reaction had become controlled by diffusion.

Tang and Gartner (T35) studied a clinker low in alkalis and in $SO_3$, but high in aluminate, which they blended with varying mixtures of calcium sulfate, calcium alkali sulfate and alkali sulfate phases. They, too, found that alkali sulfates increased the early strength; without exception, the 1-day strengths obtained using blends of gypsum or hemihydrate with aphthitalite, syngenite or calcium langbeinite were greater than those obtained at the same ratio of total $SO_3$ to $Al_2O_3$ with the calcium sulfates alone, calcium langbeinite and syngenite being especially effective. The efficacy of calcium langbeinite as a set-controlling agent was earlier recognized by Moir (M12). At 28 days, in contrast to the findings of Osbaeck and Jøns, there was little significant difference in strength between the cements with and without alkali sulfates, though those of the former tended to be lower.

Jelenić *et al.* (J29) found that, for pastes of alite and $C_3A$ with varying amounts of gypsum and with or without alkali sulfate, high strengths at 28 days were correlated with low $C_3A$ consumption at 1 day. The late strengths were increased, not decreased, in the presence of alkali provided that the gypsum content was suitably adjusted. Tang and Gartner (T35) similarly found little correlation between the amount of aluminate phase consumed at 2 min and the compressive strength at 1 day, but there was a negative correlation between this quantity and the strength at 28 days. They concluded that a reduced initial aluminate consumption tended to improve not only the workability of the fresh paste, but also the ultimate strength of the hardened material.

Ramachandran *et al.* (R39) found that the rate of reaction of $C_3S$ at ages up to at least 28 days was substantially increased by addition of NaOH. Strengths were unaffected up to 7 days, but were lowered at 28 days. SEM of fracture surfaces showed that the NaOH affected the morphology both of the C–S–H and of the CH.

## 7.7 Kinetics and modelling of the hydration process

### *7.7.1 Experimental data*

The kinetics of cement hydration are concerned with the relations between the degree of hydration $\alpha$ and the age $t$, and with the factors that influence them. Curves of $\alpha$ against $t$ will be described as kinetic curves. From the practical standpoint, the kinetic curve controls the way in which the physical properties develop as curing proceeds.

$\alpha$ may relate either to an individual clinker phase or to the cement as a whole. Because cement is a mixture of phases that react at different rates, there are problems in determining, and even in defining, $\alpha$ for the whole cement; it is defined here as the mass fraction of the cement that has reacted, irrespective of phase. In principle, it may be obtained by summing the amounts of the individual phases that have reacted, which in turn can be determined by QXDA or in other ways. Because of the experimental difficulty and questionable precision of this approach, less

direct methods have often been used, based on the determination of such quantities as non-evaporable water, cumulative heat evolution (C45), or chemical shrinkage (K39). It has normally been assumed, with varying degrees of justification, that these quantities are proportional to $\alpha$ as defined above.

Major influences on the kinetic curve of a cement include the phase composition of the clinker, the particle size distribution of the cement and the RH and temperature regimes during curing. Other influences include the w/c ratio, the content and distribution of admixtures, including gypsum, the reactivities of individual clinker phases and probably others, such as the microstructures of the clinker and of the cement particles. Brown *et al.* (B118) reviewed some factors that could control the kinetics of hydration.

By definition, the kinetic curve of a cement is the weighted sum of the curves for its constituent phases as they occur in that cement. The reactivities of individual clinker phases are considered in Section 4.6 and some effects of particle size distribution, which is a particularly important variable, in Section 4.1.4. Although many data relating particle size distribution directly to strength exist, much less is known about its relation to degrees of reaction. Parrott and Killoh (P35) presented data indicating that the rate of hydration, as represented by that of heat evolution, was proportional to the specific surface area during the period of hydration in which the rate was controlled by nucleation and growth, but not subsequently, when it was controlled by diffusion.

The rates of reaction of the clinker phases are greatly influenced by the RH of the atmosphere in which curing occurs. For a typical Portland cement paste of w/c ratio 0·59 cured at 20°C and 100% RH, Patel *et al.* (P33) found the fractions of the alite, belite, aluminate and ferrite phases hydrated after 90 days to be respectively 0·94, 0·85, 1·00 and 0·51. If the RH was lowered to 80%, the corresponding values were 0·77, 0·19, 0·83 and 0·32. The hydration rate of the belite thus appears to be especially sensitive to RH. On the basis of earlier data from the literature, Parrott and Killoh (P35) concluded that the effect of RH on the hydration rate ($d\alpha/dt$) of each of the phases could be represented by a factor $\{(RH - 0{\cdot}55)/0{\cdot}45\}^4$.

Copeland and Kantro (C46), using QXDA, found that alite and belite in a Portland cement hydrated more rapidly at w/c = 0·65 than at w/c = 0·35. Heat of hydration data (C45) indicated that the rate of hydration in Portland cement pastes is higher at w/c = 0·6 than at w/c = 0·4 at all ages from 1 day to 6·5 years. Taplin (T46) found that at low w/c ratios the rate was significantly reduced at later ages. Based on this last result, Parrott and Killoh (P35) considered that $d\alpha/dt$ was reduced by a factor $f(w/c)$ which applied only at values of $\alpha$ greater than $1{\cdot}333 \times w/c$:

$$f(w/c) = \{1 + 4{\cdot}444(w/c) - 3{\cdot}333\alpha\}^4 \qquad (7.6)$$

In contrast to these results, Locher (L42), working with pure $C_3S$, found that hydration was more rapid at a low w/c ratio.

Temperature has a large effect, especially in the earlier stages of hydration; for example, from QXDA, Copeland and Kantro (C46) found that in a Portland cement paste of w/c = 0·57, the fraction of the alite hydrated at 2 days was 0·28 at 5°C, 0·63 at 25°C and 0·81 at 50°C. Apparent energies of activation calculated from such data were 41 kJ mol$^{-1}$ at $\alpha = 0{\cdot}6$ and 26 kJ mol$^{-1}$ at $\alpha = 0{\cdot}7$; for belite, a value of 56 kJ mol$^{-1}$ at $\alpha = 0{\cdot}4$ was obtained. The decrease in the apparent energy of activation in the case of alite was attributed to a gradual change in rate control from a chemical process to diffusion.

### 7.7.2 *Interpretation of kinetic data*

The kinetics of cement hydration are dominated by the effects associated with the particle size distribution of the starting material, and attempts to explain them in which this is ignored can lead to very misleading results (B112,B119,J30,K40–K42,T47). Even laboratory-prepared samples with close distributions (e.g. 2–5 $\mu$m; K21) are far from monodisperse from the kinetic standpoint. Two approaches to the resulting problems of interpretation will be considered.

Bezjak, Jelenić and co-workers (B112,B119,J30) assumed that during the hydration of each particle, up to three processes were rate-controlling at different stages. The first was nucleation and growth of a product. The second was a process occurring at a phase boundary. The third was a diffusion process. Each supplanted a predecessor when it became the slowest of the three, at a time that depended on the initial radius $r$ of the particle; more than one rate-determining process could thus operate simultaneously. Given the rate equations and appropriate rate constants, it was possible to calculate the value of $\alpha$ at any desired time for a particle of given radius, and, by summing the amounts of material that had hydrated for particles of all sizes, the value of $\alpha$ for the whole material.

In the rate equations relating $\alpha$ to $t$ for a single particle, the first did not involve $r$. In the second, a function of $\alpha$ was proportional to $(t - t_0)/r$, where $t_0$ is the time at which the process became rate-determining. In the third, a function of $\alpha$ was proportional to $(t - t_0)/r^2$. Kinetics represented by equations of the second and third of these types are described as linear and parabolic, respectively. It was shown that the kinetic curves of a number of alite and cement pastes, some of which contained added alkali sulfates, could be satisfactorily explained (B119). For the cements, diffusion became virtually the sole rate-controlling process at values of $\alpha$ varying between about 30% and 60%. This appears to agree broadly with the evidence from apparent energies of activation noted in the previous section.

Knudsen (K40–K42) assumed that the rate equation relating $\alpha$ to $t$ for a single particle could be either linear or parabolic. Like Bezjak *et al.*, he also assumed that the total amount of material reacted was the sum of the amounts calculated for all the individual particles, and thus, given the rate equation for a single particle, the rate constant and the particle size distribution, obtained the value of $\alpha$ for the whole material. In contrast to Bezjak *et al.*, he concluded that the results were highly insensitive to

the precise form of the rate equation, and that all that could be learned about the latter from the kinetic curve was whether it was linear or parabolic, and the value of the rate constant. Using data from various sources, Knudsen concluded that, for the values of $\alpha > 0{\cdot}15$ to which his model was applicable, some cements followed linear kinetics for virtually the whole range of values up to $\alpha = 1$, and others parabolic kinetics. A change from linear to parabolic kinetics could be produced by adding $CaCl_2$, and the possibility of a gradual change from linear to parabolic kinetics at high values of $\alpha$ was not excluded. It is not obvious how the conclusion that some cements show linear kinetics throughout can be reconciled with the evidence from apparent energies of activation.

Knudsen's model led to the prediction that, if linear kinetics were followed, the age at which 50% of the cement has hydrated is proportional to the fineness constant $r_0$ (or $x_0$) in the Rosin–Rammler distribution (equation 4.1); for parabolic kinetics, it predicted that this age is proportional to $r_0^2$ (K43). Evidence was presented in support of this conclusion for cements considered to follow linear kinetics. The theory did not predict any relation to the breadth of the particle size distribution, which is represented by the slope of the Rosin–Rammler curve.

In neither of these approaches is it necessary to specify the rate-controlling step more precisely than is given above. The discussion on the hydration kinetics of $C_3S$ pastes (Section 5.8) is probably substantially applicable also to cement pastes. One may speculate that in the theory of Bezjak *et al.*, the nucleation and growth of C–S–H determines the rate until the anhydrous phases cannot supply the ions sufficiently quickly. Dissolution of the anhydrous phases then becomes rate-determining until the permeability of the layer of product has decreased to a level such that diffusion takes over. It would be highly desirable to examine the implications of both theories in the light of the more recent microstructural evidence (Section 7.2). It would also be desirable to determine whether Knudsen's more pessimistic conclusion regarding the information that can be extracted from the experimental data results from a more realistic appraisal of the precision of the data, or from the differences between his assumptions and those of Bezjak *et al.*

# 8 Structure and properties of fresh and hardened Portland cement pastes

## 8.1 Fresh pastes

### *8.1.1 Workability*

Workability is a general, descriptive term that indicates the ease with which a concrete can be mixed, transported, placed and compacted to give a uniform material. There is no single measure of it, but various empirical tests that provide information on particular aspects are widely used. The most important is the slump test, in which the material is moulded by lifting away a conical container in which it was placed. The subsidence of the resulting pat provides a measure of the ability of the material to flow under its own weight. Neither this nor any of several other empirical tests that are in use gives results that are simply related to any fundamental rheological properties. Their main value is for quality control of a given concrete mix rather than for the comparison of different mixes.

The workability of a concrete mix is by no means dependent only on the physical properties of the cement paste it contains, but an understanding of it requires one of those properties. For some specialist uses in which cement is used without an aggregate, the latter are directly relevant. The most important properties are concerned with rheology, and this section deals primarily with these properties in Portland cement pastes, free from admixtures, prior to setting. From the chemical standpoint, this period comprises that of initial reaction and induction period. From the practical standpoint, it includes those of mixing, placing and compaction.

### *8.1.2 Rheology; viscometry*

The resistance of a fluid to flow may be considered in terms of the situation existing between two parallel planes, one of which is moving in its own plane relative to the other. It is assumed that flow is confined to the single direction thus defined, and that the velocity varies linearly with distance in the direction perpendicular to the planes. Liquids of simple and stable molecular structure generally obey the Newtonian law

$$\tau = \eta \times \dot{\gamma} \tag{8.1}$$

where $\tau$ is the shear stress (Pa), $\eta$ is the viscosity (Pa s) and $\dot{\gamma}$ is the shear rate ($s^{-1}$), equal to the velocity of one surface relative to the other divided by the distance between them. The resistance to flow at a given temperature and pressure is thus defined by a single constant, the viscosity.

Suspensions show Newtonian behaviour only if there is no long-range structure. In varying degrees, many approximate in behaviour to the Bingham model, represented by the equation

$$\tau = \tau_0 + (\mu \times \dot{\gamma}) \tag{8.2}$$

where $\tau_0$ is the yield stress and $\mu$ is the plastic viscosity. No flow occurs until the shear stress exceeds $\tau_0$. Many more complex variants on this type of behaviour are possible; the relation between $\tau$ and $\dot{\gamma}$ may not be linear, and may show hysteresis (Fig. 8.1). The quantity $\tau/\dot{\gamma}$ for a non-Newtonian fluid is called the apparent viscosity. Its value varies with $\dot{\gamma}$ and, if hysteresis occurs, with the previous history of the sample.

In many studies on fresh cement pastes, rotational viscometers have been used to obtain flow curves in which shear rate is plotted against shear stress, including hysteresis effects. Work up to 1988 was reviewed in a book (T48) and several shorter articles (H47,L43,S86). There is general agreement that there is a yield stress below which no flow occurs, but in other respects the results from different investigations vary widely. Banfill

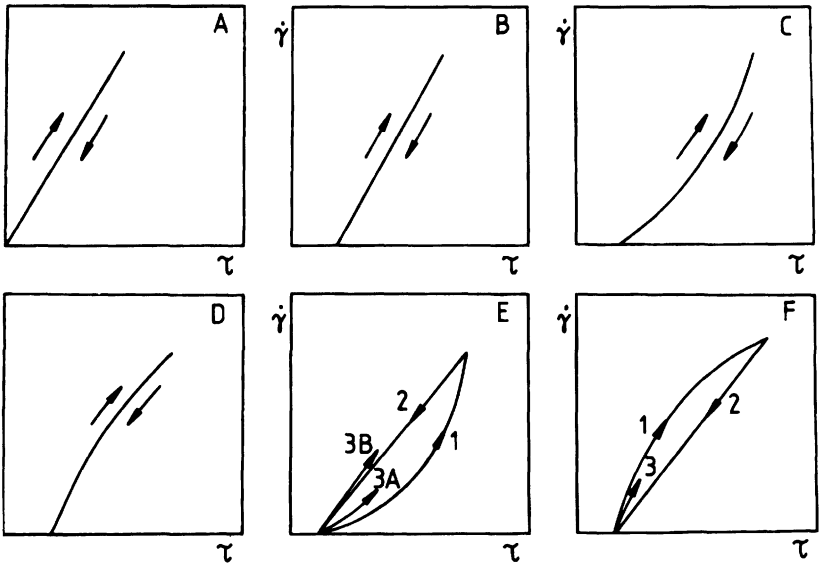


**Fig. 8.1** *Idealized plots of shear rate $\dot{\gamma}$ against shear stress $\tau$ for fluids of various types. (A) Newtonian fluid. (B) Bingham fluid. (C) Shear thinning. (D) Shear thickening. (E) Positive hysteresis: 1, 2, 3A thixotropy; 1, 2, 3B rheodestruction. (F) Negative hysteresis with antithixotropy.*

and Saunders (B120) concluded that this arose from two competing processes: breakdown of a floc structure caused by shear, and building up of structure due to continuing hydration. They considered that flow curves and hysteresis loops were of very limited value, to be used only in the clear understanding of their disadvantages. They are probably useful mainly as a comparative technique.

Tattersall and Banfill (T48) considered the structural breakdown to be partly irreversible. Because the irreversible breakdown occurs during mixing, variable results can be obtained if it is not completed before measurements begin. This problem can be avoided by high-shear mixing prior to the rheological investigation, which probably brings the paste into a condition similar to that present in a fresh concrete mix.

### *8.1.3 Oscillatory and controlled-stress rheometry*

Macroscopic flow inevitably alters the microstructure of the paste, and, while yield stress gives some information on the microstructure of the flocculated suspension, viscosity data cannot (B121,S87). In order to obtain further information from rheology on paste microstructure, it is necessary to use methods in which flow is minimized. It is also necessary that the experiments should be of sufficiently short duration that continued hydration does not complicate the results. For adequate interpretaion of rheological data, these also must be related to data relating to the course of the chemical reactions.

In an oscillatory rheometer, the strain can be oscillated through a small but increasing amplitude according to a sine function, the frequency being held constant, and the resulting stress monitored. It is also possible to hold the strain amplitude constant and to vary the frequency. The principal data obtained from these techniques are a value of the critical strain, marking the change from solid- to liquid-like behaviour, and a stress modulus $G^*$, which is a complex quantity. Its real and imaginary components are termed the storage modulus $G'$ and loss modulus $G''$, respectively; $G'$ relates to the solid component of the stress, which is in phase with the strain, and $G''$ to the liquid component. Banfill (B121) described an instrument in which a conduction calorimeter was incorporated in order to monitor the hydration reactions. Schultz and Struble (S87) concluded from oscillatory shear studies that pastes 10 min after high-shear mixing showed solid-like behaviour resulting from a flocculated microstructure which was maintained so long as the strain did not exceed $\sim 10^{-4}$. At larger strains the microstructure was disrupted, giving rise to liquid-like behaviour.

In a controlled-stress rheometer a constant small stress can be applied, and the resulting strain monitored against time during loading and after the stress has been removed. Struble and Schultz (S88) found this method to be more satisfactory than oscillatory rheometry. They used it to study cement pastes 1 min after the completion of high-shear mixing. Low applied stress (e.g. 3–4 Pa for w/c 0·50) produced an immediate strain on which was superimposed time-dependent creep. When the stress was removed, recovery was slow and far from complete. The behaviour under

load is that of a viscoelastic solid and that during recovery is that of a visccoelastic liquid. At higher applied stresses (e.g. 9 Pa) there was no instantaneous response, the strain increasing almost linearly with time throughout loading, and there was no recovery when the stress was removed. This behaviour is that of a viscous liquid. These results were explained by supposing the paste to be a flocculated suspension. A certain minimum stress was required to break down the flocculated microstructure and thus to effect a change from solid-like to liquid-like behaviour. This critical stress was sharply defined, and the values observed were reasonably consistent with the yield stresses obtained from flow curves or oscillatory shear measurements.

Struble and Lei (S89) found that the yield stress could be determined from creep-recovery curves without being exceeded. It was thus possible to obtain values at successively greater ages on a single specimen without causing structural breakdown after each determination. A study continued to the stage of initial set showed that the latter corresponded to a sharp increase in yield stress, which occurred at the end of the induction period.

### *8.1.4 Models of fresh paste structure*

Helmuth (H47) considered the cement particles in a paste to constitute a single floc, in which, however, there were regions of varying solid content. On shearing, the particles became more uniformly distributed, and the static floc structure was reformed on standing. Tattersall and Banfill (T48) considered that this model did not sufficiently explain the irreversible nature of the breakdown caused by shearing, and proposed that during the initial reaction aggregates of particles already in contact were coated with a continuous membrane of gel which, if destroyed by shearing, was replaced by separate coatings around each particle, which were less effective in binding the particles together.

It is difficult to test such models directly, as neither light nor electron microscopy is readily applied, but Uchikawa *et al.* (U15) described a method of specimen preparation for SEM examination. The paste was mixed for 3 min and, after various times, was placed on the surface of a metal sample holder already cooled in liquid $N_2$. The sample holder was then further cooled by immersion in liquid $N_2$ and the specimen was examined at $-120°C$. For a Portland cement paste without admixtures 5 min after mixing, flocs of small particles and of large particles with adhering small ones were observed, but there was no continuous floc structure. The average distance between flocs was about 3 $\mu$m. At 2 h, C–S–H and ettringite were observed on the grain surfaces and the flocs were more definite. At 6 h, the layers of hydration products were much thicker and a three-dimensional structure was formed through the linking of the larger grains through smaller ones.

To an extent that increases with the w/c ratio, fresh cement pastes exhibit the phenomenon of bleeding, i.e. settlement of the solid particles. The interparticle attractions are sufficiently strong that particles of all sizes settle at the same rate, typically about 2 $\mu m\, s^{-1}$. Settlement tends to increase the w/c ratio at the top and to decrease it at the bottom of the

sample. It decreases with increased fineness or increased early hydration rate of the cement. In a concrete, it can produce layers of water beneath aggregate particles or reinforcing bars.

## 8.2 Hardened cement pastes: models of structure

### *8.2.1 The Powers–Brownyard model*

The rest of this chapter deals with hardened Portland cement paste (hcp), which has the properties of a rigid gel. It is a relatively rigid and strong solid of high porosity and internal surface area. Variations in the relative humidity (RH) of the surrounding atmosphere cause it to gain or lose water and also produce small but important changes in volume. Powers and Brownyard (P20) described the broad structure of the material by a model based largely on evidence from total and non-evaporable water contents and water vapour sorption isotherms. Powers later modified the model in minor respects (P36).

In this model, hcp is assumed in the general case to comprise three components from the volumetric standpoint, viz. (*a*) unreacted cement, (*b*) hydration product and (*c*) capillary pores. Individual solid phases are not considered, whether in the cement or in its hydration products, which were collectively called 'cement gel'. This term may be found confusing, because it includes the CH, which forms relatively large crystals and cannot reasonably be considered part of a gel; the term 'hydration product' is substituted here. The water present in the paste was categorized as evaporable or non-evaporable, the latter being defined in the later work (P36) as that retained on D-drying. Evaporable water, when present, was considered to reside partly in the capillary pores and partly in so-called gel pores within the hydration product. This latter part was called gel water.

The content of non-evaporable water, relative to that in a fully hydrated paste of the same cement, was used as a measure of the degree of hydration. Portland cement paste takes up additional water during wet curing, so that its total water content in a saturated, surface dry condition exceeds the initial w/c ratio. Evidence from water vapour sorption isotherms indicated that the properties of the hydration product that were treated by the model were substantially independent of w/c and degree of hydration, and only slightly dependent on the characteristics of the individual cement. The hydration product was thus considered to have a fixed content of non-evaporable water and a fixed volume fraction, around 0·28, of gel pores.

The hydration product occupies more space than the cement from which it is formed, and the capillary pores were regarded as the remnants of the initially water-filled space. Their volume thus decreases, and that of the gel pores increases, as hydration proceeds. Evidence from water vapour sorption isotherms indicated that the hydration product was composed of solid units having a size of about 14 nm, with gel pores some 2 nm across (P36). The width of the capillary pores could not be determined from the available data, but they were considered to be generally much wider than the gel pores, though tending to become narrower as the

water-filled space was used up, and thus in some regions indistinguishable from gel pores.

The following symbols are used here.

$w/c$ = initial water/cement ratio, corrected for bleeding.
$w/c^*$ = critical value of w/c below which complete hydration cannot occur, typically about 0·38.
$w_t/c$ = total water/cement ratio in the saturated, surface dry state.
$w_n/c$ = ratio of non-evaporable water to cement.
$w_e/c$ = ratio of evaporable water to cement in the saturated, surface dry state, and equal to $w_t/c$ less $w_n/c$.
$V_c$ = specific volume of unhydrated cement, typically about $3{\cdot}17 \times 10^{-4}\ m^3\ kg^{-1}$.
$V_g$ = mean specific volume of the gel water, taken here as $1{\cdot}00 \times 10^{-3}\ m^3\ kg^{-1}$.
$V_n$ = mean specific volume of the non-evaporable water ($m^3\ kg^{-1}$).
$D_w$ = density of the pore solution in fresh paste, taken here as $1000\ kg\ m^{-3}$.
$m_g$ = mass of gel water per unit mass of cement in a fully hydrated paste, typically about 0·21.
$m_n$ = mass of non-evaporable water per unit mass of cement in a fully hydrated paste, typically about 0·23.
$\alpha$ = mass fraction of cement hydrated.
$\alpha_{max}$ = maximum value of $\alpha$ possible at $w/c \leq w/c^*$.

### 8.2.2 *Minimum water/cement ratio for complete hydration; chemical shrinkage*

Powers and Brownyard (P20) determined the non-evaporable and total water contents of pastes of many cements made up at different w/c ratios and cured for different lengths of time. In Fig. 8.2 the ratios of evaporable water to cement in saturated, mature pastes of a typical cement are plotted against those of total water to cement. The initial w/c ratios are shown by the scale at the top; up to about 0·06 kg of water per kg of cement is taken up during wet curing. The data show a distinct break at $w/c = 0{\cdot}38$, and are fitted by the equations

$$w_e/c = w_t/c - 0{\cdot}227 \quad \text{for } w/c > 0{\cdot}38 \tag{8.3}$$

$$w_e/c = 0{\cdot}482 \times w_t/c \quad \text{for } w/c < 0{\cdot}38 \tag{8.4}$$

The value of $w_t/c$ at the break is 0·44.

Similar results were obtained for other Portland cements. In the following interpretation of them, the small changes in total paste volume that occur during curing are ignored, and any air entrapped or deliberately introduced during mixing is regarded as being outside the system. Because the hydration product was considered to occupy more space than the cement from which it is formed, and since the total volume of the paste scarcely changes on hydration, complete hydration cannot occur if w/c is below a certain value. For the cement under discussion, this value is 0·38, and a mature paste of this w/c ratio consists entirely of hydration

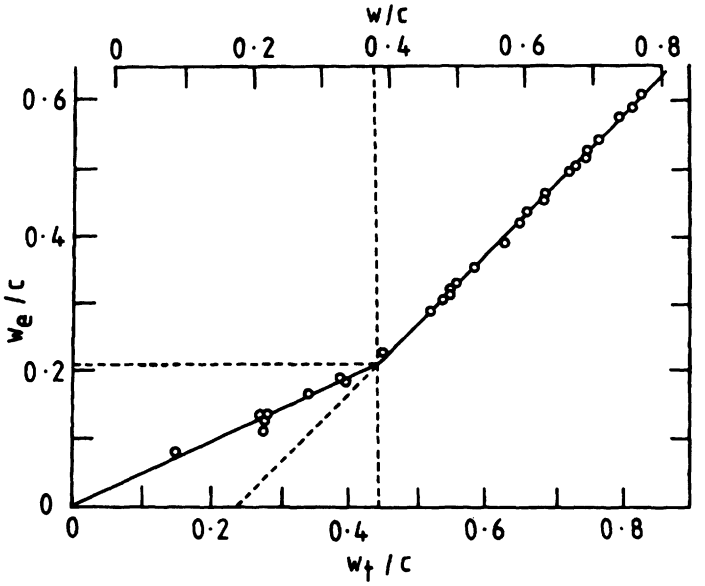


**Fig. 8.2** *Relations between the initial (w/c), total ($w_t/c$) and evaporable ($w_e/c$) water/cement ratios for saturated, mature pastes of a Portland cement. After P36.*

product. The latter contains, per kg of cement, 0·227 kg of non-evaporable water and, in the saturated condition, 0·211 kg of gel water, making a total of 0·438 kg. The pastes with $w/c < 0{\cdot}38$ consist of unreacted cement and hydration product, and thus have $(w_e/c)/(w_t/c)$ equal to 0·211/0·438, or 0·482. The pastes with $w/c > 0{\cdot}38$ consist of hydration product and capillary pores, which in the saturated condition are filled with water, and thus have $w_e/c$ equal to $w_t/c - w_n/c$.

Most investigators appear to have agreed with the observation that complete hydration cannot occur if w/c is below a value in the region of 0·38, but Rössler and Odler (R40) reported that hydration was complete in a paste with $w/c = 0{\cdot}22$, and further investigation may be required. On the Powers–Brownyard theory, the value of the minimum depends on the volume ratio of hydration product to cement, which in turn depends on the gel porosity of the hydration product. It was assumed that this porosity was fixed by the inability of new particles to nucleate in pores smaller than a certain size and by that of existing particles to grow beyond a certain size.

If a paste having $w/c < 0{\cdot}44$ is cured under sealed conditions, there will be insufficient water to fill the gel pores completely, and the capillary pores will be empty. The effective RH will be low, and hydration will become very slow or stop, even though free space remains. This phenomenon is called self-desiccation. Even at higher w/c ratios under sealed conditions, partial emptying of the capillary pores will retard hydration, and can produce irreversible changes in pore structure which reduce the

final strength. It is therefore important to provide an adequate supply of water during curing. If a paste is kept in contact with an excess of water during curing, the total volume of paste and water decreases. This effect is called chemical shrinkage, and may be used to follow the course of hydration. For this purpose, it has the merits that hydration need not be stopped and that the determination can readily be automated. Knudsen and Geiker (K39) described a device for automated determination on up to 30 samples.

### 8.2.3 Calculation of volumetric quantities

This section gives expressions and values for some important volumetric quantities. The data for the cement discussed in the previous section are adopted as typical.

(1) The *total volume of paste* per unit mass of cement is $V_c + (w/c)/D_w$, where $V_c$ is the specific volume of the cement and $D_w$ the density of the pore solution in the fresh paste. Assuming a value of $3{\cdot}17 \times 10^{-4}\,m^3\,kg^{-1}$ for $V_c$ and one of $1000\,kg\,m^{-3}$ for $D_w$, this gives $3{\cdot}17 \times 10^{-4} + (w/c)/1000\,m^3\,kg^{-1}$.

(2) The *volume of hydration product* per unit mass of cement reacted is obtained by considering the special case of a fully hydrated paste having the critical w/c ratio, w/c*, in which only hydration product is present; it is $V_c + (w/c^*)/D_w$. For the general case, it is thus $[V_c + (w/c^*)/D_w] \times \alpha$, where $\alpha$ is the degree of hydration. Inserting the values of $V_c$, w/c* and $D_w$, this gives $7{\cdot}0 \times 10^{-4} \times \alpha\ m^3\,kg^{-1}$.

(3) The *volume of unreacted cement* per unit mass of cement is $V_c \times (1-\alpha)$, or $3{\cdot}17 \times 10^{-4} \times (1-\alpha)\,m^3\,kg^{-1}$.

(4) The *specific volume of the non-evaporable water* $V_n$ is obtained by taking the volume of hydration product less those of the cement from which it was formed and the gel water, and dividing by the mass of non-evaporable water. This gives $[(w/c^*)/D_w - V_g m_g]/m_n$, or $0{\cdot}74 \times 10^{-3}\,m^3\,kg^{-1}$.

(5) The *maximum degree of hydration* $\alpha_{max}$ for a paste with $w/c \leq w/c^*$ may be calculated by equating the total volume of paste to the sum of the volumes of unreacted cement and hydration product; it is $(w/c)/(w/c^*)$, or $(w/c)/0{\cdot}38$. This assumes that an unrestricted supply of water is available during curing. If no such water is available, the degree of hydration is limited by the amount of water present initially to a maximum value of $(w/c)/(m_n + m_g)$, or $(w/c)/0{\cdot}44$.

(6) The *ratio of the volume of hydration product* to that of the cement from which it is formed may be calculated by dividing the former quantity by the volume of cement reacted per unit mass of cement, which is $\alpha \times V_c$, giving $1 + [(w/c^*)/(D_w \times V_c)]$. This gives a value of 2·20.

(7) The *porosity of the hydration product* is given by dividing the volume of gel pores per kg of reacted cement by that of the

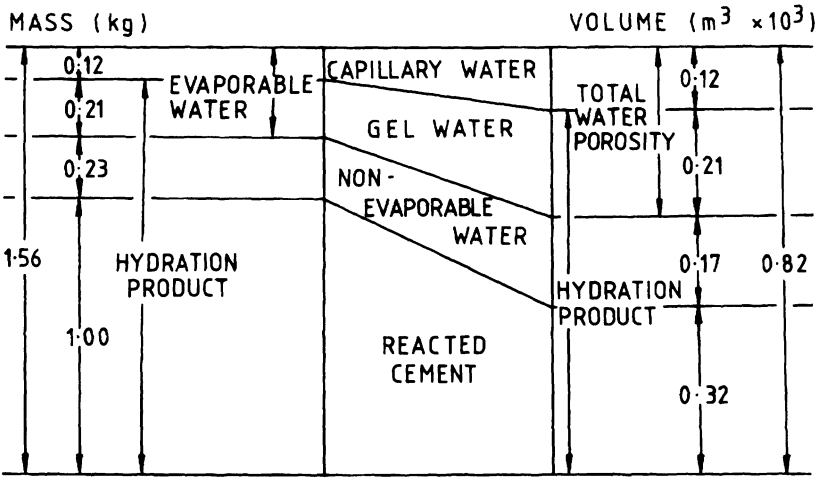


**Fig. 8.3** *Illustration of the Powers–Brownyard description of a fully hydrated and saturated Portland cement paste of initial water/cement ratio 0·5. All quantities refer to 1 kg of cement.*

hydration product. This gives $V_g \times m_g/[V_c + (w/c^*)/D_w]$, or 0·30. The value of 0·28 given by Powers and Brownyard was obtained assuming a different value for $V_g$. It should be noted that this quantity is the volume of gel pores relative to that of all the hydration products, including the CH.

Figure 8.3 shows the mass and volume relationships for a fully hydrated, saturated paste of w/c ratio 0·5, calculated using the above expressions and values. Following Powers and Brownyard, the hydrated cement is treated from a purely volumetric standpoint as a composite of reacted cement, non-evaporable water and gel water. The specific volume of the non-evaporable water was assumed to be $0{\cdot}73 \times 10^{-3} m^3 kg^{-1}$, and that of the capillary and gel water to be $1{\cdot}00 \times 10^{-3} m^3 kg^{-1}$. The results are approximate, for several reasons; for example, the pore solution is in reality not pure water, but an alkali hydroxide solution with a specific volume (for 0·3 M KOH) of about $0{\cdot}986 \times 10^{-3} m^3 kg^{-1}$.

### 8.2.4 *Later models of cement gel structure*

Brunauer and co-workers (B52,B122) considered that the gel particles of the Powers–Brownyard model consisted of either two or three layers of C–S–H, which could roll into fibres. D-drying caused irreversible loss of interlayer water, and the specific surface area could be calculated from water vapour sorption isotherms, which gave values in the region of $200 m^2 g^{-1}$ for cement paste. Sorption isotherms using $N_2$ give lower values of the specific surface area; this was attributed to failure of this sorbate to enter all the pore spaces.

Feldman and Sereda (F35,F36) regarded the gel as a three-dimensional assemblage of C–S–H layers, which tended to form subparallel groups a few layers thick and which enclosed pores of dimensions ranging from interlayer spaces upwards (Fig 8.4). They considered that much of the gel water of the Powers–Brownyard model was interlayer water. Unlike Brunauer, they considered that the loss of interlayer water on D-drying was reversible; consequently, sorption isotherms using $N_2$, not water, gave a true measure of the specific surface area. In a modification of this model, Daimon *et al.* (D45) considered that the gel consisted of particles having an internal structure similar to that shown in Fig. 8.4, together with pores having an equivalent radius of 1·6–100 nm. The smaller pores within the gel particles were 0·6–1·6 nm in equivalent radius, and pores of both types tended to have narrow entrances.

In Wittmann's (W25,W26) 'Munich model', hcp is described as a xerogel (a gel from which the dispersion medium is absent), together with the crystalline constituents. The xerogel is considered to consist of separate particles, for which no particular internal structure is assumed. Emphasis is placed on the role of water molecules adsorbed on, or lying between, these particles. Below 50% RH the particles were considered to be in contact, but at higher humidities, intervening water molecules were considered to exert a disjoining pressure, which to some extent kept them apart. The model was used primarily in the development of a theory of dimensional changes.

The Powers–Brownyard model explains why complete hydration does not occur if w/c is below a certain value, and provides a partial explanation of the dependence of some important physical properties, especially

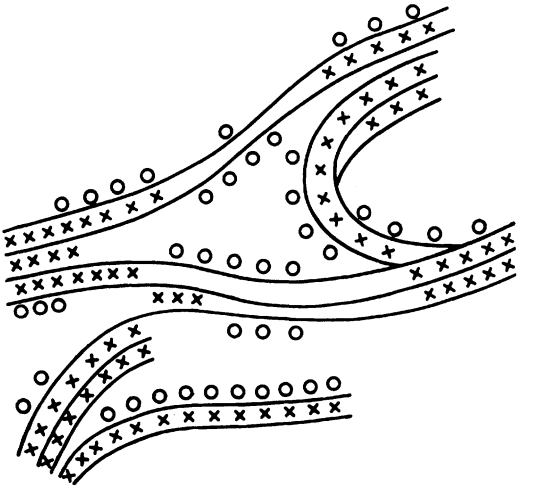

**Fig. 8.4** *Feldman–Sereda model of the structure of the C–S–H gel of Portland cement paste, showing C–S–H layers (lines), interlayer water molecules (crosses) and adsorbed water molecules (circles). After R41.*

compressive strength, on w/c and degree of hydration. No other satisfactory explanation of the minimum w/c needed for complete hydration appears to have been given, and the most important feature of the model is probably the conclusion that a given volume of cement can react only if an additional volume of free space approximately 1·2 times as great is available. The direct evidence that the relevant characteristics of the hydration product are independent of w/c and degree of hydration was, however, based largely on data from water vapour sorption isotherms for severely dried pastes, the interpretation of which has been strongly criticised (F17). Further tests of the correctness of the hypothesis are needed.

The Feldman–Sereda model was based on studies of sorption properties, porosities and relations between water content and physical properties. Alone among the proposed models, it is clearly compatible with the microstructural evidence and with the probable relationships between C–S–H gel and crystalline compounds. It is incompatible with that of Brunauer, but not with the essential features of that of Powers and Brownyard in its original form if the nature of the gel porosity is reinterpreted. Calculations of bound water (Section 7.4.4) indicate that about a third of the gel porosity of the Powers–Brownyard model is interlayer space, the remainder being micro or fine meso porosity* of the kind shown in Fig. 8.4. However, as that figure illustrates, the boundary between interlayer space and micropores is ill defined.

The models differ in whether, to what extent, or on what scale the gel is regarded as being composed of separate particles. The microstructural evidence suggests that the situation differs with the region considered, the outer product being more nearly particulate in nature than the inner product. Powers (P36) discussed his model in relation to the meagre evidence on microstructure then available. He recognized that the inner and outer products might differ in microstructure and that the porosities defined in the model could be means, but considered that the hydration product would tend towards a uniform porosity. Subsequent progress in the study of microstructure by electron microscopy and of pore structure by other methods, and in mathematical modelling of microstructure, has begun to provide answers to these and similar questions.

## 8.3 Mathematical modelling of microstructure and properties

### *8.3.1 Introduction*

Mathematical modelling has the objective of quantifying knowledge of the hydration process and microstructure of the resulting material in a manner that permits the prediction of experimentally accessible properties from similarly accessible inputs, thus allowing the effects of changes in inputs or assumptions contained in the model to be examined. Necessary inputs comprise such data as the composition and distributions of size and shape of the cement grains, w/c ratio and curing conditions, and

* The International Union of Pure and Applied Chemistry has adopted the following definitions of pores by width: micropores, <2 nm; mesopores, 2–50 nm; macropores, >50 nm.

typical outputs include mass or volume fractions of phases in a paste or concrete, content of non-evaporable water, cumulative heat evolution or physical properties such as strength, porosity or permeability defined in various ways. One can distinguish between fundamental models, which are based on simulation of the developing microstructure at the level of individual particles or regions of anhydrous phases, hydration products and porosity, and empirical or non-fundamental models, in which empirical equations play an essential part. Both types have merits and limitations.

### 8.3.2 Calculation of porosities and of volume fractions of solid phases

The calculation of porosities and volumes of phases is an essential preliminary stage in the development of most types of model. In the Powers–Brownyard model, the volume of capillary pores per unit mass of cement is obtained by subtracting the volumes of hydration product and of unhydrated cement from the total volume; using the symbols defined in Section 8.2.1, this gives $[(w/c) - \alpha(w/c^*)]/D_w$. The volume of gel pores per unit mass of cement is equal to $m_g \times V_g \times \alpha$. Expressed as fractions of the total volume, the capillary porosity is $[w/c - \alpha(w/c^*)]/[(D_w \times V_c) + w/c]$ and the gel porosity is $m_g V_g \times \alpha/[V_c + (w/c)/D_w]$. In all the above expressions, the maximum possible degree of hydration $\alpha_{max}$, equal to $(w/c)/(w/c^*)$, must be substituted for $\alpha$ if $w/c \leq w/c^*$.

Powers and Brownyard defined the total porosity as the sum of the capillary and gel porosities. This definition is adhered to here, but note that some later workers have used the term 'total porosity' in other senses. As hydration proceeds, the capillary and total porosities decrease and the gel porosity increases. Table 8.1 gives some values of the three types of porosity obtained from the above formulae, using the data given in Section 8.2.2 as typical.

In Section 7.4.4, a method is described for calculating the mass fractions of each phase in a cement paste. Given the w/c ratio and the density of the cement ($\sim 3150\,kg\,m^{-3}$), the total volume of paste may be

**Table 8.1** *Calculated porosities, based on the Powers–Brownyard model*

| w/c ratio | Fraction of cement hydrated $\alpha$ | Capillary porosity | Gel porosity | Total porosity |
|---|---|---|---|---|
| 0·3 | 0·00 | 0·49 | 0·00 | 0·49 |
| 0·3 | 0·79 | 0·00 | 0·27 | 0·27 |
| 0·4 | 0·00 | 0·56 | 0·00 | 0·56 |
| 0·4 | 1·00 | 0·03 | 0·29 | 0·32 |
| 0·5 | 0·00 | 0·61 | 0·00 | 0·61 |
| 0·5 | 1·00 | 0·15 | 0·26 | 0·41 |
| 0·6 | 0·00 | 0·65 | 0·00 | 0·65 |
| 0·6 | 1·00 | 0·24 | 0·23 | 0·47 |

**Table 8.2** *Calculated volume percentages and porosities, based on phase composition and densities*

| | Alite | Belite | Aluminate | Ferrite | Insol. res. | C–S–H | CH | AFm | AFt | Hydro-garnet | Hydro-talcite | Pores |
|---|---|---|---|---|---|---|---|---|---|---|---|---|
| Saturated | 1·0 | 0·6 | 0·0 | 1·0 | 0·1 | 48·7 | 13·9 | 11·1 | 3·6 | 2·2 | 1·8 | 16·0 |
| 11% RH | 1·0 | 0·6 | 0·0 | 1·0 | 0·1 | 36·2 | 13·9 | 11·1 | 3·6 | 2·2 | 1·8 | 28·5 |
| D-dry | 1·0 | 0·6 | 0·0 | 1·0 | 0·1 | 27·6 | 13·9 | 8·3 | 2·4 | 2·2 | 1·4 | 41·5 |

Calculated for a 14-month old paste with w/c = 0·5, from the mass percentages in Table 7.3 and water contents of phases in Table 7.4. Assumed densities ($kg\,m^{-3}$): alite, 3150; belite, 3300; aluminate, 3060, ferrite, 3570; insoluble residue, 2650; C–S–H, 1900, 2180, 2700; CH, 2240; AFm, 2010, 2010, 2400; AFt, 1775, 1775, 2380; hydrogarnet-type phase, 3100; hydrotalcite-type phase, 2000, 2000, 2300. Where three values are given, the first is for the saturated state, the second for material equilibrated at 11% RH, and the third for D-dried material.

calculated, and using the mass fractions and densities of the phases the volume of each phase may be obtained. The porosity is then obtained by difference. This calculation may be performed for any desired drying condition, provided the densities and water contents proper to that condition are used. Table 8.2 gives the results of such calculations for the paste to which the data in Table 7.3 relate. The porosities calculated for the saturated and D-dry conditions are similar to the capillary and total porosities for mature pastes obtained by the Powers–Brownyard method and given in Table 8.1.

Figure 8.5 includes porosities derived from calculated phase compositions for 18-month-old pastes of a typical Portland cement at varying w/c ratios and corresponding to (A) the D-dried state, (B) a state that includes all bound water, including that present in interlayer spaces, but

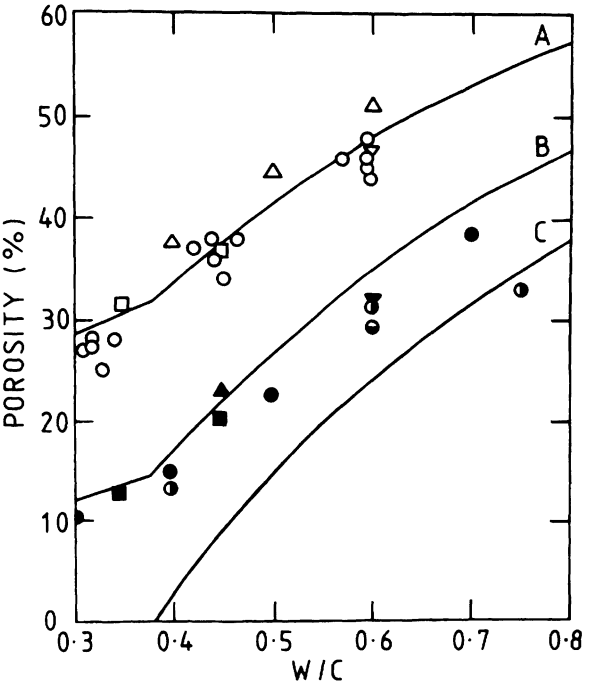


**Fig. 8.5** *Relations between porosities (volume percentages) and water/cement ratio for mature Portland cement pastes. The experimental data are for pastes at least 8 months old, and the calculated curves refer to a typical cement aged 18 months. Open symbols: total porosities. Solid or half-solid symbols: mercury porosities. Curve A: total porosity. Curve B: free water porosity. Curve C: capillary porosity. References to data:* ○ *(P20);* □ *(S90);* △ *(F37);* ▽ *(M80);* ■ *(S91);* ▲ *(F38);* ● *(O21);* ▼ (M80); ◒ (D46); ◑ *(H48). In the last two cases, porosities by volume were estimated from data referred in the original sources to masses of dried paste, assuming the latter to have contained 0·23 kg of water per kg of cement having a specific volume of* $3{\cdot}17 \times 10^{-4}\ m^3\ kg^{-1}$.

no water in larger pores and (C) capillary porosities, as defined by Powers and Brownyard. Conditions (B) and (C) are possibly realized approximately by taking material not previously exposed to an atmosphere below saturation and equilibrating it at 11% RH and about 90% RH, respectively (F18,Y5). The porosities defined by condition (B) will be called free water porosities.

Parrott and Killoh (P35) and Parrott (P37–P39) used a similar procedure and extended it to produce a comprehensive model in which empirical equations were employed. In essence, it contained three steps, as follows.

(1) The degree of hydration of each clinker phase was calculated at 56 ages, using rate equations that took into account the effects of temperature, RH and w/c ratio (P35). In so far as the clinker phases were treated separately, the simultaneous existence of more than one rate-determining step was assumed. Allowance was made for the effect of particle size distribution.

(2) The phase composition of the paste by mass and by volume, and the non-evaporable water content, were calculated. Using the w/c ratio and densities of phases, porosities were then calculated. Refinements allowed some deviation from the Powers–Brownyard postulate of a fixed volume ratio of gel porosity to C–S–H, and volumes of pores having diameters above and below 4 nm were calculated separately. The heat evolved was assumed to be the sum of the amounts given by each clinker phase, which in turn were assumed to be proportional to the fractions of those phase that had reacted. Extensions of the treatment permitted the effects of admixture of the cement with flyash to be considered.

(3) The compressive strength, permeability to water and methanol exchange rate were calculated, using empirical equations relating them to the porosity.

Typical results for the volume fractions of pores larger than 4 nm in mature pastes were approximately 0·26, 0·16 and 0·07 for w/c ratios of 0·65, 0·50 and 0·35 respectively (P37). For the two higher w/c ratios these results are near the capillary porosities of Powers and Brownyard, but for w/c 0·35 the latter value is zero.

Jennings and Tennis (J26) used a procedure broadly similar to those described above to develop a model with the prime objectives of predicting porosities and specific surface areas determinable by sorption procedures using $N_2$. The C–S–H was assumed to be of two types, of which only one was accessible to $N_2$. Both were assumed accessible to $H_2O$. The mass fraction of the C–S–H accessible to $N_2$, and the volumes of the two types or regions to which the C–S–H was assigned, were obtained using empirical equations based on limited sets of experimental data; a constant specific surface area ($392\,m^2\,g^{-1}$) was assumed for the C–S–H. The results were compared with a wider range of data for porosities and specific surface areas determined using $N_2$.

### 8.3.3 Microstructural models

Early versions of a fundamental microstructural model of $C_3S$ hydration (J31,S92) led to a more detailed one due to Garboczi and Bentz (B123,G73). In this model, a region of paste was represented by a three-dimensional array of pixels. Initially, a given pixel could be assigned to either $C_3S$ or water, the particles of $C_3S$ having realistic distributions of size and shape. As hydration proceeded, pixels were removed from the $C_3S$ surfaces, and pixels of C–S–H and CH were produced at their expense and that of the pore solution, in proportions that respected the known reaction stoichiometry and volume relations. The pixels of the product were allowed to migrate in a random way, subject to rules designed to produce a proper representation of the developing microstructure. Tests of the model included comparisons with BSE images and calculations of parameters related to the pore structure. The degree of connectivity of each phase could be calculated; irrespective of w/c ratio, that of the capillary porosity fell rapidly as the latter decreased from 40% to 20%. This conclusion agrees well with the experimental observations described in Section 8.7. Although the model related to pure $C_3S$, it was shown that it should apply without serious error to cement.

A phase is said to percolate if a continuous path can be traced through it from one side of the system to the other, and the volume fraction at or above which such paths exist is called the percolation threshold. If the volume fraction is less than this, the phase is entirely in the form of isolated regions. Brown *et al.* (B124) summarized percolation theory more fully. The $C_3S$ model (B123,G73) predicted the existence of percolation thresholds for capillary pores, C–S–H and CH at about 18%, 17–18% and 12–15% respectively. The similarity between these values appears not to be accidental, as values in the region of 16% are found for a wide range of comparable systems. A single curve was shown to hold for the relation between total capillary porosity and the fractional connectivity of the capillary pores, irrespective of w/c ratio. The fractional connectivity approximated to 100% at a capillary porosity of 60%.

The degrees of hydration at which the percolation thresholds were reached were also calculated. For a $C_3S$ paste with $w/c = 0{\cdot}5$, the percolation of the capillary pores ceased at about 86% hydration, and those of C–S–H and CH began at approximately 25% and 55%, respectively. The C–S–H was completely connected by 50% hydration, but the quantity of CH formed was shown to be insufficient to give a fractional connectivity above 0·9 even at complete hydration.

Two-dimensional models were also computed, and for given conditions gave apparent degrees of connectivity much lower than those existing in three dimensions. Thus, the CH was generally discontinuous in two-dimensional sections. This agrees with SEM observations on polished surfaces.

Properties calculated from the model included ionic diffusivities and water permeabilities (Section 8.7). The model was extended to deal with mortars and concretes, including the microstructure and properties of the interfacial zone (Section 12.1.4) and pastes, mortars and concretes containing silica fume (Section 9.7.2).

## 8.4 Experimental methods for studying pore structure

### 8.4.1 General points

The problems of defining and determining densities of finely porous solids, indicated in Section 5.2.3, apply to hcp. A determination of the density of such a material is also one of porosity, since both properties are related to the solid volume; the porosity per unit volume of material is equal to $1-[m_s/(D_s \times V)]$, where $m_s$ and $D_s$ are, respectively, the mass and density of the solid and $V$ is the total volume. The density and porosity determined by any method entailing contact with a fluid can vary with the extent to which the solid has been dried, how it has been dried and the fluid employed. Fluids may differ in their abilities to penetrate the pore system, and the pore structure may be altered both during drying and by the action of the fluid subsequently introduced.

These comments apply also to studies of pore size distribution or specific surface area, which have been widely studied using sorption isotherms or, in the former case, mercury intrusion porosimetry (MIP). Gregg and Sing (G74) have described these methods. In both cases, the material must first be dried to water contents lower than those likely to be encountered in the normal environment of the material, and the effects can be serious and difficult to allow for. The amount of water considered to form part of the solid obviously affects the definition of porosity, but the extent and manner of drying also affect the pore size distribution.

The most widely used drying procedures have been desorption at ordinary temperatures, including D-drying, or at elevated temperatures, and solvent replacement. Freeze drying has also been used (K44). In solvent replacement, the specimen, normally in a saturated state, is immersed in an organic liquid such as methanol. The course of replacement can be followed from the mass change; it has been claimed that all the pore water can be replaced (D47,P40). The organic liquid is then removed. Because of the lower surface tension, one might expect that less damage would occur as the liquid evaporates, and several investigators have concluded that this is the case (D47,H48,P40). In contrast, Beaudoin (B47,B125) concluded that straight-chain aliphatic alcohols seriously affect the pore structure, partly through reaction with CH. Methanol and other organic liquids are retained strongly by cement or $C_3S$ pastes, with resulting effects on the TG and DTA curves (Section 5.1.2). It does not necessarily follow that the pore structure is affected; this applies especially to the coarser part of the distribution, which is probably the more important for many of the physical properties.

Porosities have sometimes been reported as percentages by volume of the paste and sometimes as volumes per unit mass of dried paste. The first is the more meaningful, especially as in the latter case the water content of the material has not always been given. A similar comment applies to specific surface areas (L44).

### 8.4.2 Determination of porosities by pyknometry

Total porosities are obtained experimentally from the loss in mass when a saturated paste is D-dried or subjected to some procedure regarded as

equivalent, such as heating to constant mass at 105°C. Reabsorption of water by materials thus dried gives identical results (D47). The procedures should be carried out under $CO_2$-free conditions. A value for the specific volume of the evaporable water must be assumed; this has usually been $1{\cdot}00 \times 10^{-3}\ m^3\ kg^{-1}$. Figure 8.5 includes typical values thus obtained.

Powers and Brownyard (P20) found that porosities of D-dried pastes obtained using helium as the pyknometric fluid were lower than those obtained using water. Feldman (F37) confirmed this and found that a lower value was also obtained using methanol; if a D-dried sample was exposed to helium, the latter flowed in quickly at first, and then more slowly. The porosities calculated from the initial, rapidly accepted volumes of helium agreed with those obtained with methanol. If the material was dried only by equilibration at 11% RH, the porosities obtained with helium, methanol or saturated aqueous CH were all similar to those obtained for D-dried pastes using methanol. For D-dried pastes, the porosities obtained using helium were 23·3%, 34·5%, 42·1% and 53·4% for w/c ratios of 0·4, 0·5, 0·6 and 0·8 respectively. The corresponding values obtained with water were 37·8%, 44·8%, 51·0% and 58·7%; these are included in Fig. 8.5. Day and Marsh (D47) confirmed that porosities obtained by admitting methanol or propan-2-ol to an oven-dried paste were substantially lower than total porosities; however, if the undried paste was treated with the organic liquid, the volume exchanged was closely similar to the total porosity.

Feldman (F37) explained his results in terms of the Feldman–Sereda model as follows. If the paste is D-dried, water is lost from the interlayer spaces. If the sample is immersed in water, this water is reabsorbed, and the total porosity therefore includes the volume of the interlayer space. Methanol does not penetrate into this space, and helium does so only slowly, so that lower porosities are obtained. If the sample is equilibrated at 11% RH, the interlayer spaces are largely filled, and the lower value is obtained irrespective of the fluid used. The helium porosities reported by Feldman were near the calculated free water porosities.

### *8.4.3 Sorption isotherms; specific surface areas*

Sorption isotherms, using water, $N_2$ or other sorbates, have been widely used to study the pore structure of hcp. The results obtained by different investigators show considerable variations, which arise in part from differences in the conditions of preliminary drying.

Desorption of water from a saturated paste at ordinary temperature is a slow process. Figure 8.6 shows results for a fully hydrated $C_3S$ paste of w/c 0·5, in which each point represents the results of a separate experiment on a slab 1 mm thick (G75). Loss of water is especially slow at 30–80% RH. Parrott and co-workers (P40,P41) similarly found that in the initial desorption, equilibrium was reached within a few days at RH < 30%, but that at RH values of 40–80% many weeks were needed; there were indications that larger pores emptied through smaller ones. Drying at these humidities led to a coarsening of the pore structure,

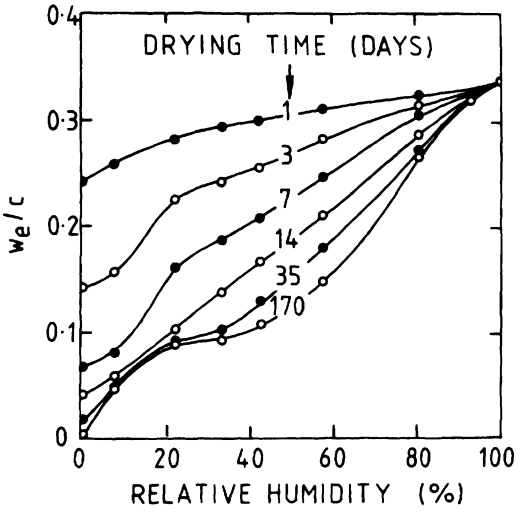


**Fig. 8.6** *Desorption curves for an initially saturated $C_3S$ paste of w/c ratio 0·5, hydrated for 5·8 years at 25°C in the form of slab samples 1 mm thick. Each point represents the result of a separate experiment in which the sample was exposed to an atmosphere of given relative humidity for the drying time shown. After G75.*

which was indicated by a marked reduction in the specific surface area accessible to $N_2$, from over $100\,m^2\,g^{-1}$ at 90% RH to around $30\,m^2\,g^{-1}$ at 10% RH, and was also associated with irreversible shrinkage (P42). On resaturation, the higher surface area was regained, but the pore size distribution did not completely revert to that originally found.

Water sorption isotherms for hcp show marked hysteresis. Powers and Brownyard (P20) found that, while it was difficult to obtain reproducible desorption curves, the low-pressure part of the water vapour resorption curve varied little with w/c ratio, between different Portland cements, or, if allowance was made for the contents of unreacted cement, with the degree of hydration. This was their main direct evidence for the conclusion (Section 8.2.1) that the properties of the hydration product considered in their model were essentially independent of these variables. However, the water sorption isotherms obtained by different investigators have varied considerably (e.g. P20,S93), and it is not clear to what extent the above conclusion would stand had different desorption conditions been used.

In principle, isotherms at low partial pressures of the sorbate may be used to determine specific surface areas by the Brunauer–Emmet–Teller (BET) method (G74). In this method, it is assumed that molecules of the sorbate are adsorbed on surfaces that can include the walls of pores, provided that the distance between molecules on opposing walls is large compared with molecular dimensions. From a plot derived from the isotherm, and given the effective cross-sectional area of the sorbate

molecule, the specific surface area of the sorbent and the net heat of adsorption are obtained. Using water as sorbate, specific surface areas of about 200 $m^2$ per g of D-dried paste have typically been obtained for mature cement pastes of normal w/c ratios (P20,H49); however, much of the water has been shown to enter the vacated interlayer spaces, thus rendering the BET equation at best only partially applicable (F35).

Using $N_2$ or other non-polar sorbates, widely varying and usually much lower values have been obtained. Lawrence (L44), reviewing earlier studies, noted that for well-cured pastes the values ranged from under 10 to nearly 150 $m^2 g^{-1}$, and even higher values, up to 249 $m^2 g^{-1}$, have been reported (L45). In contrast to values for fully hydrated pastes obtained using water, the $N_2$ areas tend strongly to increase with w/c ratio, but are also much affected by the conditions under which the sample has been dried. It would appear that the value obtained using water, whatever its precise significance, is dominated by the structure at or near the individual layer level and is thus relatively insensitive to coarser features of the structure. The much lower values obtained using $N_2$ may arise through inability of the latter to penetrate interlayer spaces; this would imply that they can give information about structural features at a somewhat coarser level. Alternatively, based on the model of Jennings and Tennis (J26), $N_2$ penetrates only one of two types of C–S–H, which may correspond to particular regions.

### 8.4.4 Pore size distributions

The hysteresis shown by sorption isotherms of hcp, whether using water, $N_2$, or other sorbates, indicates the presence of mesopores (G74). At partial pressures above those to which the BET theory applies, capillary condensation occurs. If a liquid forms a meniscus in a cylindrical pore, its vapour pressure is lowered to an extent that increases with decreasing pore radius. Using an equation due to Kelvin, or other procedures ultimately derived from it, the isotherm may be used to estimate pore size distributions in the approximate range of 1–30 nm and may give indications regarding the shapes of the pores. It may be necessary to allow for the fact that the meniscus forms in a pore narrowed by an adsorbed layer of sorbate. From an early study of this type on D-dried cement pastes, Mikhail *et al.* (M81) showed that the size distribution of the pores available to $N_2$ was probably unimodal and that with increase in w/c from 0·35 to 0·7 it shifted to higher values in both the low and the high parts of the distribution. It is difficult to reconcile this conclusion with the unvarying pore size distribution within the gel implied by the model of Powers and Brownyard.

Lawrence and co-workers (L44,L46,L47) concluded from sorption data using nitrogen and butane that the microstructure partly collapses during normal drying. This agrees with Parrott and co-workers' (P40,P41) conclusion, noted above. Pastes that had been rapidly dried were likely to be closest in structure to undried pastes; the sorption results indicated that their structures were dominated by platey particles or lamellae that formed slit-shaped mesopores and micropores. Slow drying produced

small pores more nearly cylindrical or spherical. Methanol treatment at least partially prevented the microstructural collapse, but did not always produce an increase in the recorded surface area, though it always caused a change in the shape of the isotherm; this was possibly due to chemisorption of the methanol.

Using $N_2$ sorption on samples solvent-dried by methanol exchange, Hansen and Almudaiheem (H48) found the volumes of pores with diameters smaller than 4 nm and accessible to $N_2$ to be 0·052 ml, 0·035 ml and 0·038 ml per g of dry paste for mature pastes of w/c ratio 0·4, 0·6 and 0·75 respectively. These results correspond to volume porosities of about 9%, 5% and 4% respectively.

Patel *et al.* (P33) determined the volumes of pores smaller than 4 nm or 37 nm in methanol-exchanged samples, using a methanol sorption method in which porous glass granules of known and approximately monodisperse pore size were used as a reference standard. Using also the total porosity, the volumes in the ranges larger than 4 nm and 37 nm were also obtained. For a cement paste of w/c 0·59 cured for 90 days at 100% RH, this gave values of approximately 47% for the total porosity, 17% for pores above 4 nm, and 12% for pores above 37 nm. For a paste of w/c ratio 0·71 cured in the same way, the corresponding values were approximately 57%, 36% and 18%. These results indicate volumes of pores below 4 nm considerably greater than those reported by Hansen and Almudaiheem.

Parrott *et al.* (P19) used butane sorption to determine the volume of pores smaller than 50 nm. For a 28-day-old alite paste of w/s 0·59, a volume porosity of 27% was obtained.

### *8.4.5 Mercury intrusion porosimetry (MIP)*

This method is based on the fact that a liquid that does not wet a porous solid will enter its pores only under pressure. If the pores are assumed to be cylindrical, the pressure $p$ needed to force the liquid into them is given by the Washburn equation

$$p = -4\gamma \cos\theta / d \tag{8.5}$$

where $\gamma$ is the surface energy of the liquid, $\theta$ is the contact angle, and $d$ is the pore diameter. For Hg, $\gamma = 0{\cdot}483\ \mathrm{N\,m^{-1}}$. For $\theta$, values between 117° and 140° have been variously assumed. In a critical review, Good (G76) concluded that, while a case for 180° could be made, it was probably best to assume one of 130° in the absence of direct experimental data. The maximum pressure employed is typically around 400 MPa, which allows pores of nominal diameter down to about 3·5 nm to be intruded.

Typical results (Fig. 8.7) show that the distribution moves to smaller values as hydration proceeds. The observed porosity is mainly in the 3–1000 nm range for young pastes, and in the 3–100 nm range for mature pastes. For mature pastes of low w/c ratio, which according to the Powers–Brownyard theory consist entirely of hydration product, nearly all the porosity is below 50 nm (S90). The porosities obtained using mercury at the maximum pressures employed will be referred to as mercury porosities.

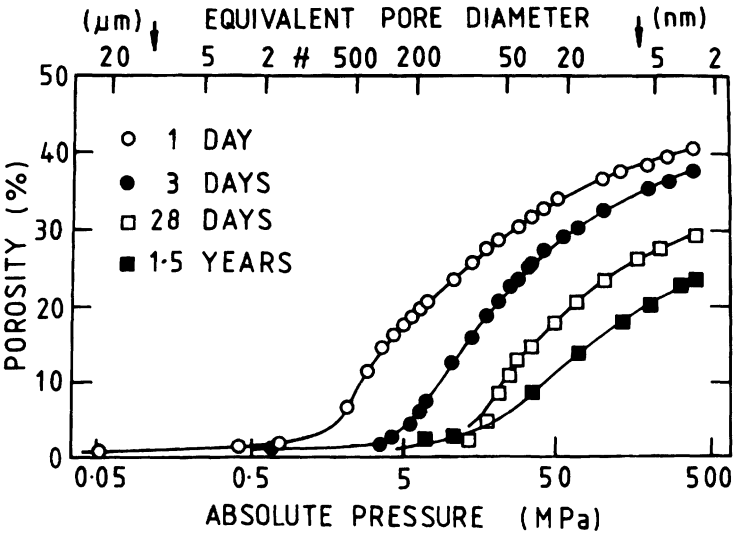


**Fig. 8.7** *Mercury porosimetry curves for a Portland cement paste (w/c ratio 0·47) at various ages. After F38.*

Typical values for mature pastes (Fig. 8.5) are somewhat lower than the calculated free water porosities.

MIP has been very widely used in the study of cement pastes, and the results obtained by it have been reasonably self-consistent, but it is doubtful whether the pore-size distributions thus obtained are even approximately correct. They may still have some comparative significance.

(1) The method does not measure the distribution of pore sizes, but that of pore-entry sizes (D48). If large pores can be entered only through small pores, they will be registered as small pores. Previous suspicions that this effect is of major significance with cement pastes were supported by the results of computer modelling of the entry of mercury into cement pastes (G77).

(2) The delicate pore structure of the paste is altered by the high stress needed to intrude the mercury. This effect was first shown in studies on composite cements (Chapter 9), in which mercury was intruded, removed and reintruded into mature pastes. Contrary to earlier conclusions, it also occurs with pure Portland cement pastes (F39).

(3) As with other methods in which the paste has first to be intensively dried, the pore structure is also altered by the removal of the water. Isopropanol replacement followed by immediate evacuation and heating at 100°C for 2 h has been reported to cause the least damage (F39).

(4) It is not clear whether the method registers the coarsest part of the porosity, intruded at low applied pressures.
(5) The assumption of cylindrical pores and of a particular contact angle may be incorrect.

The results obtained by MIP are grossly at variance with those obtained using SEM techniques, described in Section 8.4.6 (K45). The latter show that, even in mature pastes at all but low w/c ratios, there is much porosity coarser than 1 $\mu$m, whereas MIP shows virtually none. The coarse porosity detectable by SEM is partly present in hollow-shell grains. The failure of MIP to register the coarse porosity probably results from effects (1) and (4) listed above.

The volumes of pores wider than 4 nm found using methanol sorption (P33,P39) are much smaller than those indicated by MIP. On the other hand, Hansen (H50) found that, for solvent-exchanged pastes, the sum of the volumes of pores below and above 4 nm, obtained using $N_2$ sorption and MIP respectively, agreed with the total porosities.

### *8.4.6 Scanning electron microscopy*

Parrott *et al.* (P19) impregnated alite pastes with a resin, and prepared polished surfaces which were etched with acid to dissolve the cement paste before examination by SEM. Subsequently, backscattered electron imaging of unetched polished surfaces, with image analysis, has provided a more direct approach (S49,S94). Pores down to a size of some 500 nm can be identified, and the optimum magnification is probably about ×400; for a cement paste with w/c 0·5, aged 28 days, a volume porosity in the region of 13% was obtained (S94). Assuming that sufficient data are obtained to achieve an adequate level of statistical significance, area fractions of phases determined from two-dimensional sections are equal to volume fractions in three dimensions, but there are inherent major difficulties in obtaining three-dimensional information about such features as pore connectivity from two-dimensional sections (B123,S94). The porosities observable by SEM methods appear to be lower than the capillary porosities, but not grossly so; this suggests that much of the capillary porosity in the 28-day-old paste was coarser than 500 nm. The inner product appears to contain no coarse porosity observed in the SEM, if hollow-shell grains are excluded. Capillary porosity thus appears to reside exclusively in the outer product.

The porosities determined by image analysis showed high linear correlations with those obtained by methanol sorption, despite the fact that this provides data on much finer pores. Capillary porosities have also been determined using ultraviolet fluorescence microscopy with image analysis (J32).

### *8.4.7 AC impedance spectroscopy*

Studies on the electrical properties of cement pastes have the merit of being applicable to undried material. Tamás *et al.* (T49) summarized and extended earlier studies on cement pastes in which hydration processes were monitored from changes in AC conductivity at low frequencies. Subsequently, more extensive data have been obtained from studies in

which AC impedance and phase angle are determined over a wide range of frequencies (e.g. 10 mHz–15 MHz). This method was first applied to cement systems by McCarter and co-workers (M82,M83) and progress was reviewed in 1994 by Christensen *et al.* (C47). The results are commonly expressed in Nyquist plots of imaginary versus real components of impedance (Fig. 8.8). The real component increases with decrease in frequency. The low-frequency arc (L$R_B$) arises from electrode effects, and is relevant to corrosion of reinforcement. The high-frequency or bulk arc ($R_B$H) can provide information on the microstructure.

The pore solution in a cement paste has a relatively high conductivity, while the solid constituents have a low one. The paste can therefore be modelled by an appropriate assemblage of capacitors and resistors, which is used in interpreting the data. Xu *et al.* (X2) concluded that the diameter of the high-frequency arc depended mainly on the concentrations in the pore solution and the pore size distribution and total porosity. Christensen *et al.* (C47) considered that the most useful parameters were the resistance at the intersection of the two arcs ($R_B$ in Fig. 8.8) and the frequency at which the maximum in the bulk arc ($f_{MAX}$) was obtained. The depression of the centre of the bulk arc below the horizontal axis should also be capable of providing information, but its significance is not fully understood. $R_B$ represented the DC resistance of the material and, taken in conjunction with the conductivity of the pore solution and an appropriate geometrical factor, could be used to predict water permeability and ionic diffusivity. From $f_{MAX}$, an estimate of the dielectric constant can be obtained. Extremely high values observed just after set were

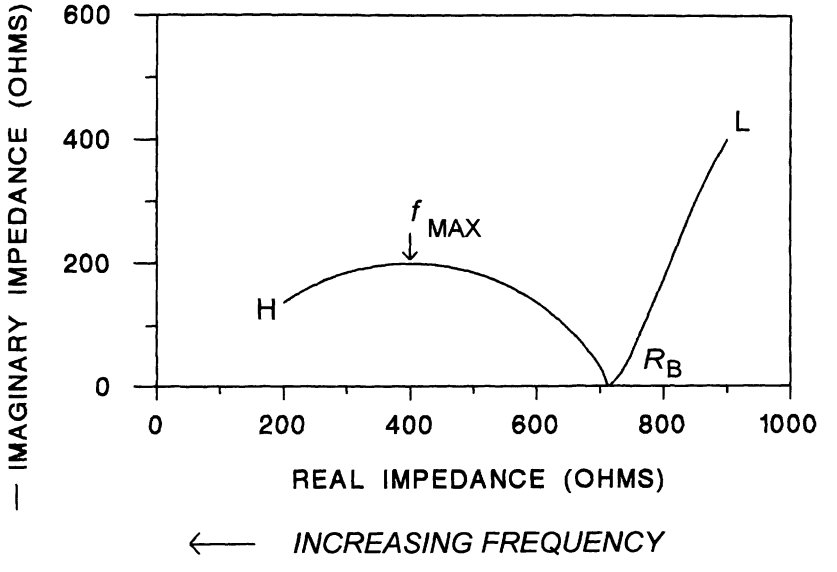


**Fig. 8.8** *General form of a typical AC impedance spectrum of a cement paste (Nyquist plot), based on data from several sources.*

attributed to an effect known as dielectric amplification arising from the association in the material of capillary pores with thin layers of relatively non-conducting solid. The pores were considered to provide many almost purely conductive channels which stretched across the entire length of the system, and which were blocked by very thin barriers provided by the hydrated material. Each such barrier contributed an abnormally high capacitance, and all were in parallel. In principle, information can be obtained on the distribution of pore sizes and the thickness of the product layers separating the pores.

### *8.4.8 Other methods*

The remaining methods to be described are also ones that can be applied to undried material. Small-angle X-ray scattering gives information on the areas of surfaces between regions of markedly different electron density. For saturated, mature cement pastes of w/c 0·4–0·6, Winslow and Diamond (W27,W28) obtained values of 700–800 $m^2$ per g ignited mass, decreasing to around 200 $m^2 g^{-1}$ on D-drying. The decrease with loss of water was reversible if the specimen was not heated. Correction for CH and unreacted clinker phases would increase the values for the saturated pastes to around 1000 $m^2 g^{-1}$. The authors were uncertain whether the method would be sensitive to an interlayer of water molecules, but the value obtained is about what would be expected for layers of C–S–H thus separated. The decrease on drying could be attributed to the coming together of the layers, and its reversibility agrees with the hypothesis that the loss of interlayer water on D-drying is reversible. The very high X-ray intensity obtainable from a synchrotron source has allowed the method to be extended to pastes at early ages (W29); the surface area scarcely changed until the the time of final set, and increased steadily thereafter. Information on fractal types and dimensions on scales of 3–150 nm was also obtained (W30).

Small-angle neutron scattering may be used in a somewhat similar way. It is especially sensitive to concentrations of H atoms. A study of the 3–25 nm range by this method showed a bimodal distribution of pores peaking at approximately 5 nm and 10 nm, but accounting for less than 2% of the total porosity (A21,P43). The pores were considered to be approximately spherical, and on heating the material at 105°, partial collapse of the pore structure was observed, with loss of the 10 nm peak.

Proton NMR by pulsed techniques to permit the study of relaxation effects provides information on the distribution of protons, and thus of water molecules, between different environments. An early study (S95) indicated that, at RH < 70%, the evaporable water in hcp was in an environment similar to that of the interlayer water in clay minerals or in certain crystalline hydrates. Subsequent work (B126,M84,M85,S96) has given indications of the distributions of both chemically bound and unbound water among a number of environments and has provided information on changes in pore structure and specific surface area. The method can be applied most effectively only to materials very low in iron or other paramagnetic atoms.

Low-temperature calorimetry (B127,S97) has been used to study coarse porosity. The method is based on the fact that water in pores freezes at a lower temperature than water in bulk. The ice forms through the advance of a front, analogous to the intrusion of mercury or the desorption of water. Hysteresis effects indicated the existence of necks in the pores, and the occurrence of up to three distinct peaks on curves of apparent heat capacity against temperature was interpreted as indicating maxima in the pore size distribution. Coarsening of the pore structure on drying was confirmed.

## 8.5 Strength

### *8.5.1 Empirical relations between compressive strength and porosity*

The physical properties of concrete are only partly determined by those of the cement paste that it contains. These properties will be considered here only for hcp and to the extent that chemical or microstructural studies have contributed to an understanding of them. Other aspects are treated elsewhere (e.g. M86).

Factors determining the compressive strength of a cement paste include: (i) the characteristics of the cement, such as clinker composition and microstructure, gypsum content and particle size distribution; (ii) the w/c ratio and the contents of air and of any admixtures present in the mix; (iii) the mixing conditions; (iv) the curing conditions, especially temperature and RH; (v) the age; (vi) the manner of testing, including the water content of the specimen. The effects of temperature and admixtures are considered mainly in Chapter 11, and some additional factors relevant to mortar or concrete are considered in Section 12.1. In various ways, the factors listed above determine the degrees of hydration of the clinker phases and the phase composition and microstructure of the hardened paste, which in turn determine its physical properties, including strength.

Many empirical relations between compressive strength and one or more of these variables have been proposed. Thus, Feret's law (1892) states that the strength is proportional to $[c/(c+w+a)]^2$, where $c$, $w$ and $a$ are the volumes of cement, water and air respectively, and various authors have reported equations based on regression analyses relating strength to cement composition and other variables (e.g. A22,A23). The generality of such equations appears to be limited, probably because of the difficulty of taking into account all the relevant parameters.

The porosity of the hardened paste, appropriately defined, is strongly correlated with strength. As seen in Section 8.3.2, it depends primarily on the degree of hydration and the w/c ratio. In this discussion, the following symbols are used:

$\sigma$ = compressive strength

$\sigma_0$ = hypothetical maximum compressive strength attainable

$p$ = porosity, which has usually been taken to mean total porosity

$p_o$ = hypothetical porosity at or above which the strength is zero

$A$, $B$, $C$, $D$ and $E$ are constants.

Powers (P36) found that cement pastes of various degrees of hydration and w/c ratio conformed to the relation

$$\sigma = \sigma_0 X^A \tag{8.6}$$

where $X$ is a quantity called the gel/space ratio, and equal to the volume of hydration product divided by that of hydration product plus capillary porosity, both quantities being defined as in Sections 8.2.1 and 8.3.2. The value of $A$ was about 3·0 if non-evaporable water was used as a measure of the degree of hydration, and typical values for $\sigma_0$ were 90–130 MPa. This equation breaks down for mature pastes of low w/c ratio, because it implies that the strength does not then depend on the w/c ratio. In reality, strength increases with decreasing w/c ratio, even though some of the cement does not hydrate.

Several empirical relationships between porosity and strength, originally found to hold for other materials, have been applied to cement pastes, viz.

$$\sigma = \sigma_0(1-p)^B \quad \text{(B128)} \tag{8.7}$$

$$\sigma = \sigma_0 \exp(-Cp) \quad \text{(R42)} \tag{8.8}$$

$$\sigma = D \ln(p_0/p) \quad \text{(S98)} \tag{8.9}$$

$$\sigma = \sigma_0(1-Ep) \quad \text{(H51)} \tag{8.10}$$

Equation 8.7 is similar to that of Powers, but unreacted cement is considered equivalent to hydration product. Some of these equations break down at zero or high porosities, but for a wide range of intermediate porosities, assuming suitable values of the constants, any of them can give a reasonable fit to a given set of data. Rössler and Odler (R40) concluded that equation 8.10 was the most satisfactory. A relation identical to that of this equation, using capillary porosity, is implicit in a figure presented earlier by Verbeck and Helmuth (V7).

### 8.5.2 *Relations between strength and microstructure or pore size distribution*

There are several indications that the compressive strength does not depend solely on porosity. In general, procedures that accelerate early reaction and thus increase early strength, such as increase in temperature or addition of certain admixtures, tend to decrease later strength. It is unlikely that they significantly alter the porosity of the mature paste, but they may affect the microstructure. If one extends consideration to a wider range of materials than normally cured Portland cement pastes, the relation between strength and porosity is markedly dependent on the broad characteristics of the microstructure. Jambor (J33) concluded that both the volume and the specific binding capacities of hydration products must be considered.

Feldman and Beaudoin (F40) showed that, while the strengths of Portland cement pastes could be fitted to a curve in accordance with equation 8.8, materials of a broadly similar type but composed largely of

denser, crystalline particles were, for a given porosity, stronger at low porosities and weaker at high porosities (Fig. 8.9, curves AB and CD). These materials comprised hot-pressed cement pastes (Section 11.9.1) and autoclaved cement pastes to which no silica had been added (Section 11.7). Feldman and Beaudoin considered that, while porosity was the major factor controlling strength, the morphology and density of the particles were also important. At high porosities, the better bonding properties of ill-crystallized material augmented the strength, but at low porosities the greater intrinsic strength of the dense, crystalline particles was more important. In agreement with Bozhenov *et al.* (B129), they concluded that the highest strengths for a given porosity could be obtained from an appropriate blend of the two types of particles. Such a blend could be realised in autoclaved cement–silica materials (curve EF).

The size and shape distribution of the solid particles in a cement paste is related, though in a complex way, to that of the pores, and other workers have attempted to relate strength to pore size distribution. From studies on autoclaved materials, Mindess (M87) concluded that, for a given porosity, the strength increased with the proportion of fine pores. Jambor (J33) similarly found relations between strength and average pore size. The weaker materials, with relatively coarse pores, were ones containing dense, crystalline phases, and broadly resembled those represented by the high-porosity end of curve CD in Fig. 8.9. Odler and Rössler (O22) concluded from a study of cement pastes cured for various combinations of w/c, temperature and time that while the main factor influencing strength was

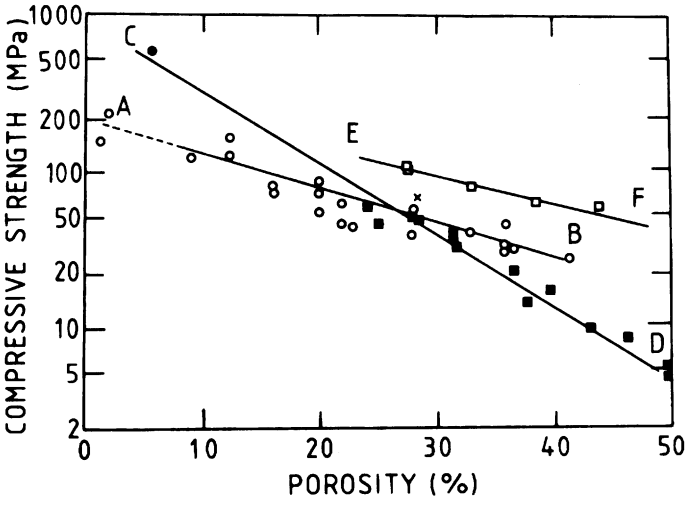


**Fig. 8.9** *Relations between compressive strength (log scale) and porosity; data from various sources for Portland cement pastes cured at ordinary temperatures (open circles), hot-pressed Portland cement paste (solid circle), autoclaved pastes of Portland cement, sometimes with added sulfur (solid squares) and autoclaved pastes of Portland cement with 50% (open squares) or 30% (cross) of added flyash. After F40.*

porosity, pores with a radius below 10 nm were of negligible importance. This conclusion, which was based on results of MIP, was supported by the observation that the specific surface area, which depends on the content of very small pores, had very little effect on the strength. For a given porosity, a given volume of hydration products contributed more to the strength than the same volume of unreacted cement, but this effect was distinctly less than that of porosity.

These results suggest that, in attempts to relate strength to porosity, the total porosity should not be used, the capillary or free water porosity or the volume of pores above a certain size being more appropriate. Parrott and Killoh (P35), in relation to their modelling of properties, similarly considered the volume, size and continuity of the larger pores to be the relevant quantities.

### *8.5.3 Mechanisms of failure*

Strength cannot be explained by relating it empirically to porosity or pore size distribution; it is necessary to know what holds the material together and what happens when it fails. Cohesion has often been attributed to the interlocking of fibrous or acicular particles. This could be important in the more porous parts of the material, but in the material as a whole, attractive forces between those parts of adjacent layers of C–S–H or other phases that are in contact are probably more important, both within particles and, in so far as the material is particulate, between them. The attractive forces could be direct, or indirect, through interposed water molecules. Even for D-dried material, analogies with crystalline tobermorite and jennite indicate that much interlayer water is still present (Section 5.4).

Various authors have discussed the application of fracture mechanics to cement paste (A24,B130,E4,J33,P44). As in other brittle materials, failure occurs through the initiation and spread of cracks, which originate in places where the local stress is high. Hardened cement pastes are about ten times as strong in uniaxial compression as in tension. It is probable that the ultimate mechanisms of failure are essentially similar, but that the cracks propagate more readily under tension. The relations between microstructure and strength must thus be sought in the features that give rise to high local stresses and in those that favour or, conversely, that arrest the spread of cracks. This is consistent with the conclusion that porosity is a major factor but not the only one; Beaudoin and Feldman (B130) discussed some others, in addition to those noted above. The strength, however measured, is less for a saturated paste than for a dry one. In principle, this is readily explained, as the entry of water molecules between particles could weaken the attractive forces between them and thereby favour the initiation or spread of cracks. A disjoining pressure is created (Section 8.2.4).

## 8.6 Deformation

### *8.6.1 Modulus of elasticity*

Curves of uniaxial compressive stress against strain for hcp are non-linear and vary somewhat with the strain rate. Caution is therefore needed in

comparing values of Young's modulus obtained in different investigations, results obtained at very low stresses by the dynamic method in which a resonance frequency of vibration is determined being higher than ones given by static or slow loading methods and averaged over greater ranges of stress. Using the dynamic method, Helmuth and Turk (H52) obtained values of 20 000–30 000 MPa for saturated, mature pastes. Trends with w/c and degree of hydration, and relations with porosity, were similar to those for compressive strength. For saturated pastes, Helmuth and Turk found

$$E = E_0(1 - p_c)^3 \tag{8.11}$$

where $E$ is Young's modulus, $E_0$ is its value extrapolated to zero porosity, and $p_c$ is the capillary porosity. For two cements, Helmuth and Turk found $E_0$ to be approximately 30 000 MPa. The same equation held equally well for total porosity if values around 75 000 MPa were used for $E_0$. They also found (H53) that, for a series of pastes 6–7 months old, the irreversible shrinkage at 47% RH was linearly related to the total porosity, whereas the reversible shrinkage was practically independent of the porosity.

Sereda *et al.* (S93) found that, as with compressive strength, the values obtained depend on the RH at which the sample is conditioned, but that the effect is in the opposite direction, saturated pastes having higher moduli than dried pastes. This was attributed to stiffening of the structure through entry of water molecules into interlayer sites, possibly augmented by stronger bonding between adjacent layers (F36,S93,S99). Hysteresis occurred, and was explained by assuming that entry and exit of water begins at the edges of the layers, and that the modulus depends primarily on whether the central parts of the layers are filled. Compacts made by compressing bottle hydrated cement at 100–750 MPa gave results similar to those for pastes.

### 8.6.2 Creep and shrinkage

Cement pastes expand slightly during wet curing; a small shrinkage, called autogenous shrinkage, occurs during sealed curing. A saturated paste shrinks on being dried. This effect, if it occurs in the absence of loading, is called drying shrinkage. Basic creep is slow deformation that occurs under a constant external load in the absence of drying. It is superimposed on the elastic strain that occurs when the load is applied. If drying and loading occur simultaneously, the deformation is greater than the sum of the two effects occurring separately. The excess deformation is called drying creep. Both shrinkage and creep have reversible and irreversible components. Both have important implications for the design and durability of concrete structures.

The changes in length, or more properly in volume, that occur through shrinkage broadly parallel ones in water content (V7). Shrinkage is complicated by the effects of moisture gradients in the specimen, and to

minimize these and the resulting mechanical constraints it is necessary to study thin slices of material. Wittmann (W26) obtained data for specimens of varying thickness and extrapolated to zero thickness. Creep decreases with age before loading and with decreasing w/c ratio (V7). If the material is heated at 110°C before loading and kept dry during test, creep almost disappears. It reappears on re-exposure to water. In contrast, increase in temperature from 10°C to 60°C during loading increases creep. Heating before loading causes the irrecoverable component of creep to decrease even if the specimen is kept saturated (P45,P46). Standing at ordinary temperature, drying at 110°C and heating under saturated conditions are all forms of ageing, which produce a more stable structure. Irreversible creep may also be a form of ageing in which a similar effect is produced by stress (F41) and which occurs less readily if a more stable condition has already been reached through some other cause.

The interaction between shrinkage and creep implies that any full explanation requires that they be considered together. The dependence of both effects on the amount of water in the material also suggests a relationship, and, more precisely, that the properties are ones of the gel, and thus predominantly of the C–S–H. Analogy with the behaviour of more highly ordered forms of C–S–H suggests that changes in interlayer water content and thus also in layer thickness play a part in shrinkage, but changes in pore structure could equally well be important. The behaviour in a mortar or concrete is unlikely to depend solely on effects that apply to a bulk paste; the interfacial transition zone adjacent to the aggregate surfaces is likely to have a major effect.

Many theories have been proposed in relation to both shrinkage and creep, but none has received universal acceptance (H54,M86,X3). All imply changes either in the characteristics or relative positions of the gel particles or in the pore structure, or both, but inadequate knowledge of the relevant features of the microstructure has in most cases precluded descriptions in terms of any but the most generalized microstructural models. For both shrinkage and creep, more than one mechanism probably operates; the dominant mechanism for shrinkage is probably not the same for different ranges of RH. Several of the theories have been formulated into mathematical expressions that agree with the data over a limited range, but, as Xi and Jennings have pointed out (X3), this has not proved sufficient to establish the correctness of the mechanism. Any comprehensive theory must not only be able to explain the observations at the macroscopic level, but also be capable of being tested at the microstructural level. For this to be possible, more detailed knowledge of the pore structure and of the interactions between the various phases is needed, both for bulk paste and for the interfacial transition zone adjacent to aggregate surfaces. Direct observations of shrinkage in the environmental SEM, in which the specimen is maintained in a humid atmosphere, have been reported (X3), and constitute a promising approach. A pressing need is for data that could provide a basis for fundamental, microstructural modelling of the type that has proved fruitful in the understanding of permeability and diffusion.

## 8.7 Permeability and diffusion

### 8.7.1 Permeability to water

The permeability of concrete and the rates at which ions and gases diffuse in it are of major importance for durability. Only the behaviour of cement paste will be considered. Brown *et al.* (B124) reviewed relations between permeability and porosity. Under certain experimental conditions permeability to water obeys D'Arcy's law:

$$dq/dt = K_1 \cdot A \cdot \Delta h/l \qquad (8.12)$$

where $dq/dt$ is the flow in $m^3 s^{-1}$, $K_1$ is the permeability in $m s^{-1}$, $A$ is the cross-sectional area in $m^2$, $\Delta h$ is the head of water in metres, and $l$ is the thickness of the specimen in metres. $K_1$ depends on the viscosity of the liquid, the temperature and the properties of the material. Important conditions are that the sample is completely saturated, steady flow is maintained, and osmotic effects, such as might be caused by concentration gradients in dissolved ions, are absent. Feldman (F42) gave a review, including references to experimental techniques.

Powers and co-workers (P20,P36,P47) determined values of $K_1$ of hcp for various combinations of w/c and age. They assumed that the capillary pores in the paste were initially continuous, but that at a certain stage in hydration they became segmented into isolated cavities, so that the water could only travel through the gel pores, causing the permeability to decrease to a very low value. They concluded that the age at which the capillaries became discontinuous increased with w/c. For a typical cement, it was about 3 days at w/c = 0·4, 1 year at w/c 0·7 and unattainable at w/c > 0·7. Reinterpreting some of these data, Verbeck and Helmuth (V7) concluded that the permeability was directly related to the capillary porosity.

Subsequent studies have shown that $K_1$ depends on the volume and connectivity of the larger pores. Mehta and Manmohan (M88) and Nyame and Illston (N18) found linear relations between $\log K_1$ and estimates of the maximum continuous pore radius, obtained from MIP, and other quantities derived from the pore size distribution and degree of reaction. A high proportion of the flow appears to be through pores wider than about 100 nm. Typical values of $\log K_1$ for mature pastes cured at ordinary temperatures range from around −13·4 at w/c 0·3 to around −11·8 at w/c 0·7 (G78,H55,M88,M89,N18). $K_1$ increases with temperature (G78,M89).

Hooton (H56) noted some pitfalls in the experimental determination of permeabilities and in the practical utilization of the results. In an experimental determination, accurate results will not be obtained unless the sample has been vacuum saturated; and, even if it is, equilibrium flow in accordance with D'Arcy's law may not occur because water is being used up to continue hydration. In practice, a concrete sample is probably not often saturated throughout; if it is not, capillary forces, as well as the pressure difference, affect the rate of flow. Applications of results obtained with pastes to concrete are further complicated by the presence in the latter of cracks, poorly compacted areas and other inhomogeneities.

### *8.7.2 Diffusion of ions and gases*

Ushiyama and Goto (U16) studied the diffusion of ions in a Portland cement paste of w/c ratio 0·4 cured at 20°C for 28 days. Fick's second law was shown to be followed when a steady state had been reached. For $Li^+$, $Na^+$ and $K^+$, diffusion coefficients of $1{\cdot}4–3{\cdot}3 \times 10^{-12}\,m^2\,s^{-1}$ were obtained. That of $Cl^-$ was somewhat greater, especially if the balancing cation was $Ca^{2+}$ or $Mg^{2+}$. It was shown that CH and MH crystallized at the surface of the specimen, suggesting that CH within the specimen had dissolved.

Other studies on $Na^+$ and $Cl^-$ (C48,G79,H57,P48) have given results in substantial agreement with those above. At ordinary temperatures, the diffusion coefficients obtained have been $10^{-11}$ to $10^{-13}\,m^2\,s^{-1}$ for $Na^+$ and $10^{-11}$ to $10^{-12}\,m^2\,s^{-1}$ for $Cl^-$. The activation energies are reported to be $84\,kJ\,mol^{-1}$ for $Na^+$ and $50\,kJ\,mol^{-1}$ for $Cl^-$ for w/c ratios of 0·35–0·45 (G79), or $42–45\,kJ\,mol^{-1}$ for $Cl^-$ at w/c ratios of 0·4–0·5 and $32\,kJ\,mol^{-1}$ for w/c = 0·6 (P48). These activation energies are much higher than those found for diffusion of the same ions in a dilute solution, which are typically below $20\,kJ\,mol^{-1}$. One study (G79) showed little apparent variation in diffusion coefficients with w/c ratio or age, but another (H57) showed increases with w/c ratio and decreases as hydration proceeded.

Studies on the permeability and diffusivity of concrete to gases, reviewed by Feldman (F42), have provided only slight information regarding the mechanism of transport through the cement paste or the relations to its pore structure. It cannot be taken for granted that their relation to pore structure is the same as that for water permeability.

Garboczi and Bentz (G80) calculated ionic diffusivities in a saturated paste from their model of paste structure. For this purpose, the system was treated through the analogy of a random network of electrical conductors. Based on experimental data, conductances were assigned to contacts between adjacent pixels within and between capillary pores, C–S–H and the electrodes. For the C–S–H, data for diffusion of $Cl^-$ were used. The results were in reasonable agreement with experimental data, which were available for the higher degrees of hydration. At porosities above 18%, the dominant pathways were through capillary pores, with some contribution from gel pores in the C–S–H; at lower porosities, they were through isolated isolated regions of capillary pore space linked by gel pores. This conclusion is similar to that relating to water permeability, discussed above. A single curve relating the relative diffusivity (diffusivity relative to that of the ions in free water) to the capillary porosity was found to apply to all the simulation data points for plain $C_3S$ pastes at capillary porosities up to 60%.

# 9 Composite cements

## 9.1 Introduction

A composite cement is a hydraulic cement composed of Portland cement and one or more inorganic materials that take part in the hydration reactions and thereby make a substantial contribution to the hydration product. This definition excludes admixtures, such as $CaCl_2$, that influence the hydration process but do not themselves contribute substantially to the product. The inorganic materials will be called mineral additions; other terms, such as supplementary cementing materials (SCMs), are also used. The most important are flyash (pulverized fuel ash), ground granulated blastfurnace slag (ggbs), natural pozzolanas and silica fume (microsilica). The mineral addition may be ground together with the cement clinker and gypsum, or mixed with Portland cement when the latter is used. In British usage, these procedures are called intergrinding and blending respectively. In US usage, the term 'blended cements' is widely used as a synonym for composite cements of either type.

Composite cements are used for various reasons. The necessity for utilizing waste materials and decreasing overall energy consumption is becoming increasingly obvious. Flyash and slag are waste materials produced in large quantities, and concretes made with them, or with natural pozzolanas, can have properties similar to those of ones made with pure Portland cements at lower cost per unit volume. Concretes made using composite cements can have properties that are desirable for particular purposes, such as slower and decreased total heat evolution in massive structures, improved durability or, especially with silica fume, strengths above the normal range.

Mineral additions may be broadly categorized as pozzolanic materials or latent hydraulic cements. Neither type reacts significantly with water at ordinary temperatures in the absence of other substances. Pozzolanic materials are high in $SiO_2$ and often also in $Al_2O_3$; they are sufficiently reactive that mixtures of them with water and CaO produce C–S–H at ordinary temperatures and thereby act as hydraulic cements. If they contain $Al_2O_3$, calcium aluminate hydrates or aluminate silicate hydrates are also formed. Because they are low in CaO, this component must be supplied in stoichiometric quantity. In a composite cement, it is provided by the Portland cement through decreased formation of CH and

decreased Ca/Si ratio of the C–S–H. Flyash low in CaO, natural pozzolanas and silica fume are examples of pozzolanic materials.

Latent hydraulic cements have compositions broadly intermediate between those of pozzolanic materials and Portland cement. They act as hydraulic cements if mixed with water and a minimal amount of some other substance that serves as a catalyst or activator. Ggbs is a latent hydraulic cement. When mixed with Portland cement, it is activated by the CH and alkali which the latter produces. As will be seen, the hydration products of the Portland cement clinker are also modified. The proportion of a latent hydraulic cement in a composite cement can be higher than that of a pozzolanic material. Some materials, such as finely ground $CaCO_3$, though used in relatively small proportions and having neither pozzolanic nor latent hydraulic properties, are conveniently considered along with mineral additions.

In this chapter and elsewhere, w/s denotes the ratio $w/(c+p)$ and 'percentage replacement' the quantity $100p/(c+p)$, where $w$, $c$ and $p$ are the masses of water, Portland cement and mineral addition respectively.

## 9.2 Blastfurnace slag

### *9.2.1 Formation, treatment and use in composite cements*

Blastfurnace slag is formed as a liquid at 1350–1550°C in the manufacture of iron; limestone reacts with materials rich in $SiO_2$ and $Al_2O_3$ associated with the ore or present in ash from the coke. If allowed to cool slowly, it crystallizes to give a material having virtually no cementing properties. If cooled sufficiently rapidly to below 800°C, it forms a glass which is a latent hydraulic cement. Cooling is most often effected by spraying droplets of the molten slag with high-pressure jets of water. This gives a wet, sandy material which when dried and ground is called ground granulated blastfurnace slag and often contains over 95% of glass.

In an alternative treatment, called pelletization, the molten slag is partially cooled with water and flung into the air by a rotating drum. The resulting pellets vary in size from a few mm to around 15 mm. The proportion of glass decreases with increasing pellet size. Pelletization has advantages to the steel manufacturer of lower capital cost, decreased emission of sulfurous gases, and formation of a drier product, which can also be sold as a lightweight aggregate, but the glass content of the size fraction used to make composite cements can be as low as 50%.

The composition of the slag must be controlled within relatively narrow limits to ensure satisfactory and economic operation of the blastfurnace, and depends on that of the ore. It therefore varies considerably between plants, but that of a given plant is unlikely to vary much unless the source of the ore is changed. Table 9.1 gives ranges and means for slags typical of those produced in Western Europe. For a wider range of steel-producing countries, the contents of major components are: MgO, 0–21%; $Al_2O_3$, 5–33%; $SiO_2$, 27–42% and CaO, 30–50% (S100). The densities of granulated or pelletized blastfurnace slags are typically 2880–2960 kg m$^{-3}$.

**Table 9.1** *Chemical compositions of some blastfurnace slags* (D49)*

| | Mean | Minimum | Maximum | | Mean | Minimum | Maximum |
|---|---|---|---|---|---|---|---|
| $Na_2O$ | 0·39 | 0·25 | 0·50 | $TiO_2$ | 0·55 | 0·49 | 0·65 |
| MgO | 5·99 | 3·63 | 8·66 | MnO | 0·64 | 0·34 | 1·31 |
| $Al_2O_3$ | 13·29 | 10·26 | 16·01 | FeO | 1·24 | 0·29 | 9·32 |
| $SiO_2$† | 33·48 | 31·96 | 37·29 | $S^{2-}$ | 0·94 | 0·68 | 1·25 |
| $P_2O_5$ | 0·13 | 0·00 | 0·34 | $F^-$ | 0·16 | 0·06 | 0·31 |
| $SO_3$ | 0·04 | 0·00 | 0·19 | $Cl^-$ | 0·019 | 0·003 | 0·050 |
| $K_2O$ | 0·70 | 0·44 | 0·98 | Ign. loss | 0·42 | 0·00 | 1·04 |
| CaO | 42·24 | 37·92 | 44·38 | Total‡ | 99·68 | | |

* Means, minima and maxima for 27 slags representative of French and Luxembourg production in 1980.
† Total $SiO_2$; insoluble residue, mean, 0·41%, minimum, 0·00%, maximum, 1·32%.
‡ Corrected for $O^{2-}$ equivalent to $S^{2-}$, $F^-$ and $Cl^-$.

In composite cements, the granulated or pelletized slag is blended or interground with Portland cement or clinker. Ternary mixes containing also, for example, natural pozzolanas are used in some countries. Slags vary considerably in grindability, but are usually harder to grind than clinker. Intergrinding may therefore produce a cement in which the slag is too coarsely, and the clinker too finely, ground. For this and other reasons, there can be a case for separate grinding, at least with some combinations of clinker and slag (S101). The relative proportions of clinker and slag vary widely; the content of slag can be over 80%, but up to 45% is more usual. Specifications and terminology based on them vary in different countries. In current (1996) British standards, cements with up to 35% of slag are called Portland slag cements, and ones with 36–85% of slag are called blastfurnace cements.

In this chapter, unless otherwise stated, the term 'slag' is used to mean granulated or pelletized blastfurnace slag, and 'slag cement' to mean composite cements consisting essentially of these materials with Portland cement or clinker. In these cements, the slag reacts considerably more slowly than the alite, and strength development is therefore slower to an extent that increases with the proportion of slag. For equal 28-day strengths, replacement of a Portland cement by one containing 65% of slag can lower the compressive strength by almost a half at 2 days, but increase it by about 12% at 91 days (S100). Workability is similar to that obtained with Portland cements. The rate of heat evolution at early ages and the total heat evolution are both reduced. Fuller comparisons would have to take account of the proportion of slag, the particle size distributions of clinker and slag, and the fact that slags vary in reactivity.

### *9.2.2 Factors affecting suitability for use in a composite cement*

The suitability of a slag for use in a composite cement depends primarily on its reactivity, though grindability and contents of water and of undesirable components, especially chloride, must also be considered.

Reactivity most obviously depends on bulk composition, glass content and fineness of grinding, though these are probably not the only factors and the relations with composition and glass content are complex.

Several investigators have found that the presence of a small proportion of crystalline material finely dispersed in the glass improves grindability or reactivity or both (S100). Demoulian *et al.* (D49) found that the highest strengths at 2–28 days were given by slags containing about 5% of crystalline phases and that increase in the content of the latter up to 35% produced only small decreases in strength. They attributed the beneficial effect of small contents of crystalline phases to mechanical stress in the glass and provision of nucleation sites for hydration products, and the smallness of the decrease at high contents to a consequent change in the glass composition, which through the separation of merwinite was enriched in $Al_2O_3$.

Smolczyk (S100) reviewed relations between composition and hydraulic properties. Many attempts have been made to assess slags on the basis of moduli based on bulk composition, of which $(CaO + MgO + Al_2O_3)/SiO_2$ is one of the simplest and most widely used. Minimum values for this ratio (e.g. 1·0) have sometimes been incorporated into standard specifications. This and similar moduli express the fact that hydraulic activity is broadly favoured by more basic composition, but the effect of $Al_2O_3$ content is complex and none of the proposed moduli has proved valid for the detailed comparison of slags other than ones of relatively similar compositions produced within a given plant. A regression analysis of compressive strengths on compositions for composite cements made using a wide range of west European slags (S102) showed that increase in $Al_2O_3$ content above 13% tended to increase early strengths but to decrease late strengths. MgO in amounts up to 11% was quantitatively equivalent to CaO. Minor components were found to have important effects: that of MnO was always negative, but those of $P_2O_5$ and of alkalis were more complex.

### 9.2.3 *X-ray diffraction and microstructure of slags*

Regourd (R43) reviewed structural and other aspects of slags. XRD patterns show an assymetric, diffuse band from the glass peaking at about 31° $2\theta$ ($CuK_\alpha$; $d = 0{\cdot}29$ nm) and extending from about 20° to about 37° and a weaker band at about 48° $2\theta$ (0·19 nm). Crystalline phases, if present in sufficient quantity, give superimposed, sharper peaks; melilite and merwinite are the most usual. Neither periclase nor lime is found and, since it is present either in the glass or in these inert, crystalline phases, MgO is not a potential cause of expansion, as it may be in a clinker (S103).

Glass contents have been determined by light microscopy and by difference from QXDA determinations of crystalline phases (R43,R44, S104,U17). Investigators have differed as to how well the results of the two methods agree. Both will fail if the individual crystalline regions are below a certain size, which is much smaller for QXDA than for light microscopy, but light microscopy complements QXDA by providing

microstructural information and does not depend on a possibly uncertain choice of reference standards. Image analysis with the SEM is a further possible method.

Individual grains of ground granulated or pelletized slag are markedly angular. The melilite and merwinite occur as inclusions in the glass, ranging in size from ones easily detectable by light microscopy to dendritic growths in which the individual dendrites are less than 100 nm wide (D49,S104). The melilite crystals may be zoned (U17). Metallic iron can occur. Crystalline inclusions and gas-filled pores can be very unevenly distributed; even in slags high in crystalline material, grains consisting only of glass may be seen using light microscopy (D49). In slags of high glass content, the composition of the glass is reported to be uniform, but near to melilite crystals it can be lower in $Al_2O_3$ (U17).

Some workers using small-angle X-ray scattering and light and electron microscopy have found evidence of phase separation within the glass (R43,S104), but others have concluded that this does not occur (U17); slag glasses may vary in this respect.

### 9.2.4 *Internal structures of slag glasses*

The internal structures of slag glasses have been widely discussed in terms of the classical theory of network-forming and network-modifying elements. On this model, the glass structure is based on a continuous, though incompletely connected, anionic network composed of O, Si and the other relatively electronegative elements, and its charge is balanced by the calcium and other electropositive elements. Consideration of the compositions of typical slag glasses (Table 9.2) suggests that this model, which has proved valuable for more acidic glasses, may be unrealistic for slags. Some important atomic ratios, derived from the data in Table 9.2, are: $O/Si = 4{\cdot}4$; $O/(Si + Al) = 3{\cdot}0$; $O/(Si + Al + P + Mg + Fe + Mn) = 2{\cdot}5$. These values indicate that nothing resembling a continuous network can be formed by the Si, Al and O atoms alone. Dron and Brivot's (D50) model, in which the network-forming atoms are present in straight or branched chains of various lengths, is more realistic. Studies of six slags, using $^{29}Si$ NMR and IR spectroscopy, TMS and an alkali extraction method, showed the predominant silicate species to be in all cases monomer and dimer (U17). The bulk compositions were all near that in Table 9.1.

Evidence on the coordination of aluminium and magnesium in slag glasses is conflicting. From molar refractivities and other evidence, Chopra and Taneja (C49) concluded that both the aluminium and the

**Table 9.2** *Atom ratios in a typical ground granulated blastfurnace slag*

| $K^+$ | $Na^+$ | $Ca^{2+}$ | $Mg^+$ | $Fe^{2+}$ | $Mn^{2+}$ | $Ti^{4+}$ | $Al^{3+}$ | $Si^{4+}$ | $P^{5+}$ | $O^{2-}$ | $S^{2-}$ | $F^-$ |
|---|---|---|---|---|---|---|---|---|---|---|---|---|
| 0·6 | 0·5 | 30·7 | 6·1 | 0·7 | 0·3 | 0·3 | 10·6 | 22·4 | 0·1 | 98·5 | 1·2 | 0·3 |

For the mean of the analyses in Table 9.1; referred to 100 ($O^{2-} + S^{2-} + F^-$).

magnesium are tetrahedrally coordinated, as in melilites. X-ray spectroscopic results have been held to favour tetrahedral coordination of the aluminium (G81) or a mixture of tetrahedral and octahedral coordination (Y7). From electron paramagnetic resonance, Royak and Chkolnik (R45) concluded that magnesium, aluminium and titanium could each be in either tetrahedral or octahedral coordination and that increased proportions in octahedral coordination enhanced hydraulic activity. The $^{27}$Al NMR spectrum of a synthetic glass similar in composition to typical slag glasses showed the Al to be in distorted tetrahedral coordination (R46).

Structural defects affect reactivity; four samples of the same slag liquid, cooled at different rates, differed in reactivity, though all were shown by XRD to be completely glassy (F43). Photoelectric emission data showed that they contained different numbers of defects.

Granulated or pelletized slags are materials formed under markedly non-equilibrium conditions, and it is not surprising that their hydraulic activities are not determined solely by bulk composition and glass content. Reactivity may be presumed to depend on glass composition rather than on bulk composition. For a given combination of glass content and bulk composition, further effects varying reactivity could thus include the following:

(1) crystallite size and morphology, through their effects on stress in the glass or nucleation sites for hydrated phases
(2) the bulk composition of the crystalline material, through its effect on that of the glass, and the profile of compositional variation in the glass near the crystallite surfaces, which could produce regions of either enhanced or decreased reactivity
(3) the degree of phase separation within the glass
(4) the coordination numbers of the aluminium and magnesium, and the distributions of atoms and bonding patterns within the glass; e.g. variation in the number of Si–O–Al linkages compared with those of Si–O–Si and Al–O–Al
(5) the numbers and types of electronic or structural defects.

### 9.2.5 *Hydration chemistry of slag cements*

Daimon (D51), Regourd (R47) and Uchikawa (U18) have reviewed slag cement hydration. Many XRD studies have shown that the principal hydration products are essentially similar to those given by pure Portland cements, but the quantities of CH found by this or other methods are in varying degrees lower than those which would be given by the Portland cement constituent if the slag took no part in the reaction (C50,K46, R47,S105). With percentage replacements above about 60%, the CH content may pass through a maximum and then decrease. The magnesium in the slag enters a hydrotalcite-type phase (F44,G82,H58,K47,R48).

The microstructures of slag cement pastes are also essentially similar to those of pure Portland cement pastes, apart from the lower CH contents

(H58,R43,U13,U18,U19). As with the clinker phases, layers of inner product form at the boundaries of the slag grains and gradually extend inwards. A light-microscopic study indicated that these were only 0·5 $\mu$m wide after 90 days (K46). Backscattered electron images with another slag (H58) showed them to be barely detectable at 28 days, but up to 10 $\mu$m wide at 6 months and up to 15 $\mu$m wide at 14 months. In the older pastes, fully reacted relicts of slag particles were abundant. A TEM study (R48) showed that, with increasing proportion of slag in the blend, the microstructure of the outer product (dried by the high vacuum of the instrument) becomes progressively less fibrillar and more foil-like in character. It was suggested that this could decrease the connectivity of the pore system and thereby account for the low permeabilities of slag-cement pastes. This matter is discussed further in Section 9.7.

Luke and Glasser (L30,L48) made a comparative study of methods for determining the content of unreacted slag. The most satisfactory was a modification of that of Demoulian *et al.* (D52), in which constituents other than unreacted slag were dissolved using an alkaline solution of EDTA in aqueous triethanolamine. Other extraction methods gave unacceptably high residues with pastes of Portland cements. This may explain the very wide variation between results given in the literature. Lumley *et al.* (L49), using a further modification of the method of Demoulian *et al.*, found that at w/s ratios of 0·4–0·6 and 20°C, 30–55% of the slag reacted in 28 days and 45–75% in 1–2 years. The degree of reaction varied with the slag and decreased with the content of slag in the blend and with decrease in w/s.

Vernet (V8) showed that the $S^{2-}$ ion in granulated or pelletized slags is almost entirely contained in the glass and that it is released at the rate at which the latter reacts. He showed that it probably entered an AFm phase. Sulfide-containing phases of this type have been synthesized (D27,V8); one also containing iron was intensely green in colour and may account for the characteristic colour of slag cement pastes (V8). Although $S^{2-}$ in AFm phases is very easily oxidized (V8), significant aerial oxidation does not seem to occur in the bulk of a slag cement paste. Observations on a sulfide-containing Portland cement (B131) suggest, however, that in slag cements some oxidation of the $S^{2-}$ by the $Fe^{3+}$ present in the Portland cement component may occur. Small amounts of thiosulfate have been detected in the pore solutions of slag cements (G83,L37).

### 9.2.6 *X-ray microanalysis*

The mean Ca/Si ratio of the C–S–H is lower than that found in pastes of plain Portland cements (H4,H58,R36,R48,U19). Richardson and Groves (R48) found from TEM analyses that it decreased with the proportion of slag in the blend, from around 1·8 for plain Portland cement pastes to 1·1–1·2 in the extreme case of a paste of an alkali-activated slag containing no Portland cement. These last values were near that of the unreacted slag. For a blend with 50% slag, values in the region of 1·55 were obtained. There was no significant difference in Ca/Si ratio between the C–S–H present in the outer product or as inner product of the slag or

clinker. In contrast, another investigation (H58) showed the inner product of the clinker to have a higher Ca/Si ratio than that of the slag.

Richardson and Groves (R48) found that the mean Al/Ca ratio of the C–S–H increased with the Si/Ca ratio, in accordance with equation 7.3. The mean Al/Ca ratio is thus approximately 0·10 for a blend with 50% slag and 0·19 for a paste of alkali-activated slag. The significance of the latter result is discussed in Section 9.2.9.

Harrisson *et al.* (H4,H58) represented the results of X-ray microanalyses of individual spot analyses in all parts of the microstructure other than unreacted clinker grains on plots of Al/Ca ratio against Si/Ca ratio and of Mg/Ca ratio against Al/Ca ratio (Figs. 9.1 and 9.2). If the analyses of the inner product of the slag are excluded, the plot of Al/Ca against Si/Ca is broadly similar to plots obtained for pure Portland cement pastes, and may be interpreted in the same way (Section 7.3.5) as indicating the presence of C–S–H, an AFm phase and small proportions of CH. Taken together, the results in the two figures show that the inner product of the slag has an approximately constant Si/Ca ratio of 0·62, and ratios of Mg/Ca and of Al/Ca that vary from point to point on a micrometre scale but are related to each other by the equation shown in Fig. 9.2. This was interpreted (H58) as indicating mixtures in varying proportions of C–S–H having Si/Ca 0·62, Al/Ca 0·09 with a

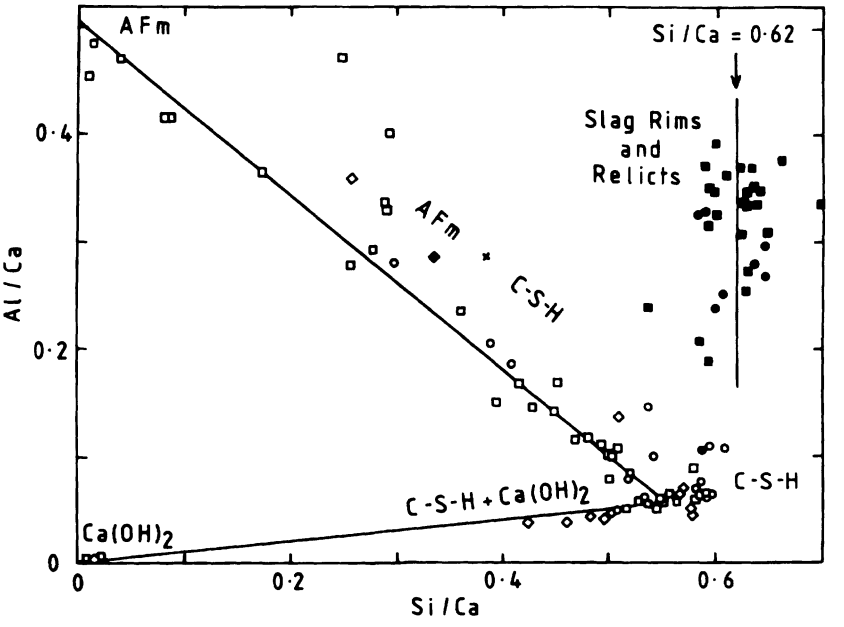


**Fig. 9.1** *Si/Ca and Al/Ca atom ratios from individual X-ray microanalyses of a slag cement paste (40% slag; w/s = 0·5) hydrated for various times at 25°C. Mg/Si < 0·15: ◇, 28 days; □, 6 months; ○, 14 months. Mg/Si ≥ 0·15: ◆, 28 days, ■, 6 months; ●, 14 months. From H58.*

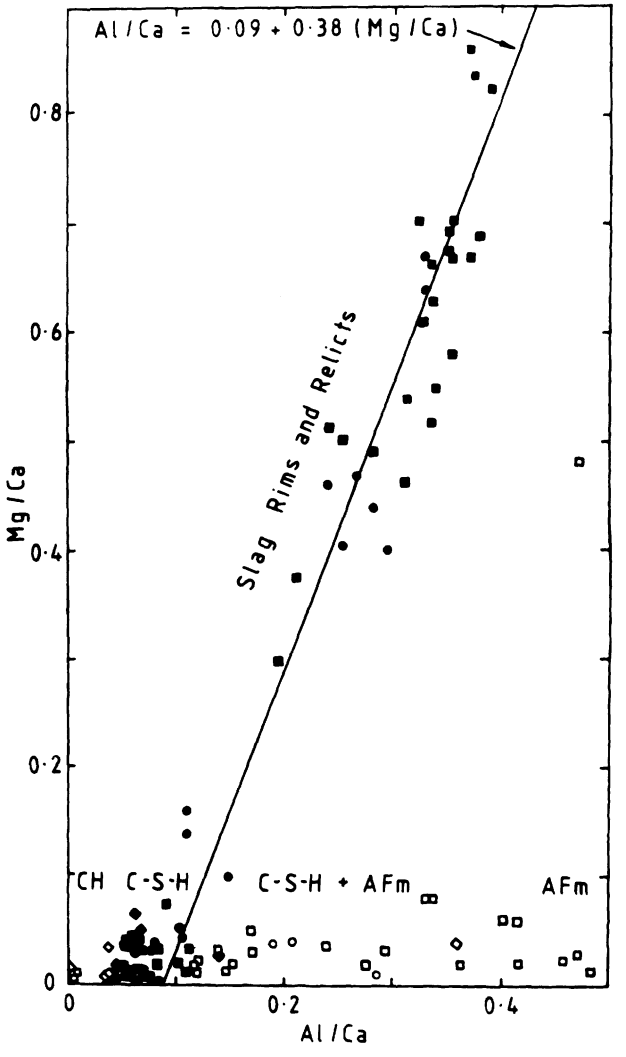


**Fig. 9.2** *Al/Ca and Mg/Ca atom ratios from individual X-ray microanalyses of the same slag cement paste as in Fig. 9.1. Si/Ca < 0·5:* ◇, *28 days;* □, *6 months;* ○, *14 months. Si/Ca ≥ 0·5:* ◆, *28 days;* ■, *6 months;* ●, *14 months. From H58.*

hydrotalcite-type phase having Al/Mg 0.38. Similar results have been obtained by subsequent investigators, though values varying between 0·23 and 0·52 have been reported for the Al/Mg ratio of the hydrotalcite-type phase (B132,G82,R48). In some slag cement pastes, the constituent phases of the slag inner product appear to be randomly though not uniformly mixed at the micrometre level (e.g. H58), but in other cases distinct zones enriched in C–S–H and in the hydrotalcite-type phase have been observed (B132,F44,T50).

The AFm phase formed in pastes of slag cements approximates to monosulfate at early ages but appears to take up increasing proportions of $S^{2-}$ as hydration proceeds (G82). With slags high in $Al_2O_3$ or blends high in slag, there are indications that a phase higher in $Al_2O_3$, possibly strätlingite, is also formed (G82). Some of the AFm phase is present in the slag inner product (Figs 9.1 and 9.2).

### 9.2.7 *Stoichiometry of slag cement hydration*

An approximate estimate of the stoichiometry of slag hydration can be obtained as follows (Table 9.3).

(1) Assume that the MgO from the slag enters a hydrotalcite-type phase, for which one must assume an Mg/Al ratio (e.g. 2·5).
(2) Assume that the $SiO_2$ from the slag enters C–S–H, for which one must assume a Ca/Si ratio, and also, using equation 7.3, an Al/Ca ratio (e.g. Ca/Si 1·55, Al/Ca 0·09).
(3) Assume that the remaining $Al_2O_3$ is contained in an AFm phase; this probably also contains the $S^{2-}$ released from the slag.
(4) The amount of CaO released from the slag will be insufficient to account for that in the C–S–H and AFm phase. The deficiency is made up by decreases in the content of CH and the Ca/Si ratio of the C–S–H formed from the Portland cement or clinker.

Comparison of the average proportions, compositions and densities of the phases present in the inner product of the slag with corresponding data for the unreacted slag suggests that little net movement of either $Mg^{2+}$ or $O^{2-}$ in or out of the latter occurs when it reacts, but that substantial fractions of the $Al^{3+}$, $Si^{4+}$ and $Ca^{2+}$ are expelled and an equivalent amount of $H^+$ taken up (H58). The ions thus released contribute to the outer product; as explained above, more $Ca^{2+}$ is provided by the Portland cement or clinker to alter the atom ratios to those in a mixture of C–S–H and AFm phase.

For any specified drying condition, the observed water contents of slag blends are lower than those of comparable plain Portland cement pastes (C50,H58,H59). In some typical cases of mature pastes, the bound

**Table 9.3** *Calculated mass balance for hydration of a granulated blastfurnace slag in a blend with Portland cement*

| | $SiO_2$ | $Al_2O_3$ | CaO | MgO | $S^{2-}$ |
|---|---|---|---|---|---|
| Total supplied by slag glass | 33·0 | 11·8 | 41·0 | 9·5 | 1·1 |
| Hydrotalcite-type phase | | 4·8 | | 9·5 | |
| C–S–H | 33·0 | 3·9 | 47·7 | | |
| AFm | | 3·1 | 6·8 | | 1·0 |
| Supplied by Portland cement | | | 13·5 | | |

All values are in g per 100 g of reacted slag glass. The basis of the calculation and compositions assumed for the hydration products are explained in the text.

water contents decreased from around 27% for plain Portland cement to 22–24% for blends containing 70% of slag (H59). Mass-balance calculations lead to a similar conclusion (H58), which appears to hold for composite cements in general.

### 9.2.8 Activation of slag glasses

If ground granulated or pelletized blastfurnace slag is placed in water alone, it dissolves to a small extent but a protective film deficient in $Ca^{2+}$ is quickly formed, and inhibits further reaction (K21,R49). Reaction continues if the pH is kept sufficiently high. The pore solution of a Portland cement, which is essentially one of alkali hydroxides, is a suitable medium. The supply of $K^+$ and $Na^+$ ions is limited, but these ions are only partially taken up by the hydration products, and the presence of solid CH ensures that the supply of $OH^-$ is maintained. The slag can similarly be rendered active by $OH^-$ ions supplied in other ways, such as sodium hydroxide or silicate (Section 9.2.9). Although several hypotheses have been proposed, the mechanism of the attack on the slag glass is not established. If it is similar to that suggested for the clinker phases (Section 4.6.1), one would expect reactivity to increase with the fraction of the oxygen atoms bonded only to calcium and a single silicon, or, especially, to calcium and a single aluminium atom.

Calcium sulfate accelerates the reaction of slag glasses, probably because precipitation of ettringite provides a sink for the $Ca^{2+}$ and $Al(OH)_4^-$ ions released from the slag. It is often described as an activator, but is not very effective unless a little alkali is also present (R47) and is perhaps more properly described as a powerful reactant. The calcium sulfate present in a slag cement thus contributes to increasing the activity of the slag. The reaction between slag and $CaSO_4$ is utilized to a much greater extent in supersulfated cements.

### 9.2.9 Alkali-activated slag cements

These were pioneered by Glukhovsky *et al.* (G84) and their properties were reviewed by Wang *et al.* (W31). Typically, they consist of ggbs with 3·5–5·5% of $Na_2O$, added usually as NaOH or sodium silicate. Desirable properties include rapid hardening, high strength development, low heat of hydration, low permeability and good resistance to chemical attack, but problems exist with quick setting, possible likelihood of alkali silica reaction, efflorescence and high drying shrinkage.

As noted in Section 9.2.6, the main hydration product is C–S–H typically having Ca/Si 1·1–1·2 and Al/Ca around 0·19. Studies of pastes of alkali activated slag or synthetic slag glass by NMR and ELNES (electron energy loss near-edge structure) showed that the aluminium in the C–S–H substituted for silicon exclusively in bridging sites of dreierketten having a mean chain length of 4·83 tetrahedra (B133,R46,R50). Substitution of silicon by aluminium in these sites was almost complete.

A hydrotalcite-type phase is also formed; AFm phase appears also to be formed with some, but not all, slags (R48,W32). If NaOH is used as

activator, the C–S–H is relatively highly ordered C–S–H(I) (Section 5.4.4), but with sodium silicate it is less crystalline (W32). An early conclusion (G84) that zeolites are formed on hydration was not confirmed for pastes cured at ordinary temperature (W32), but they would possibly be formed in ones cured at elevated temperatures.

### *9.2.10 Supersulfated cements*

Supersulfated cements consist of 80–85% of slag with 10–15% of anhydrite and about 5% of an activator, which is usually Portland cement clinker, and are somewhat more finely ground than Portland cements. A slag high in $Al_2O_3$ is preferred. XRD shows that the main hydration products are C–S–H and ettringite. The content of the latter reaches a limit in about 3 days, by which time virtually all the anhydrite has reacted (K46,S104). More water is taken up during curing than with Portland or normal slag cements, and contents of non-evaporable water are higher. TEM examination of replicas (M90) confirmed the formation of ettringite, some crystals of which were over 120 $\mu$m long.

Kondo and Ohsawa (K46) studied a cement with 80% of slag (18·5% $Al_2O_3$), 15% $CaSO_4$ and 5% $C_3S$. At 3 days, 91% of the $CaSO_4$ and 22% of the slag had reacted, and the content of non-evaporable water was 26%. To convert all the $SO_3$ supplied by the $CaSO_4$ into ettringite, about 19% of the slag would have to react, which agrees well with the observed value. The quantity of ettringite formed would be 43%, referred to the ignited mass. The high content of non-evaporable water is difficult to explain, as ettringite normally loses at least a half of its water on being dried under the conditions used; however, XRD indicated that the ettringite formed from the cement was particularly resistant to dehydration, and a little non-evaporable water would also have been contributed by the C–S–H. Daimon (D51) reported broadly similar results.

## 9.3 Flyash (pulverized fuel ash) low in CaO

### *9.3.1 Properties*

Flyash is ash separated from the flue gas of a power station burning pulverized coal. It must be distinguished from the coarser ash that collects at the bottom of the furnace; the most uniform and highest quality ash is likely to be that produced by efficient, base-load power stations. Ravina (R51) summarized the technology. The chemical and phase compositions depend on those of the minerals associated with the coal and on the burning conditions. In general, anthracitic or bituminous coals give ashes high in glass, $SiO_2$, $Al_2O_3$ and $Fe_2O_3$ and low in CaO, whereas sub-bituminous coals or lignites give ashes higher in CaO and often also in crystalline phases. The flyash used in Europe and Japan to make composite cements typically contains under 10% of CaO. The American designations of Class F and Class C fly ash, though based on contents of ($SiO_2 + Al_2O_3 + Fe_2O_3$) above and below 70% respectively, correspond approximately to low- and high-CaO ashes in the sense used here. Section 9.3 deals exclusively with flyash containing less than about 10% of CaO.

**Table 9.4** *Chemical and phase compositions and density of a typical flyash low in CaO and high in glass (W33)*

*Chemical composition (%)*

| $Na_2O$ | MgO | $Al_2O_3$ | $SiO_2$ | $P_2O_5$ | $SO_3$ | $K_2O$ | CaO | $TiO_2$ | $Mn_2O_3$ | $Fe_2O_3$ | C | $H_2O$ | Total |
|---|---|---|---|---|---|---|---|---|---|---|---|---|---|
| 1·5 | 1·6 | 27·9 | 48·7 | 0·2 | 1·2 | 4·2 | 2·4 | 0·9 | tr. | 9·5 | 1·5 | 0·3 | 99·9 |

*Phase composition (%)*

| Quartz | Mullite | Hematite | Magnetite | Carbon | Glass* | Density ($kg\,m^{-3}$) |
|---|---|---|---|---|---|---|
| 2·8 | 6·5 | 1·6 | 1·9 | 1·5 | 86 | 2220 |

* By difference.

Kokubu (K48) and Regourd (R43) reviewed the major characteristics of flyash. Others (H60,T51,W33,W34) have described the flyash produced in the UK more fully. Table 9.4 gives data for a good quality ash. SEM (e.g. R52) shows such flyash to contain a high proportion of spherical and largely glassy particles, formed by the rapid cooling of droplets of liquid. Etching with HF (R52) or partial hydration (H61) reveals inclusions of prisms of mullite and smaller crystals of quartz, which are less reactive. Hollow spheres, called cenospheres, occur; ones that contain smaller spheres are called plerospheres. $K_2SO_4$, $CaSO_4$, hematite ($Fe_2O_3$) and magnetite ($Fe_3O_4$) may be present as smaller particles adhering to the surfaces of the spheres. The iron oxides and quartz also occur as separate, angular particles. Carbon, if present in sufficient amount, forms porous particles that can be either spherical or irregular in shape (R52). For the more finely divided ashes, 50% by mass is in particles smaller than about 10 $\mu$m; for the coarser ones, the corresponding size is around 40 $\mu$m.

XRD patterns of flyash include a diffuse band from the glass, which for ashes low in CaO peaks at 22–23° $2\theta$ (CuK$\alpha$). This is slightly above the value for vitreous silica. Possibly in all such ashes, the glass shows phase separation on a 5–15 nm scale (Q1). The proportion of glass and other amorphous aluminosilicates, if any, may be determined by difference from QXDA on the superimposed peaks of the crystalline phases (D15); allowance should be made for the content of amorphous carbon. The same method shows that, in many ashes, the FeO and $Fe_2O_3$ are mainly present as magnetite and hematite. Hubbard *et al.* (H60) found a correlation between the $K_2O/Al_2O_3$ ratio and the percentage of amorphous aluminosilicates. Since it is overwhelmingly the latter that takes part in the pozzolanic reaction, they suggested that this ratio, multiplied by 10, might be used as a pozzolanic potential index (PPI).

Due to the presence of hollow spheres and spongy material, the density of flyash is difficult to define. The smaller spheres are not readily broken by grinding, and values of 2100–2400 kg m$^{-3}$, increasing with iron oxide content, are typical (K48), but these must be influenced by the presence of carbon and voids, as $Al_2O_3$–$SiO_2$ glasses have densities of 2500–2700 kg m$^{-3}$ and the densities of the crystalline constituents range from 2650 kg m$^{-3}$ (quartz) to 5240 kg m$^{-3}$ (hematite). Mather (M91) found that fine grinding of a particular flyash caused the density to increase from 2440 to 2780 kg m$^{-3}$. Watt and Thorne (W33) found that the mass distributions of density for five flyashes all peaked at 2500–2600 kg m$^{-3}$, and this is probably a reasonable estimate of the true density of the reactive part of the material.

### *9.3.2 Factors governing suitability for use in composite cements*

Important properties governing the suitability of a flyash for use in composite cements are the content of unburned carbon, the ability to decrease the water demand of the concrete and the pozzolanic activity. The second property partly depends on the first. An excessive content of carbon also produces a discoloured concrete and interferes with the action of some concrete admixtures, especially air-entraining agents. The

effect on water demand is important because the pozzolanic reaction of the flyash is slow, and to obtain a specified 28-day strength, the w/s ratio must be lower than for an otherwise similar mix containing a pure Portland cement. Early work, reviewed by Kokubu (K48), established that partial replacement of cement by a good quality flyash increases the workability. Typically, to produce a concrete with the same 28-day strength and the same slump as one made using a pure Portland cement and the same coarse and fine aggregate, some of the cement and some of the fine aggregate are replaced by flyash and the content of water per unit volume of concrete is decreased.

The enhanced workability of concrete containing good quality flyash has generally been attributed to the fact that the latter is largely composed of smooth, spherical particles (K48), together with the increased proportion of paste and the decreased formation at this stage of hydration products. Uchikawa (U18) reviewed rheological sudies. Flyash containing a high proportion of coarse (>45 $\mu$m) material is unsuitable for blending but may be suitable for intergrinding, because the effect of the latter is largely to separate particles present in agglomerates and to break up some of the larger cenospheres; the spherical particles are not otherwise damaged (M92).

Chemical tests of pozzolanicity have proved of limited use for evaluation, because the 28-day strength depends much more on the w/s ratio than on this property, and there appears to be no effective substitute for direct testing of the relevant properties on mortars or, preferably, on concretes. The degree of pozzolanic activity is, however, important for the development of strength and decrease in permeability at later ages. For equal 28-day strengths, the strengths at 91 days or more normally exceed those of otherwise similar concretes made with plain Portland cements.

### 9.3.3 *Rates of consumption of clinker phases and flyash, and contents of calcium hydroxide*

Uchikawa (U18) reviewed the hydration chemistry of flyash and other composite cements. Flyash cements differ from pure Portland cements notably in (i) the hydration rates of the clinker phases, (ii) CH contents, which are lowered both by the dilution of the clinker by flyash and by the pozzolanic reaction, (iii) the compositions of the clinker hydration products and (iv) formation of hydration products from the flyash. The two last aspects cannot be wholly separated.

Calorimetric studies show that flyash retards the reaction of alite in the early stage of reaction (G85,H61,J34,W35), but with one exception (W35) studies on the middle stage show the alite reaction to be accelerated (D15,H61,K49,L50,T39). SEM shows that C–S–H and CH are deposited on the surfaces of flyash grains before these have started to react significantly (D42). The accelerating effect is probably due mainly or entirely to the provision of additional nucleation sites on the flyash, and occurs with other fine powders (K50). A QXDA study showed that the aluminate and ferrite react more rapidly in the presence of flyash, but with

belite there was no detectable effect up to 28 days and a marked reduction in rate of consumption thereafter (D15).

Figure 9.3 shows typical results for the contents of CH in interground cements containing various proportions of flyash. At early ages, the CH content, referred to the mass of clinker, increases with increasing proportion of flyash due to the acceleration of the alite reaction, but at later ages it decreases due to the pozzolanic reaction. The decreases would, of course, be greater if the CH contents were referred to the total ignited mass, including the flyash.

SEM (H61) showed that the glass in one flyash cement was heavily etched after 7 days and that many of the particles up to 1–2 $\mu$m in size were consumed within 28 days. The crystalline phases appeared to be inert. A QXDA study of another flyash cement (D15) confirmed an earlier report (K48) that the ratio of mullite to quartz does not change on hydration, and supported the view that the crystalline phases in flyash do not react significantly within 1 year. In contrast, a TEM study (R53) of a 1-year-old specimen indicated that some, at least, of the quartz reacts at a rate comparable to that of the glass.

Quantitative data on the rate of consumption of flyash are few and somewhat variable. Those based on differences between the CH contents of pure Portland and flyash cements are suspect, because the calculation involves the effects of flyash substitution both on the rate of consumption of the clinker phases and on the compositions of the products, which are not fully understood. Unreacted flyash has been directly determined by dissolution of the other phases with HCl (C51) or with salicylic acid in methanol followed by HCl (T39), chemical separation of the residual flyash followed by QXDA determination of its content of crystalline

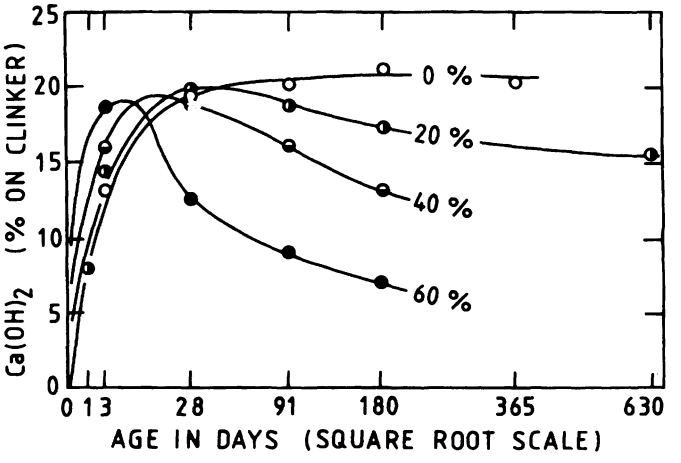


**Fig. 9.3** *Calcium hydroxide contents of pastes of Portland–flyash cements containing 0, 20, 40 and 60% of low-CaO flyash. From T39.*

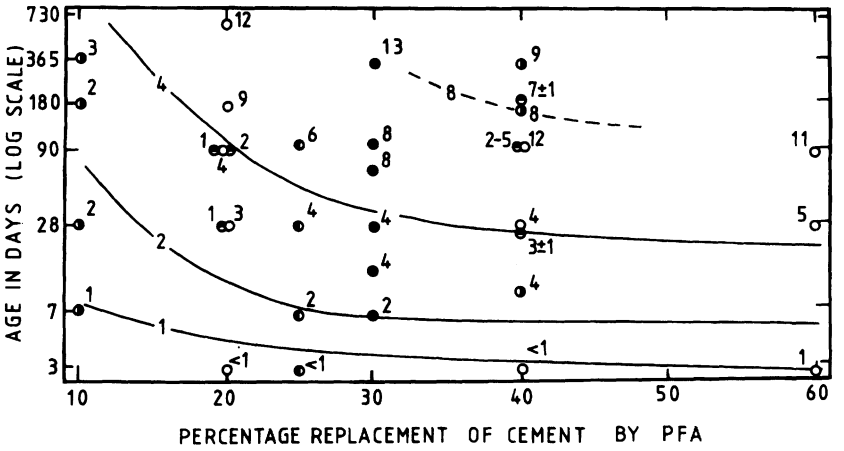


**Fig. 9.4** *Degrees of reaction of low-CaO flyash in pastes of Portland–flyash cements hydrated at 15–25°C. Numbers beside points denote g of flyash reacted per 100 g of composite cement at the indicated age and percentage of flyash in the composite cement. The curves of equal quantity of flyash reacting are based on the more typical of the results. Sources of data:* ◑ *(K49,K51);* ○ *(T39);* ◓ *(U18,U20);* ◐*(C51);* ● *(D15).*

phases (D15) and a trimethylsilylation method (U20). A method based on EDTA extraction was found unsatisfactory (L48).

Figure 9.4 shows results from several investigations on flyash cements at or near 20°C. The tentative curves of equal mass of flyash reacted are based on the more typical of the data. Such curves are necessarily U-shaped if extended over the entire range of flyash content from 0 to 100%. The discrepancies between the results of different investigations, which are especially marked at the later ages, probably arise partly from experimental errors and partly from differences in the reactivity of the flyash or the conditions under which it was used. It is difficult, however, to reconcile the higher values shown with the amounts of CH present on any reasonable assumptions concerning the stoichiometry (Section 9.3.5).

Of the flyash characteristics that influence reactivity, the glass content appears to be much the most important, but specific surface area, glass composition and the effect of stress in the glass caused by the crystalline inclusions may also be relevant (U18). Of external factors, the RH, temperature (C51) and alkali content of the cement are probably the most important. Sulfate ion may also enhance reactivity by promoting the removal of $Al^{3+}$ from the glass (U18). The rates of the pozzolanic reaction and of strength development are more sensitive to temperature than are those of hydration and strength development for pure Portland cements (e.g. H62).

### *9.3.4 Microstructure and compositions of the hydration products*

Backscattered electron and X-ray images obtained in the SEM (O23,S36, U18) show that the microstructures of hardened pastes of cement or $C_3S$

with flyash broadly resemble those of pure Portland cements, though, as would be expected, there is considerably less CH. Reaction rims may be seen around the flyash particles in sufficiently old pastes.

The hydrated material has been analysed by X-ray microanalysis and analytical electron microscopy. In a 3-day-old paste, that formed in situ from alite or belite did not differ significantly in composition from the corresponding product in pure Portland cement pastes (H4), but at later ages Ca/Si is lower and Al/Ca higher (R35,R36,R53,T39,U18,U19). Ca/Si is typically about 1·55, but the value decreases with age and ratio of flyash to clinker. Uchikawa (U18,U21) reported a value of 1·01 for a 4-year-old paste with 40% replacement of cement by flyash. Several of the studies (R35,T39,U18,U21) showed that the C–S–H was higher in alkalis if flyash was present, but one cannot tell to what extent K or Na apparently present in the C–S–H has been deposited from the pore solution on drying. For material close to the flyash particles in a 10-year-old mortar, Sato and Furuhashi (S106) found a Ca/Si ratio of 1·1–1·2.

For the microstructure as a whole, a general impression of compositions can be obtained by plotting the Al/Ca ratios of individual spot analyses against the Si/Ca ratios, as for Portland or slag cement pastes (Fig. 9.5; compare Figs. 7.6 and 9.1). For the paste to which Fig. 9.5 relates, the inner product of the alite or belite had mean Si/Ca = 0·61 (Ca/Si 1·63) and

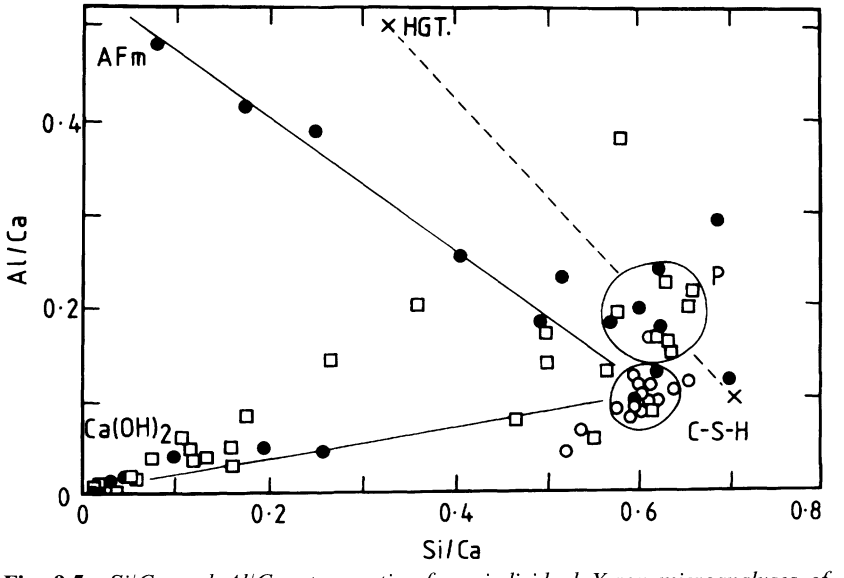


**Fig. 9.5** *Si/Ca and Al/Ca atom ratios from individual X-ray microanalyses of a 91-day-old paste of a Portland–flyash cement (28% of a flyash low in CaO; w/s = 0·5). Open circles, inner product from alite or belite; open squares, regions near to flyash particles, and sometimes also to CH; solid circles, undesignated product. P: suggested composition of inner product from flyash, possibly consisting largely of C–S–H and hydrogarnet (HGT). Modified from H4.*

mean Al/Ca = 0·10, with small contents of sodium, magnesium, sulfur, potassium and iron (H4). The space resolution obtainable with a polished surface does not allow reliable analysis of the material formed in situ from the flyash. Material near the flyash particles was often found to include CH; where this was not present, the analyses suggested mean Si/Ca ≈ 0·62 and mean Al/Ca ≈ 0·18. The analyses in this group were notably high in K and S (K/Ca 0·04–0·06, S/Ca 0·04–0·07). Some relatively large crystals of AFm phase found in a 6-month-old paste had compositions broadly intermediate between monosulfate, monosilicate and $C_4AH_x$.

Rodger and Groves (R53) studied ion-thinned sections of a $C_3S$–flyash paste by TEM, including microanalysis and diffraction. Most of the unreacted flyash particles consisted of impure alumina–silica glass, sometimes with inclusions of mullite. Some were of nearly pure silica glass, with or without quartz, or of iron oxides. In a 1-year-old paste, a typical alumina–silica particle about 12 $\mu$m in diameter had developed a reacted zone some 800 nm thick and consisting largely of radially fibrillar material described as C–S–H, with denser regions of hydrogarnet and a denser, outer rim of C–S–H. The hydrogarnet had a cell parameter of 1·24 nm and composition $C_{12}A_3FS_4H_{16}$. The C–S–H in the reacted zone had Si/Ca 0·70, Al/Ca 0·20 and Fe/Ca 0·14; that in the rim had Si/Ca 0·68, Al/Ca 0·09 and Fe/Ca 0·05. Both contained small amounts of potassium, sodium, magnesium, titanium, sulfur and other elements. Surprisingly, hydrogarnet was also observed in the reacted zones of flyash particles consisting of almost pure silica. It was suggested that these provided favourable nucleation sites, as the aluminium and iron must have come from outside. Concentric bands of differing apparent density within the reacted zones were sometimes observed, and had possibly formed by a Liesegang ring mechanism.

TMS evidence shows that silicate anion condensation occurs more rapidly in $C_3S$–flyash pastes than in pure $C_3S$ pastes. Mohan and Taylor (M93) found that at 1 year, about 60% of the silicon (excluding that in unreacted flyash) was present as polymer in the former case and 40% in the latter. Uchikawa and Furuta (U10) reported data showing ratios of silicon present as polymer to that present as dimer of 0.56 for a plain $C_3S$ paste 180 days old and of 0·80 for one containing flyash. These results agree with the evidence on C–S–H composition.

### 9.3.5 *Stoichiometry of flyash cement hydration*

The available data are probably too scanty and uncertain to justify any detailed discussion. Tentative calculations (T39) suggested that the amounts of flyash reacting, as shown in Fig. 9.4, are, in the main, compatible with the decreases in CH content (Fig. 9.3) and in the mean Ca/Si ratio of the C–S–H. The $SiO_2$ released from the flyash is used up, partly in lowering the Ca/Si ratio of the C–S–H formed from the Portland cement, and partly in forming additional C–S–H. $Al_2O_3$ released from the flyash is used in increasing the Al/Ca ratio of the C–S–H formed from the Portland cement and in the pozzolanic reaction; some probably enters additional AFm or hydrogarnet phases.

As with the slag cements discussed in Section 9.2.7, the water contents of flyash cements are lower for any specified drying condition than for comparable plain Portland cement pastes. Diamond and Lopez-Flores (D53) found that, for two 90-day-old pastes (30% flyash, w/s = 0·5), the non-evaporable water contents were 12·5% and 13·0%, while that of a Portland cement paste was 15·4%. Mass-balance calculations lead to a similar conclusion (T39).

### *9.3.6 The nature of the pozzolanic reaction*

The primary reaction of any pozzolanic material is an attack on the $SiO_2$ or $Al_2O_3$–$SiO_2$ framework by $OH^-$ ions. It may be supposed that the $OH^-$ ions attach themselves to silicon and other network-forming atoms, with consequent breaking of bonds between the latter and oxygen atoms. After this has occurred several times, the silicate or other oxy anion is detached from the framework. It may either remain in situ or pass into the solution. The charges of those that remain are balanced, partly by $H^+$, and partly by metal cations. Since a cement pore solution is essentially one of alkali hydroxides, the immediate product is likely to be an amorphous material with $K^+$ and $Na^+$ as the dominant cations, but the more abundant supply of $Ca^{2+}$ and the lower solubility of C–S–H and hydrated calcium aluminate or silicoaluminate phases will ensure that this is only an intermediate product. Its presence is indicated by the relatively high potassium contents observed in or near the reacting flyash particles.

The products formed in situ from the pozzolanic material are likely to reflect its composition and the situation in which $SiO_2$ and $Al_2O_3$ are readily available compared with CaO. One therefore expects to find C–S–H of low Ca/Si ratio, together with strätlingite or hydrogarnet or both. The compositions represented in Fig. 9.5 could arise from mixtures consisting largely or wholly of C–S–H and a hydrogarnet similar in composition to that found by Rodger and Groves (R53).

## 9.4 Natural pozzolanas

### *9.4.1 Properties*

Most natural pozzolanas are of volcanic origin, though some are sedimentary. Some clays and other materials that are unsuitable for use in concrete in their natural state become usable as pozzolanas if heat-treated. Both natural pozzolanas and heat-treated materials have been used with lime since ancient times, but today they are mainly used as constituents of pozzolanic cements. Several reviews are available (M94–M96).

The volcanic deposits range from unconsolidated materials to ones showing varying degrees of compaction and chemical alteration. The consolidated ones are called tuffs. Not all such materials are pozzolanic; the usual active constituents are glass high in silica and often highly porous, or zeolites, or both. Italian pozzolanas, Santorin Earth (from Greece) and some rhyolites (e.g. from the USA) are examples of poorly consolidated deposits, and trass (from Germany) is one of a tuff. Some of these materials include varying proportions of inactive minerals

(e.g. quartz, felspars, pyroxenes, magnetite) that are harmless. Others contain constituents, such as organic substances or clays, that interfere with setting or strength development. Zeolites or minerals of related types that are found in natural pozzolanas include analcime, leucite, chabazite, phillipsite and clinoptilolite. The last of these occurs in substantial quantities virtually pure. Zeolites are readily synthesized by mild hydrothermal treatment of starting materials of appropriate composition, and their formation as alteration products of volcanic glasses during cooling is easily understandable.

Diatomaceous earth is composed of the siliceous skeletons of microorganisms. It is pozzolanic, but its use in concrete is much restricted by its very high specific surface area, which greatly increases the water demand. Some clays react significantly with lime at ordinary temperatures, but while this property can be of value for soil stabilization, their physical properties preclude their use in concrete. Many clay minerals yield poorly crystalline or amorphous decomposition products at 600–900°C (Section 3.3.2), and if the conditions of heat treatment are properly chosen, these have enhanced pozzolanic properties. Heat-treated clays, including crushed bricks or tiles, can thus be used as pozzolanas; in India, they are called surkhi. Other examples of natural rocks that have been used as pozzolanas, usually after heat treatment, include gaize (a siliceous rock containing clay minerals found in France) and moler (an impure diatomaceous earth from Denmark). The heat-treated materials are called 'artificial pozzolanas', and this term is sometimes used more widely to include flyash.

Table 9.5 gives the chemical compositions of some natural pozzolanas. Many of the volcanic materials are not grossly different in composition from typical low-lime flyash, which they also resemble in having a glass high in $SiO_2$ and $Al_2O_3$ as a major active constituent. They differ in having zeolites as an additional active constituent and in their microstructure and physical properties. Some of the natural pozzolanas have high ignition losses, due wholly or partly to the presence of zeolites.

### 9.4.2 Hydration reactions

Early studies, reviewed by Malquori (M94), showed that natural pozzolanas take up CH, including that produced by Portland cement, with the formation of products similar to those formed on hydration of the latter material. They also showed that the zeolites present in many of them were at least as reactive in this respect as the glassy constituents. Zeolites are cation exchangers, but the amounts of CaO they take up are much greater than can be thus explained; moreover, cation exchange could not explain the development of strength that occurs on mixing with lime and water. It could be the initial process, but the main reaction is one in which the aluminosilicate framework of the zeolite is destroyed and C–S–H and hydrated aluminate phases are formed. The broad similarity between the chemical and phase compositions of many natural pozzolanas and flyashes suggests that one might expect to obtain similar products, though not necessarily the same rates of reaction.

**Table 9.5** *Chemical compositions of some natural pozzolanas*

| | $Na_2O$ | MgO | $Al_2O_3$ | $SiO_2$ | $K_2O$ | $SO_3$ | CaO | $Fe_2O_3$ | Loss | Total |
|---|---|---|---|---|---|---|---|---|---|---|
| Sacrofano (Italy) | | | 3·05 | 89·22 | | 2·28 | 0·77 | 4·67 | | 99·99 |
| Bacoli (Italy) | 3·08 | 1·2 | 18·20 | 53·08 | 0·65 | 7·61 | 9·05 | 4·29 | 3·05 | 100·24 |
| Segni (Italy) | 0·85 | 4·42 | 19·59 | 45·47 | 6·35 | 0·16 | 9·27 | 9·91 | 4·03 | 100·05 |
| Santorin Earth | 3·8 | 2·0 | 13·0 | 63·8 | 2·5 | | 4·0 | 5·7 | 4·8 | 99·6 |
| Rhenish Trass | 1·48 | 1·20 | 18·29 | 52·12 | | 5·06 | 4·94 | 5·81 | 11·10 | 100·00 |
| Rhyolite pumice | 4·97 | 1·23 | 15·89 | 65·74 | 1·92 | | 3·35 | 2·54 | 3·43 | 99·07 |

From a compilation in M95.

Strätlingite ($C_2ASH_8$; Section 6.1.4) was first synthesized by reaction between CH and metakaolin in suspensions at ordinary temperature (Z11). Depending on the composition and conditions, similar reactions of natural pozzolanas can yield, besides C–S–H, strätlingite, hydrogarnet or $C_4AH_x$. Sersale and Orsini (S107) studied the reactions of herschelite (a synonym for chabazite; $KNa(Si_4Al_2O_{12})\cdot 6H_2O$ approx.), analcime ($Na(AlSi_2O_6)\cdot H_2O$ approx.) and some natural pozzolanas, synthetic glasses and blastfurnace slag glasses with saturated CH solution in suspensions at ordinary temperature. In all cases, substantial amounts of CaO were removed from the solution, and XRD showed that C–S–H and one or more hydrated aluminate phases had been formed. In many cases, the presence of a 0·167 nm peak showed that the C–S–H was more specifically C–S–H(I).

Except with the slag glasses, the aluminate phase most often formed in these reactions was strätlingite. When it was not found, $C_4AH_{13}$, $C_4A\bar{C}H_{11}$ or hydrogarnet was usually detected. Sersale and Orsini considered that high concentrations of $SiO_2$ and $Al_2O_3$, which might arise through the presence of alkalis, favoured the formation of strätlingite and that high concentrations of CaO and $Al_2O_3$ favoured that of hydrogarnet; $C_4AH_{13}$ was formed from glasses high in $SiO_2$ and low in $Al_2O_3$. The reactions of the natural pozzolanas with CH in pastes were also examined. In all cases, the products were C–S–H, strätlingite and $C_4AH_{13}$ or $C_4A\bar{C}H_{11}$. In agreement with earlier results, the natural and synthetic glasses, tuffs and pure zeolites were found to be of comparable reactivity.

Costa and Massazza (C52) concluded from a study of natural pozzolanas of varied types that reactivity in mixtures with CH at w/s = 2 and 40°C depends during the first 28 days on the specific surface area and at later ages on the contents of $SiO_2$ and $Al_2O_3$ in the active constituents. A comparative study of five natural pozzolanas and three low-CaO flyashes in pastes with cement showed that the CH contents of the pozzolanic cements were considerably lower than those of the flyash cements at 3–60 days, but virtually the same at 90 days, the pozzolanas thus appearing to react more rapidly than the flyashes at early ages but more slowly later. Determinations of the unreacted mineral addition in pastes with CH showed that at 90 days 23–30% of the natural pozzolana had reacted, compared with 11–15% for the flyashes. The similarity in CH contents suggests, however, that these values may not apply to mixtures with cement.

X-ray microanalyses of $C_3S$-pozzolana pastes showed a gradual decrease in Ca/Si ratio on passing from regions near the unreacted $C_3S$ to ones near the pozzolana (O23). TMS studies of pastes of $C_3S$, $\beta$-$C_2S$ and cement with and without natural pozzolanas (M57,U10) showed that, in the presence of the latter, formation of polymeric anions is accelerated and their mean molecular weight is increased. TMS results and determinations of combined water showed that the hydration of $\beta$-$C_2S$ is almost completely suppressed in the presence of a pozzolana and that, in pastes with $C_3S$, 16–29% of the pozzolana had reacted in 180 days (M57). The effect on $\beta$-$C_2S$ hydration is similar to that found using

QXDA for flyash (D15). Chemical extraction showed 10–45% of the pozzolanas in pastes with $C_3S$ to have reacted in 28 days, compared with under 10% for a flyash (U10).

## 9.5 Silica fume (condensed silica fume, microsilica)

### *9.5.1 Properties*

Silica fume is a by-product of the production of silicon or silicon alloys by reducing quartz in an electric furnace. Some SiO is lost as a gas and is oxidized by the air, giving a very finely particulate solid. The material may require some beneficiation. High-quality silica fume consists of spherical particles of glass, typically around 100 nm in diameter, and has a $N_2$ specific surface area of 15–25 $m^2 g^{-1}$ (H63). Table 9.6 gives chemical compositions. The material formed in making elementary silicon typically contains 94–98% $SiO_2$, but for that formed in making the alloys 86–90% $SiO_2$ is more usual. The true density is about 2200 $kg m^{-3}$ but the bulk density of the freshly filtered powder is only 200 $kg m^{-3}$. This makes the material difficult to handle unless it is agglomerated into nodules or used as a slurry.

A comparative study of silica fumes from 18 sources showed considerable variation in composition and properties, one of those examined containing as little as 23% of $SiO_2$ and having a specific surface area of only 7·5 $m^2 g^{-1}$ (A25). The same study showed that in most of the samples the diffuse XRD peak from the glass accounted for 95–99·5% of the total diffracted intensity and that it peaked at the value of 0·405 nm characteristic of vitreous silica. The commonest crystalline impurities detected were KCl, quartz, metallic iron and iron silicide, and pozzolanic reactivity was found to depend more on the chemical composition and nature of impurities than on the fineness or $SiO_2$ content. A surface layer of carbon, if present, greatly decreased reactivity. Another study (D54) showed that many samples contained much larger particles, or agglomerates that were not readily broken up, and which could give rise to alkali silica reaction (Section 12.4) if used in concrete. The remainder of this section relates to silica fume that is free from such defects. Some studies on other highly reactive forms of silica are also considered here.

Viewed as a mineral addition in concrete, good-quality silica fume is characterized by its small particle size and high pozzolanic activity. In the

**Table 9.6** *Chemical compositions of silica fume from the production of elementary silicon and 75% ferrosilicon alloy (H63)*

| | Si | 75% Fe–Si | | Si | 75% Fe–Si |
|---|---|---|---|---|---|
| $SiO_2$ | 94–98 | 86–90 | $K_2O$ | 0·2–0·7 | 1·5–3·5 |
| $Al_2O_3$ | 0·1–0·4 | 0·2–0·6 | $Na_2O$ | 0·1–0·4 | 0·8–1·8 |
| $Fe_2O_3$ | 0·02–0·15 | 0·3–1·0 | C | 0·2–1·3 | 0·8–2·3 |
| MgO | 0·3–0·9 | 1·0–3·5 | S | 0·1–0·3 | 0·2–0·4 |
| CaO | 0·08–0·3 | 0·2–0·6 | Loss | 0·8–1·5 | 2·0–4·0 |

absence of a water-reducing admixture, the percentage replacement of cement is probably effectively limited by the high water demand to about 5%, but this can be increased by adding superplasticizers. By lowering the w/s ratio in such mixes to 0·2–0·3, concretes with high compressive strengths can be obtained (A26). Bleeding is also reduced. With special mixes and processing conditions, compressive strengths of up to 270 MPa have been obtained (Section 11.9).

The incorporation of silica fume in concrete has several effects, of which its strong pozzolanic property is only one. It accelerates the reactions of the clinker phases. The fine particles fill spaces between clinker grains, thereby producing a denser paste. It also densifies the interfacial transition zone between cement paste and aggregate; this increases the strength and lowers the permeability.

### 9.5.2 *Hydration reactions*

Traetteberg (T52) showed that silica fume used as an addition with cement has considerable pozzolanic activity, mainly in the period 7–14 days after mixing, and that the reaction product formed with CH probably had a Ca/Si ratio of about 1·1. Several subsequent studies have shown that the pozzolanic reaction is detectable within hours and also that the early reaction of the alite is accelerated (H42,H64,H65). Huang Cheng-yi and Feldman (H64,H65) studied the hydration reactions in some detail. In pastes with 10% or 30% replacement and w/s ratios of 0·25 or 0·45, the CH content passed through maxima usually within the first day before beginning to decrease; in those with 30% replacement, it had reached zero by 14 days. Table 9.7 gives some of the results obtained for CH content and non-evaporable water in these pastes. As with flyash cements, the non-evaporable water contents of mature pastes are considerably lower than those of comparable pastes of pure Portland cements.

**Table 9.7** *Contents of calcium hydroxide and non-evaporable water in some pastes of Portland cement with and without silica fume (percentages on the ignited mass) (H65)*

| Mass ratios in mix | | | Maximum in CH content | | Contents at 180 days (mass %) | |
|---|---|---|---|---|---|---|
| Cement | Silica fume | Water | Mass % | Age (days) | CH | Non-evaporable water |
| 1·0 | – | 0·45 | | | 16·2 | 20·7 |
| 0·9 | 0·1 | 0·45 | 11·2 | 10 | 8·3 | 15·5 |
| 0·7 | 0·3 | 0·45 | 5 | 1 | 0·0 | 15·3 |
| 1·0 | – | 0·25 | | | 10·4 | ~14·5 |
| 0·9 | 0·1 | 0·25 | 7·2 | 1 | 2·2 | ~11·2 |
| 0·7 | 0·3 | 0·25 | ~2 | 1 | 0·0 | ~12·5 |

The most satisfactory method for determining the degree of reaction of the silica fume appears to be $^{29}Si$ NMR, using the area of the $Q^4$ peak. Using this method, Sun and Young (S108) found degrees of reaction in ultra-high strength cement pastes of 9–15% at 1 day, increasing to 55–59% at 180 days. The percentages reacted did not show any clear dependence on the content of silica fume in the unhydrated cement within the range of 18–48% that was studied.

X-ray microanalyses and mass-balance calculations show that the mean Ca/Si ratio of the C–S–H decreases markedly as the content of silica fume or other forms of highly reactive silica increases, typically to values of 1·3–1·4, falling to about 0·9 when all the CH has been consumed or in regions where it is inaccessible (A27,D55,G86,L51,R36,R54,U13). Dobson *et al.* (D55) studied pastes of $C_3S$ and finely divided silica by TEM microanalysis. The inner product of the $C_3S$ had a Ca/Si ratio of 1·6, but the paste contained areas with Ca/Si 0·92. These could have formed by complete reaction of regions of aggregated silica particles. Studies by $^{29}Si$ NMR show that the rate of polymerization of the silicate anions in the C–S–H is markedly increased in the presence of reactive silica (A28,D55,G86,H66,J35,L51,Y6). For $C_3S$ pastes at an age of 28 days, Dobson *et al.* (D55) found the mean chain length to be 2·3 tetrahedra in the absence of reactive silica and 3·6 tetrahedra in its presence. The anions remained linear, with no cross-linking. Brough *et al.* (B134) reported an NMR study using $C_3S$ and reactive $SiO_2$ enriched in $^{29}Si$. The C–S–H that contained silicon atoms supplied by the pozzolana was slightly more ordered than that formed entirely from the $C_3S$, and the mean length of its silicate chains was greater. It contained no monomeric silicate. Silica fume is reported to favour the formation of AFt phase as opposed to AFm (A27).

## 9.6 Other mineral additions

### *9.6.1 Class C flyash*

Flyash formed on burning lignite or sub-bituminous coal is typically higher in CaO, MgO and $SO_3$, and lower in $SiO_2$ and $Al_2O_3$, than the low-CaO materials described in Section 9.3. Bulk chemical compositions vary widely (Table 9.8). Flyash with less than 70% ($SiO_2 + Al_2O_3$), and thus normally high in CaO, is termed Class C flyash in the USA. Some by-products of modern coal-burning technologies, designed to lower $SO_2$ and $NO_x$ emissions, are also high in CaO and $SO_3$ and have broadly similar properties (O24,S110).

As with flyash low in CaO, fine, spherical particles consisting largely of glass are the dominant constituent, but the glasses are higher in CaO. Diamond (D56) found a linear relation between the position of the glass peak in the XRD pattern and the content of CaO in the bulk analysis. This is consistent with observations on other glasses that the peak position moves to higher angles as the proportion of network modifiers increases, but the peak position does not depend only on the bulk composition because varying amounts of CaO are usually present in the crystalline phases (D57)

**Table 9.8** *Chemical compositions of some flyashes high in CaO (S109)*

| Origin | $Na_2O$ | MgO | $Al_2O_3$ | $SiO_2$ | $SO_3$ | $K_2O$ | CaO | $Fe_2O_3$ | Loss | Total |
|---|---|---|---|---|---|---|---|---|---|---|
| Montana, USA | 0·2 | 6·8 | 20·3 | 35·2 | 1·1 | 0·5 | 25·0 | 6·3 | 0·3 | 95·7 |
| North Dakota, USA | 7·3 | 7·9 | 12·5 | 30·2 | 9·6 | 0·6 | 23·6 | 4·6 | 1·8 | 98·1 |
| North Dakota, USA | 5·4 | 5·5 | 10·7 | 27·9 | 12·3 | 1·5 | 21·6 | 9·9 | 1·4 | 96·2 |
| Saskatchewan, Canada | 6·1 | 2·9 | 21·9 | 47·9 | 1·1 | 1·0 | 13·3 | 4·9 | 0·1 | 99·2 |

The particles of coal burn essentially independently of each other, and are likely to vary both in the nature and the relative amounts of the inorganic constituents and in the heating and cooling regime; this is likely to produce wide variations in the bulk chemical and phase compositions of individual flyash particles (D58). Two types of glass, differing in CaO content, can be concentrated by density separation, and the diffuse XRD peaks in general result from overlap of contributions from these two constituents (H67).

Crystalline material is present in higher proportion than in Class F flyashes and includes phases that react with water as well as ones that are inert. In a study of 27 ashes from the western USA, McCarthy *et al.* (M97) found that quartz, lime, periclase, anhydrite and a ferrite spinel were ubiquitous or nearly so. Other crystalline phases present in some cases or in minor amounts included $C_3A$, merwinite, alkali sulfates, melilites, mullite, sodalite and possibly others. The principal reactive phases are the glass, anhydrite and lime (M97,S110).

Diamond and Lopez-Flores (D53) found that at ages of 1 h to 30 days, 30% replacements of a Portland cement by any of three different high-CaO ashes produced only small decreases in the content of non-evaporable water. This contrasts with their observations on low-CaO ashes (Section 9.3.5). The non-evaporable water content depends mainly on the amount of CaO in the hydration products, and the observation thus suggests that the hydration of the high-CaO ashes occurs at a rate comparable with that of the clinker phases. Grutzeck *et al.* (G87) examined some pastes made using a high-CaO flyash and a coarsely ground Portland cement by XRD and SEM. The hydration products detected at ages of 3–56 days were essentially those given by pure Portland cements at similar ages, with the addition in all cases of strätlingite and, at 3 days, a trace of $C_2AH_8$. The SEM showed that the particles of flyash glass were replaced in situ by radial growths of fibrous C–S–H. These were barely detectable at 3 days but reaction was seen to be well advanced by 7 days. The formation of $C_2AH_8$ and strätlingite indicates substantial release of $Al_2O_3$ from the flyash, even at 3 days.

Many Class C flyashes and other coal conversion by-products set and harden on being mixed with water alone. The initial hydration products include ettringite, which can be formed in substantial amounts and appears to provide much of the early strength (S110). In some cases, marked loss of strength and increase in permeability subsequently occur, and are associated with formation of thaumasite (M98).

### 9.6.2 *Other pozzolanic or hydraulic additions*

The ash from burning of rice husks or some other agricultural wastes is high in $SiO_2$, and if burning is carried out under properly controlled conditions at 350–600°C the ground material is strongly pozzolanic (C53,J36,M99). The material thus formed consists largely of amorphous silica retaining the cellular microstructure of the original material and has a very high specific surface area. Its possible utilization in conjunction with CH or cement has received attention for reasons of economics and

energy conservation, and also because it can be used to make concrete that is very resistant to acid attack.

Rice husk ash has characteristics broadly similar to those of silica fume but can be even more strongly pozzolanic. A study of pastes made with $C_3S$ (K52) showed the CH content to pass through a maximum of 3% at 7 days, referred to the ignited mass; by 28 days, it had fallen to 1%. The hydration product was C–S–H with a mean Ca/Si ratio estimated at 1·3 by analytical electron microscopy, or 0·9–1·2 from the contents of CH and unreacted starting materials. There were indications that an initial product with a Ca/Si ratio of 0·1–0·2 was formed.

The nature and availabilities of specific industrial waste products may be expected to vary with changes in technology, including those resulting from depletion of existing sources of energy or raw materials or from increasing recognition of the need to reduce environmental damage and pollution. The new technologies for coal combustion that have already been mentioned are an example of this. Another example is provided by the Lurgi or other processess in which gaseous or liquid fuels are made from coal or lignite, which may become increasingly important as petroleum and natural gas are depleted (e.g. B135). In all these cases, residues are produced which, though of limited interest at present, could become major constituents of concrete at some future date. Some other waste materials, such as slags from production of steels or non-ferrous metals, are also of potential interest (R43).

### *9.6.3 Calcium carbonate and other mineral additions*

Composite cements may contain mineral additions other than, or as well as, ones with pozzolanic or latent hydraulic properties. These are widely described as 'fillers' but, at least in the case of limestone, which is the most important, this term is misleading because chemical reaction occurs. Regourd (R43) reviewed the use of this material, which is widely used in France in proportions up to 27%. The limestone is commonly inter-ground with the clinker, and because of its softness becomes considerably finer than the latter. For an overall specific surface area (Blaine) of $420\,m^2\,kg^{-1}$, 50% of the limestone can be below 700 nm, compared with 3 $\mu$m for the clinker. The effect on 28-day strength of partial replacement of clinker can be compensated by finer grinding of the clinker, and for equal 28-day strengths, the 1-day strength of a cement containing limestone can exceed that of one not containing it. This is due to the greater fineness of the clinker and the effects of the limestone.

The effects of the limestone are partly physical and partly chemical. As with many other finely divided admixtures, including flyash, the hydration of the alite and aluminate phases is accelerated. Because of its fineness, the material also acts as a filler between the grains of clinker, though it is unlikely to be as effective in this respect as silica fume. Chemically, the formation of monocarbonate ($C_4A\bar{C}H_{11}$) is well established (B136,I12,K53,R43). One would also expect that the replacement of ettringite by monosulfate would be inhibited (Section 7.1.2), and observations confirm that this is the case (B136,K53,V6). Klemm and Adams

(K53) found that ettringite was formed during the first 24 h and decreased in amount only slightly thereafter. Monocarbonate was detected after periods of 7–127 days, in amounts that appeared to depend on the amount and reactivity of the $CaCO_3$ present. This observation suggests that the assemblage of AFm and AFt phases produced may depend on the relative rates at which $SO_4^{2-}$, $Al(OH)_4^-$ and $CO_3^{2-}$ ions become avalable.

The maximum quantity of $CaCO_3$ that can react appears to be 2–3% with most cements, but values up to 5·8% have been reported (I12). The limit increases with the $C_3A$ content and with the proportion of limestone added. The $CaCO_3$ acts as a set-controlling agent, and can replace a substantial fraction of the gypsum.

The increased rate of reaction of the alite in the presence of limestone was demonstrated by light-microscopic and SEM determinations of unreacted clinker, SEM observations on the thickness of the zones of hydration product surrounding the alite, and XRD observations on relative contents of CH (G88). The presence of up to 25% of a filler does not greatly affect workability, but with highly reactive or finely ground clinkers there can be some acceleration of set (B137).

## 9.7 Pore structures and their relation to physical properties

### *9.7.1 Calculated porosities for pastes containing slag or flyash*

Calculations based on the mass percentages and densities of phases, similar to that outlined in Section 8.3.2 for a plain Portland cement paste, indicate that partial substitution of slag or flyash for Portland cement increases the porosity, however defined. Thus, for a 14-month-old paste of a typical ordinary Portland cement, with $w/c = 0{\cdot}5$, such a calculation gave capillary, free water and total porosities (as defined in Section 8.3.2) of 16%, 29% and 41% respectively (T38). For a similar paste in which 40% of the same Portland cement had been replaced by slag, the corresponding values were, respectively, 22%, 34% and 44% (H58). Broadly similar results are typically obtained for mature mixes containing 20% of flyash.

The dominant effect responsible for the higher porosities of pastes made from cements containing slag or flyash is the relatively low degree of reaction of the mineral addition. The effect increases with the percentage replacement and is especially marked at early ages. On the other hand, the increased proportion of C–S–H, and, for slag cements, of the hydrotalcite-type phase in the reaction products tends to lower the porosity. This effect can be dominant with silica fume or other highly reactive mineral additions.

### *9.7.2 Modelling of pore structure*

Bentz and Garboczi (B123) extended the model developed for the pore structure of $C_3S$ pastes (Section 8.3.3) to pastes containing inert and reactive mineral additions. With inert additions, the degree of hydration needed to lower the fractional connectivity of the capillary pores to any given value, including zero, was increased if the $C_3S$ was partially

replaced by the mineral addition. This effect is due to the decreased volume of hydration products. *Substitution* of inert material, however fine, for cement therefore does not lower the fractional connectivity at a constant degree of hydration. In contrast, *addition* of an inert material at a constant w/c ratio lowered the degree of hydration needed to lower the fractional connectivity to a given value. The curve relating the fractional connectivity of the capillary pores to the total capillary porosity that had been obtained for pure $C_3S$ pastes was maintained for pastes in which 10% of the $C_3S$ had been replaced by the inert addition.

Reaction of the CH formed on hydration of $C_3S$ with silica fume produces an increase in the solid volume, and with 10% replacement of $C_3S$ this led to a reduction in the degree of hydration needed to lower the capillary porosity and the fractional connectivity of the capillary pores to given values. At 20% replacement, not all the silica fume was considered to react, so that some of it acted as an inert diluent. The degree of hydration needed to achive pore discontinuity was still less than in a pure $C_3S$ paste, but less so than at 10% replacement. Chloride diffusivities calculated on the basis of the model were in reasonable agreement with experimental data (G80). At low w/s ratios and capillary porosities below 18%, transport through the C–S–H became important, and increase in the content of silica fume could further increase the relative diffusivity by replacing impermeable CH by C–S–H.

### 9.7.3 *Experimental determination of porosities and pore size distributions*

Studies on the pore structures of pastes of composite cements have presented difficulties, which probably arise from discontinuity of the pores. Mercury intrusion appears to alter the structure even more than with plain Portland cement pastes. The pastes of composite cements appear to contain relatively large but discontinuous pores, separated by walls that are broken by the mercury (D47,F39,F45,F46).

Some broad conclusions from mercury porosimetry may nevertheless be justified. Figure 9.6 compares curves obtained on first intrusion for pastes of Portland and composite cements. At early ages, the distribution of pore entry sizes in flyash or slag cement pastes is coarser than in comparable Portland cement pastes and the porosity recorded by the method at the maximum pressure is higher. This can be attributed to the relatively slow reaction of the mineral addition. At later ages, the distribution of pore entry sizes is finer than in comparable Portland cement pastes, and the curves do not tend to flatten out at high intrusion pressures. This suggests that, even at the highest attainable pressures, the mercury does not enter all the pore space.

For Portland cement pastes, mercury porosities agree with those obtained using helium except at low porosities, when they are lower (B138). For pastes containing flyash or silica fume, they tend to be higher than those obtained with either helium or alcohols (D47,F46,M100), presumably because the latter fluids cannot break into regions that are

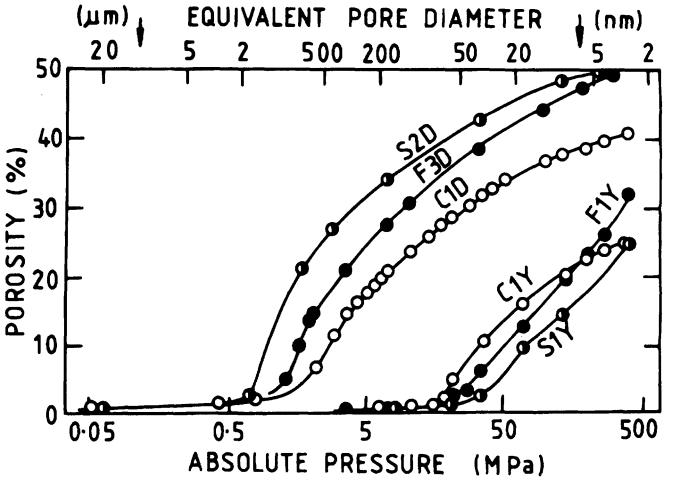


**Fig. 9.6** *Pore-entry size distributions for pastes of Portland and composite cements (w/s = 0·45, curing temperature 21°C), determined using mercury intrusion porosimetery. C1D, C1Y: Portland cement pastes cured for 1 day and 1 year. S2D, S1Y: Portland slag cement (70% slag) pastes cured for 2 days and 1 year. F3D, F1Y: Portland–flyash cement pastes (13% CaO in flyash) cured for 3 days and 1 year. After F38.*

blocked. For pastes containing silica fume, they are lower than those obtained by equilibration with water at 11% RH (F46). This supports the conclusion from the curves in Fig. 9.6 that mercury, even at high pressure, does not enter all the pore space. Feldman and Huang Cheng-yi (F46) concluded that in blends with silica fume a discontinuous pore structure was formed within 7 days.

Uchikawa *et al.* (U19) studied pastes of Portland and composite cements by $N_2$ sorption. In all cases, the pore size distributions peaked at 2 nm. Partial replacement of cement by slag increased the height of the peak, and partial replacement by flyash decreased it.

The most important conclusion from the data is that the capillary pores are markedly discontinuous in pastes made with slag or pozzolanic additions. The main reason for this is probably the lower Ca/Si ratio of the C–S–H, which causes it to have a more markedly foil-like morphology (Section 9.2.5). Much space is isolated between the foils and is inaccessible to fluids except under circumstances in which the microstructure is grossly damaged. This conclusion is strongly supported by backscattered electron images of pastes high in slag that had been intruded with a low-melting point metal, which was then dissolved away using an EDTA solution (R55). In the case of slag cements, the slag inner product appears also to contain much inaccessible porosity between lamellae of hydrotalcite-type material (F44). It is doubtful whether either mercury intrusion or sorption methods can give an accurate picture of the porosity or other characteristics of the pore system.

### 9.7.4 Relations between pore structure and physical properties

Feldman (F38) plotted the logarithms of compressive strength and Young's modulus against mercury porosity for a number of pastes, and extrapolated to zero porosity. For both quantities, the intercept at zero porosity was higher for flyash cements than for Portland cements. Slag cements also gave a higher intercept than Portland cements for Young's modulus, but the intercepts for strength were virtually identical. While the precise significance of the mercury porosities is uncertain, the results suggest that pastes of composite cements are less deformable for a given porosity than those of Portland cements and that flyash-cement pastes are also stronger. Feldman considered that this might be because the pastes of composite cements contained more C–S–H and less CH.

Partial replacement of Portland cement by a mineral addition greatly decreases the permeability to water provided the age is such that sufficient reaction of the addition has occurred. For a pastes with w/s 0·47 and 30% replacement of cement by flyash, cured at 20°C for 1 year, Marsh *et al.* (M101) found a permeability of $10^{-15.4}$ m s$^{-1}$; the corresponding paste of pure Portland cement had a permeability of $10^{-11.7}$ m s$^{-1}$. For the flyash-cement pastes, the decreases in permeability were found to run parallel to the consumption of CH in the pozzolanic reaction. The permeability is similarly decreased through the use of silica fume (H55), slag (M100,R56) or rice husk ash (M100). Its value has been correlated with pore size distribution (M100), but it is more likely to be related to the continuity of the pores (M101).

# 10 Calcium aluminate, expansive and other cements

## 10.1 Calcium aluminate cements

### *10.1.1 Introduction*

Calcium aluminate cements (CACs) are made from limestone or lime with bauxite or other aluminous material low in $SiO_2$. Their properties include rapid strength development, good resistance to sulfates and many other forms of chemical attack, and, when used with refractory aggregates, effectiveness for making refractory concrete. Their setting times are similar to those of Portland cements, but if mixed with Portland cement, alone or with slaked lime (CH) or additional gypsum, they can be used to make rapid-setting mixtures for grouting and similar applications. Other uses are as constituents of expansive (Section 10.2) and MDF (Section 11.9.3) cements. Due to their rapid hydration, heat evolution during the first day can be high, rendering them useful for low-temperature applications. In order to obtain high strengths and good durability, certain conditions must be strictly observed, including low w/c ratio ($< 0{\cdot}4$), high cement content in the concrete ($> 400\,kg\,m^{-3}$) and absence of alkaline contaminants; non-observance of these conditions has caused failures. CACs have been termed aluminous or high-alumina cements, but the former term is less specific and the latter is more appropriately used for white CACs made using purified alumina. The cements described here are those manufactured in France and the UK. They comprise Ciment Fondu, made using bauxite, and the white cements mentioned above. Those made elsewhere are similar in essential respects.

### *10.1.2 Manufacture; chemical and mineralogical compositions*

Ciment Fondu is normally made by complete fusion of limestone and bauxite at 1450–1600°C. In order to produce a cement with the desired rapid-hardening properties, both raw materials must be low in $SiO_2$. The molten clinker is tapped off continuously from the furnace, solidifies and is typically crushed and ground to a fineness of about $300\,m^2\,kg^{-1}$. Some iron is reduced to $Fe^{2+}$. The colour of cements produced from bauxite can vary from yellow-brown to black, but is commonly greyish black.

**Table 10.1** *Typical compositions of calcium aluminate cements (mass percentages)*

| Type of cement | $Al_2O_3$ | CaO | $Fe_2O_3$ + FeO | FeO | $SiO_2$ | $TiO_2$ | MgO | $K_2O$ + $Na_2O$ | $SO_3$ |
|---|---|---|---|---|---|---|---|---|---|
| Ciment Fondu | 38–40 | 37–39 | 15–18 | 3–6 | 3–5 | 2–4 | <1·5 | <0·4 | <0·2 |
| 40% Alumina | 40–45 | 42–48 | <10 | <5 | 5–8 | ~2 | <1·5 | <0·4 | <0·2 |
| 50% Alumina | 49–55 | 34–39 | <3·5 | <1·5 | 4–6 | ~2 | ~1 | <0·4 | <0·3 |
| 50% $Al_2O_3$ (low Fe) | 50–55 | 36–38 | <2 | <1 | 4–6 | ~2 | ~1 | <0·4 | <0·3 |
| 70% Alumina | 69–72 | 27–29 | <0·3 | <0·2 | <0·8 | <0·1 | <0·3 | <0·5 | <0·3 |
| 80% Alumina | 79–82 | 17–20 | <0·25 | <0·2 | <0·4 | <0·1 | <0·2 | <0·7 | <0·2 |

White CACs are usually made by sintering calcined alumina with quicklime (calcium oxide) or high-purity limestone.

Table 10.1 gives typical chemical compositions of commercially produced CACs. The essential compound in all of them, because it develops the main hydraulic activity and is consequently responsible for the strength development, is monocalcium aluminate, CA.

Most of the commercial white CACs contain CA and $C_{12}A_7$; those high in $Al_2O_3$ may also contain $CA_2$, $CA_6$ or $\alpha$-$Al_2O_3$. The crystal structures of these compounds and the phase equilibria relating to their formation were considered in Chapter 2. In the sintering process by which these cements are made, the reaction conditions are very important, as the products of a given mix can vary from a mixture of CA and $CA_2$ to the full range of phases in the CaO–$Al_2O_3$ system (S111).

In Ciment Fondu, most of the grains of the ground cement observable by backscattered imaging in the SEM are polymineralic (H68). Figure 10.1, which is of a mature concrete, includes some large, essentially unreacted grains. The major constituents are CA (medium dark) and ferrite (light). A white CAC had a broadly similar microstructure, with gehlenite and a little perovskite in place of the ferrite (S11). The texture indicates that, as would be expected from the phase equilibria (Section 2.2.2), CA is the first phase to crystallize.

Sorrentino and Glasser (S112) discussed qualitative and quantitative phase compositions of Ciment Fondu. Typically, CA makes up 40–50% of the material, and ferrite 20–40%. Other crystalline phases that can be present in various combinations include $C_{12}A_7$, $\beta$-$C_2S$, gehlenite, pleochroite, wüstite and perovskite; their individual contents are usually under 10% and often under 5%. A small proportion of glass is usually also present. The crystalline phases are mostly solid solutions. The CA contains up to about 5% of $Fe^{3+}$, expressed as $Fe_2O_3$, and a little Si (J37) The ferrite composition varies widely; Al/Fe ratios of 0·9–1·6 have been reported, with significant contents of Si and Ti (M102,R57). Gehlenite, when present in either Ciment Fondu or white CACs, seems always to be high in $Al_2O_3$ and low in $SiO_2$, possibly due to solid solution or random interlayering with $C_5A_3$ (S11) or pleochroite (S18).

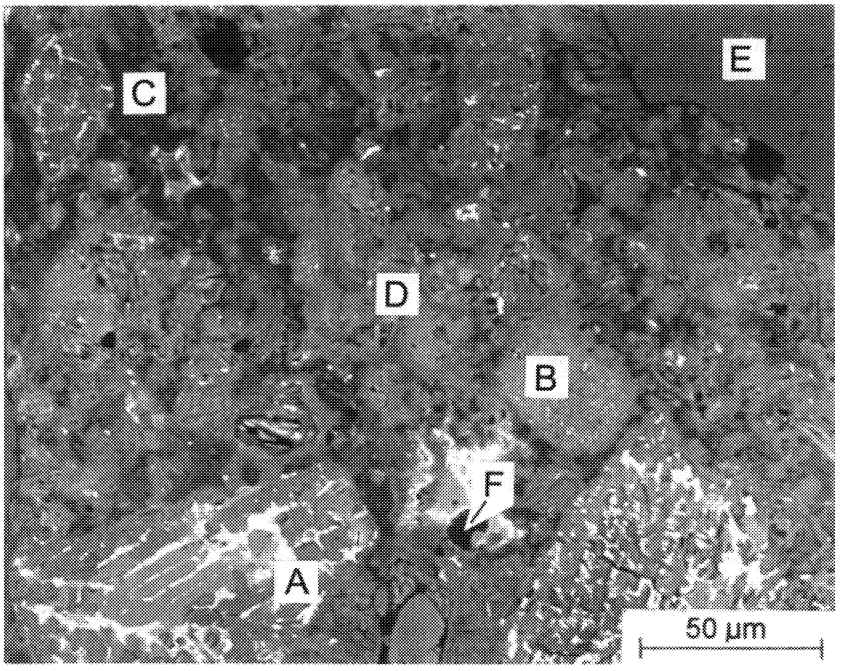


**Fig. 10.1** *Backscattered electron image of a 27-year-old Ciment Fondu concrete (total w/c 0·32); depth 10 mm beneath an external surface. A: a largely unreacted cement grain, consisting mainly of CA (medium dark) and ferrite (light). B: a cement grain that has reacted almost completely. C: $AH_3$. D: undesignated product, probably consisting mainly of $C_3AH_6$ and $AH_3$ mixed at or below micrometre level. E: aggregate. F: a pore. Courtesy M.C. Lewis and K.L. Scrivener (Imperial College, London).*

For compositions in the $CaO–Al_2O_3–Fe_2O_3–SiO_2$ system similar to those in Ciment Fondu under oxidizing conditions, the possible equilibrium assemblages of four solid phases are $CA–C_2S–C_2AS$–ferrite and $CA–C_2S–C_{12}A_7$–ferrite, where CA, $C_2AS$ and ferrite represent solid solutions (S113). Under mildly or moderately reducing conditions, either pleochroite or wüstite or both may also be present, the possible equilibrium assemblages of five solid phases being CA and ferrite together with (*a*) $C_2S$, $C_{12}A_7$ and pleochroite, (*b*) $C_2S$, $C_2AS$ and pleochroite or (*c*) $C_2AS$, pleochroite and wüstite (S114). These results imply that ferrite is always likely to be present and that $C_{12}A_7$ cannot coexist stably with $C_2AS$. Caution is needed in applying them to Ciment Fondu, because equilibrium is not necessarily reached, so that phase assemblages incompatible at equilibrium may occur.

Because of the complexity and variety of the possible phase assemblages, the wide ranges of solid solutions and departures from equilibrium arising from the nature of the manufacturing process, the calculation of

quantitative phase composition from bulk chemical analysis is difficult. Calleja (C54) obtained approximate solutions by omitting the FeO and other minor components and making suitable assumptions as to the compositions of the CA, $C_{12}A_7$ and $C_2AS$ phases. Sorrentino and Glasser (S112) also considered the effects of FeO and MgO and consequent formation of pleochroite and wüstite.

*10.1.3 Reactivities of the phases and methods of studying hydration*

In commercial CACs, the only phases that hydrate significantly at early ages are normally CA and, if present, $C_{12}A_7$. Some sintered cements made at relatively low temperatures also contain free lime or CH, which are very active in the hydration process. The reaction of $CA_2$, present in many white cements high in $Al_2O_3$, is very slow (B139), possibly because of gel formation.

In Ciment Fondu, the ferrite phase seems to play no significant part in early hydration at 20°C, but at 30–38°C over 80% can have reacted in 2 months (C55). The pleochroite seems to be unreactive. When $C_2S$ is present, silicate ions can be detected in the solution within a few minutes, but then disappear; it seems that precipitation occurs and further dissolution is inhibited. Unsubstituted $C_2AS$ does not react with water at ordinary temperatures, but the gehlenite present in a white CAC underwent substantial reaction at 40°C, perhaps due to the incorporation of $C_5A_3$ (S11). The $Na_2O$ and $K_2O$ present in CACs scarcely affect the solution equilibria at early ages, as their concentrations are very low (M103).

The hydration reactions have been widely studied using qualitative or quantitative XRD, determinations of solution compositions, thermal methods, conduction calorimetry and setting behaviour. Among the more recent studies may be noted those of Barret and Bertrandie (B99, B100), Cottin and George (C55), Rodger and Double (R58), Fujii *et al.* (F47), Bushnell-Watson and Sharp (B140,B141), Ménétrier-Sorrentino *et al.* (M104), Edmonds and Majumdar (E5–E7) and Capmas and Ménétrier-Sorrentino (C56). Other methods have included XRD using synchrotron radiation (R59,R60), neutron diffraction (C40), NMR (C57, M105,R61), TEM (C58,P49), SEM (B141,F47,H68,S11), IR (B142,P50) and Mössbauer (H69) spectroscopy, electrical properties (A29,G89,S115) and ultrasonic wave propagation (G90). These methods have been applied, according to their various characteristics, to mortars, pastes and suspensions.

*10.1.4 Hydration reactions and products*

The individual hydration products and relevant phase equilibria are described in Chapter 6. Sorrentino *et al.* (S115) reviewed hydration mechanisms. The major crystalline products formed from the calcium aluminates are $CAH_{10}$ at low temperatures, $C_2AH_8$ and $AH_3$ at intermediate temperatures and $C_3AH_8$ and $AH_3$ at higher temperatures (Fig. 10.2). With passage of time, the other products are replaced by $C_3AH_6$ and $AH_3$ at rates that depend on the temperature and other factors; this process is called conversion.

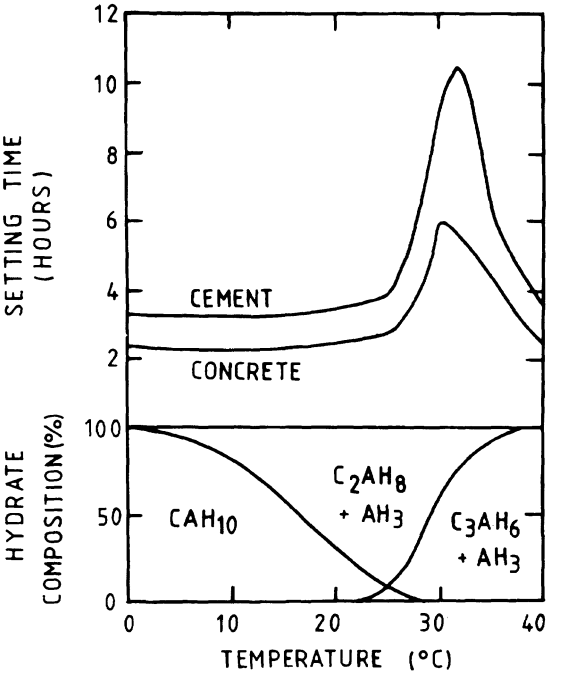


**Fig. 10.2** *Major hydration products and typical setting times for neat pastes and concretes of Ciment Fondu cured at various temperatures. From G91.*

Several investigators have reported the formation of additional, most probably amorphous products, (C57,E5–E7,F47,R61,S11). Using SEM with microanalysis, Scrivener and Taylor (S11) found an inner product of CA having Ca/Al 1·2–1·3. Using $^{27}Al$ NMR, Cong and Kirkpatrick (C57) found one or more intermediate hydration products. Those formed at or above 25°C contained 4-coordinated aluminium, which was attributed to a hitherto unreported intermediate phase. However, $C_2AH_x$ contains both 6- and 4-coordinated Al (R26). At 4°C, an intermediate product possibly containing 5-coordinated aluminium was detected. The relationships between the amorphous or intermediate products reported in the various investigations need further clarification.

In general, the results support LeChatelier's early conclusion that the hydration reactions occur by congruent dissolution followed by precipitation. Figure 10.3 shows the changes in the solution composition that occur when a typical Ciment Fondu reacts with water at 20°C, together with the metastable solubility curves for phases in the $CaO–Al_2O_3–H_2O$ system. The CaO and $Al_2O_3$ concentrations increase, at an approximately constant $CaO/Al_2O_3$ ratio somewhat greater than 1; in the experiment shown, $C_{CaO}$ reached 15 mmol $l^{-1}$ in 3 min and its maximum value of 21 mmol $l^{-1}$ in 1 h. A solid product is thus being precipitated,

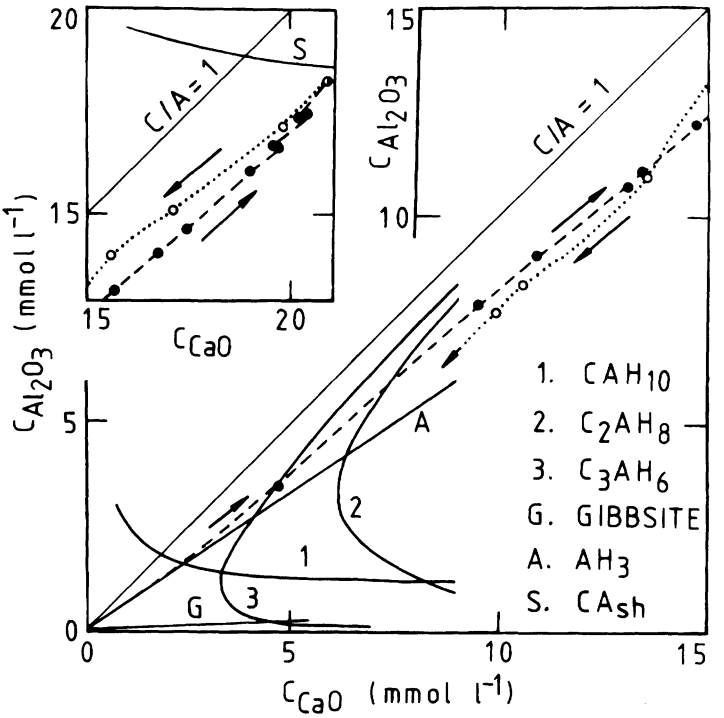


**Fig. 10.3** *The $CaO–Al_2O_3–H_2O$ system at 20°C, showing calculated solubility curves and typical path (broken and dotted lines) followed by the composition of the solution obtained on reaction of Ciment Fondu with water in a suspension with w/s = 10. $AH_3$ = poorly crystalline hydrous alumina; $CA_{sh}$ = superficially hydroxylated CA (see text). Courtesy A. Capmas and D. Sorrentino (Lafarge Corporation).*

and has a bulk $CaO/Al_2O_3$ ratio lower than 1. It has widely been regarded as alumina gel, but there are several indications that minor amounts of $C_2AH_8$ are also precipitated. SEM examination of products formed in suspensions shows the presence of foils, which could be of poorly crystalline $C_2AH_8$ (B143,M103) or of one of the amorphous phases noted in the previous paragraph. With some specimens of Ciment Fondu, the ascending curve shows minor arrests, during which $C_{CaO}$ decreases (C56,S115); two such are shown in Fig. 10.3, near $C_{CaO} = 20\,\text{mmol}\,l^{-1}$. These arrests are also manifested by temporary reversals in the generally increasing electrical conductivity (G89,M103). Determinations of bound water show, however, that the total amount of hydrated material is very small until the maxima in $C_{CaO}$ and $C_{Al_2O_3}$ are reached (B143,M103).

The subsequent course of the reaction, essentially as described by Capmas and Ménétrier-Sorrentino (C56), is as follows. An induction period occurs, during which the concentrations remain near their

maximum values, the rates of dissolution and precipitation thus being approximately equal. The products nucleate and grow; these processes begin slowly, but accelerate. Ultimately, precipitation is massive, the concentrations drop and, in a paste, setting occurs. In the experiment shown in Fig. 10.3, the concentrations began to decrease rapidly at about 2 h and the final point was recorded at 5 h.

Within minutes after mixing, the solution is supersaturated in $AH_3$, $CAH_{10}$, $C_2AH_8$ and $C_3AH_6$. As noted above, $AH_3$ and $C_2AH_8$ begin to form while the concentrations are still rising. For a cement in which CA is the only active constituent, $CAH_{10}$ subsequently becomes a more important product below about 15°C (Fig. 10.2). For cements containing $C_{12}A_7$, $C_2AH_8$ is a major product at lower temperatures.

In the conversion reaction, $CAH_{10}$ and $C_2AH_8$ redissolve and $C_3AH_6$ is formed, together with additional $AH_3$, which over time tends increasingly to approximate to gibbsite. At 5°C, this process may take many years, but at 50°C or above, the formation of $C_3AH_6$ and gibbsite is virtually immediate. The only phases in the pure $CaO–Al_2O_3–H_2O$ system stable in contact with aqueous solutions up to well above 100°C are gibbsite, $C_3AH_6$ and CH.

XRD studies using synchrotron radiation (R59,R60) showed that the formation of $C_3AH_6$ requires the prior formation of at least a small amount of $C_2AH_8$, which thus appears to be essential for its nucleation. Once nucleated, the $C_3AH_6$ can form directly from $CAH_{10}$. Below 70°C, '$\beta$-$C_2AH_8$' was detected as an intermediate phase in the formation of $C_3AH_6$ from normal, so-called $\alpha$-$C_2AH_8$. According to Scheller and Kuzel (S66), '$\beta$-$C_2AH_8$' is really $C_2AH_{7.5}$ (Section 6.1.4).

### 10.1.5 Thermodynamic calculations

When the anhydrous phases dissolve, the species present in solution in significant concentrations are $Ca^{2+}$, $Al(OH)_4^-$ and $OH^-$; $CaOH^+$ may be ignored. Taking $C_2AH_8$ as an example, the equilibrium with solution is thus represented by the equation

$$Ca_2Al_2(OH)_{10} \cdot 3H_2O \rightleftarrows 2Ca^{2+} + 2Al(OH)_4^- + 2OH^- + 3H_2O \quad (10.1)$$

The solubility product is equal to $\{Ca^{2+}\}^2 \times \{Al(OH)_4^-\}^2 \times \{OH\}^2$, where curly brackets denote species activities and $[OH^-]$ may be replaced by $2[Ca^{2+}] - [Al(OH)_4^-]$. As the concentrations are low, activity coefficients may be calculated from simplified Debye-Hückel theory. Solubility products may thus be obtained from experimental data (B99,B100,C56,N15; Table 10.2). The variations in solubility products with temperature may be represented by empirical equations of the form

$$\log_{10} K = a + bT \quad (10.2)$$

where $T$ is in °C (C56), and values of the constants $a$ and $b$ are included in Table 10.2. From the solubility products, again using activity coefficients calculated using simplified Debye-Hückel theory, one may obtain calculated solubility curves (B99,B100,C56), some examples of which are

**Table 10.2** *Equilibrium constants in the $CaO–Al_2O_3–CO_2–H_2O$ system* and constants a and b in equation 10.2 (C56)†*

| Reaction ($H_2O$ molecules in solution omitted) | | | log $K$ | Ref. |
|---|---|---|---|---|
| 1. $AH_3$ (gibbsite) | $\rightleftarrows$ | $Al^{3+} + 3OH^-$ | −33·5 | S62 |
| 2. $AH_3$ (amorph.) + $OH^-$ | $\rightleftarrows$ | $Al(OH)_4^-$ | +0·2 | B99 |
| 3. $CAH_{10}$ | $\rightleftarrows$ | $Ca^{2+} + 2Al(OH)_4^-$ | −7·6 | B99 |
| 4. $C_2AH_8$ | $\rightleftarrows$ | $2Ca^{2+} + 2Al(OH)_4^- + 2OH^-$ | −13·8 | B99 |
| 5. $C_3AH_6$ | $\rightleftarrows$ | $3Ca^{2+} + 2Al(OH)_4^- + 4OH^-$ | −22·3 | B99 |
| 6. $C_4AH_{19}$ | $\rightleftarrows$ | $4Ca^{2+} + 2Al(OH)_4^- + 6OH^-$ | −25·2 | B99 |
| 7. $CaCO_3$ (calcite) | $\rightleftarrows$ | $Ca^{2+} + CO_3^{2-}$ | −8·4 | S62 |
| 8. $C_4A\bar{C}H_{11}$ | $\rightleftarrows$ | $4Ca^{2+} + 2Al(OH)_4^- + 4OH^- + CO_3^{2-}$ | −29·3 | B101 |
| 9. $Ca^{2+} + OH^-$ | $\rightleftarrows$ | $CaOH^+$ | +1·3 | S62 |
| 10. $Al^{3+} + 4OH^-$ | $\rightleftarrows$ | $Al(OH)_4^-$ | +32·4 | B144 |

| | *Reaction* 2 | 3 | 4 | 5 | 6 |
|---|---|---|---|---|---|
| *a* | +0·05 | −9·000 | −14·469 | −23·168 | −27·837 |
| *b* | +0·0174 | +0·0604 | +0·0192 | +0·0136 | +0·1073 |

* 25°C and ionic strength $I = 0$ except for no. 10, which is for $I = 0{\cdot}1$ and 20°C.
† Recalculated to give $K$ as log to base 10.

shown in Figs 10.3 and 10.4. It is thus possible to calculate entire curves, such as that for $CAH_{10}$ at 40°C, or portions of curves, such as those for $C_2AH_8$ and $C_3AH_6$ at high $Al_2O_3$ concentrations, that are difficult or impossible to determine by experiment.

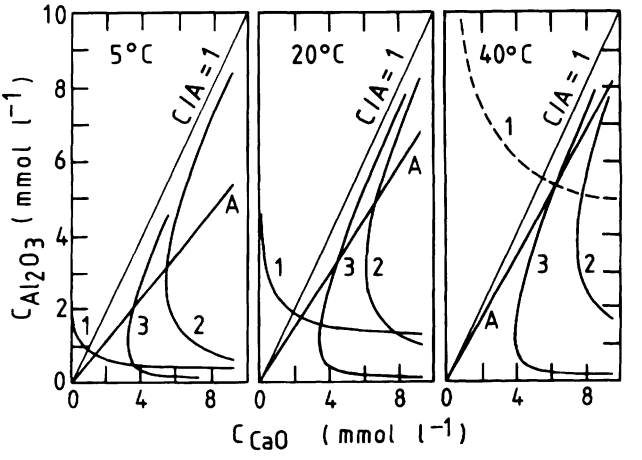


**Fig. 10.4** *Calculated solubility curves for (A) poorly crystalline $AH_3$, (1) $CAH_{10}$, (2) $C_2AH_8$ and (3) $C_3AH_6$ in the $CaO–Al_2O_3–H_2O$ system at 5°C, 20°C and 40°C. Courtesy A. Capmas (Lafarge Corporation).*

Degrees of supersaturation relative to specific hydrates may also be calculated. The solubility curve of $CAH_{10}$ is more markedly dependent on temperature than are those of $C_2AH_8$ or $C_3AH_6$. At 5°C, a solution obtained from CA rapidly becomes highly supersaturated in $CAH_{10}$, but much less so in $C_2AH_8$ or $AH_3$, but with increase in temperature this situation changes; thus $CAH_{10}$ is the major product at 5°C, but is undetectable above 30°C (C56). At 50°C, supersaturation is high only in $C_3AH_6$, which is rapidly formed.

Barret and Bertrandie (B99,B100,B145) explained the maximum concentrations reached in the CA–water reaction and the path by which they were attained. On contact with water, CA was assumed to develop a hydroxylated surface layer, termed $CA_{sh}$, of composition $Ca[Al(OH)_4]_2$, which dissolves congruently and is continuously regenerated as new areas of surface are exposed. The maximum values reached by the CaO and $Al_2O_3$ concentrations were considered to represent the solubility of $CA_{sh}$. A solubility curve was thus calculated for $CA_{sh}$, and is included in Fig. 10.3. The path of increasing concentrations was shown to pass along a narrow corridor on the $C_{CaO}$–$C_{Al_2O_3}$ diagram, enclosing compositions for which neither $AH_3$ nor $C_2AH_8$ is rapidly precipitated. These phases were immediately precipitated on passing beyond the low-CaO and high-CaO boundaries of the corridor respectively. The path was shown to correspond to a series of compositions for which the conflicting tendencies to precipitate $AH_3$ and $C_2AH_8$ were as far as possible minimized. The hydration of $C_{12}A_7$ was considered in a similar way. The $CA_{sh}$ postulated in this approach could possibly be identified with one of the amorphous intermediate phases that have been reported, but the latter appear in all cases to be more substantial than a surface layer and are in other respects not taken into account. Further work is needed in order to relate the results of the various investigations.

### *10.1.6 Setting times; mixing and placing*

The setting times of most CACs pass through a maximum at 25–30°C (Fig. 10.2). The effect has been observed with white CACs and with pure CA as well as with Ciment Fondu, and thus does not depend on the presence of phases other than CA (B140). The setting time usually shortens between 0°C and about 20°C, but at 28–30°C it can be up to 8 times as long as at 20°C. Above 30°C, it again shortens very rapidly. It appears that at 28–30°C neither $CAH_{10}$ nor $C_2AH_8$ forms readily, and that $C_3AH_6$ can only form from one or other of these phases. Several hypotheses based on difficulties of nucleation, protective coatings or both have been proposed (B140,C59,S115). The effect is not of practical importance for the setting of normal concrete mixes except possibly in the surface zone, because the heat evolved on hydration increases the temperature to more than 30°C.

The length of the induction period decreases with the C/A ratio in the solution, which is in turn affected by the presence of $C_{12}A_7$ (B99). For ratios up to 1·06, given by pure CA, it can be as long as 6–12 h, but at ratios above 1·20, immediate setting can occur. The mechanism and

products of hydration of $C_{12}A_7$ are essentially similar to those for CA, but, as might be expected from the higher C/A ratios in the solution, the products do not include much $CAH_{10}$, even at 4°C (E6).

Increase in energy or time of mixing markedly accelerates the hydration of CACs, and if excessive can even cause quick setting in the mixer. Once mixing stops, progressive thickening occurs. Samples of a given paste mixed for different times can behave very differently during placing. This factor is often forgotten, and can lead to the addition of more water during placing, with a consequent increase in porosity and decrease in strength. The rheological properties of the fresh pastes (B146,C60) and $\zeta$-potentials of suspensions (Z13) are broadly similar to those found for Portland cements (Sections 8.1 and 11.4.3). As with the latter, the water demand can be decreased by adjusing the particle size distribution. Factors affecting choice of w/c ratio are discussed in Section 10.1.8.

### *10.1.7 Microstructural development*

Cottin (C58) studied pastes of Ciment Fondu, largely by the TEM replica method. The microstructures of pastes of low w/c ratios hydrated for 7 days at 12°C were too compact to show more than occasional detail, but with pastes of w/c = 0·7 much detail could be observed in cavities exposed by fracture, which were lined with small crystals of $CAH_{10}$ and sometimes contained plates of $C_2AH_8$. The crystals of $CAH_{10}$, which were hexagonal prisms up to 1 $\mu$m long and 0·2 $\mu$m wide, were present in rounded aggregates. Hydrous alumina was seen in a paste of w/c = 1·0 hydrated at 30°C; it occurred in the lining of a cavity, mainly as rounded masses of randomly oriented platelets. Secondary electron images obtained in the SEM give similar results (H68,M103) (Fig. 10.5).

Backscattered electron images (H68,L52,S11) confirm and extend these results. Scrivener and Taylor (S11) reported an SEM and XRD study of pastes of a white CAC consisting mainly of CA and gehlenite, with minor perovskite. The clinker grains were mostly polymineralic. At 5°C, the earliest process detected was dissolution of CA, with deposition of $CAH_{10}$ in the outer product. Later, the inner product described in Section 10.1.4 was also observed. At 40°C, these processes were followed by what appeared to be successive formation of $C_2AH_8$ and $AH_3$ from $CAH_{10}$ and of $C_3AH_6$ and $AH_3$ from $C_2AH_8$. Both of these latter processes appeared to occur by dissolution and reprecipitation. The $C_2AH_8$ often formed aggregates of plates similar to those shown in Fig. 10.5B. The $C_3AH_6$ characteristically occurred as aggregates of equidimensional nodules, individually about 200 nm in diameter, which were mixed on or below a micrometre scale with flakes of $AH_3$. The latter phase also occurred in larger regions, which were apparently structureless and, rarely, as pseudomorphs after $C_2AH_8$. Some $C_2ASH_8$ was detected.

Broadly similar results were obtained for a 60-year-old field concrete, made with Ciment Fondu (C61,H70). The concrete was a pile that had been knocked over and was lying on its side in an estuary, where it had undergone repeated wetting and drying from the tide. It had probably

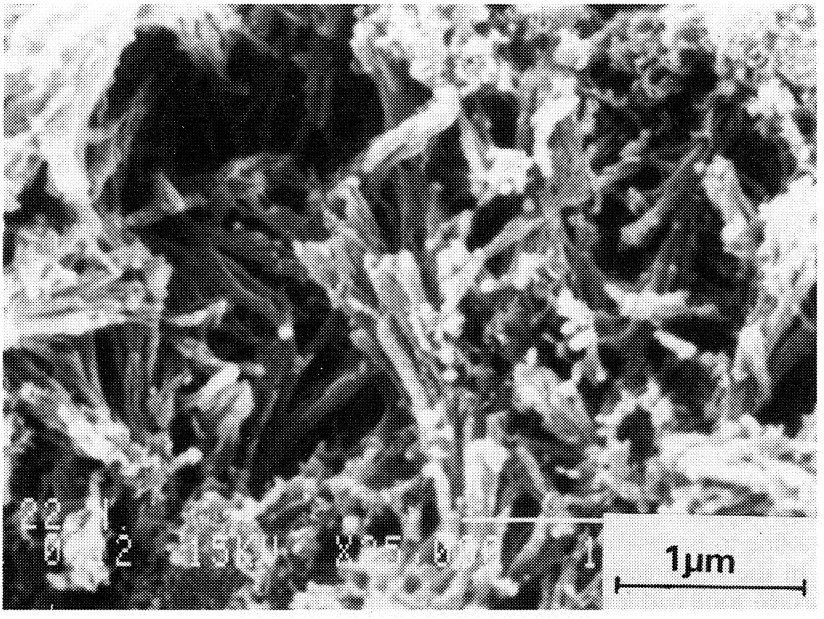


A

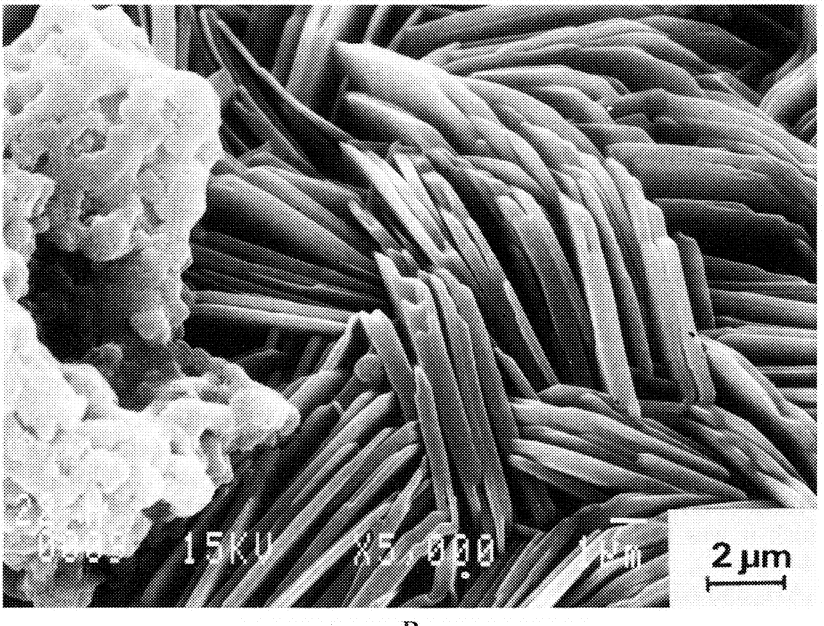


B

**Fig. 10.5** *SEM secondary electron images of the fracture surface of a paste of Ciment Fondu (w/c = 0·4) hydrated for 22 h at room temperature, showing (A) $CAH_{10}$, and (B) plates of $C_2AH_8$. Courtesy D. Sorrentino (Lafarge Corporation).*

been made at w/c = 0·6–0·7 and a cement content of 300 kg $m^{-3}$. The core material had converted, and image analysis indicated a volume porosity of 17%. The surface zone had a porosity of only 3–4% and was substantially unconverted. The river water contained $Cl^-$ and $SO_4^{2-}$, which had very minor effects that are noted in Section 10.1.11. An SEM, DTA and XRD study of Ciment Fondu pastes (H70) gave similar results.

The 27-year-old Ciment Fondu concrete shown in Fig. 10.1 had been made at a total w/c ratio of 0·32 (C61). The cement had largely reacted, apart from some large grains. Within the latter, some of the material in the regions of CA is darker than the rest, and is possibly inner product. Elsewhere in the paste, the partly or completely reacted cement grains are less clearly distinguishable from the outer or undesignated product than in typical Portland cement pastes, though some of the areas of denser and more uniform appearance, such as that marked B, are probably grains that have reacted completely apart from pinhead regions of ferrite. There are some well-defined areas of $AH_3$. These apart, X-ray microanalyses mostly appeared to correspond to mixtures of $C_3AH_6$ and $AH_3$ on a scale too fine to be resolved by this method (L52).

In the white cement and 60-year-old specimens described above, the surface zone had a more compact, less porous appearance than the bulk material. In the converted white cement paste, the porosity appeared to be unevenly distributed on a scale of some 50 $\mu$m. The mature Ciment Fondu concrete of w/c ratio 0·32 showed little porosity detectable in a backscattered image, even in material far removed from the surface.

### *10.1.8 Hardening; effects of conversion*

CACs harden rapidly as soon as the massive precipitation of hydrates begins. Relatively high proportions of water are taken up in the hydration reactions, the theoretical w/c ratios needed for complete hydration of CA being 1·14, 0·63 and 0·46 for the formation of $CAH_{10}$, $C_2AH_8 + AH_3$ and $C_3AH_6 + 2AH_3$ respectively. For this reason, and also because of the rapid heat evolution, care is needed to avoid surface drying. In blocks of concrete more than 300 mm thick, the temperature rise is sufficient to cause rapid formation of $C_3AH_6$ during hardening under normal conditions, though a surface zone may remain unconverted. Strong bonds are formed with limestone aggregates (B147,F48), apparently due to formation of $C_4A\bar{C}H_{11}$, and with synthetic aggregates high in $Al_2O_3$, which give high abrasion and corrosion resistance (G92).

Calculation based on the relevant densities shows that when CA hydrates to form $CAH_{10}$, the volume of the latter is 3·64 times that of the CA from which it was formed. For hydration to give $C_2AH_8$ and $AH_3$ (density 2.44 kg $m^{-3}$), the corresponding factor is 2·31 and for hydration to give $C_3AH_6$ and $AH_3$ it is 1·73. Conversion of $CAH_{10}$ into $C_3AH_6$ and $AH_3$ thus entails a 53% decrease in volume. The porosity of the paste therefore increases and the compressive strength decreases. Figure 10.6 shows some results for Ciment Fondu pastes. The importance of the changes increases markedly with the w/c ratio. This has been explained thus (R62). At high w/c ratios, all the CA can hydrate to give $CAH_{10}$; the changes are

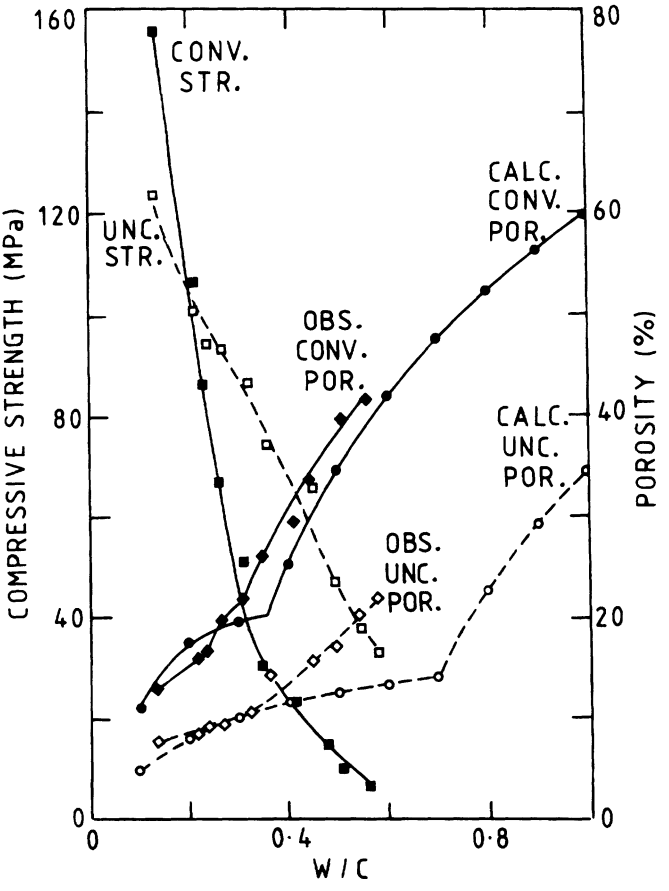


**Fig. 10.6** *Compressive strengths and observed and calculated porosities for pastes of Ciment Fondu of varying w/c ratios. The unconverted paste, which contained $CAH_{10}$, was cured for 7 days at 10°C. The converted paste, which contained $C_3AH_6$ and $AH_3$, was cured for 7 days at 70°C. After G91.*

relatively large, and the converted materials are weak and porous. At low ratios, there is insufficient space for all the CA to react to form $CAH_{10}$. When conversion occurs, much water is released, so that even if the pores contain no water, more CA can hydrate. This partially compensates for the effects of conversion, and, along with the low w/c ratio, ensures that the converted materials are strong and of relatively low porosity.

The rate of conversion at a given temperature is reduced if the RH falls below saturation. The temperatures during setting and curing also have a large effect; if they are high, subsequent conversion occurs more rapidly, even though the temperature is then low (C55). This is probably due to the presence of nuclei of $C_3AH_6$. The strength after conversion is affected by the rate at which that process occurs, perhaps because of the effect on

$C_3AH_6$ morphology (M106). Strength may also be affected by the crystallization of $AH_3$, which could reduce its pore-filling capacity and efficacy as a binder. The size of the $C_3AH_6$ crystals increases with the temperature at which they are formed; this may decrease strength. It has sometimes been said that $C_3AH_6$ is an intrinsically weak binder, but this is not correct. As with relatively dense, crystalline substances in general (F40), it gives lower strengths than less dense substances at high porosities, but higher ones at low porosities. This may be seen from the crossing of the curves in Fig. 10.6. Hot-pressed pastes of CACs, in which the binder is $C_3AH_6$ and the porosity has been reduced to about 4%, show strengths of up to 480 MPa (Section 11.9.1).

Figure 10.7 shows the results of some long-term tests of compressive strength. The initial, rapid increase, due to formation of $CAH_{10}$, is followed by a decrease due to conversion and, ultimately, by an increase due to continuing hydration. It is implicit in such results that design should be based on the assumption that conversion is inevitable, and that tests using accelerated curing should be be carried out to determine the long-term minimum strength (B148,C61,G92,G93). A rapid increase levelling off at this value should be assumed. For satisfactory strength and durability, the total w/c ratio (i.e. that including water sorbed by the aggregate) must not exceed 0·4 and the cement content must be at least 400 kg m$^{-3}$. At this cement content, a total w/c ratio of 0·4 typically corresponds to a free (i.e. effective) ratio of about 0·33. Because of the self-heating effect, the long-term minimum strength is commonly reached with such mixes within a few hours.

Conversion and its practical implications have been widely studied but not always well understood. Thus, concretes made with inadequate

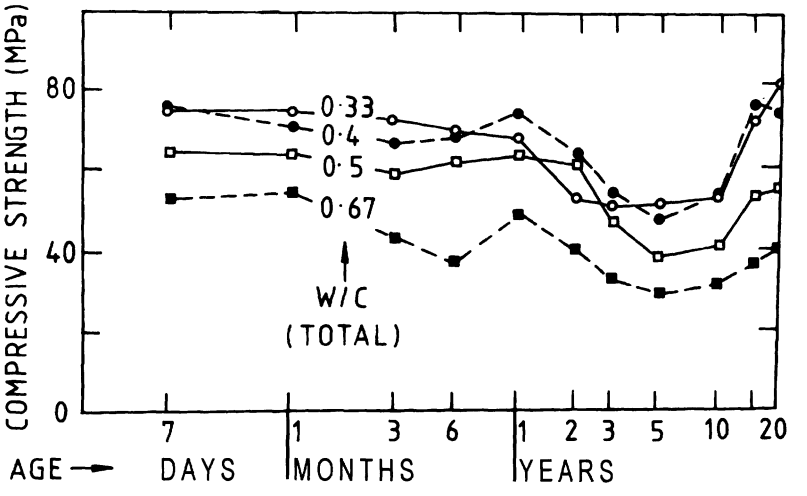


**Fig. 10.7** *Long-term compressive strengths of Ciment Fondu concretes cured for 24 h in moist air at 18C and then stored outdoors in southern France. After G92.*

cement contents and excessive w/c ratios have failed in structural applications. An extensive investigation in the UK into calcium aluminate concrete in existing buildings (B148) showed that a high level of conversion was generally reached in a few years, causing a very variable loss of strength, but that this loss was in most cases insufficient to endanger the structure. No adverse effects of corrosion on steel tendons removed from prestressed concrete beams in normal buildings were detected. The use of CACs in structural work is nevertheless not deemed to satisfy the current (1996) UK Building Regulations. In France, prohibitive restrictions were for a time placed on its use in the public sector of the construction industry, but in 1968 a new set of rules was issued after lengthy studies. Current French regulations (M107) specify the maximum total w/c ratio of 0·4 and minimum cement content of $400\,kg\,m^{-3}$ mentioned above.

Conversion is of only minor importance for the use of CACs in refractory applications and in mixes with Portland cement such as those described in Section 10.1.10.

### *10.1.9 Chemical admixtures*

Many inorganic salts affect the setting times of CACs and are effective in concentrations around 0·5% (C62,L6,R58). The effects on setting times differ greatly both in direction and in relative magnitudes from those observed with Portland cements (Section 11.5.1). The results of different investigators show apparent discrepancies, and the effects probably depend greatly on concentration, which may even reverse their direction, but there is general agreement that $Li^+$ salts and alkali or calcium hydroxides are strong accelerators and that many common inorganic salts retard. As with Portland cement, hydroxylic organic compounds, such as sugars or citric, tartaric or gluconic acids, are powerful retarders.

Rodger and Double (R58) studied the effects of several admixtures, particularly LiCl and citric acid, by XRD, conduction calorimetry and solution analyses. The samples were slurries of a Ciment Fondu hydrated at 22°C and in the absence of admixtures gave $CAH_{10}$ as the main product. In the mixes with LiCl, $C_2AH_8$ was the main product and a little $Li_2O \cdot 2Al_2O_3 \cdot 11H_2O$ was detected. The authors considered that this compound acted as a nucleation substrate for $C_2AH_8$. The very low concentrations in which the organic compounds are effective suggests that, as with Portland cement, they act by poisoning the nuclei of the hydration products, but the authors found this hypothesis incompatible with the observed solution compositions.

An experimental study of the $CaO–Al_2O_3–H_2O$ system in the presence of NaOH showed that at a concentration of $1\,mmol\,l^{-1}$ the latter had negligible effect on the equilibria, but that at $10\,mmol\,l^{-1}$ the solubility curves were displaced to lower CaO and higher $Al_2O_3$ concentrations. At $100\,mmol\,l^{-1}$, the solutions were very low in CaO, and precipitation did not occur within 28 days (P51). The effect of $OH^-$ ion on the solubility curves can also be calculated by an extension of the procedure mentioned in Section 10.1.5 (B100). The results showed large shifts in the curves at an

NaOH concentration of 40 mmol $l^{-1}$, the minimum in CaO concentration on the $C_2AH_8$ curve at 21°C being shifted from $C_{CaO} = 6{\cdot}8$ mmol $kg^{-1}$, $C_{Al_2O_3} = 2{\cdot}3$ mmol $kg^{-1}$ to $C_{CaO} = 1{\cdot}1$ mmol $kg^{-1}$, $C_{Al_2O_3} \sim 13$ mmol $kg^{-1}$. An experimental study on the effects of adding sodium phosphates of various types has been reported (B149).

Other types of admixture used with CACs include water reducers and superplasticizers (Section 11.4), which also act as retarders, and thickening agents, such as carboxymethylcellulose. Complex formulations may be used for special purposes, e.g. a ready-mix mortar for high-performance road repair might contain 55% Ciment Fondu and 45% sand, with glass fibre, Al powder, $Li_2CO_3$, Na gluconate and methyl ethyl cellulose (M108).

### *10.1.10 Mixtures with calcite, slag, gypsum or Portland cement*

Cussino and Negro (C63) reported that loss of strength in CAC mortars could be prevented by using calcareous aggregates or by adding finely ground calcite to the cement. They showed that $C_4A\bar{C}H_{11}$ was formed and concluded that this limited or prevented conversion. Fentiman (F49) confirmed the formation of $C_4A\bar{C}H_{11}$ but found that at 25°C or below $CAH_{10}$ was still the main product and that conversion was delayed but not prevented. $C_4A\bar{C}H_{11}$ seems to form at the expense of $C_2AH_8$ and $C_3AH_6$ at 25–60°C but to be unstable at or above 60°C (F49,M109). Strong concentration gradients and other local inhomogeneities (B150) may explain some of these apparently contradictory results. Equilibria involving $C_4A\bar{C}H_{11}$ have also been approached theoretically (B101,B102,D36,S75). Barret *et al.* (B101,B102) concluded that $CaCO_3$ would dissolve giving $C_4A\bar{C}H_{11}$ only at partial $CO_2$ pressures above a certain value, but that equilibrium with atmospheric $CO_2$ would not be reached within the pores of a concrete.

Majumdar *et al.* (M110) studied concretes containing equal masses of Ciment Fondu and ggbs. On water curing at either 20°C or 38°C, the compressive strengths continuously increased over a period of 1 year, whereas those of control samples made without the slag showed the normal decreases associated with conversion. Parallel studies on pastes showed that the superior behaviour of the mixes with slag were associated with formation of strätlingite.

Various combinations of CACs with calcium sulfate, Portland cement and in some cases calcium hydroxide are commonly used to make cements that set and harden rapidly. They may also dry out rapidly, due to the absorption of water in formation of ettringite. Some such mixtures also show expansive behaviour (Section 10.2.1). A simple, rapidly setting mix might contain 15–20 % ordinary Portland cement, 10–30% Ciment Fondu, 10–25% CH and 40–60% sand. More complex formulations, containing various admixtures, are used to produce self-levelling mortars. The setting times of all such mixtures depend greatly on the relative proportions, the characteristics of the individual cements and the mixing time and temperature; only laboratory tests can predict the precise behaviour of a specific mix. Figure 10.8 gives a general indication of the

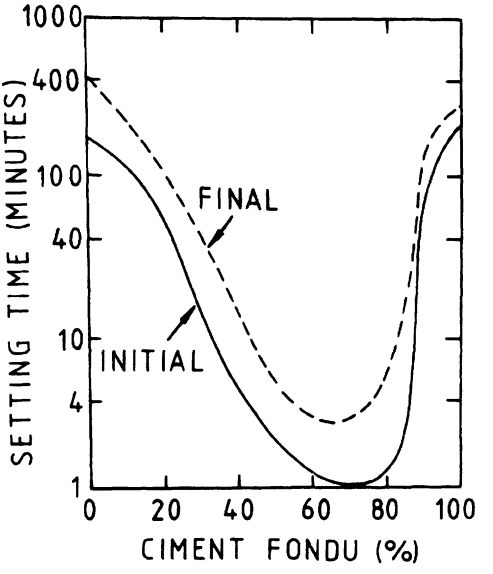


**Fig. 10.8** *Setting times of neat pastes of mixtures of Ciment Fondu and Portland cement. These are only general indications, as the times depend on Portland cement composition, mixing time, temperature and other factors. After R62.*

behaviour of neat pastes made from calcium aluminate and Portland cements. The rapid setting of the mixes high in Portland cement is possibly caused by preferential reaction of the gypsum with the CAC, and that of those high in CAC by the increase in pH due to the presence of the Portland cement. In addition to C–S–H and CH, the hydration products can include $C_4AH_{13}$ and strätlingite. Mixes of CA with sufficiently high proportions of calcium sulfate yield ettringite (C40).

### *10.1.11 Reactions of calcium aluminate cement concrete with external agents*

Concrete made with CAC is highly resistant to sulfate solutions, sea water or dilute acid solutions with $pH > 4$, including natural waters in which $CO_2$ is the only significant solute. Resistance may extend to $pH \approx 3$ if the salt formed is of sufficiently low solubility. As might be expected, resistance increases with decreasing w/c ratio and increasing cement content (C64).

Early work indicated that high resistance to attack is associated with restricted penetration by aggressive species. Thus, Midgley (M111) found that in massive, fully converted concrete exposed to a sufate-containing ground water for 18 years, penetration with formation of a substituted ettringite was limited to a depth of about 5 mm. Surface zones of hard and almost non-porous material, of the type described in Section 10.1.7,

have been very widely observed (C61,C64,H70) and probably play an important part in restricting penetration. The zones vary in thickness from a few millimetres to 25 mm, and the material in them appears often to be largely or wholly unconverted. Observations on test specimens 15 years old indicated that the permeability of the surface zone may be further decreased by carbonation (C64).

Probably on account of the surface zone, resistance can still be high with mixes made at what would now be considered an improperly high w/c ratio and low cement content. Thus, the concrete described in Section 10.1.7, that had been exposed to river water containing Cl– and $SO_4^{2-}$, was still in good condition after 60 years (C61). In this specimen, there was significant ingress of $Cl^-$ but very little of $SO_4^{2-}$. Some $C_3A \cdot CaCl_2 \cdot 10H_2O$ had formed, and was apparently intergrown with $C_2ASH_8$, but most of the $Cl^-$ seemed to be adsorbed on the $CAH_{10}$. In test cubes in which expansion and cracking had occurred, sulfate had penetrated into the core material and ettringite or gypsum or both were detected (C64).

The resistance of CAC concrete to attack by alkali hydroxide solutions is low, especially if $CO_2$ is also present, as can occur if the calcium aluminate concrete is in contact with Portland cement concrete and exposed to atmospheric $CO_2$ (R63). The combined attack by $CO_2$ and alkali has been called alkaline hydrolysis. Although more complex explanations have been postulated, the effect seems to be explainable by the destruction of both the hydrated calcium aluminates and the hydrous alumina by a combination of carbonation and alkaline leaching of $Al_2O_3$ as $Al(OH)_4^-$ ion.

In contrast to the above, carbonation in the absence of alkali increases the strength of CAC concrete (P52,R64). In sufficiently porous material in which conversion has occurred, some of the $C_3AH_6$ reacts to give calcite and hydrous alumina (P50), but in dense concrete the extent of penetration by $CO_2$ is small, probably because the pores do not contain the water necessary to promote the reaction (R64) and because they become blocked by $CaCO_3$ and alumina gel (B151). These observations support the general conclusion that the high resistance of dense calcium aluminate concretes to various forms of attack is at least in part due to effects that impede or prevent the ingress of the attacking substance. In addition to the blocking of pores by reaction products, these effects could include the rapid removal of incoming water by continued hydration.

### *10.1.12 Refractory castables*

Castable refractory concrete can be made using Ciment Fondu for use at hot-face temperatures up to 1350°C, or using white CACs for use up to 2000°C. Refractory castables can be categorized as cement castables (15–25% CAC), low cement castables (5–10%) and ultra-low cement castables having proprietary formulations that include under 5% of cement, silica fume and other admixtures. Depending on the service temperature and application, aggregates include exfoliated vermiculite, chamotte, sintered bauxite, brown or white fused alumina, chromite, etc.

A very simple formula for a wall more than 50 mm thick and for use at a hot-face temperature up to 1650°C might contain 14% of '70% $Al_2O_3$ cement', with 86% of a suitably graded aggregate of brown fused alumina and 0·2% of trisodium citrate on the mass of cement; the w/c ratio must be determined by an empirical test, as for a rapidly hardening mix, but would be $\leq 0{\cdot}4$.

When the concrete is heated, the hydration products undergo conversion and dehydration. The strength decreases to a minimum value at a temperature usually between 900°C and 1100°C, though if the cement content is sufficiently high it is still sufficient for ordinary applications. At higher temperatures, sintering reactions occur between the cement and aggregate, and the ceramic bonding that results causes the strength and resistance to abrasion to increase. The compounds formed depend on the compositions of the cement and aggregate, but typically include such high melting point phases as $CA_2$, $CA_6$ and spinel (MA).

## 10.2 Expansive cements

### *10.2.1 General*

A normal Portland cement concrete expands slightly during moist curing, but this effect is outweighed by the drying shrinkage that occurs on subsequent exposure to an atmosphere of normal humidity. If the concrete is restrained, the resulting tensile stress may be sufficient to crack it. In an expansive cement, the expansion is increased, so as to balance or outweigh the subsequent contraction. Expansive cements, which were first described by Lossier (L53), may be categorized as shrinkage-compensated or self-stressing cements.

In a shrinkage-compensated cement, the object is to balance the drying shrinkage to prevent cracking. In practice, the expansion is restrained by reinforcement and a small compressive stress of 0·2–0·7 MPa is created in the concrete, which should preferably remain under slight compression after the normal drying shrinkage has occurred. Practical uses of shrinkage-compensated cements have included such structures as multi-storey car parks or water storage tanks, in which it is desirable or essential to eliminate water leaks.

In a self-stressing cement, a larger expansion is produced, with the object of achieving greater stresses in the reinforcement and the concrete to permit the production of thin, strong articles or structures, as in mechanical prestressing. Estimates of the maximum stress that can be safely achieved have ranged from 3·5 MPa (M112) to 8 MPa (W36). Because the concrete expands triaxially, careful design and choice of curing conditions, including if necessary triaxial restraint, are essential. Self-stressing cements have been used both in the manufacture of precast pipes and other units and for in situ applications.

In any expansive cement, the amount of expansion and the period during which the expansive reaction occurs are critical. The reaction must take place after the concrete has developed some strength, but before exposure to a reduced RH places it in tension, which could cause irreversible damage.

### 10.2.2 Types of expansive cement

Probably a majority of practical expansive cements have depended on the modification of a Portland cement in such a way as to increase the formation of ettringite. Single expansive cement clinkers can be made, but it has been more usual to produce admixtures that are blended or interground with a normal Portland cement or clinker. Blending has the advantage that the fineness of the expansive admixture can be optimized, usually by grinding it more coarsely so as to delay the expansive reaction until the cement has developed the necessary strength. It also allows a single admixture to be used in differing proportions to make both shrinkage-compensated and self-stressing cements.

In a widely used US terminology, expansive cements based on Portland cement and calcium sulfate are categorized as Types K, M or S, according to the source of the additional $Al_2O_3$ that is required. Type K cements, developed by Klein and Troxell (K54), contain $C_4A_3\bar{S}$ as an essential ingredient. They are usually produced by intergrinding or blending an ordinary Portland cement clinker with additional gypsum or anhydrite and an expansive clinker containing $C_4A_3\bar{S}$. The composition of the expansive clinker can be varied considerably to utilize the raw materials most economically available; the clinkers made in the USA typically contain 8–50% of $C_4A_3\bar{S}$ with some anhydrite and usually some free lime (M112). The proportions of expansive clinker and of gypsum or anhydrite or both that are added to the Portland cement depend on the composition of the expansive clinker and the degree of expansion required. Mehta and Polivka (M112) found that Type K shrinkage-compensated cements made with Portland cement clinkers of low or moderate potential $C_3A$ content and containing 6% or more of $SO_3$ resisted chemical attack by sulfates, but that Types M and S cements did not. Table 10.3 includes some analyses of Type K cements.

Type M cements contain Portland cement, a CAC and additional calcium sulfate. They were extensively studied in the former USSR. Mikhailov (M113) described a self-stressing cement composed of Portland cement, CAC and gypsum typically in the proportions 66:20:14 and used to produce precast units. An initial cure in air followed by hot water allowed strength to be developed without formation of ettringite, which occurred during a subsequent cure in cold water. Mixtures using alumina slag as the source of the additional $Al_2O_3$ were also used, and only required curing in air followed by cold water (M112,M114).

**Table 10.3** *Compositions of Type K expansive cements produced in the USA (M112)*

| Application | MgO | $Al_2O_3$ | $SiO_2$ | $SO_3$ | CaO | $Fe_2O_3$ | Loss |
|---|---|---|---|---|---|---|---|
| Shrinkage compensation | 0·7 | 4·8 | 21·6 | 6·2 | 62·4 | 2·8 | 1·1 |
| Shrinkage compensation | 3·4 | 5·7 | 18·8 | 6·5 | 61·4 | 1·9 | 1·5 |
| Self-stressing | 2·7 | 8·4 | 14·6 | 12·4 | 57·6 | 1·6 | 1·9 |

Mixtures of CAC with gypsum (X4) or with gypsum and $C_4AH_{13}$, the latter made from CAC and lime (M113), have also been employed.

Type S cements are Portland cements high in $C_3A$ and with suitable contents of calcium sulfate; they have found little favour as too difficult to control. The $Al_2O_3$ has also been supplied in forms other than those mentioned above. Impure alunite ($KAl_3(SO_4)_2(OH)_6$), which occurs as a natural rock, has been used, either after calcination (V9) or uncalcined (W36). In the latter case it was mixed with Portland cement clinker, anhydrite and flyash or slag and was found to dissolve relatively slowly, thus suitably delaying the expansive reaction.

The possibilities of using free lime or periclase as expansive agents have also been investigated. Kawano *et al.* (K55) and Long (L54) described clinkers in which substantial proportions of free lime are present as inclusions in alite. In both cases, the raw mix included anhydrite. Long investigated and described the processes by which this microstructure was formed.

### *10.2.3 Mechanism of expansion in Type K cements*

In a Type K cement, the formation of ettringite from $C_4A_3\bar{S}$ may be represented by the equation

$$C_4A_3\bar{S} + 8C\bar{S}H_2 + 6CH + 74H_2O \rightarrow 3C_6A\bar{S}_3H_{32} \qquad (10.3)$$

Consideration of the relevant densities shows that the solid volume is approximately doubled, and it has sometimes been assumed that this is sufficient to explain the expansion. However, as the case of the normal hydration of Portland cement shows, a doubling of the solid volume does not necessarily cause significant expansion. The change in porosity must be considered, and depends on the extent to which the particles of the product are accommodated in the existing pore structure. Any adequate theory of the mechanism of an expansive reaction must be based on an understanding of the microstructure.

Odler and Jawed (O25) reviewed expansive reactions in concrete, including those produced through the use of expansive cements. Probably a majority of workers have accepted the view of Lafuma (L55) that expansion results from forces exerted by the growth of the ettringite crystals. Of other theories, the most significant in relation to Type K cements is that proposed by Mehta (M115), who attributed it to attraction of water molecules to ettringite crystals of colloidal dimensions.

Bentur and Ish-Shalom (B152,B153,I13,I14) studied mixtures of $C_4A_3\bar{S}$, $C\bar{S}$ and CH in pastes, alone or mixed with $C_3S$. Expansion did not begin until a certain critical degree of reaction, which was about 50% at 20°C, had been reached. Using SEM, light microscopy and mercury intrusion porosimetry, they confirmed earlier observations that the ettringite was formed as porous coatings around the grains of $C_4A_3\bar{S}$, which were thus effectively caused to expand; expansion began when the expanding particles came into contact and exerted pressure on each

other. In the absence of restraint, these particles could be treated as spheres, but under restraint they expanded in the directions in which the restraining forces were least. Essentially the same mechanism was described by Ogawa and Roy (O17,O26), who found that the ettringite was formed initially as very small, unoriented crystals. After the degree of reaction (defined by the quantity of ettringite formed) had reached about 50%, the ettringite developed as radial growths of longer crystals. Contact between the ettringite layers surrounding the $C_4A_3\bar{S}$ particles, and the associated expansion, began only after this stage had been reached. The change in ettringite morphology was considered to be an important first step in causing expansion.

One study on Type K cements showed no significant dependence of ettringite crystal size on the $Ca^{2+}$ concentration in the solution (K56). In contrast, other investigators have found that suspensions of $C_4A_3\bar{S}$, $C\bar{S}$ and CH at high CaO concentrations give ettringite in the form of a fine-grained coating on the $C_4A_3\bar{S}$ particles, but that in the absence of CH the ettringite forms long, thin needles (M115,N19,O27). In pastes containing $C_4A_3\bar{S}$, expansion occurs if CH is present but not if it is absent, even though ettringite is still formed (N19,O27). This parallels the behaviour of supersulfated cements (Section 9.2.10), which yield much ettringite and no CH, and do not expand significantly.

The effect of CH in favouring expansion is explained on Mehta's theory by the decreased crystal size of the ettringite (M115). On the crystal growth hypothesis, it is explained by the differing microstructural location in which the ettringite is formed (N19,O27). If the CaO concentration in the solution is high, $Al(OH)_4^-$ ions cannot migrate far from the surface of the $C_4A_3\bar{S}$, and the ettringite is precipitated on the surface of that phase. Very high degrees of supersaturation may be reached locally at that surface, and, since the pressure that can be exerted by a growing crystal increases with the degree of supersaturation, strong expansive forces can be produced. The stresses may be further increased by the fact that ettringite formation is concentrated into a relatively few places. The crystals are small due to the high degree of supersaturation. If the CaO concentration is lower, $Al(OH)_4^-$ ions can migrate more freely and the ettringite is precipitated more evenly throughout the material, under lower supersaturation. The lower degree of supersaturation would also explain the increased size of the crystals.

The balance of the evidence favours the hypothesis that expansion in Type K cements is caused by crystal growth. It is also difficult to see why ettringite crystals of the size postulated by Mehta ($\sim 1\,\mu m$ in longest dimension; M115) should attract water more strongly than C–S–H gel, which has a very much greater specific surface area. However, the same mechanism does not necessarily operate in other cases of expansion associated with ettringite formation, including even other types of expansive cements. For expansion caused by external sulfate attack (Section 12.5) or by delayed ettringite formation (Section 12.6), there is some reason to suppose that it does not.

## 10.3 Other cements

### *10.3.1 Very rapidly hardening cements*

Various methods have been used to obtain cements that set and harden rapidly. They include the use of Portland cement with admixtures and of mixtures containing both Portland and CACs, described in Sections 11.5 and 10.1.10 respectively. Another approach has been the manufacture of clinkers containing either $C_{11}A_7 \cdot CaF_2$ or $C_4A_3\bar{S}$, both of which hydrate rapidly under appropriate conditions with the formation of ettringite.

Regulated-set cement and jet cement are modified Portland cements in which the normal aluminate phase is replaced by $C_{11}A_7 \cdot CaF_2$ through the use of a raw mix containing $CaF_2$. Uchikawa and co-workers (U22,U23) gave chemical (Table 10.4) and phase compositions of two jet cements. Both contained approximately 60% of alite, 20% of $C_{11}A_7 \cdot CaF_2$, 1% of belite and 5% of ferrite. Admixtures were required to control the rate of reaction of the $C_{11}A_7 \cdot CaF_2$ and the nature of the products. One of the cements included a proprietary retarder based on citric acid, together with 2% of $CaCO_3$. The other contained 2·5% of hemihydrate. In each case, $Na_2SO_4$ (1%) and anhydrite were also present. The specific surface areas were around $550\,m^2\,kg^{-1}$.

Uchikawa and co-workers (U22–U24) studied the hydration reactions of $C_{11}A_7 \cdot CaF_2$ and jet cements, including the effects of various admixtures. A wide variety of methods was used. For the two cements mentioned above, hydrated in pastes at 20°C, the main product at 3 h was ettringite. At this stage, 40–45% of the $C_{11}A_7 \cdot CaF_2$ had reacted. SEM showed needles of ettringite, 0·5–1·0 $\mu$m thick, growing from the particles of clinker and anhydrite to form a closely knit, interlocking structure. Comparable mortars of the same age had compressive strengths of around 10 MPa. The quantity of ettringite formed was such that a high proportion of the anhydrite must have reacted. Subsequently, the content of ettringite tended to decrease slightly and some monosulphate was formed; the ettringite recrystallized, giving larger crystals. The alite hydrated to give C–S–H; calculations based on assumed reaction stoichiometry indicated that the reaction was much faster than in a Portland cement, with about 65% reacting in 1 day. The compressive and bending strengths increased rather slowly between 3 h and 24 h, but thereafter more quickly, and by 7 days the former were 32–44 MPa. The type of retarder (citric acid or hemihydrate) considerably affected the hydration reactions and the pattern of strength development. The fluoride ion was believed to enter an aluminium hydroxide fluoride.

Cements that set and harden rapidly can also be made in which the principal constituents are $C_4A_3\bar{S}$ and belite. Table 10.4 includes the chemical composition of a clinker described by Sudoh *et al.* (S116). The clinker, made from limestone, by-product gypsum, aluminous materials and clay, was burned at 1300°C. The presence of a limited amount of free lime was found to be necessary to achieve rapid strength development, and conditions such that all the $SO_3$ was bound as $C_4A_3\bar{S}$ were required to avoid atmospheric pollution. The phase composition was given as $C_4A_3\bar{S}$, 54%; $C_2S$, 32%; $C_4AF$, 5%; free lime, 9%. The clinker was

**Table 10.4** *Chemical and phase compositions of rapidly hardening materials containing $C_{11}A_7 \cdot CaF_2$ or $C_4A_3\bar{S}$*

| Material | $Na_2O$ | MgO | $Al_2O_3$ | $SiO_2$ | $SO_3$ | $K_2O$ | CaO | $Fe_2O_3$ | F | Loss | Ref. |
|---|---|---|---|---|---|---|---|---|---|---|---|
| Jet cement | 0·6 | 0·8 | 11·0 | 13·9 | 11·1 | 0·4 | 58·9 | 1·7 | 1·0 | 0·2 | U22 |
| High strength (clinker) | – | – | 28·1 | 11·2 | 7·1 | – | 52·0 | 1·6 | – | – | S116 |

interground with by-product anhydrite to a specific surface area of $400\,m^2\,kg^{-1}$; the optimum molar ratio of total $SO_3$ to $Al_2O_3$ was found to be 1·3–1·9 (20–25% $SO_3$). XRD and SEM of 1-day-old pastes showed the main product to be ettringite, the needles of which were 1–2 $\mu$m long and formed an interlocking network. A mortar made with the cement containing 20% $SO_3$ developed compressive strengths of 27 MPa at 3 h, 49 MPa at 1 day and 59 MPa at 28 days. The strength development at later ages was attributed to hydration of the $C_2S$.

For supporting and sealing the walls of roadways in coal mines, a material is required that can be transported as a slurry which remains stable for long periods while stationary in a pipeline but which when placed develops a modest compressive strength within a few hours. This can be achieved by employing two slurries that react and harden on being mixed. In one such system, one slurry contains a clinker containing $C_4A_3\bar{S}$ and the other contains anhydrite, CH, bentonite and alkali metal salts (L56). The $C_4A_3\bar{S}$ clinker, which can also be used as an expansive admixture with Portland cement, hydrates only slowly in the absence of CH. In the second slurry, the bentonite keeps the other solids in suspension and the alkali metal salts act as accelerators. In another system (B154), one slurry contains a CAC and the other anhydrite, bentonite, gypsum, lime and $Li_2CO_3$. In both cases, the products include ettringite and are of very high water content.

In most of the cements described in this section, ettringite is an important hydration product, but, as in supersulfated cements, its formation does not cause significant expansion. It is presumably formed either at a stage when the matrix of other phases is readily deformable or under conditions that allow it to be accommodated in an existing pore structure without causing disruption.

### *10.3.2 Energy reduction in the manufacture of cements*

Environmental pollution, including the emission of $CO_2$, and the depletion of resources of fossil fuels and raw materials are among the most serious problems confronting humanity today. Locher (L57) reviewed ways of decreasing the energy consumption in cement manufacture to values substantially below those characteristic of modern Portland cement production. They included the use of fluxes to lower the burning temperature, the production of cements containing more reactive forms of belite or based on belite together with highly reactive phases, replacement of alite by the chloride-containing phase, alinite, and the use of composite cements.

The burning temperature for production of Portland cement clinker can be decreased by about 150 K through the use of fluxes, but opinions have differed as to the energy saving thereby obtainable. Klemm and Skalny (K57), who reviewed the subject, estimated it at $630\,kJ\,kg^{-1}$. Christensen and Johansen (C65) considered that this figure, while possibly realistic for an inefficient, wet-process kiln, was unlikely to be so for a modern precalciner–preheater kiln, in which heat recovery is efficient. They considered a value of $105\,kJ\,kg^{-1}$ more realistic.

The compositions of many waste materials, such as slags, limit the extent to which these can be used in the production of a normal Portland cement clinker, but a wider range or higher content of waste materials might be usable in making other types of clinker. Mehta (M116) noted the possibility of using by-product gypsum, red mud (from aluminium extraction), slag and flyash in producing high-iron cements (Section 10.3.4). Some limestones unsuitable for making a normal Portland cement clinker could be used to make clinkers higher in belite. Burning at a reduced temperature might be expected to decrease the formation of $NO_x$.

In appraising the energy savings obtainable with these or other new types of cement, it is essential to consider the total energy requirements, from the winning and transport of the raw materials onwards. Locher (L57) emphasized the further need to consider not only strength development but also the durability obtainable given the curing conditions likely to be used in practice. He concluded that, with the low-energy cements that had then been investigated, the energy savings were probably no greater than those which could be achieved by use of composite cements containing slag, flyash, natural pozzolanas or fillers, the behaviour of which was well understood.

### *10.3.3 Reactive belites*

In the past few decades, very substantial improvements in energy efficiency in the production of Portland cement clinker have been made, and while further improvements may be expected, the possibilities of energy saving by this means are inevitably limited. The major component of the enthalpy change in the formation of Portland cement clinker arises from the decomposition of calcite, and a large saving could be achieved if the proportion of belite could be increased and, ideally, the formation of alite avoided. The theoretical heat requirement would be less and the clinkering temperature could probably be lowered. Because of the lower CaO content, the proportion of limestone would be reduced, less $CO_2$ would be produced and, possibly, limestone of lower purity could be used. In addition, the decreased quantity of CH formed on hydration might be expected to improve durability. The outstanding difficulty is the low rate of reaction of belite and thus also of strength development.

Methods for producing highly reactive belite or cements high in belite have recently been reviewed (C66). Attempts to increase the reactivity of belite have rested mainly on stabilization of the higher-temperature polymorphs, decrease in crystallinity or crystallite size, or combinations of these. Thus, reactive forms of belite have been obtained in the laboratory by low-temperature methods (R65,V10), but it is not clear how the latter could be effectively utilized in practice. Rapid cooling of a clinker (e.g. at $1000\,K\,min^{-1}$) increases the reactivity of belite, at least in part by preserving the $\alpha'$-polymorph (G94,S117) and may offer a more practical approach. Hillebrandite ($Ca_2(SiO_3)(OH)_2$) may be prepared hydrothermally from lime and silica at 200–250°C, and dehydrated at 500°C to give a form of $\beta$-$C_2S$ having a high specific surface area, which hydrates

rapidly in pastes at 25°C (I15,I16,O28). The hydration product is C–S–H having a Ca/Si ratio close to 2·0, so that little or no CH is formed.

*10.3.4 Cements containing belite and a highly reactive constituent.* In another approach to the problem, cements have been devised that contain belite together with a constituent, usually $C_4A_3\bar{S}$, which reacts rapidly and thereby provides sufficient early strength. Some have been proportioned in a way designed to produce rapid setting and hardening; an example is given in Section 10.3.1. Some other examples of cements based on belite and a highly reactive constituent are as follows.

(1) An alumina-belite cement (Z14) was obtained by burning at 1300°C of a mix intermediate in composition between those of Portland and calcium aluminate cements, with some gypsum. It contained 62–64% of belite, with CA, $C_{12}A_7$, $C_4A_3\bar{S}$ and $C_5S_2\bar{S}$, and was claimed to give good strength development and resistance to sulphate attack. Porsal cement (V11) is essentially similar and was made using $CaF_2$ as a mineralizer.

(2) Cements high in $Fe_2O_3$ have been described, containing high proportions of $C_2S$, $C_4A_3\bar{S}$, ferrite, and anhydrite (M116,W37). The hydration products of one such cement were reported to be AFt (ettringite), AFm, $AH_3$, $FH_3$ and C–S–H, with little CH (W37). Depending on phase composition, either normal or expansive cements can be obtained (W37).

(3) Sahu and Majling (S118) described cements made by firing mixtures of limestone, flyash and gypsum at 1200°C. The cements typically contained $C_2S$, $C_4A_3\bar{S}$ and $C\bar{S}$ as their major constituents, with smaller amounts of free lime and ferrite. The phase assemblages agreed with ones predicted from data on the $CaO$–$SiO_2$–$Al_2O_3$–$Fe_2O_3$–$SO_3$ system. The properties were broadly similar to those of Portland cements. Ettringite was a major early hydration product, and appeared to form by reaction involving the $C_4A_3\bar{S}$, anhydrite and free lime. Glasser and co-workers reviewed the hydration chemistry (W38) and the microstructure and microchemistry (A30) of cements based on $C_4A_3\bar{S}$. A clinker in which the most active phase was $C_4A_3\bar{S}$ had a spongy texture, making it easy to grind. Equant, well-shaped crystals of $C_4A_3\bar{S}$ were embedded in a matrix consisting largely of the $C_2S$ and a phase that approximated in composition to a ferrite but was possibly more properly described as a perovskite (A30).

*10.3.5 Alinite cements*

These cements were developed by Nudelman in the former USSR and patented in 1977. A mix for making Portland cement clinker is modified by adding $CaCl_2$, which allows the maximum temperature in the kiln to be reduced to 1000–1100°C. Table 10.5 gives some typical oxide compositions of the clinker. The alite is replaced by alinite, a structurally related phase containing essential $Mg^{2+}$, $Al^{3+}$ and $Cl^-$. Bikbaou (B155)

**Table 10.5** *Composition of alinite clinkers (A31)*

| | | | | | |
|---|---|---|---|---|---|
| MgO | 2·0–2·2 | CaO | 62·5–63·9 | Cl (free) | 0·04–0·12 |
| $Al_2O_3$ | 4·4–4·6 | $Fe_2O_3$ | 3·6–4·8 | Ignition loss | 0·7–1·0 |
| $SiO_2$ | 22·7–23·3 | Cl (total) | 1·0–2·9 | Free lime | <0·5 |

gave the phase composition as alinite, 60–80%, belite, 10–30%, $C_{11}A_7 \cdot CaCl_2$, 5–10%, ferrite, 2–10%, and discussed the process of clinker formation. Later work showed that a calcium chloride orthosilicate is also present (A31). This was possibly $Ca_3SiO_4Cl_2$, which is relatively highly reactive (K58). The process of formation has been further discussed (A31,B156,N20). Locher (L57) gave a survey of more general information, based partly on the patent data. The preparation of the pure compound has been described (V12,M117).

The crystal structure of alinite has been determined (I17,V12). The constitutional formula is $Ca_{9.9}Mg_{0.8}\square_{0.3}(SiO_4)_{3.4}(AlO_4)_{0.6}O_{1.9}Cl$, where $\square$ denotes a vacancy; limited variations in the Mg/Ca and Al/Si ratios are possible (V12). Alinite is tetragonal, space group $I\bar{4}2m$, with $a = 1{\cdot}0451$ nm, $c = 0{\cdot}8582$ nm, $Z = 2$, $D_x \approx 3010\,kg\,m^{-3}$ (V12), and is isostructural with the silicate sulphide mineral, jasmundite, $Ca_{11}(SiO_4)_4O_2S$ (D59). A Br-analogue has been prepared (K59).

The hydration reactions of alinite cements do not appear to have been reported, but it may be surmised that they are similar to those of Portland cements, with the probable addition to the products of $C_3A \cdot CaCl_2 \cdot 10H_2O$ and possibly also that of $Ca_2Cl_2(OH)_2 \cdot H_2O$. The $Cl^-$ is, however, not wholly and permanently combined in these or other hydration products. In tests on reinforced concrete, serious corrosion had occurred within 5 years, showing the cement to be unsuitable for such use (L57).

# 11 Admixtures and special uses of cements

## 11.1 Introduction

Admixtures for concrete are defined as materials other than hydraulic cements, water or aggregates that are added immediately before or during mixing. Materials such as grinding aids that are added to cement during manufacture are strictly called additives, though the term admixture is often used for these also. The most important admixtures are ones added to accelerate or retard setting or hardening, to decrease the quantity of water needed to obtain a given degree of workability, or to entrain air in order to increase the resistance of the concrete to damage from freezing. Mineral additions (Chapter 9) are not included here in either category.

Many materials have been used as admixtures and the potential of many more has been examined. The literature, including the patent literature and other descriptions of proprietary materials, is voluminous, and this text will attempt only to describe the effects of the most important classes of admixtures and additives in general terms and to discuss the chemistry underlying those effects at a fundamental level.

The rest of the chapter deals with the hydration chemistry of Portland and composite cements at temperatures outside the range of 15–25°C, including that of autoclave processes, and with specialized uses of cements in casing oil wells and in making very high strength materials.

## 11.2 Organic retarders and accelerators

### *11.2.1 Retarders*

Admixtures that retard setting are of value for concreting in hot weather and other purposes, including oil well cementing (Section 11.8). Many organic materials have this property; sucrose, calcium citrate and calcium lignosulfonate are examples. They are effective in low concentrations, suggesting that they act by adsorption. Taplin (T53) noted that most contain one or more groups in which O atoms are attached to adjacent carbon atoms, such as $-CO \cdot C(OH)=$, or are otherwise able to approach each other closely. He also noted that adsorption on either a clinker phase or a hydration product might cause retardation, in the latter case through interfering with growth. Young (Y8), reviewing the evidence,

concluded that adsorption on products, especially CH, was the prime cause of retardation. He considered that adsorption on anhydrous phases also occurred and that, with pure $C_3A$ or $C_3S$, it caused an initial acceleration by favouring dissolution.

Ramachandran *et al.* (R41) discussed factors affecting the efficacy of a retarder with cement. They included the ratio of retarder to cement, the time at which the retarder is added, the temperature and the compositions of the cement and of the mix. The time of initial set increases with the content of retarder and generally decreases with temperature and cement content. In a typical case, addition of 0.1% of sucrose on the mass of cement might increase the time of initial set from 4 h to 14 h, while a 0·25% addition might delay it to 6 days. Sufficiently high additions can delay setting indefinitely. Retarders are more effective with cements low in aluminate, because the latter, or their hydration products, consume disproportionate amounts of retarder. Some are more effective with cements low in alkali, perhaps because the latter destroys them. Retarders are most effective if added 2–4 min after mixing, because the aluminate has by that time reacted to some extent with the gypsum and consumes less retarder. The interactions between these and other factors are sufficiently complex that the effect of a specific retarder on a given mix should be pretested before it is used on a job. This applies to admixtures in general.

### 11.2.2 Mechanism of retardation

Thomas and Birchall (T54) obtained strong support for the hypothesis that retardation arises from adsorption on a hydration product. They

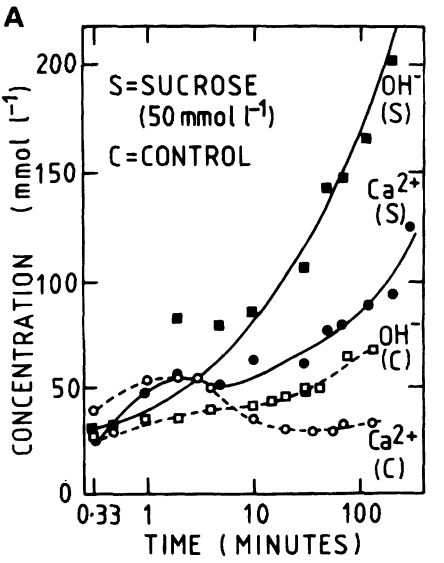


**Fig. 11.1** *Concentrations in the aqueous phase of Portland cements hydrated at w/c = 2·0 in water or in sucrose or EDTA solutions. After Thomas and Birchall (T54).*

determined analytical concentrations of calcium, silicon, aluminium, iron and $OH^-$ in the solution phases of slurries of cement (w/c = 2) with and without additions of sucrose or other sugars, at ages up to 7 h (Figs 11.1A and B). In the absence of a retarder, the concentrations of

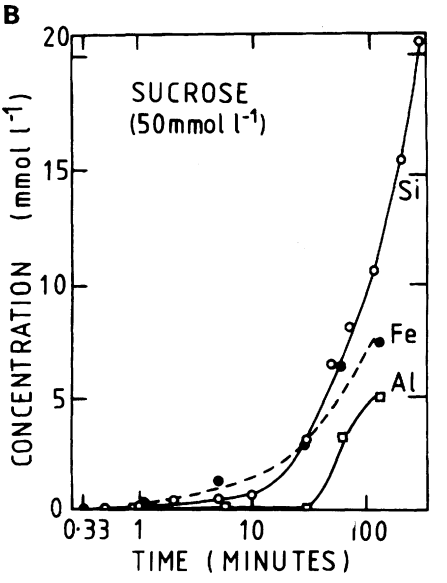


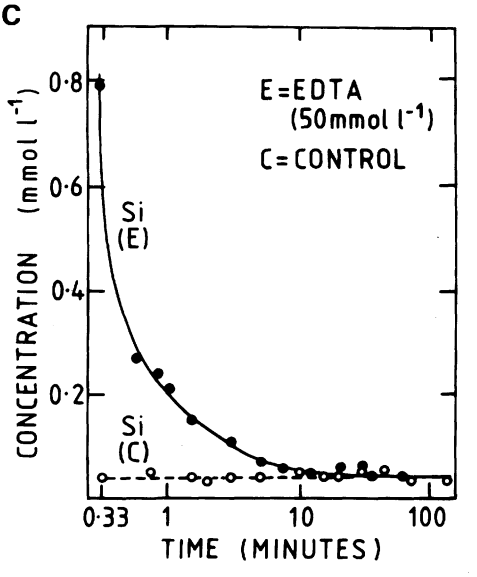


**Fig. 11.1** *(continued).*

silicon, aluminium and iron were all very low ($Si = 0{\cdot}04 \pm 0{\cdot}01$ mmol $l^{-1}$, $Al \leq 0{\cdot}01$ mmol $l^{-1}$, $Fe \leq 0{\cdot}01$ mmol $l^{-1}$), and Ca/Si ratios were in the order of 1000. In the presence of sucrose at 50 mmol $l^{-1}$, the calcium and $OH^-$ concentrations were somewhat increased, but those of silicon, aluminium and iron were increased by factors of up to 500, so that the Ca/Si ratio at 2 h had fallen to 6. The results were explained (B157, T54, T55) by supposing that poisoning of the surfaces of the hydration products allowed the $Ca^{2+}$ ions to coexist in solution with the silicate, hydroxoaluminate and hydroxoferrite ions at concentrations that were impossible if the solution was in equilibrium with the unmodified hydration products. NMR studies showed that Si–sucrose complexes were not formed.

The results of a similar study in which EDTA was used in place of sucrose further supported this conclusion (T56). The silicon concentration in this case increased rapidly during the first 20 s, but soon decreased to a value similar to that in the control (Fig. 11.1C). EDTA is a strong complexing agent for $Ca^{2+}$ in alkaline solutions; it therefore effectively removes the $Ca^{2+}$ from the system, and allows the silicate ion concentration to increase. Because it acts in the solution and not on a surface, a stoichiometric quantity (1 EDTA anion per $Ca^{2+}$ ion) is required, and the effect ceases when this is used up. Sucrose, in contrast, acts by adsorption, and much less is required. In accordance with these conclusions, EDTA has a negligible effect as a retarder when used in concentrations typical for such admixtures (T53).

Thomas and Birchall (T54) summarized and extended data on the comparative retarding effects of different sugars. They distinguished three categories. Trehalose and $\alpha$-methyl glucoside are ineffective as retarders; both are non-reducing sugars containing only 6-membered rings. Glucose, maltose, lactose and cellobiose, which are reducing sugars containing only 6-membered rings, are good retarders. Sucrose and raffinose, which are outstanding retarders, are non-reducing sugars containing 5- and 6-membered rings. The ability to solubilize CH was shown to be highest for maltose, lactose and cellobiose and lowest for trehalose and $\alpha$-methyl glucoside, and thus does not run parallel to retarding ability. This is shown also by the behaviour of EDTA, noted above.

Experiments in which calcium oxide or hydroxide was treated with sucrose solutions (B157) showed that a 1:1 Ca–sucrose complex was formed. It was concluded (B157,T54) that the retarding species was R–O–Ca–OH, where R represents the sucrose anion, which was incorporated into the surface of a growing particle of CH or C–S–H, thereby inhibiting growth. The calcium was considered to be attached to the fructose (5-membered ring) part of the molecule. Trehalose and $\alpha$-methyl glucoside were considered to be ineffective because their ability to complex calcium is very weak. The reducing sugars were considered to be less effective than sucrose or trehalose because opening of the ring allowed them to chelate Ca, giving complexes that were less readily adsorbed.

Birchall and Thomas (B157) explained the inhibition of growth of C–S–H by assuming that the Ca–O layers are the first parts of this

material to be formed, and could thus be poisoned by the retarder. Taylor (T57) earlier proposed a similar mechanism for the growth of C–S–H: starting from mononuclear complexes, such as $[Ca(H_2O)_5(OH)]^+$, repeated condensation through sharing of edges and elimination of water molecules leads to the formation of a Ca–O layer, which serves as a matrix for the formation of $Si_2O_7$ groups, and ultimately of dreierketten. He considered it unnecessary for a complete $CaO_2$ layer to be formed before silicate ions can begin to condense with it. It is most unlikely that the Si–O parts of the structure could form before the Ca–O parts because, although a column or layer of linked Ca–O polyhedra can exist without dreierketten, the reverse is not true. The manner in which the silicate tetrahedra condense is governed by the coordination requirements of the metal cations, and is entirely different if the $Ca^{2+}$ is replaced, for example, by $Mg^{2+}$.

Jennings *et al.* (J38) found that with $C_3S$, the retarding effect of sucrose was greatest if it was dissolved in the mixing water. This contrasts with the situation for cement. They concluded that the retarder was incorporated into the initial product and impeded its transformation into a second product. This explanation is compatible with that discussed above if incorporation is taken to mean adsorption on nuclei or growing particles of the second product. Although there may well be a phase transformation, this evidence does not seem to demand one. Even without one, the retarder would be more effective the sooner it was added, because a smaller area would require to be poisoned. The situation with cement differs due to the competing effect of the aluminate phase.

The broad conclusion indicated by the evidence considered in this section is that organic retarders are substances that are readily adsorbed on to the surfaces of growing particles of hydration products, especially C–S–H, and which do so in preference to complexing $Ca^{2+}$ ions in aqueous solution. The monodentate mode of attachment proposed by Thomas and Birchall (T54) explains the differences in behaviour among sugars, but its applicability in this respect to a wider range of substances has yet to be examined. It does not appear to account for the observation that the effective retarders are compounds in which two oxygen atoms are located on adjacent carbon atoms, or are otherwise able to approach each other closely.

### *11.2.3 Practical retarders*

The retarders most widely used in practice appear to be hydroxy carboxylic acids or their salts, such as citrates or heptonates, and lignosulfonates. Because of the low concentrations required, they are commonly added as solutions. Calcium or sodium lignosulfonates are waste materials from the manufacture of wood pulp, when they are formed by the breakdown of lignins. Their molecules are random, three-dimensional polymers with molecular weights of up to 50 000, probably spherical and with many sulfonate groups on their surfaces. The molecular structures are not completely known, and the element shown in Fig. 11.2 is purely illustrative of the types of local grouping that have been identified. Unpurified

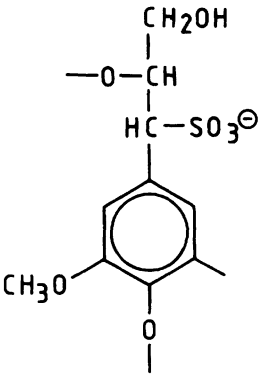


**Fig. 11.2** *Typical element of structure from a lignosulfonate anion.*

commercial lignosulfonates contain substantial proportions of sugars and related salts of sugar acids, such as gluconates, which are at least partly responsible for their retarding properties. Differing views have been expressed concerning the extent of the contribution from the lignosulfonate molecules themselves. Milestone (M118) and others have concluded that the retarding effect with $C_3A$ is largely due to the sugar acids, but Ramachandran (R66) found that, in low concentrations with cement, purified lignosulfonates were almost as effective as the unpurified material.

### *11.2.4 Organic accelerators*

Calcium formate accelerates setting and hardening in a manner similar to that of many inorganic salts (Section 11.5). Oxalic acid, added to $C_3S$, increases the extent of the initial reaction, but has no significant effect on the length of the induction period or the subsequent major stage of reaction (O14). Calcium oxalate is precipitated, and the concentration or chemical potential of $Ca^{2+}$ ions close to the surface of the $C_3S$ is thereby kept low until all the oxalic acid has been used up. Triethanolamine is added to some admixture formulations to decrease the retarding effect of the water reducer. The chemistry of its action is not well understood. Ramachandran (R67) found that, added as the sole admixture in amounts greater than 0·1%, it accelerates the reaction of the aluminate phase but markedly retards that of the silicates. At 0·5%, initial set occurs within a few minutes, but final set is delayed to over 24 h. This behaviour appears to be qualitatively similar to that of glucose, which also accelerates the initial reaction of the aluminate phase, though it delays the subsequent replacement of ettringite by monosulfate and greatly retards the hydration of the silicates.

## 11.3 Air-entraining agents and grinding aids

### *11.3.1 Air-entraining agents*

The ability of concrete to resist damage from freezing of the pore solution is increased by introducing voids into which the latter can expand. Air is entrapped on normal mixing, but is then of limited value because the

resulting voids are too large and too widely spaced. By the addition of a suitable surfactant, additional air is entrained and produces a stable foam, which persists in the hardened paste in the form of closely spaced, spherical pores. Air entrainment also improves workability. To avoid undue loss of strength, the total volume of pores should not be larger than necessary; the pores should therefore be small. The pores should not readily fill with water if the paste is saturated; small, isolated pores are most likely to meet this requirement. Klieger (K60) discussed the separations and total volumes of pores needed to provide adequate frost resistance. Typically, the pores are 10–250 $\mu$m in diameter and the average maximum distance from any point in the paste to the nearest void, called the void spacing factor, is about 150 $\mu$m.

Air-entraining agents are characteristically long-chain molecules with a polar group at one end, which therefore become concentrated at the air–liquid interface with their polar groups in the liquid and their non-polar parts out of it. Bubbles are formed by entrapment of air, but in the absence of the air-entraining agent are mostly destroyed because of the surface tension of the liquid. The air-entraining agent lowers the surface tension and stabilizes them. The inner surface of the bubble is thus composed of hydrophobic material formed by the non-polar parts of the molecules, which acts as a barrier to the entry of water during mixing or placing and on any subsequent occasion when the paste is saturated.

Air-entraining agents may be simple compounds, such as sodium salts of fatty or alkyl aryl sulfonic acids, but some are more complex (K60). The quantity of the active ingredient used is typically in the order of 0·05% on the mass of cement. As noted above, the property of air entrainment overlaps in varying degrees with the properties of retardation and water reduction. Air entrainment increases the workability of an otherwise similar concrete; by allowing the w/c ratio to be decreased, this can partly or wholly offset the loss in strength arising from the presence of the air voids.

Admixtures are known that decrease air entrainment; butyl phosphate is an example.

### *11.3.2 Grinding aids*

Grinding aids are sometimes used in clinker grinding, to decrease the energy required to achieve a given fineness of grinding or throughput. Massazza and Testolin (M119) reviewed their use. They are surfactants of various kinds, of which amines and polyhydric alcohols are possibly the most effective, and the amounts added are normally 0·01–0·1% on the mass of clinker. They appear to act mainly by decreasing agglomeration, though it has been suggested that they also aid fracture by preventing incipient microcracks from healing. There are conflicting reports on their effects on setting times, early strength and other properties. Grinding aids are clearly taken up by the anhydrous phases, and it is probably significant that the more effective are of different chemical types from retarders and water reducers, which are taken up mainly or entirely by the hydration products.

## 11.4 Water reducers and superplasticizers

### *11.4.1 Water reducers*

Water-reducing agents, also called plasticizers, allow a given degree of workability to be achieved at a lower w/c ratio. Conventional water reducers allow w/c to be decreased by 5–15%. To achieve greater decreases, they would have to be used at concentrations that would also cause excessive retardation, excessive air entrainment or flash setting. More powerful water reducers, called superplasticizers, allow w/c to be decreased by up to about 30%; these are considered in Section 11.4.2.

Water reducers act by adsorption at the solid–liquid interface, in this respect resembling retarders. There is a wide overlap between the two properties, many retarders being in varying degrees water reducers and vice versa. Both properties also overlap to some extent with that of air entrainment, which is promoted by species that act at the air–liquid interface. Conventional water reducers are typically added as solutions in concentrations of up to 0·2% on the mass of cement. Calcium and sodium lignosulfonates are widely used both as retarders and as water reducers. Their retarding effect can be decreased by treatment to lower the content of sugars and sugar acids, and can be further decreased or reversed by blending with an accelerator, or enhanced by blending with a stronger retarder. Compounds that decrease air entrainment may also be added. Other materials used as water reducers include salts of hydroxy carboxylic acids, hydrolysed carbohydrates, and hydrolysed proteins.

In general, water reducers are effective with Portland, composite and calcium aluminate cements. Many of the characteristics of retarders, described in Section 11.2.1, apply also to water reducers, and for the same reasons; thus, they are most effective if added a few minutes after mixing, and, in some cases at least, with cements low in aluminate phase and alkali.

The workability of any fresh concrete decreases with time after mixing, but this effect, which is called slump loss, is more marked if a water reducer is used. The slump nevertheless remains higher than if the latter was absent. Slump loss is caused by the slow commencement of the hydration reactions, and its increased magnitude in concrete containing water reducers is probably due to the gradual absorption of the admixture by the hydration products. Delay in adding the admixture until a few minutes after mixing minimizes it.

### *11.4.2 Superplasticizers*

Superplasticizers are also called high-range water reducers. The marked lowering of w/c ratio that they allow makes it possible to produce high-strength concretes, especially if the mix also includes silica fume. Alternatively, the use of superplasticizers at normal w/c ratios allows the production of 'flowing' concrete that is self-levelling and can readily be placed by such methods as pumping or continuous gravity feed through a vertical pipe. The greater effect compared with conventional water reducers is due to the fact that they can be used in higher concentrations, which can be over 1% on the mass of cement, without causing excessive

retardation or air entrainment. If used in similar concentrations to conventional water reducers, the degrees of water reduction obtained are also similar.

Three principal types of superplasticizer are in common use, viz. salts of sulfonated melamine formaldehyde polymers (poly(melamine sulfonate); PMS), salts of sulfonated naphthalene formaldehyde polymers (poly(naphthalene sulfonate); PNS), and modified lignosulfonate materials. Most of the available information relates to the first two types, which will alone be considered here. Both are commonly added as solutions. Commercial formulations often contain other substances added to alter setting behaviour or for other reasons.

Both PMS and PNS are, in theory, linear anionic polymers with sulfonate groups at regular intervals (Fig. 11.3). Jolicoeur *et al.* (J39) summarized chemical aspects of commercial PNS, including spectroscopic and other methods of characterization, distributions of molecular weight, and deviations from the idealized structures. The chains are often branched and may contain closed loops. The number of sulfonate groups in an individual monomeric unit, theoretically one, can also be zero or two. The mean number of sulfonate groups per monomeric unit decreases with molecular weight, e.g. from 0·80 in a low-polymer fraction to 0·66 in the most highly polymerized fraction. The distribution of molecular weight is very broad, with molecules ranging from monomer to

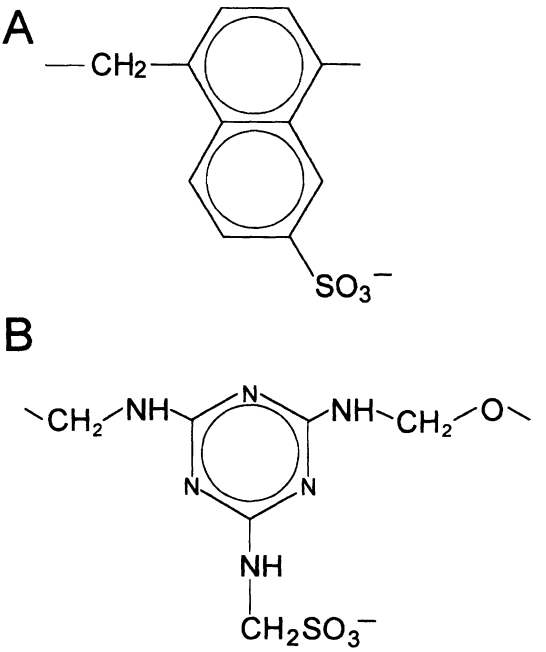


**Fig. 11.3** *Repeating units of the structures of idealized superplasticizer anions: (A) naphthalene formaldehyde condensate; (B) melamine formaldehyde condensate.*

a molecular weight of over 100 000. These and other variables markedly affect behaviour, e.g. decreases in apparent viscosity are much greater with $Na^+$, $K^+$ or $(CH_3)_4N^+$ than with $Ca^{2+}$ or $Mg^{2+}$.

Most of the characteristics of conventional water reducers are shown also by superplasticizers, at least qualitatively; thus, they are more effective if added a few minutes after mixing, retard setting and increase slump loss. Retardation of set is slight with PMS but more marked with PNS. Slump loss is considerable with both types, and is accelerated by increase in temperature. At 15°C, the enhanced fluidity typically persists for 30–60 min. Slump loss is lessened if the superplasticizer is added a few minutes after mixing, and can also be partly countered by including a retarder or, if practicable, by adding a second dose of superplasticizer before placing. Unlike conventional water reducers, superplasticizers used in normal concentrations do not cause significant air entrainment, and may even decrease the amount of entrapped air because of the greater fluidity of the mix. Air-entraining agents can be added, and must be used in higher than normal concentrations.

### *11.4.3 Mode of action of water reducers and superplasticizers*

The fact that the water-reducing effects of superplasticizers are similar to those of conventional water reducers used in similar concentrations suggests that the modes of action are similar, and that the essential difference is that the properties that limit the concentrations in which conventional water reducers can be used are weaker or absent in superplasticizers. These properties comprise retardation, air entrainment and, in some cases, flash setting.

It is widely agreed that water reduction is effected through improved dispersion of the cement grains in the mixing water; flocculation is decreased or prevented, and the water otherwise immobilized within the flocs is added to that in which the particles can move. With superplasticizers, this can be seen with the light microscope (D60,R41), or in greater detail by SEM of rapidly frozen samples (U15; Section 8.1.4). With some water reducers, retardation of hydration and increased air entrainment may contribute to the increase in fluidity at any given age, though with lignosulfonates the fluidity is increased even if air entrainment is avoided through addition of tributyl phosphate (B158), and superplasticizers in normal concentrations do not entrain air.

Adsorption of the admixture on the hydrating cement grains could decrease flocculation in at least three ways (D60). The first is an increase in the magnitude of the $\zeta$-potential; if all the particles carry a surface charge of the same sign and sufficient magnitude, they will repel each other. The second is an increase in solid–liquid affinity; if the particles are more strongly attracted to the liquid than to each other, they will tend to disperse. The third is steric hindrance; the oriented adsorption of a non-ionic polymer can weaken the attraction between solid particles.

All water reducers, including superplasticizers, appear to contain more than one polar group in the molecule, and many are polymeric. Some simple compounds that are good retarders, such as glucose, are not water

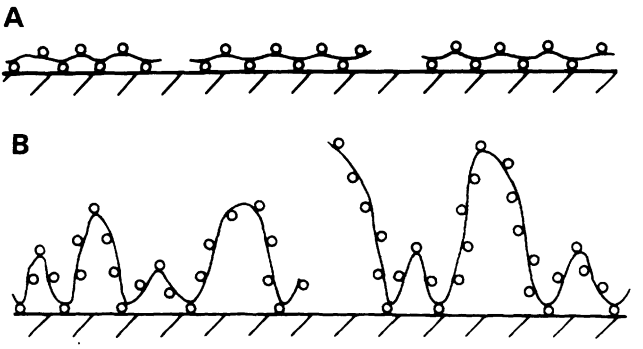


**Fig. 11.4** *Possible modes of attachment of polyelectrolyte anions to the surface of a particle of cement: (A) train and (B) loop modes. Circles represent negatively charged groups. After K61.*

reducers. Kondo *et al.* (K61) considered that polyelectrolytes were adsorbed on the solid surfaces in the ways shown in Fig. 11.4, so that some of their polar groups bind them to the solid, while others point towards the solution.

*11.4.4 Zeta potential, rheology and nature of the sorbent phases*

Ernsberger and France (E8) showed that addition of calcium lignosulfonate causes cement grains to develop a negative $\zeta$-potential. Daimon and Roy (D60,D61) studied the action of superplasticizers by determinations of $\zeta$-potential and quantities adsorbed, which they related to the flow behaviour. In the absence of admixture, the charges on the grains were too small to permit reliable determinations of the $\zeta$-potential, but with increasing contents of admixture the latter became increasingly negative, and tended towards a limit of $-30$ to $-40$ mV. Up to about 1% of PNS could be adsorbed, and the increase in $\zeta$-potential, amount adsorbed, dispersion of the grains and increase in fluidity were all positively correlated. Daimon and Roy concluded that the increase in $\zeta$-potential was the major cause of the improved dispersion. Further rheological studies (A32,R68) showed that superplasticizers decrease both the plastic viscosity and the yield stress. The major effect was on the yield stress, which could decrease almost to zero. Zelwer (Z13) found that, in the absence of admixtures, $C_3S$ and cement developed weak negative $\zeta$-potentials. That of $C_3A$ was difficult to study due to flocculation, but appeared to be positive, becoming negative on hydration.

Kondo *et al.* (K61) considered that too high a molecular weight was undesirable, as the molecules could then form bridges between adjacent particles. In contrast, Andersen *et al.* (A33) found that for sulfonated polystyrenes, the highest $\zeta$-potentials were obtained with material of high molecular weight, although this was not as strongly adsorbed as that of lower molecular weight. They concluded that the high molecular material was more likely to show loop as opposed to train adsorption (Fig. 11.4), and thus to place more of its negative charges into the diffuse double layer.

The fact that both conventional water reducers and superplasticizers are more effective if added some time after mixing provides a strong indication that adsorption probably occurs at least in part on the hydrated phases, as the anhydrous surfaces have by that time become covered with hydration products. Chiocchio *et al.* (C67) found that the optimum time for addition was at the start of the induction period. More of the admixture seems to be taken up by the early hydration products, especially of the aluminate phase, if it is added before the early reaction has subsided.

Costa *et al.* (C68) showed that superplasticizers increase the fluidity of $C_3S$ pastes much as they do that of cement pastes. Studies on individual anhydrous and hydrated compounds in aqueous and non-aqueous media indicate that calcium lignosulfonate and superplasticizers are adsorbed by C–S–H, AFm phases or CH but not by $C_3S$, $C_3A$ or $C_3AH_6$ (C68,M120,R69–R71), though they appear to be taken up by unhydrated $\beta$-$C_2S$ (C69). The admixtures also enter interlayer sites of $C_4AH_x$ and perhaps also of C–S–H (R70). Intercalation of organic molecules in $C_4AH_x$ is a well-established effect (Section 6.1.1).

Banfill (B159) noted that the amounts of superplasticizers taken up by cement were sufficient to form a layer on the anhydrous grains some 60 nm thick. He concluded that multilayer adsorption occurred and that steric hindrance was the major effect. This argument is weakened by the evidence that uptake is largely by the hydration products and that significant amounts of material are absorbed as well as adsorbed. The bulk of the evidence indicates that increase in $\zeta$-potential is the major effect.

### *11.4.5 Reasons for the enhanced dispersing power of superplasticizers*

As noted above, the difference between superplasticizers and conventional water reducers probably lies in the weaker ability of the former to act as retarders, air-entraining agents or causes of quick setting, which allows them to be used in higher concentrations. The low air-entraining ability can reasonably be attributed to the repeating pattern of polar groups, which provides the molecule with no suitable hydrophobic regions (K61). The reason for the weakness of the retarding power is less obvious. Weak retarding power implies that the hydration products can grow despite the presence of the sorbed material. This might happen because the latter can be assimilated into them, or because the individual bonds between sorbent and sorbate are sufficiently weak that the latter can be displaced by ions adding to the product. Equilibrium with the solution would ensure that the sorbate was readsorbed on the added material.

## 11.5 Inorganic accelerators and retarders

### *11.5.1 Accelerators of setting and hardening*

Calcium chloride has long been known to accelerate both the setting and hardening of Portland cement concrete. Typically, for concrete cured at 20°C, an addition of 2% of $CaCl_2 \cdot 2H_2O$ on the mass of cement might shorten the time of initial set from 3 h to 1 h and double the 1-day

compressive strength. The effect on strength decreases with time, and the final strength can be reduced. Some properties related to the microstructure of the paste, such as resistance to sulfate attack, are also adversely affected. The accelerating effects are greater at low temperatures. They increase with the amount of $CaCl_2$ used, and at 4% very rapid setting may occur; 2% is probably a reasonable limit. This gives a concentration of about $0{\cdot}3\,mol\,l^{-1}$ in the mixing water for $w/c = 0{\cdot}5$.

Calcium chloride is typically added as $CaCl_2 \cdot 2H_2O$. Chloride ion promotes corrosion of reinforcement, and in many countries, including the UK, $CaCl_2$ is no longer used in reinforced concrete. A number of other compounds, such as calcium formate, have been found to have similar properties to $CaCl_2$, but all are both more expensive and less effective.

### *11.5.2 Mode of action*

The addition of $CaCl_2$ increases heat evolution at early ages. Supported by other evidence, considered shortly, this indicates that the effects on setting and hardening are due to acceleration of the hydration reactions. Early studies, summarized by Murakami and Tanaka (M121), showed that a great many salts have effects qualitatively similar to those of $CaCl_2$. With some reservations, these effects occur with $C_3S$ pastes as well as with cement pastes, and are thus seen to be due to faster hydration of the alite.

Figure 11.5 shows heat evolution curves, obtained by conduction calorimetry, for a $C_3S$ paste with and without addition of $CaCl_2$. When the latter is present, the main heat evolution peak begins earlier and rises and falls more steeply; its maximum is reached earlier. The rate of heat evolution at the maximum is positively correlated with the reciprocal of the time at which the maximum occurs (D25). The linear relation extends to organic retarders. As these probably act by hindering the growth of C–S–H (Section 11.2.2), this evidence suggests that the accelerators act by promoting it.

Many studies have shown that both cations and anions contribute to the accelerating effect and that an approximate rank order can be established for each type of ion (C70,D25,E9,K62,K63,M121,W39). For the present such ions as $Mg^{2+}$ or $F^-$, for which precipitation of additional phases complicates the situation, will be excluded from consideration. The sequences found by different investigators vary somewhat, and are also influenced by concentration and possibly by the nature of the counter ion. Kantro's (K62) results for the cumulative heat evolution at 12 h for a 3% addition of $CaCl_2 \cdot 2H_2O$ and equivalent concentrations of the other chlorides or calcium salts are reasonably typical:

$$Ca^{2+} > Sr^{2+} > Ba^{2+} > Li^+ > K^+ > Na^+ \approx Cs^+ > Rb^+$$

$$Br^- \approx Cl^- > SCN^- > I^- > NO_3^- > ClO_4^-$$

While there are some anomalies, the effect tends to increase with increasing charge and decreasing size of the ion. $Ca^{2+}$ is considerably more

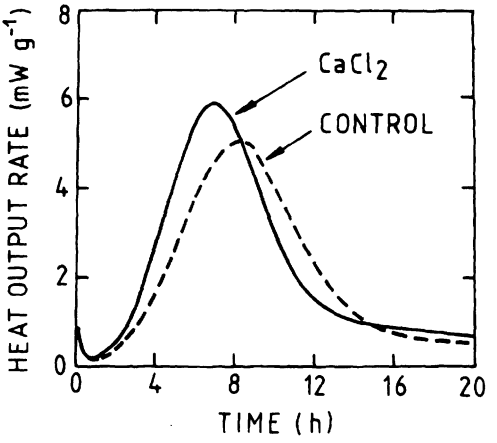


**Fig. 11.5** *Rates of heat output from $C_3S$ pastes hydrated at 25°C and w/c ratio 0·6, with and without $CaCl_2$ in a concentration of 0·0204 mol $l^{-1}$. After B70.*

effective than any other cation, suggesting that a specific effect is superimposed on a general one. At very high concentrations, some salts that accelerate in lower concentrations, such as NaCl, act as retarders.

At normal concentrations (e.g. $\leq 1$ mol $l^{-1}$), the accelerating effect of ions is sufficiently widespread to suggest that some general property of electrolytes is involved. The ranking sequences are broadly similar to the Hoffmeister series, which relates to the flocculation of hydrophilic colloids; flocculation is promoted by the action of ions that compete for the water molecules that otherwise keep the particles apart. A similar effect may influence the rate at which complexes can be transferred from the solution to the growing particles of C–S–H. Anomalies in relations to size and charge might be explained through differing degrees of solvation or complexation. It would indeed be surprising if the rate at which the C–S–H grows was not influenced by the nature and concentration of ions in the surrounding solution, and if at least one of the ions entering the solid did not have a specific and positive effect.

The hydration of hemihydrate or anhydrite shows interesting similarities to and differences from that of $C_3S$ (G53). Many foreign ions accelerate or retard hydration, but the sequences of effectiveness differ markedly from those found for $C_3S$. Excess $SO_4^{2-}$, but not excess $Ca^{2+}$, is a particularly strong accelerator. Murat *et al.* (M122) found that, for anhydrite, the effectiveness of an added cation decreased with its ionic potential $z/r$, and considered that the cations mainly affected the rate of nucleation. The relation to $z/r$ is almost the reverse of what is found with $C_3S$ hydration.

In other approaches to the problem, attempts have been made to relate the accelerating effects either to diffusion of ions (D25,K63), the pH of the bulk solution or the solubility of CH. $CaCl_2$ and other salts decrease

the pH of the solution (B70,L58,M121), but there is no apparent correlation between the magnitude of the decrease and the accelerating effect (M121) and NaOH has no significant effect on the rate of $C_3S$ hydration in the stage of the reaction under consideration (B70,G53). The latter observation also tells against the view (S119) that acceleration is due to increased CH solubility, since the latter is decreased by addition of NaOH.

### *11.5.3 Effects on the composition and structure of the hydration products*

In any attempt to understand the effects of $CaCl_2$ or other accelerators on the structure or properties of the hydration products it is essential to compare pastes at equal degrees of hydration and not at equal ages. Several early studies (e.g. R72,T12) indicated that the addition of $CaCl_2$ affects the Ca/Si ratio of the C–S–H or the degree of condensation of the silicate anions, but later work did not support either conclusion. Determinations of unreacted $C_3S$, CH and combined water confirmed that substantially more $C_3S$ reacts during the first day if $CaCl_2$ is present, but showed the latter to have no significant effect on either the Ca/Si or the $H_2O$/Si ratios of the C–S–H (L19). SEM of fracture surfaces of both young and mature samples shows that the C–S–H morphology is altered (L19,R72). At early ages, it changes from the fibrillar Type I to the honeycomb-like Type II variety. A study using TG and $^{29}Si$ NMR showed that admixture of $C_3S$ with $CdCl_2$, $Pb(NO_3)_2$ or malic acid had no significant effect on the Ca/Si ratio of the C–S–H or, if equal degrees of hydration were considered, on the ratio of $Q^1$ to $Q^2$ silicate tetrahedra, and thus on the relative amounts of dimer and larger silicate ions (C71). $CdCl_2$ is an accelerator, but $Pb(NO_3)_2$ and malic acid are retarders.

Ramachandran and Feldman (R72) determined helium porosities and densities for cement pastes containing various quantities of $CaCl_2$. They concluded that for a given degree of hydration, the effect of the latter was to increase the absolute density and thus also the porosity. At non-evaporable water contents of 12–16%, 1% or 2% additions of $CaCl_2$ slightly increased the compressive strength, but 3·5% additions decreased it.

The situation of the $Cl^-$ ion in the hardened paste is important in relation to the possibility of promoting corrosion. A study on the hydration of $C_3A$ and $C_3S$ in the presence of gypsum and $CaCl_2$ showed that $C_3A \cdot CaCl_2 \cdot 10H_2O$ was formed after all the $SO_4^{2-}$ had been used up (T58). No phase containing essential $Cl^-$ was detected in the mixes with $C_3S$ except at a 20% addition of $CaCl_2$. Ramachandran (R73) concluded from thermal and other evidence that, in cement pastes made with $CaCl_2$, much of the $Cl^-$ was chemisorbed or present in interlayer spaces, and that about 20% of it was not leachable by water. In contrast, analysis of pore solutions expressed from 35- or 70-day-old pastes of cement with NaCl additions showed that 85–98% of the $Cl^-$ was present in the pore solution (P53). This proportion was substantially lower for cements containing silica fume.

### 11.5.4 Precipitation effects; inorganic retarders and setting accelerators

Many salts precipitate additional phases when added to $C_3S$ or cement pastes. If the hydroxide of an added cation is less soluble than CH, either it or a basic or complex salt is precipitated. Examples of such precipitates are $Mg(OH)_2$ or AFm phases (K62), $Zn(OH)_2$ or $CaZn_2(OH)_6 \cdot 2H_2O$ (A34) and basic Pb nitrate or sulfate (T59). Precipitation will leave in solution all or part of the added anion and an equivalent amount of $Ca^{2+}$. The calcium salt of an added anion, if of sufficiently low solubility, is similarly precipitated; examples are provided by $SO_4^{2-}$, $CO_3^{2-}$, $PO_4^{3-}$, $F^-$, silicate, aluminate and borate. In this case, the added cation remains in solution with an equivalent amount of $OH^-$.

The salts in these categories have widely varying effects on setting and hardening. Some, such as Pb or Zn salts, phosphates or borates, are strong retarders. Others, such as Mg salts, behave as setting and hardening accelerators in much the same way as ones not precipitating additional phases. Yet others, such as carbonates, have effects ranging from flash set to retardation of set depending on the concentrations in which they are added.

Retardation is probably caused by the formation of protective layers over the cement grains; this has been demonstrated for Pb (T59) and Zn (A34) salts and carbonates (U25). In the latter case, it was shown that the layer formed at low concentrations, which caused retardation, was more compact than that formed at higher concentrations, when acceleration occurred. Evidently, more than one effect is involved, and these effects can be delicately balanced.

The chemistry underlying accelerating effects produced by salts that yield precipitates is not well understood. As with retarding effects, more than one mechanism probably operates. In cases where a cation is precipitated (e.g. with magnesium salts), the $Ca^{2+}$ released and the anion supplied would be expected to behave like the corresponding calcium salt added at the same stage. $CaCl_2$ is a less effective accelerator if added 12 h after mixing than if added immediately (C70), perhaps because by this time growth of C–S–H is becoming increasingly unimportant as a factor controlling the rate of reaction (Section 7.7.2); this may be expected to reduce the effectiveness of the liberated $Ca^{2+}$. The accelerating effect of carbonates in suitable concentrations appears to be confined to the initial stage of reaction. It occurs with alite as well as with cement (U25), and is thus associated with the behaviour of that phase. It may be due to decreased permeability of a protective layer, as suggested above, but might also be due to removal of $Ca^{2+}$ from the solution, as has been postulated for oxalic acid (Section 11.2.4).

Admixtures that accelerate the early reaction are used in shotcreting or gunniting, in which a concrete mix is sprayed from a nozzle onto a vertical or steeply sloping surface, and for other applications, such as plugging leaks against pressure, in which rapid setting is essential. Those commonly used include sodium carbonate, silicate and aluminate. Setting

can thus be caused to begin within minutes, or almost immediately, but subsequent hardening may be delayed and final strengths greatly reduced.

## 11.6 Effects of high or low temperatures at atmospheric pressure

### *11.6.1 Hydration at 25–100°C*

Precast concrete products are frequently cured at elevated temperatures below 100°C because of the increased rate of hardening that is obtained. Elevated temperatures can also arise adventitiously in mass concrete due to the heat evolved on hydration, or from subsequent exposure to a source of heat. In the case of precast concrete, various temperature cycles have been employed. In order to avoid microcracking from thermal stresses, it has generally been considered necessary to cure for some hours at ordinary temperature before raising the external temperature and to restrict the rates at which the temperature is increased and decreased. Maximum temperatures up to 100°C have been used, but if the temperature within the concrete exceeds 60–70°C serious loss of durability can occur. This could be partly due to increased microcracking, but a deleterious effect known as delayed ettringite formation (Section 12.6) can also occur. Some modern codes of practice set limits in this region (e.g. D62). The concrete may be heated using saturated steam at atmospheric pressure, and the term 'steam curing' is often used, but, to achieve better temperature control and for other reasons, other methods of heating are also widely used and the term 'elevated-temperature curing' is preferable.

### *11.6.2 Effects on kinetics, ultimate extent of hydration and microstructure*

Early work suggested that time and temperature could be regarded as equivalent from the standpoint of strength development. So-called maturity functions, based on this concept, have been used for the prediction of strength (e.g. B160), but proved to be of limited validity. In fact, increase in curing temperature accelerates hardening but the ultimate strength is generally reduced (I18,S120). Hydration rates increase markedly with temperature (A19,C46), which accounts for the increased rate of hardening. Some of the earlier studies indicated that the ultimate degrees of hydration are lower at elevated temperatures (A35,V7) but a recent XRD study (A19) showed that there is no significant variation.

The reactions of flyash, slag and other pozzolanic or latent hydraulic materials are accelerated by increasing temperature to a greater extent than are those of the clinker phases. With flyash, substantial reaction occurs within 1–2 days at 40°C or above, which may well be reached within a large pour of concrete. Under conditions simulating the temperature regime at a depth of 3 m, and using a composite cement containing 25% of flyash, about 7 kg of the latter per 100 kg of composite cement had reacted in 3 days and 10 kg in 100 days (C51). The increased rate of reaction is also shown by accelerated consumption of CH (H62).

The lowered ultimate strength of concrete cured at elevated temperatures is probably due, at least in part, to microstructural changes in the paste. Verbeck and Helmuth (V7) suggested that rapid hydration led to encapsulation of the cement grains by a product layer of low porosity, which retarded or prevented further hydration. Because the remaining product would necessarily be more porous, the material would be weaker than one of the same w/c ratio and degree of hydration in which the product was uniformly distributed. SEM examination by backscattered electron imaging of polished surfaces supports this conclusion (K64,K65). In pastes hydrated at 50°C, the hydration products were less uniformly distributed than in those hydrated at 5°C; dense hydration shells were observed around the clinker grains, and numerous large pores were present in the interstitial space. For a paste of w/c ratio 0·5, hydrated to an estimated 70% at 5°C, the porosity determined from BSE images was 4%; for one similarly hydrated at 50°C, it was 15%. Provided that allowance is made for differing degrees of hydration, sorption studies using water or nitrogen indicate distributions that become coarser with increasing temperature (A35,B57,C72,O22,S120). Mercury intrusion porosimetry shows a similar effect (K45).

For pastes cured at 50°C, the hydration shells of inner product formed from or around the larger grains appear brighter in backscattered electron images than the remaining C–S–H (K64). The grey level of this inner C–S–H approached that of the CH, making it difficult to distinguish between the two. Estimates of the Ca/Si ratio of the C–S–H in calcium silicate pastes cured at elevated temperatures have been obtained from determinations of CH and unreacted starting material (A35,B57,C46, K19, O29,O30). The results are conflicting, but tend to indicate increases in Ca/Si ratio with temperature. X-ray microanalyses also indicate this (P54,S121). There is not necessarily any real variation in the Ca/Si ratio of the C–S–H, as poorly crystalline CH closely mixed with C–S–H in the hydration shells would probably not have been determined by the methods used.

In pastes that have been cured at an elevated temperature and subsequently hydrated further at ambient temperature, the inner product of the clinker grains may be zoned, the outer part being the brighter (P54,S122). The outer and inner zones were considered to be material that had hydrated at the elevated and ambient temperatures, respectively. The difference in grey levels was accompanied by one in the totals found in X-ray microanalysis. The effect could be due to differences in porosity or composition or both. The results of X-ray microanalyses tend to suggest that they are mainly due to differences in porosity (P54,S122).

Studies on calcium silicate pastes show that the distribution of silicate anion size is shifted significantly upwards with rise in curing temperature (Sections 5.5.2 and 5.5.3). XRD gives no definite indication of any variation in crystallinity of the C–S–H with temperature up to at least 100°C.

The reactions of the aluminate and sulfate phases are much modified at temperatures of about 70°C and above. These reactions, which can

cause damage through an effect known as delayed ettringite formation, are discussed in Sections 12.6.1 and 12.6.2.

### *11.6.3 Low temperatures*

Mironov (M123) summarized the results of studies on concreting at subzero temperatures in the former USSR. Hydration continues to the extent that liquid water is present; this in turn depends on the ambient conditions and on the pore structure, and is increased by precuring at ordinary temperature. At −5°C, with 24 h precuring, hydration continues at a useful rate, but at or below −10°C it is extremely slow. Additions of $CaCl_2$ and other salts act both as accelerators and anti-freezing agents (M123,M124). These conclusions were substantially confirmed by Regourd *et al.* (R74), who examined a concrete containing 9% of $CaCl_2$ on the mass of cement that had been mixed with hot water and cast and cured for 1 year at −10°C. The long-term compressive strength and microstructure were not greatly different from those of a similar concrete cured at ordinary temperature. Calcium aluminate cements behave well at low temperatures (Section 10.1).

## 11.7 High-pressure steam curing

### *11.7.1 General*

The hardening of concrete or other materials based on calcium silicates may be further accelerated by the use of saturated steam under pressure in an autoclave. Typically in such processes, a mix containing Portland cement and finely ground quartz, in addition to aggregate, is cured for 2–4 h in saturated steam at 175°C (~800 kPa). As with elevated-temperature curing below 100°C, it is necessary to precure for a few hours at ordinary temperature, and to restrict the rate of heating, and to a lesser extent that of cooling.

Autoclave processes are used to produce a wide variety of materials, ranging from dense concretes and fibre-reinforced materials, through aerated concrete with a bulk density of 300–800 $kg\,m^{-3}$ to very low density thermal insulation materials. The cement provides strength to facilitate handling prior to autoclaving, but otherwise serves essentially as a source of CaO and $SiO_2$, and may be partly or wholly replaced by other starting materials of suitable composition. Calcium silicate bricks (P55) are made from lime and sand, which are pressed into shape when moist and autoclaved. The chemistry of the process is essentially similar to that of the cement-based materials. Aerated concretes (M125) are typically made by incorporating aluminium powder, which reacts during the initial curing below 100°C, generating hydrogen. In autoclave processes in general, both natural and waste materials of various kinds may be used as partial sources of the CaO or $SiO_2$ or both.

Early experience in making autoclaved concrete showed that the presence of siliceous material of a sufficiently reactive nature was essential for attainment of satisfactory strength. Menzel (M126) showed that the ratio of such material to cement was critical. Figure 11.6 shows his results for mixes containing Portland cement and finely ground quartz. The

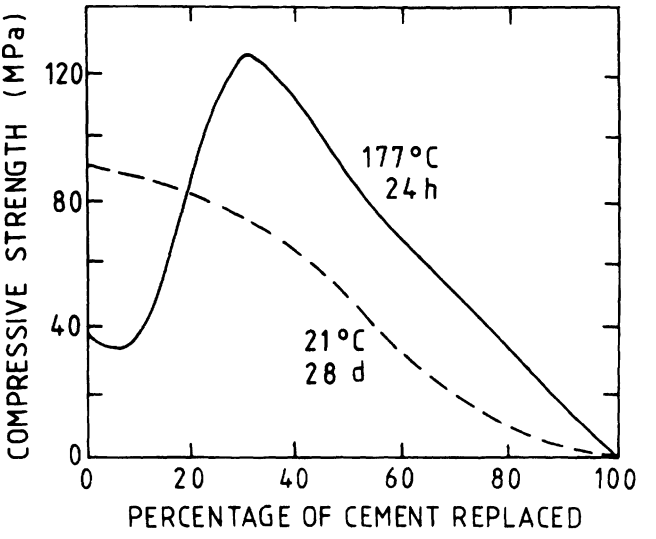


**Fig. 11.6** *Effects of partial replacement of cement by finely ground silica on the compressive strengths of mixes cured normally and in the autoclave. After M126.*

highest strengths were obtained at a quartz–cement mass ratio of about 30 : 70. The optimum ratio depends on the nature and fineness of the siliceous material.

### *11.7.2 Basic chemistry of autoclave processes*

Understanding of the chemistry of autoclave processes is due primarily to the work of Kalousek and co-workers (K34,K66–K69). Above about 150°C, for the time scales of a few hours that are used in practice, two features of cement hydration chemistry are added to those relevant at lower temperatures. Firstly, the hydration products tend to crystallize; in the absence of reactive silica, C–S–H tends to be replaced by a structurally unrelated, crystalline phase, $\alpha$-$C_2S$ hydrate. Secondly, the range of siliceous materials having effective pozzolanic properties is widened, and includes quartz and various other crystalline minerals, if sufficiently finely ground. The behaviour of the aluminate and sulfate phases differs from that occurring at 70°–100°C, and subsequent damage from delayed ettringite formation is not a potential problem.

Menzel's results were thus explained. Addition of a small amount of quartz brings the bulk Ca/Si ratio to 2·0, which is that of $\alpha$-$C_2S$ hydrate. This phase is relatively dense and crystallizes as rectangular tablets; the product is porous and weak. With larger amounts of quartz, pozzolanic reaction occurs; the CH is consumed, formation of $\alpha$-$C_2S$ hydrate is avoided, and a C–S–H of low Ca/Si ratio is formed. The porosity is reduced, and a strong material results. The optimum addition of quartz is the maximum that can be taken up; further additions act only as a

diluent, and the strength decreases. Table 11.1 gives crystal data for $\alpha$-$C_2S$ hydrate and other phases.

The optimum addition yields C–S–H with a Ca/Si ratio of 0·8–1·0. C–S–H of this composition tends to crystallize to give 1·1 nm tobermorite (Section 5.4.1). Opinions have differed as to the extent to which crystallization is desirable (K67). It has been widely found that optimum times and temperatures of autoclaving exist, which if exceeded lead to decreases in strength. As the main effect of extended time or increased temperature is likely to be an increase in the crystallinity of the binder, this suggests that, from the standpoint of strength, crystallization is either undesirable or that some optimum degree of crystallinity exists. The latter view (B129,F40) appears the more probable for relatively dense materials. It is generally agreed that crystallization decreases drying shrinkage and improves resistance to chemical attack (A36,K67,P55). Crystallization is probably favoured by low bulk density; its extent is apparently minimal in calcium silicate bricks (P55), but complete in aerated concretes (M125). In the latter materials, excessive autoclaving can weaken the material through formation of xonotlite ($C_6S_6H$).

In cement–silica materials, substantially all the $Al_2O_3$ appears to enter the C–S–H, which as its Ca/Si ratio decreases can accommodate increasing amounts of tetrahedrally coordinated Al (R23,S123). NMR results (K70)

**Table 11.1** *Crystal data for some synthetic, hydrothermally produced phases*

| Name | 1·1 nm tobermorite* | 1·1 nm tobermorite‡ | $\alpha$-dicalcium silicate hydrate |
|---|---|---|---|
| Formula | $[Ca_4(Si_{5.5}O_{17}H_2)]\cdot Ca\cdot 4H_2O$ | $[Ca_4(Si_{5.5}Al_{0.5}O_{17}H_2]\cdot Ca_{0.2}\cdot Na_{0.1}\cdot 4H_2O$ | $Ca_2(HSiO_4)(OH)$ |
| Lattice parameters | | | |
| *a* (nm) | 0·564 | 0·563 | 0·9476 |
| *b* (nm) | 0·368 | 0·369 | 0·9198 |
| *c* (nm) | 2·26 | 2·28 | 1·0648 |
| Crystal system | Orthorhombic | Orthorhombic | Orthorhombic |
| Space group | I – – –† | I – – –† | Pbca |
| *Z* | 1 | 1 | 8 |
| X-ray density ($kg\,m^{-3}$) | 2481 | 2400 | 2723 |
| References | | | |
| Structure | H33,M54 | § | H71,M127,Y9 |
| Lattice parameters | H72 | H72 | P1¶ |

* Typical data for normal tobermorite.
† Data for tobermorites relate to pseudocell. Structures not fully ordered.
‡ Typical data for anomalous tobermorite with Al and Na substitution.
§ See Section 11.7.4.
¶ Card no. 29-373.

support an early conclusion (K69) that 1·1 nm tobermorite, too, can accommodate aluminium in tetrahedral sites. Small amounts of hydrogarnet have sometimes been detected, especially in products made from raw materials high in $Al_2O_3$, such as flyash or slag. Minor amounts of jaffeite (tricalcium silicate hydrate; $C_6S_2H_3$) have sometimes been reported (A37,K68). The behaviour of the sulfate ion does not appear to be understood.

### 11.7.3 Mechanisms of reaction and equilibria

Quartz reacts relatively slowly, and substantial proportions of C–S–H having a Ca/Si ratio of about 1·75 are formed as intermediate products, which gradually react with it to give C–S–H of lower Ca/Si ratio. This process competes with the formation of $\alpha$-$C_2S$ hydrate. The conditions should be such as to minimize the latter process, since subsequent reaction of $\alpha$-$C_2S$ hydrate with quartz is slow and may not be completed in the time available. Fine grinding of the quartz and adequate mixing with the cement are therefore essential.

Several reviews of phases and equilibria in the $CaO–SiO_2–H_2O$ system have been given (R75,T60,T61). Over 20 crystalline ternary phases were listed in a 1980 review (T61), and two more have since been reported (G95,S124). Neither 1·1 nm tobermorite nor $\alpha$-$C_2S$ hydrate is an equilibrium product in the pure system at 180°C under saturated steam pressures, the stable ternary phases under these conditions possibly being truscottite ($C_7S_{12}H_3$), gyrolite ($C_2S_3H_2$), xonotlite, hillebrandite ($C_2SH$) and jaffeite, according to the composition (T60). Of these phases, only xonotlite forms readily under normal autoclaving conditions from mixtures in which the $SiO_2$ is supplied partly as quartz. It is rapidly formed from such mixtures at 200°C, and because of its good thermal stability in air is used in some autoclaved thermal insulation materials. If the $SiO_2$ in an autoclaved material is supplied in a highly reactive form, such as diatomaceous earth, the reaction takes a different course; gyrolite, or at higher temperatures truscottite, is formed as an early product, and 1·1 nm tobermorite, if formed at all, results from reaction of CaO with phases of lower Ca/Si ratio (B161).

### 11.7.4 Characteristics of hydrothermally formed C–S–H and tobermorite

Mitsuda *et al.* (M128) described the XRD patterns, morphology, IR spectra, thermal behaviour and other properties of hydrothermal preparations of C–S–H. The XRD patterns resembled those of C–S–H(I) (Section 5.4.4). TEM showed that all contained crumpled foils, but some also contained fibrous aggregates. The latter gave electron diffraction patterns corresponding to poorly crystalline tobermorite, in some cases probably intergrown at or near a single-layer level with xonotlite or foshagite ($C_4S_3H$). These results show that the distinctions between C–S–H(I), tobermorite and other crystalline phases are not sharp; materials of intermediate composition and crystallinity can exist through mixing on the nanometre scale.

1·1 nm tobermorites differ in their behaviour on heating. All lose their interlayer water at 100–300°C, but this may or may not be accompanied by shrinkage of the layer thickness to 0·93–0·94 nm (G96). Specimens that show lattice shrinkage, called normal tobermorites, crystallize as thin, pseudohexagonal plates with (001) cleavage and a tendency to elongation parallel to *b*. Those that do not, called anomalous tobermorites, tend to form smaller, more elongated crystals with major (001) and minor (100) cleavages. Apart from small differences in lattice parameters, which can be obscured by effects of ionic substitutions (H72), the XRD powder patterns are identical.

The structure of the individual layers in tobermorites is described in Section 5.4.2. In 1·1 nm tobermorites, these layers are stacked in such a way that those O atoms of the bridging tetrahedra (Fig. 5.6) that do not form part of the chain can closely approach those of the adjacent layer. A suggestion (M55,T62) that interlayer Si–O–Si links are present in anomalous tobermorites was confirmed by chemical (W40) and $^{29}Si$ NMR (K17,R23,W21) studies of silicate anion type. The compositions and densities of naturally occurring tobermorites show that the contents of the pseudocell (Table 11.1) always deviate markedly from the idealized formula $C_5S_6H_5$ (M55). There are at least three effects, as follows.

(1) The silicate chains can have missing tetrahedra, as in C–S–H(I) (Section 5.6.1). This, the sole major effect in unsubstituted normal tobermorites, is compositionally equivalent to loss of the elements of $SiO_2$ and thus increases the Ca/Si ratio and lowers the density. In the highly crystalline natural materials, the limiting composition is probably about $[Ca_4Si_{5.5}O_{17}H_2]Ca \cdot 4H_2O$, where square brackets exclude the interlayer material. In synthetic preparations, the proportion of missing tetrahedra can possibly be greater.

(2) Interlayer Si–O–Si links are formed. This effect is associated with reduction in interlayer Ca content and is probably a replacement of $(2Si–O^- + Ca^{2+})$ by Si–O–Si, and thus compositionally equivalent to loss of CaO. It decreases both the Ca/Si ratio and the density. The theoretical limiting composition is $[Ca_4Si_6O_{17}H_2] \cdot 4H_2O$, but may not be realizable.

(3) Substitution of $Si^{4+}$ by $Al^{3+}$ is balanced by an increase in interlayer $Ca^{2+}$ or introduction of interlayer alkali cations or both. All known naturally occurring anomalous tobermorites show a combination of effects (2) and (3).

1·1 nm tobermorite is readily synthesized using CH and finely ground quartz at 180°C. It is much less readily formed if amorphous silica is used. Synthetic studies show that normal tobermorite is an intermediate in the transition from C–S–H(I) to anomalous tobermorite (E10,H72). Its formation in preference to anomalous tobermorite is favoured by short time, low temperature, high Ca/Si ratio, and presence of $Al^{3+}$ in absence of alkali. The presence of $Al^{3+}$ together with alkali favours the formation of anomalous tobermorite (E10). That of alkali without $Al^{3+}$

has been variously found to impede crystallization (E10) or to favour formation of anomalous tobermorite (H72). Most of these results are readily explainable in terms of the structural differences described above. $Al^{3+}$ is also reported to accelerate the formation of tobermorite and to retard its replacement by xonotlite at temperatures around 175°C (K69). Mitsuda and Chan (M129) found the tobermorite in some aerated concretes to be anomalous. Aluminium-substituted tobermorites have cation exchange properties (K71).

Hara and Inoue (H72) studied the lattice parameters of tobermorites. They confirmed an early observation (K69) that $c$ increases with Al substitution, but found that several other variables affect the parameters to smaller extents. The $a$-axial lengths of highly crystalline, natural tobermorites appear to be lower (0·560–0·562 nm for the pseudocell) than those of the synthetic materials (M55).

## 11.8 Oil well cementing

### *11.8.1 General*

In oil well cementing (N21) a cement slurry is pumped down the steel casing of the well and up the annular space between it and the surrounding rock. The main objects are to restrict movement of fluids between formations at different levels and to support and protect the casing. More specialized operations include squeeze cementing, in which the slurry is forced through a hole in the casing into a void or porous rock, and plugging, in which the casing is temporarily or permanently blocked at a specified depth.

With current technology, oil wells are typically up to 6000 m deep. The temperature of the rock at the bottom of the well ('bottom hole static temperature') at that depth is 100–250°C. The maximum temperature of the slurry during pumping ('bottom hole circulating temperature') is in general lower but may still be as high as 180°C. The pressure experienced by the slurry during pumping is equal to the hydrostatic load plus the pumping pressure, and may be as much as 150 MPa. The entire depth of a deep well would not be cemented in a single operation, but even so, pumping can take several hours. In geothermal wells, the maximum temperatures encountered may exceed 300°C.

### *11.8.2 Types of cement and of admixture*

The slurry must remain sufficiently mobile for the pumping operation to be completed and must provide adequate strength, resistance to flow of liquid or gas and resistance to chemical attack after it has been placed. By using a high-temperature, high-pressure consistometer, in which the regime of temperature and pressure during pumping is simulated, it is possible to monitor the changes in consistency and to predict the 'thickening time' during which pumping is practicable. The thickening time is akin to final set under the simulated well conditions. The American Petroleum Institute has defined various classes of Portland cement, of which G and H are widely used. The specifications of both are typically met by sulfate-resisting

Portland cements, coarsely ground to 280–340 $m^2 kg^{-1}$ (Blaine) for Class G or to 200–260 $m^2 kg^{-1}$ for Class H (B162,N21). Free lime is minimized to permit good response to admixtures. Both classes are intended to be used as basic cements at depths down to about 2500 m, and at greater depths with suitable admixtures. In practice, admixtures of many kinds are used at most depths.

Retarders and dispersants (water reducers) are widely employed, especially in the deeper wells and also to counteract the effects of other admixtures that have incidental accelerating effects. Lignosulfonates, modified lignosulfonates, cellulose derivatives and saturated NaCl are among those used. NaCl is effective up to about 130°C, and modified lignosulfonates to at least 150°C. Superplasticizers may be used up to 150°C. Accelerators, such as $CaCl_2$ (2–4% on the mass of cement) or NaCl (2·0–3·5%) are also used. In marine locations, sea water is often used for mixing, and acts as an accelerator. Sodium chloride may be added to fresh water; in addition to its accelerating or retarding properties, it reduces damage to salt and shale strata and causes the hardened paste to expand.

Various admixtures are used to modify physical properties of the slurry, though some have incidental chemical effects that are countered by the use of further admixtures. It may be necessary to adjust the bulk density, e.g. by adding hematite to raise it, or bentonite (sodium montmorillonite) or sodium silicate to lower it. Bentonite greatly increases the water demand, but may be used together with calcium or sodium lignosulfonate and sometimes NaCl to obtain a desired combination of density, fluidity, w/c ratio and thickening time. The optimum addition of untreated bentonite is 8%, but this is reduced to 2% if the bentonite has been prehydrated, i.e. mixed with water and allowed to swell before being used. Granular, lamellar or fibrous materials are occasionally added to prevent slurry from being lost in rock fissures when lightweight or thixotropic slurries are insufficiently effective. Expanded perlite (a heat-treated volcanic material), walnut shells, coal, cellophane and nylon are examples. Nylon or other fibres have been used to increase shear, impact and tensile strength but sometimes present logistical problems. Cellulose derivatives, water reducers and latex admixtures are among admixtures that reduce loss of solution from the slurry into porous strata.

More specialized admixtures include radioactive tracers, which may be detected by devices lowered down the hole to trace the movement of the slurry. Dyes or pigments may similarly be used to check its emergence. Some of the chemicals added to drilling muds are strong retarders for cement. Proprietary 'spacer fluids' are commonly pumped ahead of the cement slurry to counteract contamination. Admixtures of paraformaldehyde and sodium chromate are sometimes also used. Addition of 5–10% of gypsum produces a thixotropic slurry, which can be pumped but which gels rapidly when stationary; this can be used to help the slurry to pass permeable formations. Gypsum, if added in appropriate proportion, also causes expansion, and it or other expansive admixtures may be used to improve the seal with the rock or casing.

### 11.8.3 Effects of temperature and pressure

At the high temperatures encountered in deep wells, pozzolanic admixtures are essential to prevent strength retrogression, as in high-pressure steam curing (Section 11.7). Silica flour (finely ground quartz) and silica sand are the most commonly used. There are few data on the effects of prolonged exposure of cement–silica mixes to hydrothermal conditions; pastes cured for 2·5–4 months at 140–170°C and saturated steam pressures are reported to have similar strengths to those so treated for shorter times, though some replacement of tobermorite by gyrolite and xonotlite was observed (I19). In a deep well, the pressure may be much above that of saturated steam; this alters the equilibria (R75,T60) and possibly also the kinetics. At 110°C or 200°C and 7–68 MPa, mixtures of cement and quartz were shown to give C–S–H(I), which began to change into tobermorite within 32–64 h (O31). In hot, geothermal wells, many phases can form in addition to or in place of those found in autoclaved cement materials (L59).

Special problems arise in cementing wells in the Arctic, where permafrost may exist to a depth of 1000 m. It is necessary that the cement should set at low temperatures, that the surrounding ground should not be disturbed by melting or erosion during drilling or cementing or in the subsequent life of the well, and that freezable liquids should not be left in the annular space. Calcium aluminate cements, and mixtures based on Portland cement and gypsum, have been used (N21).

## 11.9 Very high strength cement-based materials

### 11.9.1 General

This section deals with cement-based materials having compressive strengths much above 100 MPa or comparable uprating of other mechanical properties. Relatively modest improvements yield materials with potential specialist uses in construction. Larger ones, especially in tensile or flexural strength and fracture toughness, offer the possibility of making low-volume, high-technology materials. Roy (R76) has reviewed the chemistry and other aspects of these materials.

The compressive strength can be increased by lowering the w/c ratio. As the latter decreases, the particle size distribution of the starting material becomes increasingly important. Brunauer *et al.* (B163) described the preparation and properties of cement pastes with compressive strengths up to 250 MPa. Portland cement clinkers were ground to 600–900 $m^2 kg^{-1}$ using grinding aids and subsequently mixed at w/c 0·2 with admixtures of calcium lignosulfonate and $K_2CO_3$.

Lime–quartz materials with compressive strengths of up to 250 MPa can be made by moulding the starting materials under a pressure of 138 MPa before autoclaving (C73,T63). Portland cement pastes have similarly been pressure moulded to allow use of w/c ratios down to 0·06 and development of 28-day strengths up to 330 MPa (R77). Roy and co-workers obtained still higher strengths by hot-pressing Portland (R77,R78) or calcium aluminate (G97) cement pastes, followed by normal curing in water. A Portland cement paste pressed for 1 h at 250°C

and 345 MPa and then cured for 28 days had a strength of 650 MPa. The compressive strengths and total porosities (1·8% in the case mentioned) obeyed the Schiller relation (Section 8.5.1).

Impregnation with an organic polymer of a concrete that has already developed some strength is another way of reducing porosity and increasing strength. The concrete is first dried, and the monomer is then introduced and polymerized in situ by $\gamma$-irradiation or by including a catalyst and subsequently heating at 70–90°C (I20). Poly(methylmethacrylate) (PMMA) is possibly the most effective polymer. For maximum uptake of polymer, it is necessary to dry strongly (e.g. by heating at 150°C) and to evacuate, but useful amounts can be introduced without evacuation. Compressive strengths can be approximately doubled, and values around 220 MPa have been reported for cement–sand mortars. Vacuum impregnation of cement pastes and autoclaved materials with molten sulfur at 128°C similarly increased microhardness and elastic modulus by factors of up to 6 and 4 respectively (F50).

In general, XRD and other studies show that the phase compositions of the very high strength materials described above are similar to those of weaker ones of similar types, the proportion of unreacted clinker phases increasing with decrease in porosity. The microstructures of hot-pressed cements are dense and compact (R77); the major product detected in hot-pressed calcium aluminate cements was $C_3AH_6$ (G97). This is consistent with Feldman and Beaudoin's (F40) view that this and similar dense, crystalline phases produce high strengths if sufficiently closely welded together in materials of low porosity. The same applies to unreacted clinker phases. Pastes impregnated with PMMA or sulfur are still sufficiently permeable to water that expansion occurs on long exposure (F51). In polymer-impregnated cement pastes, there is evidence of interaction between $Ca^{2+}$ ions and carboxylate and possibly other groups of the polymer matrix (S125).

### *11.9.2 DSP concretes*

Very high strength concretes have since been obtained using Portland cements with superplasticizers and silica fume. In so-called DSP (densified systems containing homogeneously arranged ultrafine particles) materials, the use of low w/s ratios (0·12–0·22), special aggregates, including fibres, and special processing conditions allows compressive strengths of up to 270 MPa to be obtained, with good resistance to abrasion and chemical attack (H63,H73). The properties were attributed to a combination of effects. The particles of silica fume, being much finer than those of the cement, partially fill the spaces between the cement grains, and this, together with the superplasticizer, allows the latter to pack more uniformly. They also provide nucleation sites for hydration products, undergo pozzolanic reaction and improve the paste–aggregate bond.

### *11.9.3 MDF cements*

The tensile or flexural strengths of the materials described above were, in general, about one-tenth of the compressive strengths, as in normal cement

pastes or concretes. In so-called MDF (macro-defect-free) cements, Birchall and co-workers (B164,K72) obtained higher relative values of flexural strength and other mechanical properties. The materials were made by including a water-soluble polymer in a Portland or calcium aluminate cement mix. The polymer (typically PVA, i.e. poly(vinyl alcohol), poly(acrylamide) or methylcellulose) made it possible to achieve mixing at a very low w/c ratio (0·10–0·15). Subsequent high-shear mixing and pressing produced a dough that could be formed by extrusion or other techniques. The highest strengths were obtained using calcium aluminate cements; compressive strengths up to 300 MPa, flexural strengths up to 150 MPa and Young's moduli up to 50 GPa were obtained.

Kendall *et al.* (K72) considered that MDF cements owed their high strengths primarily to the absence of large flaws, which they held to be the reason for the relative weakness of normal cement pastes; they regarded the polymer essentially as a processing aid. However, the large volume fraction of polymer and the small extent of hydration of the cement that can occur in view of the low w/c ratio render this unlikely, and later work (B130,E4,K73) showed that the polymer plays an essential role in determining the physical properties of the product. In MDF (R79) cement pastes, and also in polymer-impregnated cement pastes (S125), there is evidence of interaction between $Ca^{2+}$ ions and carboxylate and possibly other groups of the polymer. In MDF pastes made with calcium aluminate cement, the polymer (PVA) was found to inhibit the normal hydration reactions of the cement, but to react with $Ca^{2+}$ and $Al^{3+}$ to give an ionically cross-linked polymer and calcium acetate. TEM showed the material to be essentially a dispersion of grains of clinker or hydration products in a continuous polymer matrix. The materials thus appear to be polymers modified by cross-linking by $Ca^{2+}$ ions, and filled with grains of largely unreacted cement, to which they are probably chemically bonded.

Unmodified MDF cements suffer severe loss of flexural strength on exposure to moisture, data quoted by Roy (R76) showing falls to 20–40% of the oven-dry values. The strength loss is accompanied by significant expansion. The effects are due to swelling of the polymer matrix, compounded by other effects, which can include further hydration of the cement grains made possible by the resulting ingress of water (R80). Russell *et al.* (R80) described four possible strategies for improving the performance of an MDF cement containing PVA in the presence of moisture. These were:

(1) increasing the temperature of pressing and drying
(2) adding a cross-linking agent (boric acid or an organic Cr(III) complex) to insolubilize the PVA
(3) incorporating an organosilane coupling agent to produce a hydrophobic polymer network at the PVA–cement interface
(4) impregnation of the cured material with a monomer that reacts with PVA

Method (4) was not investigated. Of the others, method (3) appeared to offer the most promise, but further work was needed in order to obtain consistent results.

# 12 Concrete chemistry

## 12.1 Cement paste in concrete

### *12.1.1 The interfacial transition zone*

Concrete cannot properly be described as a composite of coarse and fine aggregate in a matrix of cement paste otherwise identical with the aggregate-free material. The microstructure of the paste close to the aggregate differs from that of cement paste in bulk, and much of the paste in a concrete or mortar is in this category (D63). Because the strength and durability of concrete depend in part on features at the cement–aggregate interface, many of the studies on concrete microstructure have concentrated on this aspect. Several reviews exist (D64,M130,M131,S126).

In a study of thin sections of mortars by light microscopy and TEM, Farran and co-workers (F48,F52) showed the presence in some cases of an interfacial transition zone (ITZ) at the paste–aggregate interface. In this zone, which was up to some 35 $\mu$m wide, the paste was of increased porosity and presumably lower strength. Microhardness measurements confirmed this (L60). Further TEM studies (J40) showed that the aggregate surfaces were closely covered with poorly crystalline material, probably C–S–H.

Studies of specimens in which cement paste was cast against glass or polished surfaces of aggregates, and of fracture surfaces, showed the presence of highly oriented layers of CH on the aggregate surfaces (B165,B166, D65,G98,M132,S127). In some cases, duplex films of CH and C–S–H, typically of total thickness 1·0–1·5 $\mu$m, were reported (B165,B166). Ettringite contents were also shown to increase on approaching the aggregate surface (M132,M133,W41). A TEM study of ion-thinned sections of mortars gave no evidence of either a duplex film or of CH in contact with the aggregate surfaces, though CH was sometimes present near the interface. C–S–H was commonly present in contact with the aggregate (Z15).

### *12.1.2 Backscattered electron imaging of the interfacial transition zone*

Studies of prepared surfaces do not properly reflect the situation in a real mortar or concrete. As Scrivener and Gartner (S128) noted, the aggregate

surfaces in a real concrete or mortar are not polished, flat and widely separated, but in varying degrees irregular and close together. During mixing, the aggregate particles are in vigorous motion relative to the surrounding paste, and during setting, localized bleeding below aggregate particles or reinforcement can occur. Studies of fracture surfaces suffer from the further serious limitations that they are not representative of the bulk material, but of its weaker regions, and that X-ray microanalyses on them are at best only semi-quantitative. The high resolution provided by secondary electron images aggravates the problem of obtaining statistically representative information. Backscattered electron images (BEI) of sections cut through a mortar or concrete and then polished (S37,S128–S131) do not suffer from these limitations, and are readily combined with quantitative X-ray microanalysis and with image analysis to provide further types of quantitative information.

In any attempt to estimate distances within an ITZ from BEI of polished sections, proper account must be taken of the fact that the interfaces examined are in general not perpendicular to the section (S128,S131). Studies by BEI with image analysis (S131) showed that the ITZ is approximately 50 $\mu$m thick, though the transition to the bulk paste structure is gradual and the most marked differences were found in the so-called near ITZ within 10–20 $\mu$m of the aggregate surface. As the aggregate surface was approached within the ITZ, the average content of unreacted clinker phases decreased and the porosity increased (Fig. 12.1). The region within about 10 $\mu$m from the surface was deficient in the usual relicts of large clinker grains, indicating that it is difficult for the latter to pack close to the interface. The grains smaller than about 5 $\mu$m had often hydrated completely, giving hollow-shell grains, which were thus relatively abundant in the interfacial region.

These results gave no indication of the presence either of duplex films or of continuous layers of CH at the aggregate interfaces in normal concretes or mortars, and showed only a slight increase in average CH content as the aggregate surface was approached. Large crystals of CH were sometimes formed adjacent to the sand grains, and tended to predominate on fracture surfaces because of their good cleavage; their orientation relative to the aggregate surface varied considerably (S129). Particularly large crystals or extensive deposits of CH were found in places where local bleeding was considered to have been likely. Regions poorer in cement particles sometimes occurred on one side only of a sand grain and possibly arose from the sweeping action of the latter during mixing. The tendency to increased content of ettringite in the ITZ was confirmed.

Later work has, in general, shown larger increases in the average content of CH in the ITZ, though their extent appears to vary considerably. Thus, Bonen (B167) found that, in concretes with a variety of different aggregates, coatings of CH were usually present, either as layers or as dispersed crystals. The CH layer was commonly 2–3 $\mu$m wide but frequently thinned or, alternatively, thickened to some 8 $\mu$m. Where aggregate particles were close together, CH tended to fill the spaces between them. The increased porosity in the near ITZ was confirmed.

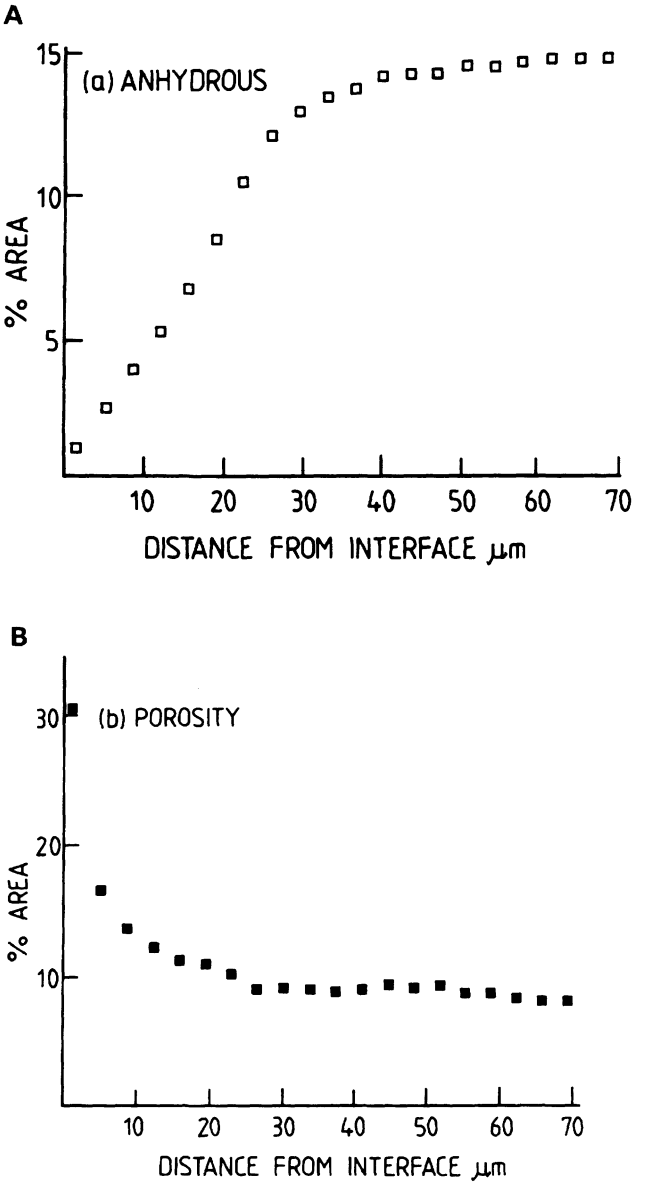


**Fig. 12.1** *Microstructural gradients in the interfacial region of a concrete: (A) unreacted clinker phases; (B) porosity, determined using SEM with image analysis. Each point represents a mean from 50 determinations, and the standard errors were approximately 10% relative. From S131.*

### 12.1.3 The nature of the paste–aggregate bond

In principle, chemical reactions between paste and aggregate could strengthen the bond by corroding the aggregate surface and thereby increasing the area of contact (F48,G99), but they could also weaken the material by creating spaces between paste and aggregate or by producing expansive forces too strong for the bond to withstand.

Struble *et al.* (S126) reviewed early work on the paste–aggregate bond. Postulated superficial pozzolanic reactions at ordinary temperatures between paste and quartz or other common siliceous aggregates appear to be unsupported by experimental evidence, except for the deleterious alkali–silica reaction (Section 12.4). On the other hand, there is considerable evidence that superficial reaction occurs with calcite aggregate and that it strengthens the bond with the paste (B168,F48,G99,M134). From XRD and SEM studies on composites of pastes cast against marble surfaces and on pastes made from cement mixed with finely ground calcite, Grandet and Ollivier (G99) concluded that $C_4A\bar{C}_{0.5}H_{12}$ was formed initially and that it was later replaced by $C_4A\bar{C}H_{11}$. The calcite surfaces were strongly pitted. This reaction, earlier postulated by Lyubimova and Pinus (L60), is noted in Section 9.6.3 in connection with the use of calcite as a mineral addition.

Monteiro and Mehta (M134) found that the calcite was similarly pitted if alite was substituted for cement and reported the appearance of an XRD peak at 0·79 nm. They considered that the reaction product, either with alite or with cement, was not a carbonate-containing AFm phase but a basic calcium carbonate. Such phases have been reported as synthetic products (S132) and as a natural mineral, defernite (P56).

### 12.1.4 Permeability of the interfacial transition zone

Winslow and Liu (W42) concluded from an investigation using MIP that the cement paste in mortars or concretes was more porous than that in a neat paste hydrated to the same extent. The increase was mainly in the larger pore entry sizes detectable by this technique. In further work, a series of mortars of differing sand contents was studied (W43). The results confirmed a suspicion that the extra porosity resided in the ITZ. For mortars made using plain Portland cement, the porosity increased sharply at a volume fraction of sand between 45% and 49%. This was attributed to the onset of percolation of the interfacial transition zone. Computer modelling indicated that an ITZ thickness of 15–20 $\mu$m would account for this result. This thickness agrees well with the SEM evidence on the thickness of the highly porous part of the ITZ closest to the aggregate surfaces. The authors concluded that percolation of the ITZ would occur in most constructional concretes, a result that agreed with the generally high permeabilities of concretes compared with those of cement pastes.

### 12.1.5 Composite cements and other topics

Partial replacement of cement by silica fume increases the strength in concrete, but not in pastes (B169). This supports the view that the effect is due to a strengthening of the paste–aggregate bond (B169,R81,S128).

Studies of concretes by backscattered electron imaging showed that the increase in porosity in the ITZ is much less marked if silica fume is present (B169,B170,R82,S133). Scrivener and Gartner (S128) found some increase in porosity, but attributed it almost entirely to the presence of hollow-shell grains. With pastes vibrated against a single piece of aggregate, in contrast, the replacement had no significant effect on the distribution of porosity within the ITZ, and some clumping of the silica fume was observed. Clumping was found to occur in pastes even when a superplasticizer was used (S133), suggesting that the coarse aggregate breaks up the clumps by crushing or shearing during mixing.

Computer modelling of the ITZ (B171) confirmed that silica fume would be expected to decrease the gradient of capillary porosity in the ITZ but indicated that it would not eliminate it completely. The model also predicted that the effectiveness of mineral additions in increasing the integrity of the ITZ would depend on both their particle size and their reactivity. Inert additions would, with some reservations, have little effect, and flyash would be less effective than silica fume, because of its larger particle size and lower reactivity. The porosity in the ITZ may also be increased by dissolution of CH (B170). An experimental study showed that partial replacement of cement by flyash can either increase or decrease the width of the ITZ, depending on the characteristics of the flyash, but that slag had relatively little effect (C74).

Interfaces of calcium aluminate cements with aggregates are discussed in Chapter 10. The ITZ between Portland cement paste and steel has been studied by SEM, using various techniques of specimen preparation (e.g. A38,B172). The major features observed have been substantial deposits of CH and, further away from the interface, a relatively weak, porous zone. Bentur *et al.* (B172) also reported the occurrence of a duplex film. Interfaces of cement or $C_3S$ pastes with zinc (A39,T64) or copper (T64) have been studied.

### *12.1.6 Effects at exposed surfaces*

The microstructures of the surface regions of a concrete differ from that of the bulk material, and are important because they have a major effect on durability. The differences have several origins. Settlement and constraints imposed by the formwork may affect aggregate distribution. Moisture gradients can be created if a surface is exposed to a drying atmosphere, retarding or even stopping hydration in the surface layers, altering the pore structure and facilitating carbonation. Water can be lost by absorption in or leakage through formwork.

Patel *et al.* (P57) moist cured blocks of cement pastes of w/c ratio 0·59 for 7 days and then sealed the prism surfaces of each and exposed the ends to air at 20°C and 65% RH. Methanol sorption data showed that, near the exposed surfaces, the pore structure was markedly coarser and the diffusion time lower. TG evidence showed that less hydration had occurred and that carbonation was increased. These effects were detectable even at a distance of 50 mm from the exposed surface. Further work confirmed the marked effect of RH on hydration rates (P33; Section 7.7.1).

Crumbie *et al.* (C75) moist-cured concrete specimens with w/c 0·4 and 0·6 in steel moulds for 24 h and then cured them in saturated CH solution for 28 days. Slices from the top, bottom, sides and bulk of each specimen were examined by methanol exchange, quantitative determination of coarse and fine aggregate and backscattered electron imaging in the SEM. The largest variations in the aggregate distribution were in the contents of coarse aggregate in the top 5 mm, which were much reduced, especially in the mix with w/c 0·6, for which the content was almost zero. The methanol-exchange data showed that the porosity and permeability increased near to all the surfaces. SEM examination of a section cut perpendicular to the top surface confirmed the increase in porosity, which was about twice as high in the outermost 200 $\mu$m as in the bulk. The surface region was also depleted in CH, but the content of anhydrous material was little affected. Despite the fact that the specimens had been placed in saturated CH, some leaching appeared to have occurred.

## 12.2 Durability: general aspects

If it is properly designed and produced for the environment in which it has to serve, concrete is an extremely durable material. If the design or production is inadequate, it may deteriorate. Some environments exist in which no concrete is durable.

Deterioration may occur through a variety of chemical or physical processes. The rest of this chapter deals with these, with emphasis on chemical processes in which the cement paste is involved. For convenience, the various forms of attack are considered separately, but examination of deteriorated concretes often shows that more than one form of attack has been operative. This is often because one form of attack renders the concrete more susceptible to damage by another. Portland and composite cement concretes are considered; calcium aluminate cements are discussed in Section 10.1.11.

The concept of a design life for concrete structures is becoming increasingly recognized (S134), failure then being defined as deterioration of properties to an unacceptable level at an age lower than the design life. To design a concrete for a specified minimum life, it is necessary to understand the processes that cause deterioration, including the rates at which these will occur under the conditions to which it will be subjected. In this last respect, a wide range of climatic, chemical and physical factors must be considered.

## 12.3 Carbonation, chloride penetration and corrosion of reinforcement

### *12.3.1 General*

Corrosion of reinforcement is probably the most widespread cause of deterioration in concrete. The expansion produced by rust formation causes the surrounding concrete to crack and spall. In a sound concrete, rusting is prevented by the high pH of the pore solution, which stabilizes an oxide film on the steel that inhibits further attack. This film is unstable

at lower pH values, which can result from carbonation or leaching, or in the presence of $Cl^-$. Sources of the latter include sea water or salt spray, de-icing salts used on roads, certain aggregates, especially those available in desert climates, and $CaCl_2$ used as an accelerator which, though now widely prohibited, can still affect older structures. Tensile stress can damage the protective film, and particular care must be taken to minimize ingress of $CO_2$ and $Cl^-$ in prestressed structures.

Carbonation begins at exposed surfaces, and spreads inwards at a rate proportional to the square root of time (K74). The thickness of the affected layer can be approximately determined by testing a section with phenolphthalein. Chloride ion from an external source similarly penetrates inwards. The age at which corrosion is liable to begin thus depends on the minimum thickness of concrete covering the reinforcement, the resistance to penetration and the conditions to which the concrete is subjected. The depth of cover needed to provide protection over a given period can be calculated (B173,S134).

The resistance to penetration depends on the permeability of the concrete, which is affected by cement content, w/c ratio, aggregate grading, degree of compaction and adequacy of curing. Lack of bonding between the steel and concrete decreases this resistance and also destroys the protection afforded by the alkaline pore solution. Microcracks are in some circumstances closed up by the products of carbonation or by ingress of dust, but this may not occur, especially under fluctuating loads, which may thus accelerate the onset of corrosion. With a dense, well made concrete, 15 mm of cover may suffice to provide virtually indefinite protection, but with a porous or poorly made concrete, it may allow corrosion to begin within a few years (B173). Important environmental factors, in addition to stress and availability of $CO_2$, $O_2$ and $Cl^-$, include RH and temperature. At low humidities, gases penetrate easily through empty pores, but lack of water may inhibit both carbonation and corrosion; at very high humidities, these effects are reversed. Chloride penetration requires the presence of water. Attack is thus most serious at intermediate humidities.

Roy (R83) reviewed carbonation and transport and reactions of chlorides. Hansson (H74) and Turriziani (T65) reviewed corrosion.

### *12.3.2 Carbonation*

Carbon dioxide dissolves in the pore solution of cement paste, producing $CO_3^{2-}$ ions, which react with $Ca^{2+}$ to produce $CaCO_3$. The $OH^-$ and $Ca^{2+}$ ions required by these reactions are obtained by the dissolution of CH and by lowering the Ca/Si ratio of the C–S–H. The CH and C–S–H carbonate simultaneously (D66).

Figure 12.2 shows a backscattered electron image of a strongly carbonated region of a concrete. X-ray microanalysis shows that the dark grains are residual clinker particles that have been largely or wholly converted into a highly porous C–S–H of low Ca/Si ratio, approaching hydrous silica. Unhydrated ferrite (bright) has escaped reaction. The matrix material is an intimate mixture of partly decalcified C–S–H and calcium carbonate. There is no significant quantity of CH.

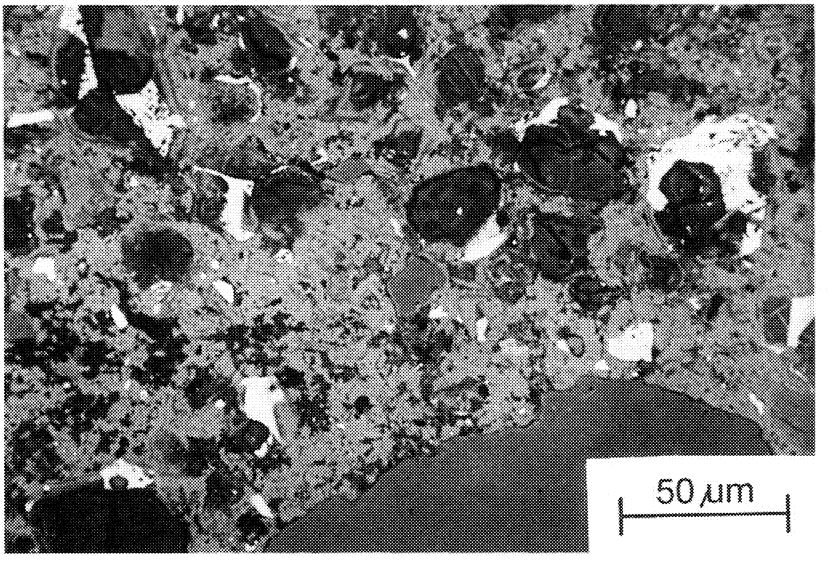


**Fig. 12.2** *SEM (backscattered electron image) of a carbonated region of a concrete. The extensive, light areas are mainly of C–S–H finely intergrown with $CaCO_3$. The very bright regions are of unhydrated clinker, and the dark particles are clinker grains that have been replaced by C–S–H of low Ca/Si ratio. Courtesy R.S. Gollop (Blue Circle Industries plc).*

Richardson *et al.* (R84) examined carbonated pastes of Portland cement with and without silica fume additions by several methods. XRD showed that the $CaCO_3$ was almost entirely in the form of calcite. Ion-thinned sections were examined by TEM. For the plain Portland cement paste, at a depth of $\sim 15\,\mu$m below the surface, in the outer product, microcrystals of calcite were intermingled with fibrils of C–S–H on a scale much below 100 nm. The outer product was clearly densified by the calcite. The inner product did not contain calcite crystals, but its Ca/Si ratio was lowered from the normal value of $\sim 1{\cdot}7$ to $1{\cdot}4$. Higher concentrations of calcite crystals were present around CH crystals and at the interface between inner and outer products. $^{29}$Si NMR showed that the $Q^2/Q^1$ ratio was higher than in uncarbonated material, but no $Q^3$ or $Q^4$ tetrahedra were present; the average chain length in the C–S–H had increased, but silica gel had not been formed. Broadly similar results were obtained for the paste containing silica fume, but the microstructure was notably non-uniform, some regions being apparently unaltered while in others the outer product contained microcrystalline calcite closely mixed with C–S–H and residual silica fume. Carbonated $C_3S$ paste was also broadly similar, but the overall level of carbonation was higher and the microcrystals were predominantly of vaterite (G100,G101).

Another NMR study showed that in carbonated $C_3S$ pastes the silicate tetrahedra were predominantly $Q^3$ and $Q^4$, indicating formation of silica

gel, but that with Portland cement the extent of silicate polymerization was smaller (T66).

The results of the phenolphthalein test show that the pH falls to 8·5 or below in the carbonated zone. Andrade *et al.* (A40) concluded that a value as low as this could only be explained if alkali cations were removed from the solution by leaching or uptake by the hydrous silica formed by decomposition of the C–S–H. In the pure $(K,Na)_2O$–$CO_2$–$H_2O$ system, a pH of 8·5 corresponds approximately to formation of $HCO_3^-$. Suzuki *et al.* (S135) studied the mechanism of carbonation of C–S–H in suspensions. Barret *et al.* (B101) discussed equilibria relevant to the carbonation of $C_4AH_x$.

Apart from the effect on reinforcement corrosion, carbonation has both good and bad effects on concrete. It markedly increases the compressive and tensile strengths of Portland cement mortars and concretes, sometimes by as much as 100%, in the regions affected. The strengths also increase if the binder is a composite cement made with 40% of slag, but decrease if this proportion is increased or with supersulfated cements (M135). The changes in strength are paralleled by ones in mass for a specified drying condition, indicating that gain in strength occurs if the uptake of $CO_2$ exceeds the loss of bound water. Carbonation also makes a specific and substantial contribution to irreversible shrinkage; as Lea (L6) pointed out, this indicates that the C–S–H is attacked. It may cause superficial crazing, and can contribute significantly to the drying shrinkage meaurements on small specimens. The reduction in permeability due to carbonation of the surface layers results in a decrease in the reversible volume changes with subsequent variations in RH.

### *12.3.3 Transport and reactions of chlorides*

The risk of chloride-induced corrosion increases with ease of migration of $Cl^-$ through the cement paste and with the ratio of $Cl^-$ to $OH^-$ in the pore solution (P58). The diffusion of $Cl^-$ through cement pastes is discussed in Section 8.7.2. In concrete, transport can also occur through regions of enhanced permeability or microcracks and diffusion is supplemented by capillary action except in a completely saturated material. Factors affecting the $Cl^-/OH^-$ ratio include the $OH^-$-concentration and the extent to which $Cl^-$ is taken up by solid phases. The $OH^-$ concentration depends on the alkali content of the cement and will often be lower for a composite than for a pure Portland cement. Chloride is partly bound in $C_3A \cdot CaCl_2 \cdot 10H_2O$ but much remains in the pore solution (M136,P53,R83,R85). With very concentrated chloride solutions, other solid phases may be formed (Section 12.7.3). Formation of $C_3A \cdot CaCl_2 \cdot 10H_2O$ may be decreased in the presence of sulfates, due to preferential formation of monosulfate or ettringite, or by carbonation, and possibly depends on the source of the $Cl^-$ (P58).

Page *et al.* (P58) determined the $Cl^-/OH^-$ ratios in the pore solutions, $Cl^-$ diffusivities and corrosion rates of embedded steel in pastes of cements of several types. With Portland cements, the $Cl^-/OH^-$ ratios decreased with potential $C_3A$ content; cements containing 30% flyash or 65% ggbs gave lower ratios than any of the Portland cements. The $OH^-$

concentrations were lower for the composite cements, and the low $Cl^-/OH^-$ ratios were presumably due to greater uptake of $Cl^-$ by the hydration products. The $Cl^-$ diffusivities increased in the sequence slag cement < flyash cement < ordinary Portland cements < sulfate-resisting Portland cement. In conformity with these results, the corrosion rates were slightly lower for the composite cements than for an ordinary Portland cement, and considerably lower than that for the sulfate-resisting Portland cement. The authors stressed the need to study a wider range of cements and chloride solutions before any general conclusions should be made. The results nevertheless indicate that binding of $Cl^-$, as well as diffusivity, plays an important part in limiting $Cl^-$-induced corrosion. A microstructural study (M137) showed greater corrosion with a silica fume cement than with a pure Portland cement; replacement of cement by silica fume may be expected both to lower the $OH^-$ concentration and to decrease the content of AFm phase able to take up $Cl^-$.

### *12.3.4 Corrosion*

The corrosion of steel in concrete is an electrochemical processes. Due to local compositional or structural variations, some areas become positively and others negatively charged, and electrical cells are set up. The anodic reaction and the principal cathodic reaction are respectively typified by the equations

$$3Fe + 8OH^- \rightarrow Fe_3O_4 + 4H_2O + 8e^- \qquad (12.1)$$

$$4e^- + 2H_2O + O_2 \rightarrow 4OH^- \qquad (12.2)$$

At the anodes, iron is dissolved and an oxide deposited. Electrons travel from anode to cathode within the metal, and $OH^-$ ions travel from cathode to anode through the solution with which it is in contact. For these processes to occur, a continuing source of oxygen is needed, and the surface of the metal must remain wet. If the pH is above about 11·5 (P53) and $Cl^-$ is absent, the oxide is deposited as a thin protective film which is virtually continuous, and the rate of attack is so low as to be insignificant. The iron is said to be in a passive condition. At a lower pH, an oxide or oxyhydroxide is deposited in an incoherent form, and corrosion is rapid.

Chloride ions cause local breakdown of the passive film, even at high pH. The regions of metal thus exposed become anodes and the unaffected areas become cathodes. Since the areas of breakdown are small, high current densities can develop at the anodes, causing pitting and localized decrease in pH, which aggravates the attack. High local ratios of $Cl^-$ to $OH^-$ in the solution favour pitting (P58).

As was noted in Section 12.3.1, corrosion may be inhibited if the permeability of the concrete to water or oxygen is low enough, and thus does not necessarily occur even if the concrete in contact with the reinforcement is carbonated. The maintenance of the passive film requires the presence of some oxygen, and if the supply of oxygen is very restricted, as in concrete buried under moist ground or in deep water, all

can be used up. In theory, corrosion can then occur through reduction of water to hydrogen, but in practice, corrosion rates are little greater than when a passive film exists (H74).

Several approaches to the prevention of corrosion have been followed, in addition to that of making concrete that is less permeable and that gives adequate cover to the steel (T65). They include

(1) cathodic protection, in which a voltage is applied between the reinforcement and a conducting paint applied to the outer surface of the concrete
(2) sacrificial anodes, in which an electropositive metal or alloy is embedded in the concrete and connected electrically to the reinforcement
(3) corrosion inhibitors, e.g. $Ca(NO_2)_2$, which appear to act by stabilizing or otherwise altering the oxide film or by scavenging oxygen
(4) inert coatings of organic materials applied to the steel
(5) galvanizing, which, however, has been considered to retard hydration and to weaken the paste–metal bond (A39,T65).

## 12.4 Alkali silica reaction

### *12.4.1 General*

The general features of alkali silica reaction (ASR) were first described by Stanton (S136). Hydroxide ions in the pore solution react with certain types of silica that can occur in the aggregate, resulting in internal stresses that can cause expansion and cracking. Failure may occur within days or only after years. On the surface of unrestrained concrete, it typically produces a random network of fine cracks with some larger cracks ('map cracking'). In reinforced concrete, the cracks tend to form parallel to the reinforcement. Thin sections show cracks that can pass through the aggregate; a characteristic gel is present. This can partly or wholly replace reactive aggregate particles and can also occur in the cracks in the aggregate or the paste, as rims around aggregate particles, or elsewhere in the paste (Fig. 12.3). The gel can exude from the concrete.

The necessary conditions for ASR in a Portland cement concrete are a sufficiently high content of alkali oxides in the cement, a reactive constituent in the aggregate and a supply of water. The $K^+$ and $Na^+$ are present in the cement as sulfates and in the silicate and aluminate phases. When the compounds containing these ions react, their anions enter products of low solubility, such as ettringite, C–S–H or AFm phases, and equivalent amounts of $OH^-$ are formed. The $K^+$ or $Na^+$ are involved at this stage only in the negative sense that, since their hydroxides are soluble, they allow the $OH^-$ to enter the pore solution. ASR is unlikely to occur in concrete made with Portland (not composite) cements if the content of equivalent $Na_2O$ ($Na_2O^e = Na_2O + 0{\cdot}66K_2O$) in the concrete is below $4\,kg\,m^{-3}$, and a practical limit of $3\,kg\,m^{-3}$ has been proposed to allow for day-to-day variations in cement composition (H75). An alternative criterion based on cement composition ($Na_2O^e < 0{\cdot}6\%$) does

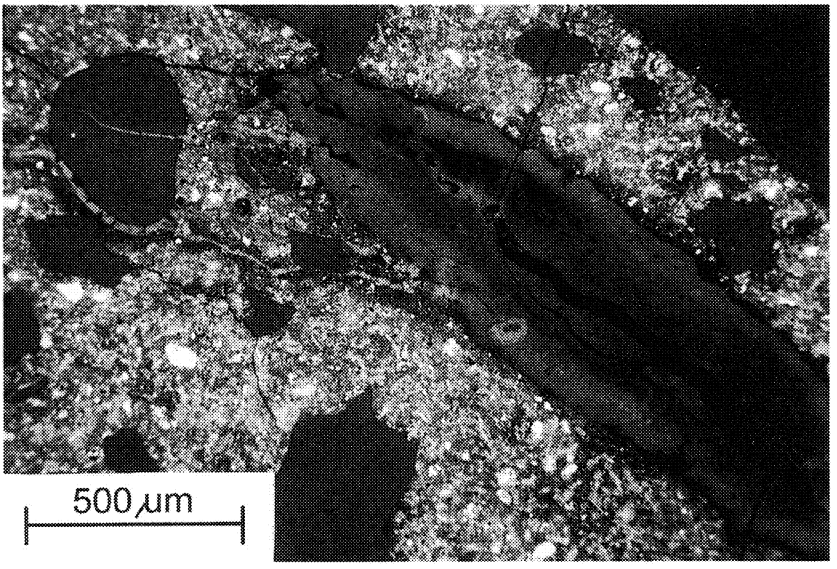


**Fig. 12.3** *SEM (backscattered electron image) of a concrete, showing a particle of a reactive aggregate, partially replaced by ASR gel, veins of which have grown out of the particle through the cement paste and another aggregate particle. Courtesy R.S. Gollop (Blue Circle Industries plc).*

not allow for varying cement content in the concrete. Alkali cations may also be supplied from external sources such as solutions of $Na_2SO_4$ (P59,T67) or NaCl (N22), mineral additions (Section 12.4.4) or aggregates. In all cases they will yield equivalent amounts of $OH^-$ except in so far as they enter solid phases or are balanced by other anions that stay in solution.

Diamond (D67) described the types of silica that can take part in ASR. They include quartz if sufficiently strained or microcrystalline, tridymite, cristobalite and glass or other amorphous forms, which occur in varying combinations in opals, flints, cherts and other rock types. Opals are especially reactive. Macroscopic, unstrained crystals of quartz appear to be unreactive but are possibly not completely inert. Some silicate minerals and volcanic glasses may undergo reactions similar to ASR.

If all other variables are fixed, a curve of expansion against the percentage of the reactive constituent in the aggregate often passes through a maximum at a 'pessimum' composition. For opals and other highly reactive constituents in mortars, this is typically under 10% (Fig. 12.4; H76) but for less reactive consituents it can be much higher and may even occur at 100%. The expansion also depends on the particle size of the reactive constituent. The results of different investigators vary considerably (H77), probably on account of differences between the materials used, but expansion appears always to be greatest for material in the 0·1–1·0 mm range and is possibly

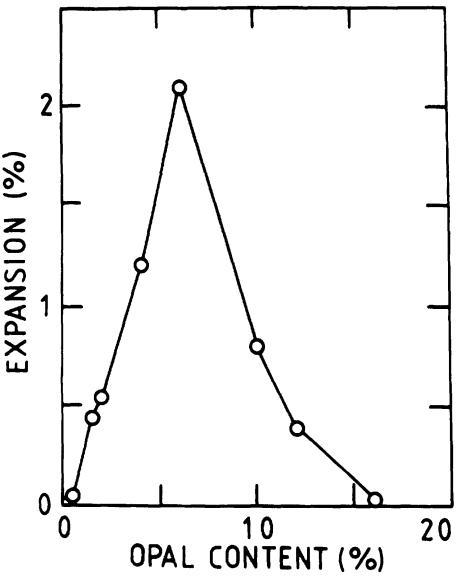


**Fig. 12.4** *Relation between the expansion of a mortar (w/c = 0·41, aggregate/cement = 2, age = 200 days) and the content of Beltane opal, expressed as a mass percentage of the total aggregate. From H76.*

zero or negligible if the particle size is below about 10 $\mu$m. At least some specimens of opal, if sufficiently finely ground, act as pozzolanas (B174).

### *12.4.2 Chemistry of alkali silica reaction*

Knudsen and Thaulow (K75) made X-ray microanalyses of the gel present in cracks in a 30-year old concrete that had undergone ASR and compared them with typical analyses of gel exuded from the surface, reported by Idorn (I21). The gel in the cracks was, in general, much higher in CaO and lower in alkalis than the exuded gel (Fig. 12.5), and its CaO content increased on moving along a crack away from its source. The authors concluded that an alkali silicate gel formed initially reacted with $Ca^{2+}$ ions from the cement paste, with which the exuded material had scarcely been in contact. The compositions of the gels were analogous to those of ones in the $Na_2O$–CaO–$SiO_2$–$H_2O$ system studied by Kalousek (K20). Regourd *et al.* (R86) made similar observations. Diamond *et al.* (D68) observed that $K^+$, but not $Ca^{2+}$, penetrated deeply into opal grains, and Bhatty (B175) found that the gel formed from $C_3S$, opal, flyash and NaOH was essentially a calcium silicate gel and gave an XRD pattern of C–S–H(I).

These results suggest that the chemistry of ASR is essentially that of pozzolanic reaction (Section 9.3.6), the different effect on concrete properties arising mainly from the difference in particle size of the siliceous

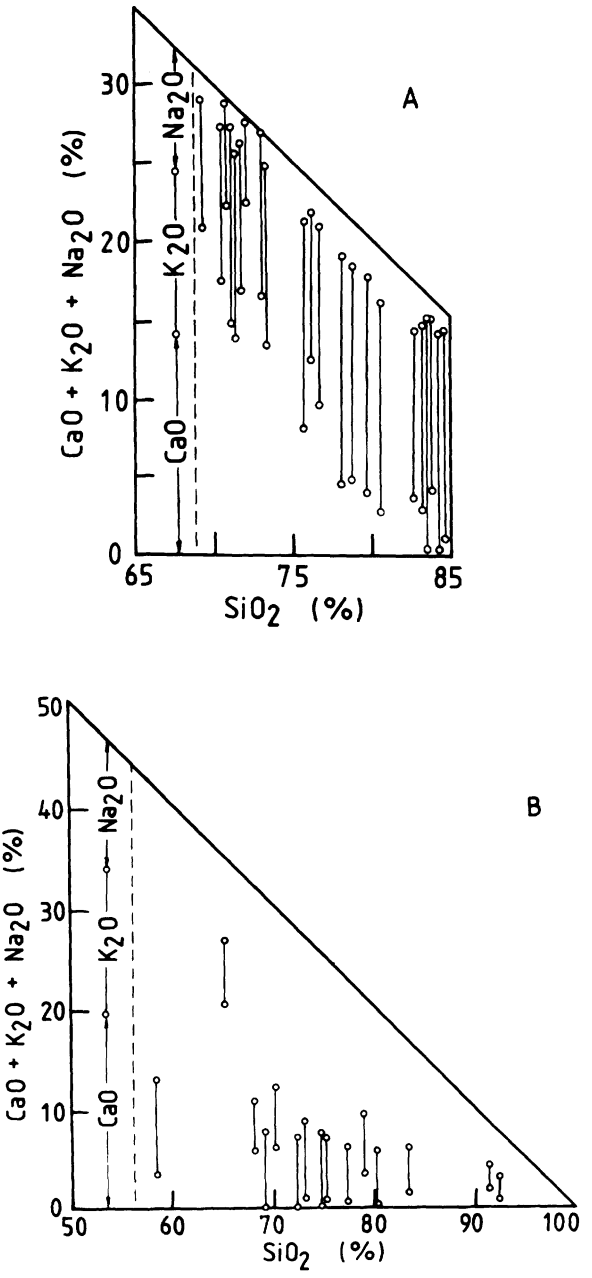


**Fig. 12.5** *Compositions of gels produced by ASR (A) in cracks or otherwise deposited within a concrete and (B) exuded to the exterior. In each case, the data are given as percentages of the ignited mass, and points to the left of the broken line merely illustrate how the results are expressed. From K75.*

material. Observations that agglomerates of silica fume can cause ASR (Section 9.5.1) reinforce this conclusion. The following explanation of the process is essentially that given by Powers and Steinour (P60) and, in more detail, by Dent Glasser and Kataoka (D69,D70). Hydroxide ions attack the silica, causing Si–O–Si bridges to be replaced by pairs of $SiO^-$ groups. This process, many times repeated, ultimately fragments the three-dimensional silica framework into separate silicate anions, which in a concentrated solution are of varying sizes. The negative charges, whether on oxygen atoms still forming part of the framework or on ones present in separate silicate ions, are balanced by the most readily available cations, which are $K^+$ and $Na^+$. The damaged framework is sufficiently deformable that, for some compositions at least, the material can imbibe water molecules and expand; if sufficiently fragmented, it can be highly mobile. In these respects it differs from C–S–H, which has a relatively rigid structure based on Ca–O layers. It is unstable in the presence of $Ca^{2+}$, which reacts with it to form C–S–H. This regenerates $OH^-$ in the solution, e.g. from CH if the latter is the source of the $Ca^{2+}$. The alkali silicate constituent of the gel can possibly itself accommodate some $Ca^{2+}$, but a point is probably soon reached at which particles of C–S–H begin to form as a separate constituent.

In pozzolanic reaction, the alkali silicate gel is formed in an environment rich in $Ca^{2+}$ and, except in a narrow zone close to the reacting surface, is quickly converted into C–S–H. In ASR, it is formed in an environment poor in $Ca^{2+}$, and massive outflows of gel may result. The cement paste cannot supply $Ca^{2+}$ fast enough to prevent much of this gel from persisting for long periods. This situation is especially marked if the alkali silicate gel forms within the aggregate particles, as is the case with opal.

The $K^+$, $Na^+$ and $OH^-$ concentrations in the pore solutions of mortars containing reactive aggregates are lowered due to uptake by the gel (D68). Kollek *et al.* (K76) showed that destructive expansion was unlikely to occur in a particular series of mortars made with pure Portland cements if the $OH^-$ concentrations in otherwise similar mortars not containing the reactive constituent had not reached 0·6 mol $l^{-1}$ by 180 days. This is a correlation and not a causal relationship, and it would be wrong to regard any concentration determined in the absence of reactive aggregate as a 'trigger' value at which the aggregate begins to react.

Cole and co-workers (C76,C77) showed from XRD, X-ray microanalysis, IR, DTA and thermal weight loss data that the rims around sandstone and siltstone aggregates in a 30-year old concrete contained an alkali-substituted okenite ($C_5S_9H_9$; M138) and a precursor phase characterized by a 1·22 nm XRD spacing. This latter phase was more highly hydrated than okenite, had formed in a wet environment and on being dried changed into okenite. A possible similarity to rhodesite [$(Ca,K,Na)_9Si_{16}O_{40} \cdot 11H_2O$] was suggested, but the latter does not change into okenite on dehydration (G102). Okenite has a structure based on silicate sheets and layers (M138), and a higher hydrate of similar structure could well exist. Similar products have been observed by other workers (B176,D71) and had previously been tentatively identified as

zeolites (C77), or jennite or tricalcium silicate hydrate (B176). These crystalline phases appear to be minor, though possibly equilibrium products of ASR.

A 'rapid chemical test' for the susceptibility of aggregates to ASR has been described (M139). The chemistry on which it is based is confused (D72).

### 12.4.3 The expansion process

Expansion due to ASR is generally attributed to imbibition of pore solution by the alkali silicate gel (V13); the resulting swelling pressure is not simply related to the expansion in absence of restraint (D69). In accordance with this hypothesis, many dried sodium silicate gels swell markedly on wetting and can develop high swelling pressures (S137), whereas the equivalent volume changes for C–S–H are small. Vivian (V13) found that reactive mortars stored for about 40 days in dry air did not expand, but if then placed in water expanded very rapidly. Expansion can also occur in a concrete that is continuously saturated; Hobbs (H75) has argued that this process is one in which a solid reactant yields a more voluminous solid product but which cannot properly be called imbibition. Osmosis has been postulated (H78), but there is no substantial evidence that a semipermeable membrane exists.

Three principal hypotheses have been proposed to account for the decreased expansion observed if the reactive material is more finely ground or present in quantities above the pessimum, as follows.

(1) The gel is more thinly distributed, and $Ca^{2+}$ ions are therefore more readily available to it, accelerating its conversion into the virtually non-expansive C–S–H (P60). The thinner distribution of the gel might also in itself decrease the expansive stresses.

(2) The gel has a lower ratio of alkali cations to $SiO_2$, which renders it less expansive. Dent Glasser and Kataoka (D73) found the expansion of the solid phases on placing silica gel in NaOH solutions to pass through a maximum at $SiO_2/Na_2O$ ratios that might reasonably have corresponded to pessimum compositions. Struble and Diamond (S137,S138) obtained broadly similar results for swelling pressures and amounts of unrestrained swelling for dried sodium silicate gels placed in water, but various anomalies led them to conclude that the swelling characteristics were probably more directly related to the anion structure of the gel. This depends not only on $SiO_2/Na_2O$ ratio, but also on drying, ageing, temperature, type of silica, carbonation and possibly other factors.

(3) The gel is formed before the paste has hardened sufficiently for damage to occur (H75,O32).

These hypotheses are not mutually exclusive, though the general slowness of pozzolanic reactions renders (3) unlikely. The evidence is insufficient to determine their relative importance, which could probably be assessed from a combination of expansion data, pore solution analyses and SEM

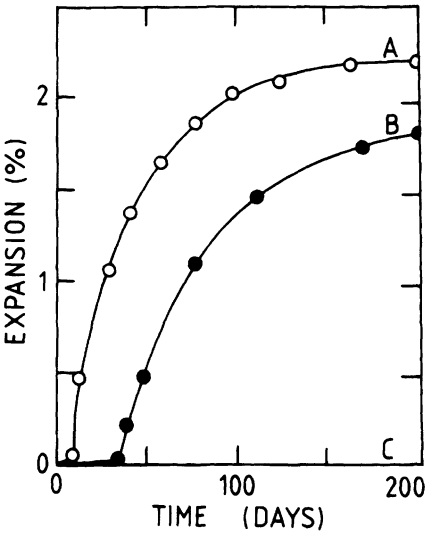


**Fig. 12.6** *Typical relations between expansion produced by ASR and age; data are for mortars with w/c = 0·41 and aggregate/cement = 2, (A) with 6·7% of Beltane opal in the aggregate and a cement with $Na_2O_e$ = 1·24%, and (B) with 4·5% of Beltane opal in the aggregate and $Na_2O_e$ = 0·8%. After H76.*

of polished sections with accompanying X-ray microanalyses made in parallel on a series of mortars of suitable ages and compositions.

Curves of expansion against time typically have the form shown in Fig. 12.6. Cracking usually begins at an expansion of 0·05–0·1%. It is unlikely that the start of the reaction is delayed, and thus probable that a certain degree of reaction can occur without producing expansion, which presumably begins when the gel can no longer be accommodated in the pore structure of the paste without producing stresses sufficient to disrupt it.

### *12.4.4 ASR in mortars or concretes made with composite cements*

The relations between expansion and the content and particle size of the reactive aggregate early suggested that expansion might be decreased by the use of pozzolanic additions, and provided that the latter do not themselves supply too much alkali this has been found to be the case. Hobbs (H79) reviewed and extended data on the effects of replacements by flyash or ggbs on expansion in mortars and concretes. In the great majority of cases, the replacements decreased expansion, though not always sufficiently to prevent failure. In a few cases in which the mineral addition was itself especially high in alkalis, expansion increased. Failure sometimes occurred at lower concrete $Na_2O^e$ contents than would have been expected if these were calculated from the contribution of the Portland cement alone. Hobbs concluded that, contrary to some earlier views, allowance must be made for the alkalis supplied by the mineral addition, and suggested that, failing a direct test of the effectiveness of a particular flyash or slag in

preventing expansion, the $Na_2O^e$ content should be calculated by adding one-sixth of the total alkali content of the flyash, or one-half of that of the slag, to the contribution from the cement.

Kollek *et al.* (K76) extended the parallel studies on expansion and pore solution compositions mentioned in Section 12.4.2 to mortars containing flyash, slag or natural pozzolanas. For each mix, several contents of the reactive aggregate (Beltane opal) were used to ensure that pessimum compositions were being compared. With a high alkali cement ($Na_2O^e = 0{\cdot}92\%$), failure occurred in the absence of a mineral addition, but was avoided at sufficiently high replacement levels of flyash, slag or one of the natural pozzolanas used. With a cement lower in alkali ($Na_2O^e = 0{\cdot}68\%$), failure did not occur in the absence of a mineral addition, but took place in mixes with either of the flyashes, most of the natural pozzolanas and one of the slags tested.

The pore solution compositions were consistent with these results. They could not be explained by assuming that the mineral additions acted as inert diluents in regard to the alkali contents of the solutions. In the mixes with flyash, failure could be correlated with an $OH^-$ concentration greater than $0{\cdot}3\,mol\,l^{-1}$ at 180 days in an otherwise similar mix not containing the reactive aggregate. The corresponding values for mixes with slags or natural pozzolanas were $0{\cdot}5\,mol\,l^{-1}$ and $0{\cdot}4\,mol\,l^{-1}$ respectively. The relations between the $OH^-$ concentration in the pore solution of a mix not containing reactive aggregate and the likelihood of failure in a mix in which one is present thus differ for the various types of cements.

The alkali cations in flyash normally occur almost entirely in the glass, and when the latter reacts may be presumed to enter the alkali-rich silicate that appears to be the initial product. When this phase is decomposed by reaction with $Ca^{2+}$, they will be distributed, like alkali cations from any other source, between the solution and the solid hydration products, on which they are probably adsorbed (Section 7.4.3). The C–S–H tends to take them up more strongly as its Ca/Si ratio decreases (B68,G72); consequently, the alkali cations released from the flyash are less effective in raising the $OH^-$ concentration of the pore solution than are those released from the cement. The method outlined in Section 7.5.2 for calculating the $OH^-$ concentration in the pore solution of a Portland cement mix was extended to cover Portland–flyash cement mixes taking this into account (T43).

## 12.5 Sulfate attack

### *12.5.1 General*

Portland cement concrete is attacked by solutions containing sulfate, such as some natural or polluted ground waters. Attack can lead to strength loss, expansion, spalling of surface layers and, ultimately, disintegration. While in test procedures and laboratory studies much attention has been paid to expansion and cracking, field experience shows that loss of adhesion and strength are usually more important (M140). The effects are minimized in a dense concrete of low permeability and by using a sulfate-resisting cement or, with reservations, composite cements.

Ground water containing sulfate is often also high in magnesium, and sulfate attack has often been discussed in terms of reaction between solid phases in the cement paste and dissolved compounds, such as $Na_2SO_4$ or $MgSO_4$, in the attacking solution. This obscures the fact that the reactions of the cations and anions in that solution are essentially separate. With $Na_2SO_4$, the reaction is one of the $SO_4^{2-}$ ions, but with $MgSO_4$ the $Mg^{2+}$ also participates. Many studies have shown that $MgSO_4$ solutions are more aggressive than $Na_2SO_4$ solutions of the same concentration. Probably a majority of studies of concrete that has been attacked have shown the presence of both ettringite and gypsum; if $Mg^{2+}$ is present, brucite and poorly crystalline serpentine ($M_3S_2H_2$) are also formed.

Sulfate attack proceeds by the inward movement of a reaction front. This is illustrated by Fig. 12.7, which shows part of a section cut through a Portland cement cube that has been attacked by a $MgSO_4$ solution. Adequate experimental procedures for studying the chemistry of sulfate attack must take account of this fact. Thus, surface layers may be progressively removed and the resulting surfaces examined by XRD or other methods (C78,W44), or a cube or other specimen may be sawn through the middle and a surface so obtained polished and examined in the SEM (B177,B178,C75,G71). The reactions that occur first are those taking place at the greatest depths.

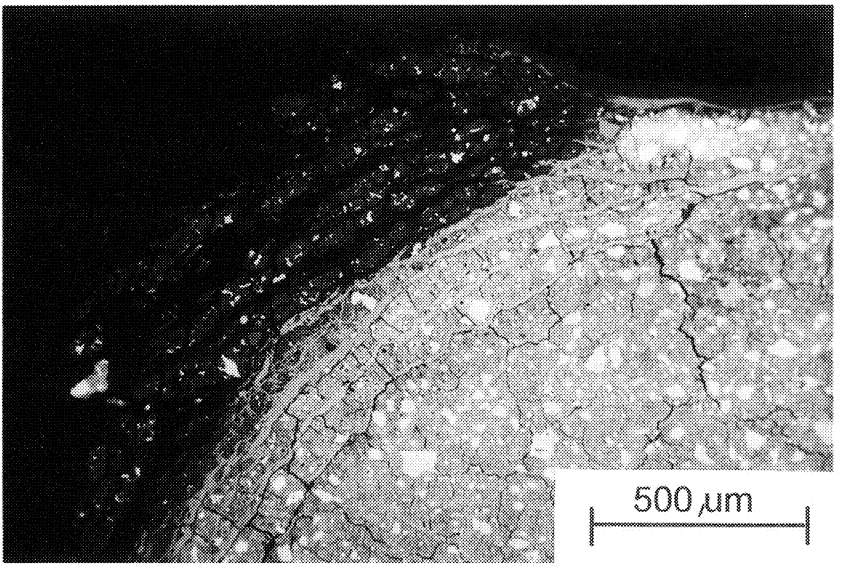


**Fig. 12.7** *SEM (backscattered electron image) of a section through a cube of Portland cement paste after storage in $MgSO_4$ solution. At the cube edge (top left) the material consists largely of magnesium silicate hydrate, with some ferrite. The veins beneath it are of gypsum. At the cube face (top right) there is a composite layer of gypsum and, outside it and barely discernible, brucite. The cement paste beneath it is darkened due to decalcification. From G71.*

### 12.5.2 Sodium sulfate solutions

Investigations on the action of 0·25–0·35M $Na_2SO_4$ solutions on plain Portland cement pastes by XRD or SEM methods (A41,C78,G71,R87, W44) have given results in good mutual agreement. The first observed change has in most cases been replacement of monosulfate by ettringite, which is formed as microcrystals intimately mixed with the C–S–H. It is readily detected by XRD, but in backscattered electron images in the SEM cannot be observed as a separate phase, though its presence can be inferred from X-ray microanalyses. Nearer to the surface, the average Ca/Si ratio of the C–S–H falls, the CH is depleted and gypsum is formed, partly as microcystals mixed with the C–S–H and partly as veins, often subparallel to the surface. Cracks, often asssociated with the gypsum veins, are formed, and there is more extensive gypsum formation and cracking at cube edges.

The formation of ettringite from monosulfate may be assumed to occur by dissolution and precipitation. It requires a supply of $Ca^{2+}$, $SO_4^{2-}$ and $H_2O$:

$$C_4A\bar{S}H_{12} + 2Ca^{2+} + 2SO_4^{2-} + 20H_2O \rightarrow C_6A\bar{S}_3H_{32} \qquad (12.3)$$

The $SO_4^{2-}$ is provided by the external solution. The $Ca^{2+}$ ions are provided partly by the CH, and, after the latter has been consumed or is less readily available, by the C–S–H, which is partly decalcified, i.e. its Ca/Si ratio decreases. At a later stage, gypsum is formed; this too requires $Ca^{2+}$. The evidence from X-ray microanalyses thus does not support the view (L6) that solutions of $Na_2SO_4$, as opposed to those of $MgSO_4$, do not attack the C–S–H.

$C_3S$ pastes are slowly attacked by 0·15 molar $Na_2SO_4$ solution; more concentrated $Na_2SO_4$ solutions also attack $\beta$-$C_2S$ pastes (T67). The action is presumably associated with formation of gypsum.

### 12.5.3 Magnesium sulfate solutions

Storage of plain Portland cement pastes or mortars in $MgSO_4$ solutions produces a composite and almost continuous surface layer of brucite and gypsum, with the brucite on the outside (A41,B177,B178,G71,G103,N23, R87,R88). At the edges of cubes, where attack has been more severe, a magnesium silicate hydrate is also formed (Fig. 12.7). For this phase, Mg/Si ratios ranging from 4:1 to 1:1 have been proposed (B178,B179, C79); Gollop and Taylor (G71) concluded from XRD and microanalytical evidence that it was poorly crystalline serpentine ($M_3S_2H_2$), and noted that this phase has ben found to be the initial product of reactions in the $MgO$–$SiO_2$–$H_2O$ system under a range of other conditions. Decalcification of the C–S–H is more marked than in $Na_2SO_4$, and leads ultimately to complete destruction of the C–S–H with formation of silica gel, but in other respects the microstructure is essentially the same as in the latter case. The increased decalcification occurs because of the low solubility of brucite, which may be assumed to lower the pH of the pore solution.

With both $Na_2SO_4$ and $MgSO_4$, sulfate-resisting Portland cements behave in a manner similar to ordinary Portland cements, but ettringite formation, decalcification of C–S–H and cracking are all much reduced (G103).

### 12.5.4 Calcium sulfate

Some aggregates, notably in the Middle East, contain gypsum, which can cause so-called internal sulfate attack. Light microscopy shows that the gypsum is replaced in situ by CH, while ettringite is formed in the cement paste, which is liable to expand (C80). The process entails counter migration of $SO_4^{2-}$ and $OH^-$ between paste and aggregate; within the paste, the reactions are presumably the same as in attack by $SO_4^{2-}$ from an external source. The effect is lessened by using either a sulfate-resisting or a rapid-hardening Portland cement, in the latter case because the paste can become less permeable before much $SO_4^{2-}$ has been released.

Despite its relatively low solubility, $CaSO_4$ present in solution can also attack concrete. In this case, the solution can provide all the ions that are needed to produce ettringite from monosulfate, and little or no dissolution of CH or decalcification of C–S–H need occur. The saturated solution also slowly attacks $C_3S$ pastes (T67); the explanation of this is not clear. The use of abnormally large quantities of finely divided gypsum interground or blended with the cement also produces expansion (Section 7.6.2).

### 12.5.5 Composite cements and sulfate attack

Partial replacement of cement by mineral additions can either improve or reduce resistance to sulfate attack. Locher (L61) found that resistance of ordinary Portland cements to $Na_2SO_4$ solutions was increased if more than 65% of the cement was replaced by slag at a constant gypsum addition of 5%, and also at lower degrees of substitution if the slag was low in $Al_2O_3$ (11%), but that it was lessened at low degrees of substitution if the slag was high in $Al_2O_3$ (18%). Broadly speaking, mineral additions are more likely to have a beneficial effect towards $Na_2SO_4$ than towards $MgSO_4$ solutions. With composite cements in general, the effect is likely to depend markedly on the degree of curing before exposure to the sulfate solution begins, because of the slow reaction of the mineral addition. Hughes (H80) found that 30% replacement of cement by flyash in a paste greatly increased the time to cracking if the paste had been cured in saturated CH solution for 12 weeks before being transferred to a $Na_2SO_4$ solution, but if the preliminary curing period was restricted to 1 week, expansion took place more quickly in the flyash–cement paste.

XRD or SEM studies have been reported for pastes or mortars containing slags (A41,G82,L61,R88), flyash (A41,C78,R88) and silica fume (A41,B177–B180,R87,R88). In general, the microstructural and chemical changes are basically similar to those found with plain Portland cements, though the extent of attack and the relative importance of different effects varies greatly. The deposits of gypsum and, in the case of attack by $MgSO_4$ solutions, of brucite often differ in form from those observed with

plain Portland cements; with $Na_2SO_4$ solutions, at least, less gypsum tends to be formed than in the latter case. With pastes of some slag blends attacked by $Na_2SO_4$, no gypsum at all was observed (G82).

### 12.5.6 Mechanisms of weakening and expansion

Susceptibility to sulfate attack depends on both physical and chemical factors. The superior resistance of dense, well-compacted concrete indicates that the ability of the sulfate solution to diffuse into the concrete is a major factor affecting the rate of attack. The high resistance to attack provided by many composite cements, such as those high in slag, can probably be attributed, at least partly, to low permeability. This appears to be the case also with calcium aluminate cements, which give concrete that is protected by a very dense and impermeable surface zone (Section 10·1.11).

Hypotheses regarding the mechanism of sulfate attack have concentrated on the cause of expansion, but, as indicated above, this is probably less important in most cases than loss of strength and disintegration. These latter effects can be attributed to the decalcification and destruction of C–S–H, which is particularly serious in the case of attack by $MgSO_4$ solutions (A41,B179,C79,R88). There is nevertheless little doubt that the availability of $Al(OH)_4^-$ ion is a major chemical factor determining susceptibility. There is abundant evidence that the resistance of plain Portland cements decreases with $C_3A$ content. $Al_2O_3$ present in monosulfate or in unreacted $C_3A$ reacts with sulfates, whereas that substituted in C–S–H or present in hydrotalcite-type phases, hydrogarnets or ettringite does not (G82,M141). This hypothesis was shown to account for the good resistance of sulfate-resisting cements and for the widely varying effects on resistance that can result from slag substitution. The good resistance of autoclaved concrete has been attributed to the absence of CH and greater crystallinity of the C–S–H and AFm phases (B181), but increased substitution of aluminium in the C–S–H may also contribute. Even with $MgSO_4$ solutions, where the action of the $Mg^{2+}$ ion is dominant, the availability of $Al_2O_3$ appears to be a major determinant of susceptibility to attack. These observations suggest that the aluminate reactions in some way intensify those of the C–S–H.

Inferior resistance to attack by $MgSO_4$ solutions by composite cements as compared with plain Portland cements has been attributed to the lower contents of CH, which through being attacked preferentially shields the C–S–H from attack (A41,R88). In contrast, the lower contents of CH in composite cements were considered to improve resistance to attack by $Na_2SO_4$ solutions, since the CH played a major part in ettringite formation.

Expansion has been widely attributed to the increase in solid volume associated with ettringite formation, but this increase is approximately the same as that occurring when $C_3S$ is hydrated to give C–S–H and CH. In none of the recent laboratory studies has the formation of ettringite in veins or other massive deposits been reported, and in one series of investigations cases no ettringite at all was detected (B177,B178). At least

three more realistic hypotheses of ettringite-related expansion have been advanced:

(1) directed crystal growth of ettringite crystals causes disruption (L55)
(2) ettringite crystals of colloidal dimensions imbibe water, which produces a pressure akin to that resulting from osmosis (M115)
(3) expansion occurs because of changes in the swelling properties of the cement gel; the formation of ettringite is incidental (T67) or has an effect that is possibly only indirect (G71).

There is no general agreement as to the relative merits of these hypotheses. The cause of expansion is not necessarily the same as in other cases in which ettringite is formed, e.g. with Type K expansive cements (Section 10.2.3). The observation (G71,W44) that expansion does not occur when the ettringite is formed, but later, tells against hypothesis (1). It is difficult to see why small crystals of ettringite dispersed in a C–S–H gel should attract water molecules any more strongly than the gel itself; this appears to be a serious objection to hypothesis (2). On the whole, some form of hypothesis (3) seems the most likely; imbibition of water by a gel can readily produce large expansive pressures. One possibility is that the immediate source of the water needed to produce ettringite is the surrounding C–S–H, which thus becomes strongly dehydrated. Expansion, perhaps enhanced by weakening of the gel as a result of decalcification, could then occur when the C–S–H regains water from an external source.

### *12.5.7 Reactions involving sulfate and carbonate*

Thaumasite ($Ca_3Si(OH)_6(SO_4)(CO_3) \cdot 12H_2O$; Section 6.2.2) can form through a combination of sulfate attack and carbonation. It can cause severe damage, but there appear to be very few cases in which it has been identified as the principal cause of deterioration. Examples are given in B182, L62 and O33; Crammond (C38) and Crammond and Nixon (C81) listed others and described relevant laboratory studies.

Thaumasite is similar to ettringite in crystal structure and morphology. It can be misidentified as ettringite, but the XRD spacings are quite distinct. The conditions conducive to its formation as a constantly high RH, a temperature of 5–10°C, adequate supplies of $SO_4^{2-}$ and $CO_3^{2-}$ ions, and presence of reactive $Al_2O_3$. Brickwork high in $SO_4^{2-}$ covered with a cement-based rendering that has cracked through drying shrinkage, and existing in a cold, damp climate, provides a typical situation for thaumasite formation (C38). Thaumasite formation can be very rapid in concretes containing finely divided $CaCO_3$ (C81). The prior formation of ettringite seems to be needed, probably as a nucleating agent; this would explain the need for a source of $Al_2O_3$. The quantity of ettringite that can be formed from a cement is limited by the amount of $Al_2O_3$ available, but, assuming a continuing source of $SO_4^{2-}$ and the presence of atmospheric $CO_2$ or some other source of $CO_3^{2-}$ ions, thaumasite formation is limited only by the available CaO and $SiO_2$. $MgSO_4$, even in very low concentrations, seems to

play an important part in initiating thaumasite formation, perhaps because magnesium silicate hydrate is also formed (C81).

Thaumasite formation thus decomposes the C–S–H and can completely destroy the binding capacity of the cement paste. Since the attack is on the silicate and not the aluminate constituents of the cement paste, sulfate-resisting Portland cement does not offer any special protection.

## 12.6 Delayed ettringite formation

### *12.6.1 Conditions of occurrence*

This term is used here to denote the formation of ettringite in a concrete, mortar or paste that has been subjected to a temperature high enough to destroy any that was earlier present. The effect can cause expansion or cracking. It has been held partly or wholly responsible for delayed damage in railway sleepers and other precast concrete products. It could also occur in concrete that has been heated adventiously through the heat evolved on hydration, or from an external source during service.

For damage to occur, a number of conditions must be satisfied. The temperature inside the concrete must be at least 65–70°C. During its subsequent life, the concrete must be in an atmosphere that is saturated, or nearly so, either intermittently or continuously. The effect of cement composition is complex and not fully understood; high contents of $SO_3$ (up to about 4%), alkalis and MgO are among factors favouring expansion, but no single factor appears to be dominant. A number of other factors affect the rate or the ultimate extent of expansion, and some may be additional necessary conditions. Of these factors, some concern the mix, some the curing conditions, and some the conditions of subsequent service or storage. Thus, for given conditions, expansion is much more rapid with quartz aggregates than with purely limestone aggregates (D74,H81,L63) or in neat pastes (L63,L64,O18); it decreases with sufficient addition of an air-entraining agent, is affected by sand grading and, with reservations, increases with w/c ratio (H81). Expansion increases with curing temperature above 70°C (L63), with repeated freeze–thaw cycling (H81) and with the presence of pre-existing cracks in the paste (F53). There is disagreement concerning the effect of precuring time before the heat treatment (H81,S139).

Alkali silica reaction has a particularly important effect in promoting expansion from delayed ettringite formation (DEF). It has been shown to have occurred in many cases of field concretes that have undergone damage from DEF (O34,S140–S142); the ASR appears always to precede the DEF. Laboratory studies support the conclusion that DEF can be promoted, and even made possible, by ASR. Diamond and Ong (D74) showed that, in the case of a mortar made with limestone aggregate and cured at 95°C, subsequent expansion was insignificant and ettringite formation limited, but that both were much increased if an alkali-susceptible aggregate was also present. In the presence of the reactive aggregate, expansion attributed to ASR began during the heat treatment and continued for some time subsequently, during which time marked cracking and expansion occurred. Subsequently, ettringite was formed

and was considered to be responsible for the subsequent additional expansion. Other laboratory investigations have confirmed the importance of ASR as a precursor to expansion for DEF (B183,S143).

It has been claimed that concretes cured at ordinary temperature have been damaged by DEF resulting from excessive $SO_3$ content in the cement, or more specifically in the clinker, and that such $SO_3$ is present in forms from which it is only slowly released (D75,M142). No data for the cements were given in support of the assertions.

### 12.6.2 *Decomposition and reformation of ettringite and the origin of expansion*

Many investigators have confirmed the early observation by Kalousek and Adams (K34) that hydrated sulfoaluminate phases rapidly become undetectable in cement pastes cured at 70–100°C. Ludwig and co-workers (G104,H39,H81) made the first extensive studies. Typically, ettringite disappears by about 70°C and AFm phases by 80–100°C. Reports have differed widely as to the persistence of monosulfate as detected by XRD, and this phase may not be so much absent as in varying degrees undetectable through deterioration in crystallinity (Section 7.4.1). As such, it could contain a major proportion of the $Al^{3+}$ and some of the $SO_4^{2-}$. Some of the latter enters the pore solution (W45), but the concentrations reached can account for only a minor proportion of the amount present. As will be seen, some is taken up by the C–S–H. A little syngenite ($K_2Ca(SO_4)_2 \cdot H_2O$) is possibly formed (S143). The quantity of $Al^{3+}$ substituting for $Si^{4+}$ in the C–S–H probably increases and, at least at the higher temperatures, some $Al^{3+}$ enters a hydrogarnet phase.

If the material that has been subjected to an elevated temperature is subsequently stored in water or saturated air at ambient temperature, ettringite is reformed. In pastes stored in water, this process can begin within days, and the ettringite is formed initially as very small crystals dispersed in the C–S–H gel (P61,S121). According to one school, the presence of a little $CO_2$ is essential to the process (S80). Later, in neat pastes, ettringite recrystallizes in any small cavities that may be present.

Expansion and cracking typically occur on a time scale of months in laboratory mortars cured at 90–100°C, or on one of years in field concretes. In mortars or concretes that have expanded, bands or veins of ettringite, typically up to some 50 $\mu$m wide, are observed (H39; Fig. 12.8). Expansion has been attributed to the formation of ettringite crystals at the aggregate interfaces resulting in pressure either from an osmotic effect or from crystal growth (D75,H39) or, alternatively, to expansion of the paste, which causes the latter to separate from the aggregate, thereby producing space in which ettringite can recrystallize, either simultaneously or subsequently (J41,M143,P54). Marusin (M143) considered that the process began with expansion of the paste, and that damage increased progressively as ettringite was deposited in cracks in the paste and at aggregate interfaces.

The ettringite veins can completely surround aggregate particles, and are then reported to have widths proportional to the size of the aggregate

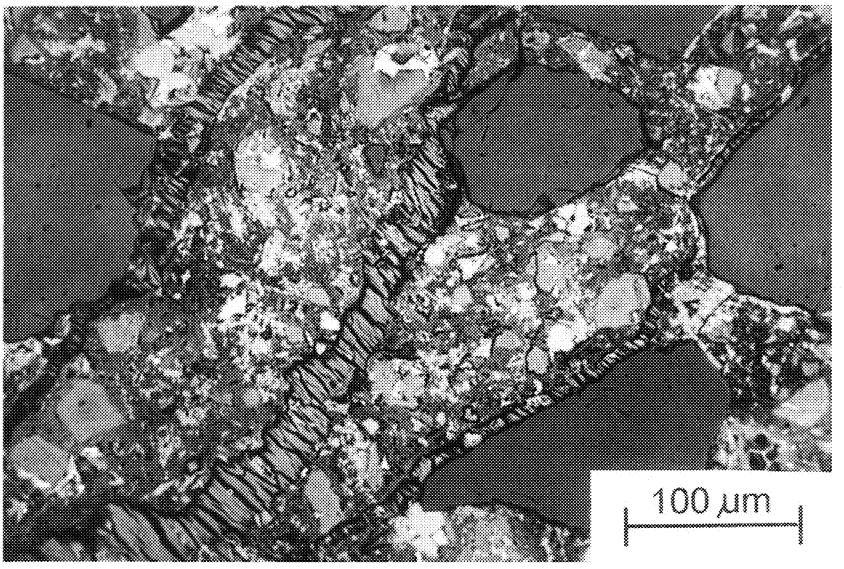


**Fig. 12.8** *SEM (backscattered electron image) of a concrete that has expanded through delayed ettringite formation. Bands of ettringite are present at aggregate interfaces and running through the paste. Courtesy R.S. Gollop (Blue Circle Industries plc).*

(J41); the only obvious explanation of this situation is that the paste has expanded uniformly. In other cases, as in D75 or Fig. 12.8, the veins follow a less regular pattern, which might be attributed to non-uniform expansion of the paste. In all cases, the ettringite in the rims or veins has presumably formed by recrystallization from the much more finely crystalline material present in the paste. If this is so, it is difficult to see how expansion can be caused by crystal growth of ettringite at aggregate interfaces or other large cracks, because the degree of supersaturation is too low in such places for any significant pressure to be developed.

Lewis *et al.* (L65) and Scrivener (S142) studied ten mortars by back-scattered electron imaging and X-ray microanalysis at various stages from one day after heat curing to the completion of expansion, if any. The mortars in which subsequent expansion occurred could be distinguished one day after the heat treatment by the average Al/Ca and S/Ca ratios of the C–S–H (Fig. 12.9). At this stage, no ettringite could be detected by XRD. When expansion occurred, the S/Ca ratios dropped to values broadly similar to those found at 1 day for the mortars that had not expanded; this was attributed to loss of ettringite through recrystallisation. These observations, and those of Fu *et al.* (F54), indicate that sorption of $SO_4^{2-}$ by the C–S–H plays an important part in the mechanism of expansion. It was suggested that the S/Ca and Al/Ca ratios of the C–S–H at an age of 1 day might provide a diagnostic test of the likelihood of subsequent expansion,

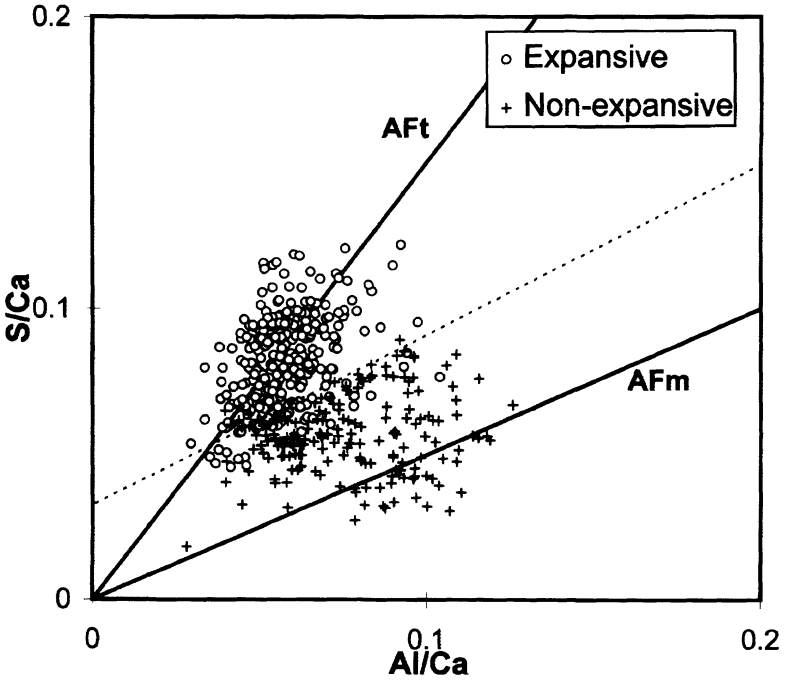


**Fig. 12.9** *Plot of S/Ca against Al/Ca for the C–S–H in a number of mortars, one day after heat treatment. The broken line separates mortars that subsequently expanded from ones that did not. Courtesy K.L. Scrivener and M.C. Lewis (Imperial College, London).*

but all the mortars were made with the same clinker, to which different amounts of calcium sulfate and other substances had been added, and the need for data obtained with a variety of different clinkers was recognized.

### *12.6.3 Effects of variation in the cement*

Early studies by Ludwig and co-workers placed emphasis on the ratio of $SO_3$ to $Al_2O_3$ (G104,H39) or a related parameter (H81) as a major factor determining whether expansion was likely to occur with a given cement. Wieker and Herr (W45) found that high-alkali cements were more liable to undergo expansion than low-alkali cements. Expansion is much reduced or eliminated with composite cements containing slag, flyash, silica fume or natural pozzolana (H81). Later work using plain Portland cements did not support the view that the $SO_3/Al_2O_3$ ratio, or a related parameter, is critical. Odler and Chen (O18) found that expansion increased with the contents of $SO_3$ and Bogue $C_3A$ separately. From a study of mortars made from 55 different cements which had been cured at 100°C, Lawrence (L64)

concluded that major factors included the contents of $SO_3$ and of MgO, which were positively correlated with expansion. He found highly significant correlations with other parameters, but mutual correlations between these rendered interpretation uncertain. From a study using five clinkers with various quantities of gypsum or anhydrite and in some cases additions of KOH or $K_2SO_4$, and ground to various levels of fineness, Kelham (K77) concluded that expansion increased with fineness and with the contents of equivalent $Na_2O$, MgO, Bogue $C_3A$ and Bogue $C_3S$. There was a pessimum content of $SO_3$ of about 4%, increasing with alkali content. From considerations of equilibria, Glasser *et al.* (G105) also concluded that expansion was likely to increase with alkali content and that there would be a pessimum $SO_3$ content in the region of 4%.

Kelham (K77) noted that most of the factors increasing expansion were ones that were linked with high early strength. This conclusion may be compared with the observation (L65) that expansion is associated with a high S/Al ratio in the C–S–H. Increased early strength implies increased formation of C–S–H, and if, as suggested in Section 12.6.2, $SO_4^{2-}$ in a loosely bound form in the C–S–H plays an important part in DEF, a high content of C–S–H at the end of the heat curing might be expected to have an effect similar to that of a high S/Al ratio in the C–S–H. If the C–S–H content is a factor, the otherwise puzzling observation that expansion increases with fineness might be explained.

### *12.6.4 Effects of aggregate and other factors*

Many of the variables noted in Section 12.6.1 as increasing the rate or extent of expansion, other than ones concerning cement properties, are ones that weaken the concrete. They include, among others, alkali silica reaction, freeze–thaw cycling, and the nature of the aggregate. The paste–aggregate bond is a particular source of weakness in any concrete and the bond of cement paste with limestone is generally considered to stronger than that with quartz (Section 12.1.3). Observations on autoclaved aerated concrete show that an extremely thin surface layer of the quartz is dissolved, thereby weakening the bond (I22). This could be described as a form of high-temperature ASR. If the same mechanism operates at lower temperatures, it would further weaken the bond between cement paste and a quartz aggregate, and would contribute to the effect of alkali in increasing expansion from DEF.

These and similar observations suggest that expansion from DEF is a relatively weak effect, which is greatly exacerbated and perhaps only made possible by some pre-existing weakness. In the absence of a sufficient source of weakness, as in an undamaged paste or mortar made with a limestone sand, the formation of ettringite is insufficient to disrupt the surrounding material, and either stops or is greatly retarded when the easily accessible space is exhausted. This situation is analogous to that existing with the normal hydration of a Portland cement in a paste of low w/c ratio. If there is a sufficient source of weakness, formation of ettringite can continue, and expansion and cracking may result.

## 12.7 Other forms of attack

### *12.7.1 Physical attack*

Concrete may be damaged by frost, and especially by repeated cycles of freezing and thawing. Damage usually begins with flaking at the surface, and gradually extends inwards, though deep cracks may occur. Damage associated with freezing does not occur unless a sufficient quantity of water is present in the pores, and is minimal in dense concrete of low w/c ratio and low permeability. It can be much reduced by air entrainment (Section 11.3). It is especially likely if freezing occurs before adequate hardening has occurred.

Various explanations have been given and may not be mutually exclusive. Early theories associated damage directly with the volume expansion that occurs on freezing; this could cause disruption if the water that freezes is sufficiently confined, e.g. between regions already frozen. The damage could also be caused by the growth of ice crystals, resulting from the migration of water as a result of differences in vapour pressure. Collins (C82) postulated a mechanism, similar to that believed to cause frost heaving in soils, in which the growth of ice lenses led to the formation of weak layers parallel to an exposed surface. Other theories (L66,P62,P63) attribute the damage to hydraulic pressure caused by the movement of water through capillaries. Powers (P62) considered that the expansion associated with freezing in the pores near the surface forced water inwards through small pores, where it could produce stresses sufficient to rupture the surrounding material. This theory led to the successful development of air entrainment. Later work showed that a properly air-entrained concrete contracts on freezing. This was attributed to migration of water out of the gel to the ice crystals, occurring because the vapour pressure of supercooled water is higher than that of ice at the same temperature (P63).

Studies using low-temperature calorimetry appear to provide clear evidence of the formation of an ice front that nucleates at at the surface and moves inwards (B127,B184). They also showed that the pattern of ice formation is much affected by the previous drying history.

Some other forms of physical attack will be briefly mentioned. Soluble salts may be drawn into a sufficiently permeable concrete by capillary action and crystallize within the pore structure when evaporation occurs (e.g. S144). Mechanical or thermal stress or drying shrinkage can all cause concrete to crack. Thermal stresses can cause damage at low temperatures even if the pores contain little or no water. The use of de-icing salts can cause surface damage, known as salt scaling; suggested causes have included rapid cooling caused by the melting of ice, osmotic effects associated with the presence of high concentrations of de-icing chemicals in the surface layers of the concrete, and chemical attack (Section 12.7.3). Surface damage from abrasion depends markedly on w/c ratio and on the quality of the surface layer of the concrete; at high w/c ratios it depends also on the properties of the aggregate. Abrasion resistance can be increased by surface treatments, e.g. with sodium silicate.

### 12.7.2 Leaching

Leaching of concrete by percolating or flowing water has sometimes caused severe damage, e.g. in dams, pipes or conduits, and is potentially important for the long-term storage of nuclear wastes. Pure water may be expected to remove alkali hydroxides, dissolve CH and decompose the hydrated silicate and aluminate phases. Reference to the equilibria discussed in Chapters 5 and 6 indicates that, for practical purposes, the ultimate residue will consist essentially of hydrous forms of silica, alumina and iron oxide, all the CaO having been lost. By this stage, the cement paste will have disintegrated. The equilibria also suggest that CH will be dissolved before the other phases are attacked, but in practice attack is likely to be simultaneous, because of the greater specific surface areas of the hydrated silicate and aluminate phases.

The rate of attack depends on the quality and shape of the concrete, the rate at which the water percolates through or flows over it, the temperature and the concentrations of solutes in the water. Attack is most likely to be serious with soft water. The partial pressure of $CO_2$ in unpolluted air at sea level is 32 Pa ($10^{-3.5}$ atm). Calculation based on the data in Table 12.1 shows that, for water in equilibrium with such air and not containing any other solutes, the significant species present are $CO_2$, $HCO_3^-$ and $H^+$, $[CO_2]$ is $0{\cdot}012\,\text{mmol}\,l^{-1}$ and the pH is 5·6. In underground waters, $[CO_2]$ may be much higher and the pH correspondingly lower.

A solution of $CO_2$ can dissolve $CaCO_3$ with formation of additional $HCO_3^-$

$$CaCO_3 + CO_2 + H_2O \rightarrow Ca^{2+} + 2HCO_3^- \qquad (12.4)$$

and can similarly dissolve CH or $Ca^{2+}$ and $OH^-$ ions from C–S–H or hydrated calcium aluminate phases. In all cases, the amount of $Ca^{2+}$ that a given volume of solution can dissolve is limited by the equilibria involving $CO_3^{2-}$ (Table 12.1). The term 'aggressive $CO_2$' is used to express this amount and the rate at which attack is likely to occur. It is properly defined as the quantity of $CO_2$ in unit volume of solution that can react with $CaCO_3$ according to equation 12.4. As Rogers (R89) and Cowie and

**Table 12.1** *Equilibrium constants in the system $CaO$–$CO_2$–$H_2O$*

| Reaction | Definition of $K$ | $\log K$ |
|---|---|---|
| $CO_2\,(\text{gas}) = CO_2$ | $[CO_2]/p_{CO_2}$ | −1·42 |
| $CO_2 + H_2O = H_2CO_3$ | $[H_2CO_3]/[CO_2]$ | −2·8 |
| $H_2CO_3 = H^+ + HCO_3^-$ | $\{H^+\}[HCO_3^-]/[H_2CO_3]$ | −3·5 |
| $HCO_3^- = H^+ + CO_3^{2-}$ | $\{H^+\}[CO_3^{2-}]/[HCO_3^-]$ | −10·25 |
| $CaCO_3\,(\text{calcite}) = Ca^{2+} + CO_3^{2-}$ | $[Ca^{2+}][CO_3^{2-}]$ | −8·35 |

From P64. Species are in solution except where stated. Square brackets denote species concentrations; curly brackets denote activities. Concentrations are in $\text{mol}\,l^{-1}$; $p_{CO_2}$ is in atm (1 atm = 101 kPa).

Glasser (C83) have noted, it has sometimes been incorrectly defined and calculated. It is smaller than the concentration of $CO_2$ present as such or as $H_2CO_3$, because when the solution dissolves $CaCO_3$ the concentrations of all the species change in accordance with the equilibria.

Rogers (R89) critically reviewed methods for determining total and aggressive $CO_2$. Natural waters may contain other anions, such as $SO_4^{2-}$, and in the earlier stages of leaching, at least, the situation is further complicated by the presence of alkali hydroxides from the cement pore solution. In any aqueous system of the type considered, the equilibrium composition of the solution and the nature of the solid phases can be calculated by setting up and solving equations for the various acid–base, precipitation and complexation equilibria and for charge and mass balance. The general principles of such calculations, and references to computer programs for solving the equations, may be found in works on natural water chemistry (e.g. P64). Cowie and Glasser (C83) applied this approach to the problem of leaching of concrete. They defined an aggressivity index as the ratio of $Ca(OH)_2$ dissolved at equilibrium relative to that dissolved by an equal volume of pure water, and described a method whereby it could be calculated.

Leaching destroys AFm and AFt phases as well as C–S–H and CH. Adenot and co-workers (A42,A43) showed that, as the surface was approached, the first phase to disappear was CH, followed in sequence by monosulfate, ettringite and C–S–H, though the last became progressively more decalcified. The zone immediately below the surface was amorphous material, approximating to silica gel with minor Ca and Al. The greater persistence of ettringite compared with monosulfate agrees with an observation that monosulfate is decomposed at or below pH 11.6, whereas for ettringite the corresponding value is 10·7 (G64).

### *12.7.3 Miscellaneous forms of chemical attack*

This section summarizes observations on the actions on concrete made using Portland or composite cements not considered above. There have been few systematic or detailed chemical studies, and the information given is based largely on results reported by Lea (L6) and Kuenning (K78).

Acids have an action similar in principle to that of water, but greatly intensified; CH is dissolved and the hydrated silicate and aluminate phases are decomposed, with removal of $Ca^{2+}$. Those giving insoluble products, such as $H_2SO_4$ or $H_3PO_4$, tend to be less aggressive for a given concentration than those that do not, such as HCl or $HNO_3$. Fattuhi and Hughes (F55) made a detailed study of the action of $H_2SO_4$. Acid attack is produced not only by Brønsted acids that are neutral molecules, such as the above, but also by ones that are cations or anions, such as $NH_4^+$, $Al(H_2O)_6^{3+}$, $H_2PO_4^-$ or $HSO_4^-$, which are thus highly aggressive. Acids attack limestone aggregates as well as cement paste. Alkalis have relatively little effect, but concentrated solutions of alkali hydroxides (e.g. 5 mol $l^{-1}$) attack concrete, probably by decomposing the hydrated aluminate phases.

Metal cations that produce hydroxides or basic salts of low solubility attack cement paste. The behaviour of $Mg^{2+}$ in $MgSO_4$ (Section 12.5.3) is

typical, and is shown by other magnesium salts. Concentrated (3 mol $l^{-1}$) solutions of $CaCl_2$ or $MgCl_2$ attack Portland cement concretes by reacting with the CH to form basic salts (S145). The reactions are expansive and may contribute to salt scaling (Section 12.7.1). With saturated NaCl, $C_3A \cdot CaCl_2 \cdot 10H_2O$ is formed, and there is some loss in strength, but the effect is much less than with $CaCl_2$ or $MgCl_2$. A composite cement containing 75% of slag was resistant to all three solutions.

Some organic compounds, such as sugar solutions, attack concrete, presumably through complexing of $Ca^{2+}$ and consequent dissolution of CH and the hydrated silicate and aluminate phases.

### 12.7.4 Sea water attack

Sea water (Atlantic Ocean) contains about 11 g of $Na^+$, 20 g of $Cl^-$, 2·9 g of $SO_4^{2-}$ and 1·4 g of $Mg^{2+}$ per l, with smaller amounts of $K^+$, $Ca^{2+}$, $Br^-$ and $HCO_3^-$ (0·08 g $l^{-1}$). The pH is usually 7·8–8·3. Massazza (M144) gave a general account, and Buenfeld and Newman (B185) discussed microstructural aspects and equilibria more fully. Attack is more serious in and somewhat above the tidal zone than on concrete that is permanently submerged. In the latter case, the combined action of $Mg^{2+}$ and $HCO_3^-$ produces a surface skin, typically consisting of a layer of brucite about 30 $\mu$m thick, overlain by a more slowly developing layer of aragonite. $CaCO_3$ is precipitated as aragonite rather than as calcite because of the presence of $Mg^{2+}$ ions. This skin tends to protect a well produced, dense concrete from further attack. To the extent that the latter occurs, the processes are those of leaching, $Mg^{2+} + SO_4^{2-}$ attack, carbonation, and chloride penetration, with the attendant possibility of corrosion of reinforcement, all of which are discussed elsewhere in this chapter. The effects of the $Mg^{2+}$ and $SO_4^{2-}$ are considerably milder than those observed with $MgSO_4$ solutions of similar concentration. The danger of corrosion decreases at depth due to the lack of oxygen.

In and above the tidal zone, cycles of saturation and evaporation tend to occur, the water being drawn in by capillary action or entering as spray, and damage may occur through salt crystallization. The protective layer of brucite and aragonite is liable to be destroyed. Mechanical damage may result from erosion due to waves, solid debris, sand or ice. Oxygen is readily available, permitting corrosion to occur.

As with concrete for use in other severe environments, the most important conditions for ensuring satisfactory performance are that it should be of high cement content, of low w/c ratio, of high strength and properly made, with adequate cover for the reinforcement, and wet cured before being exposed to sea water. Massazza (M144) concluded that pozzolanic or slag cements (> 60% slag) were more durable than pure Portland cements, and noted that lime–pozzolana mortars used by the Romans in sea works are still in good condition.

### 12.7.5 Bacterial attack

Normal sewage is alkaline and does not significantly attack Portland cement concrete directly, but severe damage can arise through formation of

$H_2SO_4$ by processes in which bacterial action plays a part. Anaerobic bacteria in the sewage decompose inorganic or organic sulfur compounds, giving $H_2S$. This passes into the air above the liquid and dissolves in the film of water on the walls above the water level, where under the influence of aerobic bacteria, oxygen oxidizes it to $H_2SO_4$. The cement paste softens and the aggregate falls out.

Preventive treatments have been of several kinds (L6). The sewage may be treated, e.g. with chlorine to oxidize the sulfides, with lime to raise the pH to above 10, which decreases the activity of the anaerobic bacteria, or with appropriate salts to precipitate the sulfide. Removal of slime and silt, in which the sulfide-forming reactions appear to occur, increase in flow and design to avoid turbulance, have been found useful. The service life of the concrete is much increased by using limestone as opposed to siliceous aggregates. Various surface treatments have been used, of which one of the most effective appears to be with $SiF_4$ gas.

Other situations in which attack by $H_2SO_4$ formed through bacterial action has been reported include cooling towers (L6) and concrete floors laid on rocks containing pyrite ($FeS_2$; P65).

### *12.7.6 Miscellaneous paste–aggregate reactions*

Destructive expansion occurs in concretes made with some aggregates containing dolomite, which reacts with OH– ions in the so-called dedolomitization reaction:

$$CaMg(CO_3)_2 + 2OH^- \rightarrow CaCO_3 + Mg(OH)_2 + CO_3^{2-} \qquad (12.5)$$

The effect was first observed with certain Canadian aggregates, which also contained calcite and clay minerals. Gillott and Swenson (G106), reviewing theories of the expansion mechanism, concluded that the expansion was due to uptake of water by the clay minerals, which were exposed as a result of the dedolomitization reaction. In contrast, Tang *et al.* (T68) concluded from an STEM study that the clay minerals were present in the matrix material of the aggregate and not as inclusions in the dolomite, and that expansion was mainly caused by the growth of brucite crystals around the surfaces of the dolomite grains; the clay minerals provided pathways through which the alkaline solution could penetrate. Destructive reactions associated with dedolomitization have also been observed with dolomitic aggregates from Bahrein (F56), in this case possibly complicated by the presence also of gypsum.

Van Aardt and Visser (V14,V15) showed that felspars can react with CH and water at ordinary temperatures to give $C_4AH_x$, alkalis and other products, and that the $C_4AH_x$ could react further with $CaSO_4$ to form ettringite. They concluded that some felspathic rocks, such as greywackes and some shales and sandstones, might be suspect as regards reactivity towards cement paste. Way and Cole (W46) confirmed the occurrence of felspar reactions, but found no evidence of deleterious reactions with granite or basalt aggregates.

Reinforcement of a cement paste or mortar with glass fibre much increases the tensile strength and toughness, but these properties deteriorate with time, especially in a moist environment. The deterioration is retarded, but not eliminated, by using a special glass high in $ZrO_2$. The glass is attacked by the alkaline pore solution, but the loss of strength and toughness may not be a direct consequence of this. Changes in the microstructure at the interface between glass and cement paste take place, and may be due both to attack on the glass and to processes occurring within the cement paste (M145,S146). Growth of products, especially CH, between the filaments of which the fibres are composed alters the mode of fracture and has been considered the dominant cause of deterioration, at least during the first year (B186).

### *12.7.7 Fire damage*

Because of its relatively low thermal conductivity and high specific heat, concrete provides good protection to steel against fire, though it may itself be extensively damaged. At low temperatures, cement paste expands on heating, but by 300°C contraction, associated with the water loss, occurs. Normal aggregates continue to expand, and the resultant stresses lead to loss of strength, spalling and cracking. Quartz expands sharply at 573°C due to polymorphic transformation, and calcite begins to contract at 900° due to decomposition. Blastfurnace slag, used as aggregate, is highly resistant (L6,P66).

Piasta *et al.* (P67) described the thermal effects on the cement paste. Below 500°C, major effects include carbonation and coarsening of the pore structure. Decomposition of CH at 450–550°C, and of $CaCO_3$ above 600°C, yield calcium oxide, which rehydrates on cooling. The resulting expansion may disrupt a concrete that has withstood a fire without actual disintegration (L6). Above 500°C, the pore structure continues to coarsen, and incipient crystallization of $\beta$-$C_2S$ occurs. Extensive carbonation occurs in fire-damaged buildings that have been left standing for a few years (H82).

# Appendix: Calculated X-ray powder diffraction patterns for tricalcium silicate and clinker phases

The patterns (T5) were calculated as described by Morris *et al.* (M22). The columns headed $d$ (nm), $I_{int}$, $h$, $k$ and $l$ in Tables A.1–A.6 give the integrated intensity pattern as defined by those authors, i.e. they refer to individual reflections, which can be components of overlaps. $I_{int}$ is the integrated intensity relative to a value of 100 for the strongest. Reflections with $I_{int} < 1{\cdot}5$ are not listed. The column headed $I_{pk}$ gives an indication of relative peak heights assuming typical experimental conditions using a diffractometer, but these depend on resolution and on any variation in cell parameters, because these factors affect separations between overlapping peaks. They take into account contributions from reflections too weak to appear in the list of integrated intensities, and their spacings sometimes differ significantly from those of the individual components. Peaks of significant intensity can arise from groups of reflections all of which are too weak to be listed individually; the most prominent are noted in footnotes to the tables. Except with $T_1$ $C_3S$, the cell parameters and compositions assumed are typical ones for phases in Portland cement clinkers. No data are available from which it would be possible to calculate a pattern for an $M_1$ alite. Reference intensity ratios $I_{hkl}/I_c$ (H26,M22) are also given. Their use is explained in Chapter 4.

**Table A.1** *Calculated XRD powder pattern for $T_1$ tricalcium silicate*

| $d$ (nm) | $I_{int}$ | $I_{pk}$ | $h$ | $k$ | $l$ | $d$ (nm) | $I_{int}$ | $I_{pk}$ | $h$ | $k$ | $l$ |
|---|---|---|---|---|---|---|---|---|---|---|---|
| 1·1108 | 2 | 3 | 0 | −1 | 1 | 0·2191 | 3 | | 5 | −2 | 1 |
| 0·5979 | 2 | | 1 | 2 | −1 | 0·2190 | 3 | | −1 | 0 | 6 |
| 0·5964 | 3 | 8 | −1 | 2 | 0 | 0·2190 | 2 | | 5 | 2 | 0 |
| 0·5937 | 4 | | −1 | 0 | 2 | 0·2186 | 4 | 11 | 2 | −6 | 2 |
| 0·3916 | 5 | 6 | 1 | −2 | 3 | 0·2183 | 4 | | 2 | 6 | −1 |
| 0·3890 | 4 | | 1 | 2 | 2 | 0·2176 | 3 | | 2 | 2 | −6 |
| | | 7 | | | | 0·2175 | 2 | | 4 | 4 | −3 |
| 0·3878 | 2 | | 3 | 0 | 0 | 0·2169 | 2 | | −4 | 4 | 1 |
| 0·3560 | 3 | 3 | 0 | −4 | 1 | | | 8 | | | |
| 0·3524 | 2 | 3 | −2 | 2 | 2 | 0·2166 | 3 | | −2 | 2 | 5 |
| 0·3459 | 2 | 3 | 3 | 1 | −2 | 0·2137 | 2 | 3 | 5 | 1 | −3 |
| 0·3063 | 34 | 38 | 1 | 4 | −3 | 0·2076 | 3 | 3 | −1 | 5 | 3 |
| 0·3044 | 33 | 43 | −1 | 4 | 1 | 0·2000 | 4 | 6 | 1 | 6 | −5 |
| 0·3027 | 35 | 44 | −3 | 0 | 3 | 0·1988 | 2 | 6 | −3 | 6 | 0 |
| 0·2990 | 8 | | 2 | 4 | −2 | 0·1986 | 4 | 7 | −1 | 6 | 2 |
| | | 19 | | | | 0·1979 | 2 | 6 | −3 | 0 | 6 |
| 0·2982 | 9 | | −2 | 4 | 0 | 0·1975 | 2 | 5 | −5 | 0 | 4 |
| 0·2969 | 10 | 15 | −2 | 0 | 4 | 0·1958 | 10 | 10 | 2 | −4 | 6 |
| 0·2805 | 2 | | −4 | 1 | 1 | 0·1945 | 8 | 9 | 2 | 4 | 4 |
| | | 100 | | | | 0·1939 | 9 | 12 | 6 | 0 | 0 |
| 0·2801 | 100 | | 3 | 0 | 3 | 0·1916 | 2 | 3 | 3 | 4 | −6 |
| 0·2777 | 42 | 51 | 0 | −4 | 4 | 0·1851 | 3 | 4 | 0 | −6 | 6 |
| 0·2755 | 42 | 53 | 0 | 4 | 2 | 0·1838 | 3 | | 5 | −4 | 3 |
| 0·2741 | 44 | 54 | −4 | 0 | 2 | 0·1837 | 2 | 7 | 0 | 6 | 3 |
| 0·2623 | 40 | | 3 | −4 | 1 | 0·1836 | 2 | | 1 | 0 | 7 |
| | | 85 | | | | 0·1833 | 2 | | 5 | 4 | 1 |
| 0·2622 | 40 | | 3 | 4 | −1 | 0·1830 | 2 | 7 | 4 | 3 | −6 |
| 0·2615 | 31 | 84 | −1 | 0 | 5 | 0·1828 | 2 | | −6 | 0 | 3 |
| 0·2588 | 2 | 2 | 1 | −5 | 3 | 0·1780 | 34 | 32 | 0 | −8 | 2 |
| 0·2473 | 3 | 5 | 3 | −1 | 4 | 0·1771 | 26 | 27 | 4 | 4 | −6 |
| 0·2462 | 2 | 4 | 2 | 5 | 0 | 0·1762 | 28 | 28 | −4 | 4 | 4 |
| 0·2454 | 2 | | −1 | 1 | 5 | 0·1654 | 2 | | 5 | −6 | 2 |
| | | 6 | | | | 0·1651 | 2 | | 5 | 6 | −1 |
| 0·2453 | 3 | | 4 | 3 | −2 | | | 18 | | | |
| 0·2382 | 2 | 3 | 4 | −3 | 2 | 0·1649 | 2 | | −1 | 0 | 8 |
| 0·2350 | 7 | 8 | 1 | −4 | 5 | 0·1647 | 16 | | −3 | −4 | 7 |
| 0·2342 | 3 | 8 | 4 | 0 | 3 | 0·1637 | 16 | 18 | 3 | 4 | 5 |
| 0·2333 | 2 | | 2 | 0 | 5 | 0·1633 | 13 | 20 | 7 | 0 | 1 |
| | | 10 | | | | 0·1554 | 10 | | 6 | −4 | 4 |
| 0·2332 | 6 | | 1 | 4 | 3 | | | 15 | | | |
| 0·2323 | 9 | 12 | −5 | 0 | 1 | 0·1554 | 9 | | 2 | 0 | 8 |
| 0·2307 | 2 | 6 | 4 | 3 | 1 | 0·1550 | 8 | 15 | 6 | 4 | 2 |
| 0·2291 | 2 | 6 | 3 | 5 | −2 | | | | | | |
| 0·2252 | 2 | 5 | 4 | 4 | −1 | | | | | | |
| 0·2207 | 3 | | 3 | −4 | 4 | | | | | | |
| 0·2204 | 2 | | 1 | −2 | 6 | | | | | | |
| 0·2201 | 13 | | 4 | −4 | 2 | | | | | | |
| 0·2197 | 19 | 44 | 0 | 0 | 6 | | | | | | |
| 0·2196 | 12 | | 4 | 4 | 0 | | | | | | |
| 0·2195 | 3 | | 3 | 4 | 2 | | | | | | |
| 0·2194 | 2 | | 1 | 2 | 5 | | | | | | |

**Table A.2** *Calculated XRD powder pattern for $M_3$ alite*

| $d$ (nm) | $I_{int}$ | $I_{pk}$ | $h$ | $k$ | $l$ | $d$ (nm) | $I_{int}$ | $I_{pk}$ | $h$ | $k$ | $l$ |
|---|---|---|---|---|---|---|---|---|---|---|---|
| 0·5949 | 4 | 11 | 4 | 0 | 2 | 0·2186 | 15 | 48 | 4 | 0 | 8 |
| | | | | | | 0·2186 | 32 | | −10 | 2 | 4 |
| 0·5940 | 7 | | 3 | 1 | 0 | 0·2186 | 5 | | −13 | 1 | 4 |
| 0·5490 | 2 | 3 | 1 | 1 | 2 | 0·2183 | 6 | | 1 | 1 | 8 |
| 0·3877 | 4 | 8 | −8 | 0 | 2 | 0·2182 | 6 | | −6 | 2 | 6 |
| | | | | | | 0·2170 | 5 | 17 | 9 | 1 | 6 |
| 0·3869 | 6 | | −1 | 1 | 4 | 0·2170 | 6 | | 12 | 2 | 0 |
| 0·3535 | 5 | 6 | 7 | 1 | 2 | 0·2166 | 6 | | −5 | 3 | 2 |
| | | | | | | 0·2071 | 2 | 2 | −10 | 2 | 5 |
| 0·3527 | 3 | | 0 | 2 | 0 | 0·1984 | 4 | 11 | 16 | 0 | 2 |
| 0·3180 | 2 | 3 | −6 | 0 | 5 | 0·1980 | 4 | | 9 | 3 | 0 |
| 0·3042 | 34 | 90 | 10 | 0 | 2 | 0·1979 | 7 | | 5 | 3 | 4 |
| | | | | | | 0·1938 | 7 | 18 | −16 | 0 | 4 |
| 0·3034 | 78 | | 4 | 2 | 2 | | | | | | |
| 0·2975 | 10 | 27 | 8 | 0 | 4 | 0·1934 | 17 | | −2 | 2 | 8 |
| | | | | | | 0·1837 | 3 | 5 | 14 | 2 | 3 |
| 0·2970 | 20 | | 6 | 2 | 0 | | | | | | |
| 0·2778 | 100 | 90 | −6 | 0 | 6 | 0·1835 | 2 | | 18 | 0 | 0 |
| 0·2753 | 43 | 99 | 12 | 0 | 0 | 0·1830 | 5 | 7 | 3 | 3 | 6 |
| | | | | | | 0·1825 | 4 | 7 | −12 | 2 | 6 |
| 0·2745 | 84 | | 2 | 2 | 4 | | | | | | |
| 0·2697 | 2 | 8 | −11 | 1 | 2 | 0·1824 | 2 | | 2 | 0 | 10 |
| 0·2694 | 2 | | 3 | 1 | 6 | 0·1768 | 58 | 50 | 14 | 2 | 4 |
| 0·2692 | 3 | | −4 | 2 | 4 | 0·1763 | 31 | 52 | 0 | 4 | 0 |
| 0·2611 | 41 | 100 | 6 | 0 | 6 | 0·1644 | 2 | 5 | 8 | 0 | 10 |
| | | | | | | | | | | | |
| 0·2609 | 80 | | −8 | 2 | 2 | 0·1644 | 3 | | −13 | 3 | 4 |
| 0·2453 | 5 | 5 | −6 | 0 | 7 | 0·1630 | 14 | 26 | −18 | 0 | 6 |
| 0·2327 | 6 | 18 | −14 | 0 | 2 | | | | | | |
| 0·2321 | 16 | | 0 | 2 | 6 | 0·1627 | 27 | | −4 | 2 | 10 |
| 0·2318 | 2 | | 6 | 0 | 7 | 0·1542 | 14 | 16 | −14 | 2 | 8 |
| 0·2299 | 2 | 1 | 3 | 3 | 0 | | | | | | |
| 0·2287 | 2 | 3 | −10 | 2 | 3 | 0·1542 | 8 | | 0 | 0 | 12 |

Pattern calculated assuming $a = 3{\cdot}312$ nm, $b = 0{\cdot}7054$ nm, $c = 1{\cdot}855$ nm, $\beta = 94{\cdot}17°$; atomic parameters given by Nishi *et al.* (N1); site occupancies $(Ca_{0{\cdot}98}Mg_{0{\cdot}01}Al_{0{\cdot}0067}Fe_{0{\cdot}003})_3$ $(Si_{0{\cdot}97}Al_{0{\cdot}03})O_5$. Other peaks of significant height: 0·3248 nm (2), −2 2 2 +; 0·3211 nm (1), 10 0 1 +; 0·2673 nm (3), −8 2 1; 0·2562 nm (2), −8 0 6 +; 0·2504 nm (1), 2 2 5 +; 0·2276 nm (2), 13 1 2 +; 0·2097 nm (2), −1 3 4 +; 0·2036 nm (1), 16 0 1 +; 0·1861 nm (1), −16 0 5 +; 0·1794 nm (2), −8 2 8 +; 0·1714 nm (1), −7 1 10 +; 0·1693 nm (2), −18 0 5; 0·1691 nm (2), 14 2 5 +; 0·1594 nm (1), −13 3 5 ; 0·1561 nm (1), −18 0 7. $I_{\bar{6}06}/I_c = 0{\cdot}742$.

Note to Table A.1.

Pattern calculated from the data of Golovastikov *et al.* (G2); $a = 1{\cdot}167$ nm, $b = 1{\cdot}424$ nm, $c = 1{\cdot}372$ nm, $\alpha = 105{\cdot}50°$, $\beta = 94{\cdot}33°$, $\gamma = 90{\cdot}00°$. The pattern includes many additional weak peaks, arising from multiple overlaps. The most prominent (spacings in nanometres and relative intensities) are 0·3717 (3), 0·1910 (3), 0·1905 (2), 0·1816 (3), 0·1800 (3), 0·1725 (2), 0·1703 (2), 0·1690 (2), 0·1621 (3), 0·1612 (2) and 0·1585 (2). $I_{303}/I_c = 0{\cdot}798$.

**Table A.3** *Calculated XRD powder pattern for a belite*

| $d$ (nm) | $I_{int}$ | $I_{pk}$ | $h$ | $k$ | $l$ | $d$ (nm) | $I_{int}$ | $I_{pk}$ | $h$ | $k$ | $l$ |
|---|---|---|---|---|---|---|---|---|---|---|---|
| 0·4891 | 3 | 3 | −1 | 0 | 1 | 0·1915 | 9 | 8 | 0 | 2 | 4 |
| 0·4651 | 10 | 10 | 0 | 0 | 2 | 0·1900 | 8 | 8 | 2 | 1 | 3 |
| 0·3830 | 7 | 7 | 0 | 1 | 2 | 0·1893 | 16 | 15 | 2 | 2 | 2 |
| 0·3786 | 6 | 6 | 1 | 1 | 1 | 0·1845 | 6 | 5 | −2 | 0 | 4 |
| 0·3375 | 8 | 7 | 0 | 2 | 0 | 0·1821 | 4 | 4 | 0 | 3 | 3 |
| 0·3237 | 9 | 9 | −1 | 1 | 2 | 0·1805 | 12 | 16 | −2 | 2 | 3 |
| 0·3173 | 6 | 6 | 0 | 2 | 1 | | | | | | |
| 0·3051 | 12 | 11 | 1 | 1 | 2 | 0·1804 | 8 | | −1 | 0 | 5 |
| 0·2874 | 26 | 24 | 1 | 2 | 0 | 0·1794 | 13 | 12 | 0 | 1 | 5 |
| 0·2818 | 14 | 19 | 0 | 1 | 3 | 0·1764 | 5 | 4 | 3 | 1 | 0 |
| 0·2793 | 100 | 100 | −1 | 0 | 3 | 0·1743 | 2 | 2 | −1 | 1 | 5 |
| 0·2778 | 81 | 94 | −1 | 2 | 1 | 0·1725 | 7 | 7 | −2 | 3 | 1 |
| 0·2742 | 88 | 88 | 2 | 0 | 0 | 0·1722 | 4 | 7 | 1 | 0 | 5 |
| | | | | | | 0·1710 | 3 | 14 | 2 | 0 | 4 |
| 0·2732 | 28 | | 0 | 2 | 2 | | | | | | |
| 0·2716 | 32 | 38 | 1 | 2 | 1 | 0·1708 | 15 | | 2 | 2 | 3 |
| 0·2615 | 69 | 60 | 1 | 0 | 3 | 0·1695 | 5 | 5 | 2 | 3 | 1 |
| 0·2540 | 16 | 14 | 2 | 1 | 0 | 0·1687 | 5 | 5 | 0 | 4 | 0 |
| 0·2446 | 17 | 16 | −2 | 0 | 2 | 0·1660 | 2 | 2 | 0 | 4 | 1 |
| 0·2438 | 8 | 16 | 1 | 1 | 3 | 0·1630 | 21 | 23 | −3 | 0 | 3 |
| 0·2407 | 13 | 24 | 2 | 1 | 1 | | | | | | |
| | | | | | | 0·1629 | 10 | | 0 | 2 | 5 |
| 0·2402 | 18 | | 1 | 2 | 2 | 0·1619 | 4 | 6 | −2 | 2 | 4 |
| 0·2326 | 3 | 3 | 0 | 0 | 4 | 0·1613 | 5 | 8 | 1 | 4 | 0 |
| 0·2299 | 3 | 4 | −2 | 1 | 2 | | | | | | |
| 0·2287 | 3 | 28 | 2 | 0 | 2 | 0·1611 | 5 | | 3 | 1 | 2 |
| | | | | | | 0·1607 | 8 | 11 | 3 | 2 | 0 |
| 0·2283 | 31 | | 0 | 2 | 3 | 0·1604 | 2 | 15 | 2 | 3 | 2 |
| 0·2199 | 18 | 18 | 0 | 1 | 4 | | | | | | |
| 0·2187 | 51 | 45 | 0 | 3 | 1 | 0·1602 | 14 | | −3 | 2 | 1 |
| 0·2166 | 19 | 18 | 2 | 1 | 2 | 0·1595 | 2 | 5 | −1 | 4 | 1 |
| 0·2152 | 2 | | −1 | 2 | 3 | 0·1591 | 3 | | −1 | 2 | 5 |
| 0·2128 | 8 | 7 | 2 | 2 | 0 | 0·1586 | 6 | 8 | 0 | 4 | 2 |
| 0·2102 | 2 | <1 | −2 | 2 | 1 | | | | | | |
| 0·2094 | 8 | 8 | −1 | 1 | 4 | 0·1585 | 2 | | −3 | 1 | 3 |
| 0·2082 | 5 | 5 | 1 | 3 | 0 | 0·1583 | 5 | 8 | 1 | 4 | 1 |
| 0·2048 | 17 | 16 | 2 | 2 | 1 | 0·1574 | 16 | 13 | −1 | 3 | 4 |
| 0·2044 | 3 | 13 | −1 | 3 | 1 | 0·1555 | 4 | 10 | −2 | 1 | 5 |
| 0·2037 | 10 | 12 | −2 | 1 | 3 | 0·1552 | 4 | | −3 | 2 | 2 |
| 0·2025 | 11 | 13 | 0 | 3 | 2 | | | | | | |
| 0·2019 | 15 | 18 | 1 | 3 | 1 | 0·1550 | 6 | | 0 | 0 | 6 |
| 0·1992 | 18 | 16 | 1 | 1 | 4 | 0·1549 | 5 | | −2 | 3 | 3 |
| 0·1980 | 31 | 28 | −2 | 2 | 2 | | | | | | |

Pattern calculated assuming $a = 0{\cdot}550$ nm, $b = 0{\cdot}675$ nm, $c = 0{\cdot}933$ nm, $\beta = 94{\cdot}40°$; atomic parameters given by Jost *et al.* (J2); site occupancies $(K_{0{\cdot}01}Na_{0{\cdot}005}Ca_{0{\cdot}975}Mg_{0{\cdot}01})_2(Fe_{0{\cdot}02}Al_{0{\cdot}06}Si_{0{\cdot}90}P_{0{\cdot}01}S_{0{\cdot}01})O_{3{\cdot}96}$. Other peaks of significant height: 0·1760 nm (3), −3 1 1; 0·1656 nm (2), −2 3 2 +· $I_{-103}/I_c = 0{\cdot}724$.

**Table A.4** *Calculated XRD powder pattern for a cubic aluminate*

| $d$ (nm) | $I_{int}$ | $I_{pk}$ | $h$ | $k$ | $l$ | $d$ (nm) | $I_{int}$ | $I_{pk}$ | $h$ | $k$ | $l$ |
|---|---|---|---|---|---|---|---|---|---|---|---|
| 0·6815 | 2 | 2 | 1 | 0 | 2 | 0·2694 | 100 | 100 | 0 | 4 | 4 |
| 0·5080 | 3 | 4 | 1 | 2 | 2 | 0·2410 | 2 | 3 | 0 | 2 | 6 |
| 0·4595 | 2 | 2 | 1 | 1 | 3 | 0·2380 | 2 | 3 | 0 | 4 | 5 |
| 0·4227 | 5 | 6 | 0 | 2 | 3 | 0·2200 | 7 | 7 | 4 | 4 | 4 |
| 0·4073 | 5 | 14 | 1 | 2 | 3 | 0·2037 | 2 | 2 | 2 | 4 | 6 |
| | | | | | | 0·1951 | 3 | 3 | 3 | 4 | 6 |
| 0·4073 | 7 | | 2 | 1 | 3 | 0·1905 | 31 | 29 | 0 | 0 | 8 |
| 0·3810 | 3 | 3 | 0 | 0 | 4 | 0·1890 | 2 | 4 | 1 | 0 | 8 |
| 0·3326 | 3 | 3 | 2 | 1 | 4 | 0·1822 | 2 | 3 | 3 | 5 | 6 |
| 0·3048 | 2 | 2 | 3 | 0 | 4 | 0·1555 | 34 | 30 | 4 | 4 | 8 |
| 0·2830 | 4 | 5 | 0 | 2 | 5 | | | | | | |
| 0·2782 | 5 | 8 | 1 | 2 | 5 | | | | | | |
| 0·2782 | 2 | | 2 | 1 | 5 | | | | | | |

Pattern calculated assuming $a = 1{\cdot}524$ nm, space group Pa3, atomic parameters given by Mondal and Jeffery (M17) and composition $(K_{0{\cdot}03}Na_{0{\cdot}06}Ca_{2{\cdot}76}Mg_{0{\cdot}08}Ti_{0{\cdot}01})(Fe_{0{\cdot}22}Al_{1{\cdot}60}Si_{0{\cdot}18})O_6$. Other peaks of significant height: 0·6215 nm (2), 1 1 2; 0·2272 nm (2), 4 2 5 +; 0·2177 nm (2), 2 3 6 +; 0·1984 nm (2), 3 1 7 +; 0·1643 nm (2), 5 5 6 +. $I_{044}/I_c = 3{\cdot}06$.

**Table A.5** *Calculated XRD powder pattern for an orthorhombic aluminate phase*

| $d$ (nm) | $I_{int}$ | $I_{pk}$ | $h$ | $k$ | $l$ | $d$ (nm) | $I_{int}$ | $I_{pk}$ | $h$ | $k$ | $l$ |
|---|---|---|---|---|---|---|---|---|---|---|---|
| 0·7553 | 2 | 2 | 0 | 0 | 2 | 0·2282 | 2 | 2 | 3 | 3 | 3 |
| 0·6846 | 3 | 4 | 1 | 1 | 1 | 0·2270 | 2 | 3 | 3 | 1 | 5 |
| 0·5104 | 5 | 6 | 0 | 2 | 1 | 0·2207 | 5 | 9 | 4 | 0 | 4 |
| 0·4414 | 5 | 5 | 2 | 0 | 2 | | | | | | |
| 0·4211 | 8 | 8 | 1 | 1 | 3 | 0·2202 | 6 | | 0 | 4 | 4 |
| 0·3840 | 2 | 2 | 2 | 2 | 0 | 0·2186 | 2 | 3 | 2 | 4 | 3 |
| 0·3690 | 2 | 2 | 0 | 2 | 3 | 0·2030 | 2 | 2 | 1 | 3 | 6 |
| 0·3423 | 9 | 9 | 2 | 2 | 2 | 0·1964 | 3 | 3 | 5 | 1 | 3 |
| 0·3389 | 2 | 3 | 1 | 1 | 4 | 0·1920 | 32 | 29 | 4 | 4 | 0 |
| 0·3353 | 4 | 7 | 3 | 1 | 1 | 0·1905 | 4 | 5 | 4 | 4 | 1 |
| | | | | | | 0·1892 | 2 | 14 | 2 | 4 | 5 |
| 0·3345 | 3 | | 1 | 3 | 1 | | | | | | |
| 0·3054 | 6 | 6 | 2 | 2 | 3 | 0·1888 | 15 | | 0 | 0 | 8 |
| 0·2812 | 5 | 5 | 1 | 1 | 5 | 0·1848 | 2 | 2 | 4 | 0 | 6 |
| 0·2720 | 31 | 49 | 4 | 0 | 0 | 0·1749 | 2 | 2 | 4 | 2 | 6 |
| | | | | | | 0·1688 | 2 | 1 | 0 | 4 | 7 |
| 0·2711 | 25 | | 0 | 4 | 0 | 0·1624 | 3 | 3 | 2 | 6 | 3 |
| 0·2693 | 100 | 100 | 2 | 2 | 4 | 0·1565 | 17 | 17 | 6 | 2 | 4 |
| 0·2431 | 3 | 3 | 4 | 2 | 0 | 0·1562 | 15 | 21 | 2 | 6 | 4 |
| 0·2392 | 2 | 3 | 1 | 1 | 6 | 0·1551 | 9 | 11 | 4 | 0 | 8 |
| 0·2374 | 4 | 4 | 2 | 2 | 5 | | | | | | |
| 0·2354 | 2 | 2 | 2 | 3 | 4 | 0·1549 | 6 | | 0 | 4 | 8 |
| 0·2310 | 2 | 3 | 2 | 4 | 2 | | | | | | |

Pattern calculated assuming $a = 1{\cdot}0879$ nm, $b = 1{\cdot}0845$ nm, $c = 1{\cdot}5106$ nm, space group Pbca; composition $(Na_{0{\cdot}292}Ca_{2{\cdot}792})(Fe_{0{\cdot}150}Al_{1{\cdot}725}Si_{0{\cdot}125})O_6$; atomic parameters given by Nishi and Takéuchi (N4). Other peaks of significant height: 0·5414 nm (2), 0 2 0; 0·5388 nm (2), 1 1 2; 0·2639 nm (2), 0 2 5; 0·2586 nm (2), 3 2 3 +; 0·2425 nm (3), 3 3 2; 0·2047 nm (2), 1 5 2; 0·2042 nm (2), 2 4 4; 0·1827 nm (2), 1 3 7 +; 0·1616 nm (2), 6 1 4. $I_{224}/I_c = 1{\cdot}94$.

**Table A.6** *Calculated XRD powder pattern for a clinker ferrite*

| $d$ (nm) | $I_{int}$ | $I_{pk}$ | $h$ | $k$ | $l$ | $d$ (nm) | $I_{int}$ | $I_{pk}$ | $h$ | $k$ | $l$ |
|---|---|---|---|---|---|---|---|---|---|---|---|
| 0·7321 | 19 | 21 | 0 | 2 | 0 | 0·1919 | 48 | 41 | 2 | 0 | 2 |
| 0·5177 | 4 | 4 | 1 | 1 | 0 | 0·1882 | 3 | 3 | 2 | 5 | 1 |
| 0·3839 | 2 | 2 | 1 | 0 | 1 | 0·1857 | 9 | 8 | 2 | 2 | 2 |
| 0·3661 | 16 | 17 | 1 | 3 | 0 | 0·1830 | 2 | 20 | 2 | 6 | 0 |
| 0·3400 | 7 | 7 | 1 | 2 | 1 | | | | | | |
| 0·2767 | 35 | 33 | 2 | 0 | 0 | 0·1830 | 21 | | 0 | 8 | 0 |
| 0·2664 | 47 | 53 | 0 | 0 | 2 | 0·1799 | 3 | 3 | 0 | 6 | 2 |
| 0·2649 | 100 | 100 | 1 | 4 | 1 | 0·1726 | 10 | 8 | 3 | 3 | 0 |
| 0·2588 | 14 | 14 | 1 | 5 | 0 | 0·1648 | 2 | 2 | 1 | 2 | 3 |
| 0·2422 | 5 | 4 | 2 | 1 | 1 | 0·1592 | 4 | 3 | 2 | 7 | 1 |
| 0·2208 | 9 | 9 | 2 | 4 | 0 | 0·1574 | 17 | 15 | 3 | 4 | 1 |
| 0·2154 | 7 | 14 | 1 | 3 | 2 | 0·1561 | 3 | 4 | 3 | 5 | 0 |
| | | | | | | 0·1535 | 21 | 17 | 1 | 4 | 3 |
| 0·2154 | 9 | | 0 | 4 | 2 | 0·1527 | 6 | 6 | 2 | 8 | 0 |
| 0·2059 | 23 | 20 | 1 | 6 | 1 | | | | | | |

Pattern calculated assuming $a = 0{\cdot}5535$ nm, $b = 1{\cdot}4642$ nm, $c = 0{\cdot}5328$ nm, space group Ibm2, atomic parameters given for $C_4AF$ by Colville and Geller (C3) and composition $Ca_2[Al_{0{\cdot}7}Fe_{0{\cdot}3}](Al_{0{\cdot}7}Fe_{0{\cdot}3})O_5$, where square and round brackets denote octahedral and tetrahedral sites respectively. $I_{141}/I_c = 1{\cdot}79$.

# References

Abbreviations used in the reference list are as follows.

| | |
|---|---|
| [2nd] SCC | *Symposium on the Chemistry of Cements* (Stockholm 1938), Ingeniörsvetenskapsakademien, Stockholm (1939). |
| 3rd ISCC | *Proceedings of the Third International Symposium on the Chemistry of Cement* (London 1952), Cement and Concrete Association, London (1954). |
| 4th ISCC | *Chemistry of Cement. Proceedings of the Fourth International Symposium* (Washington 1960), 2 vols, National Bureau of Standards Monograph 43, US Department of Commerce, Washington, DC (1962). |
| 5th ISCC | *Proceedings of the Fifth International Symposium on the Chemistry of Cement* (Tokyo 1968), 4 vols, Cement Association of Japan, Tokyo (1969). |
| 6th ICCC | *Sixth International Congress on the Chemistry of Cement* (Moscow 1974), Vols. 1, 2(1), 2(2) and 3, Russ. with Engl. preprints, Stroyizdat, Moscow (1976). |
| 7th ICCC | *7th International Congress on the Chemistry of Cement* (Paris 1980), 4 vols, Editions Septima, Paris (1980,1981). |
| 8th ICCC | *8th International Congress on the Chemistry of Cement* (Rio de Janeiro 1986), 6 vols, Abla Gráfica e Editora Ltda, Rio de Janeiro (1986). |
| 9th ICCC | *9th International Congress on the Chemistry of Cement* (New Delhi 1992), 5 vols, National Council for Cement and Building Materials, New Delhi (1992). |
| IC Cem. Microsc. | *Proceedings of the International Conference on Cement Microscopy*, International Cement Microscopy Association, Duncanville, TX. |


A1 Aggarwal, P.S., Gard, J.A., Glasser, F.P. and Biggar, G.M. (1972). *Cem. Concr. Res.* **2**, 291.

A2 Allen, W.C. and Snow, R.B. (1955). *J. Am. Ceram. Soc.* **38**, 264.

A3 Arceo, H.B. and Glasser, F.P. (1990). *Cem. Concr. Res.* **20**, 862.

A4 Andaç, Ö. and Glasser, F.P. (1994). *Adv. Cem. Res.* **6**, 57.

A5 Amafuji, M. and Tsumagari, A., in *5th ISCC*, Vol. 1, p. 136 (1969).

A6 Allen, T. *Particle Size Measurement* (2nd Edn), 454 pp, Chapman and Hall, London (1975).

A7 Anderegg, F.O. and Hubbell, D.S. (1929). *Proc. ASTM* **29**, 554.

A8 Anderegg, F.O. and Hubbell, D.S. (1930). *Proc. ASTM* **30**, 572.
A9 Aldridge, L.P. (1982). *Cem. Concr. Res.* **12**, 381.
A10 Ahmed, S.J. and Taylor, H.F.W. (1967). *Nature* **215**, 622.
A11 Allmann, R. (1968). *Neues Jahrb. Mineral. Monatsh.* 140.
A12 Ahmed, S.J, Dent Glasser, L.S. and Taylor, H.F.W., in *5th ISCC*, Vol. 2, p. 118 (1969).
A13 Aruja, E. (1960). *Acta Cryst.* **14**, 1213.
A14 Allmann, R. (1970). *Chimia* **24**, 99.
A15 Allmann, R. and Lohse, H.-H. (1966). *Neues Jahrb. Mineral. Monatsh.* 161.
A16 Abriel, W. (1983). *Acta Cryst.* **C39**, 956.
A17 Atkins, M., Macphee, D., Kindness, A. and Glasser, F.P. (1991). *Cem. Concr. Res.* **21**, 991.
A18 Abate, C. and Scheetz, B.E. (1995). *J. Am. Ceram. Soc.* **78**, 939.
A19 Asaga, K., Ishizaki, M., Takahashi, S., Konishi, K., Tsurumi, T. and Daimon, M., in *9th ICCC*, Vol. 4, p. 181 (1992).
A20 Al-Dulaijan, S.U., Parry-Jones, G., Al-Tayyib, A.-H. J. and Al-Mana, A.I. (1990). *J. Am. Ceram. Soc.* **73**, 736.
A21 Allen, A.J., Windsor, C.G., Rainey, V., Pearson, D., Double, D.D. and Alford, N.McN. (1982). *J. Phys.* **D15**, 1817.
A22 Alexander, K.M., Taplin, J.H. and Wardlaw, J., in *5th ISCC*, Vol. 3, p. 152 (1969).
A23 Aldridge, L.P., in *7th ICCC*, Vol. 3, p. VI-83 (1980).
A24 Alford, N. McN., Birchall, J.D., Howard, A.J. and Kendall, K. (1985). *J. Mater. Sci.* **20**, 1134.
A25 Aïtcin, P.C., Carles-Gibergues, A., Oudjit, M.N. and Vaquier, A., in *8th ICCC*, Vol. 4, p. 22 (1986).
A26 Aïtcin, P.-C., Sarkar, S.L. and Diatta, Y. (1987). *Mater. Res. Soc. Symp. Proc.* **85**, 261.
A27 Atkins, M., Lachowski, E.E. and Glasser, F.P. (1993). *Adv. Cem. Res.* **5**, 97.
A28 Al-Dulaijan, S.U., Al-Tayyib, A.-H.J., Al-Zahrani, M.M., Parry-Jones, G. and Al-Mana, A.I. (1995). *J. Am. Ceram. Soc.* **78**, 342.
A29 Afshar, A.B. and McCarter, W.J. (1985). *J. Mater. Sci. Lett.* **4**, 851.
A30 Andaç, Ö. and Glasser, F.P. (1995). *Mater. Res. Soc. Symp. Proc.* **370**, 135.
A31 Agarwal, R.K., Paralkar, S.V. and Chatterjee, A.K., in *8th ICCC*, Vol. 2, p. 327 (1986).
A32 Asaga, K. and Roy, D.M. (1980). *Cem. Concr. Res.* **10**, 287.
A33 Andersen, P.J., Roy, D.M. and Gaidis, J.M. (1988). *Cem. Concr. Res.* **18**, 980.
A34 Arliguie, G., Ollivier, J.P. and Grandet, J. (1982). *Cem. Concr. Res.* **12**, 79.
A35 Alunno-Rossetti, V., Chiocchio, G. and Collepardi, M. (1974). *Cem. Concr. Res.* **4**, 279.
A36 Alexanderson, J. (1979). *Cem. Concr. Res.* **9**, 507.
A37 Aitken, A. and Taylor, H.F.W., in *4th ISCC*, Vol. 1, p. 285 (1962).
A38 Al-Khalaf, N.N. and Page, C.L. (1979). *Cem. Concr. Res.* **9**, 197.
A39 Arliguie, G., Grandet, J. and Duval, R., in *7th ICCC*, Vol. 3, p. VII-22 (1980).
A40 Andrade, C., Alonso, C., Santos, P. and Macías, A., in *8th ICCC*, Vol. 5, p. 256 (1986).
A41 Al-Amoudi, O.S.B., Maslehuddin, M. and Saadi, M.M. (1995). *ACI Mater. J.* **92**, 15.

A42 Adenot, F. and Buil, M. (1992). *Cem. Concr. Res.* **22**, 489.
A43 Adenot, F. and Richet, C., in *Mechanisms of Chemical Degradation of Cement-based Systems* (eds K.L. Scrivener and J.F. Young), p. 341, E & FN Spon, London (1997).

B1 Bigaré, M., Guinier, A., Mazières, C., Regourd, M., Yannaquis, N., Eysel, W., Hahn, T. and Woermann, E. (1967). *J. Am. Ceram. Soc.* **50**, 609.
B2 Boikova, A.I., in *8th ICCC*, Vol. 1, p. 19 (1986).
B3 Boikova, A.I., Esayan, A. and Lazukin, V., in *7th ICCC*, Vol. 4, p. 183 (1981).
B4 Boikova, A.I., Fomicheva, O.I. and Zubekhin, A.P., in *8th ICCC*, Vol. 2, p. 243 (1986).
B5 Burke, E., in *3rd ISCC*, p. 50 (1954).
B6 Barnes, P., Fentiman, C.H. and Jeffery, J.W. (1977). *Acta Cryst.* **A36**, 353.
B7 Barbier, J. and Hyde, B.G. (1985). *Acta Cryst.* **B41**, 383.
B8 Bonafous, L., Bessada, C., Massiot, D., Coutures, J.-P., LeRolland, B. and Colombet, P. (1995). *J. Am. Ceram. Soc.* **78**, 2603.
B9 Biggar, G.M. (1971). *Cem. Concr. Res.* **1**, 493.
B10 Banda, R.M.H. and Glasser, F.P. (1978). *Cem. Concr. Res.* **8**, 665.
B11 Büssem, W., in *2nd SCC*, p. 141 (1939).
B12 Bertaut, E.F., Blum, P. and Sagnières, A. (1959). *Acta Cryst.* **12**, 149.
B13 Berggren, J. (1971). *Acta Chem. Scand.* **25**, 3616.
B14 Bergstrom, T.B., Hall, C. and Scrivener, K.L. (1991/2). *Adv. Cem. Res.* **4**, 141.
B15 Bachiorrini, A. (1985). *Cem. Concr. Res.* **15**, 167.
B16 Boyko, E.R. and Wisnyi, L.G. (1958). *Acta Cryst.* **11**, 444.
B17 Büssem, W. and Eitel, W. (1936). *Zeit. Krist.* **95**, 175.
B18 Bartl, H. and Scheller, T. (1970). *Neues Jahrb. Mineral. Monatsh.* 547.
B19 Brisi, C. and Borlera, M.L. (1983). *Cemento* **80**, 3.
B20 Borlera, M.L. and Brisi, C. (1984). *Cemento* **81**, 13.
B21 Brisi, C., Borlera, M.L., Montanaro, L. and Negro, A. (1986). *Cem. Concr. Res.* **16**, 156.
B22 Brotherton, P.D., Epstein, J.M., Pryce, M.W. and White, A.H. (1974). *Austral. J. Chem.* **27**, 657.
B23 Bellanca, A. (1942). *Periodico Mineral.* **13**, 21.
B24 Bereczky, E. (1964). *Épitöanyag* **16**, 441.
B25 Bogue, R.H. (1929). *Ind. Engng Chem. (Anal.)* **1**, 192.
B26 Bannon, C.A. (1995). *World Cem.* **26** (11) 4.
B27 Bye, G.C. *Portland Cement. Composition, Production and Properties*, 149pp., Pergamon Press, Oxford (1983).
B28 Bucchi, R. (1978). *Cemento* **75**, 411.
B29 Bucchi, R., in *7th ICCC*, Vol. 1, p. I-1/3 (1980).
B30 Bucchi, R. (1981). *World Cem. Technol.* **12**, 258.
B31 Bogue, R.H. *The Chemistry of Portland Cement* (2nd Edn), 793pp., Reinhold, New York (1955).
B32 Banda, R.M.H. and Glasser, F.P. (1978). *Cem. Concr. Res.* **8**, 319.
B33 Butt, Yu. M., Timashev, V.V. and Osokin, A.P., in *6th ICCC*, Vol. 1, p. 132 (1976).
B34 Barlow, D.F., in *7th IC Cem. Microsc.*, p. 243 (1985).
B35 Bucchi, R. (1981). *World Cem. Technol.* **12**, 210.
B36 Brisi, C. and Appendino, P. (1965). *Ann. Chim.* (Rome) **55**, 1213.

B37 Butt, Ju. M., Kolbasov, V.M. and Melniekij, G.A. (1974). *Zem.-Kalk-Gips* **27**, 27.
B38 Blaine, R.L. (1943). *ASTM Bull.* **123**, 51.
B39 Bensted, J. (1980). *Cemento* **77**, 169.
B40 Bensted, J. and Varma, S.P. (1974). *Cem. Technol.* **5**, 378.
B41 Bensted, J. (1976). *J. Am. Ceram. Soc.* **59**, 140.
B42 Berger, R.L., Frohnsdorff, G.J.C., Harris, P.H. and Johnson, P.D., in *Symposium on Structure of Portland Cement Paste and Concrete* (Sp. Rpt 90), p. 234, Highway Research Board, Washington, DC (1966).
B43 Barret, P., Ménétrier, D. and Bertrandie, D. (1983). *Cem. Concr. Res.* **13**, 728.
B44 Boikova, A.I., Degen, M.G., Paramonova, V.A. and Sud'ina, V.V. (1978). *Tsement* 3.
B45 Boikova, A.I., Domansky, A.I., Paramonova, V.A., Stavitskaja, G.P. and Nikushchenko, V.M. (1977). *Cem. Concr. Res.* **7**, 483.
B46 Boikova, A.I., Grishchenko, L.V. and Domansky, A.I., in *7th ICCC*, Vol. 4, p. 460 (1981).
B47 Beaudoin, J.J. (1987). *Matér. Constr.* **20**, 27.
B48 Bernal, J.D. and Megaw, H.D. (1935). *Proc. R. Soc. London* **A151**, 384.
B49 Berger, R.L. and McGregor, J.D. (1972). *Cem. Concr. Res.* **2**, 43.
B50 Bassett, H. (1934). *J. Chem. Soc.* 1970.
B51 Bentur, A. and Berger, R.L. (1979). *J. Am. Ceram. Soc.* **62**, 117.
B52 Brunauer, S. and Greenberg, S.A., in *4th ISCC*, Vol. 1, p. 135 (1962).
B53 Brown, L.S. and Carlson, R.W. (1936). *Proc. ASTM* **36**, 332.
B54 Bailey, J.E. and Stewart, H.R. (1984). *J. Mater. Sci. Lett.* **3**, 411.
B55 Bernal, J.D., Jeffery, J.W. and Taylor, H.F.W. (1952). *Mag. Concr. Res.* **2**, 1.
B56 Brown, P.W., Franz, E., Frohnsdorff, G. and Taylor, H.F.W. (1984). *Cem. Concr. Res.* **14**, 257.
B57 Bentur, A., Berger, R.L., Kung, J.H., Milestone, N.B. and Young, J.F. (1979). *J. Am. Ceram. Soc.* **62**, 362.
B58 Bentur, A., Berger, R.L., Lawrence, F.V., Milestone, N.B., Mindess, S. and Young, J.F. (1979). *Cem. Concr. Res.* **9**, 83.
B59 Brough, A.R., Dobson, C.M., Richardson, I.G. and Groves, G.W. (1994). *J. Mater. Sci.* **29**, 3926.
B60 Barret, P. and Bertrandie, D. (1986). *J. Chim. Phys.* **83**, 765.
B61 Barret, P. and Bertrandie, D. (1988). *J. Am. Ceram. Soc.* **71**, C-113.
B62 Barby, D., Griffiths, T., Jacques, A.R. and Pawson, D., in *The Modern Inorganic Chemicals Industry* (ed. R.Thompson), p. 320, Chemical Society, London (1977).
B63 Brisi, C. (1954). *Ricerca Sci.* **24**, 1436.
B64 Brunauer, S., Hayes, J.C. and Hass, W.E. (1954). *J. Phys. Chem.* **58**, 279.
B65 Babushkin, W.I., Matveev, G.M. and Mchedlov-Petrossian, O.P., *Thermodynamics of Silicates* (3rd Edn), 350pp., Publishers of Construction Literature, Moscow (1972).
B66 Brown, P.W. (1990). *J. Am. Ceram. Soc.* **73**, 3457.
B67 Brown, P.W. (1992). *Adv. Cem. Res.* **4**, 17.
B68 Bhatty, M.S.Y. and Greening, N., in *Effects of Alkalies on Cement and Concrete* (ed. S. Diamond), Publ. CE-MAT-1-78, p. 87, Purdue University, W. Lafayette, IN (1978).
B69 Barret, P., Bertrandie, D. and Ménétrier, D., in *7th ICCC*, Vol. 2, p. 261 (1980).

B70 Brown, P.W., Harner, C.L. and Prosen, E.J. (1986). *Cem. Concr. Res.* **16**, 17.
B71 Ball, M.C., Simmons, R.E. and Sutherland, I. (1984). *Br. Ceram. Proc.* (35) 1.
B72 Brown, P.W., Pommersheim, J. and Frohnsdorff, G. (1985). *Cem. Concr. Res.* **15**, 35.
B73 Brown, P.W., Galuk, K. and Frohnsdorff, G. (1984). *Cem. Concr. Res.* **14,** 843.
B74 Barret, P., in *8th ICCC*, Vol. 3, p. 86 (1986).
B75 Buttler, F.G., Dent Glasser, L.S. and Taylor, H.F.W (1959). *J. Am. Ceram. Soc.* **42**, 121.
B76 Brown, P.W. and Bothe, J.V. (1993). *Adv. Cem. Res.* **5**, 47.
B77 Bensted, J. (1979). *Cemento* **76**, 117.
B78 Bensted, J. (1976). *Tonind. Zeit.* **100**, 365.
B79 Bensted, J. and Varma, S.P. (1973). *Cem. Technol.* **4**, 112.
B80 Buhlert, R. and Kuzel, H.-J. (1971). *Zem.-Kalk-Gips* **24**, 83.
B81 Bensted, J. and Varma, S.P. (1971). *Cem. Technol.* **2**, 73, 100.
B82 Bensted, J. and Varma, S.P. (1972). *Silicates Ind.* **37**, 315.
B83 Bensted, J. and Varma, S.P. (1972). *Cem. Technol.* **3**, 185.
B84 Bannister, F.A., Bernal, J.D. and Hey, M.H. (1936). *Mineral. Mag.* **24**, 324.
B85 Bensted, J. and Varma, S.P. (1974). *Silicates Ind.* **39**, 11.
B86 Bartl, H. (1969). *Neues Jahrb. Mineral. Monatsh.* 404.
B87 Basso, R., Della Giusta, A. and Zefiro, L. (1983). *Neues Jahrb. Mineral. Monatsh.* 251.
B88 Basso, R. (1985). *Neues Jahrb. Mineral. Monatsh.* 108.
B89 Ball, M.C. (1976). *Cem. Concr. Res.* **6**, 419.
B90 Buttler, F.P. and Taylor, H.F.W. (1978). *Cemento* **75,** 147.
B91 Barret, P. and Dufour, P., in *7th ICCC*, Vol. 3, p. V-124 (1980).
B92 Brindley, G.W. and Kikkawa, S. (1979). *Am. Mineral.* **64**, 836.
B93 Brindley, G.W. and Kikkawa, S. (1980). *Clays and Clay Minerals* **28**, 87.
B94 Bokii, G.B., Pal'chik, N.A. and Antipin, M. Yu. (1978). *Sov. Phys. Cryst.* **23**, 141 (translated from *Kristallografiya* **23**, 257).
B95 Bensted, J. (1975). *Cemento* **72**, 139.
B96 Bensted, J. and Varma, S.P. (1971). *Nature Phys. Sci.* **232**, 174.
B97 Brown, P.W., in *8th ICCC*, Vol. 3, p. 231 (1986).
B98 Bailey, J.E. and Hampson, C.J. (1982). *Cem. Concr. Res.* **12**, 227.
B99 Barret, P. and Bertrandie, D., in *7th ICCC*, Vol. 3, p. V-134 (1980).
B100 Barret, P. and Bertrandie, D., in *International Seminary on Calcium Aluminates* (ed. M. Murat *et al.*), Politecnico di Torino, Turin (1982).
B101 Barret, P., Bertrandie, D. and Beau, D. (1983). *Cem. Concr. Res.* **13**, 789.
B102 Barret, P., Beau, D. and Bertrandie, D. (1986). *Cem. Concr. Res.* **16**, 785.
B103 Breval, E. (1976). *Cem. Concr. Res.* **6**, 129.
B104 Ball, M.C., Simmons, R.E. and Sutherland, I. (1987). *J. Mater. Sci.* **22**, 1975.
B105 Barret, P. and Bertrandie, D., in *7th ICCC*, Vol. 4, p. 443 (1981).
B106 Bailey, J.E. and Hampson, C.J. (1983). *Phil. Trans. R. Soc. London* **A310**, 105.
B107 Brown, P.W. (1987). *J. Am. Ceram. Soc.* **70**, 493.
B108 Barker, A.P. (1984). *World Cem.* **15**, 25.
B109 Bensted, J. and Varma, S.P. (1974). *Cem. Technol.* **5**, 440.
B110 Barnes, P., Ghose, A. and Mackay, A.L. (1980). *Cem. Concr. Res.* **10**, 639.

B111 Barnes, B.D., Diamond, S. and Dolch, W.L. (1978). *Cem. Concr. Res.* **8**, 263.
B112 Bezjak, A., Jelenić, I., Mlakar, V. and Panović, A., in *7th ICCC*, Vol. 2, p. II-111 (1980).
B113 Bonen, D. and Diamond, S. (1994). *J. Am. Ceram. Soc.* **77**, 1875.
B114 Barnes, J.R., Clague, A.D.H., Clayden, N.J., Dobson, C.M., Hayes, C.J., Groves, G.W. and Rodger, S.A. (1985). *J. Mater. Sci. Lett.* **4**, 1293.
B115 Bensted, J. (1983). *Cem. Concr. Res.* **13**, 493.
B116 Bensted, J., in *Characterization and Performance Prediction of Cement and Concrete*, p. 69, Engineering Foundation, New York (1983).
B117 Bentur, A. (1976). *J. Am. Ceram. Soc.* **59**, 210.
B118 Brown, P.W., Pommersheim, J.M. and Frohnsdorff, G. (1984). *Cem. Res. Prog.* [for] 1983, 245.
B119 Bezjak, A. and Jelenić, I. (1980). *Cem. Concr. Res.* **10**, 553.
B120 Banfill, P.F.G. and Saunders, D.C. (1981). *Cem. Concr. Res.* **11**, 363.
B121 Banfill, P.F.G in *Hydration and Setting of Cements* (eds A. Nonat and J.C. Mutin), p. 267, E & FN Spon, London (1992).
B122 Brunauer, S. (1962). *American Scientist* **50**, 210.
B123 Bentz, D.P. and Garboczi, E.J. (1991). *Cem. Concr. Res.* **21**, 325.
B124 Brown, P.W., Shi, D. and Skalny, J., in *Materials Science of Concrete II* (eds J.P. Skalny and S. Mindess), p. 83, American Ceramic Society,Westerville, OH, (1991).
B125 Beaudoin, J.J. (1986). *Cemento* **83**, 199.
B126 Barbič, L., Kocuvan, I., Blinc, R., Lahajnar, G., Marljak, P. and Zupančič, I. (1982). *J. Am. Ceram. Soc.* **65**, 25.
B127 Bager, D.H. and Sellevold, E.J. (1986). *Cem. Concr. Res.* **16**, 709, 835.
B128 Bal'shin, M.Y. (1949). *Dokl. Akad. Nauk SSSR* **67**, 831.
B129 Bozhenov, P.I., Kavalerova, V.I., Salnikova, V.S. and Suvorova, G.F., in *4th ISCC*, Vol. 1, p. 327 (1962).
B130 Beaudoin, J.J. and Feldman, R.F. (1985). *Cem. Concr. Res.* **15**, 105.
B131 Brückner, A., Lück, R., Wieker, W., Winkler, A., Andreae, C. and Mehner, H. (1992). *Cem. Concr. Res.* **22**, 1161.
B132 Barker, A.P. (1989). *Adv. Cem. Res.* **2**, 171.
B133 Brydson, R., Richardson, I.G., McComb, D.W. and Groves, G.W. (1993). *Solid State Comm.* **88**, 183.
B134 Brough, A.R., Dobson, C.M., Richardson, I.G. and Groves, G.W. (1995). *J. Mater. Sci.* **30**, 1671.
B135 Bland, C.H. and Sharp, J.H. (1990). *Adv. Cem. Res.* **3**, 91.
B136 Barker, A.P. and Cory, H.P. in *Blended Cements in Construction* (ed. R.N. Swamy), p. 107. Elsevier Applied Science, London (1991).
B137 Bombled, J.P., in *8th ICCC*, Vol. 4, p. 190 (1986).
B138 Beaudoin, J.J. (1979). *Cem. Concr. Res.* **9**, 771.
B139 Buttler, F.G. and Taylor, H.F.W. (1959). *J. Appl. Chem.* **9**, 616.
B140 Bushnell-Watson, S.M. and Sharp, J.H. (1986). *Cem. Concr. Res.* **16**, 875.
B141 Bushnell-Watson, S.M. and Sharp, J.H. (1990). *Cem. Concr. Res.* **20**, 623, 677.
B142 Bensted, J. (1982). *World Cem.* **13**, 85.
B143 Bertrandie, D. (1977). Doctorate thesis, University of Dijon, France.
B144 Baes, E.F. and Mesmer, R.E. *The Hydrolysis of Cations*, 489pp., Wiley, New York (1976).
B145 Bertrandie, D. and Barret, P., in *8th ICCC*, Vol. 3, p. 79 (1986).
B146 Banfill, P.F.G. and Gill, S.M., in *8th ICCC*, Vol. 6, p. 223 (1986).

B147 Bachiorrini, A. and Cussino, L. (1980). *Cemento* **77**, 183.
B148 Building Research Establishment, High alumina cement concrete in buildings (CP 34/75), in *Practical Studies from the Building Research Establishment*, Vol. 1, *Concrete*, p. 228, Construction Press, Lancaster (1978).
B149 Barret, P., Benes, C., Bertrandie, D. and Moisset, J., in *7th ICCC*, Vol. 3, p. V-175 (1980).
B150 Bachiorrini, A., Guilhot, B., Murat, M., Negro, A., Soustelle, M. and Fournier, A.A., in *8th ICCC*, Vol. 4, p. 376 (1986).
B151 Blenkinsop, R.D., Currell, B.R., Midgley, H.G. and Parsonage, J.R. (1985). *Cem. Concr. Res.* **15**, 276.
B152 Bentur, A. and Ish-Shalom, M. (1974). *Cem. Concr. Res.* **4**, 709.
B153 Bentur, A. and Ish-Shalom, M. (1975). *Cem. Concr. Res.* **5**, 597.
B154 Brooks, S.A. and Sharp, J.H., in *Calcium Aluminate Cements* (ed. R.J. Mangabhai), p. 335, E & FN Spon, London (1990).
B155 Bikbaou, M., in *7th ICCC*, Vol. 4, p. 371 (1981).
B156 Bikbaou, M.Y., in *8th ICCC*, Vol. 2, p. 352 (1986).
B157 Birchall, J.D. and Thomas, N.L. (1984). *Br. Ceram. Proc.* (35) 305.
B158 Bruere, G.M., in *Symposium on Structure of Portland Cement Paste and Concrete* (Sp. Rpt 90), p. 26, Highway Res. Board, Washington, DC (1966).
B159 Banfill, P.F.G. (1979). *Cem. Concr. Res.* **9**, 795.
B160 Bergstrom, S.G. (1953). *Mag. Concr. Res.* (14) 61.
B161 Buckner, D.A., Roy, D.M. and Roy, R. (1960). *Am. J. Sci.* **258**, 132.
B162 Bensted, J. (1987). *World Cem.* **18**, 72.
B163 Brunauer, S., Skalny, J., Odler, I. and Yudenfreund, M. (1973). *Cem. Concr. Res.* **3**, 279.
B164 Birchall, J.D. (1983). *Phil. Trans. R. Soc. Lond.* **A310**, 31.
B165 Barnes, B.D., Diamond, S. and Dolch, W.L. (1978). *Cem. Concr. Res.* **8**, 233.
B166 Barnes, B.D., Diamond, S. and Dolch, W.L. (1979). *J. Am. Ceram. Soc.* **62**, 21.
B167 Bonen, D. (1994). *J. Am. Ceram. Soc.* **77**,193.
B168 Buck, A.D. and Dolch, W.L. (1966). *J. Am. Concr. Inst.* **63**, 755.
B169 Bentur, A., Goldman, A. and Cohen, M.D. (1988). *Mater. Res. Soc. Symp. Proc.* **114**, 97.
B170 Bentz, D.P. and Stutzman, P.E. (1994). *Cem. Concr. Res.* **24**, 1044.
B171 Bentz, D.P., Stutzman, P.E. and Garboczi, E.J. (1991). *Cem. Concr. Res.* **22**, 891.
B172 Bentur, A., Diamond, S. and Cohen, M.D. (1985). *J. Mater. Sci.* **20**, 3610.
B173 Browne, R. (1986). *Chem. Ind.* 837.
B174 Bennett, I.C. and Vivian, H.E. (1955). *Austral. J. Appl. Sci.* **6**, 88.
B175 Bhatty, M.S.Y. (1985). *Cem. Concr. Aggr.* **7**, 69.
B176 Buck, A.D. and Mather, K., in *Effects of Alkalies on Cement and Concrete* (ed. S. Diamond), p. 73, (Publ. CE-MAT-1-78), Purdue University, W. Lafayette, IN (1978).
B177 Bonen, D. and Cohen, M.D. (1992). *Cem. Concr. Res.* **22**, 169.
B178 Bonen, D. and Cohen, M.D. (1992). *Cem. Concr. Res.* **22**, 707.
B179 Bonen, D. (1992). *J. Am. Ceram. Soc.* **75**, 2904.
B180 Bonen, D. (1993). *Cem. Concr. Res.* **23**, 541.
B181 Blair, L.R. and Yang, J.C.-S., in *4th ISCC*, Vol. 2, p. 849 (1962).

B182 Baronio, G. and Berra, M. (1986). *Cemento* **83**, 169.
B183 Bournazel, J.-P. and Moranville-Regourd, M. (1995). *Mater. Res. Soc. Symp. Proc.* **370**, 57.
B184 Bager, D.H. and Sellevold, E.J. (1987). *Cem. Concr. Res.* **17**, 1.
B185 Buenfeld, N.R. and Newman, J.B. (1986). *Cem. Concr. Res.* **16**, 721.
B186 Bentur, A., Ben-Bassat, M. and Schneider, D. (1985). *J. Am. Ceram. Soc.* **68**, 203.

C1 Chan, C.J., Kriven, W.M. and Young, J.F. (1988). *J. Am. Ceram. Soc.* **71**, 713.
C2 Colville, A.A. and Geller, S. (1972). *Acta Cryst.* **B28**, 3196.
C3 Colville, A.A. and Geller, S. (1971). *Acta Cryst.* **B27**, 2311.
C4 Colville, A.A. (1970). *Acta Cryst.* **B26**, 1469.
C5 Chatterjee, A.K. and Zhmoidin, G.I. (1972). *J. Mater. Sci.* **7**, 93.
C6 Conjeaud, M. (1975). Unpublished data quoted in G15 and M31.
C7 Chatterjee, A.K. and Zhmoidin, G.I. (1972). *Inorg. Mater.* **8**, 769 (translated from *Neorg. Mater.* **8**, 886).
C8 Castanet, R. and Sorrentino, F.P., in *8th ISCC*, Vol. 2, p. 36 (1986).
C9 Chromý, S., in *6th ICCC*, Vol. 3, p. 268 (1976).
C10 Cottin, B., Rouanet, A and Conjeaud, M., in *8th ICCC*, Vol. 2, p. 31 (1986).
C11 Chromý, S. (1982). *Zem.-Kalk-Gips* **35**, 204 (partial English translation, p. 145).
C12 Chromý, S. and Weber, M. (1981). *Zem.-Kalk-Gips* **34**, 453 (partial English translation, p. 244).
C13 Christensen, N.H. (1979). *Cem. Concr. Res.* **9**, 219.
C14 Christensen, N.H. (1979). *Cem. Concr. Res.* **9**, 285.
C15 Chromý, S. (1982). *Zem.-Kalk-Gips* **35**, 555 (partial English translation, p. 303).
C16 Chromý, S. and Hrabě, Z. (1982). *Zem.-Kalk-Gips* **35**, 368 (partial English translation, p. 221).
C17 Centurione, S.L., in *13th IC Cem. Microsc.*, p. 120 (1991).
C18 Campbell, D.H. *Microscopical Examination and Interpretation of Portland Cement and Clinker*, 128pp., Construction Technology Laboratories, Skokie, IL (1986).
C19 Conjeaud, M. and Boyer, H. (1980). *Cem. Concr. Res.* **10**, 61.
C20 Commission chimique du CETIC (1978). *Ciments, Bétons, Plâtres, Chaux* (713) 205.
C21 Copeland, L.E. and Hayes, J.C. (1953). *ASTM Bull.* **194**, 70.
C22 Copeland, L.E. and Schultz, E.G. (1962). *J. PCA Res. Dev. Labs.* **4** (1) 2.
C23 Chatterji, S. and Jeffery, J.W. (1966). *Nature* **209**, 1233.
C24 Copeland, L.E., Bodor, E., Chang, T.N. and Weise, C.H. (1967). *J. PCA Res. Dev. Labs.* **9** (1) 61.
C25 Cong, X. and Kirkpatrick, R.J. (1996). *Adv. Cem. Based Mater.* **3**, 133.
C26 Carpenter, A.B., Chalmers, R.A., Gard, J.A., Speakman, K. and Taylor, H.F.W. (1966). *Am. Mineral.* **51**, 56.
C27 Cong, X. and Kirkpatrick, R.J. (1996). *Adv. Cem. Based Mater.* **3**, 144.
C28 Currell, B.R., Midgley, H.G., Montecinos, M. and Parsonage, J.R. (1985). *Cem. Concr. Res.* **15**, 889.
C29 Clayden, N.J., Dobson, C.M., Hayes, C.J. and Rodger, S.A. (1984). *J.Chem. Soc. Chem. Comm.* 1396.
C30 Cong, X. and Kirkpatrick, R.J. (1993). *Cem. Concr. Res.* **23**, 1065.

C31 Cong, X. and Kirkpatrick, R.J. (1995). *Cem. Concr. Res.* **25**, 1237.
C32 Cong, X. and Kirkpatrick, R.J. (1995). *Adv. Cem. Res.* **7**, 103.
C33 Cong, X. and Kirkpatrick, R.J. (1996). *J. Am. Ceram. Soc.* **79**, 1585.
C34 Carlson, E.T. and Berman, H.A. (1960). *J. Res. Nat. Bur. Stand.* **64A**, 333.
C35 Courtois, A., Dusausoy, Y., Laffaille, A. and Protas, J. (1968). *Comptes rendus Acad. Sci. Paris*, **D266**, 1911.
C36 Crammond, N.J. (1985). *Cem. Concr. Res.* **15**, 431.
C37 Cohen-Addad, C. (1971). *Acta Cryst.* **A27**, 68.
C38 Crammond, N.J. (1985). *Cem. Concr. Res.* **15**, 1039.
C39 Collepardi, M., Baldini, G., Pauri, M. and Corradi, M. (1978). *Cem. Concr. Res.* **8**, 571.
C40 Christensen, A.N., Fjellvåg, H. and Lehmann, M.S. (1986). *Acta Chem. Scand.* **A40**, 126.
C41 Corstanje, W.A., Stein, H.N. and Stevels, J.M. (1973). *Cem. Concr. Res.* **3**, 791.
C42 Chatterji, S. and Jeffery, J.W. (1962). *J. Am. Ceram. Soc.* **45**, 536.
C43 Carlson, E.T. (1964). *J. Res. Nat. Bur. Stand.* **68A**, 453.
C44 Collepardi, M., Monosi, S., Moriconi, G. and Corradi, M. (1979). *Cem. Concr. Res.* **9**, 431.
C45 Copeland, L.E., Kantro, D.L. and Verbeck, G., in *4th ISCC*, Vol. 1, p. 429 (1960).
C46 Copeland, L.E. and Kantro, D.L., in *5th ISCC*, Vol. 2, p. 387 (1969).
C47 Christensen, B.J., Coverdale, R.T., Olson, R.A., Ford, S.J., Garboczi, E.J., Jennings, H.M. and Mason, T.O. (1994). *J. Am. Ceram. Soc.*, **77**, 2789.
C48 Collepardi, M, Marcialis, A. and Turriziani, R. (1972). *J. Am. Ceram. Soc.* **55**, 534.
C49 Chopra, S.K. and Taneja, C.A., in *5th ISCC*, Vol. 4, p. 228 (1969).
C50 Cesareni, C. and Frigione, G., in *5th ISCC*, Vol. 4, p. 237 (1969).
C51 Coole, M.J. (1984). *Br. Ceram. Proc.* (35) 385.
C52 Costa, U. and Massazza, F., in *Effects of Flyash Incorporation in Cement and Concrete* (ed. S. Diamond), p. 134, Materials Research Society, University Park, PA (1981).
C53 Cook, D.J. and Suwanvitaya, P., in *Fly Ash, Silica Fume, Slag and Other Mineral By-Products in Concrete* (ed. V.M. Malhotra), Sp. Publ. SP79, Vol. 2, p. 831, American Concrete Institute, Detroit, MI (1983).
C54 Calleja, J., in *7th ICCC*, Vol. 3, p. V-102 (1980).
C55 Cottin, B. and George, C.M., in *International Seminary on Calcium Aluminates* (ed. M. Murat *et al.*), Politecnico di Torino, Turin (1982).
C56 Capmas, A. and Ménétrier-Sorrentino, D., in *UNITECR'89* (Proc. Conf. Global Advances in Refractories, ed. L.J. Trostel), Vol. 2, p. 1157, American Ceramic Society, Westerville, OH (1989).
C57 Cong, X. and Kirkpatrick, R.J. (1993). *J. Am. Ceram. Soc.* **76**, 409.
C58 Cottin, B. (1971). *Cem. Concr. Res.* **1**, 177.
C59 Capmas, A., Ménétrier-Sorrentino, D. and Damidot, D., in *Calcium Aluminate Cements* (ed. R.J. Mangabhai), p. 65, E & FN Spon, London (1990).
C60 Chappuis, J., Bayoux, J.P. and Capmas, A., in *UNITECR'89* (Proc. Conf. Global Advances in Refractories, ed. L.J. Trostel), Vol. 2, p. 1157, American Ceramic Society, Westerville, OH (1989).
C61 Capmas, A. and George, C.M., in *Advances in Cement and Concrete* (eds M.W. Grutzeck and S.L. Sarkar), p. 377, American Society of Civil Engineers, New York (1994).

C62 Currell, B.R., Grzeskowiak, R., Midgley, H.G. and Parsonage, J.R. (1987). *Cem. Concr. Res.* **17**, 420.
C63 Cussino, L. and Negro, A., in *7th ICCC*, Vol. 3, p. V-62 (1980).
C64 Crammond, N.J., in *Calcium Aluminate Cements* (ed. R.J. Mangabhai), p. 208, E & FN Spon, London (1990).
C65 Christensen, N.H. and Johansen, V., in *Cement Production and Use*, p. 55, Engineering Foundation, New York (1979).
C66 Chatterji, A.K. (1996). *Cem. Concr. Res.* **26**, 1213, 1227.
C67 Chiocchio, G., Mangialardi, T. and Paolini, A.E. (1986). *Cemento* **83**, 69.
C68 Costa, U., Massazza, F. and Barrilà, A. (1982). *Cemento* **79**, 323.
C69 Costa, U. and Massazza, F. (1984). *Cemento* **81**, 127.
C70 Collepardi, M., Rossi, G. and Spiga, M.C. (1971). *Ann. Chim. (Rome)* **61**, 137.
C71 Clayden, N.J., Dobson, C.M., Groves, G.W. and Rodger, S.A., in *8th ICCC*, Vol. 3, p. 51 (1986).
C72 Collepardi, M., Massidda, L. and Usai, G. (1971). *Cemento* **68**, 3.
C73 Cole, W.F. and Moorehead, D.R., in *Autoclaved Calcium Silicate Building Products*, p. 134, Society of Chemical Industry, London (1967).
C74 Carles-Gibergues, A., Grandet, J. and Ollivier, J.P., in *Liaisons Pâtes de Ciment Matériaux Associés* [Proc. RILEM Colloq.], p.D8, Laboratoire de Génie Civil, Toulouse (1982).
C75 Crumbie, A.K., Scrivener, K.L. and Pratt, P.L. (1989). *Mater. Res. Soc. Symp. Proc.* **137**, 279.
C76 Cole, W.F. and Lancucki, C.J. (1983). *Cem. Concr. Res.* **13**, 611.
C77 Cole, W.F., Lancucki, C.J. and Sandy, M.J. (1981). *Cem. Concr. Res.* **11**, 443.
C78 Cabrera, J.G. and Plowman, C. (1988). *Adv. Cem. Res.* **1**, 171.
C79 Cole, W.F. (1953). *Nature* **171**, 354.
C80 Crammond, N.J. (1984). *Cem. Concr. Res.* **14**, 225.
C81 Crammond, N.J. and Nixon, P.J. in *6th Int. Conf. Durability of Building Materials and Components* (eds S. Nagataki, T. Nireki and F. Tomosawa), Vol. 1, p. 295, E & FN Spon, London (1993).
C82 Collins, A.R. (1944). *J. Instn. Civ. Engrs* **23**, 29.
C83 Cowie, J. and Glasser, F.P. (1991/2). *Adv. Cem. Res.* **4**, 119.

D1 Daimon, M., Hirano, Y., Tsurumi, T. and Asaga, K., in *9th ICCC*, Vol. 2, p. 17 (1992).
D2 Day, A.L., Shepherd, E.S. and Wright, F.E. (1906). *Am. J. Sci.* (4th series) **22**, 266.
D3 Dahl, L.A., quoted by R.H. Bogue in *2nd SCC*, p. 138 (1939).
D4 Duda, W.H. *Cement-Data-Book*, Vol. 1: *International Process Engineering in the Cement Industry* (3rd Edn), 636pp., Bauverlag, Wiesbaden and Berlin (1985).
D5 Davis, P., Stringer, J.A. and Watson, D., in *Making the Most of Materials – Cement*, Chapter 7, Science Research Council, Swindon (1979).
D6 Davis, P. and Longman, P.A., in *International Cement Seminar* (Proc., 19th), p. 25, Rock Products, Chicago, IL (1984).
D7 De Keyser, W.L. (1951). *Bull. Soc. Chim. belg.* **60**, 516
D8 De Keyser, W.L. (1954). *Bull. Soc. Chim. belg.* **63**, 40.
D9 De Keyser, W.L. (1955). *Bull. Soc. Chim. belg.* **64**, 395.
D10 Dreizler, I.E., Strunge, J. and Knöfel, D.F.E. in *7th IC Cem. Microsc.*, p. 100 (1985).

D11 Diamond, S. and Bonen, D. (1992). *Mater. Res. Soc. Symp. Proc.* **245**, 291.
D12 Danilov, V.V., in *6th ICCC*, Vol. 2, Part 1, p. 73 (1976).
D13 De Keyser, W.L. and Tenoutasse, N., in *5th ISCC*, Vol. 2, p. 379 (1969).
D14 Day, R.L. (1981). *Cem. Concr. Res.* **11**, 341.
D15 Dalziell, J.A. and Gutteridge, W.A. (1986). *The Influence of Pulverized-Fuel Ash upon the Hydration Characteristics and Certain Physical Properties of a Portland Cement Paste* (Techn. Rpt. 560), 28pp., Cement and Concrete Association, Slough (1986).
D16 Diamond, S., in *Hydraulic Cement Pastes: Their Structure and Properties*, p. 2, Cement and Concrete Association, Slough (1976).
D17 Double, D.D., Hellawell, A. and Perry, S.J. (1978). *Proc. R. Soc. London* **A359**, 435.
D18 Dalgleish, B.J. and Ibe, K. (1981). *Cem. Concr. Res.* **11**, 729.
D19 Davis, R.W. and Young, J.F. (1975). *J. Am. Ceram. Soc.* **58**, 67.
D20 Dent Glasser, L.S., Lachowski, E.E., Qureshi, M.Y., Calhoun, H.P., Embree, D.J., Jamieson, W.D. and Masson, C.R. (1981). *Cem. Concr. Res.* **11**, 775.
D21 Damidot, D., Nonat, A., Barret, P., Bertrandie, D., Zanni, H. and Rassem, R. (1995). *Adv. Cem. Res.* **7**, 1.
D22 Damidot, D., Nonat, A. and Barret, P. (1990). *J. Am. Ceram. Soc.* **73**, 3319.
D23 Damidot, D. and Nonat, A. (1994). *Adv. Cem. Res.* **6**, 27.
D24 Damidot, D. and Nonat, A. (1994). *Adv. Cem. Res.* **6**, 83.
D25 Double, D.D. (1983). *Phil. Trans. R. Soc. London* **A310**, 53.
D26 Dosch, W. (1967). *Neues Jahrb. Mineral. Abhandl.* **106**, 200.
D27 Dosch, W. and Keller, H., in *6th ICCC*, Vol. 3, p. 141 (1976).
D28 Dosch, W., Keller, H. and zur Strassen, H., in *5th ISCC*, Vol. 2, p. 72 (1969).
D29 Dosch, W. and zur Strassen, H. (1967). *Zem.-Kalk-Gips* **20**, 392.
D30 D'Ans, J. and Eick, H. (1953). *Zem.-Kalk-Gips* **6**, 197, 302.
D31 Dron, R., in *6th ICCC*, Vol. 2, Part 1, p. 208 (1976).
D32 Damidot, D. and Glasser, F.P. (1992). *Cem. Concr. Res.* **22**, 1179.
D33 Damidot, D. and Glasser, F.P. (1993). *Cem. Concr. Res.* **23**, 221
D34 Damidot, D. and Glasser, F.P. (1993). *Cem. Concr. Res.* **23**, 1195.
D35 Damidot, D. and Glasser, F.P. (1995). *Cem. Concr. Res.* **25**, 22.
D36 Damidot, D., Stronach, S., Kindness, A., Atkins, M. and Glasser, F.P. (1994). *Cem. Concr. Res.* **24**, 563.
D37 Damidot, D. and Glasser, F.P. (1995). *Adv. Cem. Res.* **7**, 129.
D38 Damidot, D., Birnin-Yauri, U.A. and Glasser, F.P. (1994). *Cemento*, **91**, 261.
D39 Diamond, S. and Bonen, D. (1993). *J. Am. Ceram. Soc.* **76**, 2993.
D40 Dalgleish, B.J., Ghose, A., Jennings, H.M. and Pratt, P.L., in *International Conference on Concrete of Early Ages* [Proc. RILEM Colloq.], Vol. 1, p. 137, Editions Anciens ANPC, Paris (1982).
D41 Dalgleish, B.J., Pratt, P.L. and Toulson, E. (1983). *J. Mater. Sci.* **17**, 2199.
D42 Diamond, S., Ravina, D. and Lovell, J. (1980). *Cem. Concr. Res.* **10**, 297.
D43 Diamond, S. (1981). *Cem. Concr. Res.* **11**, 383.
D44 Duchesne, J. and Bérubé, M.A. (1994). *Cem. Concr. Res.* **24**, 456.
D45 Daimon, M., Abo-El-Enein, S.A., Hosaka, G., Goto, S. and Kondo, R. (1977). *J. Am. Ceram. Soc.* **60**, 110.
D46 Diamond, S. and Dolch, W.L. (1972). *J. Coll. Interface Sci.* **38**, 234.

D47 Day, R.L. and Marsh, B.K. (1988). *Cem. Concr. Res.* **18**, 63.
D48 Dullien, F.A.L. *Porous Media–Fluid Transport and Pore Structure*, 396pp., Academic Press, New York (1979).
D49 Demoulian, E., Gourdin, P., Hawthorn, F. and Vernet, C., in *7th ICCC*, Vol. 2, p. III-89 (1980).
D50 Dron, R. and Brivot, F., in *7th ICCC*, Vol. 2, p. III-134 (1980).
D51 Daimon, M., in *7th ICCC* Vol. 1, p. III-2/1 (1980).
D52 Demoulian, E., Vernet, C., Hawthorn, F. and Gourdin, P., in *7th ICCC*, Vol. 2, p. III-151 (1980).
D53 Diamond, S. and Lopez-Flores, F., in *Effects of Flyash Incorporation in Cement and Concrete* (ed. S. Diamond), p. 112, Materials Research Society, University Park, PA (1981).
D54 Diamond, S. (1997). *Cem. Concr. Composites*, in press, Elsevier Applied Science.
D55 Dobson, C.M., Goberdhan, D.G.C., Ramsay, J.D.F. and Rodger, S.A. (1988). *J. Mater. Sci.* **23**, 4108.
D56 Diamond, S. (1983). *Cem. Concr. Res.* **13**, 459.
D57 Diamond, S. and Olek, J. (1987). *Mater. Res. Soc. Symp. Proc.* **86**, 315.
D58 Diamond, S., in *Effects of Flyash Incorporation in Cement and Concrete* (ed. S. Diamond), p. 12, Materials Research Society, University Park, PA (1981).
D59 Dent Glasser, L.S. and Lee, C. K. (1981). *Acta Cryst.* **B37**, 803.
D60 Daimon, M. and Roy, D.M. (1978). *Cem. Concr. Res.* **8**, 753.
D61 Daimon, M. and Roy, D.M. (1979). *Cem. Concr. Res.* **9**, 103.
D62 Deutscher Ausschuss für Stahlbeton [German Association for Reinforced Concrete] *Richtlinie zur Wärmebehandlung von Beton* [Guidelines for the heat treatment of concrete], 6pp., Beuth Verlag GmbH, Berlin (1989).
D63 Diamond, S., Mindess, S. and Lovell, J., in *Liaisons Pâtes de Ciment Matériaux Associés* (Proc. RILEM Colloq.), p.C42, Laboratoire de Génie Civil, Toulouse (1982).
D64 Diamond, S., in *8th ICCC*, Vol. 1, p. 122 (1986).
D65 Detwiler, R.J., Monteiro, P.J.M., Wenk, H.-R. and Zhong, Z. (1988). *Cem. Concr. Res.* **18**, 823.
D66 Dunster, A.M. (1989). *Adv. Cem. Res.* **2**, 99.
D67 Diamond, S. (1976). *Cem. Concr. Res.* **6**, 549.
D68 Diamond, S., Barneyback, R.S. and Struble, L.J., in *Alkali–Aggregate Reaction in Concrete*, Paper S252/22, CSIR, Pretoria (1981).
D69 Dent Glasser, L.S. and Kataoka, N., in *Alkali–Aggregate Reaction in Concrete*, Paper S252/23, CSIR, Pretoria (1981).
D70 Dent Glasser, L.S. and Kataoka, N. (1982). *Cem. Concr. Res.* **12**, 321.
D71 Davies, G and Oberholster, R.E., in *8th ICCC*, Vol. 5, p. 249 (1986).
D72 Dent Glasser, L.S. and Kataoka, N. (1981). *Cem. Concr. Res.* **11**, 191.
D73 Dent Glasser, L.S. and Kataoka, N. (1981). *Cem. Concr. Res.* **11**, 1.
D74 Diamond, S. and Ong, S., in *Cement Technology* (Ceramic Trans., Vol. 40, eds E.M. Gartner and H. Uchikawa), p. 79, American Ceramic Society, Westerville, OH (1994).
D75 Diamond, S. (1996). *Cem. Concr. Composites*, **18**, 205.

E1 Eysel, W. (1973). *Am. Mineral.* **58**, 736.
E2 Edge, R. and Taylor, H.F.W. (1971). *Acta Cryst.* **B27**, 594.
E3 Effenberger, H., Kirfel, A., Will, G. and Zobetz, E. (1983). *Neues Jahrb. Mineral. Monatsh.* 60.

E4 Eden, N.B. and Bailey, J.E., in *8th ICCC*, Vol. 4, p. 163 (1986).
E5 Edmonds, R.N. and Majumdar, A.J. (1988). *Cem. Concr. Res.* **18**, 311.
E6 Edmonds, R.N. and Majumdar, A.J. (1988). *Cem. Concr. Res.* **18**, 473.
E7 Edmonds, R.N. and Majumdar, A.J. (1989). *Cem. Concr. Res.* **19**, 289.
E8 Ernsberger, F.M. and France, W.G. (1945). *Indust. Engng Chem.* **37**, 598.
E9 Edwards, G.G. and Angstadt, R.L. (1966). *J. Appl. Chem.* **16**, 166.
E10 El-Hemaly, S.A.S., Mitsuda, T. and Taylor, H.F.W. (1977). *Cem. Concr. Res.* **7**, 429.

F1 Fukuda, K. and Maki, I. (1989). *J. Am. Ceram. Soc.* **72**, 2204.
F2 Fukuda, K. and Maki, I. (1989). *Cem. Concr. Res.* **19**, 913.
F3 Fukuda, K. and Maki, I. (1993). *Cem. Concr. Res.* **23**, 599.
F4 Fukuda, K., Maki, I., Ito, S., Yoshida, H. and Kato, C. (1994). *J. Am. Ceram. Soc.* **77**, 3027.
F5 Fletcher, K.E., Midgley, H.G. and Moore, A.E. (1965). *Mag. Concr. Res.* **17**, 171.
F6 Feng, Q.L., Glasser, F.P., Howie, R.A. and Lachowski, E. (1988). *Acta Cryst.* **C44**, 589.
F7 Fundal, E., in *8th ICCC*, Vol. 2, p. 139 (1986).
F8 Flörke, H. (1952). *Neues Jahrb. Mineral. Abhandl.* **84**, 189.
F9 Feng, X., Liao, G. and Long, S. (1991). *Cemento* **88**, 29.
F10 Fayos, J., Glasser, F.P., Howie, R.A., Lachowski, E.E. and Pérez-Mendez, M. (1985). *Acta Cryst.* **C41**, 814.
F11 Fundal, E. (1979). *World Cem. Technol.* **10**, 195.
F12 Franke, B. (1941). *Zeit. anorg. allg. Chem.* **247**, 180.
F13 Fierens, P. and Verhaegen, J.-P. (1972). *J. Am. Ceram. Soc.* **55**, 309.
F14 Fierens, P., Tirlocq, J. and Verhaegen, J.P. (1973). *Cem. Concr. Res.* **3**, 549.
F15 Fujii, K. and Kondo, W. (1979). *J. Am. Ceram. Soc.* **62**, 161.
F16 Feldman, R.F. and Ramachandran, V.S. (1971). *Cem. Concr. Res.* **1**, 607.
F17 Feldman, R.F., in *5th ISCC*, Vol. 3, p. 53 (1969).
F18 Feldman, R.F. and Ramachandran, V.S. (1974). *Cem. Concr. Res.* **4**, 155.
F19 Feldman, R.F. (1972). *Cem. Concr. Res.* **2**, 123.
F20 Fujii, K. and Kondo, W., in *5th ISCC*, Vol. 2, p. 362 (1969).
F21 Farmer, V.C., Jeevaratnam, J., Speakman, K. and Taylor, H.F.W., in *Symposium on Structure of Portland Cement Paste and Concrete* (Sp. Rpt 90), p. 291, Highway Research Board, Washington, DC (1966).
F22 Fujii, K. and Kondo, W. (1983). *J. Am. Ceram. Soc.* **66**, C220.
F23 Fujii, K. and Kondo, W. (1981). *J. Chem. Soc. Dalton Trans.* 645.
F24 Fierens, P. and Verhaegen, J.P. (1976). *Cem. Concr. Res.* **6**, 337.
F25 Funk, H., in *4th ISCC*, Vol. 1, p. 291 (1962).
F26 Fierens, P. and Tirlocq, J. (1983). *Cem. Concr. Res.* **13**, 41.
F27 Fierens, P. and Tirlocq, J. (1983). *Cem. Concr. Res.* **13**, 267.
F28 Feitknecht, W. and Buser, H.W. (1951). *Helv. Chim. Acta* **34**, 128.
F29 Fischer, R. and Kuzel, H.-J. (1982). *Cem. Concr. Res.* **12**, 517.
F30 Fischer, R., Kuzel, H.-J. and Schellhorn, H. (1980). *Neues Jahrb. Mineral. Monatsh.* 322.
F31 Foreman, D.W. (1968). *J. Chem. Phys.* **48**, 3037.
F32 Feldman, R.F. and Ramachandran, V.S. (1966). *Mag. Concr. Res.* **18**, 185.
F33 Fukuhara, M., Goto, S., Asaga, K., Daimon, M. and Kondo, R. (1981). *Cem. Concr. Res.* **11**, 407.

F34 Fortune, J.M. and Coey, J.M.D. (1983). *Cem. Concr. Res.* **13**, 696.
F35 Feldman, R.F. and Sereda, P.J., in *5th ISCC*, Vol. 3, p. 36 (1969).
F36 Feldman, R.F. and Sereda, P.J. (1970). *Engng J.* **53**, 53.
F37 Feldman, R.F. (1972). *Cem. Technol.* **3**, 5.
F38 Feldman, R.F., in *Effects of Fly Ash Incorporation in Cement and Concrete* (ed. S. Diamond), p. 124, Materials Research Society, University Park, PA (1981).
F39 Feldman, R.F. and Beaudoin, J.J. (1991). *Cem. Concr. Res.* **21**, 297.
F40 Feldman, R.F. and Beaudoin, J.J. (1976). *Cem. Concr. Res.* **6**, 389.
F41 Feldman, R.F. (1972). *Cem. Concr. Res.* **2**, 521.
F42 Feldman, R.F., in *8th ICCC*, Vol. 1, p. 336 (1986).
F43 Fierens, P. and Poswick, P., in *7th ICCC*, Vol. 2, p. III-112 (1980).
F44 Feng, Q.L., Lachowski, E.E. and Glasser, F.P. (1989). *Mater. Res. Soc. Symp. Proc.* **136**, 263.
F45 Feldman, R.F. (1984). *J. Am. Ceram. Soc.* **67**, 30.
F46 Feldman, R.F. and Huang Cheng-yi (1985). *Cem. Concr. Res.* **15**, 765.
F47 Fujii, K., Kondo, W. and Ueno, H. (1986). *J. Am. Ceram. Soc.* **69**, 361.
F48 Farran, J. (1956). *Rev. Matér. Constr.* (490-491) 155; (492) 191.
F49 Fentiman, C.H. (1985). *Cem. Concr. Res.* **15**, 622.
F50 Feldman, R.F. and Beaudoin, J.J. (1977). *Cem. Concr. Res.* **7**, 19.
F51 Feldman, R.F. and Beaudoin, J.J. (1984). *Cem. Concr. Res.* **14**, 785.
F52 Farran, J., Javelas, R., Maso, J.-C. and Perrin, B. (1972). *Comptes rendus Acad. Sci. Paris* **D275**, 1467.
F53 Fu, Y., Xie, P., Gu, P. and Beaudoin, J.J. (1994). *Cem. Concr. Res.* **24**, 1015.
F54 Fu, Y., Xie, P., Gu, P. and Beaudoin, J.J. (1994). *Cem. Concr. Res.* **24**, 1428.
F55 Fattuhi, N.I. and Hughes, B.P. (1988). *Cem. Concr. Res.* **18**, 545.
F56 French, W.J. and Poole, A.B. (1974). *Cem. Concr. Res.* **4**, 925.

G1 Guinier, A. and Regourd, M., in *5th ISCC*, Vol. 1, p. 1 (1969).
G2 Golovastikov, N.I.., Matveeva, R.G. and Belov, N.V. (1975). *Sov. Phys. Cryst.* **20**, 441 (translated from *Kristallografiya* **20**, 721).
G3 Ghose, A. and Barnes, P. (1979). *Cem. Concr. Res.* **9**, 747.
G4 Ghose, A. (1980). PhD thesis, University of London.
G5 Gollop, R.S. and Taylor, H.F.W. (1994). *Cem. Concr. Res.* **24**, 1347.
G6 Gartner, E.M. and Tang, F.J. (1987). *Cemento* **84**, 141.
G7 Gross, S. (1977). *Bull. Geol. Surv. Israel* (70) 1.
G8 Gazzozi, G. and Chiari, G. (1986). *Acta Cryst.* **B42**, 146.
G9 Groves, G.W. (1982). *Cem. Concr. Res.* **12**, 619.
G10 Grant, R.W., Geller, S., Wiedersich, H., Gonser, U. and Fullmer, L.D. (1968). *J. Appl. Phys.* **39**, 1122.
G11 Geller, S., Grant, R.W. and Gonser, U. (1971). *Prog. Solid State Chem.* **5**, 1.
G12 Gutt, W., in *Manufacture of Portland Cement from Phosphate Raw Materials* (Building Research Station Paper CP90/68), p. 5, HMSO, London (1968).
G13 Goodwin, D.W. and Lindop, A.J. (1970). *Acta Cryst.* **B26**, 1230.
G14 Gutt, W. (1961). *Nature* **190**, 339.
G15 Glasser, F.P. and Marr, J. (1975). *Trans. J. Br. Ceram. Soc.* **74**, 113.
G16 Gutt, W. and Smith, M.A. (1967). *Trans. Br. Ceram. Soc.* **66**, 557.
G17 Glasser, F.P. and Marr, J. (1980). *Cem. Concr. Res.* **10**, 753.
G18 Gutt, W. and Smith, M.A. (1968). *Trans. Br. Ceram. Soc.* **67**, 487.

G19 Gutt, W. and Osborne, G.J. (1967). *Trans. Br. Ceram. Soc.* **65**, 521.
G20 Gutt, W. and Osborne, G.J. (1968). *Trans. Br. Ceram. Soc.* **67**, 125.
G21 Gilioli, C., Massazza, F. and Pezzuoli, H. (1979). *Cem. Concr. Res.* **9**, 295.
G22 Gutt, W. and Osborne, G.J. (1970). *Trans. Br. Ceram. Soc.* **69**, 125.
G23 Gutt, W., in *5th ISCC*, Vol. 1, p. 93 (1969).
G24 Gutt, W., Chatterjee, A.K. and Zhmoidin, G.I. (1970). *J. Mater. Sci.* **5**, 960.
G25 Ghosh, S.N. (ed.) *Advances in Cement Technology*, 804pp., Pergamon, Oxford (1983).
G26 Goldshtein, L.Y.A. *Cement Production from Industrial By-Products (Wastes) Utilization*, 80pp., Stroyizdat, Leningrad (1985).
G27 Glasser, F.P., in *Structures and Properties of Cements* (ed. P. Barnes), p. 69, Applied Science Publishers, London (1983).
G28 Glasser, F.P., in *8th ICCC*, Vol. 6, p. 15 (1986).
G29 Gartner, E.M., in *Research on the Manufacture and Use of Cements* (ed. G. Frohnsdorff), p. 1, Engineering Foundation, New York (1986).
G30 Gilioli, C., Massazza, F. and Pezzuoli, M. (1972). *Cemento* **69**, 19.
G31 Gilioli, C., Massazza, F. and Pezzuoli, M. (1973). *Cemento* **70**, 137.
G32 Gutt, W. (1963). *Nature* **197**, 142.
G33 Gutteridge, W.A. (1984). *Br. Ceram. Proc.* (35) 11.
G34 Gille, F., Dreizler, I., Grade, K., Krämer, H. and Woermann, E. *Mikroskopie des Zementklinkers – Bilderatlas*, 75pp., with English translation of text, 20pp., Beton-Verlag GmbH, Düsseldorf (1965).
G35 Goldstein, J.I., Newbury, D.E., Echlin, P., Joy, D.C., Fiori, C. and Lifshin, E. *Scanning Electron Microscopy and X-ray Microanalysis*, 673pp., Plenum Press, New York (1981).
G36 Gutteridge, W.A. (1979). *Cem. Concr. Res.* **9**, 319.
G37 Gutteridge, W.A. (1986). Private communication.
G38 Gartner, E. and Myers, D. (1993). *J. Am. Ceram. Soc.* **76**, 1521.
G39 Groves, G.W., Le Sueur, P.J. and Sinclair, W. (1986). *J. Am. Ceram. Soc.* **69**, 353.
G40 Groves, G.W. (1987). *Mater. Res. Soc. Symp. Proc.* **85**, 3.
G41 Grudemo, Å. (1984). *Cem. Concr. Res.* **14**, 123.
G42 Greenberg, S.A. and Copeland, L.E. (1960). *J. Phys. Chem.* **64**, 1057.
G43 Grudemo, Å., in *4th ISCC*, Vol. 2, p. 615 (1962).
G44 Goto, S., Daimon, M., Hosaka, G. and Kondo, R. (1976). *J. Am. Ceram. Soc.* **59**, 281.
G45 Groves, G.W. (1981). *J. Mater. Sci.* **16**, 1063.
G46 Groves, G.W. (1983). *Phil. Trans. R. Soc. London* **A310**, 79.
G47 Gard, J.A., Mohan, K., Taylor, H.F.W. and Cliff, G. (1981). *J. Am. Ceram. Soc.* **63**, 336.
G48 Groves, G.W. (1990). *Cem. Concr. Res.*, **20**, 315.
G49 Gard, J.A., Taylor, H.F.W., Cliff, G. and Lorimer, G.W. (1977). *Am. Mineral.* **62**, 365.
G50 Gard, J.A. and Taylor, H.F.W. (1976). *Cem. Concr. Res.* **6**, 667.
G51 Grutzeck, M., Benesi, A. and Fanning, B. (1989). *J. Am. Ceram. Soc.* **72**, 665.
G52 Gartner, E.M. and Jennings, H.M. (1987). *J. Am. Ceram. Soc.* **70**, 743.
G53 Gartner, E.M. and Gaidis, J.M., in *Materials Science of Concrete I* (ed. J.P. Skalny), p. 95, American Ceramic Society, Westerville, OH (1989).
G54 Glasser, F.P., Lachowski, E.E. and Macphee, D.E. (1987). *J. Am. Ceram. Soc.* **70**, 481.

G55 Grutzeck, M.W. and Ramachandran, A.R. (1987). *Cem. Concr. Res.* **17**, 164.
G56 Gerhard, W. and Nägele, E. (1983). *Cem. Concr. Res.* **13**, 849.
G57 Greening, N.R. (1972), quoted by J.F. Young in Y9.
G58 Gessner, W., Müller, D., Behrens, H.-J. and Scheler, G. (1982). *Zeit. anorg. allg. Chem.* **486**, 193.
G59 Gessner, W. and Müller, D. (1989). *Z. Chemie* **29**, 344.
G60 Granger, M.-M. and Protas, J. (1969). *Acta Cryst.* **B25**, 1943.
G61 Gard, J.A., in *Chemistry of Cements* (ed. H.F.W. Taylor), Vol. 2, p. 243, Academic Press, London (1964).
G62 Gaudefroy, C., Granger, M.-M., Permingeat, F. and Protas, J. (1968). *Bull. Soc. franç. Mineral. Crist.* **91**, 43.
G63 Gartner, E.M., Tang, F.J. and Weiss, S.J. (1985). *J. Am. Ceram. Soc.* **68**, 667.
G64 Gabrisová, A., Havlica, J. and Sahu, S. (1991). *Cem. Concr. Res.* **21**, 1023.
G65 Glasser, F.P. and Marinho, M.B. (1984). *Br. Ceram. Proc.* (35) 221.
G66 Gupta, P., Chatterji, S. and Jeffery, J.W. (1970). *Cem. Technol.* **1**, 3.
G67 Gupta, P., Chatterji, S. and Jeffery, J.W. (1973). *Cem. Technol.* **4**, 63.
G68 Ghorab, H.Y. and El Fetouh, S.H.A. (1987). *Mater. Res. Soc. Symp. Proc.* **85**, 255.
G69 Groves, G.W. (1981). *Cem. Concr. Res.* **11**, 713.
G70 Groves, G.W. and Richardson, I.G. (1994). *Cem. Concr. Res.* **24**, 1191.
G71 Gollop, R.S. and Taylor, H.F.W. (1992). *Cem. Concr. Res.* **22**, 1027.
G72 Glasser, F.P. and Marr, J. (1985). *Cemento* **82**, 85.
G73 Garboczi, E.J. and Bentz, D.P., in *Materials Science of Concrete II* (eds J.P. Skalny and S. Mindess), p. 249, American Ceramic Society, Westerville, OH (1991).
G74 Gregg, S.J. and Sing, K.S.W. (1982). *Adsorption, Surface Area and Porosity* (2nd Edn), 303pp., Academic Press, London (1985).
G75 Grudemo, Å., *Strength–structure relationships of cement paste materials. Part 1. Methods and basic data for studying phase composition and microstructure* (CBI Research, 6:77), 101pp., Swedish Cement and Concrete Research Institute, Stockholm (1977); also private communication quoted by L.-O. Nilsson in Report TCBM-1003, Division of Building Materials, University of Lund.
G76 Good, R.J., in *Surface and Colloid Science* (eds E. Matijević and R.J. Good), Vol. 13, p. 283, Plenum Press, New York (1984).
G77 Garboczi, E.J. and Bentz, D.P., in *Advances in Cementitious Materials* (Ceramic Trans. Vol. 16, ed. S. Mindess), p. 365, American Ceramic Society, Westerville, OH (1991).
G78 Goto, S. and Roy, D.M. (1981). *Cem. Concr. Res.* **11**, 575.
G79 Goto, S. and Roy, D.M. (1981). *Cem. Concr. Res.* **11**, 751.
G80 Garboczi, E.J. and Bentz, D.P. (1992). *J. Mater. Sci.* **27**, 2083.
G81 Goto, S., Yoshii, T. and Daimon, M. (1985). *Cem. Concr. Res.* **15**, 964.
G82 Gollop, R.S. and Taylor, H.F.W. (1996). *Cem. Concr. Res.* **26**, 1013, 1029.
G83 Glasser, F.P., Luke, K. and Angus, M.J. (1988). *Cem. Concr. Res.* **18**, 165.
G84 Glukhovsky, V.D., Rostovskaja, G.S. and Rumyna, G.V., in *7th ICCC*, Vol. 3, p. V-164 (1980).
G85 Ghose, A. and Pratt, P.L., in *Effects of Flyash Incorporation in Cement and Concrete* (ed. S. Diamond), p. 82, Materials Research Society, University Park, PA (1981).

G86 Groves, G.W. and Rodger, S.A. (1989). *Adv. Cem. Res.* **2**, 135.
G87 Grutzeck, M.W., Roy, D.M. and Scheetz, B.E., in *Effects of Flyash Incorporation in Cement and Concrete* (ed. S. Diamond), p. 92, Materials Research Society, University Park, PA (1981).
G88 Gegout, P., Hornain, H., Thuret, B., Mortureux, B., Volant, J. and Regourd, M., in *8th ICCC*, Vol. 4, p. 197 (1986).
G89 Galtier, P. and Guilhot, B. (1984). *Cem. Concr. Res.* **14**, 679.
G90 Gill, S.M., Banfill, P.F.G. and El-Jazairi, B., in *8th ICCC*, Vol. 4, p. 322 (1986).
G91 George, C.M., in *Structure and Performance of Cements* (ed. P. Barnes), p. 415, Applied Science Publishers, London (1983).
G92 George, C.M., in *7th ICCC*, Vol. 1, p. V-1/3 (1980).
G93 George, C.M., in *Calcium Aluminate Cements* (ed. R.J. Mangabhai), p. 181, E and FN Spon, London (1990).
G94 Ghosh, S.N., Mathur, V.K. and Chopra, S.K. (1984). *Cem. Concr. Res.* **14**, 437.
G95 Gard, J.A., Luke, K. and Taylor, H.F.W (1981). *Cem. Concr. Res.* **11**, 659.
G96 Gard, J.A. and Taylor, H.F.W. (1957). *Mineral. Mag.* **31**, 361.
G97 Gouda, G.R. and Roy, D.M. (1975). *Cem. Concr. Res.* **5**, 551.
G98 Grandet, J. and Ollivier, J.P., in *7th ICCC*, Vol. 3, pp. VII-63, VII-85 (1980).
G99 Grandet, J. and Ollivier, J.P. (1980). *Cem. Concr. Res.* **10**, 759.
G100 Groves, G.W., Brough, A., Richardson, I.G. and Dobson, C.M. (1991). *J. Am. Ceram. Soc.* **74**, 2891.
G101 Groves, G.W., Rodway, D.I. and Richardson, I.G. (1990). *Adv. Cem. Res.* **3**, 117.
G102 Gard, J.A., Taylor, H.F.W. and Chalmers, R.A. (1957). *Mineral. Mag.* **31**, 611.
G103 Gollop, R.S. and Taylor, H.F.W. (1995). *Cem. Concr. Res.* **25**, 1581.
G104 Ghorab, H.Y., Heinz, D., Ludwig, U., Meskendahl, T. and Wolter, A., in *7th ICCC*, Vol. 4, p. 496 (1980).
G105 Glasser, F.P., Damidot, D. and Atkins, M. (1995). *Adv. Cem. Res.* **7**, 57.
G106 Gillott, J.E. and Swenson, E.G. (1967). *J. Engng Geol.* **2**, 7.

H1 Hudson, K.E. and Groves, G.W. (1982). *Cem. Concr. Res.* **12**, 61.
H2 Hahn, T., Eysel, W. and Woermann, E., in *5th ISCC*, Vol. 1, p. 61 (1969); summarized from E. Woermann, T. Hahn and W. Eysel, *Zem.-Kalk-Gips* **16**, 370 (1963); **20**, 385 (1967); **21**, 241 (1968); **22**, 235, 412 (1969).
H3 Harrisson, A.M., Taylor, H.F.W. and Winter, N.B. (1985). *Cem. Concr. Res.* **15**, 775.
H4 Harrisson, A.M., Winter, N.B. and Taylor, H.F.W., in *8th ICCC*, Vol. 4, p. 170 (1986).
H5 Harrisson, A.M., in *Proc. 4th Euroseminar on Microscopy Applied to Building Materials* (eds J.E. Lindqvist and B. Nitz), Swedish Nat. Testing and Research Inst. Building Technol. SP Report 1993:15, Borås, Sweden (1993).
H6 Hall, C. and Scrivener, K.L. (1997). *Adv. Cem. Based Mater.*, in press.
H7 Han, K.S., Gard, J.A. and Glasser, F.P. (1981). *Cem. Concr. Res.* **11**, 79.
H8 Hansen, W.C., Brownmiller L.T. and Bogue, R.H. (1928). *J. Am. Chem. Soc.* **50**, 396.

H9 Hornain, H. (1973). *Rev. Matér. Constr.* (680) 4.
H10 Henmi, C., Kusachi, I., Kawahara, A. and Henmi, K. (1978). *Mineral. J.* (Japan) **9**, 169.
H11 Henmi, C., Kawahara, A., Henmi, K., Kusachi, I. and Takéuchi, Y. (1983). *Am. Mineral.* **68**, 156.
H12 Hörkner, W. and Müller-Buschbaum, H. (1976). *J. Inorg. Nucl. Chem.* **38**, 983.
H13 Hentschel, G. (1964). *Neues Jahrb. Mineral. Monatsh.* 22.
H14 Hansen, W.C. (1928). *J. Am. Chem. Soc.* **50**, 2155.
H15 Hanic, F., Handlovič, M. and Kaprálik, I. (1980). *Acta Cryst.* **B36**, 2863.
H16 Hallstedt, B. (1995). *J. Am. Ceram. Soc.* **78**, 193.
H17 Halstead, P.E. and Moore, A.E. (1962). *J. Appl. Chem.* **12**, 413.
H18 Hanic, F., Havlica, J., Kaprálik, I., Ambrúz, V., Gáliková, L. and Urbanova, O. (1986). *Trans. J. Br. Ceram. Soc.* **85**, 52.
H19 Henmi, C. and Henmi, K. (1978). *Mineral. J.* (Japan) **9**, 106.
H20 Harker, R.I. and Tuttle, O.F. (1956). *Am. J. Sci.* **254**, 239.
H21 Hills, A.W.D. (1968). *Chem. Engng Sci.* **23**, 297.
H22 Heilmann, T., in *3rd ISCC*, p. 711 (1954).
H23 Hofmänner, F. *Microstructure of Portland Cement Clinker*, 48pp., Rheintaler Druckerei und Verlag, Heerbrugg, Switzerland (1975).
H24 Hornain, H. and Regourd, M., in *7th ICCC*, Vol. 2, p. I-276 (1980).
H25 Hjorth, L. and Laurén, K.-G. (1971). *Cem. Concr. Res.* **1**, 27.
H26 Hubbard, C.R., Evans, E.H. and Smith, D.K. (1976). *J. Appl. Cryst.* **9**, 169.
H27 Halstead, P.E. and Moore, A.E. (1957). *J. Chem. Soc.* 3873.
H28 Hansen, W. (1987) quoted by J.F. Young and W. Hansen in Y5.
H29 Hunt, C.M., in *4th ISCC*, Vol. 1, p. 297 (1962).
H30 Henderson, E. and Bailey, J.E. (1993). *J. Mater. Sci.* **28**, 3681.
H31 Harrisson, A.M., Winter, N.B. and Taylor, H.F.W. (1987). *J. Mater. Sci. Lett.* **6**, 1339.
H32 Hara, N., Chan, C.F. and Mitsuda, T. (1978). *Cem. Concr. Res.* **8**, 113.
H33 Hamid, S.A. (1981). *Zeit. Krist.* **154**, 189.
H34 Hara, N. and Inoue, N. (1980). *Cem. Concr. Res.* **10**, 677.
H35 Hara, N., Inoue, N., Noma, H. and Hasegawa, T. in *8th ICCC*, Vol. 3, p. 160 (1986).
H36 Hirljac, J., Wu, Z.-Q. and Young, J.F. (1983). *Cem. Concr. Res.* **13**, 877.
H37 Henning, O., in *The Infrared Spectra of Minerals* (ed. V.C. Farmer), p. 445, Mineralogical Society, London (1974).
H38 Hernandez-Moreno, M.J., Ulibarri, M.A., Rendon, J.L. and Serna, C.J. (1985). *Phys. Chem. Minerals* **12**, 34.
H39 Heinz, D. and Ludwig, U., in *8th ICCC*, Vol. 5, p. 189 (1986).
H40 Houtepen, C.J.M. and Stein, H.N. (1976). *Cem. Concr. Res.* **6**, 651.
H41 Henderson, E., Turrillas, X. and Barnes, P. (1994). *Adv. Cem. Res.* **6**, 173.
H42 Halse, Y., Goult, D.J. and Pratt, P.L. (1984). *Br. Ceram. Proc.* (35) 403.
H43 Harchand, K.S., Vishwamittar and Chandra, K. (1980). *Cem. Concr. Res.* **10**, 243.
H44 Helmuth, R.H., private communication.
H45 Hobbs, D.W. (1978). *Cem. Concr. Res.* **8**, 211.
H46 Hobbs, D.W. (1977). *World Cem. Technol.* **8**, 75.
H47 Helmuth, R.A., in *7th ICCC*, Vol. 3, p. VI-0/16 (1980).
H48 Hansen, W. and Almudaiheem, J. (1987). *Mater. Res. Soc. Symp. Proc.* **85**, 105.

H49 Hagymassy, J., Odler, I., Yudenfreund, M., Skalny, J. and Brunauer, S. (1972). *J. Coll. Interface Sci.* **38**, 20.

H50 Hansen, W. (1987). *J. Am. Ceram. Soc.* **70**, 323.

H51 Hasselmann, D.P.H. (1962). *J. Am. Ceram. Soc.* **46**, 564.

H52 Helmuth, R.A. and Turk, D.A., in *Symposium on Structure of Portland Cement Paste and Concrete* (Sp. Rpt 90), p. 135, Highway Research Board, Washington, DC (1966).

H53 Helmuth, R.A. and Turk, D.H. (1967). *J. PCA Res. Dev. Labs* **9** (2) 8.

H54 Hansen, W. and Young, F., in *Materials Science of Concrete II* (eds J.P. Skalny and S. Mindess), p. 185, American Ceramic Society, Westerville, OH (1991).

H55 Hooton, R.D., in *Blended Cements* (ASTM Spec. Tech. Publ. 897), p. 128, American Society for Testing and Materials, Philadelphia, PA (1986).

H56 Hooton, R.D. (1989), in *Advances in Cement Manufacture and Use*, p. 143, Engineering Foundation, New York.

H57 Halamickova, P., Detwiler, R.J., Bentz, D.P. and Garboczi, E.J. (1995), *Cem. Concr. Res.* **25**, 790.

H58 Harrisson, A.M., Winter, N.B. and Taylor, H.F.W. (1987). *Mater. Res. Soc. Symp. Proc.* **85**, 213.

H59 Hinrichs, A. and Odler, I. (1989). *Adv. Cem. Res.* **2**, 9.

H60 Hubbard, F.H., Dhir, R.K. and Ellis, M.S. (1985). *Cem. Concr. Res.* **15**, 185.

H61 Halse, Y., Pratt, P.L., Dalziel, J.A. and Gutteridge, W.A. (1984). *Cem. Concr. Res.* **14**, 491.

H62 Halse, Y., Jensen, H.-U. and Pratt, P.L., in *8th ICCC*, Vol. 4, p. 176 (1986).

H63 Hjorth, L. *Microsilica in Concrete* (Nordic Concrete Res., No.1, Paper 9), 18pp., Aalborg Portland, Denmark (1982).

H64 Huang, Cheng-yi and Feldman, R.F. (1985). *Cem. Concr. Res.* **15**, 285.

H65 Huang, Cheng-yi and Feldman, R.F. (1985). *Cem. Concr. Res.* **15**, 585.

H66 Hjorth, J., Skibsted, J. and Jakobsen, H.J. (1988). *Cem. Concr. Res.* **18**, 789.

H67 Hemmings, R.T. and Berry, E.E. (1988). *Mater. Res. Soc. Symp. Proc.* **113**, 3.

H68 Halse, Y. and Pratt, P.L., in *8th ICCC*, Vol. 4, p. 317 (1986).

H69 Harchand, K.S., Vishwamittar and Chandra, K. (1984). *Cem. Concr. Res.* **14**, 19.

H70 Houghton, S.J. and Scrivener, K.L. in *Durability of Concrete* (ed. V.M. Malhotra), p. 133, ACI SP-145, American Concrete Institute, Detroit, MI (1994).

H71 Heller, L. (1952). *Acta Cryst.* **5**, 724.

H72 Hara, N. and Inoue, N. (1980). *Cem. Concr. Res.* **10**, 53.

H73 Hjorth, L. (1983). *Phil. Trans. R. Soc. London* **A310**, 167.

H74 Hansson, C.M. (1984). *Cem. Concr. Res.* **14**, 574.

H75 Hobbs, D.W. (1986). *Struct. Eng.* **64A**, 381.

H76 Hobbs, D.W. (1981). *Mag. Concr. Res.* **33**, 208.

H77 Hobbs, D.W. and Gutteridge, W.A. (1980). *Mag. Concr. Res.* **32**, 235.

H78 Hansen, W.C. (1944). *J. Am. Concr. Inst. (Proc.)* **40**, 213.

H79 Hobbs, D.W. (1986). *Mag. Concr. Res.* **38**, 191.

H80 Hughes, D.C. (1985). *Cem. Concr. Res.* **15**, 1003.

H81 Heinz, D., Ludwig, U. and Rüdiger, I. (1989). *Concrete Precasting Plant and Technology* (11) 56.

H82 Hamada, M., in *5th ISCC*, Vol. 3, p. 343 (1962).

I1 Il'inets, A.M., Malinovskii, Yu.A. and Nevskii, N.N. (1985). *Doklady Akad. Nauk SSSR* **281**, 332.
I2 Ilyinets, A.M., Simonov, V.I. and Bikbau, M. Ya., in *8th ICCC*, Vol. 6, p. 489 (1986).
I3 Il'inets, A.M., Nevskii, N.N., Ilyukhin, V.V., Bikbau, M. Ya. and Belov, N.V. (1982). *Doklady Akad. Nauk SSSR* **267**, 641.
I4 Ichikawa, M., Ikeda, S. and Komukai, Y. (1994). *Cem. Concr. Res.* **24**,1092.
I5 Ichikawa, M. and Komukai, Y. (1993). *Cem. Concr. Res.* **23**, 933.
I6 Imlach, J.A., Dent Glasser, L.S. and Glasser, F.P. (1971). *Cem. Concr. Res.* **1**, 57.
I7 Insley, H. and McMurdie, H.F. (1938). *J. Res. Nat. Bur. Stand.* **20**, 173.
I8 Ikeda, K., Kishimoto, K. and Shima, H. (1996). *Cem. Concr. Res.* **26**, 743.
I9 Imlach, J.A. and Hofmänner, F., in *6th ICCC*, Vol. 1, p. 281 (1976).
I10 Ings, J.B., Brown, P.W. and Frohnsdorff, G. (1983). *Cem. Concr. Res.* **13**, 843.
I11 Ingram, L. and Taylor, H.F.W. (1967). *Mineral. Mag.* **36**, 465.
I12 Ingram, K.D. and Daugherty, K.E., in *9th ICCC*, Vol. 3, p. 180 (1992).
I13 Ish-Shalom, M. and Bentur, A. (1974). *Cem. Concr. Res.* **4**, 519.
I14 Ish-Shalom, M. and Bentur, A. (1975). *Cem. Concr. Res.* **5**, 139.
I15 Ishida, H., Mabuchi, K., Sasaki, K. and Mitsuda, T. (1992). *J. Am. Ceram. Soc.* **75**, 2427.
I16 Ishida, H., Sasaki, K. and Mitsuda, T. (1992). *J. Am. Ceram. Soc.* **75**, 353.
I17 Ilyukhin, V.V., Nevsky, N.N., Bickbau, M.J. and Howie, R.A. (1977). *Nature*, **269**, 397.
I18 Idorn, G., in *5th ISCC*, Vol. 3, p. 411 (1969).
I19 Imlach, B.V. and Taylor, H.F.W. (1972). *Trans. J. Br. Ceram. Soc.* **71**, 71.
I20 Idorn, G. and Fördös, Z., in *6th ICCC*, Vol. 3, p. 287 (1976).
I21 Idorn, G.M. (1961). *Danish Inst. Bldg Res. Ser., Progr. Rpt (2)*; quoted by T. Knudsen and N. Thaulow in K75.
I22 Isu, N., Teramura, S., Ishida, H. and Mitsuda, T. (1994). *J. Am. Ceram. Soc.* **77**, 2093.

J1 Jeffery, J.W. (1952). *Acta Cryst.* **5**, 26.
J2 Jost, K.H., Ziemer, B. and Seydel, R. (1977). *Acta Cryst.* **B33**, 1696.
J3 Jeevaratnam, J., Glasser, F.P. and Dent Glasser, L.S. (1964). *J. Am. Ceram. Soc.* **47**, 105.
J4 Jøns, E.C. (1980). *Cem. Concr. Res.* **10**, 103.
J5 Johansen, V. (1973). *J. Am. Ceram. Soc.* **56**, 450.
J6 Johansen, V. and Jakobsen, U.H. (1993). *World Cem. Res. Dev.* **24** (8), 32.
J7 Johansen, V. (1978). *Cem. Concr. Res.* **8**, 245.
J8 Javellana, M.P. and Jawed, I. (1982). *Cem. Concr. Res.* **12**, 399.
J9 Jost, K.H. and Ziemer, B. (1984). *Cem. Concr. Res.* **14**, 177.
J10 Jones, F.E. (1940). *J. Soc. Chem. Ind.* **51**, 29.
J11 Jennings, H.M., Dalgleish, B.J. and Pratt, P.L. (1981). *J. Am. Ceram. Soc.* **64**, 567.
J12 Jennings, H.M. and Pratt, P.L. (1980). *J. Mater. Sci.* **15**, 250.
J13 Jennings, H.M. and Parrott, L.J. (1986). *J. Mater. Sci.* **21**, 4048.
J14 Jennings, H.M. and Parrott, L.J. (1986). *J. Mater. Sci.* **21**, 4053.
J15 Jawed, I. and Skalny, J. (1982). *J. Coll. Interface Sci.* **85**, 235.

J16 Jennings, H.M. (1986). *J. Am. Ceram. Soc.* **69**, 614.
J17 Jennings, H.M. (1988). *J. Am. Ceram. Soc.* **71**, C115.
J18 Jones, F.E and Roberts, M.H., quoted by F.E. Jones in J21.
J19 Jones, F.E., in *2nd SCC*, p. 231 (1939).
J20 Jappy, T.G. and Glasser, F.P. (1991/2). *Adv. Cem. Res.* **4**, 1.
J21 Jones, F.E., in *4th ISCC*, Vol. 1, p. 205 (1962).
J22 Jones, F.E. (1944). *J. Phys. Chem.* **48**, 311.
J23 Jones, F.E. (1944). *J. Phys. Chem.* **48**, 356, 379.
J24 Jawed, I. and Skalny, J., in *International Seminary on Calcium Aluminates* (ed. M. Murat *et al.*), Politecnico di Torino, Turin (1982).
J25 Jennings, H.M. and Pratt, P.L., in *7th ICCC*, Vol. 2, p. II-141 (1980).
J26 Jennings, H.M. and Tennis, P.D. (1994). *J. Am. Ceram. Soc.* **77**, 3161.
J27 Jawed, I. and Skalny, J. (1978). *Cem. Concr. Res.* **8**, 37.
J28 Jelenić, I., Panović, A., Halle, R. and Gaćeša, T. (1977). *Cem. Concr. Res.* **7**, 239.
J29 Jelenić, I., Panović, A. and Bezjak, A. (1980). *Cem. Concr. Res.* **10**, 463.
J30 Jelenić-Bezjak, I., in *Advances in Cement Technology* (ed. S.N. Ghosh), p. 397, Pergamon Press, Oxford (1983).
J31 Jennings, H.M. and Johnson, S.K. (1986). *J. Am. Ceram. Soc.* **69**, 790.
J32 Jakobsen, U.H., Johansen, V. and Thaulow, N. (1995). *Mater. Res. Soc. Symp. Proc.* **370**, 227.
J33 Jambor, J., in *6th ICCC*, Vol. 2, Part 1, p. 315 (1976).
J34 Jawed, I. and Skalny, J., in *Effects of Flyash Incorporation in Cement and Concrete* (ed. S. Diamond), p. 60, Materials Research Society, University Park, PA (1981).
J35 Justnes, H., Sellevold, E.J. and Lundevall, G., in *Fly Ash, Silica Fume, Slag and Natural Pozzolans in Concrete* (ed. M. Malhotra), Vol. 2, p. 873, SP-132, American Concrete Institute, Detroit (1993).
J36 James, J. and Subba Rao, M. (1986). *Cem. Concr. Res.* **16**, 296.
J37 Jeanne, M. (1968). *Rev. Matér. Constr.* (629) 53.
J38 Jennings, H.M., Taleb, H., Frohnsdorff, G. and Clifton, J.R., in *8th ICCC*, Vol. 3, p. 239 (1986).
J39 Jolicoeur, C., Piotte, M., Chassé, M., Simard, M.-A., Aïtcin, P.-C., Nkinamubanzi, P.-C. and Baalbaki, M., in *Concrete: from the Material to the Structure* (Proc. RILEM Colloq., Arles, France, 1996) (preprint).
J40 Javelas, R., Maso, J.C., Ollivier, J.P. and Thenoz, B. (1975). *Cem. Concr. Res.* **5**, 285.
J41 Johansen, V., Thaulow, N. and Skalny, J. (1993). *Adv. Cem. Res.* **5**, 23.

K1 Kristmann, M. (1978). *Cem. Concr. Res.* **8**, 93.
K2 Kim, Y.J., Nettleship, I and Kriven, W.M. (1992). *J. Am. Ceram. Soc.* **75**, 2407.
K3 Kondo, R.-I., Goto, S. and Fukuhara, M., in *Review of the 32nd General Meeting*, p. 38, Cement Association of Japan, Tokyo (1978).
K4 Kaprálik, I. and Hanic, F. (1980). *Trans. J. Br. Ceram. Soc.* **79**, 128.
K5 Kurfel, A. and Will, G. (1980). *Acta Cryst.* **B36**, 2881.
K6 Kaprálik, I., Hanic, F., Havlica, J. and Ambrúz, V. (1986). *Trans. J. Br. Ceram. Soc.* **85**, 107.
K7 Kaprálik, I. and Hanic, F. (1986). *Trans. J. Br. Ceram. Soc.* **85**, 131.
K8 Kerton, C.P. and Murray, R.J., in *Structures and Properties of Cements* (ed. P. Barnes), p. 205, Applied Science Publishers, London (1983).

K9 Kirchner, G. (1986). *Zem.-Kalk-Gips* **39**, 555 (partial English translation, p. 368).
K10 Kuhlmann, K., Ellerbrock, H.-G. and Sprung, S. (1985). *Zem.-Kalk-Gips* **38**, 169 (partial English translation, p. 136).
K11 Klug, H.P. and Alexander, L.E., *X-ray Diffraction Procedures for Polycrystalline and Amorphous Materials* (2nd Edn), 966pp., Wiley, New York (1974).
K12 Knudsen, T. (1976). *Am. Ceram. Soc. Bull.* **55**, 1052.
K13 Kristmann, M. (1977). *Cem. Concr. Res.* **7**, 649.
K14 Kantro, D.L. and Weise, C.H. (1979). *J. Am. Ceram. Soc.* **62**, 621.
K15 Kantro, D.L., Brunauer, S. and Weise, C.H. (1959). *J. Colloid Sci.* **14**, 363.
K16 Kalousek, G.L. and Roy, R. (1957). *J. Am. Ceram. Soc.* **40**, 236.
K17 Komarneni, S., Roy, D.M., Fyfe, C.A. and Kennedy, G.J. (1987). *Cem. Concr. Res.* **17**, 891.
K18 Kalousek, G.L., in *3rd ISCC*, p. 296 (1954).
K19 Kantro, D.L., Brunauer, S. and Weise, C.H. (1962). *J. Phys. Chem.* **66**, 1804.
K20 Kalousek, G.L. (1944). *J. Res. Nat. Bur. Stand.* **32**, 285.
K21 Kondo, R. and Ueda, S., in *5th ISCC*, Vol. 2, p. 203 (1969).
K22 Kondo, R., Ueda, S. and Kodama, M. (1967). *Semento Gijutsu Nenpo* **21**, 83.
K23 Kuzel, H.-J. (1966). *Neues Jahrb. Mineral. Monatsh.* 193.
K24 Kuzel, H.-J. (1970). *Neues Jahrb. Mineral. Monatsh.* 363.
K25 Kuzel, H.-J. (1976). *Neues Jahrb. Mineral. Monatsh.* 319.
K26 Kuzel, H.-J. and Pöllmann, H. (1991). *Cem. Concr. Res.* **21**, 885.
K27 Kwan, S., LaRosa, J. and Grutzeck, M.W. (1995). *J. Am. Ceram. Soc.* **78**, 1921.
K28 Kuzel, H.-J. (1968). *Zem.-Kalk-Gips* **21**, 493.
K29 Kalousek, G.L., Davis, C.W. and Schmertz, W.E. (1949). *J. Am. Concr. Inst. (Proc.)* **45**, 693.
K30 Kuzel, H.-J. (1969). *Neues Jahrb. Mineral. Monatsh.* 397.
K31 Kiriyama, R., Kiriyama, H. and Takagawa, M., in *5th ISCC*, Vol. 2, p. 98 (1969).
K32 Koritnig, S. and Süsse, P. (1975). *Tschermaks Mineral. Petr. Mitt.* **22**, 79.
K33 Kuzel, H.-J. (1987). *Neues Jahrb. Mineral. Abhandl.* **156**, 155.
K34 Kalousek, G.L. and Adams, M. (1951). *J. Am. Concr. Inst. (Proc.)* **48**, 77.
K35 Kuzel, H.-J. and Meyer, H., in *15th IC Cem. Microsc.*, p. 191 (1994).
K36 Kalousek, G.M. (1965). *Mater. Res. Stand.* **5**, 292.
K37 Kjellsen, K.O., Jennings, H.M. and Lagerblad, B. (1996). *Cem. Concr. Res.* **26**, 593.
K38 Kanare, H.M. and Gartner, E.M. (1985). *Cem. Res. Prog.* [for] 1984, 213.
K39 Knudsen, T. and Geiker, M. (1985). *Cem. Concr. Res.* **15**, 381.
K40 Knudsen, T. (1980), in *7th ICCC*, Vol. 2, p. I-170 (1980).
K41 Knudsen, T., in *Characterization and Performance Prediction of Cement and Concrete*, p. 125, Engineering Foundation, New York (1983).
K42 Knudsen, T. (1984). *Cem. Concr. Res.* **14**, 622.
K43 Knudsen, T., in *8th ICCC*, Vol. 3, p. 369 (1986).
K44 Kumar, A. and Roy, D.M. (1986). *Cem. Concr. Res.* **16**, 74.
K45 Kjellsen, K.O., Detwiler, R.J. and Gjørv, O.E. (1990). *Cem. Concr. Res.* **20**, 927.

K46 Kondo, R. and Ohsawa, S., in *5th ISCC*, Vol. 4, p. 255 (1969).
K47 Kühle, K. and Ludwig, U. (1972). *Sprechsaal Keram. Glas Email Silik.* **105**, 421.
K48 Kokubu, M., in *5th ISCC*, Vol. 4, p. 75 (1969).
K49 Kovács, R. (1975). *Cem. Concr. Res.* **5**, 73.
K50 Kawada, N. and Nemoto, A. (1968). *Semento Gijutsu Nenpo* **22**, 124.
K51 Kovacs, R., in *6th ICCC*, Vol. 3, p. 99 (1976).
K52 Khan, M.H., Mohan, K. and Taylor, H.F.W. (1985). *Cem. Concr. Res.* **15**, 89.
K53 Klemm, W.A. and Adams, L.D., in *Carbonate Additions to Cement* (eds. P. Klieger and R.D. Hooton), p. 60, ASTM STP 1064, American Society for Testing and Materials, Philadelphia, PA (1990).
K54 Klein, A. and Troxell, G.E. (1958). *Proc. ASTM* **58**, 986.
K55 Kawano, T., Hitotsuya, K. and Mori, T., in *6th ICCC*, Vol. 3, p. 179 (1976).
K56 Kurdowski, W. and Thiel, A. (1981). *Cem. Concr. Res.* **11**, 29.
K57 Klemm, W.A. and Skalny, J. (1977). *Cem. Res. Progr.* [for] 1976, 259.
K58 Kurdowski, W. and Miskiewicz, K. (1985). *Cem. Concr. Res.* **15**, 785.
K59 Kurdowski, W. (1987). *Cem. Concr. Res.* **17**, 361.
K60 Klieger, P. (1966), in *Significance of Tests and Properties of Concrete and Concrete-Making Materials*, p. 530, Sp. Tech. Publ. 169A, American Society for Testing and Materials, Philadelphia, PA (1966).
K61 Kondo, R., Daimon, M. and Sakai, E. (1978). *Cemento* **75**, 225.
K62 Kantro, D.L. (1975). *J. Testing Evaln.* **3**, 312.
K63 Kondo, R., Daimon, M., Sakai, E. and Ushiyama, H. (1977). *J. Appl. Chem. Biotechnol.* **27**, 191.
K64 Kjellsen, K.O., Detwiler, R.J. and Gjørv, O.E. (1990). *Cem. Concr. Res.* **20**, 308.
K65 Kjellsen, K.O., Detwiler, R.J. and Gjørv, O.E. (1991). *Cem. Concr. Res.* **21**, 179.
K66 Kalousek, G.L. (1954). *J. Am. Concr. Inst. (Proc.)* **50**, 365.
K67 Kalousek, G.L. (1966). *J. Am. Concr. Inst. (Proc.)* **63**, 817.
K68 Kalousek, G.L., in *5th ISCC*, Vol. 3, p. 523 (1969).
K69 Kalousek, G.L. (1957). *J. Am. Ceram. Soc.* **40**, 74.
K70 Komarneni, S., Roy, R., Roy, D.M., Fyfe, C.A. and Kennedy, C.J. (1985). *Cem. Concr. Res.* **15**, 723.
K71 Komarneni, S., Roy, D.M. and Roy, R. (1982). *Cem. Concr. Res.* **12**, 773.
K72 Kendall, K., Howard, A.J. and Birchall, J.D. (1983). *Phil. Trans. R. Soc. London* **A310**, 139.
K73 Knab, L.I., Clifton, J.R. and Ings, J.B. (1983). *Cem. Concr. Res.* **13**, 383.
K74 Kondo, R., Daimon, M. and Akiba, T., in *5th ISCC*, Vol. 3, p. 402 (1969).
K75 Knudsen, T. and Thaulow, N. (1975). *Cem. Concr. Res.* **5**, 443.
K76 Kollek, J.J., Varma, S.P. and Zaris, C., in *8th ICCC*, Vol. 4, p. 183 (1986).
K77 Kelham, S. (1996). *Cem. Concr. Composites*, **18**, 171
K78 Kuenning, W.H. (1966). *Highway Res. Record* (113) 43.

L1 Lee, F.C., Banda, H.M. and Glasser, F.P. (1982). *Cem. Concr. Res.* **12**, 237.
L2 Lee, F.C. and Glasser, F.P. (1979). *J. Appl. Cryst.* **12**, 407.
L3 Louisnathan, S.J. (1971). *Canad. Mineral.* **10**, 822.
L4 Lea, F.M. and Parker, T.W. (1934). *Phil. Trans. R. Soc. London* **A234**, 1.

L5 Lea, F.M. and Parker, T.W. *The Quaternary System $CaO$–$Al_2O_3$–$SiO_2$–$Fe_2O_3$ in Relation to Cement Technology* (Building Res. Techn. Paper 16), 52pp., HMSO, London (1935).

L6 Lea, F.M. *The Chemistry of Cement and Concrete* (3rd Edn), 727pp., Arnold, London (1970).

L7 Leary, J.K. (1962). *Nature* **194**, 79.

L8 Lehmann, H., Locher, F.W. and Thormann, P. (1964). *TIZ* **88**, 489.

L9 Ludwig, U. and Ruckensteiner, G. (1974). *Cem. Concr. Res.* **4**, 239.

L10 Long, G.R., in *4th IC Cem. Microsc.*, p. 92 (1982).

L11 Long, G.R. (1983). *Phil. Trans. R. Soc. London* **A310**, 43.

L12 Locher, F.W. (1980). *World Cem. Technol.* **11**, 67.

L13 Long, G.R., in *4th IC Cem. Microsc.*, p. 128 (1982).

L14 Lerch, W. and Brownmiller, L.T. (1937). *J. Res. Nat. Bur. Stand.* **18**, 609.

L15 Lea, F.M. and Nurse, R.W. (1939). *J. Soc. Chem. Ind.* **58**, 227.

L16 Locher, F.W., Sprung, S. and Korf, P. (1973). *Zem.-Kalk-Gips* **26**, 349.

L17 Lebiedzik, J., Lebiedzik, J. and Gouda, G.R., in *3rd IC Cem. Microsc.*, p. 154 (1981).

L18 Lerch, W. and Bogue, R.H. (1926). *Ind. Engng Chem.* **18**, 739.

L19 Le Sueur, P.J., Double, D.D. and Groves, G.W. (1984). *Br. Ceram. Proc.* (35) 177.

L20 Lehmann, H. and Dutz, H., in *4th ISCC*, Vol. 1, p. 513 (1962).

L21 Long, J.V.P. and McConnell, J.D.C. (1959). *Mineral. Mag.* **32**, 117.

L22 Lentz, C.W., in *Symposium on Structure of Portland Cement Paste and Concrete*, p. 269, Sp. Rpt 90, Highway Research Board, Washington, DC (1966).

L23 Lipmaa, E., Mägi, M., Tarmak, M., Wieker, W. and Grimmer, A.-R. (1982). *Cem. Concr. Res.* **12**, 597.

L24 Lerch, W. and Bogue, R.H. (1934). *J. Res. Nat. Bur. Stand.* **12**, 645.

L25 Li, G., Le Bescop, P. and Moranville, M. (1996). *Cem. Concr. Res.* **26**, 27.

L26 Ludwig, U. and Rüdiger, I. (1993). *Zem.-Kalk-Gips* **46**, 150 (partial English translation, p.E153).

L27 Lager, G.A., Armbruster, T. and Faber, J. (1987). *Am. Mineral.* **72**, 756.

L28 Longuet, P., in *3rd ISCC*, p. 328 (1954).

L29 Lager, G.A., Armbruster, T., Rotella, F.J., Jorgensen, J.D. and Hinks, D.G. (1984). *Am. Mineral.* **69**, 910.

L30 Luke, K. and Glasser, F.P. (1987). *Cem. Concr. Res.* **17**, 273.

L31 Lachowski, E.E., Mohan, K., Taylor, H.F.W. and Moore, A.E. (1980). *J. Am. Ceram. Soc.* **63**, 447.

L32 Lachowski, E.E., Mohan, K., Taylor, H.F.W., Lawrence, C.D. and Moore, A.E. (1981). *J. Am. Ceram. Soc.* **64**, 319.

L33 Lachowski, E.E. and Diamond, S. (1983). *Cem. Concr. Res.* **13**, 177.

L34 Lachowski, E.E. (1979). *Cem. Concr. Res.* **9**, 337.

L35 Lawrence, C.D., in *Symposium on Structure of Portland Cement Paste and Concrete*, p. 378, Sp. Rpt 90, Highway Research Board, Washington, DC (1966).

L36 Locher, F.W., Richartz, W. and Sprung, S. (1976). *Zem.-Kalk-Gips* **29**, 435 (partial English translation, p. 257).

L37 Longuet, P., Burglen, L. and Zelwer, A. (1973). *Rev. Matér. Constr.* (676) 35.

L38 Lashchenko, V.A. and Loganina, V.I. (1974). *Zh. Prikl. Khim.* **47**, 645 (p. 646 in English translation).

L39 Locher, F.W., in *7th ICCC*, Vol. 4, p. 49 (1981).

L40 Locher, F.W., Richartz, W. and Sprung, S. (1980). *Zem.-Kalk-Gips* **33**, 271 (partial English translation, p. 150).
L41 Lerch, W. (1946). *Proc. ASTM* **46**, 1252.
L42 Locher, F.W., in *Symposium on Structure of Portland Cement Paste and Concrete*, p. 300, Sp. Rpt 90, Highway Research Board, Washington, DC (1966).
L43 Lapasin, R. (1982). *Cemento* **79**, 243.
L44 Lawrence, C.D., *An Examination of Possible Errors in the Determination of Nitrogen Isotherms on Hydrated Cements* (Techn. Rpt 520), 29pp., Cement and Concrete Association, Slough (1978).
L45 Litvan, G.G. (1976). *Cem. Concr. Res.* **6**, 139.
L46 Lawrence, C.D., Gimblett, F.G.R. and Sing, K.S.W., in *7th ICCC*, Vol. 3, p. VI-141 (1980).
L47 Lawrence, C.D., *The Interpretation of Nitrogen Sorption Isotherms on Hydrated Cement* (Techn. Rpt 530), 28pp., Cement and Concrete Association, Slough (1980).
L48 Luke, K. and Glasser, F.P. (1988). *Cem. Concr. Res.* **18**, 495.
L49 Lumley, J.S., Gollop, R.S., Moir, G.K. and Taylor, H.F.W. (1996). *Cem. Concr. Res.* **26**, 139.
L50 Lukas, W. (1976). *Matér. Constr.* **9**, 331.
L51 Lu, P., Sun, G. and Young, J.F. (1993). *J. Am. Ceram. Soc.* **76**, 1003.
L52 Lewis, M.C. and Scrivener, K.L. (1996). Private communication.
L53 Lossier, H. (1936). *Génie Civil.* (109) 285.
L54 Long, G.R., in *5th IC Cem. Microsc.*, p. 86 (1983).
L55 Lafuma, H. (1929). *Rev. Matér. Constr. Trav. Publ.* (243) 441.
L56 Long, G.R., Longman, P.A. and Gartshore, G.C., in *9th IC Cem. Microsc.*, p. 263 (1987).
L57 Locher, F., in *8th ICCC*, Vol. 1, p. 57 (1986).
L58 Libermann, G.V. and Kireev, V.A. (1964). *Zh. Prikl. Khim.* **37**, 194.
L59 Langton, C.A., White, E.L., Grutzeck, M.W. and Roy, D.M., in *7th ICCC*, Vol. 3, p. V-145 (1980).
L60 Lyubimova, T.Yu. and Pinus, E.R. (1962). *Kolloidn. Zh.* **24**, 491
L61 Locher, F.W. (1966). *Zem.-Kalk-Gips* **19**, 395.
L62 Ludwig, U. and Mehr, S., in *8th ICCC*, Vol. 5, p. 181 (1986).
L63 Lawrence, C.D., *Laboratory Studies of Concrete Expansion Arising from Delayed Ettringite Formation*, 147pp., BCA Publ. C/16, British Cement Association, Crowthorne (1993).
L64 Lawrence, C.D. (1995). *Cem. Concr. Res.* **25**, 903.
L65 Lewis, M.C., Scrivener, K.L. and Kelham, S. (1995). *Mater. Res. Soc. Symp. Proc.* **370**, 67.
L66 Litvan, G.G. (1972). *J. Am. Ceram. Soc.* **55**, 38.

M1 Maki, I. and Chromý, S. (1978). *Cem. Concr. Res.* **8**, 407.
M2 Maki, I. and Chromý, S. (1978). *Cemento* **75**, 247.
M3 Maki, I. (1979). *Cemento* **76**, 167.
M4 Maki, I. and Kato, K. (1982). *Cem. Concr. Res.* **12**, 93.
M5 Maki, I., in *8th ICCC*, Vol. 1, p. 34 (1986).
M6 Mumme, W.G. (1995). *Neues Jahrb. Mineral. Monatsh.*, 145.
M7 Maki, I., Fukuda, K., Yoshida, H. and Kumaki, J. (1992). *J. Am. Ceram. Soc.* **75**, 3163.
M8 Moranville-Regourd, M. and Boikova, A.I., in *9th ICCC*, Vol. 1, p. 3 (1992).

M9 Maki, I. and Goto, K. (1982). *Cem. Concr. Res.* **12**, 301.
M10 Maki, I. (1984). *Cemento* **81**, 165.
M11 Maki, I., in *Cement Technology* (Ceram. Trans. Vol. 40, ed. E.M. Gartner and H. Uchikawa), p. 3, American Ceramic Society, Westerville, OH (1994).
M12 Moir, G.K. (1983). *Phil. Trans. R. Soc. London* **A310**, 127.
M13 Mumme, W.G., Hill, R.J., Bushnell-Wye, G. and Segnit, E.R. (1995). *Neues Jahrb. Mineral. Abhandl.* **169**, 35.
M14 Moore, P.B. (1973). *Am. Mineral.* **58**, 32.
M15 Midgley, C.M. (1952). *Acta Cryst.* **5**, 307.
M16 Moore, P.B. and Araki, T. (1976). *Am. Mineral.* **61**, 74.
M17 Mondal, P. and Jeffery, J.W. (1975). *Acta Cryst.* **B31**, 689.
M18 Maki, I. (1973). *Cem. Concr. Res.* **3**, 295.
M19 Maki, I. (1976). *Cem. Concr. Res.* **6**, 183.
M20 Maki, I. (1976). *Cem. Concr. Res.* **6**, 797.
M21 Maki, I. (1974). *Cem. Concr. Res.* **4**, 87.
M22 Morris, M.C., McMurdie, H.F., Evans, E.H., Paretzkin, B. and de Groot, J.H. *Standard X-ray Diffraction Powder Patterns* (NBS Monograph 25, Section 16), 186pp., US Dept of Commerce, Washington, DC (1979).
M23 Marinho, M.B. and Glasser, F.P. (1984). *Cem. Concr. Res.* **14**, 360.
M24 Miyazawa, K. and Tomita, K., in *5th ISCC*, Vol. 1, p. 252 (1969).
M25 Maki, I., Fukuda, K., Oba, E., Yoshida, M. and Ito, S. (1995). *Cem. Concr. Res.* **25**, 863.
M26 Muan, A. and Osborn, E.F. *Phase Equilibria among Oxides in Steelmaking*, 236pp., Addison-Wesley, Reading, MA (1965).
M27 Majumdar, A.J. (1965). *Trans. Br. Ceram. Soc.* **64**, 105.
M28 Moseley, D. and Glasser, F.P. (1981). *Cem. Concr. Res.* **11**, 559.
M29 McMurdie, H.F. and Insley, H. (1936). *J. Res. Nat. Bur. Stand.* **16**, 467.
M30 Majumdar, A.J. (1964). *Trans. Br. Ceram. Soc.* **63**, 347.
M31 Midgley, H.G. (1979). *Cem. Concr. Res.* **9**, 623.
M32 McGinnety, J.A. (1972). *Acta Cryst.* **B28**, 2845.
M33 Mehrotra, B.N., Hahn, T., Eysel, W., Röpke, H. and Illguth, A. (1978). *Neues Jahrb. Mineral. Monatsh.* 408.
M34 Maki, I., Nakagawa, K., Hiraiwa, K. and Nonami, T. (1984). *Cemento* **81**, 3.
M35 Moore, A.E. (1976). *Cem. Technol.* **7**, 85, 134.
M36 Maki, I., Fukuda, K., Imura, T., Yoshida, H. and Ito, S. (1995). *Cem. Concr. Res.* **25**, 835.
M37 Maki, I., Haba, H. and Takahashi, S. (1983). *Cem. Concr. Res.* **13**, 689.
M38 Maki, I. and Takahashi, S. (1984). *Cem. Concr. Res.* **14**, 413.
M39 Miller, F.M., in *Research on the Manufacture and Use of Cements*, p. 21, Engineering Foundation, New York (1986).
M40 Mohan, K. and Glasser, F.P. (1977). *Cem. Concr. Res.* **7**, 1, 269, 379.
M41 Moir, G.K., private communication.
M42 Méric, J.P., in *7th ICCC*, Vol. 1, p. I-4/1 (1980).
M43 Maultzsch, M., Gierloff, M. and Schimmelwitz, P., in *7th ICCC*, Vol. 2, p. I-128 (1980).
M44 Midgley, H.G., in *3rd ISCC*, p. 140 (1954).
M45 Märten, A., Knöfel, D. and Strunge, J. (1994). *World Cem.* **25** (8) 49.
M46 Mohan, K. and Taylor, H.F.W. (1981). *J. Am. Ceram. Soc.* **64**, 717.
M47 Midgley, H.G. (1979). *Cem. Concr. Res.* **9**, 77.

M48 Ménétrier, D., Jawed, I., Sun, T.S. and Skalny, J. (1979). *Cem. Concr. Res.* **9**, 473.
M49 Ménétrier, D., Jawed, I. and Skalny, J. (1980). *Silicates Ind.* **45**, 243.
M50 Ménétrier, D., Jawed, I. and Skalny, J. (1980). *Cem. Concr. Res.* **10**, 697.
M51 Ménétrier, D., McNamara, D.K., Jawed, I. and Skalny, J. (1980). *Cem. Concr. Res.* **10**, 107.
M52 Melzer, R. and Eberhard, E. (1989). *Cem. Concr. Res.* **19**, 411.
M53 McConnell, J.D.C. (1955). *Mineral. Mag.* **30**, 293, 672.
M54 Megaw, H.D. and Kelsey, C.H. (1956). *Nature* **177**, 390.
M55 Mitsuda, T. and Taylor, H.F.W. (1978). *Mineral. Mag.* **42**, 229.
M56 Mohan, K. and Taylor, H.F.W. (1982). *Cem. Concr. Res.* **12**, 25.
M57 Massazza, F. and Testolin, M. (1983). *Cemento* **80**, 49.
M58 Michaux, M., Ménétrier, D. and Barret, P. (1983). *Comptes Rendus Acad. Sci. Paris* (Ser. 2) **296**, 1043.
M59 Milestone, N.B., in *7th ICCC*, Vol. 3, p. VI-61 (1980).
M60 Macphee, D.E., Lachowski, E.E. and Glasser, F.P. (1988). *Adv. Cem. Res.* **1**, 131.
M61 Macphee, D.E., Luke, K., Glasser, F.P. and Lachowski, E.E. (1989). *J. Am. Ceram. Soc.* **72**, 646.
M62 Maycock, J.N., Skalny, J. and Kalyoncu, R. (1974). *Cem. Concr. Res.* **4**, 835.
M63 Ménétrier, D., Jawed, I., Sun, T.S. and Skalny, J. (1980). *Cem. Concr. Res.* **10**, 425.
M64 Mehta, P.K. and Klein, A. in *Symposium on Structure of Portland Cement Paste and Concrete* (Sp. Rpt 90), p. 328, Highway Res. Board, Washington, DC (1966).
M65 Malquori, G. and Caruso, E. (1938). *Atti 10° Congr. Int. Chim.* (Rome) **2**, 713; *Chem. Abstr.* **33**, 8134 (1939).
M66 Midgley, H.G. and Rosaman, D., in *4th ISCC*, Vol. 1, p. 259 (1962).
M67 Moore, A.E. and Taylor, H.F.W. (1968). *Nature* **218**, 1048.
M68 Moore, A.E. and Taylor, H.F.W. (1970). *Acta Cryst.* **B26**, 386.
M69 Mylius, C.R.W. (1933). *Acta Acad. Aboensis, Math. Phys.* **7** (3), 147pp.
M70 Moenke, H. (1964). *Naturwiss.* **51**, 239.
M71 Millet, J., Bernard, A., Hommey, R., Poindefert, A. and Voinovitch, I.A. (1980). *Bull. Liaison Lab. Ponts Chaussées* **109**, 91.
M72 Majumdar, A.J. and Roy, R. (1956). *J. Am. Ceram. Soc.* **39**, 434.
M73 Mascolo, G. and Marino, O. (1980). *Mineral. Mag.* **43**, 619.
M74 MacKenzie, K.J.D., Meinhold, R.H., Sherriff, B.L. and Xu, Z. (1993). *J. Mater. Chem.* **3**, 1263.
M75 Miyata, S. (1980). *Clays and Clay Minerals* **28**, 50.
M76 Murakami, K., in *5th ISCC*, Vol. 4, p. 457 (1969).
M77 Mehta, P.K. (1976). *Cem. Concr. Res.* **6**, 169.
M78 Mather, K., in *Evaluation of Methods of Identifying Phases of Cement Paste* (ed. W.L. Dolch), p. 9, Transportation Res. Circ. 176, Transportation Research Board, Washington, DC (1976).
M79 Marchese, B. (1980). *Cem. Concr. Res.* **10**, 861.
M80 Mehta, P.K. (1981). *Cem. Concr. Res.* **11**, 507.
M81 Mikhail, R. Sh., Copeland, L.E. and Brunauer, S. (1964). *Canad. J. Chem.* **42**, 426.
M82 McCarter, W.J. and Afshar, A.B. (1985). *J. Mater. Sci. Lett.* **4**, 405.
M83 McCarter, W.J. and Brousseau, R. (1990). *Cem. Concr. Res.* **20**, 891.

M84 MacTavish, J.C., Miljkovic, L., Pintar, M.M., Blinc, R. and Lahajnar, G. (1985). *Cem. Concr. Res.* **15**, 367.
M85 MacTavish, J.C., Miljković, L., Schreiner, L.J., Pintar, M.M., Blinc, R. and Lahajnar, G. (1985). *Zeit. Naturforschung* **A40**, 32.
M86 Mindess, S. and Young, J.F. *Concrete*, 671pp., Prentice-Hall, Englewood Cliffs, NJ (1981).
M87 Mindess, S. (1970). *J. Am. Ceram. Soc.* **53**, 621.
M88 Mehta, P.K. and Manmohan, D., in *7th ICCC*, Vol. 3, p. VII-1 (1980).
M89 Marsh, B.K. (1986). PhD thesis, quoted by R.F. Feldman in F42.
M90 Midgley, H.G. and Pettifer, K. (1971). *Cem. Concr. Res.* **1**, 101.
M91 Mather, B., in *5th ISCC*, Vol. 4, p. 113 (1969).
M92 Monk, M. (1983). *Mag. Concr. Res.* **35**, 131.
M93 Mohan, K. and Taylor, H.F.W., in *Effects of Flyash Incorporation in Cement and Concrete* (ed. S. Diamond), p. 54, Materials Research Society, University Park, PA (1981).
M94 Malquori, G., in *4th ISCC*, Vol. 2, p. 983 (1962).
M95 Massazza, F. (1976). *Cemento* **73**, 3.
M96 Massazza, F. and Costa, U. (1979). *Cemento* **76**, 3.
M97 McCarthy, G.J., Swanson, K.D., Keller, L.P. and Blatter, W.C. (1984). *Cem. Concr. Res.* **14**, 471.
M98 McCarthy, G.J., Butler, R.D., Brekke, D.W., Ademek, S.D., Parks, J.A., Foster, H.J. and Solc, J. (1995). *Mater. Res. Soc. Symp. Proc.*, **370**, 179.
M99 Mehta, P.K. and Groney, P.R. (1977). *J. Am. Concr. Inst. (Proc.)* **74**, 440.
M100 Manmohan, D. and Mehta, P.K. (1981). *Cem. Concr. Aggr.* **3**, 63.
M101 Marsh, B.K., Day, R.L. and Bonner, D.G. (1985). *Cem. Concr. Res.* **15**, 1027.
M102 Muzhen, S., Kurdowski, W. and Sorrentino, F. in *9th ICCC*. Vol. 1, p. 317 (1992).
M103 Ménétrier-Sorrentino, D. (1989). Private communication.
M104 Ménétrier-Sorrentino, D., George, C.M. and Sorrentino, F.P., in *8th ICCC*, Vol. 4, p. 334 (1986).
M105 Müller, D., Rettel, A., Gessner, W. and Scheler, G. (1984). *J. Magn. Res.* **57**, 152.
M106 Midgley, H.G., in *International Seminary on Calcium Aluminates* (ed. M. Murat *et al.*), Politecnico di Torino, Turin (1982).
M107 Ministère de l'Environnement, France (1979). Circular 79-34 of 27 March 1979.
M108 Marcdargent, S. and Mathieu, A. (1989). Private communication.
M109 Midgley, H.G. (1984). *Clay Minerals* **19**, 857.
M110 Majumdar, A.J., Singh, B. and Edmonds, R.N. (1990). *Cem. Concr. Res.* **20**, 197.
M111 Midgley, H.G., in *7th ICCC*, Vol. 3, p. V-85 (1980).
M112 Mehta, P. and Polivka, M., in *6th ICCC*, Vol. 3, p. 158 (1976).
M113 Mikhailov, V.V., in *4th ISCC*, Vol. 2, p. 927 (1962).
M114 Mikhailov, V.V., in *Klein Symposium on Expansive Cement Concretes* (Sp. Publ. SP38), p. 415, American Concrete Institute, Detroit, MI (1973).
M115 Mehta, P.K. (1973). *Cem. Concr. Res.* **3**, 1.
M116 Mehta, P.K. (1980). *World Cem. Technol.* **11**, 166.
M117 Massazza, F. and Gilioli, C. (1983). *Cemento* **80**, 101.
M118 Milestone, N.B. (1976). *Cem. Concr. Res.* **6**, 89.

M119 Massazza, F. and Testolin, M. (1980). *Cemento* **77**, 73.
M120 Massazza, F. and Costa, U., in *7th ICCC*, Vol. 4, p. 529 (1981).
M121 Murakami, K. and Tanaka, H., in *5th ISCC*, Vol. 2, p. 422 (1969).
M122 Murat, M., El Hajjouji, A. and Comel, C. (1987). *Cem. Concr. Res.* **17**, 633.
M123 Mironov, S.A., in *6th ICCC*, Vol. 2, Part 1, p. 182 (1976).
M124 Mironov, S.A., Kourbatova, I.I., Ivanova, O.S. and Vyssotsky, S.A., in *7th ICCC*, Vol. 2, p. II-52 (1980).
M125 Mitsuda, T., Sasaki, K. and Ishida, H. (1992). *J. Am. Ceram. Soc.* **75**, 1858.
M126 Menzel, C.A. (1935). *J. Am. Concr. Inst. (Proc.)* **31**, 125.
M127 Marsh, R.E. (1994). *Acta Cryst.* **C50**, 996.
M128 Mitsuda, T., Kobayakawa, S. and Toraya, H., in *8th ICCC*, Vol. 3, p. 173 (1986).
M129 Mitsuda, T. and Chan, C.F. (1977). *Cem. Concr. Res.* **7**, 191.
M130 Maso, J.C., in *7th ICCC*, Vol. 1, p. VII-1/3 (1980).
M131 Massazza, F. and Costa, U., in *8th ICCC*, Vol. 1, p. 158 (1986).
M132 Monteiro, P.J.M., Maso, J.C. and Ollivier, J.P. (1985). *Cem. Concr. Res.* **15**, 953.
M133 Monteiro, P.J.M. and Mehta, P.K. (1985). *Cem. Concr. Res.* **15**, 378.
M134 Monteiro, P.J.M. and Mehta, P.K. (1986). *Cem. Concr. Res.* **16**, 127.
M135 Manns, W. and Wesche, K., in *5th ISCC*, Vol. 3, p. 385 (1969).
M136 Midgley, H.G. and Illston, J.M. (1984). *Cem. Concr. Res.* **14**, 546.
M137 Monteiro, P.J.M., Gjorv, O.E. and Mehta, P.K. (1985). *Cem. Concr. Res.* **15**, 781.
M138 Merlino, S. (1983). *Am. Mineral.* **68**, 614.
M139 Mielenz, R.C., Greene, K.T. and Benton, E.J. (1947). *J. Am. Concr. Inst. (Proc.)* **44**, 193.
M140 Mehta, P.K. in *Materials Science of Concrete III* (ed. J. Skalny), p. 105. American Ceramic Society, Westerville, OH (1992).
M141 Marchese, B. and Sersale, R., in *5th ISCC*, Vol. 2, p. 133 (1969).
M142 Mielenz, R.C., Marusin, S.L., Hime, W.G. and Jugovic, Z.T. (1995). *Concr. Int.* **17**(12), 62.
M143 Marusin, S.L., in *15th IC Cem. Microsc.*, p. 289 (1993).
M144 Massazza, F. (1985). *Cemento* **82**, 3.
M145 Majumdar, A.J. (1974). *Cem. Concr. Res.* **4**, 247.

N1 Nishi, F., Takéuchi, Y. and Maki, I. (1985). *Zeit. Krist.* **172**, 297.
N2 Nishi, F. and Takéuchi, Y. (1984). *Zeit. Krist.* **168**, 197.
N3 Niesel, K. and Thormann, P. (1967). *Tonind. Zeit.* **91**, 362.
N4 Nishi, F. and Takéuchi, Y. (1975). *Acta Cryst.* **B31**, 1169.
N5 Neubauer, J., Sieber, R., Kuzel, H.-J. and Ecker, M. (1996). *Cem. Concr. Res.* **26**, 77.
N6 Nurse, R.W. and Welch, J.H., quoted by R.W. Nurse, in *4th ISCC*, Vol. 1, p. 9 (1962).
N7 Nurse, R.W., Welch, J.H. and Majumdar, A.J. (1965). *Trans. Br. Ceram. Soc.* **64**, 409.
N8 Nurse, R.W., Welch, J.H. and Majumdar, A.J. (1965). *Trans. Br. Ceram. Soc.* **64**, 323.
N9 Newkirk, T.F. and Thwaite, R.D. (1958). *J. Res. Nat. Bur. Stand.* **61**, 233.
N10 Newkirk, T.F., in *3rd ISCC*, p. 151 (1954).
N11 Nurse, R.W. (1949). *J. Sci. Instrum.* **26**, 102.
N12 Newman, E.S. and Hoffman, R. (1956). *J. Res. Nat. Bur. Stand.* **56**, 319.

N13 Nurse, R.W., Welch, J.H. and Gutt, W. (1959). *J. Chem. Soc.* 1077.
N14 Norris, A.C. *Computational Chemistry*, 454pp., Wiley, Chichester (1981).
N15 Nikushchenko, V.M., Khotimchenko, V.S., Rumyantsev, P.F. and Kalinin, A.I. (1973). *Cem. Concr. Res.* **3**, 625.
N16 Newton, R.G. and Sharp, J.H. (1987). *Cem. Concr. Res.* **17**, 77.
N17 Neal, C. and Stanger, G. (1984). *Mineral. Mag.* **48**, 237.
N18 Nyame, B.K. and Illston, J.M., in *7th ICCC*, Vol. 3, p. VI-181 (1980).
N19 Nakamura, T., Sudoh, G. and Akaiwa, S., in *5th ISCC*, Vol. 4, p. 351 (1969).
N20 Noudelman, B.I. and Gadaev, A.I., in *8th ICCC*, Vol. 2, p. 347 (1986).
N21 Nelson, E.B. *Well Cementing*, Schlumberger Educational Services, Houston, TX (1990)
N22 Nixon, P.J., Canham, I. and Bollinghaus, R., in *Concrete Alkali–Aggregate Reactions* (ed. P.E. Grattan-Bellew), p. 110, Noyes Publ., Park Ridge, NJ (1987).
N23 Nielsen, J. in *Symposium on the Effects of Aggressive Fluids on Concrete* (Highway Res. Record, Vol. 113), p. 114. National Research Council, Washington, DC (1966).

O1 Ono, Y., Kawamura, S. and Soda, Y., in *5th ISCC*, Vol. 1, p. 275 (1969).
O2 Ono, M. and Nagashima, N., in *6th ICCC*, Vol. 1, p. 170 (1976).
O3 Ol'shanskii, Ya.I. (1951). *Doklady Akad. Nauk SSSR* **76**, 93.
O4 Ohashi, Y. (1984). *Phys. Chem. Minerals* **10**, 217.
O5 Okada, K. and Ossaka, J. (1980). *Acta Cryst.* **B36**, 919.
O6 Odler, I. and Dörr, H. (1977). *Am. Ceram. Soc. Bull.* **56**, 1086.
O7 Ono, Y., in *3rd IC Cem. Microsc.*, p. 198 (1981).
O8 Odler, I. and Zhang, H. (1996). *World Cem. Res. Dev.* **27** (2) 73.
O9 Osbaeck, B. and Jøns, E.S., in *7th ICCC*, Vol. 2, p. II-135 (1980).
O10 Odler, I., Abdul-Maula, S., Nudling, P. and Richter, T. (1981). *Zem.-Kalk-Gips* **34**, 445 (partial English translation, p. 240).
O11 Odler, I. and Dörr, H. (1979). *Cem. Concr. Res.* **9**, 239.
O12 Odler, I. and Stassinopoulos, E.N. (1982). *TIZ* **106**, 394.
O13 Odler, I. and Schüppstuhl, J. (1981). *Cem. Concr. Res.* **11**, 765.
O14 Odler, I. and Dörr, H. (1979). *Cem. Concr. Res.* **9**, 277.
O15 Odler, I. and Schüppstuhl, J. (1982). *Cem. Concr. Res.* **12,** 13.
O16 Odler, I. and Abdul-Maula, S. (1984). *Cem. Concr. Res.* **14**, 133.
O17 Ogawa, K. and Roy, D.M. (1981). *Cem. Concr. Res.* **11**, 741.
O18 Odler, I. and Chen, Y. (1995). *Cem. Concr. Res.* **25**, 853.
O19 Odler, I., in *7th ICCC*, Vol. 4, p. 493 (1981).
O20 Odler, I. and Wonneman, R., in *7th ICCC*, Vol. 4, p. 510 (1981).
O21 Odler, I. and Köster, H. (1986). *Cem. Concr. Res.* **16**, 893.
O22 Odler, I. and Rössler, M. (1985). *Cem. Concr. Res.* **15**, 401.
O23 Ogawa, K., Uchikawa, H., Takemoto, K. and Yasui, I. (1980). *Cem. Concr. Res.* **10**, 683.
O24 Odler, I. and Skalny, J., in *Materials Science of Concrete III* (ed. J. Skalny), p. 319, American Ceramic Society, Westerville, OH (1992).
O25 Odler, I. and Jawed, I. in *Materials Science of Concrete II* (eds. J. Skalny and S. Mindess), p. 221, American Ceramic Society, Westerville, OH (1991).
O26 Ogawa, K. and Roy, D.M. (1982). *Cem. Concr. Res.* **12**, 101, 247.
O27 Okushima, M., Kondo, R., Muguruma, H. and Ono, Y., in 5th ISCC, Vol. 4, p. 419 (1969).

O28 Okada, Y., Ishida, H., Sasaki, K., Young, J.F. and Mitsuda, T. (1994). *J. Am. Ceram. Soc.* **77**, 1313.
O29 Odler, I. and Skalny, J. (1973). *J. Chem. Technol. Biotechnol.* **23**, 661.
O30 Odler, I., Abdul-Maula, S and Lu Z.-Y. (1987). *Mater. Res. Soc. Symp. Proc.* **85**, 139.
O31 Oyefesobi, S.O. and Roy, D.M. (1976). *Cem. Concr. Res.* **6**, 803.
O32 Ozol, M.A., in *Alkali–Aggregate Reaction–Preventive Measures*, p. 113, Icelandic Building Research Institute, Reykjavik (1975).
O33 Oberholster, R.E., Du Toit, P. and Pretorius, J.L., in *6th IC Cem. Microsc.*, p. 360 (1984).
O34 Oberholster, R.E., Maree, H. and Brand, J.H.B., in *9th International Conference on Alkali–Aggregate Reaction in Concrete*, Vol. 2, p. 739, The Concrete Society, Wexham (1992).

P1 *Powder Diffraction File* (various formats). JCPDS International Centre for Diffraction Data, Swarthmore, PA (1989) and later supplements.
P2 Pollitt, H.W.W. and Brown, A.W., in *5th ISCC*, Vol. 1, p. 322 (1969).
P3 Ponomarev, V.I., Kheiker, D.M. and Belov, N.V. (1971). *Sov. Phys. Cryst.* **15**, 799 (translated from *Kristallografiya* **15**, 918).
P4 Phillips, B. and Muan, A. (1959). *J. Am. Ceram. Soc.* **42**, 413.
P5 Parker, T.W., in *3rd ISCC*, p. 485 (1954).
P6 Pryce, M.W. (1972). *Mineral. Mag.* **38**, 968.
P7 Pliego-Cuervo, Y.B. and Glasser, F.P. (1978). *Cem. Concr. Res.* **8**, 455.
P8 Pliego-Cuervo, Y.B. and Glasser, F.P. (1979). *Cem. Concr. Res.* **9**, 51.
P9 Pliego-Cuervo, Y.B. and Glasser, F.P. (1977). *Cem. Concr. Res.* **7**, 477.
P10 Pliego-Cuervo, Y.B. and Glasser, F.P. (1979). *Cem. Concr. Res.* **9**, 573.
P11 Péréz-Mendez, M., Howie, R.A. and Glasser, F.P. (1984). *Cem. Concr. Res.* **14**, 57.
P12 Péréz-Mendez, M., Fayos, J., Howie, R.A., Gard, J.A. and Glasser, F.P. (1985). *Cem. Concr. Res.* **15**, 600.
P13 Peray, K. *The Rotary Cement Kiln* (2nd Edn), 389pp., Arnold, London (1986).
P14 Péréz-Mendez, M. and Fayos, J., in *8th ICCC*, Vol. 2, p. 223 (1986).
P15 Petersen, I.F. and Johansen, V. (1979). *Cem. Concr. Res.* **9**, 631.
P16 Petersen, I.F. (1983). *World Cem. Technol.* **14**, 188, 220.
P17 Petersen, I.F., in *8th ICCC*, Vol. 2, p. 21 (1986).
P18 Petch, H.E. (1961). *Acta Cryst.* **14**, 950.
P19 Parrott, L.J., Patel, R.G., Killoh, D.C. and Jennings, H.M. (1984). *J. Am. Ceram. Soc.* **67**, 233.
P20 Powers, T.C. and Brownyard, T.L. *Studies of the Physical Properties of Hardened Portland Cement Paste* (Bull. 22), 992pp., Portland Cement Association, Chicago, IL (1948); reprinted from *J. Am. Concr. Inst. (Proc.)* (1947) **43**, 101, 249, 469, 549, 669, 845, 993.
P21 Parrott, L.J. and Young, J.F. (1981). *Cem. Concr. Res.* **11**, 11.
P22 Prosen, E.J., Brown, P.W., Frohnsdorff, G. and Davis, F. (1985). *Cem. Concr. Res.* **15**, 703.
P23 Pöllmann, H. (1989). *Neues Jahrb. Mineral. Abhandl.* **161**, 27.
P24 Pöllmann, H., Kuzel, H.-J. and Wenda, R. (1989). *Neues Jahrb. Mineral. Abhandl.* **160**, 133.
P25 Poellmann, H. and Kuzel, H.-J. (1990). *Cem. Concr. Res.* **20**, 941.
P26 Poellmann, H., St. Auer, Kuzel, H.-J. and Wenda, R. (1993). *Cem. Concr. Res.* **23**, 422.

P27 Passaglia, E. and Rinaldi, R. (1984). *Bull. Minéral. (Paris)* **107**, 605.
P28 Pedersen, B.F. and Semmingsen, D. (1982). *Acta Cryst.* **B38**, 1074.
P29 Posnjak, E. (1938). *Am. J. Sci.* **A35**, 247.
P30 Percival, A. and Taylor, H.F.W. (1959). *J. Chem. Soc.* 2629.
P31 Plowman, C. and Cabrera, J.G. (1984). *Cem. Concr. Res.* **14**, 238.
P32 Pratt, P.L. and Ghose, A. (1983). *Phil. Trans. R. Soc. London* **A310**, 93.
P33 Patel, R.G., Killoh, D.C., Parrott, L.J. and Gutteridge, W.A. (1988). *Matér. Constr.* **21**, 192.
P34 Pressler, E.E., Brunauer, S., Kantro, D.L. and Weise, C.H. (1961). *Analyt. Chem.* **33**, 877.
P35 Parrott, L.J. and Killoh, D.C. (1984). *Br. Ceram. Proc.* (35) 41.
P36 Powers, T.C., in *4th ISCC*, Vol. 2, p. 577 (1962).
P37 Parrott, L.J., in *Research on the Manufacture and Use of Cements*, p. 43, Engineering Foundation, New York (1986).
P38 Parrott, L.J., in *Materials Science of Concrete I* (ed. J.P. Skalny), p. 181, American Ceramic Society, Westerville, OH (1989).
P39 Parrott, L. (1987). *Mater. Res. Soc. Symp. Proc.* **85**, 91.
P40 Parrott, L.J. (1981). *Cem. Concr. Res.* **11**, 651.
P41 Parrott, L.J., Hansen, W. and Berger, R.L. (1980). *Cem. Concr. Res.* **10**, 647.
P42 Parrott, L.J. and Young, J.F., in *Fundamental Research on Creep and Shrinkage of Concrete* (ed. F.H. Wittmann), p. 35, Martinus Nijhoff, The Hague (1982).
P43 Pearson, D., Allen, A., Windsor, C.G., Alford, N.McN. and Double, D.D. (1983). *J. Mater. Sci.* **18**, 430.
P44 Pratt, P.L. (1987). *Mater. Res. Soc. Symp. Proc.* **85**, 145.
P45 Parrott, L.J. (1977). *Cem. Concr. Res.* **7**, 597.
P46 Parrott, L.J. (1977). *Mag. Concr. Res.* **29**, 26.
P47 Powers, T.C., Copeland, L.E. and Mann, H.M. (1959). *J. PCA Res. Dev. Labs* **1** (2), 38.
P48 Page, C.L., Short, N.R. and El Tarras, A. (1981). *Cem. Concr. Res.* **11**, 395.
P49 Poon, C.S. and Groves, G.W.(1988). *J. Mater. Sci. Lett.* **7**, 243.
P50 Péréz, M., Vázquez, T. and Triviño, F. (1983). *Cem. Concr. Res.* **13**, 759.
P51 Percival, A., Buttler, F.P. and Taylor, H.F.W., in *4th ISCC*, Vol. 1, p. 277 (1962).
P52 Péréz Mendez, M. and Triviño Vázquez, F. (1984). *Cem. Concr. Res.* **14**, 161.
P53 Page, C.L. and Vennesland, Ø. (1983). *Matér. Constr.* **16**, 19.
P54 Patel, H.H., Bland, C.H. and Poole, A.B. (1996). *Adv. Cem. Res.* **8**, 11.
P55 Purton, M.J. (1973). *J. Appl. Chem. Biotechnol.* **23**, 871.
P56 Peacor, D.R., Sarp, H., Dunn, P.J., Innes, J. and Nelen, J.A. (1988). *Am. Mineral.* **73**, 888.
P57 Patel, R.G., Parrott, L.J., Martin, J.A. and Killoh, D.C. (1985). *Cem. Concr. Res.* **15**, 343.
P58 Page, C.L., Short, N.R. and Holden, W.R. (1986). *Cem. Concr. Res.* **16**, 79.
P59 Pettifer, K. and Nixon, P.J. (1980). *Cem. Concr. Res.* **10**, 173.
P60 Powers, T.C. and Steinour, H.H. (1955). *J. Am. Concr. Inst (Proc.)* **51**, 497, 785.
P61 Patel, H.H., Bland, C.H. and Poole, A.B. in *18th IC Cem. Microsc.*, p. 112 (1996).
P62 Powers, T.C. (1945). *J. Am. Concr. Inst. (Proc.)* **41**, 245.

P63 Powers, T.C. and Helmuth, R.A. (1953). *Proc. [US] Highway Res. Board* **32**, 285.
P64 Pagenkopf, G.K. *Introduction to Natural Water Chemistry*, 272pp., Marcel Dekker, New York (1978).
P65 Penner, E., Gillott, J.E. and Eden, W.J. (1970). *Canad. Geotech. J.* **7**, 333.
P66 Philleo, R. (1958). *J. Am. Concr. Inst. (Proc.)* **54**, 857.
P67 Piasta, J., Sawicz, Z. and Rudzinski, L. (1984). *Matér. Constr.* **17**, 291.

Q1 Qian, J.C., Lachowski, E.E. and Glasser, F.P. (1988). *Mater. Res. Soc. Symp. Proc.* **113**, 45.

R1 Regourd, M. and Guinier, A., in *6th ICCC*, Vol. 1, p. 25 (1976).
R2 Regourd, M. (1967). *Rev. Matér. Constr.* (620) 167.
R3 Regourd, M., Bigaré, M., Forest, J. and Guinier, A., in *5th ISCC*, Vol. 1, p. 44 (1969).
R4 Rankin, G.A. and Wright, F.E (1915). *Am. J. Sci.* (4th series) **39**, 31.
R5 Regourd, M., Chromý, S., Hjorth, L., Mortureux, B. and Guinier, A. (1973). *J. Appl. Cryst.* **6**, 355.
R6 Richardson, I.G., Hall, C. and Groves, G.W. (1993). *Adv. Cem. Res.* **5**, 15.
R7 Roy, D.M. and Roy, R., in *4th ISCC*, Vol. 1, p. 307 (1962).
R8 Rowe, J.J., Morey, G.W. and Hansen, I.D. (1965). *J. Inorg. Nucl. Chem.* **27**, 53.
R9 Ragozina, T.A. (1957). *Zh. Prikl. Khim.* **30**, 1682.
R10 Ritzmann, H. (1971). *Zem.-Kalk-Gips* **24**, 338.
R11 Rivera, M., Odler, I. and Abdul-Maula, S. (1987). *Adv. Cem. Res.* **1**, 52.
R12 Rouanet, A., in *8th ICCC*, Vol. 2, p. 25 (1986).
R13 Ritzmann, H. (1968). *Zem.-Kalk-Gips* **21**, 390.
R14 Regourd, M., Hornain, H. and Mortureux, B., in *7th. ICCC*, Vol. 4, p. 477 (1981).
R15 Ramachandran, V.S. (1979). *Cem. Concr. Res.* **9**, 677.
R16 Relis, M. and Soroka, J. (1980). *Cem. Concr. Res.* **10**, 499.
R17 Richardson, I.G. and Groves, G.W. (1993). *J. Mater. Sci.* **28**, 265.
R18 Rayment, D.L. (1988). Private communication.
R19 Rodger, S.A, Groves, G.W., Clayden, N.J. and Dobson, C.M. (1988). *J. Am. Ceram. Soc.* **71**, 91.
R20 Rodger, SA., Groves, G.W., Clayden, N.J. and Dobson, C.M. (1987). *Mater. Res. Soc. Symp. Proc.* **85**, 13.
R21 Rassem, R., Zanni-Theveneau, H., Vernet, C., Heidemann, D., Grimmer, A.R., Barret, P., Nonat, A., Bertrandie, D. and Damidot, D., in *Hydration and Setting of Cements* (eds. A. Nonat and J.C. Mutin), p. 77, E & FN Spon, London, 1992.
R22 Richardson, I.G. and Groves, G.W. (1992). *Cem. Concr. Res.* **22**,1001.
R23 Richardson, I.G. and Groves, G.W. (1993). *Cem. Concr. Res.* **23**, 131.
R24 Regourd, M., Thomassin, J.H., Baillif, P. and Touray, J.C. (1980). *Cem. Concr. Res.* **10**, 223.
R25 Roberts, M.H., in *5th ISCC*, Vol. 2, p. 104 (1969).
R26 Richard, N., Lequeux, N. and Boch, P. (1995). *Eur. J. Solid State Inorg. Chem.* **32**, 649; J. Phys. III France **5**, 1849.
R27 Regourd, M., Hornain, H. and Mortureux, B. (1976). *Cem. Concr. Res.* **6**, 733.
R28 Rinaldi, R., Sacerdoti, M. and Passaglia, E. (1990). *Eur. J. Mineral.* **2**, 841.
R29 Rogers, D.E. and Aldridge, L.P. (1977). *Cem. Concr. Res.* **7**, 399.

R30 Roberts, M.H. (1970), quoted by F.M. Lea in L6.
R31 Reisdorf, K. and Abriel, W. (1988). *Zem.-Kalk-Gips* **41**, 356 (partial English translation, p. 218).
R32 Rodger, S.A. and Groves, G.W. (1989). *J. Am. Ceram. Soc.*, **72**, 1037.
R33 Rayment, D.L. and Majumdar, A.J. (1982). *Cem. Concr. Res.* **12**, 753.
R34 Rayment, D.L. and Lachowski, E.E. (1984). *Cem. Concr. Res.* **14**, 43.
R35 Rayment. P.L. (1982). *Cem. Concr. Res.* **12**, 133.
R36 Regourd, M., Mortureux, B. and Hornain, H., in *Fly Ash, Silica Fume, Slag and Other Mineral By-Products in Concrete* (ed. V.M. Malhotra), Sp. Publ. SP79, Vol. 2, p. 847, American Concrete Institute, Detroit, MI (1983).
R37 Rayment, D.L. (1986). *Cem. Concr. Res.* **16**, 341.
R38 Richardson, I.G. and Groves, G.W. (1992). *J. Mater. Sci.* **27**, 6204.
R39 Ramachandran, V.S., Beaudoin, J.J., Sarkar, S.L. and Aimin, X. (1993). *Cemento*, **90**, 73.
R40 Rössler, M. and Odler, I. (1985). *Cem. Concr. Res.* **15**, 320.
R41 Ramachandran, V.S., Feldman, R.F. and Beaudoin, J.J. *Concrete Science*, 427pp., Heyden, London (1981).
R42 Ryshkewitch, E. (1953). *J. Am. Ceram. Soc.* **36**, 65.
R43 Regourd, M., in *8th ICCC*, Vol. 1, p. 199 (1986).
R44 Regourd, M. (1985). *Chem. Scripta* **26A**, 37.
R45 Royak, S.M. and Chkolnik, J. Ch., in *7th ICCC*, Vol. 2, p. III-74 (1980).
R46 Richardson, I.G., Brough, A.R., Brydson, R., Groves, G.W. and Dobson, C.M. (1993). *J. Am. Ceram. Soc.* **76**, 2285.
R47 Regourd, M., in *7th ICCC*, Vol. 1, p. III-2/10 (1980).
R48 Richardson, I.G. and Groves, G.W. (1992). *J. Mater. Sci.* **27**, 6204.
R49 Regourd, M., Thomassin, J.H., Baillif, P. and Touray, J.C. (1983). *Cem. Concr. Res.* **13**, 549.
R50 Richardson, I.G., Brough, A.R., Groves, G.W. and Dobson, C.M. (1994). *Cem. Concr. Res.* **24**, 813.
R51 Ravina, D., in *Effects of Flyash Incorporation in Cement and Concrete* (ed. S. Diamond), p. 2, Materials Research Society, University Park, PA (1981).
R52 Richartz, E. (1984). *Zem.-Kalk-Gips* **37**, 62 (partial English translation, p. 65).
R53 Rodger, S.A. and Groves, G.W. (1988). *Adv. Cem. Res.* **1**, 84.
R54 Regourd, M., Mortureux, B., Aïtcin, P.C. and Pinsonneault, P., in *4th IC Cem. Microsc.*, p. 249 (1982).
R55 Richardson, I.G., Groves, G.W. and Rodger, S.A. (1989). *Mater. Res. Soc. Symp. Proc.* **137**, 313.
R56 Roy, D.M. and Parker, K.M., in *Fly Ash, Silica Fume, Slag and Other Mineral By-Products in Concrete* (ed. V.M. Malhotra), Sp. Publ. SP79, Vol. 1, p. 397, American Concrete Institute, Detroit, MI (1983).
R57 Rayment, D.L. and Majumdar, A.J. (1994). *Cem. Concr. Res.* **24**, 335.
R58 Rodger, S.A. and Double, D.D. (1984). *Cem. Concr. Res.* **14**, 73.
R59 Rashid, S., Barnes, P. and Turrillas, X. (1991/2). *Adv. Cem. Res.* **4**, 61.
R60 Rashid, S., Barnes, P., Bensted, J. and Turrillas, X. (1994). *J. Mater. Sci. Lett.* **13**, 1232.
R61 Rettel, A., Gessner, W., Müller, D. and Scheler, G. (1985). *Trans. J. Br. Ceram. Soc.* **84**, 25.
R62 Robson, T.D. *High-Alumina Cements and Concretes*, 263pp., Contractors Record Ltd (John Wiley & Sons), London (1962).

R63 Rengade, E., L'Hopitallier, P. and Durand de Fontmagne, P. (1936). *Rev. Matér. Constr.* (318), 52; (319), 78.
R64 Raask, E., in *International Symposium on the Carbonation of Concrete* [Proc., RILEM], paper 5.6, Cement and Concrete Association, Slough (1976).
R65 Roy, D.M. and Oyefosobi, S.O. (1977). *J. Am. Ceram. Soc.* **60**, 178.
R66 Ramachandran, V.S. (1978). *Zem.-Kalk-Gips* **31**, 206 (partial English translation, p. 144).
R67 Ramachandran, V.S. (1976). *Cem. Concr. Res.* **6**, 623.
R68 Roy, D.M. and Asaga, K. (1980). *Cem. Concr. Res.* **10**, 387.
R69 Ramachandran, V.S. and Feldman, R.F. (1971). *Cem. Technol.* **2**, 121.
R70 Ramachandran, V.S. (1972). *Cem. Concr. Res.* **2**, 179.
R71 Ramachandran, V.S. and Feldman, R.F. (1972). *Matér. Constr.* **5**, 67.
R72 Ramachandran, V.S. and Feldman, R.F. (1978). *Cemento* **75**, 311.
R73 Ramachandran, V.S. (1971). *Matér. Constr.* **4**, 3.
R74 Regourd, M., Hornain, H. and Aïtcin, P.-C. (1987). *Mater. Res. Soc. Symp. Proc.* **85**, 77.
R75 Roy, D.M. and Harker, R.I., in *4th ISCC*, Vol. 1, p. 196 (1962).
R76 Roy, D.M., in *9th ICCC*, Vol. 1, p. 357 (1992).
R77 Roy, D.M., Gouda, G.R. and Bobrowsky, A. (1972). *Cem. Concr. Res.* **2**, 349.
R78 Roy, D.M. and Gouda, G.R. (1973). *Cem. Concr. Res.* **3**, 807.
R79 Rodger, S.A., Brooks, S.A., Sinclair, W., Groves, G.W. and Double, D.D. (1985). *J. Mater. Sci.* **20**, 2853.
R80 Russell, P.P., Shunkwiler, J., Berg, M. and Young, J.F., in *Advances in Cementitious Materials* (Ceram. Trans. Vol. 16, ed. S. Mindess), p. 501, American Ceramic Society, Westerville, OH (1991).
R81 Rosenberg, A.M. and Gaidis, J.M. (1989). *Concrete International Design and Construction* **2** (4), 31.
R82 Regourd, M. (1985). *Mater. Res. Soc. Symp. Proc.* **42**, 3.
R83 Roy, D.M., in *8th ICCC*, Vol. 1, p. 362 (1986).
R84 Richardson, I.G., Groves, G.W., Brough, A.R. and Dobson, C.M. (1993). *Adv. Cem. Res.* **5**, 81.
R85 Roy, D.M., Malek, R.I.A., Rattanussorn, M. and Grutzeck, M.W. (1986). *Mater. Res. Soc. Symp. Proc.* **65**, 219.
R86 Regourd, M., Hornain, H. and Poitevan, P., in *Alkali–Aggregate Reaction in Concrete*, Paper S252/35, CSIR, Pretoria (1981).
R87 Rasheeduzzafar, Dakhil, F.H., Al-Gahtani, A.S., Al-Saadoun, S.S. and Bader, M.A. (1990). *ACI Mater. J.* **87**, 114.
R88 Rasheeduzzafar, Al-Amoudi, O.S.B., Abduljanwad, S.N. and Maslehuddin, M. (1994). *J. Mater. Civ. Engng* **6**, 201.
R89 Rogers, D.E. (1973). *New Zealand J. Sci.* **16**, 875.

S1 Skibsted, J., Jakobsen, H.J. and Hall, C. (1994). *J. Chem. Soc. Faraday Trans.* **90**, 2095.
S2 Sarkar, S.L. and Roy, D.M., in *6th IC Cem. Microsc.*, p. 37 (1984).
S3 Sinclair, W. and Groves, G.W. (1984). *J. Am. Ceram. Soc.* **67**, 325.
S4 Saalfeld, H. (1975). *Am. Mineral.* **60**, 824.
S5 Smith, D.K. (1962). *Acta Cryst.* **15**, 1146.
S6 Scrivener, K.L. and Taylor, H.F.W. (1995). *ZKG International* **48**, 34.
S7 Scrivener, K.L. and Taylor, H.F.W. (1995). *World Cem. Res. Dev.* **26** (8), 34.

S8 Swanson, H.E. and Tatge, E. *Standard X-ray Powder Diffraction Patterns,* 95pp., (NBS Circular 539, Vol. 1), US Department of Commerce, Washington, DC (1953).
S9 Saburi, S., Kusachi, I., Henmi, C., Kawahara, A., Henmi, K. and Kawada, I. (1976). *Mineral. J.* (Japan) **8**, 240.
S10 Smirnov, G.S., Chatterjee, A.K. and Zhmoidin, G.I. (1973). *J. Mater. Sci.* **8**, 1278.
S11 Scrivener, K.L. and Taylor, H.F.W, p. 41 in *Calcium Aluminate Cements* (ed. R.J. Mangabhai), E & FN Spon, London (1990).
S12 Swayze, M.A. (1946). *Am. J. Sci.* **244**, 1.
S13 Sorrentino, F. and Glasser, F.P. (1976). *Trans. J. Br. Ceram. Soc.* **75**, 95.
S14 Swayze, M.A. (1946). *Am. J. Sci.* **244**, 65.
S15 Sharp, J.D., Johnson, W. and Andrews, W. (1960). *J. Iron Steel Inst.* **195**, 83.
S16 Schlaudt, C.M. and Roy, D.M. (1966). *J. Am. Ceram. Soc.* **49**, 430.
S17 Sarkar, S.L. and Jeffery, J.W. (1979). *J. Am. Ceram. Soc.* **62**, 630.
S18 Sourie, A., Glasser, F.P. and Lachowski, E.E. (1994). *Br. Ceram. Trans.* **93**, 41.
S19 Swanson, H.E., McMurdie, H.F., Morris, M.C. and Evans, E.H. *Standard X- Ray Diffraction Patterns* 186pp. (NBS Monograph No. 25, Section 7), US Department of Commerce, Washington, DC (1969).
S20 Shame, E.G. and Glasser, F.P. (1987). *Trans. J. Br. Ceram. Soc.* **86**, 13.
S21 Smart, R.M. and Roy, D.M. (1979). *Cem. Concr. Res.* **9**, 269.
S22 Smith, J.V., Karle, I.L., Hauptman, H. and Karle, J. (1960). *Acta Cryst.* **13**, 454.
S23 Shibata, S., Kishi, K., Asaga, K., Daimon, M. and Shrestha, P.R. (1984). *Cem. Concr. Res.* **14**, 323.
S24 Spohn, E., Woermann, E. and Knoefel, D., in *5th ISCC*, Vol. 1, p. 172 (1969).
S25 Southard, J.C. and Royster, P.H. (1936). *J. Phys. Chem.* **40**, 435.
S26 Sprung, S., in *7th ICCC*, Vol. 1, p. I-2/1 (1980).
S27 Sylla, H.-M. (1974). *Zem.-Kalk-Gips* **27**, 499.
S28 Sylla, H.-M. (1977). *Zem.-Kalk-Gips* **30**, 487 (partial English translation, p. 264).
S29 Sylla, H.-M. (1981). *Zem.-Kalk-Gips* **34**, 618 (partial English translation, 1982, Vol. 35, p. 31).
S30 Sorrentino, F.P., in *Advances in Cement and Concrete* (eds M.W. Grutzeck and S.L. Sarkar), p. 65, American Society of Civil Engineers, New York (1994).
S31 Sprung, S. (1985). *Zem.-Kalk-Gips* **38**, 577 (partial English translation, p. 309).
S32 Sumner, M.S., Hepher, N.M. and Moir, G.K., in *8th ICCC*, Vol. 2, p. 310 (1986), and private communication.
S33 Sprung, S., Kuhlmann, K. and Ellerbrock, H.-G. (1985). *Zem.-Kalk-Gips* **38**, 528 (partial English translation, p. 275).
S34 St John, D.A. and McGivin, P.N., in *3rd IC Cem. Microsc.*, p. 193 (1981).
S35 Scrivener, K.L. and Pratt, P.L., in *6th IC Cem. Microsc.*, p. 145 (1984).
S36 Scrivener, K.L. (1987). *Mater. Res. Soc. Symp. Proc.* **85**, 39.
S37 Scrivener, K.L., in *Materials Science of Concrete I* (ed. J.P. Skalny), p. 127, American Ceramic Society, Westerville, OH (1989).
S38 Stutzman, P.E. (1991). *Cem. Concr. Aggr.* **13**, 109.

S39 Stutzman, P., in *Advances in Cementitious Materials* (Ceramic Trans., Vol. 16, ed. S. Mindess), p. 199, American Ceramic Society, Westerville, OH (1991).

S40 Struble, L. (1985). *Cem. Concr. Res.* **15**, 631.

S41 Smallwood, T.B. and Wall, C.D. (1981). *Talanta* **28**, 265.

S42 Struble, L.J. (1983). *Cem. Concr. Aggr.* **5**, 62.

S43 Stutzman, P.E., in *14th IC Cem. Microsc.*, p. 290 (1992).

S44 Sakurai, T., Sato, T. and Yoshinaga, A., in *5th ISCC*, Vol. 1, p. 300 (1969).

S45 Skalny, J.P. and Young, J.F., in *7th ICCC*, Vol. 1, p. II-1/3 (1980).

S46 Spierings, G.A.C.M. and Stein, H.N. (1976). *Cem. Concr. Res.* **6**, 265, 487.

S47 Spinolo, G. and Tamburini, U.A. (1985). *Zeit. Naturforschung* **A40**, 73.

S48 Shebl, F.A., Helmy, F.M. and Ludwig, U. (1985). *Cem. Concr. Res.* **15**, 747

S49 Scrivener, K.L., Patel, H.H., Pratt, P.L. and Parrott, L.J. (1987). *Mater. Res. Soc. Symp. Proc.* **85**, 67.

S50 Slegers, P.A., Genet, M., Léonard, A.J. and Fripiat, J.J. (1977). *J. Appl. Cryst.* **10**, 270.

S51 Scrivener, K.L. and Pratt, P.L. (1984). *Mater. Res. Soc. Symp. Proc.* **31**, 351.

S52 Stewart, H.R. and Bailey, J.E. (1983). *J. Mater. Sci.* **18**, 3686.

S53 Scrivener, K.L. and Pratt, P.L. (1984). *Br. Ceram. Proc.* (35), 207.

S54 Scrivener, K.L. (1984). PhD thesis, University of London.

S55 Stade, H. (1980). *Zeit. anorg. allg. Chem.* **470**, 69.

S56 Stade, H., Wieker, W. and Garzo, G. (1983). *Zeit. anorg. allg. Chem.* **500**, 123.

S57 Stade, H. and Wieker, W. (1980). *Zeit. anorg. allg. Chem.* **466**, 55.

S58 Stade, H., Grimmer, A.-R., Engelhardt, G., Mägi, M. and Lipmaa, E. (1985). *Zeit. anorg. allg. Chem.* **528**, 147.

S59 Steinour, H.H. (1947). *Chem. Revs.* **40**, 391.

S60 Steinour, H.H., in *3rd ISCC*, p. 261 (1954).

S61 Stein, H.N. (1972). *Cem. Concr. Res.* **2**, 167.

S62 Smith, R.M. and Martell, A.E. *Critical Stability Constants*, Vol. 4: *Inorganic Complexes*, 257pp., Plenum Press, New York (1976).

S63 Suzuki, K., Nishikawa, T., Ikenaga, H. and Ito, S. (1986). *Cem. Concr. Res.* **16**, 333.

S64 Stein, H.N. and Stevels, J.M. (1964). *J. Appl. Chem.* **14**, 338.

S65 Sierra, R., in *6th ICCC*, Vol. 2, Part 1, p. 138 (1976).

S66 Scheller, T. and Kuzel, H.-J., in *6th ICCC*, Vol. 2, Part 1, p. 217 (1976).

S67 Seligmann, P. and Greening, N.R., in *5th ISCC*, Vol. 2, p. 179 (1969).

S68 Schwiete, H.E. and Iwai, T. (1964). *Zem.-Kalk-Gips* **17**, 379.

S69 Schwiete, H.E., Ludwig, U. and Jäger, P., quoted by H.E. Schwiete and U. Ludwig in *5th ISCC*, Vol. 2, p. 37 (1969).

S70 Struble, L.J., in *8th ICCC*, Vol. 6, p. 582 (1986).

S71 Serb-Serbina, N.N., Savvina, Yu.A. and Zhurina, V.S. (1956). *Doklady Akad. Nauk SSSR* **111**, 659.

S72 Schwiete, H.E., Ludwig, U. and Albeck, J. (1968). *Naturwiss.* **55**, 179.

S73 Sacerdoti, M. and Passaglia, E. (1985). *Bull. Minéral. (Paris)* **108**, 1.

S74 Swanson, H.E., Gilfrich, N.T. and Cook, M.I. *Standard X-ray Powder Diffraction Patterns* (NBS Circular 539, Vol. 6), 62pp., US Dept of Commerce, Washington, DC (1956).

S75 Soustelle, M., Guilhot, B., Fournier, A.A., Murat, M. and Negro, A. (1985). *Cem. Concr. Res.* **15**, 421.
S76 Stein, H.N. (1963). *Silicates Ind.* **28**, 141.
S77 Schwiete, H.E., Ludwig, U. and Jäger, P., in *Symposium on Structure of Portland Cement Paste and Concrete* (Sp. Rpt. 90), p. 353, Highway Research Board, Washington (1966).
S78 Skalny, J. and Tadros, M.E. (1977). *J. Am. Ceram. Soc.* **60**, 174.
S79 Šatava, V. (1988). *Silikatý* **32**, 203.
S80 Strohbauch, G. and Kuzel, H.-J. (1988). *Zem.-Kalk-Gips* **41**, 358 (partial English translation, p. 219)
S81 Scrivener, K.L., in *8th ICCC*, Vol. 3, p. 389 (1986).
S82 Sarkar, A.K. and Roy, D.M. (1979). *Cem. Concr. Res.* **9**, 343.
S83 Stade, H. and Müller, D. (1987). *Cem. Concr. Res.* **17**, 553.
S84 Stade, H., Ulbricht, K. and Mehner, H. (1984). *Zeit. anorg. allg. Chem.* **514**, 149.
S85 Stein, H.H. (1961). *J. Appl. Chem.* **11**, 474.
S86 Shaughnessy III, R. and Clark, P.E. (1988). *Cem. Concr. Res.* **18**, 327.
S87 Schultz, M.A. and Struble, L.J. (1993). *Cem. Concr. Res.* **23**, 273.
S88 Struble, L.J. and Schultz, M.A. (1993). *Cem. Concr. Res.* **23**, 1369.
S89 Struble, L.J. and Lei, W.-G. (1995). *Adv. Cem. Based Mater.* **2**, 224.
S90 Sellevold, E.J. (1974). *Cem. Concr. Res.* **4**, 399.
S91 Schwiete, H.-E. and Ludwig, U. (1966). *Tonind. Zeit.* **90**, 562.
S92 Struble, L., Johnson, S., Hartmann, M., Kaetzel, L. and Jennings, H. *Manual for the Cement Hydration Simulation Model*, NIST Technical Note 1269. National Institute of Standards and Technology, Gaithersburg, MD (1989).
S93 Sereda, P.J., Feldman, R.F. and Swenson, E.G., in *Symposium on Structure of Portland Cement Paste and Concrete* (Sp. Rpt 90), p. 58, Highway Research Board, Washington, DC (1966).
S94 Scrivener, K.L. in *Advances in Cement Manufacture and Use* (ed. E. Gartner), p. 3, Engineering Foundation, New York (1989).
S95 Seligmann, P. (1968). *J. PCA Res. Dev. Labs* **10** (1), 52.
S96 Schreiner, L.J., MacTavish, J.C., Miljković, L., Pintar, M.M., Blinc, R., Lahajnar, G., Lasic, D. and Reeves, L.W. (1985). *J. Am. Ceram. Soc.* **68**, 10.
S97 Sellevold, E.J. and Bager, D.H., in *7th ICCC*, Vol. 4, p. 394 (1981).
S98 Schiller, K.K. (1971). *Cem. Concr. Res.* **1**, 419.
S99 Sereda, P.J., Feldman, R.F. and Ramachandran, V.S., in *7th ICCC*, Vol. 1, p. VI-1/3 (1980).
S100 Smolczyk, H.-G., in *7th ICCC*, Vol. 1, p. III-1/3 (1980).
S101 Stutterheim, N., in *5th ISCC*, Vol. 4, p. 270 (1969).
S102 Smolczyk, H.-G. (1978). *Zem.-Kalk-Gips* **31**, 294 (partial English translation, p. 180).
S103 Stutterheim, N., in *4th ISCC*, Vol. 2, p. 1035 (1962).
S104 Schröder, F., in *5th ISCC*, Vol. 4, p. 149 (1969).
S105 Smolczyk, H.G. (1965). *Zem.-Kalk-Gips* **18**, 238.
S106 Sato, T. and Furuhashi, I., in *Review of the 36th General Meeting*, p. 42, Cement Association of Japan, Tokyo (1982).
S107 Sersale, R. and Orsini, P.G., in *5th ISCC*, Vol. 4, p. 114 (1969).
S108 Sun, G.-K. and Young, J.F. (1993). *Cem. Concr. Res.* **23**, 480.
S109 Stevenson, R.J., Collier, J.C., Crashell, J.J. and Quandt, L.R. (1988). *Mater. Res. Soc. Symp. Proc.* **113**, 87.

S110 Solem, J.K. and McCarthy, G.J. (1992). *Mater. Res. Soc. Symp. Proc.* **245**, 71.
S111 Scian, A.N., Porto López, J.M. and Pereira, E. (1987). *Cem. Concr. Res.* **17**, 198.
S112 Sorrentino F.P. and Glasser, F.P., in *International Seminary on Calcium Aluminates* (eds M. Murat *et al.*), Politecnico di Torino, Turin (1982).
S113 Sorrentino, F.P. and Glasser, F.P. (1975). *Trans. J. Br. Ceram. Soc.* **74**, 253.
S114 Sorrentino, F.P. (1973). PhD thesis, University of Aberdeen.
S115 Sorrentino, D., Sorrentino, F. and George, M., p. 11 in *Materials Science of Concrete IV* (eds J. Skalny and S. Mindess), American Ceramic Society, Westerville, OH (1995).
S116 Sudoh, G., Ohta, T. and Harada, H., in *7th ICCC*, Vol. 3, p. V-152 (1980).
S117 Stark, J., Müller, A., Seydel, R. and Jost, K., in *8th ICCC*, Vol. 2, p. 306 (1986).
S118 Sahu, S. and Majling, J. (1994). *Cem. Concr. Res.* **24**, 1065.
S119 Stadelmann, C. and Wieker, W. (1985). *Cemento* **82**, 203.
S120 Skalny, J. and Odler, I. (1972). *J. Coll. Interface Sci.* **40**, 199.
S121 Scrivener K.L. and Taylor, H.F.W. (1993). *Adv. Cem. Res.* **5**, 139.
S122 Scrivener, K.L. (1992). *Cem. Concr. Res.* **22**, 1224.
S123 Stade, H., Müller, D. and Scheler, G. (1984). *Zeit. anorg. allg. Chem.* **510**, 16.
S124 Sarp, H. and Burri, G. (1986). *Schweiz. Mineral. Petrogr. Mitt.* **66**, 453.
S125 Sugama, T. and Kukacka, L.E. (1980). *Cem. Concr. Res.* **10**, 303.
S126 Struble, L., Skalny, J. and Mindess, S. (1980). *Cem. Concr. Res.* **10**, 277.
S127 Struble, L. and Mindess, S. (1983). *J. Cem. Comp. Lightwt Concr.* **5**, 79.
S128 Scrivener, K.L. and Gartner, E.M. (1988). *Mater. Res. Soc. Symp. Proc.* **114**, 77.
S129 Scrivener, K.L. and Pratt, P.L., in *8th ICCC*, Vol. 3, p. 466 (1986).
S130 Scrivener, K.L. and Pratt, P.L., in *From Materials Science to Construction Materials Engineering* (ed. J.-C. Maso), Vol. 1, p. 61, Chapman and Hall, London (1987)
S131 Scrivener, K.L., Crumbie, A.K. and Pratt, P.L. (1988). *Mater. Res. Soc. Symp. Proc.* **114**, 87.
S132 Schimmel, G. (1970). *Naturwiss.* **57**, 38.
S133 Scrivener, K.L., Bentur, A. and Pratt, P.L. (1988). *Adv. Cem. Res.* **1**, 230.
S134 Somerville, G. (1986). *Struct. Eng.* **64A**, 60, 233.
S135 Suzuki, K., Nishikawa, T. and Ito, S. (1985). *Cem. Concr. Res.* **15**, 213.
S136 Stanton, T.E. (1940). *Proc. Am. Soc. Civil Eng.* **66**, 1781.
S137 Struble, L.J. and Diamond, S. (1982). *J. Am. Ceram. Soc.* **64**, 652.
S138 Struble, L. and Diamond, S. (1981). *Cem. Concr. Res.* **11**, 611.
S139 Sylla, H.-M. (1988). *Beton* **38**, 449.
S140 Shayan, A. and Quick, G.W. (1992). *ACI Mater. J.* **89**, 348.
S141 Shayan, A. and Quick, G.W., in *16th IC Cem. Microsc.*, p. 69 (1994).
S142 Scrivener, K.L., in *18th IC Cem. Microsc.*, p. 375 (1996).
S143 Shayan, A. and Ivanusec, I. (1996). *Cem. Concr. Composites*, **18**, 161.
S144 St John, D.A. (1982). *Cem. Concr. Res.* **12**, 633.
S145 Smolczyk, H.G., in *5th ISCC*, Vol. 3, p. 274 (1969).
S146 Stucke, M.S. and Majumdar, A.J. (1976). *J. Mater. Sci.* **11**, 1019.

T1 Timashev, V.V., in *7th ICCC*, Vol. 1, p. I-3/1 (1980).
T2 Terrier, P., Hornain, H. and Socroun, G. (1968). *Rev. Matér. Constr.* (630) 109.

T3 Terrier, P., in *5th ISCC*, Vol. 2, p. 278 (1969).
T4 Takéuchi, Y, Nishi, F. and Maki, I. (1980). *Zeit. Krist.* **152**, 259.
T5 Taylor, H.F.W. (1989). New data.
T6 Taylor, W.C. (1942). *J. Res. Nat. Bur. Stand.* **29**, 437.
T7 Tanaka, M., Sudoh, G. and Akaiwa, S., in *5th ISCC*, Vol. 1, p. 122 (1969).
T8 Thorvaldson, T., quoted by F.M. Lea in L6.
T9 Triviño Vázquez, F. (1985). *Cem. Concr. Res.* **15**, 581.
T10 Takashima, S., in *Review of the 12th General Meeting*, p. 12, Cement Association of Japan, Tokyo (1958).
T11 Tabikh, A. and Weht, R.J. (1971). *Cem. Concr. Res.* **1**, 317.
T12 Tamás, F.D., Sarkar, A.K. and Roy, D.M., in *Hydraulic Cement Pastes: Their Structure and Properties*, p. 55, Cement and Concrete Association, Slough, UK (1976).
T13 Taylor, H.F.W. (1989). *Adv. Cem. Res.* **2**, 73.
T14 Taylor, J.C. and Aldridge, L.P. (1993). *Powder Diffraction* **8**, 138.
T15 Taylor, H.F.W. (1991), in *Advances in Cementitious Materials* (Ceramic Trans., Vol. 16, ed. S. Mindess), p. 185, American Ceramic Society, Westerville, OH (1991).
T16 Taylor, H.F.W. and Turner, A.B. (1987). *Cem. Concr. Res.* **17**, 613.
T17 Taylor, H.F.W. (1981). *Chem. Ind.* 620.
T18 Taylor, H.F.W. (1984). *Br. Ceram. Proc.* (35) 65.
T19 Taylor, H.F.W., Mohan, K. and Moir, G.K. (1985). *J. Am. Ceram. Soc.* **68**, 680.
T20 Taylor, H.F.W. and Newbury, D.E. (1984). *Cem. Concr. Res.* **14**, 93.
T21 Taylor, H.F.W. (1986). *J. Am. Ceram. Soc.* **69**, 464.
T22 Taylor, H.F.W. (1950). *J. Chem. Soc.* 3682.
T23 Taylor, H.F.W. (1992). *Zeit. Krist.* **202**, 41.
T24 Taylor, H.F.W. (1960). *Prog. Ceram. Sci.* **1**, 89.
T25 Taylor, H.F.W. and Howison, J.W. (1956). *Clay Minerals Bull.* **3**, 98.
T26 Taylor, H.F.W. (1993). *Adv. Cem. Based Mater.* **1**, 38.
T27 Taylor, H.F.W., Barret, P., Brown, P.W., Double, D.D., Frohnsdorff, G., Johansen, V., Ménétrier-Sorrentino, D., Odler, I., Parrott, L.J., Pommersheim, J.M., Regourd, M. and Young, J.F. (1984). *Matér. Constr.* **17**, 457.
T28 Taylor, H.F.W. (1985). *Mater. Sci. Monogr. 28A* (Reactivity of Solids, Part A) 39.
T29 Thomassin, J.-H., Regourd, M., Baillif, P. and Touray, J.-C. (1979). *Comptes Rendus Acad. Sci. Paris* **C288**, 93.
T30 Tadros, M.E., Skalny, J. and Kalyoncu, R.S. (1976). *J. Am. Ceram. Soc.* **59**, 344.
T31 Tong, H.S. and Young, J.F. (1977). *J. Am. Ceram. Soc.* **60**, 321.
T32 Turriziani, R. and Schippa, G. (1954). *Ricerca Sci.* **24**, 2356.
T33 Tilley, C.E., Megaw, H.D. and Hey, M.H. (1934). *Mineral. Mag.* **23**, 607.
T34 Turriziani, R. and Schippa, G. (1956). *Ricerca Sci.* **26**, 2792.
T35 Tang, F.J. and Gartner, E.M. (1988). *Adv. Cem. Res.* **1**, 67.
T36 Teoreanu, I, Filoti, G., Hritcu, C., Bucea, L., Spânu, V., Ciocanel, S. and Ivascu, M. (1979). *Cemento* **76**, 19.
T37 Taylor, H.F.W. and Newbury, D.E. (1984). *Cem. Concr. Res.* **14**, 565.
T38 Taylor, H.F.W. (1987). *Mater. Res. Soc. Symp. Proc.* **85**, 47.
T39 Taylor, H.F.W., Mohan, K. and Moir, G.K. (1985). *J. Am. Ceram. Soc.* **68**, 685.

T40 Tamás, F. and Amrich, L. (1978). *Cemento* **75**, 357.
T41 Taylor, H.F.W., in *Advances in Cement Manufacture and Use* (ed. E. Gartner), p. 295, Engineering Foundation, New York (1989).
T42 Taylor, H.F.W., in *Cement Technology* (Ceramic Trans., Vol. 40, eds E.M. Gartner and H. Uchikawa), p. 61, American Ceramic Society, Westerville, OH, USA (1994).
T43 Taylor, H.F.W. (1987). *Adv. Cem. Res.* **1**, 5.
T44 Thomas, N.L. and Double, D.D. (1981). *Cem. Concr. Res.* **11**, 675.
T45 Tang, F.J. and Tresouthick, S.W., in *9th ICCC*, Vol. 4, p. 317 (1992).
T46 Taplin, J.H. (1959). *Austral. J. Appl. Sci.* **10**, 329.
T47 Taplin, J.H., in *5th ISCC*, Vol. 2, pp. 249, 337 (1969).
T48 Tattersall, G.H. and Banfill, P.F.G. *The Rheology of Fresh Concrete*, 356pp., Pitman Books, London (1983).
T49 Tamás, F.D., Farkas, E., Vörös, M. and Roy, D.M., in *8th ICCC*, Vol. 6, p. 374 (1986).
T50 Tanaka, H., Totani, Y. and Saito, Y., in *Fly Ash, Silica Fume, Slag and Other Mineral By-Products in Concrete* (ed. V.M. Malhotra), Sp. Publ. SP79, Vol. 2, p. 963, American Concrete Institute, Detroit, MI (1983).
T51 Thorne, D.J. and Watt, J.D. (1965). *J. Appl. Chem.* **15**, 595.
T52 Traetteberg, A. (1978). *Cemento* **75**, 369.
T53 Taplin, J.H., in *4th ISCC*, Vol. 2, p. 924 (1962).
T54 Thomas, N.L. and Birchall, J.D. (1983). *Cem. Concr. Res.* **13**, 830.
T55 Thomas, N.L. and Birchall, J.D. (1984). *Cem. Concr. Res.* **14**, 761.
T56 Thomas, N.L. and Double, D.D. (1983). *Cem. Concr. Res.* **13**, 391.
T57 Taylor, H.F.W., in *Chemistry of Cements* (ed. H.F.W. Taylor), Vol. 1, p. 167, Academic Press, London (1964).
T58 Tenoutasse, N., in *5th ISCC*, Vol. 2, p. 372 (1969).
T59 Thomas, N.L., Jameson, D.A. and Double, D.D. (1981). *Cem. Concr. Res.* **11**, 143.
T60 Taylor, H.F.W., in *5th ISCC*, Vol. 2, p. 1 (1969).
T61 Taylor, H.F.W. and Roy, D.M., in *7th ICCC*, Vol. 1, p. II-2/1 (1980).
T62 Taylor, H.F.W., in *6th ICCC*, Vol. 2, Part 1, p. 192 (1976).
T63 Taylor, W.H., Moorehead, D.R. and Cole, W.F., in *Autoclaved Calcium Silicate Building Products*, p. 130, Society of Chemical Industry, London (1967).
T64 Tashiro, C. and Tatibana, S. (1983). *Cem. Concr. Res.* **13**, 377.
T65 Turriziani, R., in *8th ICCC*, Vol. 1, p. 388 (1986).
T66 Thomas, S., Meise-Gresch, K., Müller-Warmuth, W. and Odler, I. (1993). *J. Am. Ceram. Soc.* **76**, 1998.
T67 Thorvaldson, T., in *3rd ISCC*, p. 436 (1954).
T68 Tang, M.-S. Liu, Z. and Han, S.-F., in *Concrete Alkali–Aggregate Reactions* (ed. P.E. Grattan-Bellew), p. 275, Noyes Publ., Park Ridge, NJ (1987).

U1 Uchikawa, H., Hanehara, S. and Shirasaka, T., in *9th ICCC*, Vol. 2, p. 3 (1992).
U2 Uchikawa, H., Ogawa, K. and Uchida, S. (1985). *Cem. Concr. Res.* **15**, 561.
U3 Udagawa, S., Urabe, K. and Yano, T., in *Review of the 34th General Meeting*, p. 37, Cement Association of Japan, Tokyo (1980).
U4 Udagawa, S., Urabe, K., Natsume, M. and Yano, T. (1980). *Cem. Concr. Res.* **10**, 139.

U5 Udagawa, S., Urabe, K. and Yano, T., in *Review of the 31st General Meeting*, p. 23, Cement Association of Japan, Tokyo (1977).
U6 Urabe, K., Yano, T., Iwai, A., Udagawa, S. and Ikawa, H., in *Review of the 36th General Meeting*, p. 27, Cement Association of Japan, Tokyo (1982).
U7 Udagawa, S. and Urabe, K., in *Review of the 32nd General Meeting*, p. 31, Cement Association of Japan, Tokyo (1978).
U8 Udagawa, S., Urabe, K., Yano, T. and Natsume, M (1980). *Yogyo-Kyokai-Shi* **88**, 285.
U9 Udagawa, S., Urabe, K., Yano, T., Takada, K. and Natsume, M., in *Review of the 33rd General Meeting*, p. 35, Cement Association of Japan, Tokyo (1979).
U10 Uchikawa, H. and Furuta, R. (1981). *Cem. Concr. Res.* **11**, 65.
U11 Ueda, S., Hashimoto, M. and Kondo, R. (1968). *Semento Gijutsu Nenpo* **22**, 67.
U12 Uchikawa, H. (1984). *Am. Ceram. Soc. Bull.* **63**, 1143.
U13 Uchikawa, H. (1986). *J. Res. Onoda Cement Company* **38**, 1.
U14 Uchikawa, H., Uchida, S., Ogawa, K. and Hanehara, S. (1984). *Cem. Concr. Res.* **14**, 645.
U15 Uchikawa, H., Uchida, S. and Hanehara, S. (1987). *Cemento* **84**, 3.
U16 Ushiyama, H. and Goto, S., in *6th ICCC*, Vol. 2, Part 1, p. 331 (1976).
U17 Uchikawa, H., Uchida, S. and Hanehara, S., in *8th ICCC*, Vol. 4, p. 245 (1986).
U18 Uchikawa, H., in *8th ICCC*, Vol. 1, p. 249 (1986).
U19 Uchikawa, H., Uchida, S. and Ogawa, K., in *8th ICCC*, Vol. 4, p. 251 (1986).
U20 Uchikawa, H., Uchida, S. and Ogawa, K., in *The Use of PFA in Concrete* (eds J.G. Cabrera and A.R. Cusens), p. 83, Leeds University, Concrete Society and CEGB (1982).
U21 Uchikawa, H. (1985). *Cem. Concr. (Japan)* (460), 20.
U22 Uchikawa, H. and Tsukiyama, K. (1973). *Cem. Concr. Res.* **3**, 263.
U23 Uchikawa, H. and Uchida, S. (1972). *Cem. Concr. Res.* **2**, 681.
U24 Uchikawa, H. and Uchida, S. (1973). *Cem. Concr. Res.* **3**, 607.
U25 Ushiyama, H., Kawano, Y. and Kamegai, N., in *8th ICCC*, Vol. 3, p. 154 (1986).

V1 Vincent, M.G. and Jeffery, J.W. (1978). *Acta Cryst.* **B34**, 1422.
V2 Vosteen, B. (1974). *Zem.-Kalk-Gips* **27**, 443.
V3 Vásquez, T., Blanco-Varela, M.T. and Palomo, A. (1984). *Br. Ceram. Proc.* (35) 115.
V4 Viehland, D, Li, J.-F., Yuan, L.-J. and Xu, Z. (1996). *J. Am. Ceram. Soc.* **79**, 1731.
V5 Van Aardt, J.H.P. and Visser, S., in *7th ICCC*, Vol. 4, p. 483 (1981).
V6 Vernet, C., in *8th ICCC*, Vol. 3, p. 70 (1986).
V7 Verbeck, G.J. and Helmuth, R.H., in *5th ISCC*, Vol. 3, p. 1 (1969).
V8 Vernet, C. (1982). *Silicates Indust.* **47**, 85.
V9 Volkov, V.V., Kolyovski, V.P. and Yanev, Ya.D., in *6th ICCC*, Vol. 3, p. 182 (1976).
V10 Vernet, C., in *8th ICCC*, Vol. 2, p. 316 (1986).
V11 Viswanathan, V.N., Raina, S.J. and Chatterjee, A.K. (1978). *World Cem. Technol.* **9**, 109.
V12 Von Lampe, F., Hilmer, W., Jost, K.-H., Reck, G. and Boikova, A.I. (1986). *Cem. Concr. Res.* **16**, 505.

V13 Vivian, H.E. (1950). *CSIRO Bull.* (256) 60.
V14 Van Aardt, J.H.P. and Visser, S. (1977). *Cem. Concr. Res.* **7**, 643.
V15 Van Aardt, J.H.P. and Visser, S. (1978). *Cem. Concr. Res.* **8**, 677.

W1 Woermann, E., Hahn, T. and Eysel, W. (1979). *Cem. Concr. Res.* **9**, 701.
W2 Welch, J.H. and Gutt, W. (1959). *J. Am. Ceram. Soc.* **42**, 11.
W3 Winchell, A.N. and Winchell, H. *The Microscopical Characters of Artificial Inorganic Solid Substances*, 439pp., Academic Press, London and New York (1964).
W4 Williams, P.P. (1968). *J. Am. Ceram. Soc.* **51**, 531.
W5 Williams, P.P. (1973). *Acta Cryst.* **B29**, 1550.
W6 Welch, J.H., in *Chemistry of Cements* (ed. H.F.W. Taylor), Vol. 1, p. 49, Academic Press, London (1964).
W7 Welch, J.H. (1961). *Nature* **191**, 559.
W8 Welch, J.H. and Gutt, W., in *4th ISCC*, Vol. 1, p. 59 (1962).
W9 Wolter, A (1985). *Zem.-Kalk-Gips* **38**, 612 (partial English. translation, p. 327).
W10 Wagman, D.D. and 7 other authors (1982). The NBS Tables of Chemical Thermodynamic Properties, *J. Phys. Chem. Ref. Data* **11**, Suppl. 2, 392pp., American Chemical Society, Washington, DC and American Institute of Physics, New York.
W11 Williamson, J. and Glasser, F.P. (1962). *J. Appl. Chem.* **12**, 535.
W12 Weyer, I. (1931). *Zement* **20**, 560, 608, 692.
W13 Weber, P. *Heat Transfer in Rotary Kilns*, 98pp., Bauverlag, Wiesbaden and Berlin (1963).
W14 Wolter, A., in *8th ICCC*, Vol. 2, p. 89 (1986).
W15 Weisweiler, W., Osen, E., Eck, J. and Höfer, H. (1986). *Cem. Concr. Res.* **16**, 283.
W16 Woermann, E., in *4th ISCC*, Vol. 1, p. 119 (1962).
W17 Wagner, L.A. (1933). *ASTM Bull.* **33**, 553.
W18 Webb, T.L. and Heystek, H., in *The Differential Thermal Investigation of Clays* (ed. R.C. Mackenzie), p. 329, Mineralogical Society, London (1957).
W19 Williamson, R.B. (1972). *Prog. Mater. Sci.* **15**, 189.
W20 Wieker, W. (1968). *Zeit. anorg. allg. Chem.* **360**, 307.
W21 Wieker, W., Grimmer, A.-R., Winkler, A., Mägi, M., Tarmak, M. and Lipmaa, E. (1982). *Cem. Concr. Res.* **12**, 333.
W22 Wu, Z.-Q., Hriljac, J., Hwang, C.-L. and Young, J.F. (1983). *J. Am. Ceram. Soc.* **66**, C86.
W23 Wu, Z.-Q. and Young, J.F. (1984). *J. Am. Ceram. Soc.* **67**, 48.
W24 Way, S.J. and Shayan, A. (1989). *Cem. Concr. Res.* **19**, 759.
W25 Wittmann, F.H., in *Hydraulic Cement Pastes: Their Structure and Properties*, p. 96, Cement and Concrete Association, Slough, UK (1976).
W26 Wittmann, F.H., in *7th ICCC*, Vol. 1, p. VI-2/1 (1980).
W27 Winslow, D.N. and Diamond, S. (1973). *J. Coll. Interface Sci.* **45**, 425.
W28 Winslow, D.N. and Diamond, S. (1974). *J. Am. Ceram. Soc.* **57**, 193.
W29 Winslow, D.N., Bukowski, J.M. and Young, J.F. (1994). *Cem. Concr. Res.* **24**, 1025.
W30 Winslow, D.N., Bukowski, J.M. and Young, J.F. (1994). *Cem. Concr. Res.* **25**, 147.
W31 Wang, S.-D, Pu, X.-C., Scrivener, K.L. and Pratt, P.L. (1995). *Adv. Cem. Res.* **7**, 93.

W32 Wang, S.-D. and Scrivener, K.L. (1995). *Cem. Concr. Res.* **25**, 561.
W33 Watt, J.D. and Thorne, D.J. (1965). *J. Appl. Chem.* **15**, 585.
W34 Watt, J.D. and Thorne, D.J. (1966). *J. Appl. Chem.* **16**, 33.
W35 Wei, F.-J., Grutzeck, M.W. and Roy, D.M. (1985). *Cem. Concr. Res.* **15**, 174.
W36 Wu C.-W. and Wang Y.-S., in *7th ICCC*, Vol. 3, p. V-27 (1980).
W37 Wang, Y., Deng, J. and Su, M., in *8th ICCC*, Vol. 3, p. 300 (1986).
W38 Wang, L. and Glasser, F.P. (1996). *Adv. Cem. Res.* **8**, 127.
W39 Wilding, C.R., Walter, A. and Double, D.D. (1984). *Cem. Concr. Res.* **14**, 185.
W40 Winkler, A. and Wieker, W. (1979). *Zeit. anorg. allg. Chem.* **451**, 45.
W41 Wu, Z.-W., Liu, B.-Y. and Xie, S.-S., in *Liaisons Pâtes de Ciment Matériaux Associés* [Proc. RILEM Colloq.], p.A28, Laboratoire de Génie Civil, Toulouse (1982).
W42 Winslow, D. and Liu, D. (1990). *Cem. Concr. Res.* **20**, 227.
W43 Winslow, D.N., Cohen, M.D., Bentz, D.P., Snyder, K.A. and Garboczi, E.J. (1994). *Cem. Concr. Res.* **24**, 25.
W44 Wang, J.G. (1994). *Cem. Concr. Res.* **24**, 735.
W45 Wieker, W. and Herr, R. (1989). *Z. Chemie* **29**, 321.
W46 Way, S.J. and Cole, W.F. (1982). *Cem. Concr. Res.* **12**, 611.

X1 Xue, J.-G., Xu, W.-X. and Ye, M.-X. (1983). *Guisuanyan Xuebao* **11**, 276; *Chem. Abstr.* **100**, 73009c (1984).
X2 Xu, Z., Gu, P., Xie, P. and Beaudoin, J.J. (1993). *Cem. Concr. Res.* **23**, 853.
X3 Xi, Y. and Jennings, H.M. in *Materials Science of Concrete III* (ed. J.P. Skalny), p. 37, American Ceramic Society, Westerville, OH (1992).
X4 Xue J.-G., Tong X.-L., Chen W.-H., Xu J.-Zh., Xi Y.-Zh. and Zhang, Y.-Y., in *8th ICCC*, Vol. 4, p. 306 (1986).

Y1 Yamaguchi, G. and Takagi, S., in *5th ISCC*, Vol. 1, p. 181 (1969).
Y2 Yannaquis, N. and Guinier, A. (1959). *Bull. Soc. franç. Minéral. Cryst.* **82**, 126.
Y3 Yamanaka, T. and Mori, H. (1981). *Acta Cryst.* **B37**, 1010.
Y4 Yoshioka, T. (1970). *Bull. Chem. Soc. Japan* **43**, 1981, 2317.
Y5 Young, J.F. and Hansen, W. (1987). *Mater. Res. Soc. Symp. Proc.* **85**, 313.
Y6 Young, J.F. (1988). *J. Am. Ceram. Soc.* **71**, C118.
Y7 Yan R.-Zh., Ouyang, Sh.-X. and Gao Q.-Y. (1983). *Silicates Ind.* **12**, 3.
Y8 Young, J.F. (1972). *Cem. Concr. Res.* **2**, 415.
Y9 Yano, T., Urabe, K., Ikawa, H., Teraushi, T., Ishizawa, N. and Udagawa, S. (1993). *Acta Cryst.* **C49**, 1555.

Z1 Zheng, Y. and Yang, N., in *8th ICCC*, Vol. 2, p. 293 (1986).
Z2 Zeng, Y. and Yang, N. (1991). *Cem. Concr. Res.* **21**, 31.
Z3 Zhmoidin, G.I. and Chatterjee, A.K. (1984). *Cem. Concr. Res.* **14**, 386.
Z4 Zhmoidin, G.I. and Chatterjee, A.K. (1985). *Cem. Concr. Res.* **15**, 442.
Z5 Zhang, P., Chen, Y., Shi, L., Zhang, G., Huang, W. and Wu, J., in *9th ICCC*, Vol. 3, p. 201 (1992).
Z6 Zhmoidin, G.I. and Chatterjee, A.K. (1974). *Inorg. Mater.* **10**, 1584 (translated from *Neorg. Mater.* **10**, 1846).

Z7 Zur Strassen, H. (1957). *Zem.-Kalk-Gips* **10**, 1.
Z8 Ziegler, E. (1971). *Zem.-Kalk-Gips* **24**, 543.
Z9 Zur Strassen, H. (1959). *Zement Beton* (16) 32.
Z10 Zürz, A. and Odler, I. (1987). *Adv. Cem. Res.* **1**, 27.
Z11 Zur Strassen, H. and Strätling, W. (1940). *Zeit. anorg. allg. Chem.* **245**, 267.
Z12 Zur Strassen, H. (1958). *Zem.-Kalk-Gips* **11**, 137.
Z13 Zelwer, A., in *7th ICCC*, Vol. 2, p. II-147 (1980).
Z14 Zakharov, L.A., in *6th ICCC*, Vol. 3, p. 153 (1976).
Z15 Zhang, X., Groves, G.W. and Rodger, S.A. (1987). *Mater. Res. Soc. Symp. Proc.* **114**, 89.

# Index

Substances are indexed under the most commonly used designations; thus, the major phases of Portland cement clinker, natural minerals and common chemical compounds are usually indexed by name, and other chemical compounds by cement chemical formulae. Broad categories of compounds (e.g. calcium magnesium silicates) are indexed by name